2021

Out in the Open: A Geoarchaeological Approach to Open-Air Surface Archaeology in the Semi-Arid Interior of South Africa's Western Cape

Natasha Phillips

UNIVERSITY
OF WOLLONGONG
AUSTRALIA

Out in the Open
A Geoarchaeological Approach to Open-Air Surface Archaeology in the Semi-Arid Interior of South Africa's Western Cape

Natasha Phillips

Supervisors:
Alex Mackay, Zenobia Jacobs & Brian G. Jones

This thesis is presented as part of the requirement for the conferral of the degree:
Doctor of Philosophy

This research has been conducted with the support of the Australian Government Research Training Program Scholarship

The University of Wollongong
School of Earth, Atmospheric, and Life Sciences
Centre for Archaeological Science

March 2021

ABSTRACT

Southern African research into the behavioural evolution of Late Pleistocene human adaptability, flexibility, and innovation is typically pursued through the lens of rock shelter deposits. However, rock shelters only cover a very small, geographically specific area of the subcontinent, distorting our understanding of change in human-environment interaction and demography. While still under-represented and under-explored in regional syntheses, more studies are looking to open-air archaeology to fill this geographic void in Late Pleistocene research. These studies either pursue a landscape approach that prioritises spatial coverage, or site-bound excavation to maximise temporal control. However, few investigate the depositional and erosional phenomena involved in the formation of surface archaeology and its surrounding landscape.

To rectify this disparity, this thesis explores the complex spatio-temporal relationship between surface archaeology and the formation history of Uitspankraal (UPK) 7 by combining multiple interdisciplinary methods from the Earth and archaeological sciences: randomised surface survey and sampling, geomorphometry, geophysical survey, granulometry, XRD analysis, OSL dating, artefact mapping, and assemblage composition and artefact condition analysis.

UPK7 is located in the semi-arid Doring River valley and yields surface archaeology that implies occupation from the Still Bay to the Historic period. Results show that it is an eroding series of source-bordering dunes draped across a palaeoterrace and a hillslope of bedrock and colluvium. UPK7 formed through rapid but pulsed sediment accumulation over at least the last 80 ka, with periods of surface deflation and exposure that facilitated artefact redistribution. Despite the abundance of Late Pleistocene archaeology at UPK7, erosion currently outpaces deposition and deposit stabilisation. Erosion has accelerated in at least the last 5,000 years and especially within the last 300 years, suggesting feedback between Holocene aridification, an increase in oscillations between wet-dry conditions, and an increase in human-ungulate activity in the study area. Together these conditions have differentially erased younger deposits, exposing the consolidated Late Pleistocene sediment and the more ancient material it preserves.

The visibility, spatio-temporal distribution, and preservation of UPK7's surface artefacts reflect the locality's topography, the timing of their discard and the duration and process of sediment accumulation and erosion. The spatial patterning and diversity of time-diagnostic and non-diagnostic artefacts is shown to correspond with the depositional age of their underlying substrate in areas where topographic conditions minimize or reduce the impact of surface runoff, but where sediment deflation persists. When artefacts are assessed at the scale of the archaeological epoch the spatial distribution of Middle Stone Age artefacts shows a significant association with the oldest deposit, Lower Red. The spatial distribution of Later Stone Age artefacts is significantly associated with Upper Yellow sediment, as opposed to the older Lower Red substrate and the younger Indurated Sand.

The findings presented in this thesis caution against forming behavioural interpretations from spatial patterns in surface material without examining their post-depositional history and without forming an understanding of the coevolution of archaeological and landscape formation. This study underscores the need for incorporating a geoarchaeological approach into Late Pleistocene open-air research to improve southern Africa's landscape-scale insight into greater Africa's human behavioural evolution.

DEDICATION

This thesis is dedicated to the fleetingness of life and the persistence of memory

–

to those who have come and gone:

Manus Hough; my grandma, Zena Phillips; my nana, Constance Lamb-Shawcross; my poppa, Ronald Shawcross; my heart and soul, Julie Wheeler; And my wonderful four-legged and yellow beaked family: Mini Mynah, Henrietta Rose, Crystal, Kitty, and Leo Phillips.

You remind me that no matter how short life is, it is full of possibility, fed by memory, love, laughter, and curiosity.

ACKNOWLEDGMENTS

It feels like a legion of people have helped to turn this thesis into a submittable document. To start, my supervisors—Alex Mackay and Zenobia Jacobs—were instrumental in encouraging this interdisciplinary and somewhat ambitious project. Their attempts to reign in my need to cover every aspect of the Doring River valley were only slightly successful. Even so, it is from their patience, support, and critical feedback that the best parts of this thesis have taken form. Thank you, Zenobia, for believing in my ability to learn and implement OSL and for supplying me with the necessary training and resources to do this. Thank you, Alex, for giving me the opportunity and autonomy to explore, study and run amok in the Doring River valley. If you had not, I would have never had the pleasure of acquainting myself with the wonderful world of the eastern Cederberg. Considerable debt is owed to Brian Jones, who provided in-field and post-field guidance, advice, training, and analytical support for the sedimentological component of this thesis. Along with my supervisors, Brian's commitment and support throughout this venture was critical in getting my thesis across the line.

This PhD was largely funded by a University of Wollongong PhD Scholarship, while some of the equipment used for survey and data collection came from an Australian Research Council's DECRA grant (Mackay, DE130100068), and the additional spatial data collected in 2019 was supported by a separate Australian Research Council grant (FT160100139) to Alex Mackay. Collectively, this funding, the support of my family, part time work through the University of the Witwatersrand and the University of Wollongong, and the generosity of time and labour from my friends and family kept both this PhD and its candidate alive, mostly healthy, and productive. Thanks also to the South African Weather Service (SAWs), as well as Pierre-Louis Kloppers and the Department of Environmental & Geographical Science at Climate System Analysis Group (CSAG) for supplying modern and historic climate data of the Olifants-Doring catchment.

I am also extremely grateful for access to the archaeology in the Doring River and accommodation near UPK7 that was granted by and organised through the generosity and hospitality of Lilly, Wilme and the late Manus Hough (my Cederberg whanau), Fungai and Morning, Mariette and Barry Lubbe, and the Pretorius troop (Leon, Kyle, and Louisa). The OSL component of this thesis was made possible by the support, training, and guidance of the UOW laboratory team. Particular thanks go to the patience and training of Yasaman Jafari and Terry Lachlan as well as the all-hours support from my dear friends and colleagues Daniela Müeller and Maria Schaarschmidt. Heidi Brown also provided invaluable GIS support throughout my time at the University of Wollongong. Thank you so much for all your help, advice, and wonderful brain storming sessions. Thanks also to Jose Abrantes for the technical support and training with preparing the U/Th samples and supplying me with many a sample bag and great conversation.

The field seasons carried-out for this thesis were made possible by a team of incredible people, who generously gave their time, enthusiasm, and expertise. The first field season of this project involved collaboration with Alex Sumner, Sam Lin, Matt Douglass, Aara Welz, and my lead supervisor, Alex Mackay. Their time and guidance were indispensable in helping get this doctorate started and the survey marks set up. The field season of October 2014 was pivotal to how this thesis developed and made for an enjoyable and dynamic experience. A special thanks to Marika Low, Manuel Will, Weasley Flear, Ceda Byrne, and Jared Brindley for forming the River Rat team. Their company, hard work, and help with data

collection and survey at UPK7 helped this project to find its feet.

The subsequent field seasons were made possible by the assistance of a few vital people. Lily Hough, thank you so much for providing my crew and I with your family farmhouse, your warmth, company, homemade rusks (the best in the world) and hot meals. Love you heaps. Thanks to Matthew Shaw and Benjamin Marais for March 2015. It was a tough season and without your assistance, energy, company, and laughter, I would not have survived. A special thanks also goes to Marika Low for help with co-directing and assisting me with some of the hottest, hardest field seasons in the Doring. To think I would have never met you if I had not started this doctorate...Thank you for your friendship, intelligence, climbing abilities, and free spirit. You are an inspiration. Thanks to Brigette E. Cohen for making my August 2015 field season possible and memorable—your assistance and advice were invaluable, and your company was the icing on the cake. Thank you. Thanks also to my 2016 field crews whose dedication, hard work and problem-solving skills were vital to the success of each field season. Thank you, Blair McPhee, for taking time out of an already full schedule to count rocks with me in the blistering heat and relentless wind, and Brian Jones for investing your own time and money in assisting and teaching me in the ways of the intrepid geoscientist.

I will always be grateful to my awesome August 2016 team: Aurore Val, Gizelle Kotze, Morne Valentyn, Chris Thornhill, and Alex Blackwood. Your passion for my project and drive to help make it the best it could be was a gift that I hope I have the pleasure of experiencing again. Thanks also to Dominic Stratford for traveling from Johannesburg to provide me with sage geoarchaeological advice, a drone, piloting skills, and the first of a series of valuable digital surface models for UPK1 and 7. Your support over the years and your passion for South African archaeology have been pivotal in my own journey to becoming a geoarchaeologist. A big thank you also to Ian Moffat for carrying out, processing, and analysing the geophysical survey of UPK7 for this thesis, your company during the July 2017 field season was a breath of fresh air with great field banter to top it off. You also gave me valuable advice and a second opinion on the geomorphology and formation history of this locality. And finally, thank you to Matt Shaw and Chris Ames for your instrumental work in collecting and providing access to invaluable spatial data to supplement my own. I hope I have done justice to it or at least trialled what not to do for our future spatial paper…

My PhD candidature was mostly split between three countries, and I would argue I have three country's worth of family and friends to thank for making it one of the richest, most humbling, and satisfying experiences of my life. The people make the place. Thanks to my South African cohort—Aurore, Lilly and Wilme, Barry and Marion Jacoby, Kathy Kuman, Gillian Warren-Brown and Ben Maclennan, Alex Sumner, Emese Bordy, Ben Collins, Brigette, Gizelle, Morne, Kimi Chapelle and Dominic, Kathleen Dolman, Christine Steininger, Bruce Rubidge, Gerrit Dusseldorp, Vincent Fernandez, Michael Day, Katja Douze, Paloma de la Peña, Viola Schmid, Cory Dinter, Katherine Clayton, Zubair Jinnah, Jerome and Tammy Reynard, Matt Caruana, Sam Challis, Alice, Silindokuhle Mavuso, Pia Viglietti, Jonah and Kelsey, Eveline, and Fernando Abdala—for accepting me with open arms, and filling my time in southern Africa with passionate conversations, adventure, and very, very good company. I will never be the same…The University of Cape Town (UCT) was also a valuable base while I prepared for each field season. It was also where most of my field gear and samples were stored between seasons. This was organised with the

help and support of the staff in the Department of Archaeology, particularly Louisa Hutten, Jane Wilkins, and Ben Schoville. Thank you. Although UCT was my official host university in South Africa, my home was Johannesburg, and the University of the Witwatersrand was my hub. Thank you to the staff and students in the Evolutionary Studies Institute, Origins Centre, the Geography, Archaeology, and Environmental School, the Postgraduate Club, and Xia Xia, many of whom are listed above. Thanks also to my Wollongong cohort—Daniela, James Hooper and Jungmin Lee, Nuria Lahuerta, Leo Rothacker, Sara Brandolese and Davide Di Nitto, Kirti Lal, Kai Ruo Soh, Cass Venn, Maria, Martin Struck, Nico Fenwick, Jill and Chris Ames, Corey O'Driscoll, Steve Perrett, Aara, Shezani Nasoordeen, Annette Oert, Brent Koppel, Dafne Koutamanis, Jessica Walsh, Matt Shaw, Heidi, and my Wollongong bouldering crew (esp. Paul Rattenbury, Amy Kiah, Jayden Shepperd). Know that every single one of you has fed my confidence to step up, fall down, injure myself, and get back on that climbing wall. I am truly indebted to you all. To Virginia, Johnny, Poops, Missi Moo and the chickens—thank you for the cocktails, yummy meals, and backyard conversations. You are my Australian family. Thank you for keeping me mentally sober in all the right ways.

On the odd occasion when I managed to visit my home country, Aotearoa, a number of friends, mentors and colleagues were infallible in their guidance, lateral thinking, patience, and support, despite my long absences over the past few years. Thank you, Kasey Allely, Zac McIvor, Patricia Pillay, Reno Nims, Kyla Gainsborough-Waring, Simon Holdaway, Kane Ditchfield, Alex Jorgensen, Tim Mackrell, Josh Emmitt, and Rebecca Phillipps, for continuing to inspire and challenge me. I am especially grateful to Aurore, Kasey, Zac, and Simon who have helped to feed my enthusiasm and love for the past—Although rarely in person, your friendship, support, and discussions have kept me going through it all. Thank you also to my Invercargill family, Glenda and Alf McPhee, for putting up with my reclusive, workaholic ways over the many visits and Christmases we had during my candidature. Your love, support, baked goods, and endless supply of hydrating liquids have kept me going through the good and the tough times. To my parents and sister—Jacqui, Robert, and Summer Phillips—you have been there from the start, always providing support wherever and whenever I have needed it. Without you, who would I be? Thank you for believing in my ability as an archaeologist and for enabling me to become a strong, self-driven, and tenacious woman. I will also be forever indebted to Blair McPhee for his constant commitment and love. Your support through cooking, cleaning, gardening, and editing has officially won you best person award. Your knack (or is it enjoyment?) for playing devil's advocate also always has a way of ruffling the feathers that (most of the time) results in a wiser, more informed outlook and understanding. Sorry this took so long. Here's to the next 'chapter'. Love you. Thank you.

Ngā mihi maioha

CERTIFICATION

I, Natasha Phillips, declare that this thesis, submitted in fulfilment of the requirements for the award of Doctor of Philosophy, in the Centre for Archaeological Science, School of Earth, Atmospheric and Life Sciences, University of Wollongong, is my own work unless otherwise referenced or acknowledged. This document has not been submitted for qualifications at any other academic institution.

30th March 2021

Natasha Phillips
PhD candidate
Centre for Archaeological Science
University of Wollongong

AUTHOR PUBLICATIONS AND ACKNOWLEDGEMENT

This thesis presents original research produced for my PhD candidature through the Centre of Archaeological Sciences, School of Earth, Atmosphere and Life Sciences at the University of Wollongong. However, there are important areas of this research that required collaboration and the use of datasets collected for wider application by the Doring River Archaeology Project (DRAP) team (i.e., the distributional dataset for the archaeology at UPK7) or by specialists (i.e., the geophysical dataset collected, processed, and analysed by Ian Moffat) produced specifically for this thesis. Authorship of this thesis is entirely my own, unless otherwise cited, including the random survey data collection, artefact and sediment sampling and geomorphic mapping, processing, analysis, and written interpretation. The research, ideas, and findings produced in this thesis have also, to varying degrees, been incorporated into co-authored papers as part of the wider output of the DRAP. The following is a list of co-authored papers that have contributed to the dataset analysed in this thesis or received contributions from this study, with my input as either a primary or co-author.

Primary

Phillips, N, J Pargeter, M Low & A Mackay (2019) 'Open-air preservation of miniaturised lithics: experimental research in the Cederberg Mountains, southern Africa', Archaeological and Anthropological Sciences, 11(11), 5851-5877.

Co-authored

Ames, CJH, S Chambers, M Shaw, N Phillips, BG Jones & A Mackay (2020) 'Evaluating erosional impacts on open-air archaeological sites along the Doring River, South Africa: Methods and implications for research prioritization', Archaeological and Anthropological Sciences, 12(5), 103.

Low, M, A Mackay & N Phillips (2017) 'Understanding Early Later Stone Age technology at a landscape-scale: evidence from the open-air locality Uitspankraal 7 (UPK7) in the Western Cape, South Africa', Azania: Archaeological Research in Africa, 1-34.

Shaw, M, CJH Ames, N Phillips, S Chambers, A Dosseto, M Douglass, R Goble, Z Jacobs, B Jones, SC-H Lin, MA Low, J-L McNeil, S Nasoordeen, CA O'Driscoll, RB Saktura, TA Sumner, S Watson, M Will & A Mackay (2019) 'The Doring River Archaeology Project: Approaching the evolution of human land use patterns in the Western Cape, South Africa', PalaeoAnthropology.

Watson, S, M Low, N Phillips, C O'Driscoll, M Shaw, C Ames, Z Jacobs & A Mackay (2020) 'Robberg Material Procurement and Transport in the Doring River Catchment: Evidence from the Open-Air Locality of Uitspankraal 9, Western Cape, South Africa', Journal of African Archaeology, 18(2), 209-228.

Will, M, A Mackay & N Phillips (2015) 'Implications of Nubian-Like Core Reduction Systems in Southern Africa for the Identification of Early Modern Human Dispersals', PLoS ONE, 10(6), e0131824.

LIST OF ABBREVIATIONS

Technical & Temporal

AMS	Accelerator Mass Spectrometer	
asl	Above sea level	
bls	Below surface	Depth below surface or ground
C	Carbon	
C14 or ^{14}C	Radiocarbon	Radioactive isotopic dating method
$CaCO_3$	Calcium carbonate	
D_e	Equivalent dose	
DEM	Digital Elevation Model	Model of surface elevation
DRC	Dose response curve	
DTM	Digital Terrain Model	Hydrologically corrected
E4		CFG scripted Data collection software
Early LSA	Early Later Stone Age	
Early MSA	Early Middle Stone Age	
ESA	Earlier Stone Age	
Final MSA	Final Middle Stone Age	
GPS	Global Positioning System	
Gy	Gray	A measure of the amount of energy absorbed by a sample, or its dose. It has the unit's joules per kilogramme (J.kg-1)
HP	Howiesons Poort	
ICP-MS	Inductively-Coupled Plasma Mass of a Sample	Spectrometry, a technique used to analyse the chemical composition of materials
K	Potassium	
Ka	Kiloannum	Thousand years
Kya	Thousand years ago	
LED	Light Emitting Diode	
LGIT	Late Glacial Interglacial Transition	~15.6-13.3 kya
LGM	Last Glacial Maximum	~24-18 kya
Late MSA	Late Middle Stone Age	
LSA	Later Stone Age	
MIS	Marine Isotope Stage	Pertaining to this thesis: MIS 6-1
MSA	Middle Stone Age	
µ m	Micrometre	1,000 µm = 1mm
nm	Nanometre	1,000,000 nm =1mm
OD		
OES	Ostrich eggshell	
OSL	Optically Stimulated Luminescence	Optical dating method
Φ	Phi	
ppm	parts per million	10,000ppm = 1%
PH	Preheat	
Post-HP	Post-Howiesons Poort	
SAR	Single Aliquot Renarrative Procedure	
SRTM	Shuttle Radar Topography Mission	1 arc-sec (~90 m resolution)
SRZ	Summer Rainfall Zone	

SB	Still Bay	
Th	Thorium	
U	Uranium	
UTM34s	Universal Transverse Mercator 34 South	Projected coordinate system
WRZ	Winter Rainfall Zone	Biome of the Doring River valley
WGS84	World Geodetic System 1984	Geographic coordinate system
XRD	X-Ray Diffraction	
YRZ	Year-round Rainfall Zone	

People & Places

ABK	Appleboskraal	
AOA	Areas of Analysis	Specific to Low et al. (2017)
AOI	Area of Interest	
CFR	Cape Floristic Region	
DK1	Die Kelders 1	
DR	De Rif	
DRPLP	Doring River Paleo-Landuse Project	Project name between 2014-2017
DRAP	Doring River Archaeological Project	Project name from 2018 onwards
DRS	Diepkloof Rock Shelter	
EBC	Elands Bay Cave	
HRS	Hollow Rock Shelter	
KB-1	Katbakkies 1	
KKR	Klein Kliphuis rock shelter	
KRS	Klipfonteinrand Rock Shelter	
LNGKL	Lungkaal	
MRS	Mertenhof Rock Shelter	
PL	Putslaagte	
POI	Place of Interest	
UCT	University of Cape Town	
UoW	University of Wollongong	
UPK	Uitspankraal	
WITS	University of the Witwatersrand	
ML	Marika Low	
AM	Alex Mackay	
BGJ	Brian G. Jones	
MW	Manual Will	
IA	Ian Moffat	

TABLE OF CONTENTS

ABSTRACT....ii
DEDICATION....iii
ACKNOWLEDGEMENTS....iv
CERTIFICATION....vii
AUTHOR PUBLICATIONS....viii
LIST OF ABBREVIATIONS....ix
Technical & Temporal....ix
People & Places....x
TABLE OF CONTENTS....xi
LIST OF FIGURES....xix
LIST OF TABLES....xxvi
1. INTRODUCTION....1
1.1. Thesis objective and case study....3
1.2. Chapter overview....4
2. LITERATURE REVIEW....6
2.1. Introduction....6
2.2. The Origin of Modern Human Behaviour and Evidence for Complex Cognition....6
2.2.1. Anatomical origins....7
2.2.2. Behavioural origins....7
2.3. Southern African Research: The First Half of the 20th Century....9
2.3.1. Building a culture history....9
2.3.2. The rise and fall of the pluvial sequence....10
2.4. Southern African Research: The Second Half of the 20th Century....11
2.4.1. A drive for culture-stratigraphic control....11
2.4.2. The impact of chronometric dating....12
2.4.2.1. The spatio-temporal shift in the origins of human behaviour....13
2.4.2.2. Shifting the scale of Stone Age enquiry....13
2.4.2.3. Entrenchment of rock shelter research....14
2.5. The Current State of Southern African Late Pleistocene Research....16
2.5.1. Chronological control and the question of human-environment interaction....16
2.5.2. Human-environment interaction – a landscape or rock shelter perspective?....20
2.5.3. The influence of contextual bias on interpretation....24
2.5.4. Temporal control in open-air studies....25
2.6. Open-air Approaches in Southern Africa....26
2.6.1. Landscape approach and the challenge in carrying-out open-air research....26
2.6.2. Geoarchaeological methods in South Africa's open landscape....27

2.7. Conclusions....28
3. STUDY AREA: PHYSICAL SETTING....30
3.1. Introduction....30
3.1.1. Defining the limits of the study area....30
3.2. Topography and Hydrogeology....32
3.2.1. Topography....32
3.2.2. The Doring River system....34
3.3. Present Climate and Environment....38
3.3.1. Southern Africa....38
3.3.1.1. Rainfall zones....38
3.3.2. Doring River catchment....39
3.3.2.1. Local modern rainfall....39
3.3.2.2. Temperature and evaporation....41
3.3.2.3. Wind....41
3.3.2.4. Fauna and flora....42
3.4. Paleoclimate and Environment....44
3.4.1. Global-scale forcing....44
3.4.2. Paleoclimate of the Winter Rainfall Zone....46
3.4.2.1. Late Pleistocene (126-11.7 ka)....46
3.4.2.1.1. Lowland Coastal Archives....47
3.4.2.1.2. Highland Montane Archives....48
3.4.3. Summary....50
4. STUDY AREA: HUMAN SETTING....52
4.1. An Anthropogenic Landscape....52
4.1.1. Human activity in the Doring River valley in the last 300 years....52
4.1.1.1. Access and carrying capacity....52
4.1.2. Historic occupation and use of the Doring River valley prior to the 20th century....53
4.1.3. Early exploration and settlement of the Olifants-Doring catchment....53
4.1.3.1. Early Access into the Doring River valley....56
4.2. Previous Archaeological Research....57
4.2.1. Early research focus....57
4.2.2. Rock shelter excavation in the Doring River catchment....58
4.2.2.1. Klipfonteinrand Rock Shelter (KFR)....59
4.2.2.2. Hollow Rock Shelter (HRS)....61
4.2.2.3. Mertenhof Rock Shelter (MRS)....61

4.2.2.4. Putslaagte 8 (PL8)....62
4.2.2.5. Overview of rock shelter evidence....63
4.2.3. Open-air research in the Doring River valley....63
4.2.3.1. Early surveys of the Doring corridor & Putslaagte 1 (PL1)....64
4.2.3.2. Targeted and distributional surveys of the DRAP....66
4.2.3.3. Assumptions and limitations....71
4.2.4. Concluding statement....73
5. CASE STUDY AND METHODS....74
5.1. Introduction....74
5.2. Case Study: Uitspankraal 7 (UPK7)....74
5.3. Geospatial Infrastructure....80
5.4. Sedimentology: Sampling and Characterisation....81
5.4.1. Field survey....81
5.4.2. Field sampling and characterisation....84
5.4.3. Particle size: Granulometric analysis....86
5.4.4. Minerology: X-ray Diffraction (XRD) analysis....86
5.5. Geochronology: Chronometric dating....86
5.5.1. Optically stimulated luminescence (OSL) dating....88
5.5.1.1. Sample preparation....88
5.5.1.2. Equipment....89
5.5.2. Radiocarbon dating....89
5.5.2.1. Radiocarbon survey and sampling....90
5.5.2.2. Radiocarbon sample preparation and analysis....91
5.6. Surface Morphometry....92
5.6.1. Data collection....92
5.6.2. Terrain modelling and classification....93
5.6.3. Geophysical Survey....96
5.7. Archaeological Formation....97
5.7.1. Field data collection....98
5.7.1.1. Distributional responsive non-geometric (RNG) survey....98
5.7.1.2. Random sampling square (rSSQ) survey....99
5.7.1.3. Attributes and data logging....100
5.7.2. Data analysis....104
5.7.2.1. Artefact age....106
6. RESULTS: PHYSICAL ATTRIBUTES....110
6.1. Introduction....110
6.2. Geomorphological Features and Unit Characterisation....115

6.2.1. Hillslope overview....115
6.2.2. Bedrock....119
6.2.3. Tributaries....119
6.2.4. Palaeoterrace....121
6.2.5. Sand mantle....122
6.2.5.1. Lower Red with (LR) and without $CaCO_3$ (LRcc)....125
6.2.5.1.1. Samples and surface description....126
6.2.5.1.2. Grain size and mineralogy....128
6.2.5.2. Upper Yellow (UY)....131
6.2.5.2.1. Samples and surface description....133
6.2.5.2.2. Grain size and mineralogy....133
6.2.5.3. Indurated Sand (IS)....134
6.2.5.3.1. Samples and surface description....134
6.2.5.3.2. Grain size and mineralogy....137
6.2.5.4. Unconsolidated & semi-consolidated sands compared to alluvium....140
6.2.5.4.1. Samples and surface description....140
6.2.5.4.2. Grain size and mineralogy....140
6.2.5.4.3. Summary....142
6.2.5.5. Main trends in particle size and mineralogy....143
6.2.6. ERT subsurface stratigraphy....145
6.2.7. Proposed scenario for UPK7's depositional history....147
6.2.8. Summary....150
6.3. Substrate Age....151
6.3.1. OSL samples....151
6.3.2. Single grain characteristics....152
6.3.2.1. Dose recovery tests....152
6.3.3. Grain rejection....153
6.3.3.1. Dim OSL signal....154
6.3.3.2. Recycling ratio....156
6.3.3.3. OSL-IR Depletion Ratio....156
6.3.3.4. Recuperation....157
6.3.3.5. L_n/T_n Interpolation and dose saturation....157
6.3.4. Accepted grains: decay and DRC characteristics....158
6.3.4.1. Interpreting D_e distributions for age calculation....160
6.3.4.2. Scattered distributions: Identifying outliers with nMAD....160
6.3.4.3. Mixed Distributions: Identifying multiple components with FMM....161
6.3.4.4. Truncated D_e distributions....163

6.3.5. Dosimetry....163
6.3.6. Cosmic-rays and burial depth estimates....164
6.3.7. Measured dose rates....165
6.3.8. Optical age estimates....165
6.4. The Potential Impact of UPK7's Formation on Artefact Visibility and Movement....172
6.4.1. Introduction....172
6.4.2. Deposition and erosion....174
6.4.2.1. Wind, sand & vegetation....175
6.4.2.2. Rainfall & rill development....176
6.4.2.3. Trampling....178
6.4.2.4. Rate and timing of erosion....179
7. RESULTS: SURFACE ARCHAEOLOGY....180
7.1. Introduction....180
7.2. How is UPK7's Surface Archaeology Spatially Distributed and is it Random?....180
7.2.1. The spatial distribution of all artefacts....180
7.2.1.1. Testing for Complete Spatial Randomness....181
7.2.1.2. Artefact density....182
7.3. What is UPK7's Surface Archaeology Composed of and How is it Distributed?....184
7.3.1. Artefacts by material type....186
7.3.2. Artefacts by type and lithic class....189
7.3.3. Artefacts by implement....192
7.3.4. Artefacts by archaeological epoch....195
7.3.5. Artefacts by archaeological Industry....198
7.3.6. Conclusion....201
7.4. Spatial Analysis by Archaeological Component: Relatedness, Density, and Diversity....201
7.4.1. Spatial autocorrelation....201
7.4.2. Artefact density....203
7.4.2.1. Density by inferred artefact age....203
7.4.3. Artefact density and diversity....205
7.5. Artefact Spatial Patterning in Relation to Geomorphic Setting and Artefact Condition....207
7.5.1. Artefact density and elevation....207
7.5.2. Artefact visibility and sediment composition....209
7.5.2.1. Artefact density and movement....210
7.5.2.2. Artefact density and slope angle....210

7.5.2.3. Artefact size and topographic setting....211
7.5.2.3.1. rSSQ flake composition and size distributions....212
7.5.2.3.2. Size-sorting across UPK7....214
7.5.3. Summary of artefact movement....217
7.6. Exposure and Artefact Condition....218
7.6.1. Fragmentation....218
7.6.2. Weathering....224
7.7. Association Between Artefact Spatio-Temporal Patterning and Substrate Age....227
7.7.1. Artefact abundance and substrate unit....227
7.8. Inferred Age by Consolidated Substrate Unit....228
7.8.1. Association between archaeological epoch and substrate age....228
7.8.1.1. MSA artefacts....230
7.8.1.2. LSA artefacts....230
7.8.1.3. Neolithic artefacts....230
7.9. Association Between Industries and Substrate Age....231
8. DISCUSSION....235
8.1. Introduction....235
8.2. Depositional History of UPK7....235
8.2.1. Potential conditions for artefact movement....235
8.2.2. Prior to MIS 3: >58 ka....247
8.2.2.1. Formation of UPK7's palaeoterrace and colluvium foundation....247
8.2.2.2. The Lower Red....247
8.2.2.2.1. History of sedimentation....247
8.2.2.2.2. Artefact condition....248
8.2.2.2.3. Spatio-temporal dynamic between diagnostic artefacts and depositional context....249
8.2.2.2.4. Summary and scenario outcome....250
8.2.3. MIS 3: 59 to 29 ka....251
8.2.3.1. Formation of the Upper Yellow....251
8.2.3.1.1. History of sedimentation....251
8.2.3.1.2. Artefact condition....252
8.2.3.1.3. Spatio-temporal dynamic between diagnostic artefacts and depositional context....252
8.2.3.2. Indurated Sand....253
8.2.3.2.1. History of sedimentation....253
8.2.3.2.2. Artefact condition....253

8.2.3.2.3. Spatio-temporal dynamic between diagnostic artefacts and depositional context....254
8.2.3.2.4. Summary and scenario outcome....256
8.2.4. MIS 2 to MIS 1: 29 ka to present....256
8.2.4.1. Absence of younger consolidated sands....256
8.2.4.2. Semi consolidated and Unconsolidated Sand....257
8.2.4.2.1. History of sedimentation....257
8.2.4.2.2. Spatio-temporal dynamic between diagnostic artefacts and depositional context....258
8.3. The Accumulation and Preservation of Archaeology at UPK7....259
8.3.1. Review of Scenario's based on UPK7's history of formation....259
8.3.1.1. Exposure....259
8.3.1.2. Chronology....260
8.3.2. Considering scale and its implications for archaeological interpretation....261
8.3.2.1. Artefact density in relation to substrate deposition and exposure....262
8.4. Paleoclimate and Landuse Impact on Preservation and Visibility....263
8.5. Study Implications for the History of Landuse in the Doring River Catchment (Historic to Prehistoric)....264
9. CONCLUSIONS....267
9.1. Contribution and Implications....269
9.1.1. Studying the Doring River sediment stacks....270
9.1.2. Interpretation of visible archaeology....270
9.1.3. Temporal control and the scale of interpretation....271
9.1.4. Implications for palaeoenvironmental reconstruction....271
9.2. Final Words....272
REFERENCES....273
APPENDIX 1. STUDY AREA: LAND TENURE....291
1.1. Possible Indications of Recent Anthropogenic Modification at Uitspankraal....291
1.2. Eighteenth Century Loan Farm Tenure Near the Doring River Valley....293
1.2.1. Lubbe Family and land tenure along the Doring/Biedouw Rivers....294
APPENDIX 2. FIELD SEASON DATA COLLECTION: FOCUS AND ASSISTANCE....296
APPENDIX 3. SUPPLEMENTARY INFORMATION FOR CHAPTER 5: SURFACE MODELLING & E4 CODING....298
3.1. Stage 1. Image Processing in Photogrammetry....298
3.2. Stage 2. Vegetation Filtering & Bare-earth Interpolation....300
3.2.1. TIN Densification in LAStools (via Purpose-built GUIs)....301
3.2.1.1. Filtering mode parameters....301

3.2.2. Qualitative comparison of filtering parameters.....302
3.2.2.1. Visual assessment of filtering quality.....303
3.2.3. Filtering results.....304
3.3. Stage 3. DTM Creation and Accuracy Assessment.....308
3.4. Hydrological Conditioning.....313
3.5. E4 Script for RSSQ Clast Data Collection.....314

APPENDIX 4. SUPPLEMENTARY RESULTS FOR CHAPTER 6.....329
4.1. Sediment Sample Field Notes (Excluding RSSQs).....342
4.1.1. Unconsolidated Sand (UCS) and Semi-Consolidated Sand (SCS).....342
4.1.2. Indurated sandy deposit (IS).....346
4.1.3. Upper Yellow unit (UY).....352
4.1.4. Lower Red sediment with and without calcium carbonates (LRcc & LR).....356
4.2. RSSQ Surface and Sediment Sample Field Notes.....369
4.2.1. Unconsolidated Sand.....369
4.2.2. Indurated Sand.....376
4.2.3. Upper Yellow.....383
4.2.4. Lower Red.....385
4.2.5. Lower Red with CaCO3.....388
4.2.6. Heuweltjie.....398
4.2.7. Colluvium.....401
4.2.8. Summary of frequency of rSSQ with calcium carbonate inclusions and/or features.....405
4.3. Grain Size Results.....407
4.4. XRD Results.....410
4.5. Supplementary Information for Grain Size and Mineralogical Analysis.....417
4.6. OSL Sample Context.....419
4.7. Radial Plots.....423
4.7.1. Indurated Sediment (IS): Loamy sand - slope wash/aeolian accumulation.....423
4.7.2. Upper Yellow (UY): Sandy loam – aeolian.....424
4.7.3. Lower Red (LR): Sandy loam – aeolian.....426
4.7.4. Lower Red with CaCO3 (LRcc): Loamy sand – aeolian.....429
4.8. Cosmic Dose Burial Depth Scenarios.....434
4.9. DirectAMS Analysis Report.....436
4.9.1. Report by DirectAMS conventional radiocarbon age determinations and calculations.....437
4.9.2. Radiocarbon samples and age calibration.....438

LIST OF FIGURES

1.1. Map of southern Africa showing the location of the case study within the Doring River watershed....4

The frequency of publications on site-specific chronometric datasets published over a fifty year period, from 1962-2012....13

2.2. Stacked timeline for the MSA and LSA based on Lombard et al.'s (2012, p.125) South African and Lesotho Stone Age sequence....18

2.3. Percentage and number of chronometrically dated cave/rock shelter and open-air contexts included in the SALSA sequence for each Stone Age....22

2.4. Rock shelter and open-air site locations of southern Africa grouped by Stone Age....23

3.1. Map of the Olifants-Doring Catchment system, showing the hydrology, farm rainfall gauges in the study area (Uitspankraal)....31

3.2. Elevation profile of the Olifants-Doring Basin from its south-western to north-east extent.... 33

3.3. Geological map of the Doring River (secondary) catchment, showing the main lithological groups, catchments, and rivers mentioned in text....35

3.4. Soil map of the Doring River catchments E2-E4 (secondary) and the boundaries of the Tertiary (E24) and Quaternary catchments (E24J)....37

3.5. Map from Carr et al. (2015, p.28, figure 2.3) of dominant oceanic and atmospheric circulation patterns, with the major oceanic currents....39

3.6. Comparison of thirty-year mean monthly precipitation (1983-2013) between four farms within the Doring River catchment....40

3.7. Thirty-year record (1983-2013) of mean annual precipitation....41

3.8. Windrose diagram....42

3.9. Biomes in South Africa showing location of Olifants and Doring Rivers, and all Late Pleistocene archaeological sites....43

3.10. The three chorological systems used in this thesis....45

3.11. Sea level variations over the past 35 ka based on ice-volume data....46

4.1. Early Cederberg settler farms extending to the Doring River valley by 1727....54

4.2. The Cape Colony between 1652 and 1806 showing the 1798 settler 'Frontier'....55

4.3. Select photographs of archaeology-baring sediment stacks, with examples of time-sensitive stone artefacts....65

4.4. Western view of Putslaagte 1, with Doring River to the right and Putslaagte valley to the left of image....66

5.1. A nested map series of the study area, archaeological sites mentioned in text and UPK7, shown at different spatial scales....76

5.2. Map of UPK7 artefact clusters and sediment units, with photographs of example pieces....78

5.3. Detail of UPK 7's 2015 record of the spatial distribution of time-diagnostic artefacts against 2010 aerial imagery....79

5.4. Monumentation of survey mark....81

5.5. Summary of main categories and variables used to describe (sub)surface characteristics, inclusions, and features during rSSQ survey....83
5.6. Sand auguring adjacent to section cut 1 at UPK7....85
5.7. Photographs of sampled combustion features....91
5.8. Map series showing the 2019 orthomosaic, final DTM, hill shade, and vegetation crown height outputs....93
5.9. Workflow involved in DTM creation....94
5.10. Calculating average slope for rSSQs from DTM cell values....96
5.11. Laying and measuring the length of ERT cable line....97
5.12. Example of the rSSQ survey strategy....100
6.1a. A. The horizontal extent of exposed sedimentary units across UPK7....116
6.1b. B. The vertical depiction of the surface profile line....117
6.2. Photographs of an eroding sediment mound in the southwestern slope (Exposure 1a) of UPK7..118
6.3. Circular stone ruins to the immediate east of the eastern tributary and at UPK9....118
6.4. Historic stone buildings at UPK9....119
6.5. Photos of the exposed western bank of the eastern tributary showing the Palaeoterrace....120
6.6. UPK7 western tributary and palaeoterrace....122
6.7. Aerial image of a possible heuweltjie is exposed on the consolidated sediment....124
6.8. North-east facing photograph of a residual island of consolidated sediment separated from the main stack....124
6.9. Diagram of soil catena, illustrating different erosion and deposition zones on a hillslope....125
6.10. Aerial photo from 2016 UAV survey footage of Exposure 1b's middle zone....127
6.11. Photograph of OSL Cut 1L and detail of precipitates and termite frass....128
6.12. Grain size distributions for alluvium (a), semi- and Unconsolidated Sand samples (b), Upper Yellow (c) and Indurated Sand (d), and Lower Red sediment samples (d) collected at or adjacent to UPK7....129
6.13. Mineral composition from XRD analysis of inferred LR, LRcc, and Colluvium samples....130
6.14. **a-b.** Photographic example of $CaCO_3$ occurring as either nodules in rSSQ 56 or veins in LRcc OSL Cut 8....131
6.15. Photo showing the consolidated surface of Exposure 2....132
6.16. Profile photo of Section Cut 1, showing visible sampling locations....135
6.17. OSL cut 9 profile showing location of OSL sample tube 91080/UOW-2006....136
6.18. OSL Cut 3 profile showing location of OSL sample tube 90020/UOW-1802....137
6.19. Grain size distributions of IS samples collected in 50 cm intervals from Section cut 1 and associated auger hole....138
6.20. Mineral composition from XRD analysis of inferred IS samples, collected from OSL and section cuts at UPK7....138
6.21. Mineral composition from XRD analysis of UCS, SCS and Alluvial samples collected from or adjacent to UPK7....142

6.22. Scatter plots of the percentages of sand and silt as well as mean and mode grain size plotted as a function of stratigraphic level....144
6.23. Scatter plots of sorting (phi) and mode 2 grain size as a function of stratigraphic level....144
6.24. Scatter plot of the percentage of quartz, feldspar and clay minerals plotted as a function of stratigraphic level....145
6.25. Stratigraphic results of two ERT profiles....146
6.26. Photographs of Doring River riffle zone and sand dominated channel proximate to UPK7....147
6.27. **a-b.** Windblown sand and its distribution near Appleboskraal, Lungkaal and steep western flank of the Doring River....148
6.28. **a-b.** Aeolian activity in the Doring River valley....148
6.29. North facing photograph and inset of semi-consolidated and unconsolidated dune sand, palaeoterrace and sandstone bedrock exposed in UPK7's eastern tributary....150
6.30. Map of UPK7 showing the locations of OSL samples collected from consolidated and unconsolidated sediment....151
6.31. Dose recovery test results for sample 90022/UOW-1803....153
6.32. Radial plot of dose recovery test results for sample 90022/UOW1803 for the selected preheat combination C....153
6.33. Representative example of decay curves for a grain with OSL signals after test dose stimulation and regenerative dose....154
6.34. Normalised decay curves for the regenerative and test dose, and the DRC of one grain with a poor recycling ratio....156
6.35. Example of an IR sensitive grain....157
6.36. Example DRCs from sample UoW-1832 showing two grains rejected under criterion 7 and 8....158
6.37. Typical OSL Ln and Tn decay curves and DRCs of single grains from one representative sample of each sediment unit....159
6.38. Map of UPK7 showing the locations and ages of OSL samples collected from consolidated and unconsolidated sediment....168
6.39. Surface profiles A-B and C-D showing the location and results of OSL samples and the surface distribution of the four main sediment units....169
6.40. Distribution of OSL ages for UPK7 relative to a single, calibrated radiocarbon determination, and four different chronological systems....171
6.41. Topographic map of UPK7 showing vegetation and slope angles....173
6.42. Examples of the basic processes and structure of dune formation and slope erosion....174
6.43. Zones of erosion and deposition on the northern side of UPK7....176
6.44. Flash flooding at UPK1....177
6.45. Photograph of an historic stone hearth at UPK9....179
7.1. Distribution of individual artefact point locations recorded within the RNG survey boundary....181
7.2. Two-dimension spatial Kolmogorov-Smirnov goodness-of-fit test for Complete Spatial Randomness (CSR)....182

7.3. Hot-cold spot Geti-Ord Gi* map showing areas of random and significantly high and low artefact counts....183
7.4. Map series comparing the artefact point patterns of five major archaeological components....185
7.5. Artefact counts by material type....186
7.6. Map series comparing the artefact point patterns of eleven different material types....188
7.7. Frequency of artefact types and lithic classes in the RNG dataset for UPK7....190
7.8. Map series comparing the artefact point patterns of eight artefact types and lithic classes....191
7.9. Bar graph showing implement types identified during RNG survey at UPK7....192
7.10. Map series comparing the artefact point patterns of thirteen different implement types....194
7.11. Bar graph of artefact frequencies by Archaeological epoch....195
7.12. Map of the location and pattern of artefacts associated with a specific archaeological epoch....197
7.13. Bar graph of artefact frequencies by typo-technological Industry....198
7.14. Point location and pattern of artefacts associated with a specific archaeological Industry....200
7.15. The distribution and density of MSA, LSA, and Neolithic artefacts at UPK7....204
7.16. Linear regression of the number of artefact types within three archaeological categories plotted as a function of log transformed artefact density....206
7.17. Artefact density as a function of elevation....208
7.18. Proportion of artefacts on units with different degrees of sediment compaction....209
7.19. Artefact density as a function of slope....211
7.20. Distribution of RNG-survey-derived maximum artefact dimensions for UPK7....212
7.21. rSSQ composition by artefact class and break type, showing the distribution of maximum dimensions between each category....213
7.22. Maximum dimension distributions for intact and broken implements and flakes....219
7.23. Comparative map series of artefact weathering....220
7.24. Stacked percentage graphs of the relative proportions of intact and broken implements by different hillslope settings....221
7.25. Stacked percentage graphs of the relative proportions of intact and broken flakes by different hillslope settings....223
7.26. Comparison of artefact frequencies between archaeological epochs within each consolidated substrate....229
7.27. The proportion of artefacts identified on each consolidated sediment unit, grouped by Industry....232
8.1. Photograph of historic stone hearth at UPK9....257
A1.1. Topographic Map comparison (3219 AB) from 1960 to 2003 of the Doring-Biedouw River confluence and surrounding farmland of Uitspankraal....292
A1.2. Loan farms tenured by mixed-race and Khoisan farmers in the 18th Century....294
A1.3. Location map of the Lubbe family farms between 1725-1830....295
A3.1. Agisoft PhotoScan reported figure of camera locations and image overlap....299
A3.2. Locations of UPK7 2019 UAV ground control points and their associated error estimates....300
A3.3. Location map of stacked profile lines in a range of topographic and vegetation settings....305

A3.4. Comparing filter modes in profile for a range of topographic and vegetation scenarios.....306
A3.5. Histogram distributions showing the elevation difference between las control points and two interpolation methods.....309
A3.6. Profile stacks interpolated using two different interpolation methods showing elevation and surface modelling results for bare-earth and unfiltered models.....311
A3.7. Map showing areas where large z-value differences occur between the interpolated surface and the subset of control las points.....312
A4.1. Map of UPK7 and its immediate surrounds showing the location of all sediment samples listed in Table 1.....329
A4.2. Plot of grain size versus distance from the Doring River for unconsolidated sediment samples at UPK7.....341
A4.3. Plot of grain size versus distance from the Doring River for all sediment samples at UPK7.....341
A4.1.1. SCS sampling locations for sediment samples 91065 and 91066.....342
A4.1.2. UCS sampling location for sample 91067.....343
A4.1.3. Photographs of UCS and SCS sampling surface details and settings for 91068 and 91069.....344
A4.1.4. Photos showing the location of OSL sample UNL-3808.....345
A4.1.5. IS sampling location for sediment sample 90020.....346
A4.1.6. IS sampling location for sediment sample 91080.....349
A4.1.7. Section cut 1 (SC1) showing profile of spade cut section and auger hole.....351
A4.1.8. UY sampling location for sediment sample 90016.....352
A4.1.9. UY sampling location for sediment sample 90024 (context).....354
A4.1.10. UY sampling location for sediment sample 90024.....355
A4.1.11. LRcc sampling location for sediment sample 90018.....357
A4.1.12. LRcc sampling location for sediment sample 90026.....358
A4.1.13. LRcc sampling location for sediment sample 90028.....360
A4.1.14. LRcc sampling location for sediment sample 90030.....362
A4.1.15. LR sampling location for sediment sample 90022.....364
A4.1.16. LR sampling context and section detail for sediment sample 90022.....365
A4.1.17. LR sampling locations for sediment samples 91153 and 91155.....367
A4.1.18. LR sampling location for sediment sample 91157.....368
A4.2.1. UCS sampling location for sediment sample 91003.....369
A4.2.2. UCS sampling location for sediment sample 91004.....370
A4.2.3. UCS sampling location for sediment sample 91008.....371
A4.2.4. UCS sampling location for sediment sample 91060.....372
A4.2.5. UCS sampling location for sediment sample 91061.....373
A4.2.6. UCS sampling location for sediment sample 91147.....374
A4.2.7. UCS sampling location for sediment sample 91148.....375
A4.2.8. IS sampling location for sediment sample 91000.....376
A4.2.9. IS sampling location for sediment sample 91002.....377
A4.2.10. IS sampling location for sediment sample 91005.....378

A4.2.11. IS sampling location for sediment sample 91006.....379
A4.2.12. IS sampling location for sediment sample 91007.....380
A4.2.13. IS sampling location for sediment sample 91010.....381
A4.2.14. IS sampling location for sediment sample 91011.....382
A4.2.15. UY sampling location for sediment sample 91009.....383
A4.2.16. UY sampling location for sediment sample 91150.....384
A4.2.17. LR sampling location for sediment sample 91001.....385
A4.2.18. LRcc sampling location for sediment sample 91051.....386
A4.2.19. LR sampling location for sediment sample 91056.....387
A4.2.20. LRcc sampling location for sediment sample 91050.....388
A4.2.21. LRcc sampling location for sediment sample 91049.....389
A4.2.22. LRcc sampling location for sediment sample 91048s28.....390
A4.2.23. LRcc sampling location for sediment sample 91053.....391
A4.2.24. LRcc sampling location for sediment sample 91054.....392
A4.2.25. LRcc sampling location for sediment sample 91055.....393
A4.2.26. LRcc sampling location for sediment sample 91057.....394
A4.2.27. LR(cc?) sampling location for sediment sample 91058.....395
A4.2.28. LRcc sampling location for sediment sample 91149.....396
A4.2.29. Heuweltjie/LRcc sampling location for sediment sample 91046.....398
A4.2.30. LR sampling location for sediment sample 91048.....399
A4.2.31. LR sampling location for sediment sample 91047.....400
A4.2.32. Colluvium sampling location for sediment sample 91059.....401
A4.2.33. Colluvium sampling location for sediment sample 91051.....402
A4.2.34. Colluvium sampling location for sediment sample 91052.....403
A4.2.35. Frequency of rSSQ with calcium carbonate inclusions and/or features by sediment unit.....405
A4.5.1. Scatter plot of the percentages of sand and silt plotted as a function of stratigraphic level.....417
A4.5.2. Scatter plot of mean and mode 1grain size (μm) plotted as a function of stratigraphic level.....417
A4.5.3. Scatter plot of sorting (phi) plotted as a function of stratigraphic level.....418
A4.5.4. Scatter plot of the percentage of quartz, feldspar and clay minerals plotted as a function of stratigraphic level.....418
A4.5.5. Scatter plot of mode 2 grain size (μm) plotted as a function of stratigraphic level.....418
A4.7.1. Radial plots, De values, OD, and accepted grain counts for Sample 90020/UOW-1802.....423
A4.7.2. Radial plots, De values, OD, and accepted grain counts for Sample 91080/UOW-2006.....424
A4.7.3. Radial plots, De values, OD, and accepted grain counts for Sample 90016/UOW-1801.....424
A4.7.4. Radial plots, De values, OD, and accepted grain counts for Sample 90024/UOW-1804.....425
A4.7.5. Radial plots, De values, OD, and accepted grain counts for Sample 91153/UOW-2012.....426
A4.7.6. Radial plots, De values, OD, and accepted grain counts for Sample 91155/UOW-2013.....427
A4.7.7. Radial plots, De values, OD, and accepted grain counts for Sample 91157/UOW-2014.....428
A4.7.8. Radial plots, De values, OD, and accepted grain counts for Sample 90018/UOW-1800.....429
A4.7.9. Radial plots, De values, OD, and accepted grain counts for Sample 90022/UOW-1803.....430

A4.7.10. Radial plots, De values, OD, and accepted grain counts for Sample 90026/UOW-1832.....431
A4.7.11. Radial plots, De values, OD, and accepted grain counts for Sample 90028/UOW-1833.....432
A4.7.12. Radial plots, De values, OD, and accepted grain counts for Sample 90030/UOW-1834.....433
A4.9.1. Photographs of the sampled combustion feature at UPK7 exposed in Indurated Sand (IS) 439
A4.9.2. The CRA of Sample 91071 (D-AMS 021123, 4510 ± 30 BP) is shown intercepting the SHCal13 atmospheric curve.....440
A4.9.3. Photographic compilation of the built hearth at Lungkaal.....441
A4.9.4. Photograph of hearth at Lungkaal taken from above.....442
A4.9.5. One of two hearths at UPK9.....443

LIST OF TABLES

2.1. The number of LSA and MSA sites with radiocarbon ages published in Wadley (1993) and Thackeray (1992).....15

2.2. The South African and Lesotho Stone Age Sequence from Lombard et al. (2012, p.125 Table 1).....19

3.1. Farm rainfall gauge records tabulated relative to the Uitspankraal farm (Doring-Biedouw confluence).....40

4.1. Characteristics of major technocomplexes as they occur in Doring River / Cederberg rock shelter sequences.....60

4.2. Site summary from the DRAP distributional surveys.....69

5.1. Subsample details for each carbon sample submitted to DirectAMS for radiocarbon dating.....92

5.2. List of selected artefact attributes recorded during UPK7 RNG and rSSQ survey.....103

5.3. Characteristics of Regional Industries for the ESA, MSA, LSA, and Neolithic.....108

6.1. Identified sedimentary units that contribute to the foundation and sand mantle of UPK7, listed in their stratigraphic sequence.....111

6.2a. Dominant characteristics are summarised for each unit, including their stratigraphic relationship with other units, their thickness, location, colour and sedimentary structures.....113

6.2b. Texture and common inclusions summarised for each unit.....114

6.3. List of Exposure names and their average aspect.....123

6.4. Preheat combinations applied to five sets of 300 single grains.....152

6.5. Dose recovery test results for sample 90022/UOW-1803.....152

6.6. The total number of single-grains measured, accepted, and rejected for each sample at UPK7....155

6.7. Single-grain OSL results for samples collected from UPK7, organised by sedimentary context..162

6.8. Environmental dose rate results for OSL samples collected from UPK7, organised by sedimentary context.....166

6.9. Single-grain OSL results for samples collected from UPK7, organised by sedimentary context..167

6.10. UPK7 Hillslope zones and their elevation ranges for each exposure.....175

7.1. Material type counts and percentages for artefacts recorded within the RNG survey area at UPK7.....187

7.2. The counts and percentage of artefact types and lithic classes recorded within the RNG survey area at UPK7.....190

7.3. Implement type counts and percentages.....193

7.4. Summary of time-diagnostic artefacts recorded during 2019 RNG-survey at UPK7, grouped by archaeological epoch.....195

7.5. Summary of time-diagnostic artefacts recorded during 2019 RNG-survey at UPK7, grouped by archaeological Industry.....199

7.6. Results from Moran's I Global Spatial Autocorrelation test, using K-nearest neighbour.....202

7.7. Artefact abundance and nearest neighbour results for artefacts classified by Industry.....205

7.8. Artefact count by sediment type and the proportion of each within the survey area.....210

7.9. rSSQ composition by artefact class and break type.....213

7.10. Flake frequencies by slope angle, exposure, and hillslope position.....214
7.11. The distribution of flake maximum dimensions by hillslope position for each exposure.....215
7.12. Nonparametric Wilcoxon test of differences between the median maximum dimensions of flakes by hillslope position.....216
7.13. The total number and frequency of broken compared to intact implements.....221
7.14. Pearson's Chi-square test for independence and significance for implement breakage when implements are considered across different hillslope contexts.....222
7.15. The total number and frequency of broken compared to intact flakes.....223
7.16. Pearson's Chi-square test for independence and significance for flake breakage across different hillslope contexts.....223
7.17. The number and percentage of hornfels artefacts that do or do not show signs of weathering.....224
7.18. Comparison of the observed count and percentage of hornfels artefacts with weathering for each hillslope context.....225
7.19. Chi-square tests for independence.....226
7.20. Expected proportions of artefacts on consolidated substrate units.....227
7.21. Comparison of artefact counts and conditional frequencies across each consolidated deposit by archaeological epoch.....228
7.22. The number and conditional frequencies of artefacts assigned to each Industry listed by sediment unit.....232
7.23. Contingency analysis of archaeological Industries by sediment unit.....233
8.1. Four scenarios that could lead to the current state of substrate exposure at UPK7.....238
A1.1. Lubbe Family land tenure in the Doring River Catchment during the 18th Century.....295
A3.1. Control point RMSE.....300
A3.2. Total Control point RMSE.....300
A3.3. Four modes of filtering using LAStools.....302
A3.4. Classification results for filtered and unfiltered las point clouds.....302
A3.5. Two Interpolation methods and the parameters.....303
A3.6. Meaning of good, fair, and poor in filter quality assessment.....304
A3.7. Qualitative comparison of filters.....307
A3.8. Qualitative assessment of Type I and II errors for each filter mode.....308
A3.9. Unfiltered and filtered classification statistics.....310
A3.10. Mean difference in elevation between interpolated surfaces and LAS subsampled points.....310
A4.0.1. Sediment sample index.....330
A4.0.2. Soil descriptions for all samples and their associated unit-wide summaries.....332
A4.1.1. Log of sediment samples from Section Cut 1 that were subjected to XRD analysis.....350
A4.2.1. rSSQ summary tables showing the rSSQ frequency of different surface characteristics by sediment unit.....406
A4.3.1. Results of particle size analysis on sediment samples collected from the river and modern terrace and across the sand mantle of UPK7.....407

A4.4.1. Results of XRD analysis on sediment samples collected from the river and modern terrace and across the sand mantle of UPK7 (grouped).....410
A4.4.2. Results of XRD analysis on sediment samples collected from the river and modern terrace and across the sand mantle of UPK7.....412
A4.6.1. OSL samples collected from UPK7.....419
A4.8.1. OSL burial depth scenarios.....434
A4.8.2. Estimated burial depths for each OSL sample.....435
A4.9.1. Conventional radiocarbon age (CRA) determinations & calculations.....437
A4.9.2. Calibrated radiocarbon determinations.....440

CHAPTER 1.
INTRODUCTION

Southern Africa contributes one of largest bodies of evidence for the evolution of human behaviour during the Late Pleistocene. Most of this evidence comes from rock shelter deposits. Since the 1950s, developments in rock shelter excavation and archaeological science challenged Eurocentric perspectives of Africa's role in the anatomical and behavioural origins of our species, eventually shifting entrenched views of Africa from the backwaters of human evolution to the forefront of origins research. As a consequence, research interest in southern Africa's Middle Stone Age (MSA) has intensified. The temporal resolution made possible by the development of radiometric dating methods has also shifted research interest away from culture histories towards a more nuanced understanding of the interplay between humans and their environment. However, as the increased temporal, ecological and behavioural resolution imparted by this evidence has grown, it has become increasingly apparent that our overreliance on rock shelters has introduced bias into our understanding of human behavioural change, especially when modelled across multiple sites and regions.

Despite growing interest in landscape archaeology and regional scale reconstructions, the wealth of Late Pleistocene archaeological evidence that exists across southern Africa's open landscape is generally side-lined in favour of a continued focus on the (re)excavation of rock shelter deposits. Rock shelters are favoured and prioritised for their potential to yield datable, well-preserved organic material, and finely stratified deposits. However, rock shelters are confined to specific geological and topographic conditions. This geographically limits regional models to specific locations of southern Africa, to the exclusion of large parts of the subcontinent's interior.

The relatively minor role that open-air archaeology has played in studies of Late Pleistocene human behavioural research is due in part to a legacy of methodological developments that have evolved through rock shelter excavation alone. This is perpetuated by the perception that rock shelter excavation offers a higher yield of information for the resources invested in obtaining that evidence (Ames et al 2020). This is further compounded by the perceived (lack of) integrity of archaeology in most open-air contexts, where it is more often found in a state of exposure rather than burial. Thus, despite their rarity, buried sites are often prioritised due to the stratigraphic control they afford (Kuman 1989). In contrast, surface archaeology is viewed as a) temporally compromised due to being subject to subsequent discard activity and/or b) spatially compromised due to erosional processes. This perception often lands open-air archaeology with the label 'palimpsestic' (i.e., Sampson 1968, pp.13, 16, 93). This is despite the reality that all assemblages, irrespective of their context (buried, surface, open, closed), are 'palimpsests', or rather, are time-averaged aggregates of accumulated activity that are strongly influenced by their respective sedimentary histories (Rezek et al. 2020). It is from this system that behavioural inferences are made possible (Bailey 2008; Binford 1981). Therefore, the behavioural interpretations put forth by any study that fails to account for the formation history of an archaeological sample remains questionable.

Rock shelter archaeology differs from open-air archaeology in several fundamental ways, including in the intensity of human activity that occurs within the confines of a rock shelter compared to an

open-landscape, the rate and kind of sediment accumulation, weathering, and erosion involved in the formation of their deposits, and the length of time artefacts are exposed before and/or after burial. Surface archaeology represents a period of exposure during the formation history of its respective archaeological setting. However, without the presence of overlying sediment it is difficult to temporally bracket this period with confidence. The lack of chronometric control of surface archaeology often restricts open-air research to framing behavioural change using artefacts considered to be limited in their occurrence to certain temporal windows. The temporal sensitivity of those artefacts, of course, is generally assessed from their prevalence in dated sequences recovered from rock shelters. This has the effect of locking open-air chronologies into a rock shelter sequence of change while also limiting behavioural interpretation to the temporal scale and technological forms defined by the Stone Age or Industry a given artefact is grouped under. Heavy reliance on identifying and tracking time-diagnostic artefacts across a landscape often limits behavioural interpretation to these artefacts, to the exclusion of non-diagnostic archaeology (although see` Sampson *et al.* 2015). Together the deficit in chronometric ages and the dependence on typology and technology results in behavioural interpretations considered to be ill-matched with the resolution of rock shelter chronologies and their research questions. As a consequence, much of South Africa's Late Pleistocene archaeology is excluded from regional and inter-regional reconstructions of the evolution of human behaviour.

Despite these challenges, the few studies that have dedicated time to investigating southern Africa's abundant open-air archaeology have demonstrated the potential of the open system for both informing and challenging the working narrative built from rock shelter evidence (e.g., Jerardino 2012; Kandel *et al.* 2015; Kandel & Conard 2012; Mackay *et al.* 2014; Oestmo *et al.* 2014; Sampson & Bousman 1985; Sampson 1968; Sampson *et al.* 2015). However, there is a scarcity of South African studies that employ geoarchaeological methods to investigate the formation of open-air contexts and the dynamic between the depositional history of a landscape and the spatio-temporal organisation of its archaeology. Investment in developing a similar understanding in rock shelter settings demonstrates the importance of formation to contextualise and constrain artefacts in time and space (Shahack-Gross 2017).

The process of implementing geoarchaeological methods in rock shelters has enriched MSA research and been fundamental to developing our current knowledge of human behavioural evolution in southern Africa (e.g., Ames et al. 2020; Goldberg et al. 2009; Mackay et al. 2019; Miller et al. 2013; Williams 2017). However, with a few exceptions (i.e., Fuchs *et al.* 2008; Oestmo *et al.* 2014; Toffolo *et al.* 2017; van Aardt *et al.* 2015), southern African Late Pleistocene open-air research lags behind local and international programs which employ geoarchaeological methods to contextualise Late Pleistocene and Holocene open-air archaeology (Araujo et al. 2013; Barich et al. 2006; Braun et al. 2013; Cruz-Uribe et al. 2003; Davies et al. 2016; Enloe 2006; Fitzsimmons et al. 2014; Foley et al. 2017; Holdaway & Fanning 2014; Inglis et al. 2019; Koopman et al. 2016; Kuzmin et al. 2007; Lotter et al. 2016; Lotter & Kuman 2018; Lukich et al. 2020; Sahle et al. 2014; e.g., Schick 1986; Schmidt et al. 2016; Stahlschmidt et al. 2018). Such studies demonstrate the importance of understanding the formation and post-depositional history of open-air archaeology, irrespective of its perceived condition or spatial integrity. They also emphasise the need to develop research objectives aimed at investigating the archaeological record across

multiple spatial and temporal scales—a perspective that runs counter to the singular drive for high resolution in southern African Late Pleistocene research.

Rather than focus all our energies on increasing the resolution of behavioural information and by extension narrowly prioritising sites that will provide this information, research focus needs to be directed at behavioural aggregates that provide a multiscale perspective of human behavioural change. As it stands, two questions are raised:

1. By deliberately ignoring coarse-scale aggregates (both spatial and temporal), what aspects of the evolution of human behaviour are we missing? And,
2. By considering the formation of open-air contexts what scales of aggregation are we working with and how can this inform our understanding of Late Pleistocene human-environment interactions?

1.1. Thesis objective and case study

The objective of this thesis is to investigate the formation of surface archaeology in relation to its sedimentary system in the semi-arid, Succulent Karoo landscape of the Doring River valley (Figure 1.1). The Doring River valley is located in the Western Cape region—one of the most thoroughly studied regions in southern Africa—with a long history of landscape-orientated research for both the Late Pleistocene and Holocene (e.g., Hallinan 2013; Jerardino 2012; Kandel & Conard 2012; Klein *et al.* 2004; Manhire 1987, 1993; Manhire *et al.* 1986; Parkington 1976, 2000; Parkington *et al.* 1992; Parkington *et al.* 1986; Sealy *et al.* 1986; Wiltshire 2011).

In the last decade, the Doring River catchment has been the subject of intensive open-air and rock shelter investigations as part of the Doring River Archaeology Project (DRAP). Although this project was driven by the need to expand the Late Pleistocene sample into open-air contexts, it is yet to produce a dedicated study on the formation and geoarchaeology of the valley's surface archaeology. Instead, the DRAP has prioritised technological studies and open-air-rock shelter comparison over the investigation of the depositional history of the Doring River's open-air archaeological contexts.

To rectify this, the following study presents a geoarchaeological investigation of Uitspankraal 7 (UPK7; Figure 1.1), one of 16 known artefact-bearing 'sediment stacks' along the Doring River valley (Shaw et al. 2019) to understand the formation history, taphonomy and spatio-temporal organisation of its surface archaeology. To varying degrees, sediment stacks have been described as large areas of hard bare earth and vegetated sand, with the former exposing surface scatters of Later and Middle Stone Age archaeology (Low *et al.* 2017; Mackay *et al.* 2014; Phillips *et al.* 2019; Shaw *et al.* 2019; Will *et al.* 2015). They appear geomorphologically distinct from the surrounding colluviated hillslope and modern terrace sands, which encouraged early valley surveys to target these areas through a combination of field walking and Google Earth exploration. Consequently, there is also a deficit in survey data for the surrounding, less archaeologically visible landscape.

The aim of this study is to determine the formation history of the sediment stack and associated archaeology of UPK7. This will provide a point of comparison for future geoarchaeological investigations into the surrounding landscape, including less archaeologically visible stretches of the valley system. To achieve this objective six main questions will be investigated:

1. What is a 'sediment stack' in the sense the DRAP has used the term, and how did the one at Uitspankraal 7 form?
2. When did it form?
3. What are the main processes of deposition and erosion at UPK7?
4. How have these processes promoted or inhibited the visibility and movement of its associated archaeology over time?
5. How does the inferred age of UPK7's archaeology relate to its formation history? What temporal scale(s) of archaeological formation are we working with?
6. How recently has surface exposure of UPK7's archaeology occurred, and what are the implications for its future?

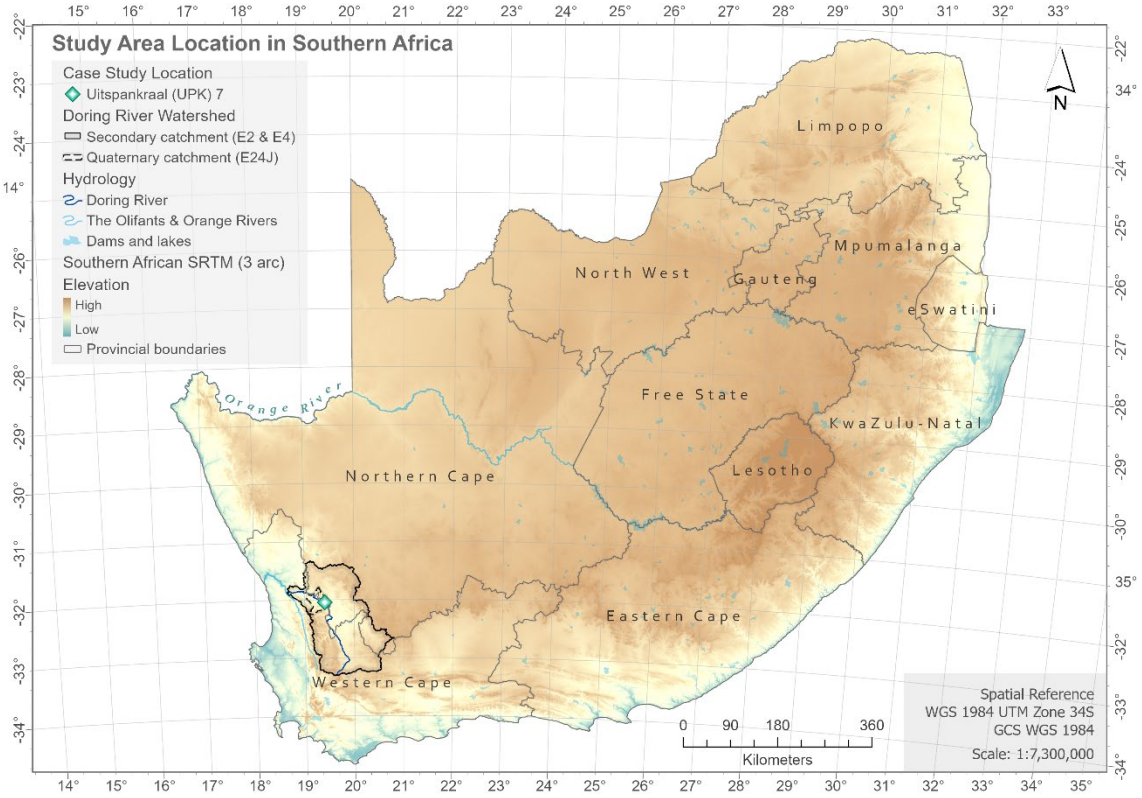

Figure 1.1. Map of southern Africa showing the location of the case study (green-white diamond) within the Doring River watershed (including the Doring River's secondary [solid black line] & quaternary [dashed black line] catchments). Three major rivers are shown: the Doring River (dark blue), the Orange River (labelled), and the Olifants River (light blue line, west of the Doring R.). Each province and landlocked country is demarcated by grey borders and underlain by an SRTM elevation map (dark blue = low elevation, dark brown = high elevation), sourced from a hole-filled 90 m DEM (originally processed by Jarvis et al. (2008)).

1.2. Chapter overview

The following study is presented over eight chapters to investigate each research question. Chapter 2 is divided into two sections, each with a central aim: The first is to provide an historical background of published literature on the last century of southern African Late Pleistocene archaeological research. This section reviews the main body of evidence used to reconstruct Late Pleistocene human behavioural change in Africa, and southern Africa's contribution to this growing dataset. The focus of this first section is on how human behavioural change has been investigated since the early 20th century and how behaviour is linked with paleoenvironmental change. It demonstrates the perpetuation of the contextual bias that is at

the heart of the thesis. The second section reviews the contribution of open-air archaeology to southern Africa Late Pleistocene research. The purpose of this section is to demonstrate the potential impact of this bias by reviewing discrepancies that exist between the rock shelter narratives and open-air findings. The question of behavioural and preservation bias is presented. Lags in the development of southern African open-air methods and theory are compared to the relatively well-developed techniques employed to study rock shelters and their deposits.

Chapter 3 introduces the study area and its physical environment. The objective of this chapter is to contextualise the Doring River valley within the physical setting and climate of its catchment, the Western Cape region, and southern Africa's Winter Rainfall Zone.

Chapter 4 follows with the anthropogenic background of the Doring River catchment's land use history and its multi-faceted relationship with the formation of the Doring River valley's archaeology. It ends with a critical review of the archaeological research carried out in the Doring River catchment to date and presents a refined series of questions that tie the main aim and questions of this thesis to the published interpretations produced in the study area by the DRAP. This chapter provides the background for why the case study Uitspankraal (UPK) 7 was selected for this thesis and for the methods employed in this study.

Chapter 5 outlines the methods and materials used to carry-out the field survey, sampling, and data collection of geomorphological, sedimentological, geophysical, and archaeological information for this study. This is followed by an outline of the laboratory preparation and analysis of this information to obtain geospatial, chronometric, and archaeological results for developing a depositional history of UPK7's landform and surface archaeology.

Chapter 6 presents the results and analysis of UPK7's sedimentology, geochronology and surface condition. This provides a depositional context for Chapter 7, which investigates the assemblage composition, spatial patterning, and condition of UPK7's non-diagnostic and time-diagnostic surface artefacts.

Chapter 8 provides an interpretation of the depositional history of UPK7 and a discussion on how the archaeology has formed throughout this history. This is followed by a discussion of the implications of this study's findings in relation to the palaeoenvironmental and anthropogenic history outlined in Chapters 3 and 4, and the published interpretations of UPK7's archaeology that were presented at the end of Chapter 4.

Chapter 9 is the final and concluding chapter. It outlines the key findings of this thesis, emphasising the importance of open-air geoarchaeology, and clarifying the study's contribution to our understanding of the formation and archaeology of UPK7, and the broader implications for archaeological research in the Doring River valley and the southern African Late Pleistocene. Intended as a pilot study to a broader landscape scale project, this research demonstrates several important aspects of open-air research that will need to be considered and implemented in the future, with recommendations given throughout the chapter.

CHAPTER 2.
LITERATURE REVIEW

2.1 Introduction

The following chapter is divided into three sections. The first section presents the period and place of interest, including a synthesis of the archaeological evidence for human evolution over the last 300 ka (thousand years) in Africa. The second section focuses on southern Africa and how its history of Stone Age research has moulded the way Late Pleistocene human behaviour is currently approached. The third and final section looks at the state of southern Africa's open-air archaeological research and the necessity for instilling a geoarchaeological approach as a baseline method to the study of its surface archaeology.

2.2 The Origin of Modern Human Behaviour and Evidence for Complex Cognition

Since the 1980s, the biological and behavioural origins of *Homo sapiens* have been traced back to Middle and Late Pleistocene Africa (Behar et al. 2008; Bräuer 1984; Cann 1988; Cann et al. 1987; Endicott et al. 2010; Hublin et al. 2017; McBrearty & Brooks 2000; Richter et al. 2017; Tishkoff et al. 2009; Vigilant et al. 1991)—diverging from our closest hominin ancestor more than 500,000 years ago [500 kya] (Gómez-Robles 2019; Meyer et al. 2016). A distinctly modern form of behaviour becomes increasingly evident from at least 200 kya, with earlier evidence going as far back as 500 kya (Wilkins & Chazan 2012), signifying the capacity for complex cognition during the early history of *Homo sapiens* evolution (Willoughby 2020; Wurz 2019) and possibly earlier as Middle Pleistocene hominins evolved and developed their behavioural repertoire (McBrearty & Brooks 2000; McBrearty et al. 2006; Wilkins & Chazan 2012).[1] By the end of the Late Pleistocene (~12 kya) modern humans had proliferated, interbreeding with other hominins beyond Africa (post-50 kya; Green et al. 2010; Prüfer et al. 2014; Reich et al. 2010), and successfully traversing, modifying and adapting to nearly every terrestrial environment on Earth. Throughout this time the world went through considerable change (Blome et al. 2012), involving the disappearance of entire ecosystems and the substantial modification of coastlines due to oscillating sea levels (Stewart & Jones 2016). The interplay between the evolution of modern humans and the natural environment has been a dominant theme in Late Pleistocene research for over a century. However, despite the amount of scholarship invested in understanding this dynamic, the origins and cause of human behavioural evolution within Africa are still largely unresolved (Willoughby 2020).While this thesis is not concerned with human behavioural evolution *per se*,[2] the drive to characterise and identify the evolution of behaviour in humans has both stimulated and, to an extent, distorted approaches to Late Pleistocene research in Africa, as this chapter will discuss.

[1] For discussion and debate concerning the concept and complexity of modernity and the use of terms such as 'complex cognition', 'modern human behaviour' and 'cultural modernity', the reader is referred to McBrearty & Brooks (2000), Shea (2011), Ames et al. (2013), and Wadley (2015).
[2] Ibid.

2.2.1 Anatomical origins

Current anatomical and behavioural evidence for the origin of modern humans is geographically and temporally disjointed. Fossil and genetic evidence place the early evolution of *Homo sapiens'* within the late African Middle Pleistocene (see Mounier & Mirazón Lahr 2019; Wood et al. 2020). The oldest fossil evidence for an early form of *Homo sapiens* dates to 315 ± 34 ka and comes from the North African site, Jebel Ihroud, in Morocco (Hublin et al. 2017; Richter et al. 2017). These fossils were found in the same depositional unit as stone artefacts considered characteristic of the Middle Stone Age (MSA), making it the earliest example of a direct association between such tools and *H. sapiens*. Similar fossil evidence, with an age of ~260 ka, was found at the southernmost end of the continent, at the southern African site of Florisbad (Grün et al. 1996; Stringer 2016), whereas the first unequivocal remains of anatomically modern humans (AMH) come from southern Ethiopia, in East Africa, and date to ~195 ka (Brown et al. 2012; McDougall et al. 2005). The geographic spread and mosaic composition of archaic and modern anatomical features refutes earlier assumptions of a single origin and unidirectional evolution for our species, suggesting a more complex pan-African process (Hublin et al. 2017). Such geographic and temporal complexity is also reflected in the behavioural evidence, with a temporal lag of 100 ka between the earliest anatomical evidence of AMH and the convincing detection of modern behaviour in the archaeological record (Stewart et al. 2016).

2.2.2 Behavioural origins

Early evidence for modern behaviour increases annually, pushing ages further back into the Late Pleistocene and strengthening its presence in different areas of the African continent, in turn weakening models that argue for a single origin and punctuated evolution of behavioural modernity in *Homo sapiens* (McBrearty & Brooks 2000; Stewart & Jones 2016). Transient evidence for modern behaviour—in the form of hafting, long distance transport of artefacts and raw materials, and heat treatment of stone—appears before 160 kya (Wilkins et al. 2012). However, an unambiguous, persistent archaeological signal is not apparent until the Late Pleistocene MSA, from 100 kya (e.g., Bouzouggar et al. 2007; Henshilwood et al. 2009). What follows is an exponential growth in the frequency and diversity of evidence for novel behaviour (Wadley 2013, 2015). However, as with the fossil evidence, archaeological signifiers of modern behaviour do not provide a continuous, geographically traceable narrative of progression or linear evolution. Rather they manifest across the continent as temporally pulsed concentrations of technological innovation, considered indicative of an iterative process of behavioural change (McBrearty & Brooks 2000), brought about through the dynamic interplay between social, biological and environmental conditions.

These signals include evidence for the exploitation of coastal resources in north, south and east Africa (Henshilwood & Marean 2003; Marean et al. 2007; McBurney 1967; Singer & Wymer 1982; Steele et al. 2019 and citations therein; Volman 1978; Walter et al. 2000), such as the threading of marine and ostrich eggshell beads in Morocco, Kenya and Tanzania (Bouzouggar et al. 2007; Henshilwood et al. 2004; Henshilwood & Marean 2003; Miller & Willoughby 2014; Steele et al. 2019; Vanhaeren et al. 2013), as well as the use of ostrich eggshell containers at Diepkloof rock shelter in South Africa (Texier et al. 2010),

the creation of compound paints and adhesives (Henshilwood et al. 2011; Wadley et al. 2009), and the engraving of geometric designs into the surface of eggshell and ochre (Henshilwood et al. 2009; Henshilwood & Dubreuil 2011; Henshilwood et al. 2014; Mackay & Welz 2008; Texier et al. 2010).

Technological evidence dramatically diversified within the last 100 ka, with novel approaches to stone knapping and organic tool production that differ markedly from the MSA's characteristic Levallois prepared core technology. Such technological innovations include the production of bone implements found in South Africa (i.e., Sibudu, Klasies River, Blombos rock shelters and Peers Cave, d'Errico & Henshilwood 2007; d'Errico et al. 2020; Henshilwood & Sealy 1997; Henshilwood et al. 2001) and North Africa (Bouzouggar et al. 2007) as well as pressure flaking (Mourre et al. 2010), retouch, the miniaturization of stone tools (Pargeter 2016), and evidence of heat treatment (Brown et al. 2009; Schmidt et al. 2020; Villa et al. 2009; Villa et al. 2010; Wadley & Prinsloo 2014). Finally, an understanding of animal behaviour, especially as it relates to the anticipation of specific environmental conditions, is suggested in the possible use of snares and stone tip poisons (Wadley 2015).

Most of these innovations manifest as concentrated accumulations in the latter part of the MSA, and have been characterised as distinctive technological complexes, including the Still Bay and Howiesons Poort in southern Africa, and the Aterian in North Africa (cf. Dibble et al. 2013; Henshilwood & Dubreuil 2011; Scerri 2017) as well as wholesale assemblage replacement (technology and typology) that is particularly acute in the LSA record (i.e., the ELSA, Robberg, Oakhurst, Wilton). The knowledge required to select, extract, process and produce these technologies demonstrates a strong capacity for complex cognition during the Late Pleistocene MSA (Wadley 2015). This plethora of evidence paints a picture of a species that had an intimate knowledge of its resources—particularly with respect to the mechanical properties of stone, and the edible, medicinal and poisonous properties of plants. It also implies that during the latter part of the MSA, humans had the ability to multi-task, forward plan, and undertake analogical reasoning—mental attributes considered essential qualities of modern humans (Ambrose 2010; Wadley 2013, 2015; Wadley & Prinsloo 2014).

Southern Africa is especially prolific in early evidence for modern behaviour, yielding one of Africa's oldest and richest archives of Late Pleistocene MSA and LSA archaeology (Brown et al. 2009; Foley & Lahr 2003; Henshilwood & Marean 2003; Marean 2010; Marean et al. 2007; McBrearty & Brooks 2000; cf. Wilkins & Chazan 2012). As a result, it has one of the most well-developed chrono-stratigraphic sequences for Late Pleistocene human history in the continent (see Lombard et al. 2012), has proved pivotal in encouraging research in Africa generally, and helped to establish protocols for how Late Pleistocene human history in Africa is approached, sampled and ultimately interpreted. However, its dominance in reconstructions of Late Pleistocene human behaviour is largely due to the long history and continuing focus of scholarship in this area, coupled with a surface geology conducive to the formation of rock shelters and caves that preserve long sequences of Late Pleistocene archaeology. These factors have introduced bias in where archaeological information is sourced from, not only for the African narrative, but also within the subcontinent. The subsequent sections of this chapter focus on the bias in the construction of the southern Africa record, considering its history of scholarship and how this has informed the dominant perspective and approach used to build its Late Pleistocene MSA and LSA narrative.

2.3 Southern African Research: The First Half of the 20th Century

2.3.1 Building a culture history

For most of the last century, scholarship on the archaeology of southern Africa was invested in developing a culture history of typo-technological change, explained largely through cultural evolutionism (Mackay 2016a). Differences observed in its stone technology were thought to represent a record of linear progression from a state of cultural simplicity to complexity. Culture histories helped to organise and track these differences over time from a physical source or origin, with the view that simpler cultures were replaced by more sophisticated ones (e.g., Burkitt 1928, p.4). Earlier attempts to describe South African material—using European nomenclature and the challenges this posed (i.e., Johnson (1907); Péringuey (1911)—inspired the development of a classification system specific to South Africa (Clark 1959). This system, published in Goodwin and Van Riet Lowe's (1929) seminal work *The Stone Age cultures of South Africa*, laid the foundations for a culture history of behavioural evolution (cf. the strictly Afrikaans nomenclature proposed by Van Hoepen 1932; see Underhill 2011, p.5 and citations therein)—first in South Africa and thereafter for the rest of the continent (Clark 1957; Mitchell 2002).

South African archaeology was divided into three Stone Ages: Earlier, Middle, and Later (ESA, MSA, LSA). In line with the racial perspectives of the time, Goodwin and Van Riet Lowe (1929) proposed a 'hypothetical evolutionary series' to reconstruct and track the evolution of cultures from North to South Africa—classifying differences in stone implements as discrete cultural traditions or Industries of technology for each Stone Age. Stone implements were organised into common types and further grouped into Industries (e.g., the Sill Bay in the MSA, the Smithfield and Wilton Industries in the LSA; Goodwin & Van Riet Lowe 1929, p.6). In surface contexts that lacked stratified material, stone implements were considered older if relatively larger and 'cruder', showing a greater depth of patination and a tendency to be heavily 'crusted' (e.g., Van Riet Lowe's seriation of Smithfield "A" relative to "B" and "C"; Goodwin & Van Riet Lowe 1929, p.172). It was assumed that innovative technology in South Africa was introduced from the more technologically adept cultures in the north, made explicit by Goodwin and Lowe's (1929, p.98) declaration that:

> …we owe both the flake implements in the Fauresmith Industry and the basis of the Middle Stone Age to a "Mousterian" influence or infiltration, not necessarily from Europe, but certainly from the north.

This perspective was held in human origins research for nearly a century, consigning Africa to humanity's 'cultural backwaters' (Breuil 1945; Butzer 1971; cf. Clark 1975; Lombard 2012; McBrearty & Brooks 2000). Furthermore, the large temporal scale of the Stone Age System and its associated Industries was such that the endeavour to determine a cause for culture change was sought in the phasing of global scale climatic periods, often resulting in environmentally deterministic models of cultural change (e.g., the Pluvial system, see below).

Southern Africa's budding cultural sequence was based on a combination of open-air and rock shelter assemblages, including both buried and surface material (Burkitt 1928; Goodwin & Van Riet Lowe 1929; Johnson 1907). However in reflecting on this, Burkitt (1928, p.14) noted that "…South African

archaeologists have not, as yet, paid enough attention to the obtaining of stratigraphical evidence". This sentiment was echoed by Goodwin & Van Riet Lowe (1929, p.268), with the added emphasis on the need for greater control during excavation:

> It does not seem unnecessary to appeal once again for more careful archaeological excavation with the intention of discovering stratification and association, with considerably less of the body-snatching methods of the ingenuously amateurish grave-robber.

The sample sizes and lack of contextual data given for many of the collections studied by Goodwin meant that some Industry divisions proposed for their Stone Age System—chiefly the MSA—were riddled with inter-regional and chronological uncertainty, in such cases being labelled as 'Variations' (e.g., the Howiesons Poort Variation; Goodwin & Van Riet Lowe 1929, p.100). Chronological uncertainty meant that many Industries were interpreted as regional divisions that overlapped in the timing of their use, suggesting that cultures or traditions did not follow a clear synchronic history of diffusion or cultural evolution. For instance, the MSA Industries of the Cape Flat Complex—the Still Bay, Mossel Bay and Howiesons Poort—were interpreted by Goodwin (1931, p.31) to be contemporaneous, representing regional and contextual variants of the same period, with assemblages from Peers Cave (Skildegat) and Cape St Blaize Cave supporting their temporal lumping and regional division (Goodwin & Malan 1935).

Goodwin and Van Riet Lowe were acutely aware of the limits in the geographic coverage of their sample. Despite the range of collections studied by Goodwin across the subcontinent (listed in Goodwin & Van Riet Lowe 1929, pp.47-51), the main focus of his work was on the collections housed at the South African Museum that were mostly sourced from the southern Cape. Moreover, the long-term field efforts by Van Riet Lowe were focused on open-sites in the Orange Free State. Overall, Goodwin noted that the distribution of their data mostly came from railroad-country—particularly in the south-eastern half of South Africa—with sporadic coverage in the north-west from geological prospecting (Goodwin & Van Riet Lowe 1929, p.45). During the 1930s and 40s, efforts to establish a culture-stratigraphic sequence by both authors are described by Underhill (2011, p.6) as largely synthetic—lacking the required systematic approach and stratified contexts required to gain more chronological control for their culture historic narrative.

2.3.2 The rise and fall of the pluvial sequence

During and after World War II, research on southern Africa's Stone Age steadily grew, and the need for greater connection between culture change, chronology and environmental shifts encouraged the development of a climatic stratigraphy that was based on the theory of pluvial phasing and glaciation, the idea being that precipitation increased at lower latitudes as glacial conditions increased in the northern hemisphere (Deacon & Lancaster 1988). Thus, it was considered a globally applicable sequence for chronology building and applied throughout the 1930s to 1950s by sub-Saharan researchers, with a four-phase "East African Pluvial Sequence" formally proposed by Leakey at the 1947 Pan-African Conference of Prehistory in Nairobi (Clark 1950; Korn & Martin 1957; Leakey & Solomon 1929; Smuts 1932; Söhnge et al. 1937; Van Riet Lowe 1929; Wayland 1934).

Throughout South Africa, geomorphological studies set about fitting geological and associated

archaeological sequences to each Pluvial phase, providing a much-needed chronological structure for archaeological research and enabling the cross-correlation of climate change inter-regionally (e.g., Korn & Martin 1957; Mabbutt 1957; Söhnge et al. 1937; Van Riet Lowe 1929). A founding example is Van Riet Lowe's work with geologists Adolf Paul Gerhard Söhnge and Dirk Visser on the Vaal and Caledon River surveys. Van Riet Lowe used the pluvial-glacial sequence to produce southern Africa's first climatic-culture-stratigraphy, which involved fitting the alluvial geological sequence of terrace deposits and their associated material culture to East African pluvial cycles and northern hemisphere glaciation (Deacon & Lancaster 1988; Malan 1970; Van Riet Lowe 1929).

The Pluvial scheme enabled scholars to link paleoenvironmental and cultural change at the geological scale. However, by the 1960s, the limitations of the Pluvial system were becoming apparent, with the lack of adequate supporting evidence linking pluvial cycles with glaciation—particularly when projecting an East African precipitation signal onto other areas of the continent—culminating in calls by Cooke (1957) and Flint (1959) to abandon it as a formal dating method. Based on Milankovitch principles of orbital forcing, Bernard (1962) subsequently hypothesised that changes in insolation would affect climate at different latitudes in variable ways, introducing an important concept that precipitation can vary globally thereby weakening chronological frameworks that were built on long-term global climatic trends from northern hemisphere datasets (Deacon 1989).

2.4 Southern African Research: The Second Half of the 20th Century

2.4.1 A drive for culture-stratigraphic control

The second half of the 20th century represents a pivotal time in establishing the conceptual and methodological foundations of southern Africa's current approach to data collection and Stone Age enquiry. This was happening during a time when the discipline was going through major theoretical and methodological reform. The most notable was the formation of New Archaeology in the 1960s, which encouraged a more scientific, process orientated approach and anthropological perspective over the imperialistic approach of culture history. This coincided with a scientific revolution in archaeology brought about by Willard Libby's development of radiocarbon dating in the 1950s. The first radiocarbon dates in South Africa were carried-out on three samples from Florisbad and Cave of Hearths (Libby 1954). This was also the first open-air Stone Age site dated by radiocarbon in Africa. However, the cumulative impact of this revolution was not fully realised in southern Africa until nearly a decade after the first publication of ages in 1949 (Arnold & Libby 1949; Libby et al. 1949) (see below).

The period following the abandonment of the Pluvial system and leading up to the application of radiocarbon dating left southern Africa without a reliable chronological framework capable of linking cultural and environmental change across the subcontinent. This meant that enquiry into the South African Stone Age was targeted at rectifying the issues of classification, sampling, and stratigraphic control. Although this period helped to refine southern African relative dating methods, it also reinforced a dependence on culture historic frameworks. The prioritisation of developing a geographically coherent cultural-stratigraphy is evident in Clark et al. (1966) summary of the 1965 Burg-Wartenstein Symposium, which outlined a series of recommendations on the naming protocols and structuring of the African Stone

Age. These emphasised the dominant, dual objectives of South African archaeology at the time: to establish a reliable chronology and an inter-regionally standardised classification system to enable reconstruction of culture change at the (sub)continental scale (Clark et al. 1966). A precise cultural-stratigraphic nomenclature—including dropping Goodwin and Van Riet Lowe's tripartite system—was believed to be essential to achieving these objectives (Clark et al. 1966).

These recommendations reinforced the importance of building a sequence of culture change through careful recording and excavation of stratified contexts, which promoted a shift in sampling strategy from surface collection to excavation (Clark et al. 1966; Volman 1981). Culture-stratigraphic sequences were repeatedly updated, culminating in the production of the first chrono-stratigraphic sequences for the South African ESA, MSA (i.e., Singer & Wymer 1982; Volman 1981, 1984), and LSA (i.e., Deacon 1984). Despite a concerted effort by Sampson (1974) to exclude Goodwin and Van Riet Lowe's Stone Age system from his South African culture-stratigraphic sequence, its use continued in subsequent chronological frameworks (i.e., Deacon & Deacon 1999; Lombard et al. 2012; Singer & Wymer 1982; Volman 1984).

The methodological developments of Mason (1962), as well as the use of ecological frameworks by Clark (1959), also pre-empted a subtle shift in South African archaeological thinking from the descriptive, imperialist tradition of culture histories to the more anthropologic and science focused principles of New Archaeology (e.g., Binford & Binford 1968; see Underhill 2011, p.7). As a consequence, the subsequent decade of MSA and LSA research also shifted in its scale of enquiry. From the late 1960s, a growing number of researchers sought to tie the culture historic chronologies of cultural evolution to more anthropological and ecological lines of enquiry—a movement heralded by the teachings of Raymond R. Inskeep, the work of John Parkington, and the interdisciplinary advancements of Hilary J. Deacon (e.g., Inskeep 1978; Parkington 1972; see Schrire 2010). As a result, excavation and analytical methods became more standardised and technologically refined, increasing the resolution of evidence for human-environment interaction and behavioural evolution.

2.4.2 The impact of chronometric dating

During the 1960s and 70s the growing application of radiometric dating techniques transformed Stone Age research in southern Africa. Among other things, radiocarbon dating pushed back the antiquity of human behavioural evolution, increased the temporal resolution of chronological frameworks, and enabled the correlation of multiple behavioural, biological, and environmental proxies. This helped to shift archaeological enquiry from broad evolutionary and environmental trends to landscape-scale questions concerning the interaction between social and ecological change.

2.4.2.1. The spatio-temporal shift in the origins of human behaviour

The advent of chronometric dating had a profound impact on our understanding of Africa's role in the timing and history of cognitive complexity in *H. sapiens* (e.g., Cann 1988; Stringer & Andrews 1988; Wainscoat et al. 1986). With the 1967 establishment of a dedicated radiocarbon facility in Pretoria, stratified localities across South Africa were increasingly subjected to radiocarbon dating (see Figure 2.1; Beaumont & Vogel 1972; Mason et al. 1973; Vogel & Beaumont 1972). This method provided greater temporal

control and resolution, helping to refine southern Africa's chronological sequence and push back the age of Industries associated with the initial appearance of modern human behaviour from the LSA into the MSA (Clark 1975; McBrearty & Brooks 2000; Vogel & Beaumont 1972). This elevated Africa from evolution's 'cultural backwaters' to the forefront of origins research, instigating a newfound interest in the MSA and LSA and dramatically increasing the number of rock shelter excavations across southern Africa.

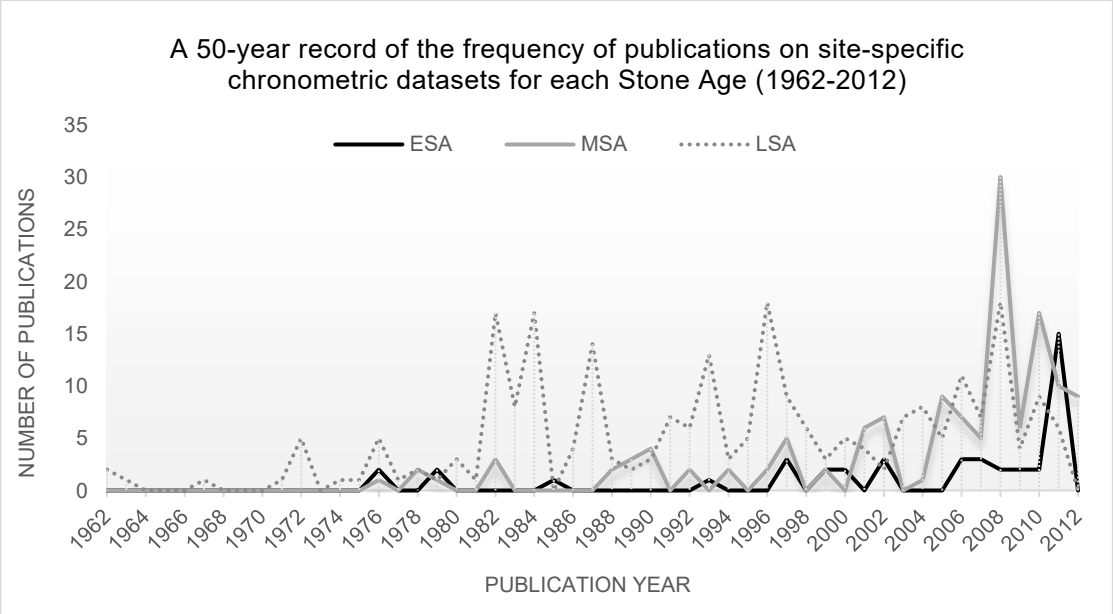

Figure 2.1. The frequency of publications on site-specific chronometric datasets published over a fifty-year period, from 1962-2012. Data sourced from Lombard et al. (2012, pp.128-140, Appendix A).

2.4.2.2. Shifting the scale of Stone Age enquiry

From the 1960s, the applicability of different dating methods and the timing of their availability for each Stone Age impacted the way LSA and MSA research was approached, particularly in terms of the scale of human behavioural change that could be detected and tested by their respective researchers. Radiocarbon dating made it possible to study human behavioural change at a finer temporal resolution for archaeology younger than 40 ka, providing a method of directly and indirectly dating material culture in addition to and independent of time-diagnostic artefacts. This enabled LSA research to investigate social and ecological trends of hunter-gatherer lifeways. However, it's temporal limit perpetuated dependency on culture historic units in MSA research, restricting the depth and resolution of enquiry to broad scale trends in typo-technological change and glacial scale shifts in climate and environment.

By the early 1970s, growing interest in landscape archaeology in LSA research exposed the divide between open-air and rock shelter studies, with Parkington's (1972, p.242) remark that "the concentration on cave sites as distinct from 'open' sites is unhealthy and needs to be rectified". Such rectification is evident in the growth in landscape scale research during the 1990s. However, this was primarily focused on the better-preserved Holocene and terminal Pleistocene archaeology, which could also be more easily temporally constrained using radiometric methods. Open-air MSA research during this time served to demonstrate the abundance of archaeology outside the confines of a rock shelter. However, with poor organic preservation and without an absolute dating method, it also emphasised the difficulties of

reconstructing the chronology of open-air archaeology across the landscape, especially in the face of erosion and the absence of stratigraphy.

2.4.2.3. Entrenchment of rock shelter research

Sampson's (1968) extensive open-air field work in the Orange Free State was a rare exception in an increasingly rock shelter-centric research paradigm. His project was driven by the impending damming and subsequent flooding of the Orange River valley, threatening an extensive record of palaeontological and archaeological remains (Sampson 1968, p.iii). The urgent need to salvage information on the archaeology in this area resulted in two years (1965-67) of survey and the excavation of five localities (Elandskloof 13, Orangia 1, Zeekoegat 27 and 12, Dagbreek 1) and included two MSA quarries (Sampson 1968). The '*The Middle Stone Age Industries of the Orange River Scheme Area*', (Sampson 1968) is an exceptional example of South African MSA open-air research that was systematic in its approach and dedicated to developing and integrating open-air archaeology on a massive landscape scale. It provided quantifiable evidence of the abundance of archaeology in the interior, in which Sampson (1968, pp.103-104, Tables 10 and 11) recorded >16,000 stone artefacts from 26 localities, six of which were from buried contexts. However, his work also underscored the difficulty in constructing a chronology and establishing artefact and assemblage association within an archaeological landscape dominated by surface artefacts. One of the main concluding remarks Sampson (1968, p.107) made about the state of South Africa's interior archaeology centred on the issue of MSA artefact preservation and stratification:

> There are no deep caves in this area because the local rock types are not suited to their formation. Deep sealed deposits containing cultural material earlier than the Later Stone Age are therefore absent. Local conditions of rainfall and vegetation preclude the accumulation of deep stratified sequences in open sites. Rapid and widespread erosion of the river and stream banks does however expose a large number of Middle Stone Age occurrences.

Due to South Africa's overriding interest in building an inter-regionally applicable culture-stratigraphy, Sampson's (1968) observations served to reinforce the growing sentiment that most of South Africa was erosional, lacking stratigraphy beyond the sediment traps of rock shelters, and rendering it incapable of yielding chronologically informative evidence for Late Pleistocene behavioural change. The issues of chronological control and preservation in South Africa's interior—despite artefact abundance—gave additional impetus to prospect for, and (re)excavate coastal rock shelters throughout the 1970s and 80s (e.g., Deacon 1979). With exceptions (e.g., Kuman 1989), this solidified the dismissal of the interior and intensified Late Pleistocene research in regions with geological conditions conducive to rock shelter formation—particularly the southern Cape coast—shifting the geographic bias from coastal and south-east inland coverage that had been in place since the 1930s, to coastal and near-coastal coverage around the perimeter of southern Africa.

The higher levels of preservation of Holocene and (to a lesser degree) terminal Pleistocene archaeology, and the availability of radiocarbon dating for these periods, enabled LSA studies to shift to a finer resolution in the ethnographic and ecological inquiry of hunter-gatherer lifeways and to assess these across a wider range of buried contexts. This is exemplified in the settlement system modelling of

Parkington and colleagues (e.g., Deacon 1976; Parkington 1976; Parkington 1972; Parkington & Mellars 1990; Parkington et al. 1986; Sealy et al. 1986) and by the surge in publications on radiometrically dated LSA samples from the 1980s—the only Stone Age with radiometric determinations published before 1975 (Figure 2.1). The lack of an appropriate dating method for MSA research prior to the mid-1990s limited interpretation of technological change to the same resolution as their associated culture historic unit. Thus, human behavioural evolution was presented as long periods of cultural stasis punctuated by sudden shifts in technology (Mackay 2016a).

Table 2.1. The number of LSA and MSA sites with radiocarbon ages published in Wadley (1993) and Thackeray (1992), respectively, compared to the total number of dated sites using multiple chronometric methods* for the same regions published in Lombard et al. (2012, pp.128-140, Appendix A)

	LSA		MSA	
Source	1993a	2012b	1992c	2012b
Sites (n)	26	171	24	50

*e.g., radiocarbon, luminescence, U-series a Wadley 1993, pp. 248-253; b Lombard et al 2012, pp. 128-140; c Thackeray 1992, p. 401

Taphonomic bias coupled with low site numbers initially helped to maintain models of modern human behavioural evolution that favoured a European origin. Throughout the 1980s, artefacts typically associated with innovative technology in the Upper Palaeolithic sites of Europe and south west Asia (e.g., human burials, decorative items, engravings of art) were thought to have only minimal occurrence in the MSA deposits of sub-Saharan Africa, whilst being relatively abundant in LSA assemblages after 40 ka (e.g., Deacon 1979). This pattern was interpreted as a 'human revolution' that occurred in Eurasia ~40-50 kya, in which sustained modern human behaviour was only fully realised after AMH successfully migrated out of Africa (e.g., Bar-Yosef 1998; Binford 1985; Klein 1989, 2000, 2008; Mellars 1996; Noble & Davidson 1991; Tattersall 1995).

The 'human revolution' model was eventually overturned in the 1990s as a combined consequence of chronometric methods capable of dating beyond the radiocarbon limit (e.g., luminescence and U-series dating) and the dramatic growth in archaeological research on the MSA (shown in Figure 2.1 and Table 2.1; McBrearty & Brooks 2000; Thackeray 1992). Rather than a sudden, punctuated evolution of human behaviour in Eurasia, this growing body of evidence supported a gradual pan-African accretion of cognitively complex behaviour that transpired over the last 300/250 ka (Henshilwood & Marean 2003; McBrearty & Brooks 2000; Willoughby 1993, 2006).

2.5 The Current State of Southern African Late Pleistocene Research

As noted earlier in this Chapter, studies of the MSA have recently become synonymous with questions relating to the evolution of modern human behaviour. This has led to a disproportionate focus on technocomplexes like the Still Bay and Howiesons Poort during which rates of cultural change and evidence for complex cognition both appear to increase. In contrast, the preceding and subsequent technocomplexes have received comparatively less attention, being considered generally technologically heterogenous periods that are difficult to characterise precisely.

Counter to traditional expectations, regional syntheses of southern Africa's Late Pleistocene human behavioural evolution do not present a continuous progression of technological change from simple to complex. Rather, southern Africa's MSA and Late Pleistocene LSA archaeology frequently present a temporally pulsed pattern of technological change and fluctuation in the number and geographic spread of Late Pleistocene-bearing sites (e.g., Figure 2.2; Mackay et al. 2014a). The sequence of these pulses defies easy interpretation, especially with respect to tracking human cognitive evolution. The Still Bay and Howiesons Poort technocomplexes appear and disappear during the latter part of the MSA, within a window of roughly 75-58 ka, before evidence for complex cognition becomes a permanent fixture of the LSA, from late MIS 2 (e.g., Figure 2.2). A decrease in archaeological evidence in the southern Cape during MIS 3—despite evidence for continued occupation in regions to the east (Wadley 2015)—further complicates the expected scenario of continuous occupation and evolution of technological innovation across southern Africa. Growing evidence for stone tool variability is also proving increasingly difficult to define within the culture-stratigraphic frameworks of the preceding century, leading some to argue for its abandonment (e.g., Shea 2014, 2019; Wilkins 2020) while others look to and continue to develop to regionally-sensitive frameworks (e.g., Sampson 2001; Sampson 1974; Sampson 1984; Sampson 1996, 2000; Sampson et al. 1989; Will et al. 2015).

2.5.1 Chronological control and accounting for behavioural variability

Despite the extensive scientific developments that southern African Late Pleistocene research has undergone since the 1965 Burg-Wartenstein symposium, a robust, subcontinent-wide chrono-stratigraphic framework that can account for behavioural variability remains elusive (Loftus et al. 2016; Mackay et al. 2014a; Wadley 2015). In an attempt to remedy this, Lombard et al. (2012) compiled an updated South African and Lesotho Stone Age (SALSA) sequence (presented in Table 2.2 and illustrated in Figure 2.2) and accompanying dataset (see Lombard et al. 2012, pp.128-140, Appendix A). The SALSA sequence combined many of the elements set forth by the culture-stratigraphies of the preceding century, retaining the Stone Age System along with many of the Industries first defined by Goodwin & Van Riet Lowe (1929), while considering technological change as broad traditions or 'technocomplexes' rather than cultures (Clark et al. 1966; Lombard et al. 2012, p.124; Table 2.2). In the hope of broadening its applicability, each technocomplex was also associated with a Marine Isotope Stage—the intention being to provide a broad chronological framework for the entire Stone Age, as opposed to linking technological change with paleoenvironmental shifts (Lombard et al. 2012, p.126).

Lombard et al. (2012, p.126) sought to capture technological variability in the SALSA dataset by

providing a breakdown of site-specific 'Variations' in material culture that exist for each technological complex, echoing the foundational work of the 1920s. The SALSA sequence gives the impression that variation is definable at the Industry level, with only minimal temporal variability evinced in the overlap of age ranges for each technocomplex (see Table 2.2 and Figure 2.2). However, stone tool variability is a recurring feature of each technocomplex *and* Industry in the SALSA dataset—particularly when defined by more than one site or region—indicating that the southern African Stone Age is characterised more by technological variability between regions than by common subcontinent-wide traditions.

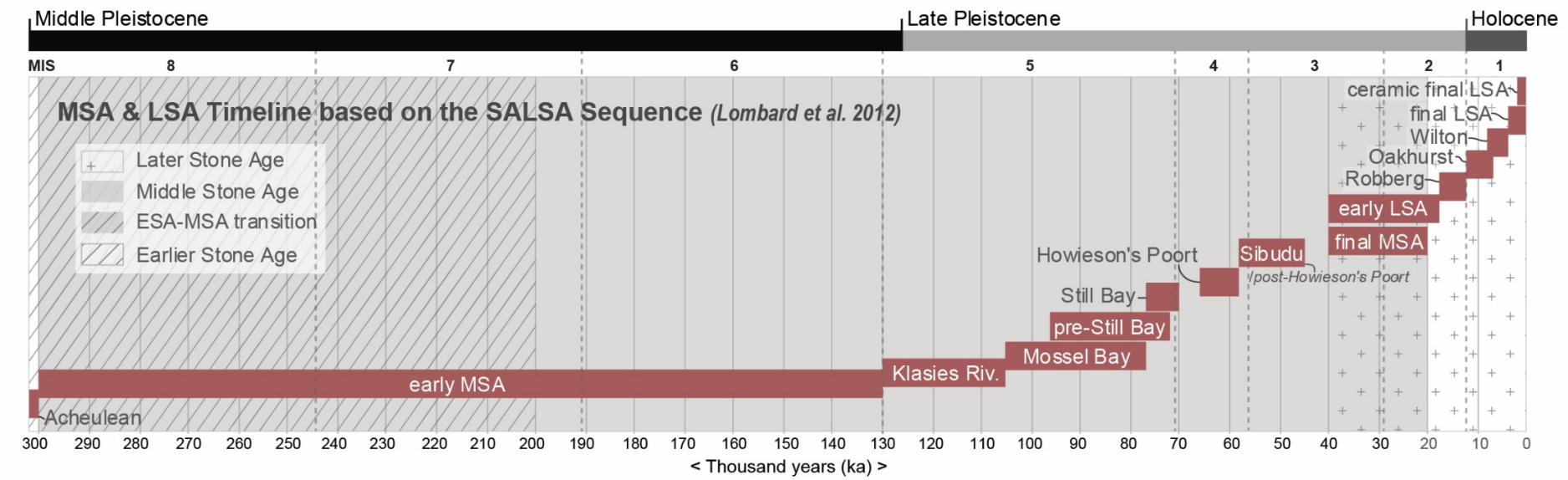

Figure 2.2. Stacked timeline for the MSA and LSA based on Lombard et al.'s (2012, p.125) South African and Lesotho Stone Age sequence (see Table 2.2)

Table 2.2. The South African and Lesotho Stone Age Sequence from Lombard et al. (2012, p.125 Table 1).

Period	SAL technocomplex	Also known as (including regional variants)	Broadly associated MISs
Later Stone Age <40 ka	*ceramic final Later Stone Age* <2 ka	ceramic post-classic Wilton, Late Holocene with pottery (Doornfontein, Swartkop)	MIS 1
	final Later Stone Age 0.1–4 ka	post-classic Wilton, Holocene microlithic (Smithfield, Kabeljous, Wilton)	MIS 1
	Wilton 4–8 ka	Holocene microlithic (Springbokoog)	MIS 1
	Oakhurst 7–12 ka	Terminal Pleistocene/early Holocene non-microlithic (Albany, Lockshoek, Kuruman)	MIS 1
	Robberg 12–18 ka	Late Pleistocene microlithic	MIS 2
	early Later Stone Age 18–40 ka	(informal designation); Late Pleistocene microlithic	MIS 2 to MIS 3
Middle Stone Age >20 to <300 ka	*final Middle Stone Age* 20–40 ka	(informal designation) MSA IV at Klasies River, MSA 4 generally	MIS 2 to MIS 3
	Sibudu 45–58 ka	late MSA/post-Howieson's Poort or MSA III at Klasies and MSA 3 generally (all informal designations)	MIS 3
	Howieson's Poort 58–66 ka		MIS 3 to MIS 4
	Still Bay 70–77 ka		MIS 4 to MIS 5a
	pre-Still Bay 72–96 ka	(informal designation)	MIS 4 to MIS 5
	Mossel Bay 77–105 ka	MSA II at Klasies River, MSA 2b generally (Pietersburg, Orangian)	MIS 5a–c
	Klasies River 105–130 ka	MSA I at Klasies River, MSA 2a generally (Pietersburg)	MIS 5d–e
	early Middle Stone Age 130–300 ka	(informal designation)	MIS 6 to MIS 8
Earlier Stone Age >200 ka	*ESA-MSA transition* >200–600 ka	(informal designation) (Fauresmith, Sangoan)	MIS 7 to MIS 15
	Acheulean 300 ka-1.5 Ma		MIS 8 to MIS 50
	Oldowan 1.5–2 Ma		MIS 50 to MIS 75

The contrast between the SALSA sequence and its dataset demonstrates the continued difficulty in presenting technological change as a top-down sequence of subcontinent-wide trends as they tend to understate regional variability and give the impression of inter-regional contemporaneity in technological change (Inskeep 1967; Mackay et al. 2014a; Orton 2014). Added to the difficulty in organising and describing stone tool variability is the challenge of explaining its temporal and geographic pattern. The geographic scale of later Pleistocene behavioural change between broadly defined climatic regions was also found to vary through time, leading Mackay et al. (2014a, p.46) to conclude that:

> Technological and occupational systems were not always in agreement across southernmost Africa and the efficacy of universal industrial schemes, particularly where attention is not given to underlying causes, is questionable.

Ongoing difficulty in describing technological variability with an inter-regionally defined culture-stratigraphic framework has prompted some studies to reject the SALSA sequence in favour of broader more inclusive terminology (i.e., Orton (2014), and Beaumont et al. (1995); Deacon (1984); in a similar vein to earlier approaches in Humphreys & Thackeray (1983)), or restricting chronological reconstructions to regionally-specific chrono-stratigraphic and chronometric sequences (e.g., Will et al. 2015). Since stratigraphic sequences of change from one technocomplex to another are often consistent between sites at the regional scale they are taken to indicate that diagnostic artefacts, in conjunction with a stratified sedimentary system, can continue to provide reliable chronological markers for long-term change in and between contexts with and without chronometric control—even if the source and composition of this change is still fervently contested and not entirely understood.

A third view is that culture-stratigraphic frameworks are inaccurate representations of behavioural variability and unnecessary given the availability of chronometric methods for building regional chronologies (see also Shea 2011; Shea 2014, 2019; Wilkins 2020). However, the issue with this latter argument is that there are still few well-dated sites in southern Africa. Although chronometric dating

methods can assist with building inter-site chronologies of Late Pleistocene behavioural change, their application and accuracy depend on what materials and sediments can be dated, their availability, preservation, and strength of association with the archaeology. Despite the application of radiocarbon dating to southern African Stone Age archaeology since the 1960s few sites have been dated thoroughly enough—often requiring re-dating—to provide the appropriate degree of chronological resolution or precision to confidently show contemporaneity in the timing and duration of LSA technocomplexes for the entire subcontinent (Loftus et al. 2019; Loftus et al. 2016; Pargeter et al. 2017; Pargeter & Low 2018).

The same can be said for the application of luminescence methods in MSA deposits. A site-specific example of this is the apparently irresolvable differences in age estimates obtained by two different labs for Still Bay and Howiesons Poort-bearing deposits at Diepkloof Rock Shelter (Feathers 2015; Guérin et al. 2013; Jacobs et al. 2013; Jacobs et al. 2008; Tribolo et al. 2013; Tribolo et al. 2009). This demonstrates that, like radiometric dating, optical dating is not as simple as a mark or range on the calendar—it represents a relatively young group of dating approaches that are constantly being refined and improved. As it stands, luminescence ages produce large errors that limit the resolution of chronological reconstructions of behavioural change in MSA studies (Mackay et al. 2014a, p.31).

2.5.2. Human-environment interaction – a landscape or rock shelter perspective?

At every level of geographic enquiry—be it at the site, catchment, regional, or inter-regional scale—southern Africa's Late Pleistocene research is aimed at furthering investigation into the "subtle links between climate, environment, and human evolution" (Wurz 2019, p.125). The collective interest in understanding the evolution of behavioural change in relation to climatic and environmental shifts inspired the need for a system like the Pluvial Scheme to be developed in the 1950s. It also catalysed more ecologically driven research questions during the 1960s and 70s and developments in isotope and pollen analysis from this time. However, as Wilkins et al. (2017) observed:

> …even at the largest scale of MIS and glacial/interglacial cycles, there is a huge degree of disagreement on how exactly early modern humans responded to these changing environmental conditions, even on a broad, time-averaged scale.

They put this down to the lack of regional palaeoenvironmental records preserved in long sequence sites. However, even the most well studied and dated regions in southern Africa (i.e., the southern and Western Cape coast) present a fragmented record. The most comprehensive are Pinnacle Point, Blombos, Klasies, and Sibudu, which occur in the coastal and near-coastal zones of southern Africa, and their dominance in MSA literature biases sample coverage to these regions and their environmental conditions—with a clear deficit in the sampling of southern Africa's interior (Mackay 2016b, p.3). Their dominance results in regional sequences that are sensitive to the addition or removal of a single locality from the regional sample—the removal of a single shelter from the southern African Late Pleistocene narrative would significantly change our understanding of early human behaviour (Mackay 2016b, p.3). This cautions against the assumption that a single site provides a comprehensive history of socio-environmental change and human-environment interaction (Mackay 2016b, p.3)—no single site is capable of representing the history of a region's occupation. Acknowledgement of this bias has also prompted renewed efforts over the last decade to increase the rock shelter/cave sample. This is done through prospecting surveys for

unknown rock shelter sites in underexplored parts of the subcontinent (Fisher et al. 2013; Steele et al. 2016) and by implementing re-excavation/dating programs of known cave and shelter deposits to MSA levels (e.g., Diepkloof, Bushmans, Elands Bay Cave, Border Cave, and Klipfonteinrand; Backwell et al. 2018; Mackay et al. 2019; Porraz et al. 2013; Porraz et al. 2016; Porraz et al. 2015).

Efforts to attain palaeoecological and climatic evidence in long-sequenced sites and the expansion of rock shelter research into old and new regions are contributing to a broader understanding of Late Pleistocene behavioural variability across southern Africa. However, publication of rock shelter focused multi-site syntheses and single-site sequences are unable to account for behavioural variability across the landscape without studying Late Pleistocene material culture outside the confines of a single site-type. The geologically-dependent and thus geographically bound nature of rock shelter and cave sites, as well as assumptions about their function—they are often recognised as both residential bases and activity-specific settings (e.g., Oestmo et al. 2014)—prompts the question of whether the behaviour associated with these deposits is representative of landscape scale human-environment interaction, or if it is more closely tied to rock shelter specific use and its reorganisation throughout the Late Pleistocene (Parkington & Mellars 1990). Ethnographic examples suggest the latter (e.g., Binford 2001; Kelly 1995), demonstrating that hunter-gatherers tend to spend the majority of their time in the open landscape. This implies that rock shelters will only account for a small component of the behavioural repertoire that manifests across a landscape.

However, the shift in focus from open-air to rock shelter investigations during the 1960s has deeply entrenched a site-type sampling bias in MSA and Pleistocene LSA datasets. For the MSA this bias has been further exacerbated by a research emphasis on human behavioural evolution, and its attendant focus on sites with excellent stratigraphic resolution and organic preservation. Open-air sites, in contrast, are not only typically overlooked, but have seen only limited application of chronometric dating methods. Although methods like OSL dating have been successfully applied in open-air studies with Late Pleistocene archaeology, there is still a heavy reliance on typo-technologically diagnostic artefacts for developing chronological frameworks beyond the rock shelter. This is partly due to the rarity of stratified sites in the open-air and the dominance of surface archaeology—the spatio-temporal integrity of which is questioned.

The difficulty in associating open-air artefacts with chronometric ages in surface contexts and the lack of investigation into this association is one of the main reasons why open-air studies remain under-represented in southern Africa's Late Pleistocene syntheses. This is apparent in the proportion of dated context types that contribute to the SALSA sequence (Lombard et al. 2012, pp.128-140, Appendix A), demonstrating the prevailing, heavy reliance on cave/rock shelter evidence. Based on their dataset, cave/rock shelters contribute to more than half the dated sites in the SALSA dataset for all Stone Age periods (Figure 2.3), with the MSA displaying the greatest bias between the two contexts—only four open air localities are listed for this period.[3]

[3] The marked difference in site numbers between each Age not only reflects the uneven focus of stone-age researchers, but also shows the discrepancy in the number of dedicated dating programs and the delayed availability of dating methods for each Age since the 1960s.

Figure 2.3. Percentage and number of chronometrically dated cave/rock shelter and open-air contexts included in the SALSA sequence for each Stone Age. A site-type category could not be allocated to six localities (all of which are dated to the LSA) and were excluded from this graph. Data sourced from Lombard et al. (2012, pp.128-140, Appendix A).

The dependence on rock shelters raises the question: to what degree is a rock shelter and cave-based narrative biasing the spatial pattern and pulsed sequence observed for Late Pleistocene human behavioural change and human-environment interaction (Hallinan & Parkington 2017; Mackay et al. 2014b; Oestmo et al. 2014)? Although southern Africa has an abundance of rock shelters—many of which yield well-preserved archaeological deposits—they only account for a small portion of its total surface area (Figure 2.4), typically congregating in geologically conducive zones such as the quartzite and sandstone formations of the Table Mountain Group along the Cape Fold Belt (CFB) or the Clarens Formation of the Orange Free State, Lesotho, and the Lebombo Mountains. Moreover, much of Late Pleistocene southern Africa is now either under water (Marean et al. 2020) or existed in landscapes lacking the requisite geology for rock shelter formation (Sampson 1968). As a consequence, extensive areas of the southern African landscape are under-represented in Late Pleistocene research (Hallinan & Parkington 2017; Kuman 1989; Mackay 2016b; Parkington & Mellars 1990; Figure 2.4).

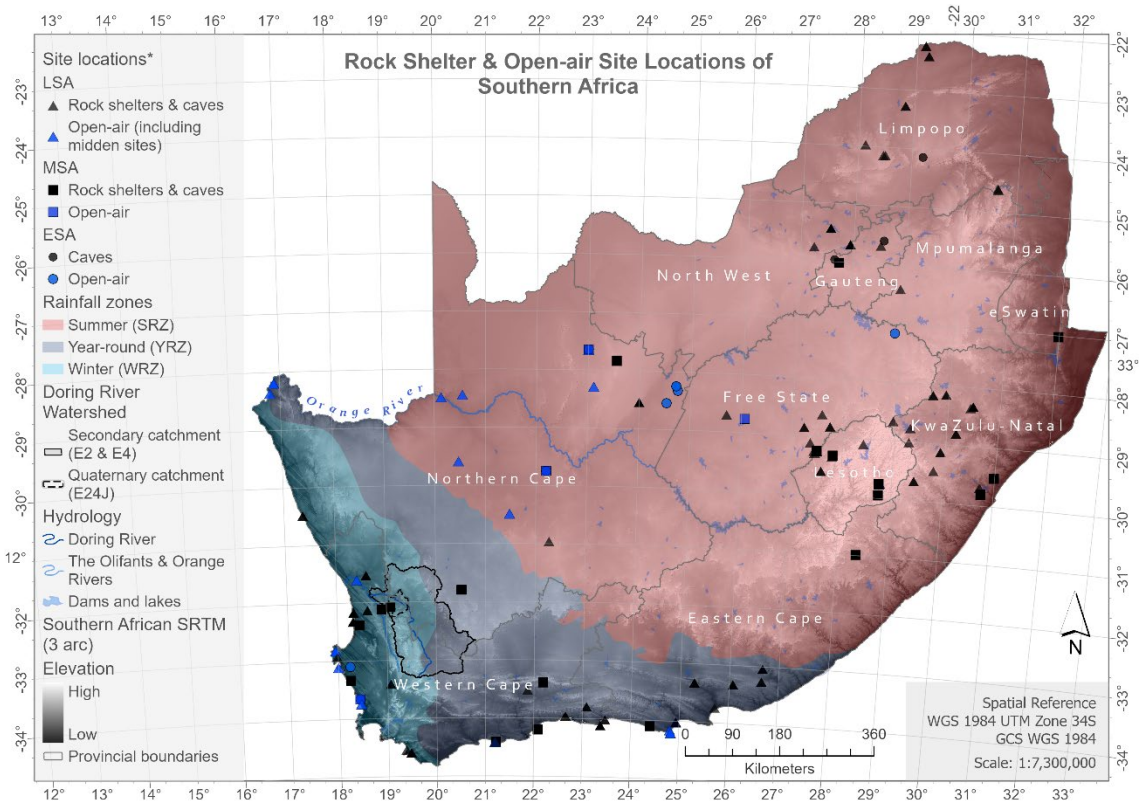

Figure 2.4. Rock shelter (black markers) and open-air (blue markers) site locations of southern Africa grouped by Stone Age (ESA as circles, MSA as squares, LSA as triangles). Sites pertain to those listed in Lombard et al. (2012, appendix A)(*). The study area location of the Doring River watershed is outlined (including the Doring River's secondary [solid black line] & quaternary [dashed black line] catchments). Three major rivers are shown: the Doring River (dark blue), the Orange River (labelled), and the Olifants River (west of the Doring R.). Each province and landlocked country is demarcated by grey borders and underlain by an SRTM elevation map (dark blue = low elevation, dark brown = high elevation), sourced from a hole-filled 90 m DEM (originally processed by Jarvis et al. (2008)).

Van Riet Lowe and Sampson's work in the Orange Free State testify to the wealth of archaeological evidence that exists across a southern African landscape otherwise devoid of rock shelters and cave formation. Moreover, Sampson's work in the interior repeatedly demonstrates that Karoo technology does not fit tidily into a chronostratigraphic sequence—complicated by the fact that rock shelters do not occur in close proximity to this region of study and chronological control has proven problematic as a result of the erosional state of much of the archaeology under investigation. Thus, the archaeology in this area is difficult to place in subcontinent-wide Stone Age reviews, despite occupation in this region spanning at least 700,000 years (Sampson et al. 2015).

At the turn of the century, the surveys, and excavations for the Geelbek and Anyskop Archaeological Survey Project (GAASP; Langebaanweg 1998, 2002) quantitatively revealed the abundance of archaeological evidence in near-coastal settings, collecting a total of 30,000 artefacts (stone, shell, and bone), spanning the entire Stone Age. More recent examples of MSA and LSA Late Pleistocene archaeological abundance in the open-air include the systematic surveys in the Olifants-Doring Basin, in the Western Northern Cape interior (Hallinan & Parkington 2017; Hallinan & Shaw 2015; Low et al. 2017; Mackay et al. 2014b; Shaw et al. 2019). Buried Late Pleistocene archaeology such as that excavated within the Doring watershed, at Putslaagte 1 (Mackay et al. 2014b), or the interior site of Florisbad (Kuman 1989; Kuman et al. 1999), also run counter to pre-conceived notions that beyond the protective bounds of a rock

shelter/cave southern Africa is an erosional landscape, rarely capable of trapping sediment long-term and thereby incapable of preserving buried Late Pleistocene material culture.

2.5.3 The influence of contextual bias on interpretation

A number of well-known and more recently identified discrepancies that exist between the Late Pleistocene occupation histories of rock shelters and those from open-air contexts emphasise the importance of incorporating open-air findings into Late Pleistocene MSA research and explanatory models.

One of the main discrepancies between rock shelters and open-air contexts for MSA archaeology is observed between the Still Bay and Howiesons Poort. The Still Bay is a recurring and often abundant feature in open-air contexts, while the Howiesons Poort is rarely observed (Mackay et al. 2018). In contrast, the Howiesons Poort is inter-regionally prolific and abundant in rock shelters throughout southern Africa (Mackay et al. 2014a; Miller et al. 2013), while the Still Bay occurs less frequently.

Despite its known presence in unstratified open-air contexts since the beginning of last century, the Still Bay was only observed intermixed with the Howiesons Poort deposits such as Peers Cave or as a limited signal in other southern Cape rock shelters until the 1990s. It was thus excluded as a culture historic unit in South Africa's MSA sequence (Keller 1969; Sampson 1974; Volman 1981). However, the continued growth in rock shelter excavation resulted in the identification of the Still Bay in the deeply stratified deposits of Blombos Cave on the southern Cape coast, as well as shelter and cave sites in the Western Cape (i.e., Hollow Rock Shelter, Diepkloof and Mertenhof) and KwaZulu-Natal (i.e., Sibudu and Umhlatuzana, (Archer 2017; Evans 1994; Henshilwood & Sealy 1997; Henshilwood et al. 2001; Högberg & Larsson 2011; Lombard et al. 2010; Rigaud et al. 2006; Wadley 2007). Consequently, less than two decades after its exclusion, the Still Bay was reinstated as a formal Industrial complex. This demonstrates the weight that the stratified structure of rock shelters had, and continues to have, over open-air surface archaeology, despite the repeated occurrence of Still Bay artefacts in open-air contexts and their association with MSA archaeology. Today the Still Bay represents one of the most well studied and chronometrically dated technocomplexes in southern Africa.

Another example of the combined effects of sampling and contextual bias is evident in the decline of dated MIS3 evidence for rock shelter-derived archaeology from ~58 ka in the regions of the southern Cape coast and Western Cape. While this is interpreted as regional abandonment, excavation of the Western Cape interior open-air site, Putslaagte 1 (PL1), yielded evidence that indicates that the Doring and Putslaagte River system were frequented by hunter-gatherers during MIS 3 (Mackay et al. 2014b). However, the flaking systems used were different to those typically observed in rock shelter deposits (Mackay et al. 2014b), with the technological analysis of the buried artefacts at Putslaagte 1 suggesting people were employing different modes of reduction during the late MSA, not otherwise observed in late MSA deposits of regionally proximate rock shelters (Mackay et al. 2014b).

Examples from rock shelters, as opposed to regional abandonment, are also evident for the LSA megamiddens on the west coast. These are dated to the Holocene (~3000-2000 BP), supporting a scenario of long-term recurring use of coastal resources during a time when the occupation of rock shelters in the region declines (Jerardino 2012).

These examples suggest that rock shelters only capture part of a region's landuse and occupation

history and are unlikely to represent the entire suite of human-environment interaction in a given region. It also shows that typo-technological markers, identified and defined in rock shelter contexts, are not a comprehensive and thus entirely reliable reference for determining and tracking technological trends in all contexts. This holds even when dealing with associated archaeology within the same technocomplex. For example, Low et al. (2017) observed that material selection and modes of reduction for early LSA assemblages between the Putslaagte 8 rock shelter and the open-air locality Uitspankraal 7—within the same catchment—differ in approach to resource type and proximity as the conditions of the Doring River system and its surrounding geology change. They suggest that artefact composition changes as the landscape and its resources change. Therefore, if one geologically specific site-type is prioritised over another our understanding of landuse and the interaction between humans and their environment will remain limited to these contexts and the range of behaviours that are often associated with them.

2.5.4. Temporal control in open-air studies

There is growing recognition that rock shelters form a small part of a continuous behavioural landscape with the potential to broaden perspectives on the dynamic between Late Pleistocene humans and their environment. However, the majority of southern Africa's prehistoric archaeology occurs as surface scatters of stone artefacts which often exist within an erosion-dominant system. Thus there is the ever-present conundrum of chronological control and the (in)ability to constrain open-air archaeology to spatio-temporal scales for comparative analyses across a landscape and its surrounding region(s). Several approaches have been employed to help circumvent or overcome this issue. One such approach is to work to the strength of the open-air by maximising the spatial coverage of surface archaeology, while chronological control is obtained using stone technology considered diagnostic of specific rock shelter technocomplexes or their regional variants (Hallinan & Parkington 2017). This approach restricts investigations of human behaviour in open-air settings to rock shelter chrono-stratigraphic frameworks (i.e., the SALSA sequence) and the behavioural and temporal connotations that these frameworks permit.

Another way time is defined in open-air contexts is to focus on buried sites. Traditionally viewed as 'sealed' or 'intact' archives of open-air human activity, buried archaeology is the most common type of open-air site included in synthetic reconstructions of Late Pleistocene human behaviour (e.g., PL1, Vleesbaai and Florisbad). Buried open-air archaeology is approached using similar methods to those employed in rock shelter excavations, including geochronometric techniques to establish a minimum and maximum age for the encased archaeology. It is often found preserved as a single horizon or lens of material encased within naturally accumulated sediment. Buried artefacts that show minimal reworking, and a clustered spatial structure are either interpreted as a time-averaged aggregate or single behavioural event. For Late Pleistocene deposits, OSL dating can be performed on the quartz or IRSL on the feldspar component of the underlying and overlying deposit to obtain a burial age for the deposit and its associated archaeology. The ability to obtain chronometric ages for these contexts means they can be incorporated into chronological syntheses (e.g., Fuchs et al. 2008). However, as a landscape that is dominated by surface artefacts without stratification, southern Africa's open-air research continues to rely heavily on rock shelter-defined technocomplexes and their chronostratigraphic associations as a way to control for time and trace behavioural change.

2.6 Open-air Approaches in Southern Africa

Open-air surface archaeology constitutes the bulk of southern Africa's available evidence for Late Pleistocene human behaviour. However, the historical narrative of southern Africa's open-air research is one of repeated, isolated, and unsuccessful attempts to revive this context as a valuable contributor to reconstructions of human behavioural evolution. Thirty years ago—in a similar vein to this section—Parkington (1990) assessed the representativeness of his own and previous regional radiocarbon chronologies for South Africa (Deacon & Thackeray 1984), compiled for dated Holocene and terminal Pleistocene sites. Despite the growth in dated sites since this publication, many of the observations made by Parkington (1990) still apply to the MSA and Late Pleistocene components of culture-stratigraphic frameworks like the SALSA sequence: that terminal Pleistocene records are almost entirely rock shelter-derived, and that many of the typo-technological markers used to build culture-stratigraphic frameworks are based on this dominant site-type and applied to open-air archaeology without exploring their appropriateness.

This dependence on rock shelters constrains the way open-air archaeology is viewed and studied. For example, if artefacts found in open-air settings are similar to those from rock shelters they can be incorporated into the culture historic system. However, if open-air assemblages fail to resemble those from rock shelters – even if they are part of a single system of technological organisation – it is not possible to incorporate them into the current behavioural narrative. Consequently, open-air archaeology will either conform to rock shelter assemblages and their behavioural narratives or be overlooked in interregional and continental histories. This perspective either leads to data collection methods that restrict open-air survey to artefact classes considered temporally informative for assessing particular behaviours across a landscape or to restrict regional reconstructions to materials and contexts that can be chronometrically dated. The latter approach being the concluding recommendation by Parkington (1990). Thus, for the few who endeavour to study southern Africa's Late Pleistocene open-air archaeology, temporal control and the issue of preservation remain central challenges.

2.6.1 Landscape approach and the challenge in carrying-out open-air research

Standard practice in southern African open-air surveys involves recording the spatial distribution of temporally diagnostic stone tool forms and flaking systems—found as surface clusters that are typically interpreted as undisturbed—either through the systematic sampling and recording of artefacts by way of transects or other geomorphic units, or through the less systematic means of field walking and/or drive-by survey. Preliminary field surveys are intended to identify the presence or absence of archaeological remains in a landscape. However, they also act as the founding structure for more intensive research strategies and, despite initial intention, have often formed the basis of *a priori* behavioural interpretations.

A common approach is to focus on the main advantage that open-air contexts have over the site-bound restrictions of rock shelter excavation: space. An excellent example of this is the work by Hallinan (2013; Hallinan & Parkington 2017), who investigated landscape-scale behavioural change by examining the use of different landforms and the degree to which hominins changed their approach to water and lithic resources over the Middle and Late Pleistocene.

The over-reliance on typo-technological systems conflates time and behaviour into a single unit

of analysis, making it difficult to temporally link or disassociate the behavioural interpretations of surface artefacts from the temporal unit and scale they are associated with. The behavioural sequence observed in rock shelter deposits cannot be tested without an independent means of controlling time in open-air settings, and this level of control is impossible to attain without having a strong understanding of how the study area and its larger physical context has formed and changed through time. A formational approach can clarify both the kinds and scale of archaeological questions that can be asked of an open-air context, rather than repeatedly trying to repurpose those posed specifically for rock shelter deposits onto archaeology with a very different formation history. For example, Thompson et al. (2014) restricted sampling to cores that are technologically characteristic of the MSA in order to understand landscape provisioning in Malawi's Karonga district. However, they were clear in isolating out the limitations of this approach as it restricted the kind of behaviour (resource acquisition, provisioning strategies) considered observable over this larger timescale.

Since the surveys carried out by Sampson, there have been a number of research projects that have included or solely considered Late Pleistocene open-air archaeology. The notable few (e.g., Fisher et al. 2013, in Pondoland; Hallinan & Parkington 2017; Kandel & Conard 2012, west of the Cape Fold Belt; Mackay et al. 2014b; Shaw et al. 2019, in the interior of the Western Cape) demonstrate the value of landscape survey and the larger scale perspective gained beyond rock shelter sites.

However, while every archaeological context requires an approach that is catered to its unique condition, there are few projects in southern Africa that employ the necessary level of geoarchaeological detail that might allow regional scale inter-project comparison. By overlooking post-depositional processes as mechanistic factors in the formation of an assemblage, its spatial patterning is interpreted behaviourally and often couched within a narrative of long periods of behavioural stasis interspersed with abrupt pulses of change. Inadvertently removing the potential for landscape change during and after its history of use likely biases our understanding of how, when, and why early humans changed in their interaction with their environment.

Only a handful of projects carry-out dedicated investigations into the post-depositional alteration of buried and surface artefacts in order to better understand the relationship between the archaeology, its spatial organisation and its formation history (e.g., Geelbek Dunes - Conard et al. 1999; Dietl et al. 2005; Felix-Henningsen et al. 2003; Kandel & Conard 2012; Kandel et al. 2003; and in the southern Cape - Oestmo et al. 2014). The lack of such an approach can result in a reflexive treatment of assemblages as unaltered, primary examples of past behaviour as well as limiting behavioural interpretation to the broadest temporal and spatial scales—its surrounding landscape often held constant as a static backdrop to the socio-economic exploits of hunting, gathering and social interaction. Moreover, such studies tend to leap from the temporally large-scale units of the stone age system—ESA, MSA, and LSA—to the event scale of the activity zone (e.g., butchery sites, knapping floors), despite the recognition of time-averaging (Stern 1994).

2.6.2 Geoarchaeology in South Africa's open landscape

Since the 1990s, chronometric and geoarchaeological developments have introduced a suite of new tools for dating Late Pleistocene open-air contexts—methodologies that were put to good use nearly 20 years ago by the GAASP (Fuchs et al. 2008). Employing a host of geoarchaeological methods (i.e., luminescence

dating, geomorphological recording, sedimentary, taphonomic and artefact spatial analyses and movement experiments), the GAASP sought to contextualise and chronologically frame both buried and surface archaeology in relation to the formation of the surrounding dune fields of Langebaanweg. This project employed state-of-the-art equipment and software for surveying and recording the distribution of individual finds across an entire dune system. Their objective was to capture the spatial signatures of hominin behaviour at a larger scale than is possible in caves and rock shelters. The GAASP is a rare example of an open-air project in southern Africa implementing geoarchaeological and fabric analysis methods similar to and developed in East Africa in the 1980s (e.g., Schick 1986). Without the interdisciplinary and geoarchaeologically oriented methods employed by the GAASP, these developments would appear to have almost gone unnoticed in studies on southern Africa's Late Pleistocene surface archaeology until very recently.

Since the GAASP, implementation of a geoarchaeological approach has not been adequately replicated in other areas of southern Africa—one that is especially necessary for developing our understanding and interpretation of surface archaeology. Until we have a better understanding of the constraining factors involved in the depositional and formation histories of open-air surface archaeology, our knowledge of Late Pleistocene behavioural change at the landscape-scale will remain restricted to isolated points in geologically conducive parts of the southern African landscape. By investigating the composition of archaeological remnants from the Late Pleistocene across an environmentally and geologically variable landscape we can begin to test the more isolated, yet stratigraphically controlled, occurrences of behavioural change from proximately located rock shelters.

2.7 Conclusions

Southern African open-air archaeology lacks the necessary research investment required to become an integral component of the Late Pleistocene MSA and LSA narrative. Time and again the study of archaeology in open-air settings is renewed and subsequently over-shadowed by findings from rock shelters. In the quest for modern human origins, the need for broader insight into human adaptability and sociality at the landscape-scale is repeatedly trumped by datable deposits and an interest in rare objects considered indicative of cognitive complexity and/or symbolic expression. As a result, human origins research continues to be dominated by trait-specific discoveries, with open-air research repeatedly directed at large-scale surveys without the requisite investigation into the formation of both archaeology and sedimentary context.

An approach that considers behavioural and palaeoenvironmental evidence from a range of contexts is essential to achieve a landscape-scale perspective of human evolution during the Late Pleistocene, especially as this relates to the origin and development of cognitive complexity in response to both social and environmental stimuli. However, successfully aligning and supplementing archaeological inference across these different contexts requires developing our understanding of how these contexts and their wider landscape have, in themselves, evolved. While open-air surface studies are on the rise in southern African Late Pleistocene research, there is limited incorporation of geoarchaeological techniques into understanding the processes by which surface archaeology forms. Few examples exist in southern African Late Pleistocene research where the geochronology of surface archaeology has been investigated,

despite their global florescence since mid-last century. Understanding the factors that constrain the formation of open-air archaeology across different sedimentary systems is a necessary prerequisite to building a landscape-scale narrative of Late Pleistocene human behavioural evolution.

This thesis presents a geoarchaeological study of an open-air context, located at the fringe of the Cederberg mountains and the arid Karroo. The objective is to investigate how a geoarchaeological approach to open-air surface archaeology and the formation of its sedimentary context can help inform our current understanding of Late Pleistocene human behavioural change in southern Africa. Part of this investigation involves exploring how technocomplexes—based on regionally defined rock shelter sequences—relate to this formation and if a chronological sequence is discernible at this temporal scale for Late Pleistocene surface artefacts.

The study presented in the subsequent chapters is intended to be a pilot study for future geoarchaeological investigations of open-air Late Pleistocene surfaces in the Doring River catchment. By approaching open-air surface remains holistically, using geoarchaeological methods, this thesis aims to increase the efficacy of open-air sampling in southern Africa—adding to the few open-air projects that employ geoarchaeological methods—with the goal of developing our understanding of the post-depositional formation of surface artefacts in a semi-arid inland context in southern Africa. The core aim is to understand the dynamics and dominant constraining factors involved in preserving, exposing, and removing surface archaeology and controlling its temporal composition.

This work has local implications for our catchment-wide understanding of Doring River surface archaeology relative to rock shelter and buried remains. It increases the archaeological sample size in a context and locality that is underrepresented, despite its importance to our understanding of Late Pleistocene human history. It also contributes to ongoing regional and global developments of geoarchaeological methods to investigate surface archaeology in Late Pleistocene research.

CHAPTER 3.
STUDY AREA: PHYSICAL SETTING

3.1 Introduction

The Doring River valley is the study area of this thesis. This chapter presents the physical, climatic, and environmental setting for the valley system at the scales of catchment, region, and subcontinent. The objective is to introduce the study area as it exists today, followed by a review of the Holocene and Late Pleistocene conditions that influenced short- and long-term changes in the formation of the landscape and the archaeology it preserves.

3.1.1 Defining the limits of the study area

The Doring River valley lies east of the Cederberg Mountains (hereafter simply 'Cederberg') and forms part of a larger, environmentally diverse Olifants-Doring[1] Basin. The Olifants-Doring Basin branches out across both the Western and Northern Cape of South Africa, encompassing the northern limb of the Cape Fold Belt and the western fringe of the Karoo. While the 'Doring River valley' is the catchall term used for the study area throughout this thesis, its location and extent refers to a specific portion the Doring River and its network of tributaries. This portion is nested within a multitiered system of catchments termed primary, secondary, tertiary, and quaternary by the Department of Water, Agriculture and Forestry (Conrad et al. 2012, p.3, map 1; Maherry et al. 2013). The primary catchment refers to the Olifants-Doring Basin (Figures 3.1 and 3.2).

For clarity and to maintain some comparability across disciplines, the 'Doring River catchment' is the title used herein to refer to the secondary level catchment that combines Water Management Areas E2 and E4 within a single watershed (see Figure 3.1). The 'study area' refers to a section of the Doring River valley located within the Quaternary catchment E24J (Figure 3.1). 'Places of interest' or POI refer to the open-air archaeological exposures identified within the study area which will be introduced in Chapter 4. One of these POI has been selected for detailed investigation as a localised case study in this thesis (Figure 3.1). The Doring River Archaeology Project (DRAP) study area encompasses the central, northern section of the Doring River (Figure 3.1). Its south-eastern boundary is slightly upriver from the Biedouw-Doring confluence and extends north-west for ~40 km, ending where the Brak tributary meets the Doring (Figure 3.1). Beyond the valley, the quaternary catchment E24J spans ~53 km from north-east to south-west to include the Bos, Biedouw, and Putslaagte tributaries in their entirety (Figure 3.1).

[1] The 'Doring' is also referred to as 'Doorn' which is the Afrikaans equivalent and still in use today.

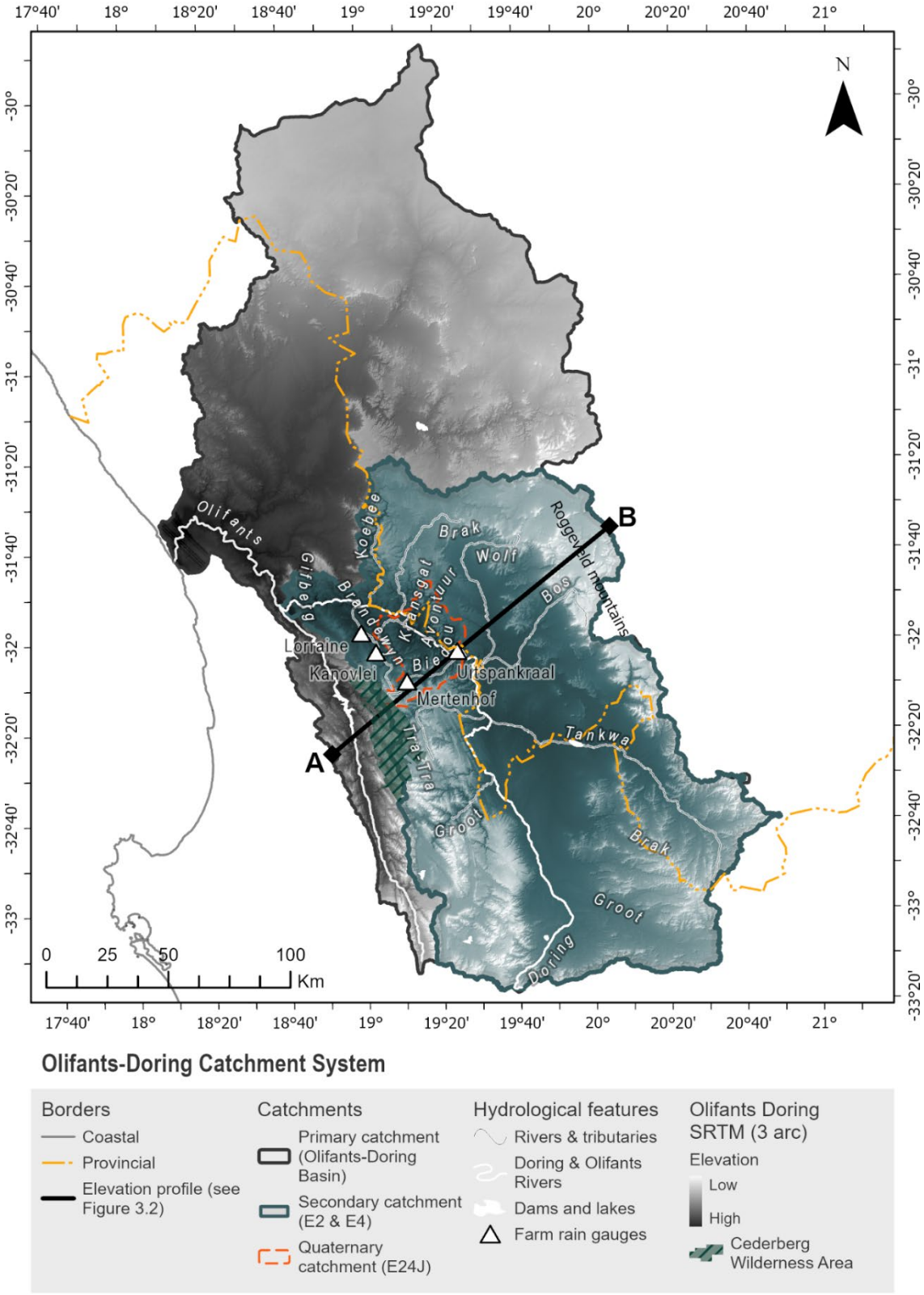

Figure 3.1. Map of the Olifants-Doring Catchment system, showing the main hydrological features (in white), farm rainfall gauges (see below for details), and the primary (black outline), secondary (dark green outline & area) and quaternary (orange dash line) catchments of the study area (Uitspankraal). See Figure 3.2 for related A-B elevation profile. Western-Northern cape boundary is shown crossing the length of all three catchments (yellow dash-dot line). The hillshade derives from a hole-filled 90 m SRTM DEM originally processed by Jarvis et al. (2008).

3.2 Topography and Hydrogeology

3.2.1 Topography

Southern Africa encompasses the countries of South Africa, Lesotho, and Swaziland. Together they form a topographically complex subcontinent most notable for its band of coastal lowlands that form a narrow perimeter around a horse-shoe shaped belt of tectonically formed marginal escarpment (>1000 m asl; (Moore et al. 2009). The Cape Fold Belt makes up its western and southern limits, while south of the Zambezi River the high elevation Drakensburg-Maluti Mountain Group contributes to southern Africa's eastern margin and interior (Moore et al. 2009). Situated within South Africa's Western Cape, the western highlands of the Doring River catchment form part of the northern arm of the Cape Fold Belt. Its tributaries range between 1500 m to 1000 m above mean sea level (amsl) cutting wide, linear valleys across the rugged terrain of the Cederberg Figures 3.2 and 3.3 Quick & Eckardt (2015). From here they travel down more than 1300 m of the Cape Supergroup's hard quartzitic sandstone to meet the Doring River channel below (Figure 3.3). The catchment's north-eastern extent also starts high above present-day sea level (~1200 m amsl), beyond the Roggeveld and Hantam Mountains (Figure 3.3). Eastern tributaries traverse the Karoo's dry terrain, winding their way across and down the broad benches of the Karoo's mesas (Figure 3.2). The catchment is one of the main contributors to the Olifants River and a dominant watershed in the Cederberg region. Together, the two rivers and their respective (secondary) catchments form the Olifants-Doring Basin, draining a total area of 48,891 km^2 (Figure 3.1; Maherry et al. (2013)). Farther west lies the coastal plains of the Sandveld, a sandy belt of lowland plains, meandering streams, springs, and marine and estuarine ecosystems.

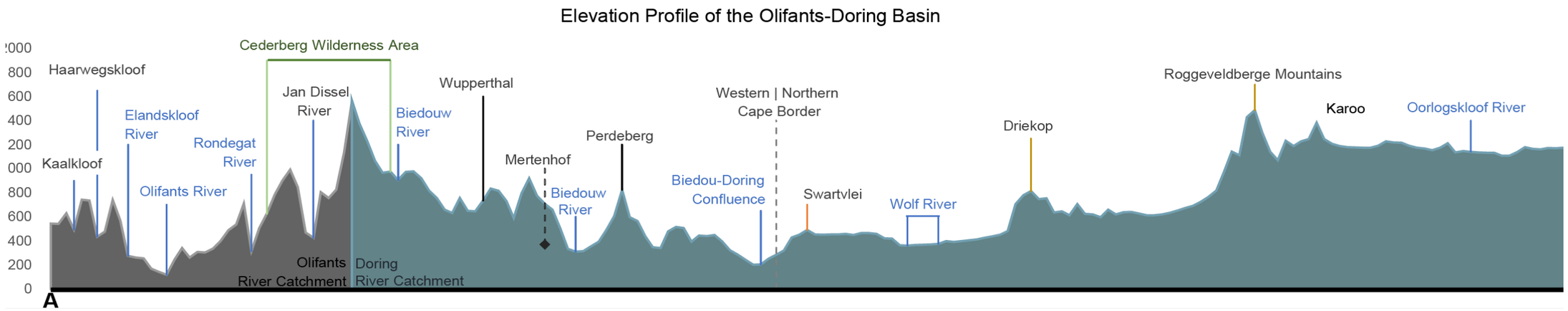

Figure 3.2. Elevation profile of the Olifants-Doring Basin from its south-western to north-east extent, as depicted in Figure 3.1. The Biedouw-Doring confluence represents the northernmost boundary of the thesis study area and is highlighted in blue. Terrain elevations derive from a 24 m resolution DEM. Elevations were exported from CapeFarmMapper 2018) using the ESRI Profile Service.

3.2.2 The Doring River system

The Doring River is an important water source to a drought-prone environment. From its origin in the Ceres-Karoo, to its confluence with the Olifants River, the Doring River cuts a 300 km north-west course, separating the arid mesa-butte terrain of the Karoo in the east from the better watered peaks and broad-linear valleys of the Cederberg in the west. Its vast and complex network of non-perennial and seasonal tributaries branch out over the north-eastern, leeward side of the Cederberg, and the westernmost extent of the Karoo's arid interior (Figure 3.1). Within its first 150 km, the main channel receives over half of its runoff from its confluence with the perennial Groot River, before connecting with the Tankwa and Tra-Tra Rivers (Figure 3.1; Paxton & King 2009). The geology along this first stretch is complex. From south-east to north-west, it is composed of the mudstones, siltstones, and sandstones of the Beaufort Group, followed by the alternating shales and siltstones of the Ecca Group, which dominate the Karoo. Where the Tankwa, Tra-tra and Doring Rivers meet, they cut through the converging tillites and diamictites of the Dwyka Group, the quartzitic sandstones of the Witteberg Group, and the shales and sandstones of the Bokkeveld Group (Conrad et al. 2012). The Ecca geology of the eastern extent of the catchment and the Roggeveld-Hantam Mountains, is riddled with igneous intrusions of Karoo Dolerite (Figure 3.3). These form sills and dykes throughout the Karoo, providing valuable aquifers in an environment where evapotranspiration outstrips precipitation (Fortuin & Woodford 2006:11; Grab 2015, p.6; Grab & Knight 2015).

As the Doring River arcs north-west and into the study area, it receives more water from the Bos and Biedouw Rivers (Figure 3.1). Carving through the sedimentary rocks of the Bokkeveld Group, its course exposes the Ceres and Biedouw Formations, sculpting steep cliffs of alternating shale and sandstone (Figure 3.3). The softer shales of the Bokkeveld Group dominate and widen the valley as the Doring River passes Lange Kaal, through the DoringBos, towards its confluence with the Putslaagte River (Figure 3.3). Once the Doring River passes Putslaagte and beyond the bounds of the study area, it arcs west towards its outlet in the Olifants River. Along this stretch, the geology shifts again to the quartzitic sandstone, shale and tillite geology of the Table Mountain Group. The channel bed of the Doring River is composed of quaternary sands and riffles of water-worn boulders. They alternate depending on the morphology of the river and the velocity of channelled water when the river is in flood. Water holes are often located immediately downstream of the riffles where the speed of flowing water cuts a deeper zone in the channel bed. The long stretches of alluvium are exposed, dried, and deflated seasonally as the Doring River ceases to flow during the summer months.

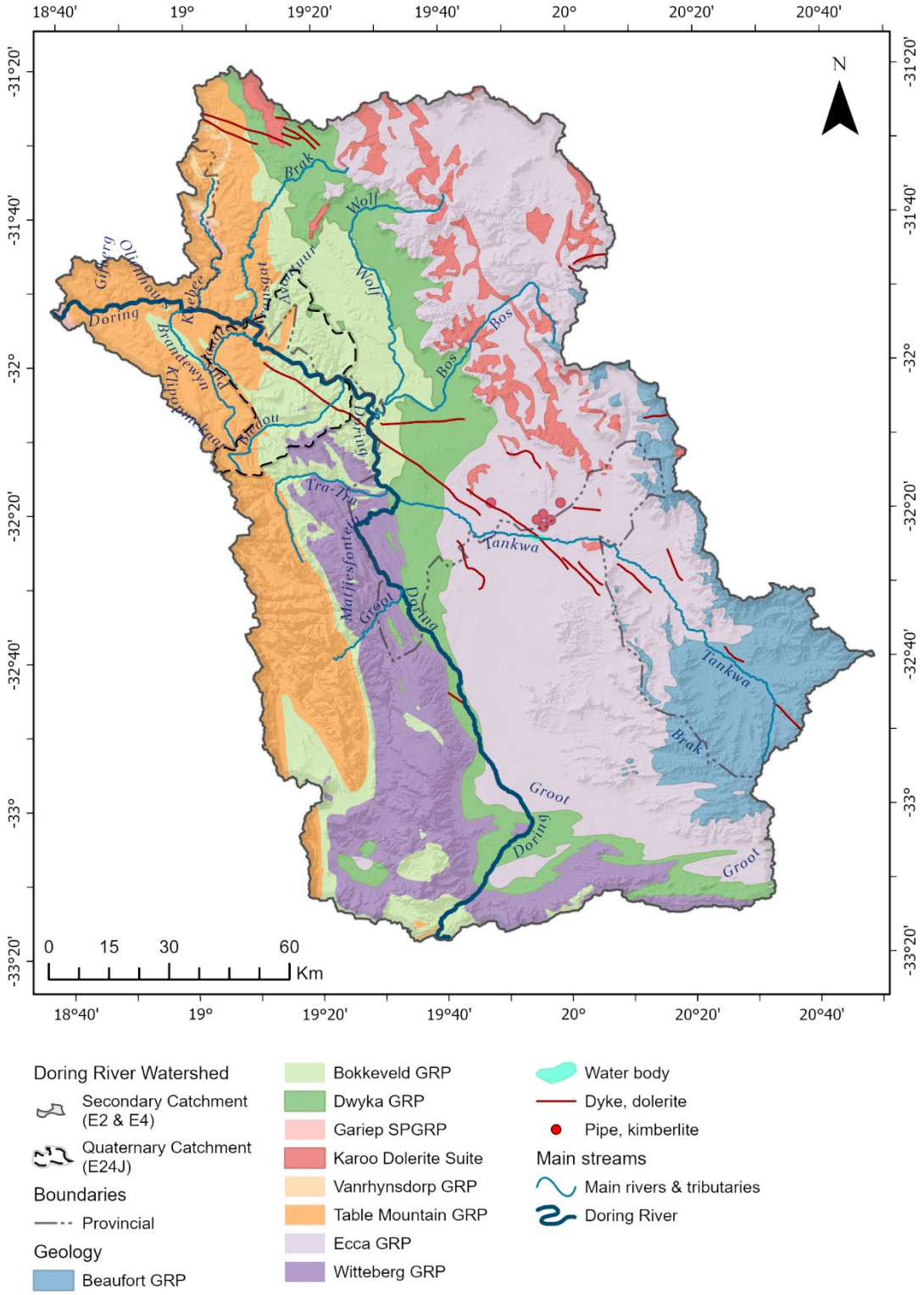

Figure 3.3. Geological map of the Doring River (secondary) catchment, showing the main lithological groups, catchments, and rivers mentioned in text. The hillshade derives from a hole-filled 90 m SRTM DEM originally processed by Jarvis et al. (2008). The geological base layers were modified from the 'RSA 1 Million Geological map' digital dataset, which is the intellectual property of the Council for Geoscience and is used herein by permission (https://geoscience.org.za/cgs/).

Together the south-western and north-eastern tributaries feed a diverse range of workable raw materials into the Doring River valley, making this landscape a rich resource of lithic materials for the procurement and manufacture of stone tools, evident from the abundant scatters of stone artefacts exposed

throughout the valley and its tributaries (e.g., Hallinan & Shaw 2015; Mackay et al. 2014; Shaw 2017). Quartzite and fine-grained sandstone are the dominant outcrop geology in the catchment and also occur as cobbles in the tributaries and main river channel. Quartz pebbles can be found eroding out of Table Mountain Group sandstone in the western catchment. The Doring River supplies hornfels cobbles to the valley as it cuts through dykes of Karoo Dolerite and associated baked Beaufort Group mudstone in the south. The only currently known primary silcrete sources are Agtesfontein and Swartvlei, which occur as geological accretions on plateaus overlooking the Biedouw and Doring River valleys. There is no local outcropping source for chert, although it is present in the archaeological record. At a minimum, chert occurs as river pebbles along the Doring River channel that may have been derived from the Dwyka tillite. However, its occurrence is unpredictable and usually in small quantities.

The Doring River Valley—from the Bos River to the Doring Bos—is dominated by leptosols, while the plateau to its north and west are mostly cambisols, which also form the dominant soils of the Doring Bos and its immediate tributaries (Figure 3.4). The calcaric cambisols or calcisols to the north-east of the Bos River will supply the Doring River channel with carbonates. Upriver of the Bos-Doring confluence the valley's landscape is comprised of Solonchaks soils. Dotted throughout the region are indurated circular features typically ~20 m in diameter most likely to reflect ancient termitaria produced by southern harvester termites (*Microhodoteres viator*, McAuliffe et al. 2019). The oldest of these formations antedate 20,000 years.

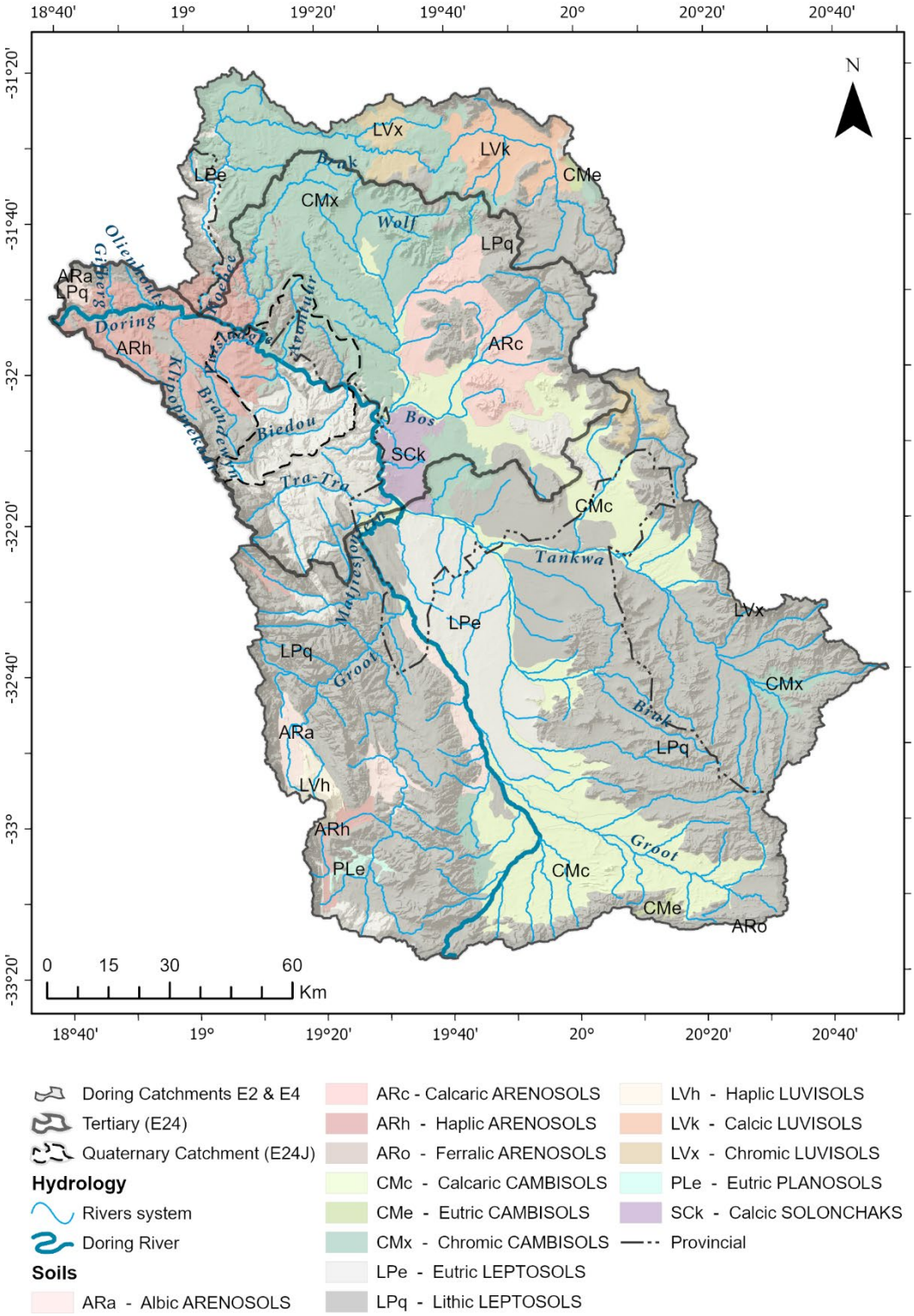

Figure 3.4. Soil map of the Doring River catchments E2-E4 (secondary) and the boundaries of the Tertiary (E24) and Quaternary catchments (E24J). The hillshade derives from a hole-filled 90 m SRTM DEM originally processed by Jarvis et al. (2008). Soil data from 1:1M SOTER for the GLADA partner countries Argentina, China, Cuba, South Africa, Senegal and The Gambia, and Tunisia 2008); Dijkshoorn et al. (2008).

3.3 Present Climate and Environment

3.3.1 Southern Africa

The Doring River catchment is subject to southern Africa's complex, highly seasonal climatic system. Terrestrial and oceanic temperature and moisture loads interact to produce strong convection cells across the subcontinent (Chase & Meadows 2007). The main terrestrial circulation systems are the tropical and subtropical high-pressure cells of the Inter Tropical Convergent Zone (ITCZ), and the low-pressure temperate westerlies that circulate south of the continent. These interact with the warm Agulhas southward currents of the Indian Ocean and the cold northward Benguela current in the south Atlantic Ocean, introducing ocean nutrients to the south and west coast, and significant moisture loads carried inland from the east (Cohen et al. 2017; Deacon & Lancaster 1988, p.13; Marean 2010; Parkington 2010). Interplay between this climatic system and South Africa's tectonically altered landmass result in subcontinent level and regionally variable environmental conditions, producing strong east to west, and coast to interior gradients in moisture, where humidity drops and evaporation generally increases westward and inland (Deacon & Lancaster 1988). As a result, three seasonally and geographically distinct precipitation zones can be differentiated across the subcontinent Chase & Meadows (2007): the Winter Rainfall Zone (WRZ; Figure 3.5), Summer Rainfall Zone (SRZ), and Year-round Rainfall Zone (YRZ).

3.3.1.1 Rainfall zones

As the ITCZ shifts south during the summer months of October-March, an influx of subtropical easterlies carries summer rainfall into the northern and eastern parts of the subcontinent. However, in the south, circumpolar westerlies introduce temperate low-pressure disturbances during the winter, providing year-round precipitation (Figure 3.5 and 2.4). The Doring River's winter flow from the Cederberg largely derives from the equatorward shift in the westerly's temperate frontals. This forms the WRZ, delivering winter rainfall to the southern and western margins of the subcontinent, where > 66% precipitation occurs between the months of April to September (Figure 3.5 & 2.4, Chase & Meadows 2007). Summer rainfall occurs over most of the northern and eastern regions of southern Africa (Figure 2.4), delivering rain to the Karoo and Kalahari as well as the eastern coastal margins between the months of October and March. A narrow band of overlap in winter and summer rainfall also exists, marking the modern extent of the YRZ. This extends along the Southern Cape coast and inland, into the adjacent Cape Fold mountains (Figure 3.5 & 2.4, Chase & Meadows 2007; Deacon & Lancaster 1988, p.13).

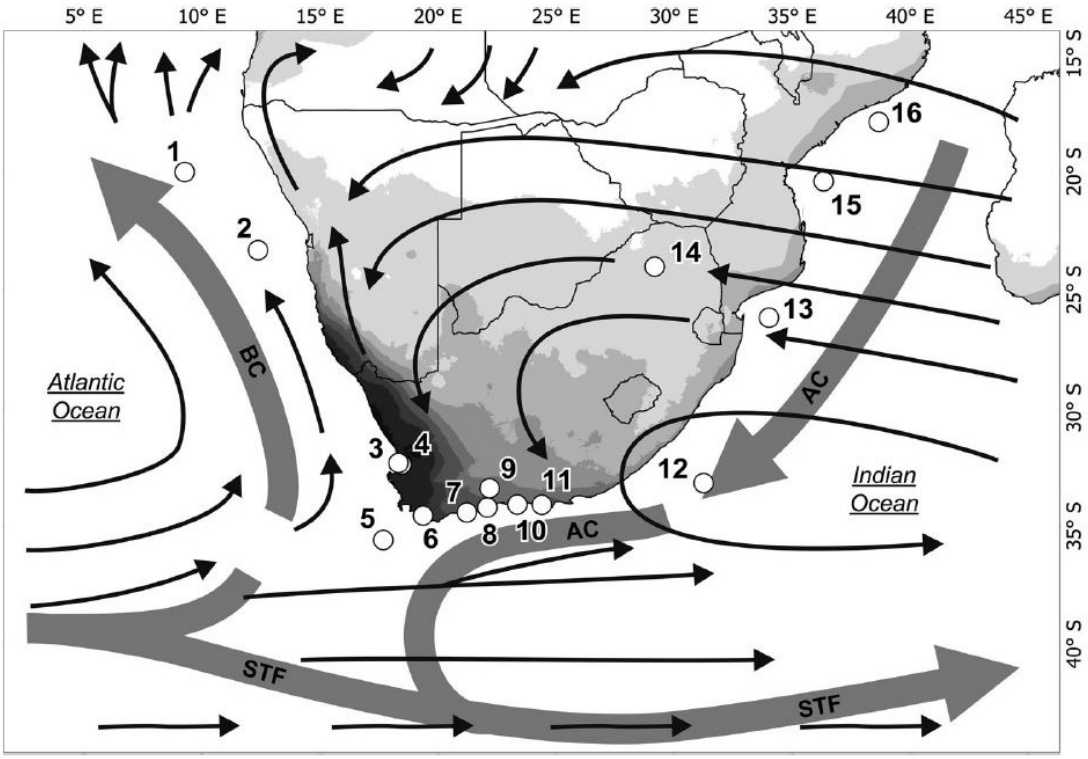

Figure 3.5. Map from Carr et al. (2015, p.28, figure 2.3) of dominant oceanic (thick arrows) and atmospheric (thin arrows) circulation patterns, with the major oceanic currents (the Benguela Current [BC] and Agulhas Current [AC]), including the subtropical front (STF) labelled. Winter precipitation frequencies are indicated as graduated shading: from 0 to 80% rainfall represented as light to dark shading, respectively. Palaeoenvironmental sites that yield marine and terrestrial evidence are indicated by white circles. Sites numbers: (1) MD962094, (2) GeoB 1711-4, (3) Elands Bay Cave, (4) Diepkloof, (5) MD962081, (6) Die Kelders, (7) Blombos Cave, (8) Pinnacle Point-Crevice Cave, (9) Boomplaas Cave, (10) Nelson Bay Cave, (11) Klasies River, (12) MD962007, (13) MD962048, (14) Cold Air Cave, (15) MD79257, (16) MD79254.

The sizes and positions of all three zones have shifted, expanded, and contracted throughout the Late Pleistocene and Holocene. While the modern extent of the WRZ encompasses the southern coast and Western Cape, it was significantly larger during the last glacial period, between ~32-17 ka (see also Chase & Meadows 2007; Schuller et al. 2018). Currently, summer rainfall in the study area only occurs in the form of occasional thunderstorms, not enough to shift seasonality or reduce aridity.

3.3.2 Doring River catchment

3.3.2.1 Local modern rainfall

Localised climate variability over shorter distances within the Doring River catchment is also apparent in modern rainfall records logged at farms close to or within the study area. Thirty-year monthly rainfall records from four local farms at Uitspankraal, Mertenhof, Kanovlei and Lorraine present localised, decadal trends in rainfall, from east to west, across the catchment that imply a highly variable climate (Figure 3.6). These records derive from daily rain gauge readings, collected at each farm by the Hough, Lubbe, Kanovlei and Lorraine families.

The rain gauge at Uitspankraal farm is located <1 km from the Doring-Biedouw confluence. Its precipitation readings reflect the region's strong seasonally driven trend in winter rainfall, with a recorded

maximum winter precipitation average of 35 ± 10 mm in June and a drop to below 10 mm between the summer months of October and March. However, the study area's location on the western fringe of the Karoo is also indicated by the slight rise in precipitation between October and January, before dropping again in the later part of summer (Figure 3.6). This is due to early summer thunderstorms that bring flash flooding to the area from the north-east.

Mertenhof farm (342 m asl) is located at the head of the Biedouw River, ~25 km south-west of the Biedouw-Doring confluence. Although it is the most proximate data source to Uitspankraal farm, compared to Kanovlei and Lorraine, Mertenhof's yearly rainfall average (256 mm/yr) differs the most from the annual precipitation mean (190 mm/yr) recorded near the Biedouw-Doring confluence. Kanovlei, on the other hand, is higher in elevation than Uitspankraal, farther west than Mertenhof and yet it has experienced similar precipitation totals to Uitspankraal, and markedly lower amounts compared to Mertenhof (Table 3.1).

Table 3.1. Farm rainfall gauge records tabulated relative to the Uitspankraal farm (Doring-Biedouw confluence). Highlighted station relates to the closest farm to the case study (see Figure 3.2 for locations). Mertenhof, Kanovlei, and Lorraine rainfall data source: Mariette and Barry Lubbe. Uitspankraal farm data source: Manus and Lily Hough.

Station	Station ID	Coordinates (dd)	Type	Distance (km)*	Altitude (m asl)	Annual mean (mm/yr[1])	SD (±)
Lorraine	local farm	18.99E, 31.98S,	rain gauges	40	184	249	25
Uitspankraal	local farm	19.41E, -32.05S	rain gauges	0	200	190	26
Kanovlei	local farm	19.05E, -32.05S	rain gauges	34	324	194	17
Mertenhof	local farm	19.19E, 32.16S	rain gauges	24	342	256	16

*The Doring-Biedouw confluence – the most proximate locality to thesis Case Study UPK7; ^Approximate Euclidean distance from Uitspankraal farm

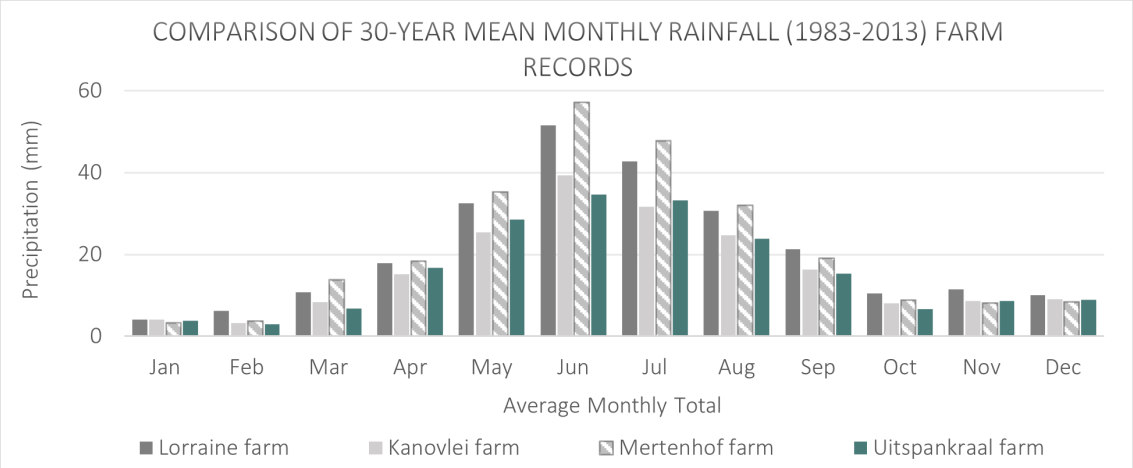

Figure 3.6. Comparison of thirty-year mean monthly precipitation (1983-2013) between four farms within the Doring River catchment: Mertenhof, Kanovlei, Lorraine, and Uitspankraal. Mertenhof farm's rainfall gauge is a direct ~24 km south-west from Uitspankraal Farm (Biedouw-Doring River confluence), at the head of the Biedouw River valley. Kanovlei and Lorraine farms are located ~34 and ~40 km from Uitspankraal farm, respectively (see Figure 3.2 for locations). Mertenhof, Kanovlei, and Lorraine rainfall data source: Mariette and Barry Lubbe. Uitspankraal farm data source: Manus and Lily Hough.

Both Lorraine and Kanovlei farms are located within the same parent farm, Elizabethfontein. However, Lorraine farm is located farthest west from the Uitspankraal rain gauge and is situated at the lowest altitude out of all four rain gauge localities (184 m asl, Table 3.1). Despite this relatively low elevation, it yields the second highest annual rainfall mean (249 mm/yr), after Mertenhof (256 mm/yr). Such localised variance between altitude and precipitation trends over short distances demonstrates the degree of topographically dependant microclimatic diversity across the Doring River catchment. This makes it difficult to compare the amplitude of short-term catchment-wide patterns in climate change. However, comparison of each farm's 30-year record of annual rainfall totals, from 1983-2013, indicates a similar pattern in the rise and fall of moisture levels at each locality (Figure 3.7). This demonstrates that the relative amplitude of precipitation between these localities are well maintained from year to year.

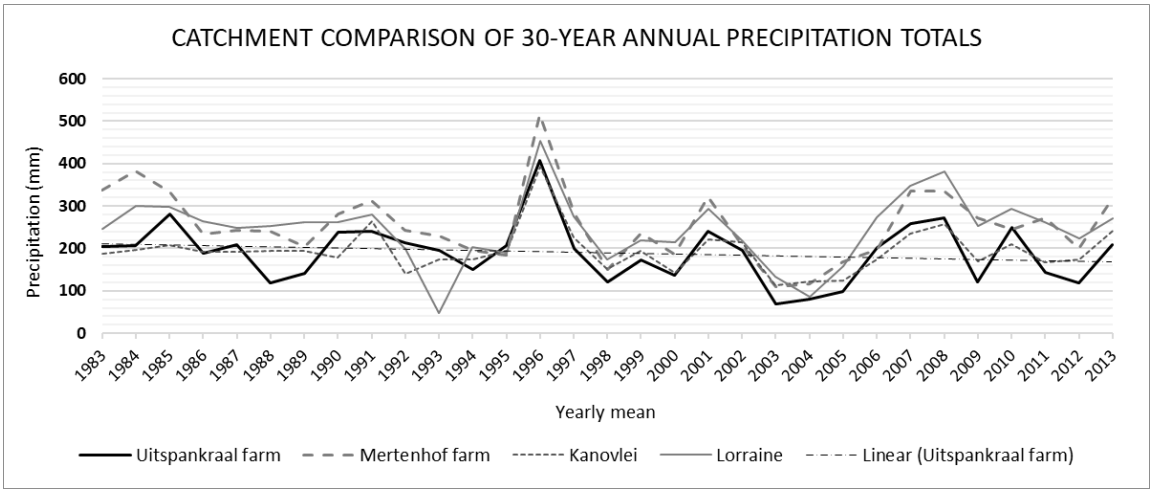

Figure 3.7. Thirty-year record (1983-2013) of mean annual precipitation at the head of the Biedouw River valley at Mertenhof (~24 km south-west of Uitspankraal Farm and the Biedouw-Doring confluence). The linear trend for Uitspankraal farm shows a ~50 mm fall in the precipitation average over the last thirty years Mertenhof, Kanovlei, and Lorraine rainfall data source: Mariette and Barry Lubbe. Uitspankraal farm data source: Manus and Lily Hough.

3.3.2.2 Temperature and evaporation

Overall temperatures for the Olifants-Doring Basin fluctuate in their extremes, between a mean low of -3 to 3°C in July, during the wet winter, and a mean high of 39 to 40°C in January, during the dry summer (Fortuin & Woodford 2006). The potential evaporation average per annum is roughly 10 times higher than precipitation across the study area, varying between ~1600-2700 mm/yr from south to north and west to east (Fortuin & Woodford 2006:11, Figure 5).

3.3.2.3 Wind

Surface winds in southern Africa are tied strongly to anticyclonic circulation. Coastal winds as a general rule, are stronger than in the interior, and are particularly pronounced in the Southern and Western Cape (Deacon & Lancaster 1988, p.16). The dominant wind direction in the western interior follows a seasonal pattern, whereby winter months are dominated by north-north-easterlies and summer months experience south-south-westerlies. Farther into the interior, northerlies and north-westerly wind patterns prevail throughout the year (Deacon & Lancaster 1988, p.16).

According to Meteoblue wind simulations of the study area (within a 30 km radius of 32.03°S 19.4°E), the dominant annual wind direction is a westerly (Figure 3.8; Meteoblue 2017b, c). The next most frequent wind direction is an east-north-easterly. The westerlies attain speeds of >28 km/h annually, compared to east-north-easterlies, which attain a max of >12 km/hr. When the latter occasionally shifts to a more easterly direction, windspeeds increase to >19 km/hr (Figure 3.8). Wind and precipitation levels are negatively correlated (Meteoblue 2017a), and the east-west polarity in dominant wind directions and speeds are tied directly to seasonality. Westerly winds occur during the drier months of summer (November/December to March). East-north-easterlies dominate the wet winter season (March to October).

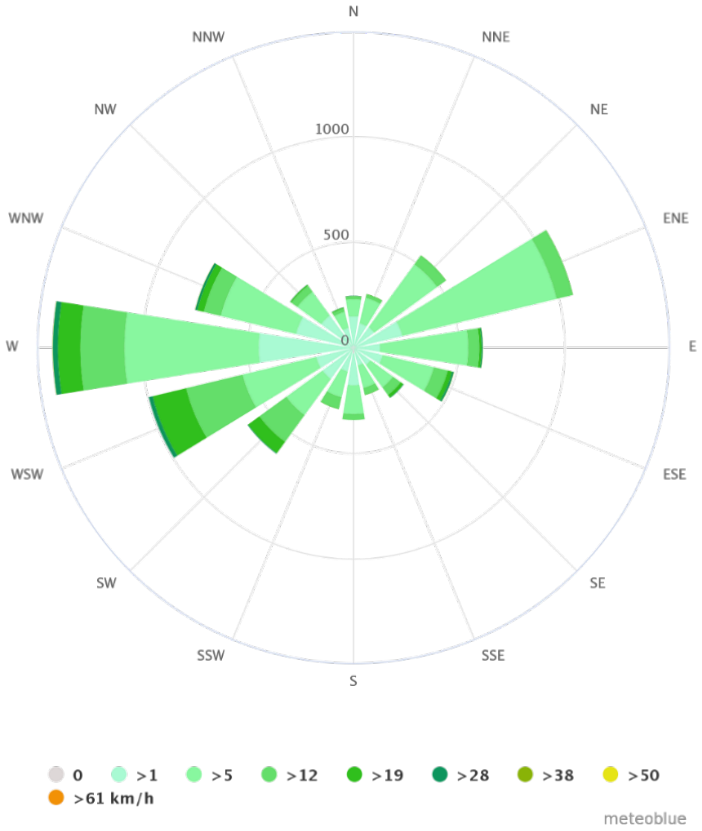

Figure 3.8. Windrose diagram for location 32.03°S 19.4°E showing annual hourly counts for wind direction and speed. Source: Meteoblue (2017b).

The mobilisation of finer sandy deposits and dunes are likely most active during the latter part of the dry season (January to March/April). The highest potential for erosion from rainfall possibly occurs at the start of the winter wet season in response to the occasional summer thunderstorms in January. Spring (July through to August/September) is the most stabilising and conducive period for soil formation. With the highest levels of humidity and low to no stock activity, factors encouraging stabilisation, such as vegetation growth, will directly affect the consolidation of sandy deposits prior to the advent of westerly wind increase and decreased precipitation levels in the months following.

3.3.2.4 Fauna and flora

The Doring River valley and most lowland areas of its catchment are set in lowland Succulent Karoo (Figure 3.9). Mountain Fynbos covers the southern and northernmost extents of the Doring River's main channel,

and borders the easternmost escarpment of the catchment system (Quick & Eckardt 2015). The Doring River valley is composed of riparian flora juxtaposed against the low-lying bush of succulent Karoo vegetation that favours rocky and sandy conditions with low pedogenic potential.

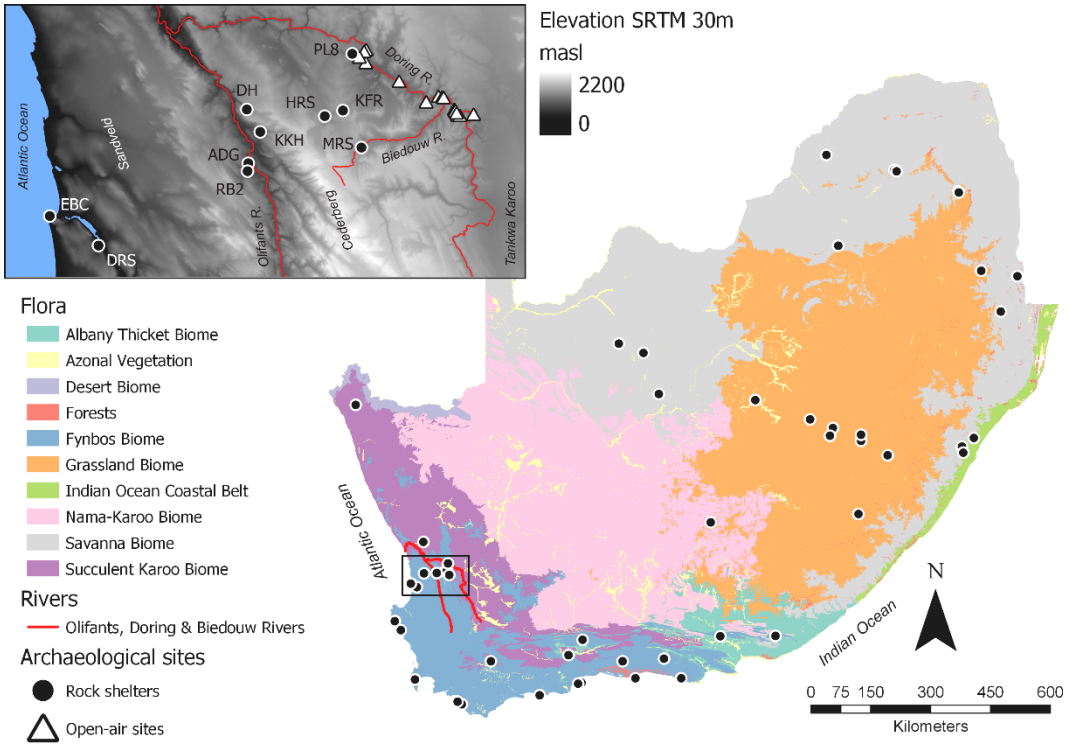

Figure 3.9. Biomes in South Africa showing location of Olifants and Doring Rivers, and all late Pleistocene archaeological sites for which co-ordinate data could be found. Note the absence of sites from the Nama-Karoo and Succulent Karoo biomes of the western interior. Inset box shows locations of open sites in the Doring River valley (triangles) and rock shelters mentioned in-text (circular markers) in the study area set against the SRTM 90 m DEM processed by Jarvis et al. (2008). Site abbreviations: HRS=Hollow Rock Shelter, KFR=Klipfonteinrand (both 1 & 2), KKH=Klein Kliphuis, MRS=Mertenhof, PL8=Putslaagte 8, ADG = Andriesgrond, RB2 = Renbaan 2, DH = De Hagen Cave, EBC = Elands Bay Cave, DRS = Diepkloof Rock Shelter.

During the dry summer months, the Doring River slows, and gradually increases in salinity (Hendriks & Rossouw 2009). At its driest (i.e., between the months of November and March), the Doring River ceases to flow. During the early part of the dry season, waterholes form in channel depressions, trapping fish and providing a temporary source of water for wildlife (e.g., baboons, ostriches, and hyrax). These waterholes gradually increase in mineral content, salinity and refuse, decreasing in quality and making them unsustainable for drinking and irrigation (Paxton 2008; Paxton & King 2009). While the seasonal flow of the Doring River is almost always guaranteed, water availability in the wider landscape is less predictable, particularly as one moves farther into the interior, away from the Cederberg. The timing and duration of river discharge also changes from year to year as it is mostly dependent on rain and snowfall entering tributaries connected with Ceres and the Cederberg. While the river provides a vital source of fresh water in a currently semi-arid landscape, it also inhibits direct movement from one side of the catchment to the other for most of the wet season. Only in the drier spring and autumn months, and throughout the summer, is the river easily passable, within the quaternary catchment bounds of E24J. However, during the summer, the river has slowed, ceased flowing altogether, or is reduced to increasingly stagnant pools of water.

3.4 Palaeoclimate and Environment

The resolution and availability of palaeoclimatic and environmental archives become coarser and more disparate the farther back you go, with older, locally derived records often producing contradictory results. To compensate, multiple sources of information are presented here to cover a range of possible palaeoenvironmental and climatic scenarios relevant to the study area. The following section highlights moisture and temperature trends detected globally, across the WRZ, and within the catchment, including large scale shifts in climate that are detectable at the austral continent and regional levels. These inferences derive from archives stored in deep-sea and ice-sheet cores, providing global scale knowledge on changes in sea level, glacial cycling, and terrestrial dust loads.

Local terrestrial archives provide high resolution, albeit discontinuous records. Intraregional trends in changing temperature and moisture levels are often detected in southern Africa from the analysis of local archives (e.g., stable isotope, pollen, and phytolith data, and records of dune formation). Local archives are often highly susceptible to environmental changes in their immediate setting (e.g., highland versus coastal or inland archives), with the differences in the timing of faunal and floral responses to changes in local rainfall, groundwater and soil nutrient levels more often influencing results on changing moisture levels. Drawing from these various archives, the following section provides a review of Holocene and later Pleistocene climate and environmental records (glacial cycles, and changes in sea level, moisture, temperature, and vegetation) for the study area and its wider catchment.

3.4.1 Global-scale forcing

At the global scale, southern hemisphere models of palaeoenvironmental change are often based on correlated oxygen isotope archives from deep-sea and Antarctic ice-sheet cores. These archives track global temperature fluctuations associated with the growth and retreat of terrestrial ice-sheets (Deacon & Lancaster 1988; Imbrie et al. 1984; Waelbroeck et al. 2002). Oscillations in ice volume correlate with cyclical shifts in the Earth's orbit (i.e., eccentricity: ~100 ka cycle), axial tilt (i.e., obliquity: 41 ka cycle), and wobble (i.e., precession: 26 ka cycle). This supports the astronomical theory of orbital forcing, which suggests that changes in Earth's insolation are the main triggers of worldwide shifts between glacial and interglacial phases (Hays et al. 1976; Imbrie 1980; Imbrie & Palmer 1986). Based on this correlation, cycles are divided into Marine Isotope Stages (MIS; Railsback et al. 2015). Even-numbered stages represent glacial (colder) phases, while odd-number stages represent interglacial or warmer phases.

Figure 3.10 shows the various MIS for the Late Pleistocene and Holocene epochs, their duration in relation to oscillations from warm to cold climatic conditions, and the timing and duration of associated African Stone Age divisions (after Stewart & Jones 2016). All three nomenclatures are used interchangeably throughout this text. The Late Pleistocene (~128 – 11.7 ka years) is associated with MIS 6 to 2, while MIS 1 represents the current Holocene interglacial (11.7 – 0 ka years). During MIS 5 (130–71 ka) southern Africa experienced a relatively warm interglacial that stands in sharp contrast to the glacial climates of the preceding MIS 6 (191–130 ka) and subsequent MIS 4 (71–57 ka; Stewart & Jones 2016). MIS 3 (57–29 ka), while warmer than MIS 4 and 2 (30–11.7 ka), is characterised by an amplified frequency of high and low temperatures. A severe drop in temperatures occurred during MIS 2, which is known as the Last Glacial Maximum (LGM, ~30-21 ka). The start of the current interglacial, MIS 1 (from ~11.7 ka),

tracks the main phase of deglaciation (~16.5-8.2 ka) that involved rapid warming and significant rise in seas level (by ~120 m). This current interglacial is also known as the Holocene epoch and is characterised by frequent, extreme shifts in climate and increasingly more arid conditions in the WRZ (Chase et al. 2019; Chase & Quick 2018).

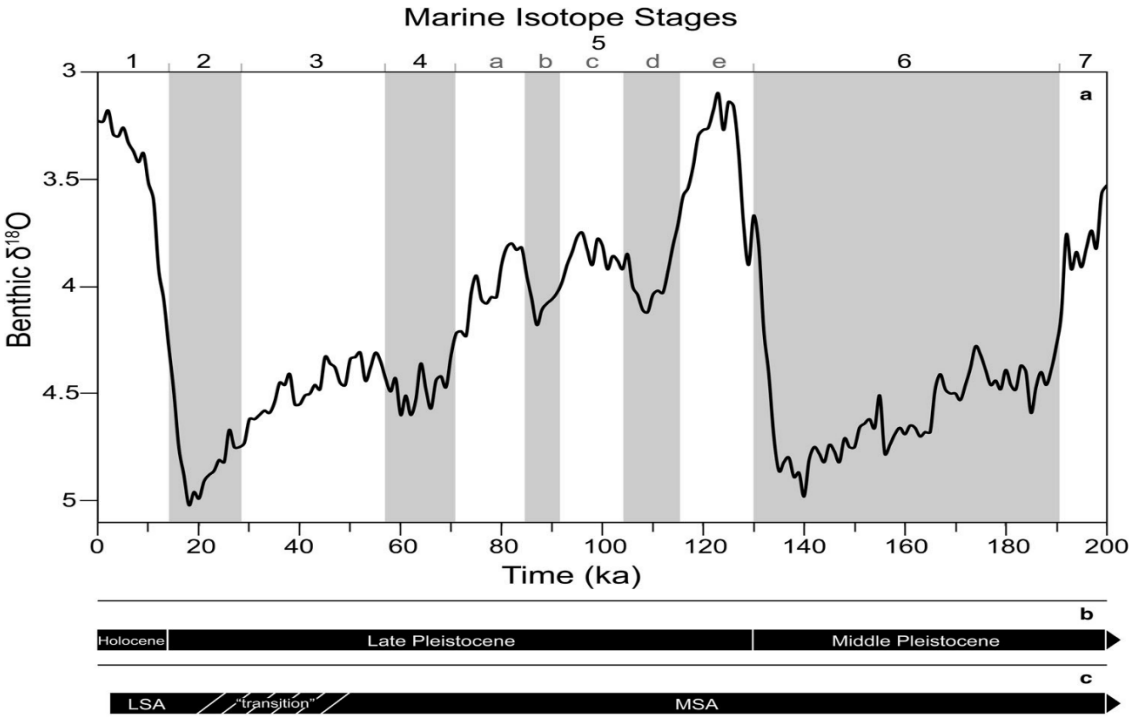

Figure 3.10. The three chronological systems used in this thesis pertain to Marine Isotope Stages 6-1, the geological epochs of the Pleistocene and Holocene and the archaeologically defined Stone Age System covering the southern African Earlier, Middle and Later Stone Ages (ESA, MSA, and LSA). MIS time ranges are based on global ice volume and deep ocean temperatures determined from average global benthic isotope 18O frequencies: MIS 6 from 191-130 ka, MIS 5 from 130-71 ka, MIS 4 from 71-57 ka, MIS 3 from 57-29 ka, MIS 2 from 29-11.7 ka, and MIS 1 from ~11.7 ka. Source: from Stewart & Jones (2016, Figure 1.1) based on results from the LR04 stack analysis presented in Lisiecki & Raymo (2005) and the revised age for the Pleistocene-Holocene transition in Walker et al. (2009).

Fluctuations in sea ice volume had long-term effects on southern Africa's surrounding oceanic and terrestrial temperatures, moisture availability and sea level. Each glacial period is marked by lower sea levels than the preceding interglacial (Figure 3.10) and is characterised by a rapid increase in ice volume. Secondary fluctuations in sea level characterize the Holocene records, which show that sea levels oscillated frequently from high to low, decreasing in amplitude over time (Compton 2011; Jerardino 1995; Meadows & Baxter 1999).

Hemispheric differences also exist during deglaciation due to differences in Earth and ocean deformation during the rapid unloading of ice. As a result, local sea-levels can vary significantly from the global average (Lambeck et al. 2014). Fluctuations in ice volume and its effect on locations in the southern hemisphere, far from the former ice margins (i.e., the southeast coast of southern Africa), provide Late Pleistocene sea level readings, during MIS3, from ~ 35 ka (Figure 3.11; Lambeck et al. 2014). A variety of indicators have also been employed to determine sea-level fluctuations along the west and east coasts of southern Africa (i.e., archaeological, geomorphological, biological, and sedimentological evidence; for a recent review see Cooper et al. (2018)).

At the onset of the glacial maximum (~30 ka), sea level fell rapidly by ~40 m (within ~2000 years) (Lambeck et al. 2014). This was followed by a gradual drop to an estimated sea level (esl) of -134 m at the start of MIS2, between 29 and 21 ka (Figure 3.11). From ~21 ka, deglaciation involved a brief, rapid rise in sea level of ~10-15 m. This was held constant after ~18 ka until the main phase of deglaciation continued from ~16.5 to 8.2 ka, resulting in a total sea level rise of ~120 m. The rate of sea level rise fluctuated throughout the later part of the Late Pleistocene, increasing between ~14 and 12 ka with a rise of ~40 m, and another rapid rise following the Younger Dryas (YD, ~12.9-11.7 ka; Lambeck et al. 2014). From the Mid-Holocene there is an overall trend of slowing sea level rise until ~150 years ago (Lambeck et al. 2014). However, a mid-Holocene highstand with sea levels rising by ~2 to 4 meters between 7.3 and 6 ka cal BP also occurred during this time (Isla 1989), as well as several <1-2 m amplitude oscillations during the Late Holocene (Although see Angulo et al. 2006; Cooper et al. 2018; Isla 1989; Khan et al. 2015).

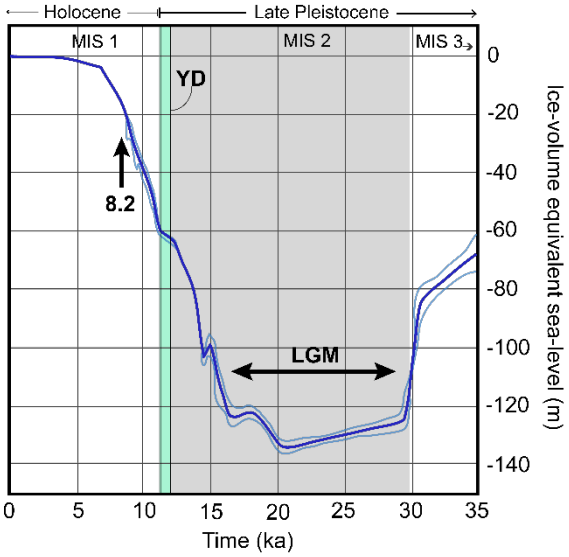

Figure 3.11. Sea level variations over the past 35 ka based on ice-volume data (modified from Lambeck et al. 2014)

Increase in ice volume is correlated to the cooler, wetter conditions of the last glacial period (MIS 2) in the WRZ, which is thought to have increased evaporation in the south Atlantic, lowered sea levels, and increased humidity levels on land. At the regional scale, glacial cycles are also thought to be responsible for increasing the impact of temperate and tropical atmospheric convection cells on southern Africa's environment. By extension, these shifts influenced the type, dominance, and distribution of biota across the subcontinent and the position, expansion, and contraction of the rainfall zones.

3.4.2 Palaeoclimate of the Winter Rainfall Zone

3.4.2.1 Late Pleistocene (126-11.7 ka)

There are several palaeoenvironmental archives available from the WRZ that date to the Late Pleistocene, most of which derive from lowland, coastal contexts (i.e., Elands Bay Cave, Diepkloof, Grootdrift site, Klaarfontein Springs, Rietvlei and Cape Flats, Die Kelders). However, the most proximate archives to the study area, which date to the last glacial or earlier, come from the Cederberg (i.e., Die Rif, Driehoek Vlei,

and Pakhuis Pass). While these sites occupy settings that differ in altitude and modern environmental settings (i.e., coastal and montane) they give insight into the timing, duration and degree of region-wide shifts in climate within the WRZ. They also have the potential to indicate the degree of climatic variability that occurred over time between relatively proximate localities. However, it should be noted that these records provide a more reliable history of changing temperature than they do of moisture, which is often riddled with spatiotemporal complexity (Chase et al. 2019).

3.4.2.1.1 Lowland Coastal Archives

According to coastal lowland archives in the WRZ, the second half of the Late Pleistocene (MIS 4-2) was cooler and wetter than the Holocene (MIS 1; e.g., Baxter 1996; Klein & Cruz-Uribe 2000; Meadows & Baxter 1999; Parkington 2000; Schalke 1973). The earliest regional evidence for this comes from macro and micro-mammalian remains together with frost-shattered roof spall from Die Kelders cave. These records indicate wetter, cooler conditions, with greater humidity, and grassier vegetation in the coastal lowlands between ~70-60 ka (Butzer 1984; Feathers & Bush 2000; Klein & Cruz-Uribe 2000; Schwarcz & Rink 2000). Continuation of more humid, cooler conditions from MIS 4 to MIS 3 are suggested by roof spall and an increase in forest taxa found in Diepkloof Rock Shelter, dated to ~60-50 ka (Chase & Meadows 2007).

Farther north, beyond the current limits of the WRZ, the timing and duration of wetter, cooler conditions are dated to 128-71 ka, based on faunal evidence from Boegoeberg 1, located 450 km north of Elands Bay Cave, along the north-west coastal margins of South Africa. These regionally derived indicators of increased moisture and decreasing temperatures during the Late Pleistocene MIS 4/3, broadly correlate with marine and terrestrial archives from deep-sea cores in the south Atlantic Ocean and geomorphological indicators farther north, in the Namib desert (Klein et al. 1999; Lancaster 2002; Scott et al. 2004; Stuut et al. 2002). Moreover, the expansion of the Antarctic ice-sheet during MIS 4 is thought to be a primary factor in increasing precipitation along the western coastal plains of South Africa (Quick 2009).

Elands Bay Cave provides the longest multiproxy record of palaeoenvironmental shifts for the west coast. However, like many rock shelter sedimentary archives, this is not a continuous record of the environmental conditions in this region. Rather it reflects the episodic history of human occupation. As mentioned above, the signal for environmental change dates to a minimum age of 40 ka cal BP and is associated with palynological evidence for wetter conditions during this time (Cartwright & Parkington 1997; Cowling et al. 1999; Parkington 2000). Continued increase in humidity from >40-37 ka cal BP are indicated from the presence of forest taxa observed at Elands Bay Cave and are supplemented by similar records at the Cape Province sites of Rietvlei and Cape Flats (Baxter 1996; Chase & Meadows 2007; Meadows & Sugden 1993; Parkington 2000; Schalke 1973). These conditions are shown to prevail in the coastal lowlands throughout the Late Quaternary until 100 cal BP (Cartwright & Parkington 1997). However, pulses of dry, cold, conditions are dated to ~21.7 ka cal BP and again between 16.8 and 12.3 cal BP, with temperatures increasing between 12.3 to 8 ka cal BP and again at ~4 ka cal BP, indicating aridification from the end of MIS 2.

In the Sandveld, macrofaunal evidence from Elands Bay Cave suggests early Holocene moisture levels were double (>400 mm/annum) what they are today (200-250 mm/yr; Klein & Cruz-Uribe 1987).

However, wood taxa suggest aridification, indicated by a shift from forest taxa, mesic thicket, and Proteoid fynbos in the Late Pleistocene (21.7 ka cal BP-12.3 ka cal BP), to the xeric thicket and shrubland from 12.3- 8 ka cal BP (Cartwright & Parkington 1997). The later dominating the west coast biome from ~4 ka BP (Cartwright & Parkington 1997).

The dominance of xeric taxa along the west coast is also dated to between 8-4 ka cal BP (mid-Holocene) based on pollen records of a sediment core taken from the Verlorenvlei Springs' Grootdrift site (Baxter 1996; Meadows & Sugden 1993). However, Klaarfontein Springs pollen and isotope records lag this trend. Providing one of the longest Holocene sediment archives in the west coast lowlands, Klaarfontein Springs indicates wetter mid-Holocene conditions (4-2.5 cal BP), followed by increased aridification of the Sandveld region in the late Holocene (from 2.5 ka cal BP to 950 cal BP). Mollusc shell analysis from Grootdrift and Klaarfontein Springs, also indicate a period of increased moisture during the latter part of the mid-Holocene (between ~5-4 ka cal BP at Grootdrift and 4-2 ka cal BP at Klaarfontein Springs), followed by drier conditions in the late Holocene (Carr et al. 2015). Carr and colleagues suggested that late Holocene aridification in the west coast's Sandveld reflects an increase in the duration and intensity of summer droughts as a hydro-climatic response to increased upwelling and sea-surface temperatures from the Atlantic Ocean's Benguela current (see also Chase et al. 2011; Farmer et al. 2005).

Declining humidity, followed by increase in temperature at the end of MIS 2, are suggested by reduced water availability, shifts in faunal composition and biome structure reflecting the gradual onset of Holocene aridification. A trend thought to result from the long-term shift in dominance between tropical and temperate circulation cells in response to orbital forcing (Carr et al. 2016). Together, the palaeoenvironmental archives from the coastal lowlands suggest cooler and wetter conditions during the Late Pleistocene, following by a pulsed sequence of drier to wetter conditions throughout the Holocene coupled with a general increase in temperature, becoming drier and seasonally more acute from at least the mid-Holocene (~3 ka cal yr. BP; Carr et al. 2015).

3.4.2.1.2 Highland Montane Archives

Within the WRZ, palaeoenvironmental archives in highland, montane settings derive from sites in the Cederberg (e.g., Pakhuis Pass, De Rif, Driehoek VleiSneeuberg Vlei, and Truitjes Kraal 4), farther south in the Swatruggens Mountains, and Table Mountain in the Cape Peninsula (i.e., Cecilia Cave). Palynological evidence from the Cederberg (Pakhuis Pass and Die Rif), dated to the last glacial period (MIS 2), indicate a complex environment of locally dependent fluctuations in temperature and moisture. At Pakhuis Pass, hyrax middens record minor changes in the frequency of pollen taxa and stable isotope data that indicate changes in water availability. From these archives, (Scott & Woodborne 2007a, b) registered cooler, drier conditions between 22 and 21 ka cal BP, followed by increased moisture and temperatures between 21 and 19 ka cal BP, which is suggested to indicate the southward displacement of the WRZ and an increase in summer rainfall along the western fringe of the Karoo (Gasse et al. 2008; Scott & Woodborne 2007b). From 19 to 17.5 ka cal BP temperature and moisture levels drop once again. Increase in Dodonaea from 16 ka cal BP suggests an increase in drier, warmer conditions after the last glacial to interglacial transition (Scott & Woodborne 2007a, b). Trends in aridification support the coastal lowland patterns of climate change. However, Pakhuis Pass indicates pulses in moisture and temperature levels that contradict

the timing recorded in records analysed west of the Cederberg.

In a wetland setting, in the highest parts of the Cederberg, pollen records from sediment cores taken from Driehoek Vlei and Sneeuberg Vlei, suggest that the high-altitude environment of this mountain range was characterised by vegetation stability from the Late Pleistocene, with only minor indications of variability in taxa frequencies (Meadows & Sugden 1993). However, a steady decline in Clanwilliam cedar (*Widdringtonia cedarbergensis*) prior to 17.6 ka cal BP, which continues to near extinction today, suggests that environmental conditions were more favourable for the growth of these trees during the last glacial period. Based on this evidence, Meadows and Baxter (1999) inferred a cooler, wetter climate during the LGM compared to the Holocene.

Overall, highland montane records indicate prevailing wetter, cooler conditions during the last glacial, and warmer, drier conditions during the Holocene epoch, supporting the trend observed at lowland coastal sites. However, De Rif yields a high resolution and relatively continuous 28 ka sequence that contradicts both, with hyrax middens recording a decline in moisture during the LGM. The contrast may say more about the geographic positions of these archives in the Cederberg (Chase et al. 2019). For instance, Pakhuis Pass is located on the Karoo side of the mountain group north-east of De Rif and although it is in the rain shadow of the Cederberg, high moisture content during this time could indicate increased summer rainfall during the LGM, brought on by stronger easterlies (Quick 2009; Tyson 1999). De Rif, in contrast, is located on the western side of the Cederberg and was more likely prone to westerly oceanic and atmospheric input (Quick 2009). This inference is supported by coincident fluctuations in sea levels and ice sheet volume and recorded moisture rise and fall at the site during the last glacial period. For example, rise in the moisture levels surrounding De Rif coincide with increased Antarctic Sea ice volume in the southern Atlantic, between ~26.5 – 22.5 ka cal BP and again between 20.5 to 18.5 ka cal BP. Between these two spikes in moisture, De Rif experienced an episode of aridity between ~22 and 21 ka cal BP, during which time sea ice volumes in the Southern Ocean were lower.

Similar to coastal lowland archives, the general trend in Holocene climate change for the Cape Fold Belt's western ranges is one of warming and vegetation stability, with oscillating moisture and temperature levels increasing in variability from ~2.5 ka cal BP (Quick 2009). The stability and homogeneity of fynbos dominated montane vegetation, observed in the Late Pleistocene, appears to have prevailed at higher altitudes (Meadows & Sugden 1993; Sugden & Meadows 1989). Fynbos vegetation, adapted well to the shallow soils of the Table Mountain Group's quartzitic sandstone, maintained dominance in the western highlands for at least 28 ka (Quick 2009). At lower elevations vegetation became more mosaic (fynbos, succulents, and thicket), and the decline in Clanwilliam cedar continues to today (Meadows & Sugden 1990, 1991; Meadows & Baxter 1999). However, fluctuations in water availability are observed for all highland sites dated to the Holocene and show increase in the amplitude and frequency of oscillating moisture and temperature (Scott 1994; Scott & Woodborne 2007a, b). Poor resolution of many of these sites make correlations in climate change in the highlands with the last glacial – interglacial transition and Younger Dryas difficult to detect (Quick 2009). However, Quick's (2009) analysis of stable isotopes $\delta^{13}C$ and $\delta^{15}N$ of hyraceum at De Rif indicate water efficiency fluctuations that broadly correlate with the LGM (~24-18 kya), and the Younger Dryas, (12.9-11.7 kya). Despite locally derived evidence for climatic variability, De Rif middens confirm the shift to drier, more arid conditions throughout the

Holocene.

Like the lowland coastal plains, the Cederberg experienced more humid, warmer conditions during the early Holocene (Scott & Woodborne 2007b). However, the abrupt increase of Dodonaea, observed in hyraceum pollen taxa frequencies at Pakhuis Pass, suggests the onset of rising temperatures, and reduction in moisture, began prior to the Holocene, at ~16 ka cal BP. Following this shift, Pakhuis Pass also indicates that temperatures continued to rise between ~16 and 9.5 ka cal BP, while wet conditions—although following a general trend of decline—prevailed (Scott & Woodborne 2007b). Holocene montane temperatures and moisture levels appear to increase in their variability throughout the Pakhuis Pass midden sequence from ~2.5 ka cal BP.

The trend from cooler, wetter conditions in the Late Pleistocene to warmer, drier conditions in the Holocene are generally expressed in both the highland and coastal records for the WRZ. Compared to the Late Pleistocene, a more detailed, higher quality archive is available for reconstructing the Holocene palaeoenvironment. Both coastal and montane archives suggest that the Holocene experienced aridification over the course the last 11.7 ka, particularly within the last 2 ka. However, a pattern of increased frequency and amplitude in abrupt shifts between dry-wet and colder-warmer conditions characterise the mid- to late Holocene.

3.4.3 Summary

Southern Africa's climate results from the complex interaction between terrestrial and oceanic circulation systems that divide the subcontinent into three seasonally distinct climatic zones: the summer rainfall zone, winter rainfall zone and year-round rainfall zone. The Doring River catchment is situated in the winter rainfall zone, which receives >66% of its moisture from westerly frontals over winter. Its modern climate is mostly temperate to hot, with wet winters and dry summers, and the occasional summer thunderstorm from the summer rainfall zone in the north-east. The physiography and underlying geology of the Doring River catchment play an important part in controlling the catchment's diverse and highly variable local climate and vegetation structure. While it exists within the seasonal regime of the WRZ, the Doring River valley is one of the driest areas within the catchment. The main channel cuts a deep river valley to the east of the Cederberg, placing it within the arid setting of its rain shadow. This limits rainfall to ~200 mm/yr. Together, low precipitation levels and a deep water table, measuring more than 19 m below ground level, result in limited groundwater river supply in a valley with annual evaporation >2700 mm (Conrad et al. 2012, pp.7, Map 5; Fortuin & Woodford 2006, pp.14, Figure 5). In contrast, the north-western limits of the catchment rise >900 m above the Doring River valley, receive >1000 mm of winter rainfall from the westerlies, contribute three to four times more groundwater to the Tra-Tra, Biedouw and Brandewyns tributaries, and experience nearly half the evaporation of the Doring River valley (~1560 mm/a; Fortuin & Woodford 2006). During winter and spring, the very mountains that restrict rainfall in the Doring River valley, also supply this dry landscape with a valuable source of water by way of its river channel.

Geographically well-distributed environmental archives for both the Late Pleistocene and Holocene are limited, which often results in contradictory interpretation of a region's palaeoenvironmental history (Chase et al. 2018, p.36). High resolution terrestrial archives are mostly Holocene in age, with high quality datasets becoming more disparate in the Pleistocene (Chase et al. 2018, p.36; Holmgren et al. 2003).

As a result, environmental change during the Late Pleistocene is often framed by global trends in glacial cycling, brought about by orbital forcing. This is supplemented by more local archives, which provide episodic insight into climatic variability from the last glacial period.

In the last 200 ka southern Africa has experienced extreme climate shifts, influencing sea level and the development of diverse biomes. Global changes in climate indicate cycles of glacial and interglacial conditions that can be divided into Marine Isotope stages. The Late Pleistocene (126-11.7 ka) spanned two warm interglacials (MIS 5 and 3) and two cold glacials (MIS 4 and 2), each respectively resulting in the rise and fall of sea levels and the contraction and expansion of the coastal plains of the subcontinent. The final and current interglacial of MIS 1 marks the final stages of rising sea levels after the LGM (~20 ka) and increasingly arid conditions throughout the Holocene. More characteristic of this latest epoch is the greater frequency and amplitude of shifts between climatic extremes. Local archives of pollen, phytolith, flora and fauna from the coastal lowlands and highlands of the Cederberg show a general warming of Holocene temperatures. However, changes in inferred moisture level vary between archives. It is likely that the study area experienced wetter, cooler conditions during the Late Pleistocene's last glacial period, while conditions in the Holocene have grown increasingly unpredictable, with aridification and flooding events increasing with time, particularly in the last ~3 ka. Based on local farm records, that trend of declining humidity continues to present.

The palaeoenvironmental record from Pakhuis Pass is the closest archive to the Doring River valley and the best indicator of the last 28 ka of climate and vegetation on this side of the Cederberg. The suggestion that moisture increased during MIS 2 due to the expansion of the Summer Rainfall Zone during this time, would have several potential effects on the study area. This includes increased pedogenic potential, with consolidation of pre-existing deposits in the study area, reduction in the amount of time the Doring River channel was dry and, thus, the amount of time available for river channel sands to dry and be transported by wind. River crossing by humans and fauna would also be affected during times of increased precipitation in the catchment.

While the general degree of aridity that occurs in the study area has continued to intensify since the Late Pleistocene, the dynamic of relative dryness between the eastern and western catchment, either side of the Cederberg, likely prevailed over the last 200 ka. However, despite the study area's dry environment and reliance on rainfall from the west, the Doring River supplies its lower valley system with a seasonally predictable source of fresh water every year. This topographically complex catchment also covers a diverse range of environments, cuts into the Table Mountain and Karoo Super Groups, and shifts from fynbos vegetation in the western highlands to drought resistant succulent Karoo flora in the east (Figures 3.3 and 3.9). Together these variables, and the different timescales at which they change, have had a direct impact on the carrying capacity of the Doring River valley, its sedimentary structure and cycles of deposition and erosion during the Holocene and Late Pleistocene.

CHAPTER 4.
STUDY AREA: HUMAN SETTING

4.1 An Anthropogenic Landscape

The Doring River catchment has a history of human activity that extends back to the Middle Pleistocene (see Chapter 2). This is preserved in the stratified rock shelter deposits of the Doring River's western catchment and the archaeologically-rich sediment 'stacks' exposed throughout the Doring River valley (Mackay et al. 2014b; Shaw et al. 2019). Archaeology preserved in the Doring River valley is not only shaped by the physical setting and environmental history of its region and catchment, but also by the human activity that took place prior to, during and after its discard. Therefore, any archaeology associated with Late Pleistocene human activity in the Doring River valley should be considered within the historical context that influenced its formation, preservation, and visibility. The major, most recent transformation of landuse in the Olifants-Doring catchment is the advent of European farming and this review begins there, before discussing previous research on the rock shelters and open-air archaeology of the study area.

4.1.1 Human activity in the Doring River valley in the last 300 years

4.1.1.1 Access and carrying capacity

The introduction of European farming methods in the last 300 years intensified landuse in the Olifants-Doring catchment. However, traversing the rugged terrain of the Cederberg to access the Doring River valley coupled with the low carrying capacity of its semi-arid environment has kept this part of the catchment relatively underdeveloped and sparsely populated compared to the west (Fortuin & Woodford 2006). Population numbers are currently low in the Doring River catchment, with an estimate of five or less individuals per square kilometre compared to the southern portion of the Olifants River (>20 people/km2; Fortuin & Woodford 2006, figure 7). However, those who live in the valley and its tributaries reside and/or farm here year-round.

The low mean annual precipitation for most of the Doring River valley (<200 mm) limits agricultural practice to livestock grazing (Neumark 1957) and dryland farming (Appendix 1). The fractured hydrogeology of the Cape Supergroup enables access to subterranean aquifers throughout the south and western catchment, supporting pivot irrigation for crop farming and even citrus farms in these areas (Conrad et al. 2012). However, large stretches of the Doring River valley, particularly between its confluence with the Bos River and the DoringBos, rely almost entirely on pumped water supply from the Doring River, restricting crop farming to small sections of land close to the channel and where sufficient borehole and spring water supplies are available.

Sheep and goat grazing is one of the main forms of land use in semi-arid areas of the Cederberg and has been a regular presence in the Doring River valley since the early 18th Century. The rugged, rocky, and steep nature of the narrower sections of the Doring River valley are especially conducive to goat grazing, and even though it was "…uniformly condemned as a cause of erosion…" in South Africa by the 1950s (Neumark 1957, p.74), Boer goats still form one of the main grazing animals around the Doring-Biedouw River confluence. Erosion caused by overgrazing, even at relatively low levels, has likely

increased within the last century (see Appendix 1). Extensive erosion is particularly evident in areas surrounding abandoned stone structures, fields demarcated by fence lines (i.e., Klein Hoek 1, see Ames et al. 2020), and where trackways have formed, and roads have been constructed (further details in Appendix 1).

4.1.2 Historic occupation and use of the Doring River valley prior to the 20th century

Occupation and landuse in the Doring River valley underwent numerous shifts since its early occupation by European settlers in the 18th Century, evident by the numerous stone structures now in ruin found scattered throughout the valley system. Many of these structures are extensive and show multiple additions, suggesting they were occupied over extended periods of time, possibly for more than one generation. The reason behind their abandonment is unknown. However, based on the present-day conditions of the Doring River's environment, their location may have proven untenable for long-term use, especially if attempts were made to subsist solely off the flow of the Doring River (Mitchell 2009). Despite this, the presence of these structures in the landscape act as locational markers of where domestic and agricultural activity would have been intensive.

4.1.3 Early exploration and settlement of the Olifants-Doring catchment

European farmers have utilized the Olifants-Doring catchment since its early exploration by Cape settlers in the late 17th Century (Mitchell 2009; Figure 4.1). A map published by (Neumark 1957) depicts the growing extent of the Cape Colony between 1652 and 1806 (see Figure 4.2), with stock and dryland farming carried out year-round by 1730 (Figure 4.1; Mitchell 2009). According to Neumark (1957), the colony was restricted to present day Cape Town and the west coast Sandveld, Koue Bokkeveld, and Olifants municipalities from 1710, which was held at least until 1750. In 1798, the "Frontier" is shown extending along and just beyond the present-day provincial boundaries of the Western and Northern Cape, north-east of the Hantam Mountains and the Doring River (Figure 4.2). Although the Doring River valley is depicted and was legally recognised as outside the Colony's bounds prior to the 19th Century, it was held as contested grazing by settlers from the early 18th Century (Walker 1930; Neumark 1957).

Figure 4.1. Early Cederberg settler farms extending to the Doring River valley by 1727 (from Mitchell 2009, p.49, figure 3.4).

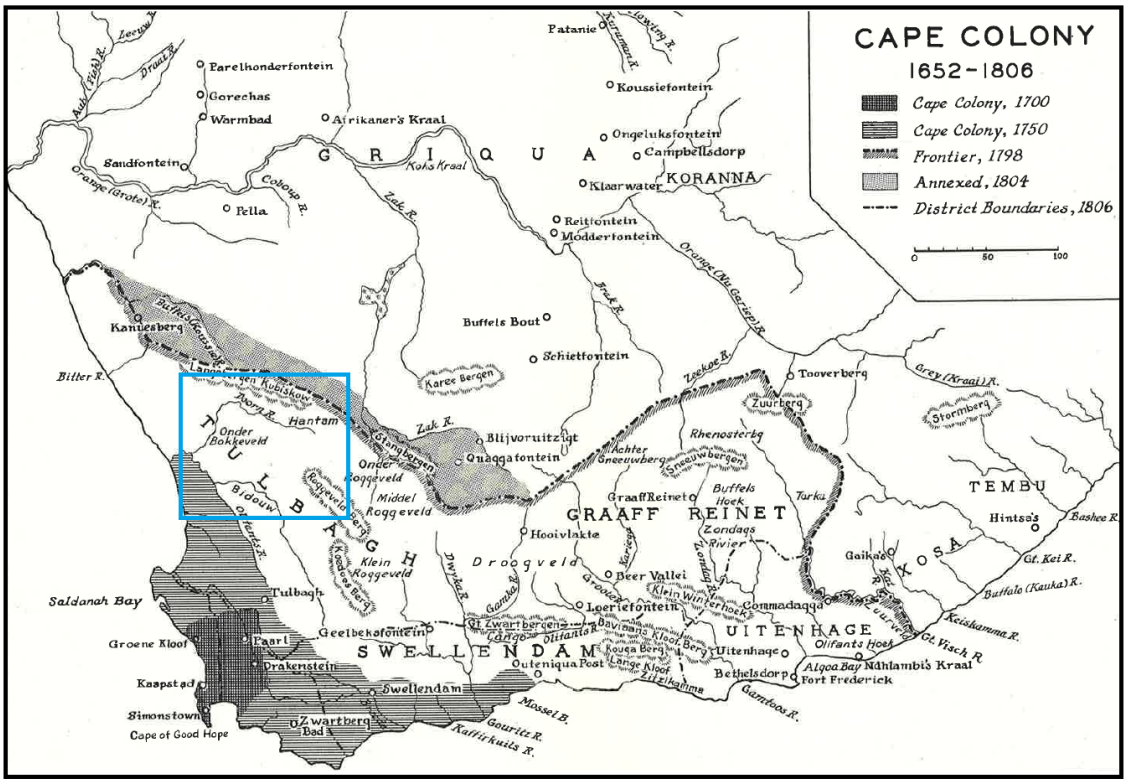

Figure 4.2. The Cape Colony between 1652 and 1806 showing the 1798 settler 'Frontier' north-west of the Doring River and Hantam mountains. Study area framed (blue box). From From Neumark (1957, p.19).

The economical ease with which settlers could become grazers in the interior encouraged their expansion north from the Cape Colony (Neumark 1957). The earliest settler land claims for grazing stock in the Olifants were made by the 18th Century (Mitchell 2009). From this time, farmers in the Cederberg were in possession of multiple, large plots of land with equally large stock counts (Mitchell 2009; Neumark 1957). However, they tended to anchor themselves to a particular location, building their homesteads at these localities while grazing lands in different parts of the region (Neumark 1957, p.25, quoting Percival's 1804 observations).The prioritization of larger units of land in different locations enabled farmers to reap the benefits of seasonal yields in different parts of the Olifants-Doring catchment and Karoo (Mitchell 2009). While this often gave early farmers the reputation for being nomadic, Neumark (1957) argued that seasonal grazing was essential for overcoming the low carrying capacity of these farms.

Stock farming in the interior intensified during the 1730s as a reaction to the deterioration of the Cape wine and wheat economy around this time (Neumark 1957). However, increasing competition for resources and land between Khoisan and the Colony culminated with the Frontier War of 1739. This reinforced the Colony's dominance and monopoly over the region to the permanent detriment of the Khoikhoi and San. With Khoisan resistance supressed, the Cederberg became more intensively settled from the mid-1700s and in 1834, the Cederberg, including the Doring River, was subsumed into the Cape Colony.

Settlement and land use increased and continued to expand from the mid-1700s, with sheep farming becoming the dominant form of grazing between 1770 and 1779 (Neumark 1957). An exponential increase in stock numbers is recorded for the 1770s where "…each farmer in the Roggeveld, the Bokkeveld, the Karroo, and the Cambedo possessed from 1,000 to 3,000 sheep" (Neumark 1957, p.248, citing Sparrman 1785), with sheep numbers in Stellenbosch growing from 12,470 in 1701 to 111,217 in 1793 (Neumark

1957, table 3). However, the distribution and size of land farmed in the region was not spread evenly across the landscape. The more remote and topographically variable character of the Doring River catchment had a strong influence on the timing and intensity of settler occupation along its main channel and tributaries.

4.1.3.1 Early Access into the Doring River valley

Selecting land for farming was largely determined by topographic and environmental factors (Walker 1930). With the Doring River being the major water source in an otherwise nutrient-poor landscape, grazing, dryland farming, and eventual settlement was prioritised around its channel. However, accessing and crossing the river valley likely impeded its occupation by early settlers, especially if transport was by wagon. It is difficult to access and cross the Doring River due to the rugged mesa-butte terrain of the surrounding catchment and the often-steep transition from these plateaus into its valley (Amschwand 2003). However, this merely hindered rather than barred access into the valley in the 18th Century, with loan farms in the catchment appearing as early as 1727 (Mitchell 2009) and likely increasing after the Frontier War of 1739.

Wagon access enabled the growth of more permeant, albeit contested, settlement in the valley (Mitchell 2009), which was initially provided by passes leading to land up-river from the Olifants-Doring confluence, prior to the 20th Century. Valley access and river crossings or 'drifs' are present throughout the landscape today. However, only a few routes were available in the 1700s—one being the Nardouws Kloof Pass, which was "…travelled via the Outspan at Elizabethsfontein and across the farm Wagenpads Leegte to Bloemfontein" (Amschwand 2003, p.27). Access to the Biedouw River and its confluence with the Doring River was greatly improved by the construction of the Pakhuis Pass in 1877. Botterkloof Passes was also developed in 1877, becoming the main wagon track to access the Bokkeveld and Hantam in the east.

While Pakhuis Pass was shorter and still possible to traverse prior to its development in 1877, it proved a more difficult route to take and saw less use prior to the late 19th Century (Amschwand 2003). For this reason, access through Pakhuis Pass and into the Biedouw River to its confluence with the Doring River would have only been possible by horse and on foot, but difficult if travelling by wagon. Semi-arid conditions and difficulty in traversing this landscape would have limited the intensity of farming and occupation of this part of the Doring River valley as well as access to building materials beyond what was at hand from the surrounding valley system.

The semi-arid landscape of the Doring River valley has a low carrying capacity making it vulnerable to erosion during times of intensive use by humans and animals. This has possibly been exacerbated by increased Holocene aridity promoting flash-flooding and high winds. Thus, the introduction and intensification of stock farming, road development and shelter construction over the last 300-200 years has likely catalysed erosion in the area, possibly exposing previously buried archaeological assemblages on consolidated sediment, making them increasingly vulnerable to weathering, entrainment, and eventually loss.

With this recent history of landuse and potential erosional conditions in mind, the following sections provide a background for the open-archaeology recently studied in the Doring River valley, beginning with the surveys and rock shelter excavations of Holocene and Late Pleistocene archaeology the

Olifants-Doring Basin and more broadly the Cederberg region. This is followed by an overview of more recent rock shelter excavations in the Doring River catchment and a critical review of the subsequent open-air surveys across the Doring River valley.

4.2 Previous Archaeological Research

4.2.1 Early research focus

Archaeological research in the Doring River catchment is nested in the early regional explorations of the Cederberg. The Cederberg is one of the most intensively surveyed and excavated archaeological regions in South Africa. However, this work has primarily been directed at the better-preserved and radiometrically datable Holocene record, beginning with the rock art surveys of the 1940s (Johnson 1959; Johnson & Rabinowitz 1955). These early surveys and shelter-specific investigations of the 1960s and 1970s were mainly targeted at recording rock art (Maggs 1967) and shelter excavations of Holocene occupation, with research interest centred on elucidating the historical tensions between hunter-gatherers and pastoralists, the seasonality of resource availability, and movement between the coast and the interior.

De Hagen Cave, in the Cederberg, was one of the first in a series of shelter excavations that contributed to a regional understanding of LSA settlement patterns between the Western Cape's coastal and inland rock shelter sites (Figure 3.9; Parkington & Poggenpoel 1971). Later excavations included those of Andriesgrond and Renbaan 2, near the Olifants and Kransvleikloof Rivers (west of the Cederberg mountains; (Anderson 1991; Kaplan 1987; Parkington 1978), Klipfonteinrand 1 and 2, east of Pakhuis Mountain (Nackerdien 1989; Thackeray 1977), and Aspoort, west of the Tankwa-Karoo and south of the Cederberg (Smith & Ripp 1978). These early studies produced evidence of seasonally driven movement between the coast and interior throughout the Holocene LSA, together with the excavation and survey of sites along the present Atlantic coastline and Sandveld (i.e., Elands Bay Cave, Diepkloof and deflation hollow sites).

Research by the University of Cape Town (UCT) Spatial Archaeology Research Unit expanded on the rock shelter excavations of the 70s and 80s to include large-scale surveys in the region, incorporating data from surface archaeology into their rock art surveys and shelter excavations. The overall goal was to develop a landscape-scale understanding of LSA settlement patterns, with a continued focus on the differential adaptations of Late Holocene populations between coastal and inland (~4000-300 years BP; Manhire et al. 1986; Parkington et al. 1980). Various landforms (e.g., deflation hollows, talus slopes, kopjes) were surveyed and compared in the Sandveld and Olifants River valley to support occupation trends observed in excavated shelters. It is worth noting, however, that the majority of this research was centred on the dynamic between hunter-gatherer and herder populations within the last 2000 years due to the temporal resolution that could be attained from well-preserved environmental and behavioural proxies across multiple sites (Manhire et al. 1986; Rijssen 1984). Thus, the lack of an appropriate dating method for Pleistocene LSA deposits and any context without time-diagnostic artefacts older than the radiocarbon dating limit of 40 ka was often excluded from regional frameworks (Parkington 1990).

From this research, two places of recurring activity were identified in the Sandveld: deflation hollows and rock shelters. The intensity and timing of their use was argued to demonstrate a shift from pre- to post-ceramic archaeology in the region. Deflation hollows are blowouts in the coastal sandsheet

(sandveld) that yield a dominant archaeological signal from the century immediately prior to herding. They are characterised as low-lying places, often located proximate to rivers and their tributaries, and are noted for their poor viewshed over the surrounding landscape. Rock shelters show an increase in use after the appearance of pastoralist activity relative to concentrated occurrences in open-air contexts. Late Holocene deposits show grass bedding and ash found in association with sheep remains, pottery fragments and adzes. Their presence in the topographically complex and less accessible hinterlands suggests the deliberate targeting of places with a greater outlook of the lower plains and hence increased predictability of resources.

It is argued that competing pressures, brought about by the arrival of pastoralism in the Western Cape ~2000 years ago manifested ecologically and through ritual (Parkington et al. 1986). The latter was inferred from the intensification of painting in the interior relative to the coast by hunter-gatherers, interpreted as a way for them to enhance social cohesion, preserve a value system under threat, and maintain access to wild resources as pressure along the more favourable lowlands in the west pushed hunter-gatherer populations into the less nutrient-rich, topographically variable interior (Parkington et al. 1986). Between ~3000 and 1800 BP, large midden sites are the dominant feature of coastal subsistence prior to the introduction of pastoralism. Domestic sheep were introduced to the Western Cape between 2000 and 1600 BP (Coutu et al. 2021). After this time, the archaeological record yields evidence of both sheep and pottery throughout the region, implying that pastoralism was one of the main subsistence strategies in use from this time.

4.2.2 Rock shelter excavation in the Doring River catchment

Despite the region's continued growth in research since the 1990s, the Doring River valley has, until very recently, received less attention compared to the western part of the Olifants-Doring Basin (i.e., the Olifants River valley and Cederberg mountains). However, within the last decade, knowledge about the archaeology of the Doring River system has grown as a result of renewed excavations of rock shelters in the south-western zone of the Doring River catchment. The most proximate to the Doring River valley are Putslaagte 8 (~2 km north-west), Klipfonteinrand 1 and 2 (~13 km south-west), Hollow Rock Shelter (17 km south-west), and Mertenhof (~19 km south-west; Figure 3.9). These natural structures have eroded out of the silica-rich sandstone and quartzite geology of the Table Mountain Group and have the dual advantage of being proximate to the Fynbos and Succulent Karroo biomes as well as occurring adjacent to or within ~5 km of a tributary that connects the Doring River to their location (Figure 3.9). Together they represent over half the excavated rock shelters in the Cederberg and yield a combined depositional sequence of material culture that spans at least 80 ka of human, climatic, and ecological change.

Inter-site comparisons as well as questions of occupational redundancy and coastal/interior interaction have become central topics of investigation and debate in Late Pleistocene literature (reviewed by Mackay 2016b). As a consequence, the last decade has witnessed a resurgence in research on the interior rock shelters of the Doring River's Western Cape catchment, many previously studied for their Holocene deposits (i.e., Klipfonteinrand (Bluff 2017; Low 2019; Mackay 2012; Mackay et al. 2019; Pargeter & Low 2018; Thackeray 1977), Mertenhof (Schmidt & Mackay 2016; Will et al. 2015; Williams 2017), Hollow Rock Shelter (Evans 1994; Feathers 2015; Högberg 2014, 2016; Högberg & Larsson 2011; Högberg & Lombard 2016; Larsson 2010a; Schmidt & Högberg 2018), and Putslaagte 8 (Low & Mackay 2016;

Mackay et al. 2015; Plaskett 2012)). More recent studies were motivated by the paucity of interior rock shelter excavations that focus on the Late Pleistocene record and the need for a more refined chrono-stratigraphy to compare against coastal and near-coastal sites. The following sections present the chronostratigraphic sequence of each rock shelter.

4.2.2.1 Klipfonteinrand Rock Shelter (KFR)

The rock shelters of Klipfonteinrand 1 and 2 (32° 4'18.00"S, 19° 7'48.00"E) are in the rain shadow of the Cederberg mountains, ~27 km west of the Doring-Biedouw confluence and east of Pakhuis Pass (Figure 3.9). The closest tributaries to the rock shelters are the seasonally flowing Biedouw and Brandewyn Rivers, located ~10 km and ~4 km south and west of the shelter, respectively. Both are tributaries of the Doring River, supplying it during the winter months with rain from the northern and central ranges of the Cederberg. Permanent springs occur at Salmanslaagte, 2 km to the north of these sites.

Klipfonteinrand 1 and 2 were first excavated in 1969 and 1987 by John Parkington and colleagues, focusing on the Late Holocene units as an inland example with which to compare the coastal record of Elands Bay Cave (Nackerdien 1989; Parkington 1976). In 2011 and 2012, the front and rear deposits of Klipfonteinrand 1 were re-excavated by Alex Mackay and colleagues to clarify its Late Pleistocene technological units and chronological sequence (see Mackay 2012; Mackay et al. 2019). They excavated two separate trenches at the front and rear of the shelter that together yield a chronostratigraphic sequence covering the early MSA, Howiesons Poort, Robberg, and Oakhurst technocomplexes (Table 4.1). Historic removal of sediment from the shelter by a recent landowner likely resulted in the loss of the Late Holocene deposits at Klipfonteinrand 1 (Mackay 2012; Thackeray 1977; Volman 1981).

Only minor typo-technological overlap exists between material recovered from the front and rear deposits at Klipfonteinrand 1. The front trench is MSA-dominated (early MSA and Howiesons Poort) with a relatively homogenous, and bioturbated matrix compared to the better-preserved, LSA-dominated sequence at the rear of the shelter. The rear trench yields technology that is indicative of the Oakhurst, Robberg and Howiesons Poort Industries. Though there is no discernible post-Howiesons Poort unit at Klipfonteinrand 1, a single ‘Nubian’ Levallois core occurs at the top of the Howiesons Poort in proximity to two unifacial points (Mackay, pers. comm., 2021). Publications focus on the MIS 2 component of the rear sequence, owing to its more intact sedimentary structure (Low 2019; Mackay et al. 2019).

Table 4.1. Characteristics of major technocomplexes as they occur in Doring River / Cederberg rock shelter sequences. Raw material characteristics are not the most common rock types – those are generally hornfels and quartz, but rather the raw materials that seem to become distinctively more common in those periods. (Summarised from Low 2018; Low & Mackay 2016; Low et al. 2017; Mackay 2016b; Mackay et al. 2019; Mackay et al. 2015; O'Driscoll & Mackay 2020; Shaw et al. 2019; Watson et al. 2020).

Technocomplex	Age range (ka)	Raw material characteristics	Flaking systems	Tool types	Other features	Sites
'Neolithic'	<2	Quartz	Unknown	Unknown	Pottery	PL8, KFR2, MRS
Wilton	6-2	Silcrete, chert, & quartz	Bladelets	Thumbnail scrapers		KFR1, KFR2
Early Holocene	10-6	Quartzite	Large flakes	Round scrapers		KFR1
Oakhurst	16-10	Hornfels, quartzite	Large flakes, flaks wider than long	Naturally backed knives, scaled pieces, core scrapers	Limited core transport	KFR1, MRS
Robberg	22-16	Silcrete, quartz	Bladelets	None	Transport of silcrete cores	PL8, KFR1, MRS
Early LSA	25-22	Hornfels	Blades	None	Limited core transport	PL8
Late MSA	50-33	Hornfels, quartzite	Flakes	Scaled pieces	Transport of cortical flakes	PL8
Post-Howiesons Poort	60-50	Silcrete, hornfels	Flakes and blades	Unifacial points	'Nubian' Levallois cores	MRS
Howiesons Poort	71-60	Silcrete, chert	Blades	Backed pieces and notched blades	Transport of silcrete cores	KFR1, MRS
Still Bay	75-71	Quartzite	Flakes, bifacial thinning flakes	Bifacial points	Limited core transport	MRS
Early MSA	>75	Quartzite	Flakes, convergent flakes, large blades	Notched and denticulated pieces		PL8, KFR1, MRS

Deposits dating to between ~22 and 16 ka cal BP conform with the defining characteristics of the Robberg, broadly congruent with Elands Bay cave near the west coast (Porraz et al. 2016) and Putslaagte 8 (see below; Low & Mackay 2016; Mackay et al. 2019): increased use of silcrete, laminar production and small blade, or bladelet, technology dominate, bipolar technology forms a minor component of the assemblage, and retouched pieces are rare and occur mostly in the form of pieces esquillees—(Low 2019). Changes in technological composition include a decline in silcrete and a rise in quartz and hornfels—the latter dominating the subsequent Oakhurst assemblage—and a decrease in overall blade size. Change in reduction technique possibly reflects changes in material use and the availability of raw materials over time and/or where people were moving through the landscape (Low 2019).

Artefacts dating from ~16 to 13 ka cal BP are consistent with the Oakhurst technocomplex, typically defined by an increase in the size of flakes, and flakes with higher width to length ratios. Their

increase in size seems to track an increase in the use of materials that occur in larger packages, such as outcropping quartzite and large river cobbles of hornfels sourced from the Doring River. At Klipfonteinrand 1, hornfels dominates the Oakhurst assemblage, with quartzite and quartz also occurring in high frequencies, whereas silcrete artefact frequencies are comparatively low. Differences in technological composition are more marked between the Robberg and Oakhurst deposits, evinced by the increase in retouch artefacts, a decrease in blade production, and the disappearance of silcrete. Core frequencies also decline, and laminar production disappears. Quartz is the only material employed to produce blades in these units. The appearance of marine shell in deposits dated to 2-4 ka, and the increase of hornfels at sites along the western coastal plains indicate interaction between the coast and the interior from the mid to late Holocene (Mackay 2016a).

4.2.2.2 Hollow Rock Shelter (HRS)

Hollow Rock Shelter (32° 5'24.94"S, 19° 5'14.62"E) occurs at the edge of a sandstone platform overlooking Brandewyn River which is connected to the Biedouw River through a network of faults in the south and its outlet into the Doring River to the north (Figure 3.9). As the crow flies, Hollow Rock Shelter is ~4.5 km south-west of Klipfonteinrand, ~12 km from Mertenhof Rock Shelter, ~18 km from Putslaagte 8, and ~31 km west of the Biedouw-Doring confluence.

Hollow Rock Shelter is a large, eroded sandstone boulder that provides a low-lying, arch-roofed hollow that has trapped roughly 30 cm of sandy sediment, deposited at least 70 kya. Discovered in 1991 and first excavated in 1993 (Evans 1994) and 2008 (Larsson 2010a, b), the chronometric dating and typo-technological analysis of this sediment revealed a chronology of shelter occupation that dates entirely to the Still Bay (Table 4.1), from ~72 to 80 ka (Högberg 2014). Together with Blombos Cave (Henshilwood et al. 2001), this site helped to reinstate the Still Bay lithic assemblage in southern Africa's chronostratigraphic sequences (Evans 1994)—nearly 60 years after the first recording of Still Bay in Peers Cave and Dale Rose Parlour.

Technological studies were carried-out on the bifacial points, their thinning flakes, and blades of the densest samples retrieved from excavation (Högberg 2014, 2016; Högberg & Larsson 2011; Högberg & Lombard 2016)—excluding the analysis of the Levallois flakes, unifacial points, retouched pieces, denticulate blades, non-thinning flakes, debris, and a variety of different core types, all of which date to the same time range (Högberg 2014, p.145). It should also be noted that although blades and bifacial point technology are the dominant component of the Hollow Rock Shelter sample and were discarded over the same period of shelter use, they represent different production strategies (Högberg & Lombard 2016).

4.2.2.3 Mertenhof Rock Shelter (MRS)

Mertenhof Rock Shelter (~32°08'58.9"S, 19°14'15.3"E) is a sandstone shelter in a narrow valley overlooking the Biedouw River, ~25 km south-west of its confluence with the Doring River (Figure 3.9). Codirected by Alex Mackay and Aara Welz, four seasons of excavations at Mertenhof (2013 to 2017), have uncovered a long sequence of discontinuous occupation over the last ~100 ka, yielding technology characteristic of late Holocene, Robberg, late MSA, post-Howiesons Poort, Still Bay and early MSA (Table 4.1). A brief report of the excavation was included in Will et al. (2015), to supplement a more in-depth

analysis of Nubian core reduction systems from the post-Howiesons Poort strata. Chronometric ages, determined using OSL, constrain the timing of human occupation at Mertenhof Rock Shelter to the later part of MIS3, with ages ranging from ~51 to 22 ka (Williams 2017).

The Late Holocene was identified in Mertenhof's upper units, yielding loose bedding, a crusted matrix of dung, ostrich eggshell, bone, and glass beads, with lithic material dominated by quartzite and hornfels. The Red and Grey Brown Series yielded technology indicative of the Robberg and terminal Pleistocene (i.e., rotated, small platform cores, and bladelets). In addition to the dominant materials of quartzite and hornfels there is a higher frequency of silcrete use than in the late Holocene layers. Within the same series, three poorly preserved burials of small children were also recovered. Underlying this, a series composed of two units (Light Grey and Lower Red) produced a low-density sample of artefacts characteristic of the MSA and possibly associated to the Late MSA (<50 ka), yielding faceted and dihedral platforms on flakes, Levallois points, and backed microliths. Hornfels dominates, while quartz forms a minor component. Technology in the underlying deposit series (Dark Grey Series), conforms well with the later post-Howiesons Poort of rock shelters in the region (i.e., Klein Kliphuis), including Levallois and discoidal cores, and unifacially retouched and Levallois unretouched points, suggesting a possible flow of ideas, materials, and people across the catchment during MIS 3. The two units underlying this (WSS and RGS) provide assemblages associated with the early post-Howiesons Poort and Howiesons Poort (WSS) and Still Bay (RGS). The former includes numerous elevated proportions of silcrete, unifacial points, notched blades and more than 100 backed artefacts; 'Nubian' Levallois cores occur only at the transition between the Howiesons Poort and post-Howiesons Poort, where backed artefacts are replaced by unifacial points. The Still Bay in RGS latter includes about a dozen bifacial points made from a mix of raw materials, with quartzite dominant overall. In the lowermost units artefact density drops, quartzite dominance increases, and the retouched component comprises mainly simple notches and denticulates on large flakes and blades.

4.2.2.4 Putslaagte 8 (PL8)

Putslaagte 8 (31°56'16.72"S, 19° 9'19.35"E) is located in the low-lying valley of the ephemeral Putslaagte tributary. This feeds directly into the Doring River, ~26 km downriver from the Doring-Biedouw confluence (Figure 3.9). Due to the minimal flow in the tributary and unlikely presence of pooled water sources in the sandy base of the Putslaagte valley, the Doring River would have provided the most proximate water source for people using this shelter (Mackay et al. 2015). Two contiguous square meters were excavated at the site in 2010. Despite bioturbation, particularly in the lowermost units, a combination of AMS and OSL dating methods produced a chrono-stratigraphically sound sequence of shelter use that spans more than 75 ka, from the Holocene to the Late Pleistocene (Low & Mackay 2016). Putslaagte 8 is one of the few rock shelters in the study area to yield artefacts dated to within the Late Holocene, 700–150 cal yr BP (Table 4.1; Mackay et al. 2015). The next closest shelters that yield Late Holocene stone artefacts are De Hangen in the Cederberg, and Renbaan and Andriesgrond, in the Olifants River catchment (Plaskett 2012).

Unlike Klipfonteinrand, Putslaagte 8 lacks reliable technological and chronometric evidence for the mid-Holocene. Spits with OSL ages less than 17 ka were associated with the Oakhurst based on typo-

technological features considered regionally characteristic of the period (i.e., bipolar technology, naturally backed knives and the presence of ostrich eggshell (OES) and marine shell). Late Pleistocene LSA technocomplexes include assemblages conforming to region-wide characteristics defining the early LSA (~22-25 ka) and Robberg (~18-21 ka). MSA units (i.e., early MSA [>76 and 69-81 ka], Still Bay and Howiesons Poort to post-Howiesons Poort [58–71 ka], and late MSA [~33-45 ka]) are also present in the lower units of the site, yielding pulsed evidence of shelter use from MIS 3 to 5 (~33 to >76; Table 4.1; Mackay et al. 2015). An overview of PL8's Late Pleistocene LSA and mid-late Holocene deposits is provided in Mackay et al. (2015), with more detailed analyses performed on assemblages dated to between ~25-17 ka and the late Holocene by Low & Mackay (2016) and Plaskett (2012), respectively. Differences in lithic material use between Putslaagte 8 and other rock shelters in the catchment and wider region, as well as between Putslaagte 8 and the Doring River valley, are thought to represent change in raw material preference and source availability specific to Putslaagte 8's position within the wider landscape (Low & Mackay 2016; Low et al. 2017; Plaskett 2012).

4.2.2.5 Overview of rock shelter evidence

Each site has helped to expand on and refine the chrono-stratigraphic sequence of technological change in the Doring River catchment (Table 4.1). In most cases, publication of these findings provides a detailed assessment of the technological composition of Late Pleistocene MSA and LSA assemblages which indicate variation in the different modes and intensity of lithic reduction at each site. Thus, their findings help to develop a more nuanced understanding of tool production, use, and transport within their respective rock shelters and across the wider landscape. For the most part the typo-technological sequence identified in these shelters conforms well to inter-regional patterns of technological change.

The main trends observed from rock shelters in the Cederberg's marginal interior include evidence for localised lithic resource procurement during the early MSA, a predominance of denticulates during the MSA of MIS 5, and weak shelter signals during MIS 3 that include the post-Howiesons Poort and Late MSA Industries (Mackay et al. 2015). There is also a relatively late transition from the MSA to the LSA (<33 ka) in the interior compared to the coast, followed by a shift from distinct resource divisions during the early MIS 2 to an increase in coastal-interior interaction, exchange, and/or resource complementarity in the later part of MIS 2 (Mackay et al. 2015). The late MSA (~50-33 ka) yields the weakest signal for the Late Pleistocene deposits in the catchment, while mid-Holocene deposits are rare. One exception to the latter, is the first excavations at Klipfonteinrand 1 that yielded lithic technology associated with early to mid-Holocene shelter use (Thackeray 1977), and a human burial, with an age of 3825 ± 85 cal BP (Pta-1642; Mackay 2012). At almost all sites, Robberg and Howiesons Poort occupation produced the densest assemblages of artefacts, consistent with regional trends (Mackay et al. 2014a).

4.2.3 Open-air research in the Doring River valley

Consistent with southern African Late Pleistocene research of the last 50 years, the Western Cape interior has a deficit of open-air research, despite the abundance of Late Pleistocene archaeology found on and beneath its surface. This information-bias and the prioritisation of a landscape scale perspective motivated the 2013 excavation of Putslaagte 1 and the reconnaissance surveys along the Doring River valley (Mackay

et al. 2014b). Not only did the findings from these explorations challenge the regional occupation histories of the Western Cape (see Chapter 2), but they also revealed a landscape abundant in Late Pleistocene and Holocene buried and surface archaeology distributed along the Doring River valley. This prompted the formation of the Doring River Archaeological Project (DRAP, formerly the Doring River PaleoLandscape Project, from 2013-present), representing one of the few long-term, landscape scale research projects dedicated to open-air archaeology in South Africa—nearly a decade after the last GAASP. This project marks a shift in research interest in the catchment from rock shelter excavation to the open-air study of Late Pleistocene archaeology.

The DRAP has produced a series of published studies with "the long-term objective…to explore lithic technological organisation as a window into the evolution of human planning and mobility through the Late Pleistocene and Holocene" (Shaw et al. 2019, p.402). They prioritise technological analysis and the spatiotemporal distribution of stone artefacts across several high visibility, archaeologically-rich sediment stacks—a discontinuous set of erosional sediment mounds 6-10 m high occurring intermittently along the valley—located between the Bos and the Putslaagte outlets in the Doring River valley. Their findings emphasise the inadequacies of rock shelter datasets as representative of landscape scale patterns in human-environment interaction, by identifying patterns in landuse, and stone tool provisioning and reduction over the last 100 ka not apparent in the regional rock shelter sequence (Mackay et al. 2014b). The typo-technological composition of clustered surface artefacts identified on the sediment stacks of Uitspankraal 7 and 9 were also compared to rock shelters assemblages at Putslaagte 8, Klipfonteinrand and Mertenhof, tying together a landscape scale narrative of lithic provisioning and reduction that varied in response to resource proximity (Low & Mackay 2018; Low et al. 2017; Mackay et al. 2018; Watson et al. 2020).

The proximity of these shelters to the Doring River valley and its immediate tributaries make it possible to investigate Pleistocene and Holocene movement and resource use as a continuous network across an interior catchment, one that varies in geomorphology, ecology, and climate. One of the pivotal outcomes of the intensification of archaeological investigation within the Doring River catchment is the realisation that an exclusively shelter-specific focus is inadequate for understanding broader patterns of human land-use and movement—both within the catchment and between the interior and coast. The need for a landscape-scale perspective, coupled with an appreciation of the abundance of surface archaeology in the Doring River valley, now drives systematic efforts to study this open-air context (Low et al. 2017; Mackay et al. 2014b; Shaw et al. 2019; Will et al. 2015).

4.2.3.1 Early surveys of the Doring corridor & Putslaagte 1 (PL1)

The DRAP began as a reconnaissance effort in 2013, involving the survey of exposed archaeology on sediment stacks along the river in addition to the excavation of the sediment stack Putslaagte 1 (Mackay et al. 2014b). Early survey and subsequent studies along the Doring River corridor roughly pertain to the Doring River zone of the quaternary catchment, E24J (Figure 3.1). Mackay and colleagues identified at least 16 isolated sediment stacks, including Putslaagte 1, most of which yielded surface archaeology in high densities on both sides of the river channel (Figure 4.3). These stacks were characterised as terrace and slack water landforms on account of their similar compositions, (i.e., highly denuded sandy sediment often

found built up above and adjacent to the Doring River channel and connecting tributaries) and the rate of sedimentation suggested by similar OSL ages from upper and lower parts of a profile (i.e., Putslaagte 1; (Mackay et al. 2014b). However, investigation of the formation of these localities in relation to the surrounding valley is yet to be performed.

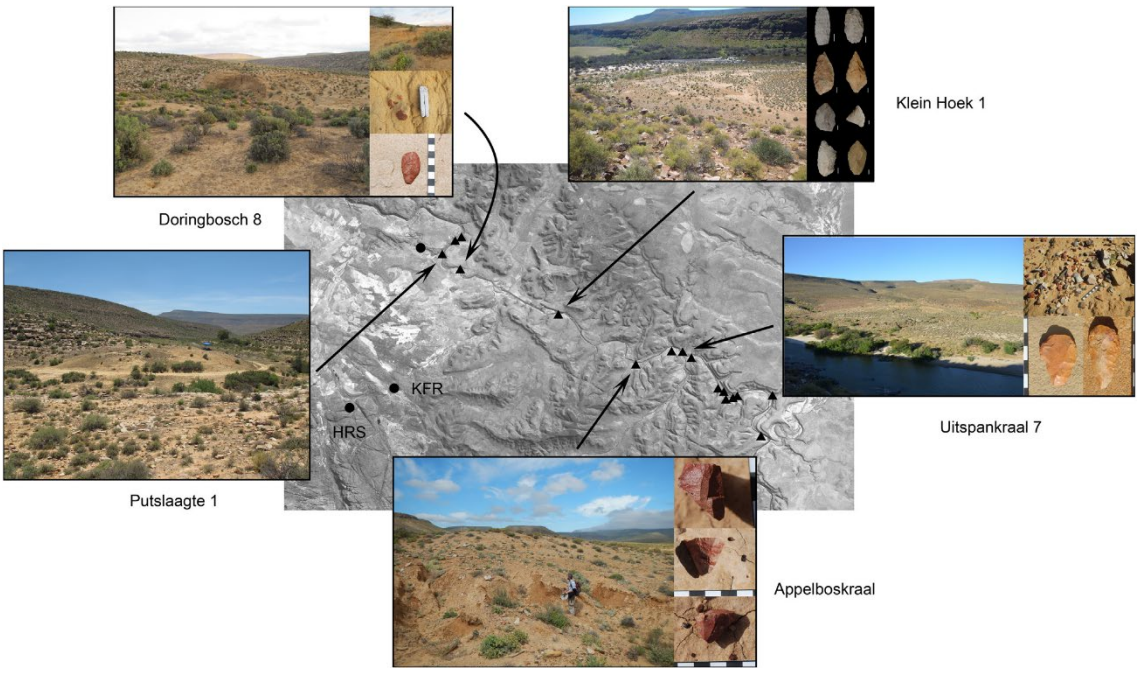

Figure 4.3. Select photographs of archaeology-bearing sediment stacks (Doringbosch 8, Klein Hoek 1, Putslaagte 1, Appleboskraal, and the case study, Uitspankraal 7), with examples of time-sensitive stone artefacts. Each locality is depicted in relation to their location along the Doring River valley and surrounding landscape. See Figure 5.1 for map details. Figured sourced from Mackay et al. (2014b).reconnaissance surveys of the Doring River Corridor. Source: Mackay et al. (2014b, Figure 4).

Drawing on typo-technological associations with regional rock shelter technocomplexes, Mackay and colleagues tracked temporally diagnostic artefacts at each locality and reported a collective record of surface archaeology spanning at least the last 200 ka, with MSA archaeology dominating most scatters. This was confirmed with the excavation and OSL dating of Late Pleistocene artefacts at Putslaagte 1, with two OSL samples from lower deposits taken 700 mm apart returning within-error ages of 58.8 ± 5.3 and 60.8 ± 5.2 ka, associating deposit burial with the end of MIS 4 and the beginning of MIS 3. These ages antedate the use of post-Howiesons Poort and Late MSA technology (Mackay et al. 2014b)—a period during which the regional rock shelter record suggests low intensity occupation or abandonment (Mitchell 2008).

Sediment directly overlying these burial ages preserved abundant evidence of stone knapping (6674 stone artefacts from a 2 m^2 pit; Figure 4.4). Technological analysis revealed the absence of retouched artefacts, laminar reduction and silcrete typical of late MIS 4/early MIS 3 reduction systems associated with the Howiesons Poort and post-Howiesons Poort. Thus, by process of elimination, coupled with sediment age, the assemblage was determined to be a Late MSA variant. This presents a mode of stone artefact reduction not observed in the Late MSA rock shelter record of southern Africa's summer rainfall region, taken to indicate inter-regional technological fragmentation during the later MIS 3 (Mackay et al. 2014b). If the chronological placement and typo-technological interpretation of Putslaagte 1's buried archaeology

is correct, then the abundance and different mode of Late MSA core reduction at this interior, open-air locality indicates reorganisation in the way humans interacted with their environment rather than total regional abandonment, challenging rock shelter-derived regional occupation histories (Mackay et al. 2014b).

This study is a cautionary example of the inherent limitations in applying rock shelter defined Industries and their temporal proxies to the landscape as a whole. Without the chronometric control attained in this study, the typo-technological composition of the buried assemblage would not be enough to confidently associate it with the Late MSA. This work provided the chronological framework for investigating questions of mobility, transportation, and provisioning. However, due to concerns over bioturbation, it is limited by the lack of ages from the upper sediments to cap the depositional history of its archaeology, rendering its chronological framework open-ended and the temporal scale for behavioural interpretation open to debate.

Figure 4.4. Western view of Putslaagte 1, with Doring River to the right and Putslaagte valley to the left of image (a), surface archaeology at Putslaagte 1 (b), and excavation pit, showing southern profile (c). Source: Mackay et al. (2014b, Figure 3).

4.2.3.2 Targeted and distributional surveys of the DRAP

In addition to the preliminary survey and excavations mentioned above, the DRAP has also produced several intensive examinations of the spatial, technological, compositional, and chronological signals of the exposed archaeology across several sites within the catchment (i.e., UPK9 and UPK7). These were carried-out as part of a series of targeted surveys at UPK7, (2014-2015) and UPK9 (2014 and 2019). The objective was to record the technological composition and spatial distribution of typo-technologically coherent artefact clusters (Low et al. 2017; Will et al. 2015).

One study compared the technological composition of an isolated dense scatter of surfaces artefacts at UPK7 and Early LSA and Robberg-bearing deposits at the Putslaagte 8 rock shelter. Analysis revealed relatively low frequencies of hornfels cores at Putslaagte 8 compared to the open-air context, whereas quartz components, including cores, were observed in abundance at Putslaagte 8 and absent from UPK7 (Low et al. 2017). This difference was interpreted as representing source-proximate acquisition and core reduction, with preferential blade transport from the two localities, reflecting UPK7's local source of hornfels from the Doring River channel, and the immediate proximity of Putslaagte 8 to quartz pebbles in

the conglomerates forming the shelter. The high frequency of hornfels blades in Putslaagte 8 supports this inference, suggesting the transport and eventual discard of hornfels blades away from their place of manufacture (i.e., Putslaagte 8 which is located ~2.5 km from the Doring channel; (Low & Mackay 2016).

The dominance of quartzite and hornfels in artefact assemblages at all Doring River open air sites is consistent with their local availability along the river. Equally, however, this makes the variable occurrence of rarer materials like silcrete, quartz and chert observed at each locality noteworthy. Quartz and chert occur more often and in greater quantities in rock shelter assemblages, closer to their source in the Cape Fold Belt system. Thus, their occurrence at localities such as UPK9, UPK7 and Doring Bos 8 is potentially indicative of the scale of mobility that existed between the Doring River valley and its wider catchment.

In addition to the Early LSA lithic scatter at UPK7, a second cluster was identified amongst a dense scatter of surface artefacts. Clustering was determined visually based on the spatially constrained accumulation of silcrete artefacts and typo-technology considered characteristic of the post-Howiesons Poort (i.e., points and blades produced using specific 'Nubian' Levallois core reduction techniques, unifacial points, scraper and the preferential selection of silcrete; Low et al. 2017). This cluster was found overlying more weathered, nodulated sediment than the Early LSA scatter, and located in the central southern slope of the sediment stack, south-west of the Early LSA distribution. Support for the inferred age of both clusters was based on the appearance of underlying deposits and how weathered they were compared to an OSL-dated consolidated sediment unit sampled on the far side of the locality, which returned two ages dating to ~30 ka (Late Pleistocene LSA, MIS2). In contrast to this, the unconsolidated sands were dated to within the last century (~0.07 ka; Shaw et al. 2019). These samples, together with a single sample collected from UPK9 form the only chronometric ages for comparing against the Stone Age and Industry level ages of time-diagnostic artefacts at both localities.

The Early LSA scatter is believed to overlie the consolidated sand, associated with a maximum discard age of ~30 ka, based on Early LSA rock shelter occurrences in southern Africa (~18-40 ka; Lombard et al. 2012) and the catchment (~22-25 ka at PL8; see Low & Mackay 2016). Given the more weathered, nodular appearance of the sediment underlying the post-Howiesons Poort cluster Will et al. (2015) regarded this unit and its overlying surface artefacts as older than the 30-ka consolidated sands. Thus, the condition of the underlying sediment was employed in both studies to support the inferred age of each cluster. This provided a framework of chronological association for non-diagnostic artefacts of the same cluster at the temporal scale of the Industry. However, the limited coverage and general paucity in chronometric ages for these sediments coupled with the lack of a dedicated study of the formation and sedimentology of the deposits at this locality means that the inferred relative chronology of UPK7's surface archaeology is based on untested assumptions about the depositional history of the locality and thus the spatio-temporal integrity of the archaeology. As a result, the interpretations presented in both studies are only as strong as their typo-technological association with rock shelter Industries and their chrono-stratigraphic sequences. Moreover, the spatial and topographic separation of the two clusters meant that the stratigraphic position between them was not demonstrable.

Following these studies, the DRAP carried-out large-scale, systematic surveys of visible surface artefacts (cores and implements) across the consolidated sediments of six sediment stacks throughout the

Doring corridor: Putslaagte 1 (PL1), Doring Bos 8 (DB8), Klein Hoek 1 (KH1), Uitspankraal 1 (UPK1), UPK7 and UPK9 (see (see Shaw et al. 2019). The distributional coverage of this dataset enables the spatial patterning and composition of each sediment stack's surface artefacts to be assessed and compared. Thus, providing a means of testing the validity of the clustering observed in Low et al. (2017) and Will et al. (2015), and to build a landscape scale narrative about the occupation history of the valley and technological trends in reduction and discard behaviour relative to rock shelter findings.

A qualitative overview of the spatial distribution and composition of each locality's surface archaeology has been published in (Shaw et al. 2019). Their results indicate horizontal variability in the abundance, density, and distribution of time-sensitive and technologically informative artefacts, within and between each locality, largely supporting the horizontal patterns observed in earlier reconnaissance and targeted surveys. The combined temporal coverage of the six survey localities suggests a long history of repeated occupation of the valley system from at least the Middle Pleistocene through to historic times (see Table 4.2), with the presence and abundance of each technocomplex considered representative of context-specific occupation trends across the region.

Table 4.2. Site summary from the DRAP distributional surveys carried-out in 2018 and 2019 (Phase 1), providing information on the survey coverage, artefact count and density, dominant and notable lithic materials present at each site (>2%), together with recognised culture historic units and their associated stone ages and epochs. Published OSL ages for UPK9, UPK7, and Putslaagte 1 are given without additional context. For this the reader is referred to their respective sources: Watson et al. (2020), Shaw et al. (2019), and Mackay et al. (2014b). Table information sourced from Shaw et al. (2019) and supplemented from the DRAP Phase 1 dataset.

Site	Location[#]	Distance from DBC[&] (km)	Height above river (m)	Area (m^2)	Artefact N	Density (artefact* n/m^2)	Artefact materials[+]	Industries[^]	Stone Age Association[^]	Epoch[^]	OSL ages (ka)
UPK9	32° 2'17.69"S, 19°24'30.26"E	0	15-30	27,013	9486	0.35	quartzite, hornfels, quartz, chert, pottery, ochre, silcrete, ironstone, glass	Robberg (22-16 ka), Oakhurst (14-8 ka), Wilton (8-12 ka), post-ceramic (<2 ka)	LSA, Neolithic, Historic, MSA, ESA	Middle, Late, and terminal Pleistocene; Middle and Late Holocene	~27 ka
UPK7	32° 2'12.02"S, 19°24'17.38"E	0.5	12-26	42,326	4285	0.1	quartzite, hornfels, quartz, silcrete, chert, ochre, sandstone	Still Bay, Howiesons Poort, post-Howiesons Poort, late MSA, eLSA, Robberg (22-16 ka), Oakhurst (14-8 ka), Wilton (8-12 ka), post-ceramic (<2 ka)	MSA, LSA, Neolithic, Historic, ESA	Middle, Late, and terminal Pleistocene; Middle and Late Holocene	~30, ~0.07
UPK1	32° 2'15.24"S, 19°23'19.10"E	2	14-31	96,699	1252	0.01	quartzite, hornfels, pottery, ochre, quartz, silcrete	Achuelean, Still Bay, Howiesons Poort, post-Howiesons Poort, Early/Late MSA, Wilton	MSA, Neolithic, ESA, LSA, Historic	Middle and Late Pleistocene	-
KH1	32° 0'3.32"S, 19°17'10.61"E	12.5	9-17	19,432	6747	0.35	hornfels, quartzite, chert, silcrete, quartz, sandstone	ESA, Still Bay, post-Howiesons Poort, late MSA, Early LSA, Robberg	MSA, LSA, ESA	Middle and Late Pleistocene	-
DB8	32° 0'6.31"S, 19°16'37.36"E	13.5	3-21	29,538	1814	0.06	hornfels, quartzite, quartz, chert, silcrete	Still Bay, Howiesons Poort, post-Howiesons Poort, late MSA, eLSA, Robberg (22-16 ka), Oakhurst (14-8 ka), Wilton (8-12 ka)	MSA, LSA, ESA	Middle, Late, and terminal Pleistocene; Middle and Late Holocene	-
PL1	31°56'37.53"S, 19°10'31"E	24.5	6-14	2941	636	0.22	hornfels, quartzite, silcrete	post-Howiesons Poort, late MSA	MSA, LSA	Late Pleistocene	~58-61

[#] Locations given in degree minutes seconds based on the WGS1984 geographic coordinate system; DBC: Doring-Biedouw confluence; [*] Cores, implements, pottery, ochre (>30 mm). Flakes excluded from sample; [+] Dominant and minor-but-notable (>2%) lithic material components; [^] Inferred temporal and typo-technological association based on Rock Shelter technocomplexes and chronometric ages, orders by artefact frequency using the DRAP Phase 1 dataset.

Common trends that were observed between rock shelters and sediment stacks include the regular and often dense occurrence of Robberg and Oakhurst, and the limited occurrence of Early LSA technology (Shaw et al. (2019). Their work also confirmed the disparity between the abundant, high-density records of Howiesons Poort technology in rock shelters and its sparse occurrence in open-air settings (Hallinan 2013; Hallinan & Parkington 2017). However, their restricted coverage within the Doring River corridor to the surface of highly exposed sediment stacks may fail to capture the landscape distribution of Howiesons Poort artefacts. Moreover, the end products denoting the Howiesons Poort Industry were possibly discarded at different stages of reduction across the landscape and thus do not conform to the expected form for identifying Howiesons Poort assemblages. Their discard pattern could also reflect a more dispersed, highly mobile approach to land use and not accumulate in the same place over time, rendering this Industry as 'invisible' beyond the sediment traps of the rock shelters.

There is also the question of preservation, whereby the smaller size of Howiesons Poort backed and notched pieces make them more vulnerable to entrainment and burial than the typically larger, heavier bifacial implements associated with other MSA Industries (i.e., the bifacial foliates of the Still Bay). One counter to this is that clusters of microlithic artefacts, characteristic of the Robberg, occur at UPK9, indicating that small artefacts diagnostic of Industries more than 10,000 years old have been preserved in the Doring River valley, despite their current exposure. Whatever the reason for the absence or rarity of time-diagnostic artefacts, caution is required when using this trend as evidence for an absence of activity during their period of use in rock shelters, without first investigating preservation bias. Nor can this trend be considered representative of differences in provisioning strategies or discard behaviour between different contexts without sampling across different landscape settings—not just sediment stacks singled out due to their highly visible archaeology and geomorphic conditions.

Other discrepancies between the open-air and rock shelter archaeology noted during the DRAP surveys include strong Late MSA and Late Holocene Wilton signals in the former compared to their relative absence in the latter. Their presence within the same catchment, but outside the confines of the rock shelter emphasise the limited ability to capture the full occupation history of a landscape without the inclusion of open-air archaeology.

Shaw et al. (2019) also identified visible differences in the dominance of LSA and MSA artefacts between sediment stacks, even for localities with less than 500 m separating them (i.e., the dominance of MSA over LSA artefacts at UPK7 compared to the LSA dominant scatters at UPK9). Again, without an understanding of the formation history of these localities such differences cannot be confidently interpreted as the result of subtle changes in land use, i.e., due to decreasing reliance on river channel sources during the LSA compared to the MSA (as in Hallinan & Parkington 2017), or change in provisioning strategies due to changes in climatic conditions between glacial/interglacials (as in Mackay et al. 2018), or due to differences in the formation and preservation of deposits and the associated archaeology at each of these sediment stacks.

Industry level clustering has been suggested due to spatially structured distributions of similar artefacts with variance between Industries in their horizontal extent and density (Mackay et al. 2014b; Shaw et al. 2019). In accordance with Will et al. (2015) and Low et al. (2017), they suggest that clusters of temporally similar technology are behavioural aggregates, indicative of intact, repeated stone tool

manufacture that has occurred within the same Industry-defined time bin, despite clear indications of erosion at each locality.

Several explanations were proposed by Shaw and colleagues for variation in core and implement density between localities, including depositional visibility in the case of low-density sites (i.e., UPK1 and DB8) and differential erosion in the case of UPK7. However, this dynamic is less clear at UPK9, KH1 and PL1, which yield high artefact densities in high visibility contexts. Shaw and colleagues suggested that differential distribution of Industry-specific clusters observed at localities like UPK9 possibly reflects the preferential use and occupation of surfaces that are sandy, rock free and proximate to water (after Sampson 1984). The abundance of surface archaeology recorded at each locality is also a possible indication of source proximity (i.e., hornfels river cobbles, quartzite cobbles and surrounding outcrop). The abundance of cores in particular, support this proposition, with cores often being quite rare in shelter contexts, but shown to dominate the artefacts at each sediment stack (Shaw et al. 2019). This could reflect a strategy of 'gearing up' at these localities, as suggested in the analysis by Lin et al. (2016) of MIS3 technology at Putslaagte 1 (see above).

4.2.3.3 Assumptions and limitations

Thus far, the DRAP has produced research that presents landscape scale interpretations of human-environment interaction that tie open-air typo-technological assessment of surface and buried archaeology to catchment and regional rock shelter sequences. In doing so, these studies present a history of occupation and land use behaviour that both conforms to and challenges rock shelter evidence covering the last 100 ka. This work underscores the merits of including the open-air perspective when modelling human-environment interaction across a landscape and region. It demonstrates that without this information, rock shelters fall short in capturing major shifts in occupation (i.e., human activity during the later MIS3) as well as the more nuanced dynamics of stone tool reduction and resource exploitation between people and their surrounds. However, despite the DRAP's progress in investigating open-air archaeology in a systematic way. Across multiple localities, it has failed to generate robust links between observation on the one hand and behavioural interpretation on the other. This is due to three critical limitations:

1. There are no dedicated studies of sediment stack formation.
2. There is an absence of chronometrically dated sediment units to reconstruct the depositional history of each locality.
3. There is an over-reliance on the visual evaluation of surface archaeology to define and interpret their spatial association, integrity, and age.

The lack of significant work carried-out on the formation of the Doring River valley's sediment stacks limits what can be said about their history and the processes involved in sediment accumulation, transformation, and erosion. This is evident in the varied ways the geomorphology of each sediment stack has been described (i.e., as palaeoterrace, slack water deposits, dunes, and in more general terms as sediment stacks). This inadvertently invites the assumption that all sediment stacks share the same depositional history, which can lead to the extrapolation of findings from one locality to account for all localities and their respective archaeology. An understanding of the unique formation histories of these localities can help isolate the main processes involved in preserving and exposing their archaeology, the potential duration of artefact exposure as well as possible localised changes in environmental conditions.

Fundamental to establishing the depositional history of these sediment stacks is to develop a geochronology for the timing and rate of sediment accumulation and erosion. This requires the application of suitable chronometric dating techniques coupled with a sampling strategy that allows for the differential timing and spatial extent of deposit accumulation and erosion across a given locality. Although OSL burial ages were produced for some localities (i.e., PL1, UPK7 and UPK9), these were preliminary and restricted in number and thus coverage (e.g., Mackay et al. 2014b; Shaw et al. 2019; Watson et al. 2020).

Establishing a geochronology that is embedded in the sedimentary and geomorphic formation for these localities will also aid in contextualising and independently testing the inferred chronology of time-diagnostic artefacts. As it stands, the inferred age of artefact clusters—based on their typo-technological associations with rock shelter and buried open-air assemblages (specifically, Putslaagte 8, Mertenhof, Klipfonteinrand, and Putslaagte 1)—is problematic due to the small proportion of artefacts (i.e., 7.2% of the entire DRAP Phase 1 dataset) which reflect the forms observed in rock shelter assemblages (Shaw et al. 2019, p.406). Not all tool forms in rock shelters can be expected to manifest at the same frequency, time or at all in open-air settings and vice versa. Thus, chronometric dating of underlying sediment and archaeological features, such as hearths, are necessary for providing an independent means of testing the ages of time-diagnostic artefacts and to determine the timeframe within which both time-diagnostic and non-diagnostic artefacts can be temporally constrained.

Some attempt has been made to corroborate inferred artefact ages at UPK7 and UPK9 with reference to OSL ages sampled from consolidated deposits exposed at each locality (e.g., Shaw et al. 2019; Watson et al. 2020). However, due to the absence of a dedicated geoarchaeological study, the sedimentological composition and stratigraphic relationship of these samples have not been established, nor is there a clear understanding of how their formation relates to the surface archaeology in question. For example, how does the timing and duration of artefact accumulation relate to deposit formation? What is the timing and duration of surface and artefact exposure? And do artefacts remain on the deposit they were originally discarded on, or have they since lagged onto an older deposit or moved onto a younger deposit?

Although technologically and spatially focused studies from the DRAP acknowledge the presence of active erosion (Shaw et al. 2019; Will et al. 2015) and sometimes inspect it (Low et al. 2017), the experimental and simulation study of Phillips et al. (2019) is used in place of an archaeological study. In this work, a moderately sloped area at UPK7—devoid of artefacts—with exposed hard surface conditions was used to investigate the vulnerability of surface artefacts to entrainment and attrition for 22 months and then projected over extended intervals of time (Phillips et al. 2019). This study used a replicated LSA microlithic assemblage of freehand and bipolar cores, flakes, and blades. These were placed within the upper zone of a minor hillslope of moderate gradient (10-11º) and their spatial disaggregation recorded either side of the wet season. Artefact displacement occurred rapidly (abruptly for flakes in the first recording and more steadily downslope in subsequent seasons), to the point that simulation of artefact movement and attrition under the current surface conditions showed assemblage disaggregation within a few centuries and complete loss within a millennium, in which case the assemblage would have either been incorporated into the surrounding sand dune or removed by way of rill channel into the riverbed in the south.

Phillips et al. (2019) is drawn on to support the view that exposure and high visibility of surface

artefacts happened recently, with artefact abundance and clustering cited as additional supporting evidence for a spatially intact assemblage (Shaw et al. 2019). This helps to justify the temporal bracketing of clusters based on the dominant Industry or Stone Age present. Consequently, through a kind of cyclical reasoning, clusters are employed as both brackets constraining the duration and timing of artefact accumulation, as well as proxies for artefact condition, preservation, and the duration of exposure. This approach inadvertently conflates behaviour with time and preservation, potentially undermining the massive amount of spatial and typo-technological data collected, analysed, and published upon by the DRAP to date. Consequently, without an understanding of the periodicity of sediment accumulation and erosion occurring at each locality, the chronological interpretations put forward regarding both the timespan and spatial integrity of artefact accumulation remain questionable.

Moreover, clusters of time-diagnostic artefacts identified at each locality have largely depended on visual assessment. However, there is the ever-present danger of the human eye seeing pattern where it might not exist. For this reason, at a minimum, the spatial distribution and structure of surface archaeology needs to be tested for complete spatial randomness. Artefact density is also often used as an indicator of the duration of accumulation, with low density clusters interpreted as single events of activity, while high densities of clasts are considered aggregates of long-term accumulation. Again, however, spatial association has only been established through visual assessment. Moreover, artefact density (and clustering) could reflect any number of processes (i.e., topographic, sedimentological, biological or behavioural; Knight & Stratford 2020), thus requiring in-depth consideration of these processes to understand the source(s) of artefact spatial patterning.

The experiment and simulation study published in Phillips et al. (2019)—carried out in supplementation to this thesis—demonstrated that artefacts exposed under the current climatic conditions and human landuse can result in assemblage disaggregation and attrition beyond a 5-metre survey zone within 1000 years of discard (outlined above). This was supported by a RUSLE analysis of the erosion potential and risk of artefact attrition at Klein Hoek 1, suggesting rapid and on-going erosion associated with dispersed sets of diagnostic artefacts (Ames et al. 2020). Despite both studies contributing to the DRAP's published output, the processes of erosion over time, and as a modifying factor in the distribution, condition, and inferred age of the surface archaeology at these localities is yet to be fully investigated and published (although see comments on erosional potential in Ames et al. (2020) and size-sorting in Low et al. (2017)). This calls into question the validity of the assumed spatial integrity and age of the surface archaeology at these localities.

4.2.4 Concluding statement

The assumptions made by the DRAP concerning the spatial integrity, age and preservation of surface archaeology exposed on each sediment stack need to be investigated using geoarchaeological methods. Without this, the landscape scale interpretations of human activity remain questionable. The objective of the following chapters is to rectify the lack of chronometric control and insight into the depositional history of the surface archaeology studied by the DRAP, using the archaeologically rich locality, UPK7, as a case study.

CHAPTER 5.
CASE STUDY AND METHODS

5.1 Introduction

In the preceding chapter, three fundamental issues were identified with the DRAP's research on the open-air archaeology of the Doring River valley: (1) the formational context of the surface archaeology has not been studied and is not well understood, (2) the geochronology is poorly developed, and (3) a dedicated study of artefact spatial integrity has not been performed. Each of these issues will be dealt with in this thesis in their listed order. This study employs a combination of earth science and archaeological methods to investigate the depositional history of UPK7 and its surface archaeology across a range of spatial and temporal scales (specified below). This approach takes its inspiration from the international (Holdaway & Fanning 2014 and citations therein) and more proximate projects (i.e., Felix-Henningsen et al. 2003; Fuchs et al. 2008; Kandel & Conard 2012; Kandel et al. 2003) that employ geoarchaeological methods to investigate Holocene and Late Pleistocene open-air archaeology.

The objective of this chapter is to outline the geoarchaeological methods and materials employed to investigate the depositional history (i.e., sedimentology, chronology, surface morphometry) and spatial integrity of the surface archaeology. It begins by introducing UPK7 as the selected case study, followed by an outline of the spatial infrastructure used to interlink the spatio-temporal data collected on its sedimentology, chronology, surface morphometry, and archaeology. The subsequent sections present the methods employed to account for the issues listed above. They start by focusing on the methods used to investigate the sedimentology and chronology of the locality, followed by the characterisation of UPK7's surface condition and morphometry. The latter connects the depositional history of UPK7 to the formation of the archaeological record by determining the hillslope and surface conditions that can inhibit or promote the visibility, movement, and weathering of artefacts, thereby influencing their spatial patterning. The final section outlines the approach, methods and materials employed to investigate the spatial organisation of the surface archaeology and its relationship with UPK7's depositional history.

5.2 Case Study: Uitspankraal 7 (UPK7)

At least 16 sediment stacks yielding concentrations of visible surface archaeology were identified and recorded by the DRAP (Shaw et al. 2019; Figure 5.1; Appendix 2). Of these, Uitspankraal 7 (UPK7) was selected as the primary case study for this thesis. The location, geomorphology, and archaeology of UPK7, together with previous research on this locality provides an appropriate starting point for carrying-out a geoarchaeological investigation of the DRAP open-air dataset.

UPK7 is located within the bounds of Uitspankraal farm, at the south-eastern end of the study area and 0.5 km downriver from the Biedouw-Doring River confluence (Figure 5.1). This locality is on the northern side of the Doring River, making it difficult to access from the south when the river is in flood. It occurs at the southern toe of a long colluvial hillslope, bounded on its western and eastern sides by two tributaries (Figure 5.1). The closest sediment stack to UPK7 is UPK9, which is located ~250 m east of UPK7's eastern tributary. UPK9 also yields surface archaeology, associated with the ESA, MSA, and LSA,

but is dominated by the LSA. Historic artefacts, features, and landscape modifications were also observed across and proximate to this locality (i.e., a saddle badge dated to 1851, glass, ceramics, fencing wire, stone buildings, historic hearths, a dirt road that runs from the river to a northern plateau on its eastern side, trackways, powerlines, and runoff trenches to divert surface water off the road). Unlike UPK9, UPK7 appears devoid of stone structures or other historic modifications (e.g., roads, stone hearths, building, drainage). This suggests that UPK7 was subjected to less historic activity, possibly due to its separation by the eastern tributary. However, this may not have been an inhibiting factor for grazing.

UPK7 is also one of the most thoroughly surveyed and analysed sediment stacks in the study area, which is evident from the preceding review (Chapters 3 & 4) and published research by the DRAP (Low et al. 2017; Phillips et al. 2019; Shaw et al. 2019; Will et al. 2015). Thus, the spatio-temporal assumptions and behavioural interpretations presented in each of these published works can be tested.

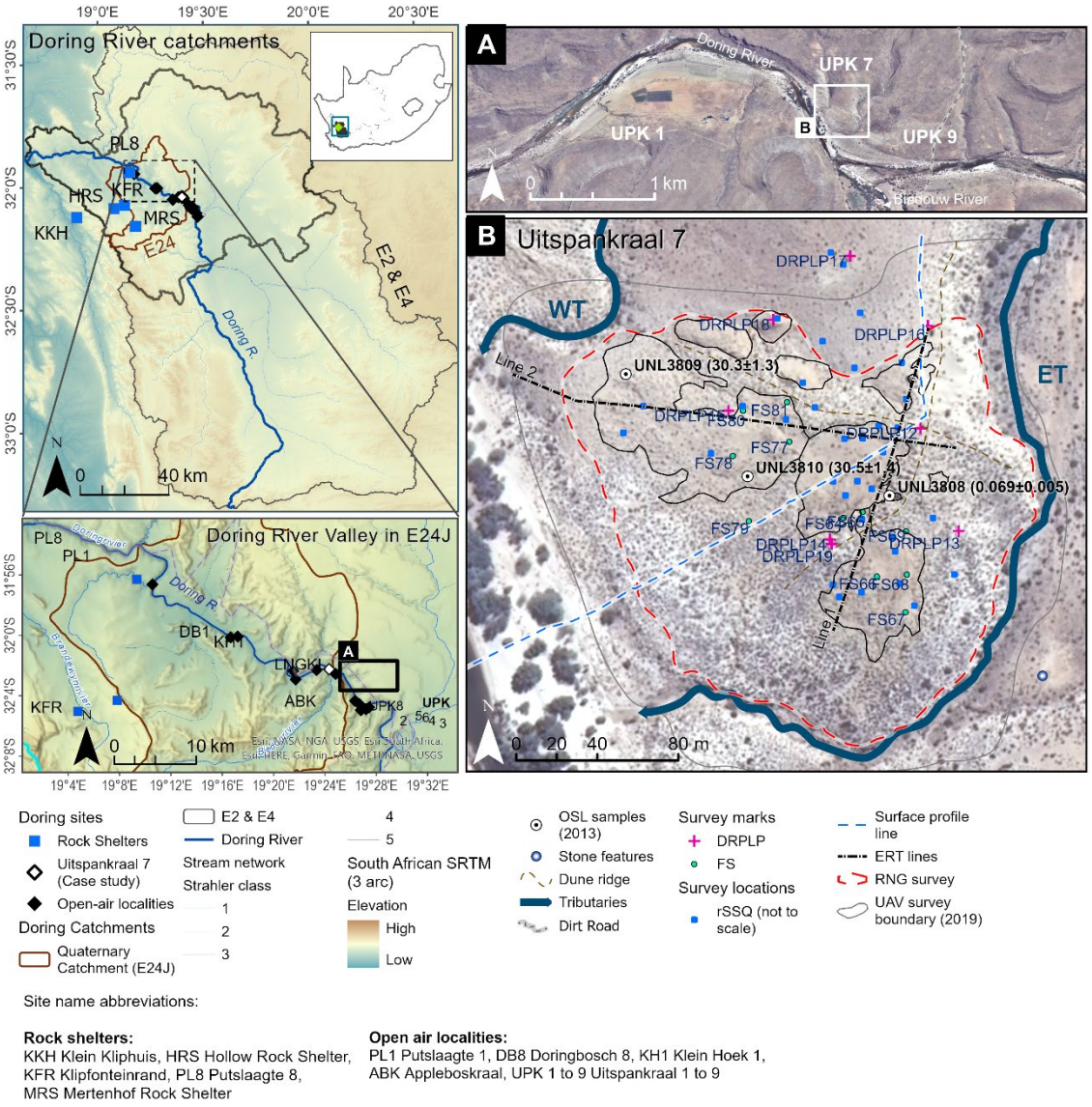

Figure 5.1. A nested map series of the study area, archaeological sites mentioned in text and UPK7, shown at different spatial scales. Site locations are depicted within southern Africa (see inset), the Doring River secondary catchment (catchment's E2 & E4), and a detail of the Doring River valley quaternary catchment, E24J (brown polygon), underlain by catchment digital elevation models (DEMs) and the river system (blue lines). Rock shelters are shown as blue squares, open-air sites as black diamond, and the location of UPK7 as a white diamond. Map (A) shows aerial footage of the Doring-Biedouw confluence and the location of UPK7 in relation to other proximate sediment stacks (UPK 9, and UPK1). Map (B) depicts an aerial of UPK7, the location of consolidated and vegetated loose sand, surface rills and the western (WT) and eastern tributaries (ET). See legend for further details on symbology and site name abbreviations. The Doring River catchment map (E2 and E4) is set against a hole-filled 90 m SRTM DEM processed by Jarvis et al. (2008). The Doring River valley E24J inset uses the World Hillshade, owned by Esri and processed by Esri, Airbus DS, USGS, NGA, NASA, CGIAR, N Robinson, NCEAS, NLS, OS, NMA, Geodatastyrelsen, Rijkswaterstaat, GSA, Geoland, FEMA, Intermap, and the GIS user community (URL: https://services.arcgisonline.com/arcgis/rest/services/Elevation/World_Hillshade /MapServer).

Three OSL samples were previously collected from two deposits at this locality (UPK7-1/UNL3808, UPK7-2/UNL3809, UPK7-3/UNL3810) as part of the 2013 reconnaissance survey (Figure 5.1). Two samples (UNL3809 and UNL3810) were collected from partly consolidated yellow sand, which date to at least the last glacial period (30.3 ± 1.3 ka and 30.5 ± 1.4 ka; Shaw et al. 2019, p.411). A third sample (UNL3808) was collected from semi- to unconsolidated vegetated sand that dates to within the last century (0.069 ± 0.005 ka; Shaw et al. 2019, p.411). The additional OSL samples were sent to different laboratories, prepared, and analysed under slightly different conditions. A full report on the preparation and measurement of these samples can be found in the SOM of Shaw et al. (2019). However, the complex geomorphology of the locality's land surface was not formally studied when these samples were collected and the sediment units are unlikely to be restricted to these two deposits—early geospatial surveys indicate the presence of a series of sedimentary units and a range of erosional and depositional features, within and beyond the main archaeological exposure (Figure 5.2). These are compared in the Discussion Chapter 8 to the results attained from the OSL analysis presented in Chapter 6.

The exposed surface of UPK7 also yields an inferred chronology that spans two glacial and two interglacial periods—from at least the Late Pleistocene early MSA to the late Holocene ceramic LSA (MIS 5 to MIS 1). Visual assessment of UPK7's surface artefacts suggested high levels of spatial integrity, despite its denuded surface (Low et al. 2017; Mackay et al. 2014b; Shaw et al. 2019; Will et al. 2015). This was inferred from the clustered occurrence of technologically similar and time-diagnostic artefacts in patches across the locality (see Figures 5.2 and 5.3). These clusters are associated with the Still Bay (bifacial points), Post-Howiesons Poort (unifacial points), Early LSA (small blades and platform cores), Oakhurst, mid-Holocene Wilton, and late Holocene (pottery; see Figures 5.2 and 5.3). Moreover, opportunistic refit sets were identified in both the post-Howiesons Poort and Early LSA clusters, and in non-diagnostic, low density clusters on the lower hillslopes of UPK7's consolidated sediment. The lack of clear defining characteristics for identifying middle and late Holocene artefacts—except late Holocene pottery use—meant that its occurrence at UPK7 remains uncertain. Clustering is mostly observed at the top of the sediment stack along with the highest artefact densities, raising the question of a preservation bias and differential disaggregation of artefacts between the top and low areas of the locality. However, refit sets found in the lower hillslope zones run counter to poor spatial integrity.

Added to the typo-technological studies at this locality is the actualistic investigation of current and simulated stone tool response to exposed surface conditions on UPK7's consolidated sediment (Phillips et al. 2019). This work provides a baseline expectation for how long it would take for exposed artefacts of UPK7's consolidated sediment to lose spatial structure (if initially clustered) under current climatic conditions over a given duration of exposure, and the kinds of clasts/artefact classes more likely to disperse.

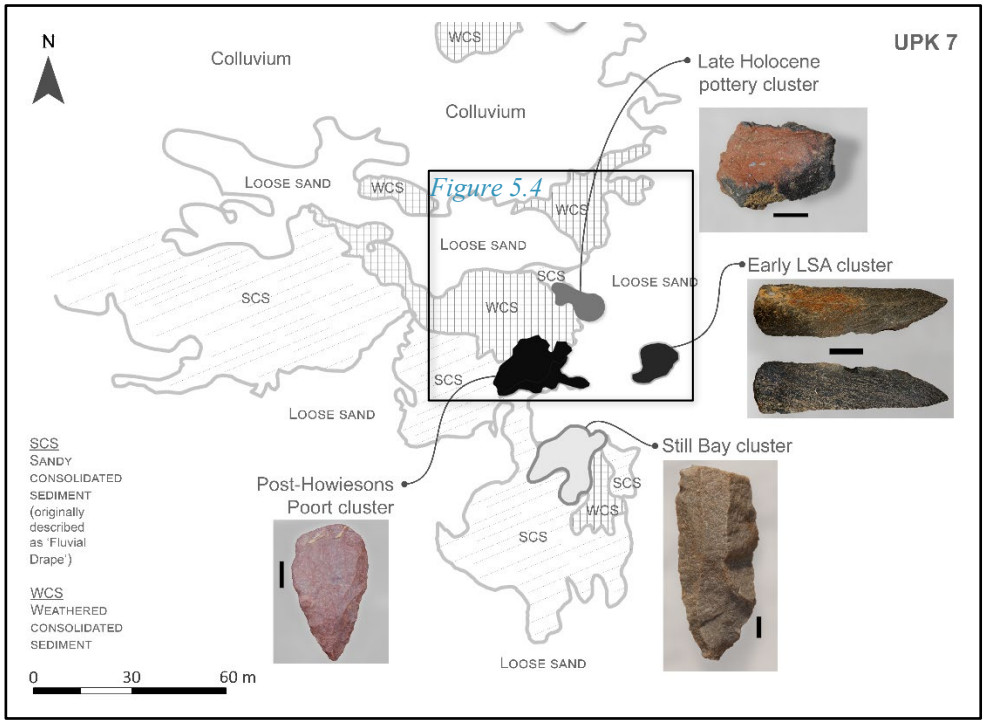

Figure 5.2. Map of UPK7 artefact clusters and sediment units, with photographs of example pieces (photo scale = 10 mm): dorsal and ventral side of a hornfels burin blade from the Early LSA scatter, pottery fragment from the Late Holocene cluster, silcrete Levallois point from the post-Howiesons Poort cluster, and a unifacial point from the Still Bay cluster. Modified from Will et al. (2015) to clarify the estimated extents of each sediment unit. Black box refers to Figure 5.3, below.

One area that requires clarification before outlining the methods for this study is the notion of site and how the DRAP localities relate to this. The following study does not treat UPK7 as an archaeological site in the classic sense (Dunnell 1992), since the visible extent of the artefact scatters may reflect multiple cultural and non-cultural processes acting at different spatial and temporal scales. Moreover, it does not form the basic unit of analysis for the surface archaeology—the artefacts themselves do. Instead, UPK7 is treated as a sample location, nested within of the Doring River valley and catchment. This location represents a specific set of geomorphic characteristics that make it both a continuous, yet differential part of the surrounding landscape (Butzer 2008; Holdaway & Fanning 2014). For this reason the physical and anthropogenic environment presented in the preceding study area chapters is drawn on at the start of the results to provide a macro and mesoscale context (i.e., regional, catchment, and valley) for understanding UPK7's sedimentology and geomorphology, and to help determine the main process(es) involved in their formation and, ultimately, its impact on the archaeological record at the micro-(locality) scale (Butzer 2008).

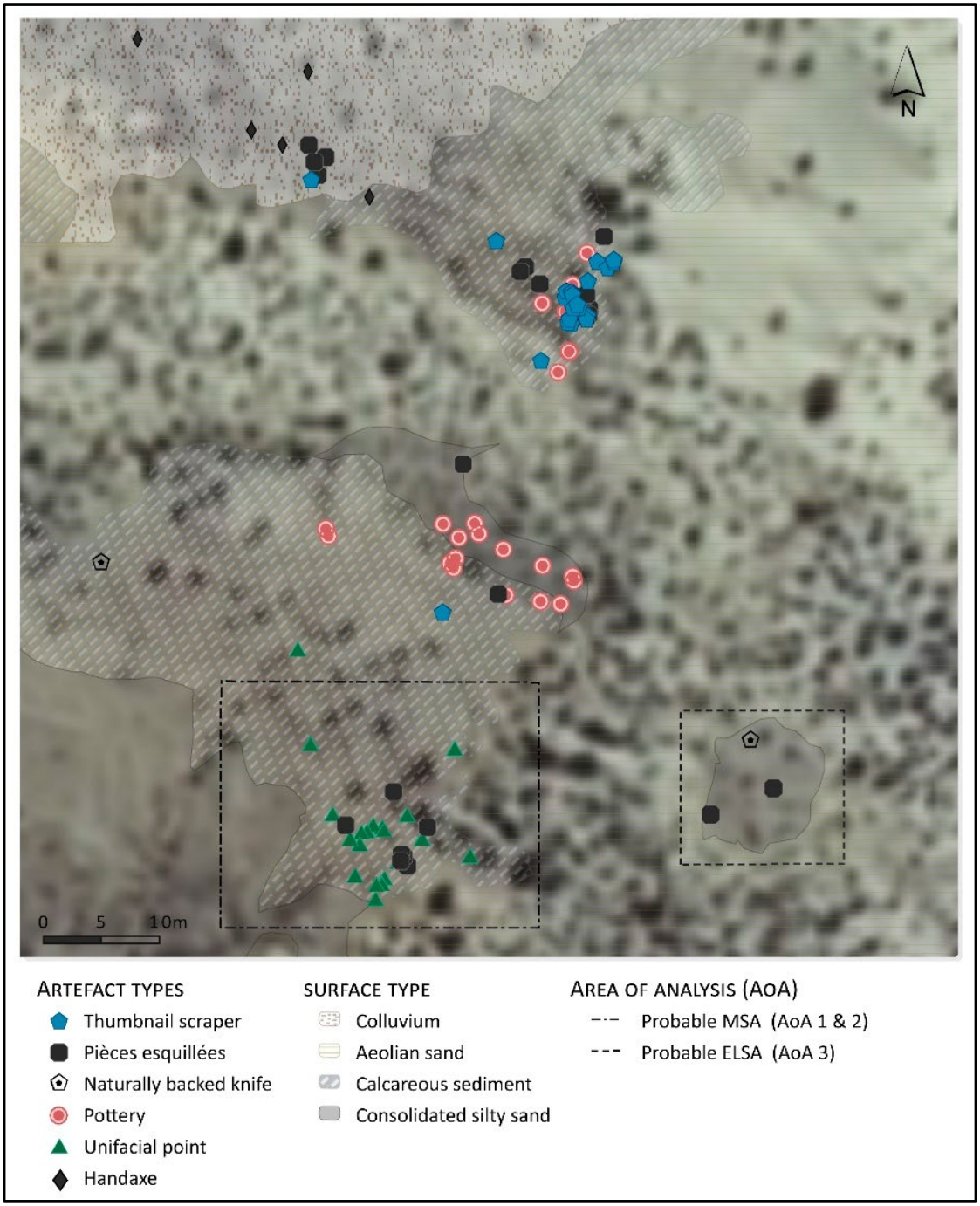

Figure 5.3. Detail of UPK 7's 2015 record of the spatial distribution of time-diagnostic artefacts against 2010 aerial imagery showing vegetation coverage as dark patches contrasted against the sand-coloured surfaces of consolidated and unconsolidated sediment. See legend for more detail. Dashed lines indicate areas of analysis (AoA) for the post-Howiesons Poort and Early LSA clusters. Map sourced from (Low et al. 2017).

5.3 Geospatial Infrastructure

A scale-based, multi-proxy approach relies heavily on geospatial data. Geospatial control is essential for interlinking environmental and cultural data across multiple spatial and temporal scales (Butzer 2008; Holdaway & Fanning 2014). For this reason, a range of geospatial methods was employed for sedimentological, chronological, geomorphic, and archaeological data collection, and the resulting datasets were processed, managed, and analysed within a Geographic Information System (GIS), using ESRI's ArcGIS Pro (2.7). Setting up the baseline infrastructure for Real-Time Kinematic (RTK) and Total Station survey is outlined below, while additional details on geospatial and archaeological survey are given in the subsequent sections.

Fieldwork for this thesis began in 2014 under the original project name 'Doring River Paleo Landscape Project' (DRPLP) and, on average, involved several field seasons per year, organised either side of the seasonal extremes of the Cederberg's summer and winter months. The collection of geospatial data relied on reference to semi-permanent survey marks installed across UPK7 (see Figure 5.1 and 5.4). Each survey mark was set into the ground with concrete, its position marked with a 100 mm nail, and labelled with the prefix 'DRPLP', followed by a unique number (Figure 5.4). In the case of UPK7, five survey marks were established in this way, DRPLP 12 to 16, and a further three were set with 500 mm length rebar (DRPLP 17, 18 and 19).[1] Additional survey marks were later established, independent of the 'DRPLP#' range, to increase coverage across the site for topographic total station mapping. These are composed of a single 100 mm nail inserted into consolidated sediment with green spray paint and attributed the tag 'FS#' (FS64-69 and FS77-81; Figure 5.1). They were originally intended to act as temporary survey marks during the March 2015 field season and have surprisingly stood the test of time (x,y,z checked over 5 field seasons from 2015 to 2017) to be used repeatedly in subsequent seasons.

[1]Concrete and nail survey marks were also setup at two other localities during the 2014 field-work series: DRPLP 1 to 5 at Uitspankraal 1, and DRPLP 6 to 11 at Appleboskraal (ABK).

Figure 5.4. Monumentation of survey mark made by excavating into sediment, to a spade's depth and setting a 100 mm nail into the centre of a block of levelled concrete. Each concrete marker was engraved with the original project name 'DRPLP' and allocated a unique ID. DRPLP16 is depicted. Five survey marks were setup at UPK 7 in this way in August 2014. Due to Baboon disturbance, DRPLP14 had to be removed and a new survey mark, DRPLP19, set up close to where DRPLP14 was originally installed. DRPLP19 is a 0.5 m length rebar (10 mm diameter) that was hammered into the ground (as of 2016).

The locations of each concrete survey mark, together with a series of temporary ground control points (GCP's) for unmanned aerial vehicle survey (see below), were recorded with a Real Time Kinematic Digital Global Positioning System (RTK DGPS). Coordinates were recorded in the WGS84 geographic system (degrees, minutes, seconds) and projected to WGS84 UTM 34S. Elevations were recorded using GNSS ellipsoid heights and converted to orthometric heights using the SA2010 geoid model (Chandler & Merry 2010). Base station coordinates were logged by an RTK equipped DGPS over a 7-hour period and post-processed using the Canadian Geodetic Survey of Natural Resources Canada's web based Precise Point Positioning service (CSRS-PPP, 2018). Trimble Geomatics Office (version 1.63) was used to correct all control point positions recorded with an RTK rover, based on the post-processed base station outputs. By resectioning from each survey mark, the project total station (Nikon C-Series) was employed for locality level survey of artefact and sampling locations as well as its geomorphology. Season-to-season positional integrity of each survey mark was checked prior to the commencement of data collection.

5.4 Sedimentology: Sampling and Characterisation

5.4.1 Field survey

With the field assistance and supervision of Brian Jones and Ian Moffat, a series of sediment units were identified, surveyed, sampled, and characterised over six field seasons from 2014-2017, using the methods outlined below. The relationship between deposits and their potential depositional hierarchy was estimated by mapping with a total station the juncture between two sediment units and classifying the sedimentological and lithological characteristics in each (surface texture, particle size and roundness, sorting, consistency, presence of carbonates) using a Wentworth scale and hand lens. A juncture or discontinuity is defined as any detectable change/break in the sedimentological/lithological characteristic between two or more geological bodies that directly contact one another. Together with their topography, these characteristics are used to distinguish between sedimentary and pedogenic processes involved in the

formation and/or post-depositional development of each sediment unit. At the time of field work, we did not have permits to excavate test pits through artefact-rich surfaces. Thus, complete profiles were not available and all stratigraphic information was obtained from existing surface and rill exposures. For this reason, formation models are reconstructed from surface and near-surface observations combined with subsurface data from geophysical survey.

The mapped junctures were cleaned and assessed in ArcGIS Pro against aerial as well as orthomosaic imagery. The latter were produced in PhotoScan from imagery collected with an unmanned aerial vehicle (UAV) (see the section on geomorphology below for details on UAV-survey and terrain modelling). Based on these datasets, a series of polygons was produced to represent the exposed spatial extent of each sediment unit. Each sediment unit was allocated a temporary vertical context ID (e.g., 'v_context: 004') to denote the initial interpretation of their relative depositional position. This was reassessed, critiqued, and updated as additional surface survey and subsurface sampling was carried-out and analysed. The final stage of analysis involved giving each deposit a 'stratigraphic unit' number and name (i.e., Unconsolidated Sand (UCS): Strat unit no. 6) to denote a hypothesised order of deposition and to give each deposit a descriptive reference code.

Sixty-four sediment samples were collected from across the locality (see Figure A4.1 and Table A4.1) for in-field characterisation and post-field analysis (i.e., grain size analysis, X-ray diffraction (XRD), and optically stimulated luminescence dating, as detailed below). These were collected from the subsurface of exposed deposits (as part of an opportunistic and random sample square survey strategy), from geological section cuts, and along a transect that ran the length of the locality (from the colluvium in the north to the river channel in the south; Figure 5.1 and Figure 6.2). The location (x,y, and z) of each sediment sample was recorded with the project total station and allocated a field sample ID that was stored and linked with their associated sedimentary unit in a GIS. After analysis of subsampled material, their field IDs, associated notes, and location were joined with their respective laboratory IDs and associated results.

Subsurface samples were also collected as part of the random sample square (rSSQ) survey of UPK7's surface archaeology (Figure 5.5). The horizontal extent of units that were observed underlying and surrounding UPK7's archaeology was used to demarcate areas for randomised subsampling. The unit size of 1 x 1 m was chosen to standardise the size of each survey area, while also constraining the surface area to what could be adequately processed by field crews within the allotted time. With the exception of the final rSSQ survey season in August 2016, there were never more than two members involved in field work, constraining the amount of data collected and area covered for any given season. To randomly select a sample square, grids of 1 x 1 m squares were draped across each sediment unit using the Fishnet Tool in ArcGIS 10.4. Each square was then allocated a feature ID and the resulting table was imported into Excel (MS Office 2016). Square IDs were sorted sequentially and randomly selected from a list of substrate-specific squares using the formula 'RAND()'. The True North coordinates of each randomly selected square were imported into the project total station (Nikon C-Series) and staked-out in real-time across each depositional unit.

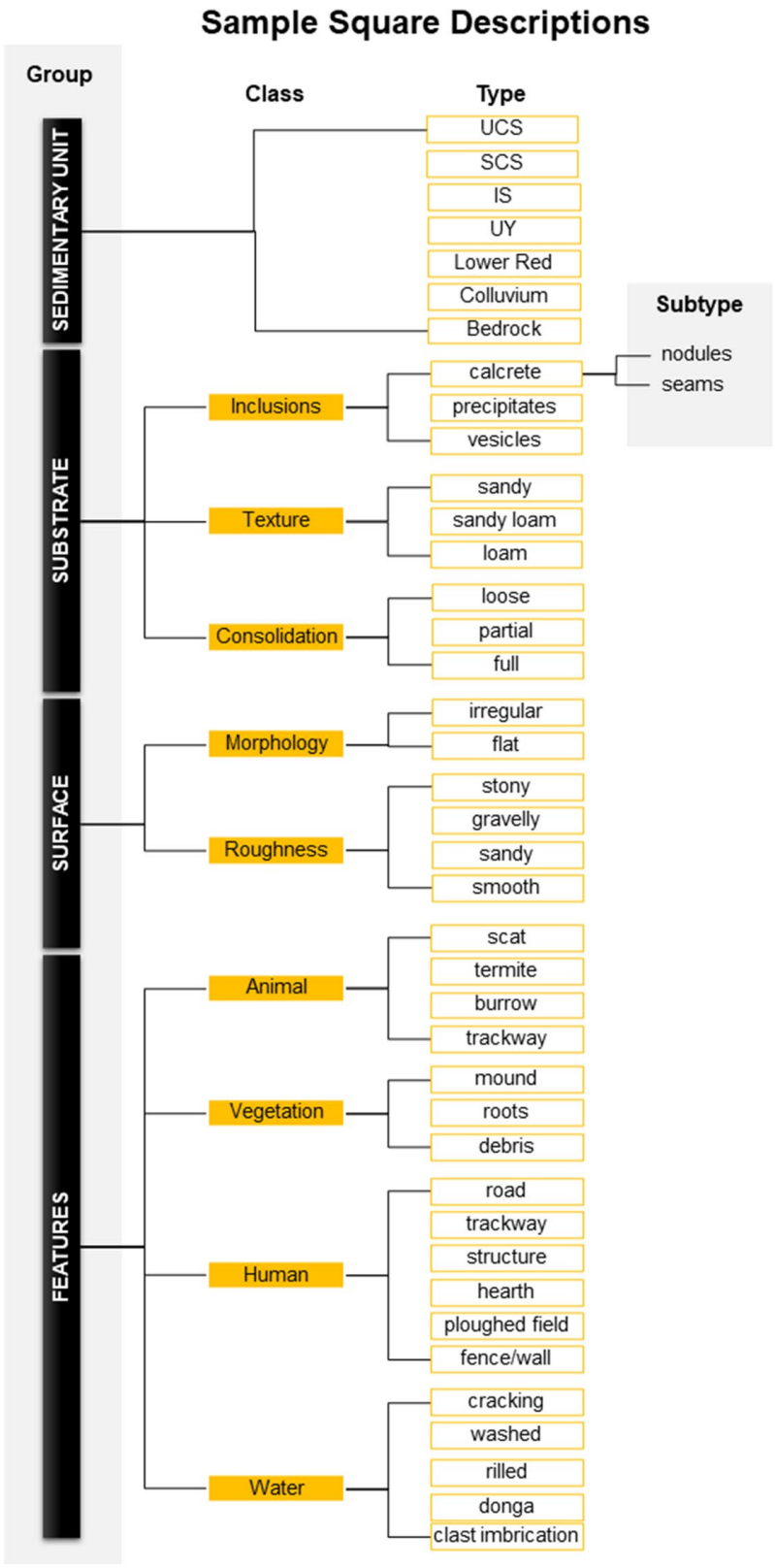

Figure 5.5. Summary of main categories and variables used to describe (sub)surface characteristics, inclusions, and features during rSSQ survey.

As the corners of each rSSQ were located they were marked out with 100 mm nails, their locations (xyz) recorded, and the rSSQ given an area ID. Due to the time-consuming nature of this process, a variant of this approach was employed in the final season to trial for future survey. This involved locating the centre points of rSSQ using a handheld GPS and nailing out the location of their respective corner points using a 1 m^2 metal frame. Six squares at UPK7 were marked out using this method and were orientated on a magnetic north axis to visually indicate the use of a different sampling strategy. All other recording steps were kept constant.

To keep track of survey progress, a handheld GPS (Trimble Juno, via ESRI's ArcPad) was used to record the location and survey status of each square, which was updated after the completion of mapping, attribute recording, and surface characterisation. Square status records also prevented the inadvertent 'cleaning' of rSSQs before each stage of data collection (archaeological survey, attribute recording and sediment sampling) was completed, especially during seasons where multiple people were working at different times on the same square. GPS waypoints also enabled fast relocation of squares during subsequent field seasons if they were staked-out, but their content not yet recorded.

5.4.2 Field sampling and characterisation

The characterisation of exposed sediment units and their (sub)surface conditions were conducted with reference to standards outlined in Jahn et al. (2006), Coe (2011) and Schoeneberger et al. (2012). Assessing surface and subsurface relationships between deposits involved cleaning back sediment with a trowel and/or geological pick (depending on degree of sediment consolidation), recording the location of junctures and describing macro level differences between sediment units. This was made by eye and with the use of a hand lens (10x magnification), classifying the average texture, colour, composition, and consistency of a deposit with reference to a Wentworth scale and Munsell Colour Chart (dry sediments only). Sediments were tested for carbonates using HCl (37% strength). Surface roughness and morphology as well as any features of erosion, vegetation, and human or animal modification were also recorded and photographed (Figure 5.5). These features can inhibit and/or promote artefact visibility and movement.

To determine the depth and transition between unconsolidated to consolidated deposit horizons a section was cut into vegetated sandy sediment that had been exposed part way by a rill on the southern slope of the locality (Figure 5.6). The section was excavated with a spade and cleaned with a trowel by cutting back into the eastern face of the rill. When it became too deep to excavate further a sand auger was used, reaching a total depth of 3.7 m (Figure 5.6). A series of sediment samples were collected and mapped-in every 300-500 mm below surface level to the base of the pit and any transitions and their locations below surface recorded.

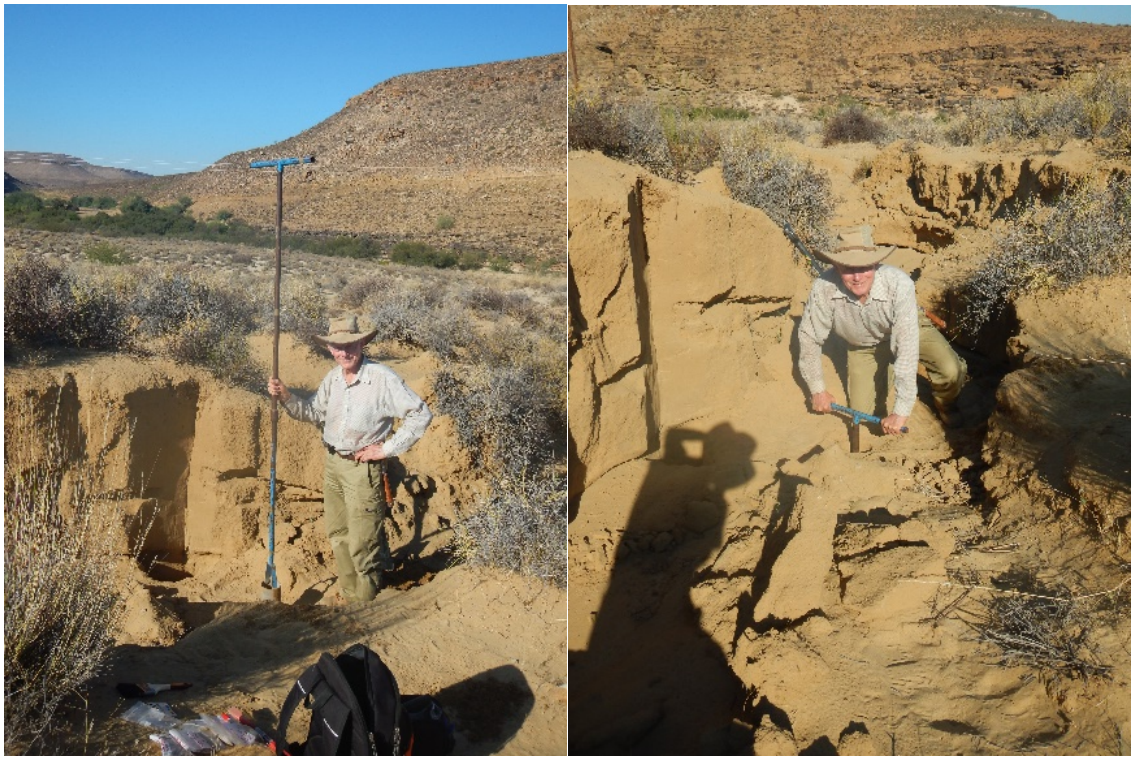

Figure 5.6. Photograph of Brian Jones (approximately 1.7 m tall when standing) sand auguring adjacent to section cut 1 at UPK7 to a total depth of 3.7 m.

Section cuts were also made across the consolidated sediment of the locality for optically stimulated luminesce (OSL) dating and to provide sediment samples for tying in the sedimentology and burial age of the sediment unit. Sections were cut with a spade, chisel, and geological pick and the base and top of the cut as well as the sample location were recorded using the project total station (Table A4.1). Due to the hardness of the sediment, these pits were often limited to a maximum depth of ~350 mm below ground level. Stainless steel tubes measuring 20 mm in diameter by 300 mm in length and 18 mm in diameter by 450 mm in length were used to take sediment samples for OSL dating. These were hammered into each section at a depth of 200-300 mm. A polystyrene plug was inserted into the contact end of the tube to help pack and protect the sample from light and accidental overflow during collection. The metal tube was selected over PVC due to the general hardness of the deposits in the research area. Sediment samples were also collected for dosimetry, X-ray diffraction (XRD) and particle size analysis from the deposit immediately surrounding the OSL tube. The profile and depth below surface (m bls) of each section cut was described, logged, and photographed before and after sediment samples were collected (see Appendix 4.1). After sampling, tube ends were sealed with polystyrene plugs and duct tape for transport to the UOW OSL laboratory. The tube itself was labelled with sample date, unique ID, name of the deposit, and an arrow indicating the insertion end of the tube. The same ID was also used for a sample's recorded total station position to form a geospatial link to its depositional context.

During rSSQ sampling, care was taken to extract samples without disturbing overlying archaeology. This involved finding a surface proximate to, yet devoid of overlying artefacts. The sample surface and square context were photographed, and the surface characteristics described (i.e., clast size and distribution, presence, or absence of duricrust, vegetation, rills, biological activity). In addition to photographic reference, any surface features forming the surface of the rSSQ were noted (e.g., vegetation,

rills, clast density and size range). A spade/trowel was used to clean back and cut into surface sediment before collecting ~100 g of sediment in a Ziplock bag. Each sample bag was allocated a unique ID and their sample location was recorded with a total station that was used to link the location of the sample with the rSSQ, its sediment and surface description, sediment sample, and archaeological content in a geodatabase.

5.4.3 Particle size: Granulometric analysis

To understand the depositional energy involved in the formation of each sedimentary unit and the type of sources contributing to this, particle analysis and direct attribute logging were carried out on sampled units. For subsurface fractions, OSL and surface profiles were subjected to laser particle-size analysis at UOW using a Malvern Mastersizer 2000. To disaggregate and prepare samples for laser counting, they were dry sieved, removing organic material, disaggregating any consolidated components, and removing any clast inclusions measuring above 2 mm in diameter. Prior to measuring the sizes, the samples were dispersed in water and subjected to 2 minutes of ultrasonic treatment to disaggregate the fine fractions. These samples were not pre-treated by wet sieving and any potential calcium carbonate component was not removed which may affect readings of the clay sized component of a sample. Results from laser counting were plotted on a grain sized curve, with multiple samples from the same substrate presented in a single graph to assess spatial variation in particle composition across the same depositional unit. Moreover, representative curves of each deposit were plotted in a single graph to compare size sorting.

5.4.4 Minerology: X-ray Diffraction (XRD) analysis

XRD analysis was applied to loose sediment samples taken from sections cut for OSL sampling and surface profiles to assess whether minerology differs between each sediment unit and to trace the potential source of sediment across the study area. Additional samples were collected from the dried riverbed and tributary deposits that bound both localities to test whether they share a common mineralogical signature to the sandy deposits that drape the locality. Bulk samples were homogenised in a Tema crusher and XRD analysis was conducted at UOW using a Philips X-ray diffractometer and Siroquant software, applying the Rietveld-based approach (Taylor 1991).

5.5 Geochronology: Chronometric Dating

A range of chronometric methods was used to date samples collected throughout the Doring River valley (i.e., optical, radiocarbon, and uranium-thorium dating). OSL dating using the single-grain single aliquot regenerative (SG-SAR) protocol was the main chronometric method used at UPK7 as it can return ages beyond the radiocarbon limit of ~50 ka, while also providing ages for the Holocene (Duller 2015; Jacobs et al. 2015). Thus, this method has the potential to return burial ages for deposits underlying archaeology that are Late Pleistocene in age or younger. Sand-sized quartz is also a common mineral found in the study area, providing adequate sample supply.

Single-grain measurements enable the identification and elimination of individual grains exhibiting aberrant luminescence behaviour that would otherwise increase error in D_e estimates when grains are combined using multi-grain aliquot methods. Employing a single-grain method increases the accuracy and precision of an age estimate. Moreover, the ability to assess the behaviour of individual grains means

that post-depositional disturbances can be assessed in samples showing non-homogenous bleaching caused by fluvial deposition, or the mixing of younger and older grains from possible vertical displacement of younger sediments (e.g., bioturbation, desiccation crack formation, ploughing). This provides additional insight into the possible formation of a deposit, hypothesised from in-field geomorphological characterisation and sedimentary analysis (outlined in detail above).

Several issues need to be kept in mind, including the possibility of the partial bleaching of an OSL signal as there are indications of slope wash at UPK7, most evident in the rills and dongas that cut across its consolidated surface. Moreover, slope-wash introduces complications of beta microdosimetry. In the case of the latter, the presence of carbonates reworked into a deposit can return higher dose estimates if these are proximate to individual grains sampled for OSL analysis (Murray & Roberts 1997).

In addition to OSL dating, nodular calcrete samples were also excavated from multiple locations (UPK7, UPK1 and UPK9) during field work to compare the U/Th isochron ages of extensive calcium carbonate-rich deposits identified at each locality. Each sample was cut with a rock saw and resin impregnated before being submitted for U/Th dating at the Wollongong Isotope Geochronology Lab. However, U/Th isochron ages were only obtained from two samples collected from UPK9, while the other samples proved too detrital. The sampling locations, collection and analytical methods, and results for the UPK9 samples were published in Shaw et al. (2019, SOM Table 3) and will be referred to in the subsequent results chapters.

Radiocarbon dating was also employed to determine the timing of hearth use and sediment exposure at UPK7 and throughout the valley. Depending on preservation, radiocarbon dating can provide a minimum record for human presence in a landscape, the kinds of plants and fauna available at the time of occupation, an independent dating method to compare the timing of deposit burial and deposit exposure, and thus provide a temporal 'envelope' for surface artefact accumulation from maximum and minimum ages (e.g., Fanning & Holdaway 2001). While a similar approach would be useful for this study, prehistoric hearths are very rare in the Doring River valley (e.g., clusters of fire cracked rock overlying baked earth)—an interesting conundrum in itself, but one that is beyond the scope of this thesis. Despite their scarcity, any hearth or combustion feature observed at UPK7 and in the surrounding landscape was recorded and their samples submitted for analysis (see below for details). Samples were collected to determine the minimum age for sediment exposure and rate of erosion. With respect to the latter, the hearth age and height above ground were recorded from the foundations of hearths found pedestalled above a deflated surface. These can be used to calculate the amount of time it has taken since hearth use for the surrounding sediment to deflate to its current level—providing an estimate of rate of erosion.

The preceding sections on survey and sediment sampling include information on the collection and recording of OSL sediment samples. The following sections present details on sample preparation and measurement for OSL dating and the methods involved in recording, collecting, and preparing samples for radiocarbon dating. More detail about the measurement and analysis of OSL samples is provided in the results (Chapter 6.2).

5.5.1 Optically stimulated luminescence (OSL) dating

A deposit's burial age can be determined using optically stimulated luminescence (OSL), together with an

understanding of its relative depositional sequence. Quartz is a common, naturally occurring dosimeter in the study area that records the timing of its last exposure to sunlight or high temperatures. This is estimated from the amount of energy its crystal lattice has stored from the radioactive decay (e.g., alpha, beta, gamma) of radionuclides (uranium [U], thorium [Th], and potassium [K]) for the duration of its buried state. This energy increases at a constant rate until its release in the form of luminescence (light photons) upon exposure to an electron stimulant (e.g., sunlight, temperatures above ~300°). Both the amount of energy stored in a quartz grain (Paleodose [De]) and the rate of radioactive decay in its depositional environment (Annual dose [Dt]) are measured to calculate when it was last exposed and emptied by one of these stimulants, before beginning its next 'recharging' phase upon reburial. The formal equation for calculating the age of a dosimeter is

$$\text{AGE} = \text{Total luminescence} / \text{Annual rate of luminescence acquisition}$$
$$\text{OR}$$
$$\text{AGE} = \text{Palaeodose (De)} / \text{Annual dose (Dt)}$$

where the paleodose is divided by the annual does to obtain a deposits burial age.

5.5.1.1 Sample preparation

Quartz grains were extracted from 12 samples collected at UPK7 for OSL measurement (Table A4.1). Following standard laboratory procedures set out by Wintle (1997), all OSL samples and related sediments were prepared and analysed under red-light conditions at the UOW OSL Laboratory and allocated UOW laboratory IDs (prefixed by 'UoW'; Table A4.1). Sediment was subsampled from the centre of the tube for equivalent dose (D_e) measurements. The first 20 mm of sediment at each end of a tube was scraped off for dose rate determination and decontamination of light exposed grains. These were weighed, dried in an oven (set to 50°C), then weighed again for water content calculations. Water content (WC) for sample bags consistently returned lower values (at least 35% less on average) than tubes. It is not clear which is more representative of the deposit's WC. However, secondary moisture acquisition is known to occur in cores during storage. For this reason, a standard WC of 5.0 ± 1.3 was employed for analysis. Dosimetry samples were subsequently homogenised in a ball mill and left to sit for one week before being analysed in a thick source alpha counter (TSAC) and low-level beta counters (GM-25-5 multi-counter) (see Chapter 6.2.5 for further details on dosimetry).

Samples for quartz-based D_e analysis were wet-sieved into multiple grain-size fractions from 90-300 µm-diameter. Grains measuring 212-180 µm in diameter were selected for further preparation and analysis, while the other fractions were archived. To remove carbonates from the 180-212 µm fraction, hydrochloric acid (HCl) was added to the sample in 1 L of water (not distilled). If no reaction (effervescence) was observed, then samples were left in this state for 24-48 hours. In rare cases when minor reaction occurred, samples were left for an additional 24 hours, stirring to check the sample's state. Once treated, samples were rinsed with clean water and oxidised in a solution of hydrogen peroxide (H_2O_2, 32%) to remove organic matter. Following the same procedure for waiting period and rinsing, samples were then sieved again to isolate out the 180-212 µm-diameter grains. Any reaction to HCl or H_2O_2 and, therefore, the presence of carbonates and organic matter was recorded.

Once isolated, quartz grains were density separated from heavy minerals and Na- and K-feldspars with a sodium polytungstate solution and distilled H_2O at densities of 2.7 and 2.62 g/cm^3, respectively. To remove the quartz grain's alpha irradiated rind and any remaining feldspars, they were etched using 40% hydrofluoric acid for 40 minutes. Etched samples were left to sit for another 24 hours before being handled. They were subsequently dry-sieved to extract 180 µm-diameter grains for dating.

5.5.1.2 Equipment

Two automated Risø DA-20 TL/OSL readers (Risø 2 and 4) in the UOW OSL lab were used for OSL measurement (Bøtter-Jensen et al. 2000, p.527). Both are fitted with single-grain laser attachments. All samples were irradiated with calibrated $^{90}Sr/^{90}Y$ beta sources. A 10 mW 532 nm (green) light Nd:YVO4 solid-state diode-pumped laser was used for optical stimulation. With three lenses, the Risø laser focusses light at a target of approx. 20 µm in diameter. At 90% power, with a power density of about 45 W/cm^2, measurement is rapid, whilst maintaining a location to location precision of 3 µm (Bøtter-Jensen et al. 2000, p.527). Ultraviolet light, emitted upon stimulation, was detected by a photomultiplier tube (PMT, Electron Tubes Ltd 9635Q) that is fitted with a 7.5 mm thick filter to detect ultraviolet light while simultaneously blocking LED wavelengths (Hoya U-340). Standard Risø single-grain aluminium discs (Bøtter-Jensen et al. 2000) were set with 100 (10 x 10) individual 180-212 µm-diameter quartz grains per disc. These were analysed using the single-aliquot regenerative-dose procedure (SAR), originally described by Murray & Wintle (2000). Prior to measuring the natural and regenerated luminescence signal, each grain was desensitised by preheating at a set temperature and held for 10s (PH_1). Preheating temperatures derive from a series of dose recovery tests, the results of which are given in Chapter 6..3.2 Individual grains were also subjected to a series of tests to assess the applicability of the SAR procedure for D_e determination. Further details on the methods, analysis and equipment used for obtaining a D_e and dose rate from each sample alongside their results are provided in Chapter 6.3.

5.5.2 Radiocarbon dating

Radiocarbon (^{14}C) dating is used for dating dead organic carbon materials (Taylor 2018). Samples of charcoal and charcoal-rich sediment were submitted for radiocarbon dating using Accelerator Mass Spectrometry (AMS). Given the ^{14}C half-life of ~5700 years, this method measures the number of ^{14}C atoms left after its decay into ^{14}N, relative to concentrations of ^{12}C or ^{13}C as well as correcting for isotopic fractionation (Rapp & Hill 2006). Radiocarbon dating can reliably estimate the age of a carbon sample between 300 years (200 ^{14}C years) and ~40,000 years—with ages beyond this becoming increasingly unreliable due to the decay rate of ^{14}C. The lower dating limit results from short-term fluctuations in solar magnetic intensity (post-1500s), the combustion of industrial fossil fuels from the late 1700s reducing relative ^{14}C concentrations, and the detonation of thermonuclear weaponry increasing ^{14}C in the atmosphere, particularly between 1955 and 1963 (Taylor 1997; Taylor & Bar-Yosef 2014). Any ages within the upper and lower dating limits were calibrated, those below the lower limit are considered 'modern', or in the case of the southern African samples 'historic'. Since all samples collected during this study derive from southern hemisphere terrestrial contexts, the SHCal13 calibration curve is used (Hogg et al. 2016).

5.5.2.1 Radiocarbon survey and sampling

To record and collect samples from combustion features for radiocarbon, reconnaissance survey and sampling was carried-out along the Doring River valley between Uitspankraal 2 and Klein Hoek 1 (Figure 5.1). This field work was carried out under the guidance of Brian Jones with the objective of ground truthing the study area's mesoscale geomorphic features and sediment units at and between several localities (Uitspankraal 1 *to* 9, Appleboskraal, Lungkaal, Klein Hoek 1, and Putslaagte 1; Figure 5.1).

In the case of recording combustion features, any feature that showed evidence of concentrated burning was recorded using a handheld GPS (Trimble Juno) and sampled for charcoal—allocating the same sample ID to both the waypoint and double bagged charcoal/bulk sample. Only four combustion features were identified: Two hearths that were interpreted as historic at the time of sediment and charcoal collection, found at UPK9 (Figure 5.7 D) and Lungkaal (Figure 5.7 B), and two combustions features that were interpreted as prehistoric—possibly Holocene in age (from Lungkaal and UPK7, Figure 5.7 A and C, respectively; Table 5.1). One of these potential prehistoric combustion features appeared more classically hearth-like, by the clustering of fire-cracked rock and heavily baked (rubified), scooped-shape earth visible directly beneath these rocks (Figure 5.7 D), while the other at UPK7 was no more than a dark grey and charcoal speckled shadow (~400 mm in diameter) with sandstone cobbles scattered across and adjacent to it (Figure 5.7 C, also see Appendix 4.9 for details and photographs of sampled features). Although not possible during this survey, it would be worth collecting orientated archaeomagnetic samples on the overlying stone clusters during future survey and sampling to provide additional insight into their integrity. Care was taken when sampling each combustion feature to: A) have minimal impact on the feature, and B) handle the samples using only clean equipment to prevent contamination, C) to only collect charcoal pieces from beneath hearth stones, if possible, or charcoal-rich sediment from the subsurface of only one half of the combustion feature, after removal of the surface layer. In the case of the latter, separate equipment was used to excavate the surface and sample the subsurface. However, collecting the bulk sample proved difficult due to the hardness of the sediment, hence a sample could only be extracted from 20 mm below the surface. Care was also taken to select sediment without faunal remains and/or roots.

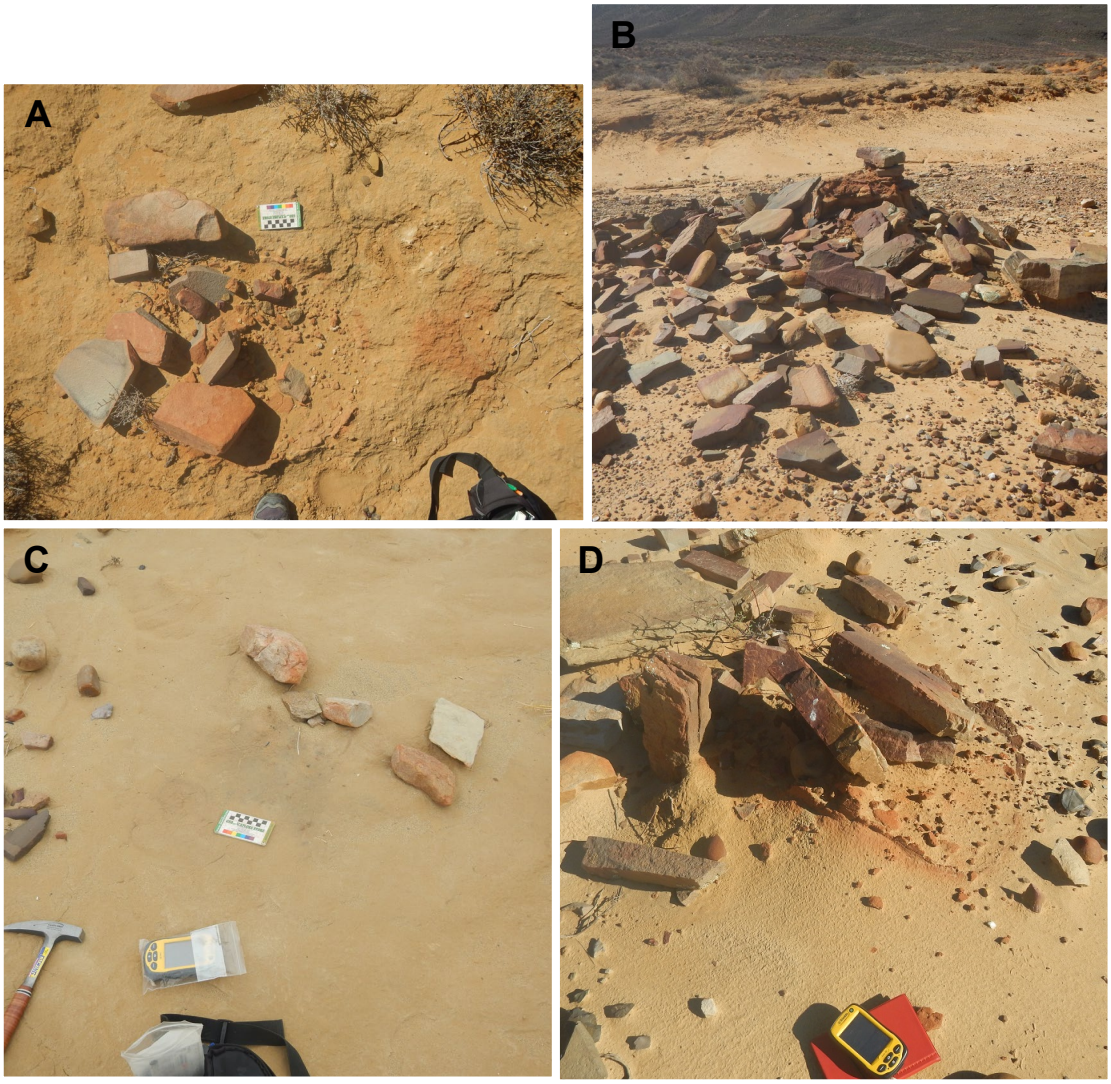

Figure 5.7. Photographs of sampled combustion features: a) fire scoop and b) stone hearth at Lungkaal, c) concentrate area of charcoal, stone scatter, and charcoal rich sediment at UPK7, and d) fire scoop at UPK9.

5.5.2.2 Radiocarbon sample preparation and analysis

To further minimize potential contamination for intrusive carbon material a subsample from each charcoal/bulk sediment sample was picked under a microscope using sterilized tweezers. This involved identifying and removing roots and microfauna under the microscope during bulk carbon extraction (sample 91071), and selection of a subsample of well-formed wood charcoal from the three charcoal samples (91118, 91119, 91130). Charcoal within the bulk sample appeared to be coated in fine clay particles. Four samples were submitted for radiocarbon dating, three charcoal and one bulk carbon sample. Table 5.1 lists the submission details for each sample. Sample collection in the field was done with a clean trowel, without contact from other carbon sources. Samples were submitted to DirectAMS for analysis. Their report is presented in Appendix 4.9, along with the calibrated results for UPK7's bulk carbon sample 91071 (D-AMS 027123).

Table 5.1. Subsample details for each carbon sample submitted to DirectAMS for Accelerator Mass Spectrometry (AMS) measurement and analysis

N	D-AMS ID	Sample ID	Material	Location	Feature/location description	Depth (cm)	Expected age
1	D-AMS 027123	91071	bulk carbon	UPK7	Possible prehistoric hearth. Charcoal extracted 0.5 cm below exposed surface	0.5-1	Holocene
2	D-AMS 027124	91118	charcoal	LNGKL	Prehistoric hearth feature. Charcoal extracted from beneath fire cracked rocks	0-0.5	Holocene
3	D-AMS 027125	91119	charcoal	LNGKL	Historic hearth. Charcoal extracted from between stone building blocks	0-0.5	<200 years
4	D-AMS 027126	91130	charcoal	UPK9	Historic hearth. Charcoal extracted from beneath baked building stone	0-0.5	<200 years

5.6 Surface Morphometry

Geomorphic conditions play a critical role in the operation and impact of erosional and depositional processes on locality formation and artefact preservation. Thus, UPK7's geomorphology is crucial for interlinking the locality's depositional history with its archaeology. While the topography of a landform changes in response to environmental and anthropogenic processes at multiple scales, these processes also operate in response to the form of the landform itself (Shreve 1972). Thus its morphology is "…not only the consequence of past processes, but is also a factor that affects the course of present erosion, and hence [its] future morphology…" (Lane & Richards 1997, p.2). The following sections outline the geospatial and geophysical methods employed to record the extent and morphology of UPK7's sediment units.

5.6.1 Data collection

A digital terrain model of UPK7 was produced from UAV-imagery collected in 2019. From this DTM it was possible to characterise the main features of UPK7's hillslope morphology, hydrology, and vegetation cover, proving essential for investigating the relationship between the spatial patterning of surface archaeology and erosional processes such as runoff. As mentioned earlier, the orthometric imagery produced from this dataset was also used as a reference for checking and refining the extents of each sediment unit. Multi-rotor UAV flyovers were performed over UPK7 in February 2019 using a DJI Mavic Pro UAV equipped with a standard 12-megapixel camera (FC220 model, focal length 4.7 mm) with a resolution of 4000 x 3000, a pixel size of 1.56 μm^2 and a pitch of between - 90° and + 30°, yaw and roll at 0° and 90° horizontally and vertically (www.dji.com/mavic/info; Ames et al. 2020a). Survey entailed flying the UAV at an average altitude of ~40 m above ground. Image capture occurred over a single flight session, totalling 191 images in 2019. This was performed during optimal conditions (i.e., minimal cloud cover, high sun angle, and low winds). Figure 5.8 presents the orthomosaic output, showing survey extent and lighting conditions. UPK7's tributaries form the eastern and western bounds of the footage with the main exposure captured in its entirety. The colluvium in the north is truncated, while the south extent of the model stops short of the modern river terrace, capturing an outcropping bolder-rich paleo-terrace. The following outlines the methods used to model UPK7's topography, and map surface roughness (i.e., vegetation coverage and rill location).

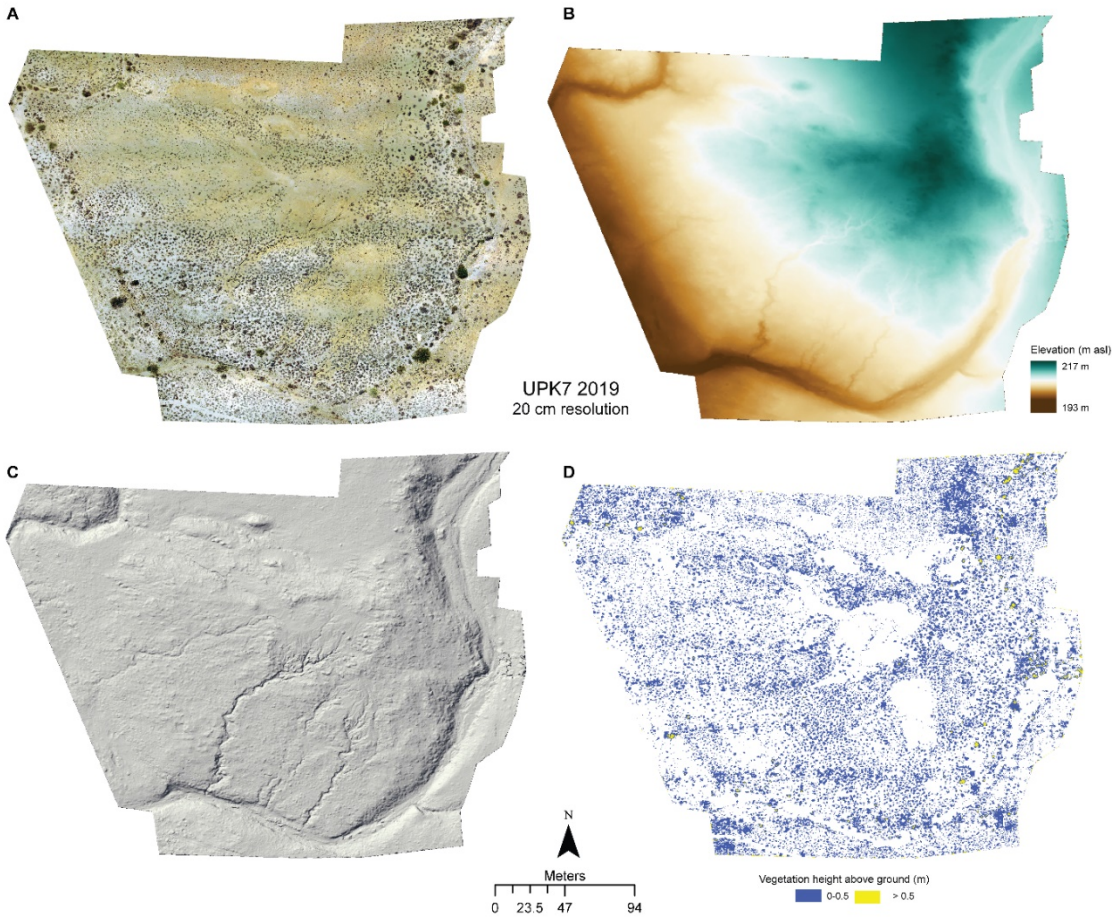

Figure 5.8. Map series showing the 2019 orthomosaic (A), final DTM (B), hill shade (C), and vegetation crown height (D) outputs.

5.6.2 Terrain modelling and classification

A three-stage workflow was employed to produce a DTM from the 2019 UAV survey of UPK7: Stage 1. Image processing, Stage 2. Vegetation filtering, and Stage 3. DTM creation (see Figure 5.9). This process draws from the previous efforts and guidance of Dietrich (2015), Chambers (2019) and Anders et al. (2019), as well as the user manual for Agisoft PhotoScan (version 1.4) and the LAStools readme files and community forum (http://groups.google.com/group/lastools).

Stage 1 in Figure 5.9 involved processing UAV imagery using structure from motion (SfM) photogrammetry in Agisoft PhotoScan (v1.4; AgiSoft 2018) to produce a georeferenced dense point cloud for digital elevation modelling (see Appendix 3.1). This followed the basic protocol outlined by Dietrich (2015), while drawing on Chambers (2019) and Anders et al. (2019) for additional parameter details and process specifications (i.e., equipment specifications and recommended tie point values for dense point cloud processing). Image processing for dense point cloud extraction involved seven steps: photo preparation, geotagging, photo alignment, georeferencing, alignment optimisation, ground control point error-checking, and dense point cloud creation—the details of which are outlined in Appendix 3A (see also Figure 5.9).

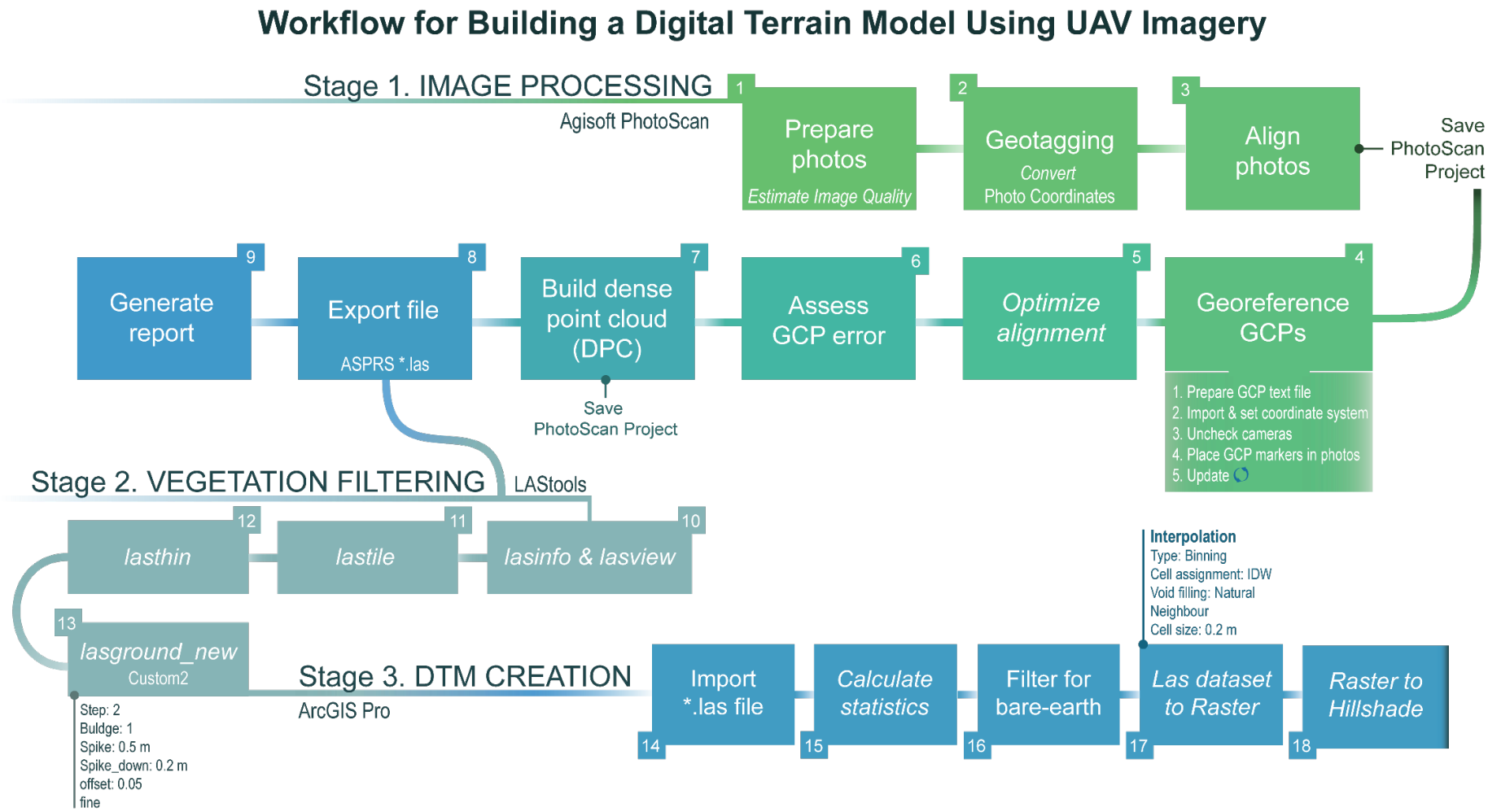

Figure 5.9. Workflow involved in DTM creation. Abbreviations: GCP = ground control point

The second stage involved filtering vegetation from the digital surface model (DSM, Appendix 3.2). The presence, density, and varying heights of vegetation above the land surface can distort terrain heights in a digital terrain model (DTM), decreasing the computational accuracy in runoff and erosion analyses across a land surface. Anders et al. (2019) outlined and compared several methods ('off-the-shelf' and customised algorithms) available for filtering vegetation to reduce this error. Two techniques proved the most useful for filtering out shrubs and trees: the vector-based technique, Triangular Irregular Networks (TIN) densification, and a dual method colour-based process 'ISL_VI', that uses an excessive greenness vegetation index (VI) and Iterative Surface Lowering (ISL) algorithm. The ISL_VI method provided the best results for shrubs, while the TIN densification algorithm returned the best all-round results for tree and shrub covered surfaces. The combination of riparian and succulent Karoo vegetation within the Doring River valley presents a scenario where land surface coverage can vary from tree to shrub to rocky and barren surfaces. To account for this variability and to standardise the processing methods employed for modelling the different sediment stacks across the Doring River valley, the TIN densification algorithm was selected for producing a digital surface model of UPK7.

A series of modules that form part of the LAStools software package (Isenburg 2019) were used for bare-earth classification and vegetation filtering (see Appendix 3.2.1). Points classed as vegetation (class 1) were filtered out, leaving the remaining bare-earth points (class 2) for digital terrain modelling (DTM). Assessment of different filtering parameters, interpolation methods, and the final production of UPK7's DTM were carried-out in Esri's ArcGIS Pro 2.4.2. The methods involved in filtering and interpolating the 2019 dense point cloud are outlined in Appendix 3.2, along with an assessment of each parameter for inclusion in the final DTM. The final DTM and its geomorphological outputs (i.e., slope, hydrology, and erosion potential) are used throughout the results Chapters 6 and 7.

Prior to producing a bare-earth digital elevation model (DEM) or 'DTM', the bare-earth, vegetation and rilling features were classified, providing a record of the extent and distribution of features that are indicative of the dominant depositional and erosional processes at this locality (i.e., wind and rain). Appendix 3.2 provides information on process and results of DTM creation and an assessment of the integrity and accuracy of surface interpolation, including details about the refinement and classification of the dense point cloud in LAStools and ArcGIS Pro, and DTM interpolation, testing, and selection.

DTM creation involved thinning a PhotoScan generated dense point cloud, filtering out vegetation with nature mode in LAStool's 'lasground_new' module, manually preserving rill and tributary integrity in ArcGIS Pro and applying triangulated irregular network (TIN) interpolation to create a final DTM output. TIN interpolation uses TIN defined cells and natural neighbour association to produce a continuous 2.5D elevation model of UPK7's surface (Figure 5.8B). The surface model was also hydrologically conditioned to produce a depression-less digital elevation model (DEM, Figure 5.8C)—unrestricted by small internally draining imperfections (sinks; see Appendix 3.4 for details). This enables assessment of the flow of water across its surface and the potential impact this can have on the location and movement of surface artefacts. Vegetation distribution and height values were also obtained from canopy height data by subtracting the DTM from the DSM using the Raster Calculator in ArcGIS Pro (Figure 5.8D).

The hydrologically corrected 2019 DTM was also used to calculate the average slope for each rSSQ, obtained from the median of the 2019 DTM-derived slope cell values that occur within and intersect

with a given square's perimeter (Figure 5.10). The distribution of slope values for each square varies in terms of normality, therefore the median values for all squares were used, irrespective of distributional normalcy.

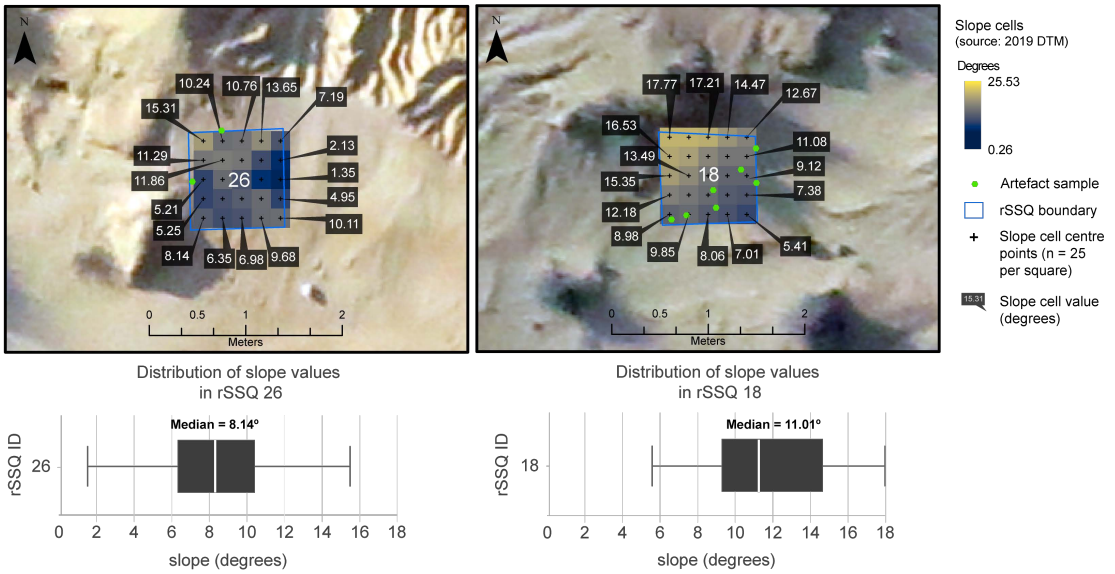

Figure 5.10. Calculating average slope for rSSQs from DTM cell values

5.6.3 Geophysical survey

A geophysical survey was carried-out at UPK7 in 2017 to investigate the relationship between its surface and subsurface deposits, their spatial extent, and morphology. Electrical resistivity tomography (ERT) was employed to attain a subsurface reading of the locality's lithology and bedrock, to determine their morphology, and horizonal and vertical extent (~1 m resolution to ~15 m depth penetration) and their potential influence on the geomorphological arrangement of the locality's exposed deposits. Data collection and analysis were carried out by Ian Moffat (Flinders University). Moffat's report detailing ERT data acquisition and processing are presented here, and the results are outlined in the Results Chapter 6.2.6 under '*ERT subsurface stratigraphy'*. Two ERT lines were laid out crossing over at a high point on the western side of the survey locality (Figure 5.11). An ERT line was formed from multiple cable sections depending on the total length of the area being covered. ZZ Flash-Res Universal cables were used with 64 electrodes and an electrode spacing of 1 m (depending on the survey line). Data was collected using Wenner, ZZ and (for some lines) the Dipole-Dipole Arrays at 120 V for 1 second. Electrodes were watered using salty water before acquisition and contact resistance was measured to ensure high data quality. Line 1 was setup along a NE-SW bearing running from survey mark DRPLP16 to DRPLP14/19. Line 2 (Line 2) extends from east to west, running perpendicular and cutting through Line 1, along exposure 1 and down to the western tributary (Figure 6.1).

Figure 5.11. Laying and measuring the length of ERT cable line no. 2 (approx. 60 m), which runs from east to west (photo facing east). This photo shows line 2 traversing loose sands with vegetation and consolidated sediment. The latter is covered by stone artefacts of varying material types and sizes. Photo taken by Ian Moffat. Author pictured (H: 1.63 m).

Transect setup involved laying out measuring tape in 30 m long runs to create the axis of a transect. Titanium pegs were inserted into the deposit at 1 metre intervals. To increase contact between metal peg and surrounding sediment, saline water (~2 cups of salt/5 L of water) was poured on the pegged earth. Cables were run along the transect and clipped to each peg. Once the first and last pegs are setup, they are used as control markers for spatial reference. Static GPS survey of each end-control peg involved setting up a GPS receiver on a tripod over the top of each marker. Their positions were recorded as a series of points for one hour, averaging their location during post-field processing. During resistivity measurement, cable lines were walked, and the context of each peg was recorded by noting the sedimentary unit. Sediment descriptions and surface types recorded during this earlier survey helped to contextualise the position of the resistivity cable with the underlying surface deposits. Photographs of exposed deposit type were taken along each transect. The locations of the end pegs were recorded with a static GPS unit and elevation and depth below surface were derived from the DEM for this locality. Sediment samples, together with deposit exposure, extent and topography were also recorded along a north-east to south-west transect to produce a surface profile of UPK7 (see below for details).

5.7 Archaeological Formation

A geoarchaeological approach to the formation of the archaeological record is embedded in the principles of uniformitarianism, in which the physical mechanisms of formation behaved in the past as they do in the present (Holdaway & Fanning 2014; Rapp & Hill 2006). Testable expectations for how artefacts—as clast and deposits—can respond to the transformative processes of deposition, erosion and *in-situ*

pedogenesis are dependent on experimental and observational research (Rapp & Hill 2006). This includes the experimental study that was carried out at UPK7, which provides a local example of the impact of current conditions and erosional processes on surface assemblages (Phillips et al. 2019). As mentioned in the preceding chapter, that study presented a case for the rapid disaggregation and eventual attrition of exposed artefacts at UPK7 under the current semi-arid conditions. This provides a baseline expectation for the duration of artefact exposure depending on their spatial composition. Thus, by considering the spatial composition and condition of surface artefacts in relation to their sedimentological, geochronological, and geomorphic setting it is possible to determine the impact processes of deposition and erosion have had on artefact preservation and their spatio-temporal organisation.

The following outlines the methods and materials used to explore the above relationships between UPK7's surface artefacts (i.e., their spatial patterning, condition and inferred temporal composition), their physical context, and their depositional history. This begins with an outline of the methods employed during field data collection of artefact spatial and attribute data and is followed by a summary of published interpretations for the spatial patterning and integrity of UPK7's surface archaeology and the approaches taken to investigate each of these interpretations.

5.7.1 Field data collection

Artefact recording provides data on variability in surface scatter composition/distribution relative to topography and erosional (e.g., rilling) and depositional (e.g., sand deposits, vegetation) features. Two archaeological datasets were used to investigate the spatio-temporal patterning, visibility and integrity of UPK7's surface archaeology. One captures the point pattern, typo-technological and taphonomic composition of UPK7's surface archaeology as they are distributed across the locality's sediment units. The other captures a random sample of each sediment unit's clast content (artefacts and non-cultural clasts) to supplement and test their composition, density, and condition, and to test the distributional dataset. The following subsections outline the survey methods and data collection protocols employed to produce, process, and analyse each archaeological dataset.

5.7.1.1 Distributional responsive non-geometric (RNG) survey

Distributional survey of UPK7 was carried-out in 2019 as Phase I in a three-phased data collection programme for the Doring River Archaeology Project (DRAP; Ames et al. 2020b; Shaw et al. 2019). The goal of Phase I was to systematically map and record the location of all cores, retouched flakes, ground stone artefacts, ochre, pottery, and beads exposed across a locality's surface and, from this dataset, identify coherent clusters of surface artefacts for future, detailed technological analysis (Phase II) and excavation (Phase III). Unretouched flakes and fragments were not recorded during Phase 1, and do not contribute the distributional dataset to be used here. For the purpose of this study, the dataset provides broad information on the spatial distribution and density of the surface archaeology across UPK7's sediment units—including a five-metre buffer beyond the surveyed area. It provides a global (locality-wide) point pattern for all artefacts (except unretouched flakes) enabling assessment of how this pattern changes depending on their condition, size, and inferred age relative to their topographic, substrate and surface context.

The survey method outlined below is referred to as a 'Responsive Non-Geometric' (RNG) survey

throughout the thesis. RNG survey denotes an approach that responds to and is bound by the natural extent and spread of the archaeology rather than by an arbitrary survey unit (i.e., transects and sample squares). To obtain a comprehensive coverage of the artefact-bearing sediment units, as well as sediment units that immediately surrounded these high visibility areas, a series of linear transects or field walking guides were strung out 5 metres apart and orientated along the short axis of the locality. Data collection and processing involved the use of a range of ESRI applications, including ArcGIS Collector, in conjunction with custom-designed data entry forms (XLSForm) using Survey 123, as well as ArcGIS Online (AGOL) and ArcGIS Pro. See Ames et al. (2020b) for a detailed outline of the 2019 design and implementation of the DRAP MobileGIS method.

Individual artefact locations (x, y, z) were recorded with an Apple iPad Mini 4s using the ESRI ArcGIS Collector platform. These were linked to Bad Elf Surveyor Pro GNSS receivers via Bluetooth connection which provides 2-3-metre positional accuracy and ~0.2 m precision (Ames et al. 2020b). This was deemed accurate enough for maintaining the relative spatial organisation of the individual artefacts, their neighbours, and any patterns in clustering that may exist relative to the boundaries of a sedimentary unit (Ames et al. 2020b). However, as a precaution, the spatial accuracy of this dataset was checked prior to analysis. Although a limit of 2 m was set as the maximum amount of error allowed for mapping in the position of an artefact, some artefacts were still recorded above this value. Thus, if the measurement accuracy of an artefact's location data was over 2 m, it was excluded from the spatial analysis.

5.7.1.2 Random sampling square (rSSQ) survey

In addition to sedimentological and surface characterisation, rSSQ survey was also used as a random subsample of the archaeological scatter, providing a dataset that supplements and tests the 2019 RNG dataset. The rSSQ dataset was collected over the course of five field seasons, between 2015 and 2016. This involved recording the locations and attributes of artefacts and non-cultural clasts. A size threshold of ≥ 10 mm was used—10 mm below the threshold reported in Will et al. (2015) for the Post-Howiesons Poort cluster—to determine if artefacts were being masked by the standard threshold of 20 mm used in publications, and to detect possible size-sorting resulting from sheet wash entrainment (see below). Once the boundaries of an rSSQ were laid out, the location of every exposed artefact and non-cultural clast (NCC) (≥10 mm size cut off) was flagged with a nail and a unique ID tag (blue duct tape), and its coordinates (x, y, and z) were recorded using the total station's reflectorless mode (to reduce stadia 'wobble' and z-value error, e.g., Figure 5.12).

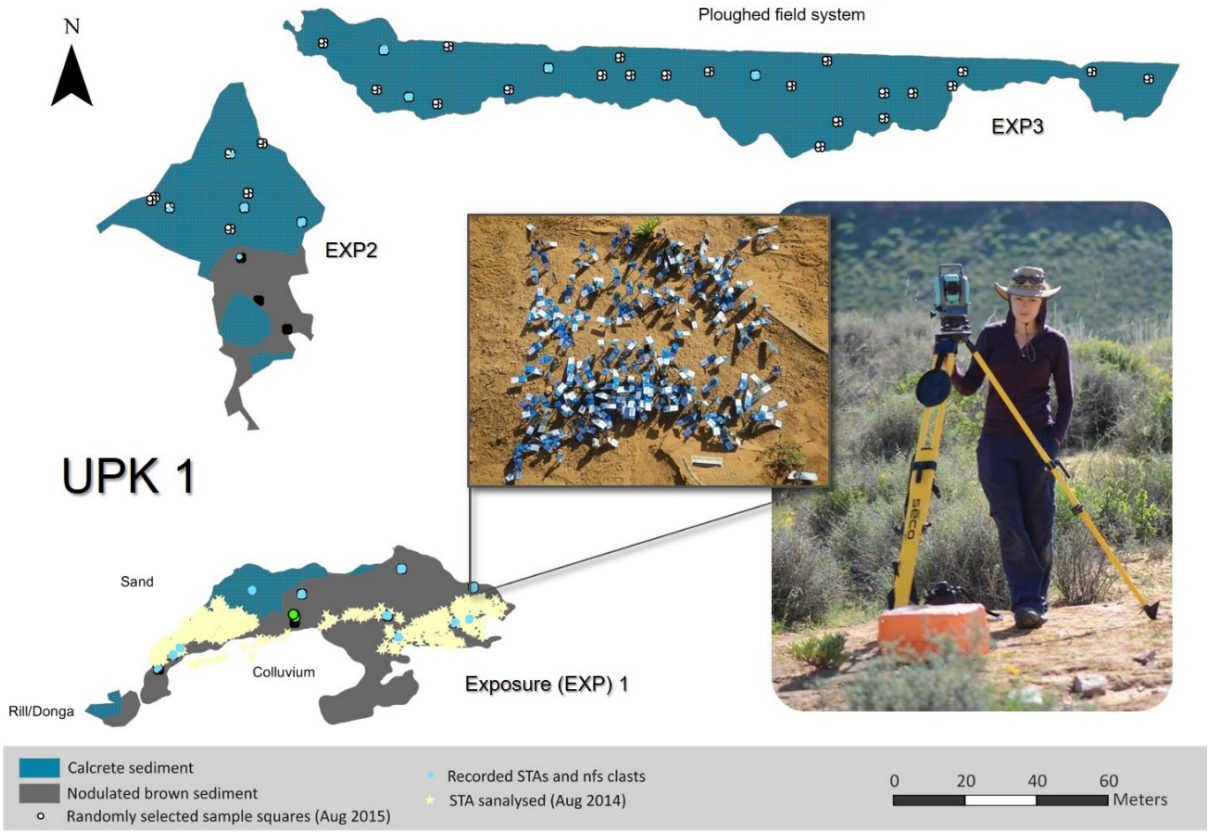

Figure 5.12. Example of the rSSQ survey strategy employed at UPK1 and UPK7. The map shows the extent of the exposed sediment units at UPK1, the location of rSSQs as well as the distribution of artefacts recorded in August 2014 as part of a pilot study for this thesis and the DRAP. Artefacts and non-cultural clasts within an rSSQ are shown nailed and tagged in the accompanying photograph as well as a photo (author pictured) of the project total station (Nikon C-Series) used to record their individual locations.

5.7.1.3 Attributes and data logging

Considered part of the sedimentary system, finds were treated as proxies for both depositional processes and behavioural change. An infield analysis non-collection strategy ('catch-release' approach) was employed during data collection for both survey strategies, in which artefacts were returned to their place of repose once their attributes were recorded. This approach helps to conserve the archaeological record and allows future surveys of the same dataset. It also precludes an archaeological collection permit.

During RNG survey, a comprehensive record of material, morphological and technological attributes were logged for each artefact, provided in Shaw et al. (2019, see SOM Table 1). However, only attributes pertaining to the objectives of this study are listed in Table 5.2. The iPad minis were used to collect attribute and metric data on each artefact, the latter through Bluetooth-connected digital callipers. Their in-built cameras also enabled regular photographic recording of time-diagnostic artefacts. The attributes and locations of all cores, retouched flakes, implements (i.e., grindstones, hammerstones, anvils), unworked quartz crystal, ochre, and pottery were recorded, without a size cut-off. While flakes are often the most prevalent lithic class in a stone artefact assemblage, the priority of Phase I survey was to maximise coverage and the collection of time-sensitive information. Thus, flakes were excluded from data collection under the assumption that the frequency of artefacts was high enough at the locality to represent the general

spatio-temporal patterns and variation in the surface archaeology of UPK7.

However, flakes are particularly valuable indicators of lithic reduction and post-depositional modification. Flakes are often smaller and less resilient than cores and, thus, more likely to break when trampled and budge under fluvial force—traveling farther downslope before resettling. For this reason, flakes were included in rSSQ data collection along with all other artefact types, and stone artefact classes. Together these are referred to as 'finds' and their attributes recorded with reference to Holdaway & Stern (2004) and Andrefsky (2005) (see Table 5.2).

After recording the location of individual finds within an rSSQ, find attributes were logged using digital callipers, scales, field laptops and the data entry software E4 (v4.5; McPherron & Dibble 2009). Each find was allocated a unique ID during survey and attribute logging. At the end of each field day these were used to connect find location and attribute data in a single geodatabase using the 'Spatial Join' tool in ArcGIS Pro. E4 was configured specifically for rSSQ attribute recording (see Appendix 3A for CFG script). Conditional statements were used to skip any variables that did not pertain to a given object, reducing data entry time. E4 stores entered data as an MDB file for processing and management in Microsoft Access. It was chosen as the data entry software for its simplicity and programmable intuitiveness and was easily adapted to the project's data entry requirements and updated throughout the season.

During the post-processing of both datasets, attributes were organised into three categories, each contributing to a different aspect of archaeological analysis: clast attributes, typo-technological attributes, and artefact condition. Clast attributes provide information on the type of clast (artefact or non-cultural clast), its size (maximum dimension) and material type (see Table 5.2). Clast type distinguishes between objects that show clear signs of modification by humans (artefacts) and those that do not (non-cultural). Typo-technological attributes provide information on the typological, technological, and temporal components of the surface scatter. Artefact condition consists of artefact attributes indicative of trampling and weathering that can result from exposure and burial. The degree of surface weathering of a stone artefact was recorded as patination, discolouration, or decayed. These categories are used as hierarchical indicators of surface weathering, with patination demonstrating the least and decay indicating the most weathering. Each raw material responds to weathering differently, especially when exposed to repeated wet and wet cycles. For this reason, analysis of surface weathering was restricted to hornfels. Hornfels is very sensitive to chemical weathering (Sandy & Cole 1982) and is also the second most prolific material type found at UPK7 (after quartzite), making it ideal for comparing the relative degrees of weathering across the locality (see Chapter 7.6.2 for additional details regarding weathering and hornfels). In addition to changes in surface condition, edge rounding was noted to occur on many artefacts. All hornfels artefacts were examined for weathering states across UPK7. In-hand specimens of unweathered 'fresh' hornfels appears dark grey to black in colour, very fine-grained, homogeneous, and dense in composition. Although not implemented in this study, future studies would benefit from the standardisation of colour coding hornfels patination using in-field spectrometers, in a similar vein to Sampson et al.'s (2015) use of the Munsell system. Occasionally the hornfels shows fine banding, which has minimal effect on their fracturing planes. Fresh hornfels artefacts have sharp edges, while weathered hornfels artefacts show rounded edges.

Under laboratory conditions patination occurs quickly when exposed to wet-dry cycles (Sandy & Cole 1982). Lightly patinated hornfels appears dark grey in colour, while extended exposure and weathering

results in further discolouration of its outer rind, to a light grey, almost white colour. Discolouration to a lighter grey cortex is expected to occur after a longer period of exposure. A hornfels artefact, described as ‘decayed’ denotes extreme weathering and thus the longest period of artefact exposure to wet-dry cycles. Similar to the initial stage of patination, rounding of a knapped edge may occur after manufacture and discard, likely as a result of abrasion by wind-blown sand. This state is thus assessed independently of the three surface conditions. In the rare case when the surface condition of an artefact has been recorded as showing multiple stages of weathering (i.e., recorded as both patinated and discoloured) the stage representing the greatest degree of weathering was chosen for inclusion in the following assessment.

Table 5.2. List of selected artefact attributes recorded during UPK7 RNG and rSSQ survey. Attributes not listed, but included as part of the Phase I data collection protocol can be found in the supplementary material of Shaw et al. (2019, SOM Table 1).

Category	Fields	Dataset	Attributes
Clast	Clast type	rSSQ	artefact, 'non-cultural' clast
	Maximum dimension	RNG	continuous (measurement)
		rSSQ	continuous (measurement)
	Material type	RNG	chert, glass, hornfels, igneous rock, ironstone, ochre, quartzite, sandstone, silcrete, pottery, quartz, indeterminate
		rSSQ	chert, dolerite, hornfels, ironstone, ochre, pottery, quartz, quartzite, sandstone, shale, silcrete, non-diagnostic
Typo-technology	Artefact type & Lithic class	RNG	core, core-on-flake, core-tool, tool, worked ochre, unworked piece, pottery, bead
		rSSQ	core, core-on-flake, tool, flake, flaked piece, heat shatter, pottery
	Implement type	RNG	backed pieces, bead, bored stone, burin, denticulate, hammerstone, grindstone, anvil, notched piece, bifacial point, bifacial other, pieces esquillees, unifacial point, scraper, undiagnostic tool
		rSSQ	anvil, backed piece, burin, denticulate, end scraper, hammer, notched piece, undiagnostic, pieces esquillees, scraper other, end scraper, unifacial point
	Archaeological Epoch	RNG	ESA, MSA, LSA, Neolithic, Historic
	Industry	RNG	Acheulean, Early MSA, Still Bay, Howiesons Poort, Post-Howiesons Poort, Late MSA, Early LSA, Robberg, Oakhurst, Wilton
	Cortex coverage	RNG	0%, 1-25%, 26-50%, 51-75%, 76-100%
Artefact condition	Implement Fragmentation	RNG	yes, no
	Flake Fragmentation	rSSQ	complete, longitudinal, transverse
	Surface condition		
	Patination	RNG	yes, no
	Discolouration	RNG	yes, no
	Decayed	RNG	yes, no
	Edge condition		
	Edge rounding	RNG	yes, no

Artefact attributes are drawn from multiple categories to supplement analysis into artefact spatial patterning, visibility, movement. The RNG dataset provides information for all three components, while rSSQ survey does not include information on the inferred age of finds. Together, the datasets attained from the RNG and rSSQ surveys provide morphological, technological, and chronological information on surface artefacts to test the assumptions of density, clustering, and spatio-temporal relatedness and to assess artefact spatial integrity and condition against their depositional and erosional contexts (Low et al. 2017; Will et al. 2015).

5.7.2 Data analysis

Previously published interpretations of the spatial patterning, integrity, and temporal composition of UPK7's surface archaeology state that:

- There is a spatial pattern to UPK7's surface archaeology—they are not randomly distributed.
- UPK7's surface archaeology varies in density between the top and bottom of the stack, with the highest artefact densities observed at the top of the stack.
- Artefact visibility results from the recent exposure of consolidated sediments.
- Clustered artefacts and high artefact densities are indicative of high spatial integrity and recent/short-term exposure.
- Artefacts are clustered by Industry.
- That time-diagnostic artefacts are constrained temporally by the underlying land surface (i.e., surface type, gradient, and maximum depositional age).
- Some Industries are over-represented relative to their presence in local rock shelter sequences, and some are under-represented.

Moreover, the preliminary inferences presented in Ames et al. (2020a); Phillips et al. (2019), Shaw et al. (2019, p.404) and Ames et al. (2020a) hypothesise recent erosion is most likely a result of historic grazing practices. Therefore, younger sediments and their associated Late Pleistocene and Holocene LSA artefacts are expected to be most prone to erosion and weathering. In contrast, older, harder sediment units associated with Late Pleistocene MSA artefacts are expected to show the highest levels of spatial coherence (i.e., clustering, poorly size-sorted) and less evidence for artefact weathering (i.e., fragmentation, edge rounding, surface discolouration, and feature decay).

Investigation into each interpretation and the 'recent exposure' hypothesis is carried-out in two stages with analysis involving a combination of qualitative and quantitative methods. The first stage of enquiry introduces the surface archaeology found at UPK7, followed by an examination of its spatial distribution across the locality's entire surface (irrespective of substrate)—testing for complete spatial randomness at different levels of assemblage composition (i.e., all artefacts irrespective of type, followed by artefact/lithic class, raw material type, archaeological epoch, and Industry).

If a non-random pattern is found at any of these levels, the spatial organisation of surface artefacts will be assessed for locality-wide post-depositional modification. The objective of the second component is to determine if spatial patterning is the result of preservation bias or substrate age, and if this applies to surface scatters across the entire locality or changes due to other factors. This involves the examination of artefact spatial patterning (distribution, density, and diversity) at multiple scales: the locality-wide (global) scale, by hillslope, and by substrate unit in relation to visibility, size-sorting, artefact condition, and inferred artefact age.

Investigation into the spatial patterning (where, what and how) of UPK7's surface archaeology is broadly structured around the following questions that are separated into two stages of enquiry:
Stage One – Detecting and characterising artefact spatial patterning:

1. What is the composition of UPK7's surface archaeology?
2. Is UPK7's surface archaeology spatially patterned or randomly distributed at the scale of:
    a. the archaeological population? and/or
    b. an archaeological component (i.e., artefact class, material type, archaeological epoch, archaeological Industry)?

Stage Two – Determining the constraining factors of artefact spatial patterning:

3. Have post-depositional processes influenced artefact spatial patterning by inhibiting/promoting:
    a. artefact visibility (e.g., artefact frequency depends on surface and substrate composition – hard versus soft)?
    b. artefact movement (e.g., artefact size is negatively responsive to slope position)?
    c. artefact condition (i.e., fragmentation and weathering, e.g., artefact condition corresponds with hillslope conditions)?
4. If there is a discernible relationship between the spatial patterning of surface archaeology and post-depositional processes, does this hold across the entire locality, irrespective of substrate type and age? Or does this relationship differ depending on the hillslope and/or substrate an artefact is found on?
5. If they differ by substrate, is there a spatio-temporal association between inferred artefact age and the underlying deposit age?

UPK7's Early LSA cluster was the only assemblage previously subjected to an assessment of condition and size-sorting to determine post-depositional alteration (Low et al. 2017). Minimal evidence of weathering in the form of edge rounding from abrasion, chemical deterioration of surface features, and patination of hornfels (the dominant material in the scatter – see Figure 4.3 inset) was detected (Low et al. 2017). These results will be considered in light of the given study's finding in the discussion Chapter 7. However, it should be noted that the results for size-sorting were not reported.

The first stage of enquiry involves determining if there is a quantifiable pattern in artefact density, clustering, and diversity, beginning with a visual assessment of the composition and spatial distribution of the surface archaeology in relation to its topographic setting and sediment units. This was followed by spatial and categorical analyses of artefact density, spatial relatedness, and diversity also in relation to topographic setting (i.e., elevation, slope, and hillslope position) and sediment unit. Analysis included descriptive, nonparametric, parametric, and spatial statistics across multiple programs (i.e., R, JMP Pro (14.1), MS Excel, and ArcGIS Pro). This stage of analysis draws on the RNG dataset's distributional point pattern for all artefacts and by assemblage components (i.e., artefact type and lithic class, material, implement type, inferred age). It also draws on the rSSQ dataset to test the relationship between diversity and density, creating diversity indices of artefact types and lithic classes, material types, implement type, and artefact size. If spatial variation is detected during the first stage of analysis, then the second stage investigates the possible cause of this variation. The mapped extents and surface morphometry of UPK7's

substrates are used throughout the second stage of analysis to investigate whether artefact spatial patterning is associated with specific hillslope conditions and/or sediment units, to help determine whether artefact composition and spatial distribution are the result of the main processes involved in hillslope and sediment formation (age) and erosion (duration of exposure). Artefact density is assessed against hillslope conditions using artefact location data from both datasets. To determine if spatial patterning is the result of visibility, the spatial distribution of artefacts will be assessed in relation to depositional features that have the potential to inhibit exposure (i.e., unconsolidated, or loose sediment versus consolidated or hard sediment). Contingency analysis is performed between artefact frequency and substrate type to determine if there is a significant association between each variable and the strength of this association.

Visibility is assessed through contingency analysis to determine the association between artefact frequency and substrate composition (loose versus consolidated). Artefact movement is also assessed to determine if artefact density/clustering results from disaggregation and/or artefact attrition as a result of runoff. This can be detected where artefact density shows a negative correlation with hillslope angle or in size-sorted artefacts where artefact size is negatively responsive to slope position. To determine if surface artefacts are organised across UPK7's sloped surface as a result of runoff, the randomly recorded location and maximum dimensions of rSSQ flakes were assessed for size sorting by topographic setting—this entailed the non-parametric analysis of median differences between hillslope zones in JMP Pro. The impact of rill development and proximity on artefact movement is also assessed. This involved producing buffer zones extending out from the centre of each rill at 0.5 m intervals in ArcGIS Pro and assessing artefact counts and median max dimension as a function of distance from rill channel and rill development (or stream order, denoted by Strahler class). This will provide a controlled assessment of the degree of size sorting due to surface wash of the identified archaeology at fixed distances away from the rill system.

The condition of artefacts in relation to their topographic and depositional contexts were also assessed by pulling together data from the geomorphological results and both the RNG and rSSQ datasets. Specifically, assessment of the extent and variation in artefact fragmentation was assessed based on the proportional frequencies of artefact breakage by topographic and substrate setting, and their association tested using a Pearson's Chi-square test for independence. This analysis draws from spatial and attribute information on implement breakage from the RNG dataset as well as flake breakage from the rSSQ dataset. Categorical data analysis and Chi-square tests for independence were also carried-out to investigate the relative states of weathering in relation to different topographic and depositional contexts. Information on artefact location, raw material, and clast condition data from the RNG dataset were used to analyse the surface and edge condition of these artefacts by topographic and substrate setting.

5.7.2.1 Artefact age

In stratified contexts (e.g., cave, rock shelter and midden sites), independent dating is made possible through the analysis of the deposit and/or direct dating of sediment or well-preserved organic matter. In the case of the former method, the assumption is that an artefact found within a deposit is an integral part of the deposit's sedimentation process and therefore 'shares' its depositional age. However, in surface contexts association between non-diagnostic archaeological objects can only be temporally constrained through a combination of spatial associations—proximity to a time-diagnostic and/or directly dated artefact or feature

(i.e., a hearth), and/or its underlying deposit, depending on its spatial integrity. Burial ages of underlying deposits provide maximum ages for overlying surface archaeology, and thus help to test the technological Epoch and Industry-based observations inferred from diagnostic surface artefacts. For example, if we are to follow the stratigraphic ordering of Industries identified in southern African rock shelters, then the deposit age underlying the post-Howiesons Poort cluster at UPK7 (analysed by Will and Mackay et al., 2015) should be no younger than 50 ka (see Table 5.3), and probably, given the presence of 'Nubian' Levallois cores, no younger than 55 ka. If a younger age is returned then several behavioural or post-depositional possibilities may explain this outcome: e.g., 1, post-Howiesons Poort artefacts were moved onto a younger surface from an older surface due to either cultural or non-cultural mechanisms; 2, the cluster and its diagnostic artefacts are not indicative of the post-Howiesons Poort; or 3, technology resembling the post-Howiesons Poort occurs later in the Doring River valley than in the rock shelter sequence. Moreover, the highly clustered distributions of similar artefacts should not rest on much older sediment units, because the implied duration of exposure should have resulted in their disaggregation (Phillips et al 2018). Thus, the analysis of time-diagnostic artefacts at UPK7 involves determining their spatial structure, spatial relatedness, the age of the artefact's underlying substate and the nature of their spatio-temporal association by assessing the effect of post-depositional processes on artefact spatial integrity.

The spatial distribution of inferred artefact ages recorded during RNG survey are assessed in relation to their taphonomic context and the geochronological findings presented in this study. Time sensitive artefacts, deemed 'diagnostic' of an Industry and Archaeological Epoch (or Stone Age), were recorded throughout each stage of the RNG survey. Assignment of culture historic units to time-diagnostic artefacts were based on the prevailing chrono-stratigraphic framework established for the region and supplemented by excavated sites within the catchment (see Table 5.3 and citations therein). A reference collection was assembled from stratified catchment examples (i.e., Klipfonteinrand, Mertenhof, Putslaagte 8 and Putslaagte 1) and referred to throughout survey (Shaw et al. 2019). This helped to maintain consistency throughout the field season and to reduce inter-surveyor bias. Table 5.3 lists the regional chrono-stratigraphic sequence of each archaeological epoch and associated Industries as well as a list of the main technological attributes that characterise each Industry.

Analysis involved an assessment of spatial patterning of inferred ages (i.e., at the archaeological epoch and industry scale) to determine if they are clustered. Their spatial distribution is also assessed in relation to substrate extent and age to determine if it corresponds with the depositional history of the locality. Spatial analysis of time-diagnostic artefacts at the level of the archaeological epoch combines visual assessment with analyses of their density and contextual association. Density analysis was performed using the Optimized Getis-Ord Gi* Hot Spot tool in ArcGIS Pro, while association between archaeological epochs and substrate age were determined based on their observed and expected proportional frequencies by substrate unit, testing for independence using the Pearson's Chi-Square goodness-of-fit test.

Table 5.3. Characteristics of Regional Industries for the ESA, MSA, LSA, and Neolithic

Epoch	Industry	Marine Isotope Stage (MIS)	Age (ka) (approx.)		Technological characteristics	Raw material selection
			Regional*	Local^		
ESA	Acheulean	>8	>200/300		LCTs** (handaxes, cleavers, picks), large flakes (>100 mm in length)	Local
	Fauresmith		500-280/150		LCTs and small handaxes, blades, and points	Local
MSA	Early MSA	5-8	80-300	>76	Highly variable. Denticulates, Levallois points, long blades	Local
	Still Bay	5	70-80 (70-110)	72-87	Bifacial points, bifacial thinning flakes	Some silcrete
	Howiesons Poort	4	60-65 (60-110)	58-71	Backed artefacts, notched blades, blades	Silcrete
	Post-Howiesons Poort	3/4	50-60	?	Unifacial points, scrapers, Levallois points, blades	Some silcrete
	Late MSA	3	30-50	33-50	Highly variable. Blanks. Types incl. points, flakes	Local
LSA	Early LSA	2/3	18-40	22-27	Highly variable. Bipolar reduction common, pieces esquillees (scaled pieces), retouch is rare. Local signal: hornfels blade production.	
	Robberg	2	12-18	16-23	Microlithic. bipolar technology, small blades, single platform bladelet cores, pieces esquillees, retouch rare.	Increase in fine grain materials (i.e., chert, silcrete)
	Oakhurst	1	7-12	13-17	Large side-struck flakes, scrapers, naturally backed knives, retouch uncommon otherwise, blades and bladelets rare.	
	Wilton	1	4-8	3.6-6	Microlithic. Retouch common and standardised, small convex scrapers and backed pieces & geometrics, blades & bladelets common.	
	Final LSA	1	0.1-4	?	Highly variable. Scrapers, segments, backed bladelets, adzes, large unretouched flakes.	Fine grain materials (chert, quartz, silcrete)
Neolithic	Ceramic final LSA/Late Holocene (pottery	1	<2	1.7-0.2	Pottery, long end scrapers, backed artefacts (retouch frequency variable).	Fine grain materials (i.e., chert, quartz)

*Industries and their associated regional ages mostly pertain to those described for the modern year-round and winter rainfall zones (Deacon 1984; Herries 2011; Jacobs 2010; Jacobs et al. 2013; Jacobs & Roberts 2008, 2015; Jacobs et al. 2008; Lombard et al. 2012; Lotter & Kuman 2018; Mackay et al. 2014a; McNabb & Beaumont 2012; Mitchell 1988; Tribolo et al. 2013; Wadley 1993; Wurz 2013). Ages in parentheses refer to older ages obtained from Diepkloof Rock Shelter, published in (cf. Feathers 2015; Jacobs & Roberts 2015, 2017); Tribolo et al. (2013); ^local ages derive from dated catchment sites Putslaagte 8, Klipfonteinrand, and Hollow Rock Shelter (Högberg 2014; Low & Mackay 2016; Mackay et al. 2019; Mackay et al. 2015; Mackay et al. 2014b; Shaw et al. 2019); **Large Cutting Tools (LCT). Table modified from Will et al. (2015). Dashed horizontal line indicates a transitional Industry.

Density analysis could not be applied to time-diagnostic artefacts at the Industry level due to sample size. According to Shaw et al. (2019: table 4), the Industries identified on the consolidated and semi-consolidated sediments at UPK7 include the Still Bay (n = 19), Howiesons Poort (n = 11), post-Howiesons Poort (n = 51), Late MSA (n = 95), Early LSA (n = 55), Robberg (n = 36), Oakhurst (n = 59), Wilton (n = 49), and Pottery-period (n = 178) fragments. When these numbers are divided into multiple contexts, their low frequencies preclude the application of most statistical analyses. Thus, in a similar vein as Ames et al. (2020a), nearest neighbour cluster analysis was performed using ArcGIS Pro to supplement and test visual interpretation of clustering. A contingency analysis was also performed to compare the observed frequencies of Industry diagnostic artefacts to expected frequencies for each underlying substrate unit. However, in some cases artefact counts were below 5, precluding a Pearson chi-squared test of association for determining a relationship between substrate units.

CHAPTER 6.
RESULTS: PHYSICAL ATTRIBUTES

6.1 Introduction

The objective of this chapter is to present the results of the field sampling and analysis of UPK7's main lithological and sedimentary units, including the identification and characterisation of each unit, their stratigraphic association, relationships and depositional age, and the main processes involved in their formation. The following sections describe each sedimentary unit in the proposed order of their deposition (from oldest to youngest deposit), beginning with the basal units of bedrock, hillslope colluvium and palaeoterrace (subsections 6.2.2 to 6.2.4). This is followed by a description of the overlying sand mantle (subsection 6.2.5; Table 6.1) and the results of the electrical resistivity survey (subsection 6.2.6) to provide insight into the stratigraphy and subsurface topography of UPK7's basal units. The characterisation of the lithological units concludes with a proposed scenario for the formation of UPK7's sand mantle (subsection 6.2.7). This is followed by the results and analysis of the OSL ages of the sand mantle's consolidated units (section 6.3). The final section presents an appraisal of the dominant processes involved in UPK7's formation to establish their potential impact on the visibility and movement of its archaeology (section 6.4), analysed in detail in Chapter 7 (*Results: Surface Archaeology*).

Table 6.1. Identified sedimentary units that contribute to the foundation and sand mantle of UPK7, listed in their stratigraphic sequence.

	Unit	Abbreviations	Description
	Modern terrace	MT	The actively aggrading landform. The most recent terrace (T0) to have formed at the base of the bank-attached bar, south of and parallel to UPK7's palaeoterrace.
Sand Mantle	Unconsolidated Sand	UCS	The most extensively exposed and youngest unit. An extensive sand sheet and dune of unconsolidated and semi-consolidated sand. Low-lying, shallow-rooting vegetation intermittently covers this unit.
	Indurated Sand	IS	Indurated sandy sediment, with a crusted surface, prone to rilling and rarely vegetated.
	Upper Yellow	UY	Consolidated sand with dispersed inclusions of calcrete nodules (i.e., rhizoliths).
	Lower Red	LR or LRcc	Consolidated red sediment with and without veins or nodulated inclusions of calcium carbonate (cc).
	Palaeoterrace	PT	Composed of alluvium and riffle boulders forming a bank-attached paleochannel bar (observed as an exposed boulder bed and bench of colluvium).
	Colluvium	C	Composed of hillslope cobble and pebble-sized float to the north of, and beneath, the sand mantle.
	Bedrock	BR	Composed of clastic sedimentary rock from the Ceres Subgroup (Devonian Period, Palaeozoic Era) of the Bokkeveld Group (see section 3.2.2). Its dominant lithological units include alternating sandstone and shale. South or upriver of UPK7 the Doring also cuts through the quartzitic sandstone and mudrock of the Witteberg Group. The river's north-eastern catchment carves into shales and sandstones of the Karoo Ecca Group and diamictite of the Karoo Dwyka Group. Its south-western catchment carves through the quartzitic sandstone of the Cape Table Mountain Group.

Table 6.2A and B define the dominant characteristics of each identified lithological unit at UPK7, including any incipient soil B-horizons (i.e., the zone of cement accumulation observed in profile; see Table A4.0.2 for soil descriptions by individual sample). It should be noted that B-horizons do not necessarily indicate an erosional break, particularly in dry regions where they can occur well below the sediment surface. Where possible, the basal and upper contact for each unit is given. In some cases, more than one unit of contact was observed and is listed accordingly (Table 6.2A). The basal and upper contact fields are clear indicators of the disconformities that exist throughout UPK7's stratigraphic profile, with missing units suggesting differential erosion across the site. Because trench excavation and coring were not possible visibility was limited to surface and natural exposures. For this reason, the thickness of individual units was estimated from the results of the electrical resistivity survey and/or naturally exposed sections (i.e., the exposed sides of gullies and tributaries). Exposed sections were cleaned back prior to measurement. Thus, unit thickness should be taken as an estimated, minimum value since either the tops of each unit have likely eroded and/or the base of each unit was not exposed due to excavation restrictions.

Matrix colour lists the dominant lithochromic colour of a unit's matrix in the form of Munsell® notations (hue, value, chroma) and/or name (i.e., 7.5 10 YR, yellow brown; Table 6.2A). These derive from the dry, exterior, and crushed determination of unit samples using the Munsell® colour chart. The sample range in mean particle size, sorting, rounding, and consistency are provided for each unit to characterise their texture class (Table 6.2B). Particle size was determined from the numerical portion of sand, silt and clay that was measured from the fine earth fraction (< 2 mm) of each unit's sample set (see Chapter 5, subsection 5.4.3), while sorting, rounding and consistency are collated from sediment samples and in-field descriptions presented in Appendix 4. The dominant sedimentary structures are also given for each unit (Table 6.2A). Sedimentary structure is defined here as '...the natural organization of soil particles into discrete soil units (aggregates or peds) that result from pedogenic processes' (Jahn et al. 2006, p.44). Mottles are areas of sediment where the colour differs from that of the matrix (Schoeneberger et al. 2012, pp.2-9 to 2-12). They are attributed to pedogenesis or weathering as opposed to the source rock, e.g., Mottling refers to secondary soil colours not associated with compositional properties. Redoximorphic features are a type of mottle associated with wetness. Lithochromic mottles are a type of mottling associated with variations of colour due to weathering of parent materials. Note that mottling was not identified in UPK7's sedimentary or lithological units.

Table 6.2A. Dominant characteristics are summarised for each unit, including their stratigraphic relationship with other units, their thickness, location, colour and sedimentary structures. Listed in their stratigraphic sequence.

Unit	Basal contact	Upper contact	Thickness (m)		Sample Depth (bls m)[b]	Elevation (m asl)[c]	Distance from River	Matrix Colour	Sedimentary Structures[d]
			Observed	ERT[a]					
Modern Terrace/ Alluvium (T0)	PT; BR	None	-	-	0-0.5	192-195	16-40	-	Structureless-single grain (weak)
UCS/SCS	SCS; IS; LRcc	None	0.6-1.4	5	0-0.7	202-215	127-248	10 YR 6/4 (light yellowish brown)	Structureless-single grain and layered (thin laminations, weak)
IS	UY?; LRcc	UCS; SCS	0.1-3.7	4	0-2.7	202-211	142-222	Yellowish brown	Massive and layered (weak, thin laminations); fine surface cracking; crusted surface of varying thicknesses (10-20 mm); porous.
UY	LR; LRcc	UCS; SCS	0.28-0.32	2-5	0-0.24	214-215	243-268	10 YR 5/6, (yellowish brown)	Massive and blocky subangular; crusted surface; porous
LR/LRcc	LRcc; C	LR; UY; IS; UCS	0.3-0.8	3-7	0-0.6	208-218	201-261	Yellowish to reddish brown	Structureless-massive (cemented)/blocky-subangular to angular; desiccation cracks and carbonate infilling; crusted surface; porous
Palaeoterrace	BR	LR; UY; IS; UCS	2.6	8	-	-	-	-	Granular
Colluvium	BR	LR; UCS	-	1.5	0-0.05	207-212	223-259	7.5 YR 7/6 to 7.5YR 5/6 (reddish yellow to strong brown)	Granular; fine desiccation cracking; crusted
Bedrock	Not visible	C; PT	-	-	-	-	-	Reddish to light grey	Massive; layered

[a]Electrical Resistivity Tomography; [b]Below surface (bls); [c]Above sea level (asl); [d]Source: FAO (1990)

Table 6.2B. Texture and common inclusions summarised for each unit. Listed in their stratigraphic sequence.

Unit & Sample IDs	Texture						Inclusions
	Vol. Weighted Mean Particle Size Sample Range (µm)[a]	Particle Size Class[a]	Sorting (Std Dev phi Φ)[b]	Rounding	Consistence (dry)	Texture Class[a]	
Modern Terrace/ Alluvium (T0)	374-559 µm	Medium sand	Poorly sorted (1.03-1.21)	-	Loose	Sand	None
UCS/SCS	203-417 µm	Medium sand	Moderately to poorly sorted (0.50-1.20)	Medium sphericity; subangular to subrounded	Loose	Sand	Fine roots; insect burrows
IS	140-225 µm	Fine to medium sand	Poorly to very poorly sorted (1.53-2.10)	-	Indurated, hard, smooth	Loamy sand	Small calcrete nodules; fine roots; insect burrows
UY	119-157 µm	Very fine to fine sand	Poorly to very poorly sorted (1.98-2.20)	-	Indurated, slightly hard to hard	Sandy loam to loam	Effervescent; calcrete nodules (≤60 mm diameter); fine roots; stone artefacts
LR/LRcc	95-500 µm	Very fine to medium sand	Poorly to very poorly sorted (1.37-2.56)	Moderate to high sphericity; subrounded and subangular	Indurated, slightly hard to very hard	Sandy loam to loamy sand	Insect burrows/casts; hard small calcrete nodules (≤55 mm diameter); salt crystallisation; fine roots; pores; rugose biocrusts
Palaeoterrace	-	-	-	-	-	-	-
Colluvium	100-750 µm	Fine to medium sand	Very poorly sorted (2.47)	Moderate sphericity, subrounded	Compacted, hard	Sandy loam to loam	Stoney (5-300 mm max. dimensions), clay coating on quartz grains
Bedrock	-	-	Well sorted	-	Lithified, extremely hard, cemented	Sand	Quartz grains

[a]Source: FAO (1990); [b]Source: Folk et al. (1957)

6.2 Geomorphological Features and Unit Characterisation

The main geomorphological features together with the lithological and sedimentological units that contribute to the landform of UPK7 were identified during field work and remote survey are outlined in the following subsections.

6.2.1 Hillslope overview

UPK7 is located on a northern bank of the Doring River (~195 m asl), at the tail-end of the Biedouw-Doring River confluence, a long medium-gradient hillslope that forms the nose slope of an interfluve of the Doring River (Figure 5.1a & b). Its landform of sandy, vegetated sediment rises ~20 m above a channel floor of alluvium and outcropping mudrock and sandstone of the Bokkeveld bedrock (Ceres Subgroup), gradually increasing in elevation from the modern river terrace in the south-west (196 m asl) to a dune crest in the north-east (216 m asl; Figure 5.1). Diffusive weathering as a result of sheet wash, mass movement, and slope creep from the plateau's interbedded rock sequence has produced a rectilinear hillslope of outcropping mudrock and sandstone bedrock, covered by colluvium and shallow rooting succulent (Tankwa Karoo) vegetation (Figure 3.3 & 3.9, see Chapter 3). Cutting into either side of the hillslope are two ephemeral tributaries, the western and eastern tributary (Figure 6.1a,b). These have scoured down through bedrock, introduced coarse, matrix-supported material to the valley floor, and partly exposed a palaeoterrace in the process (i.e., Figure 6.5). The hillslope is also pocked by heuweltjies (Figure 6.1)—large circular sediment mounds, or remnants of mounds, that are visually distinct from the surrounding colluvium (Ames et al. 2020; Cramer et al. 2016; Midgley et al. 2012; Potts et al. 2009). The hillslope is defined by a foundation of bedrock and colluvium in the north and palaeoterrace in the south-west (see Figure 6.1). The palaeoterrace is covered by a mantle (or 'stack') of loose sand and consolidated sediment that yields archaeology (Mackay et al. 2014). The modern channel features (i.e., riffle boulders, alluvium) and associated terrace—about 5 m above the channel floor—form UPK7's modern riparian margin (Figure 6.1).

Structural features—historic or otherwise—were not observed on the sediment stack or on the length of its hillslope (Figure 6.1). However, there is an unusual erosional feature that rises above the sediment stack's consolidated substrate, which is covered and encircled by medium to large sandstone river cobbles (Figure 6.2). This topographic anomoly could be indicative of a destabalised structure that capped and protected the underlying substrate while surrounding sediment deflated. Another possibility is that it is a remnant coppice dune, which could also protect overlying and proximate archaeological material as the surrounding surface deflated, giving the appearance of a concentrated area of activity. There are also circular stone ruins to the immediate east of the eastern tributary and at UPK9, indicating that the surrounding area has been repeatedly used and modified for farming and grazing purposes (Figure 6.3). The circular cluster of foundation stones next to the eastern tributary have lost their original structure and are possibly older than the historic stone buildings farther east (Figure 6.4). These stone clusters are possibly the deflated remnants of historic herder huts or small kraal. Such huts were called 'lammerhok' and were used by individual sheperds living with stock herds who moved across fenceless terrain to graze. Their use depleted with the widespread establishment of fencing and the implementation of the first Fencing Act in 1883 (Van Sittert 2002).

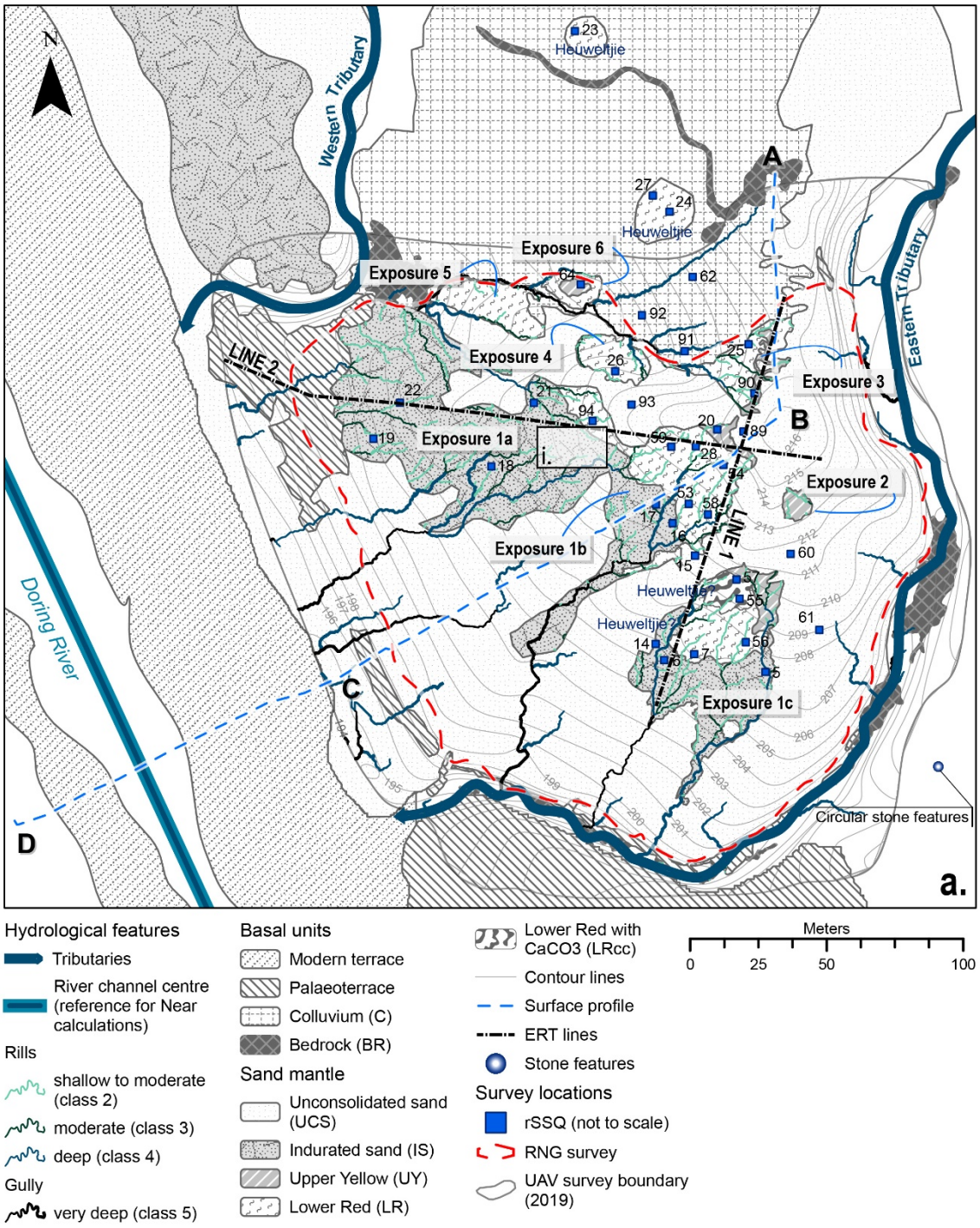

Figure 6.1a. The horizontal extent of exposed sedimentary units across UPK7. Map (a) also shows the location and unit number of each rSSQ, exposure numbers, elevation, hydrological features, the location of the circular stone features to the southeast of the Eastern Tributary, the location and orientation of ERT lines 1 and 2 (black dashed lines), and the surface profile line from A to D (blue dashed line) depicted in profile in Figure 6.1b (below).

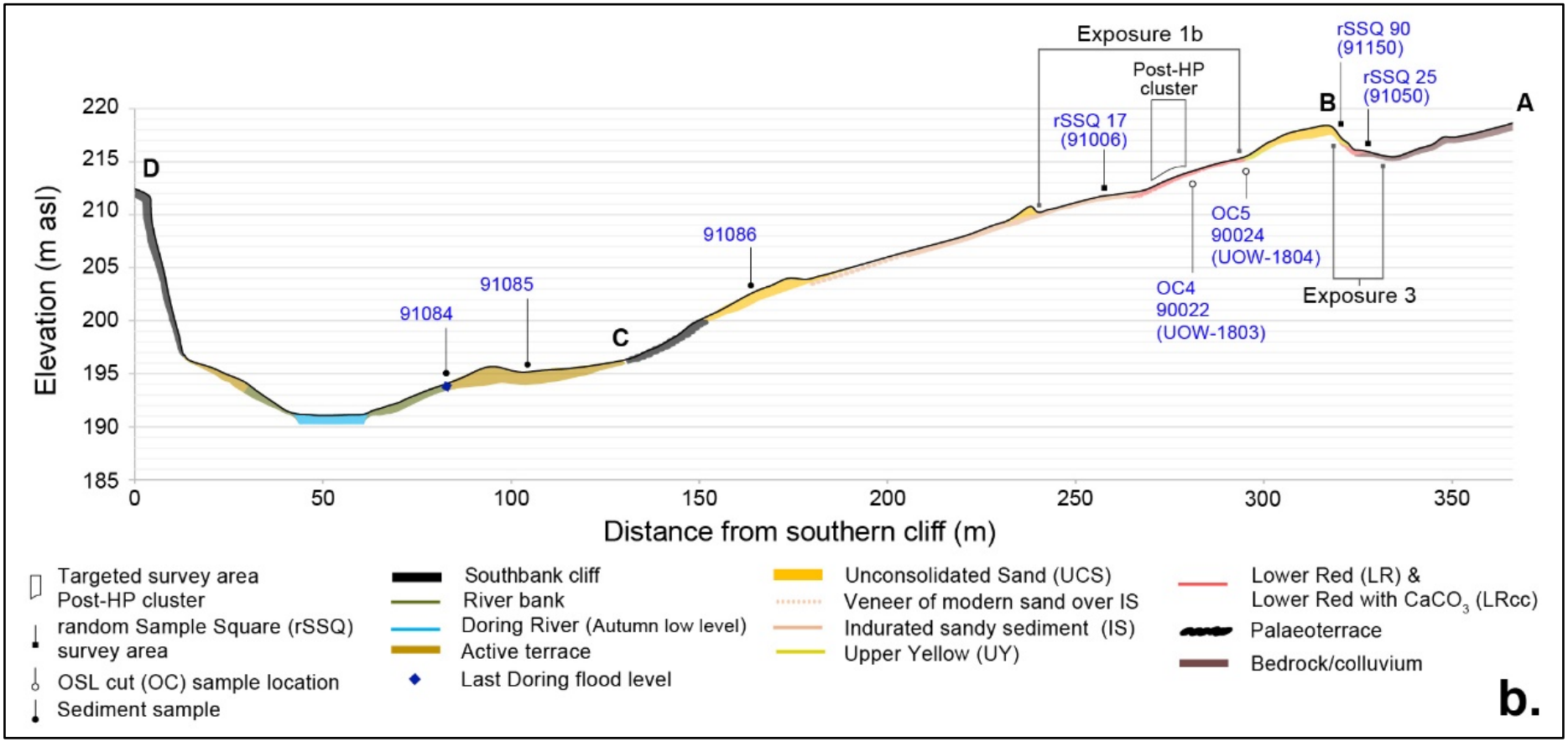

Figure 6.1b. The vertical depiction of the surface profile line (shown in Figure 1.6a [above] as a blue dashed line) facing downriver (north-west) showing the topography and horizontal extent of exposed sedimentary units observed across UPK7, between A and D. The surface profile (b) also shows proximate sediment and OSL sample locations collected along or close to the transect, the location of consolidated sediment exposures, 1b and 3. Note transect orientation shifts from a north-south bearing to a north-east to south-west bearing between B and D (see Figure 6.1a above).

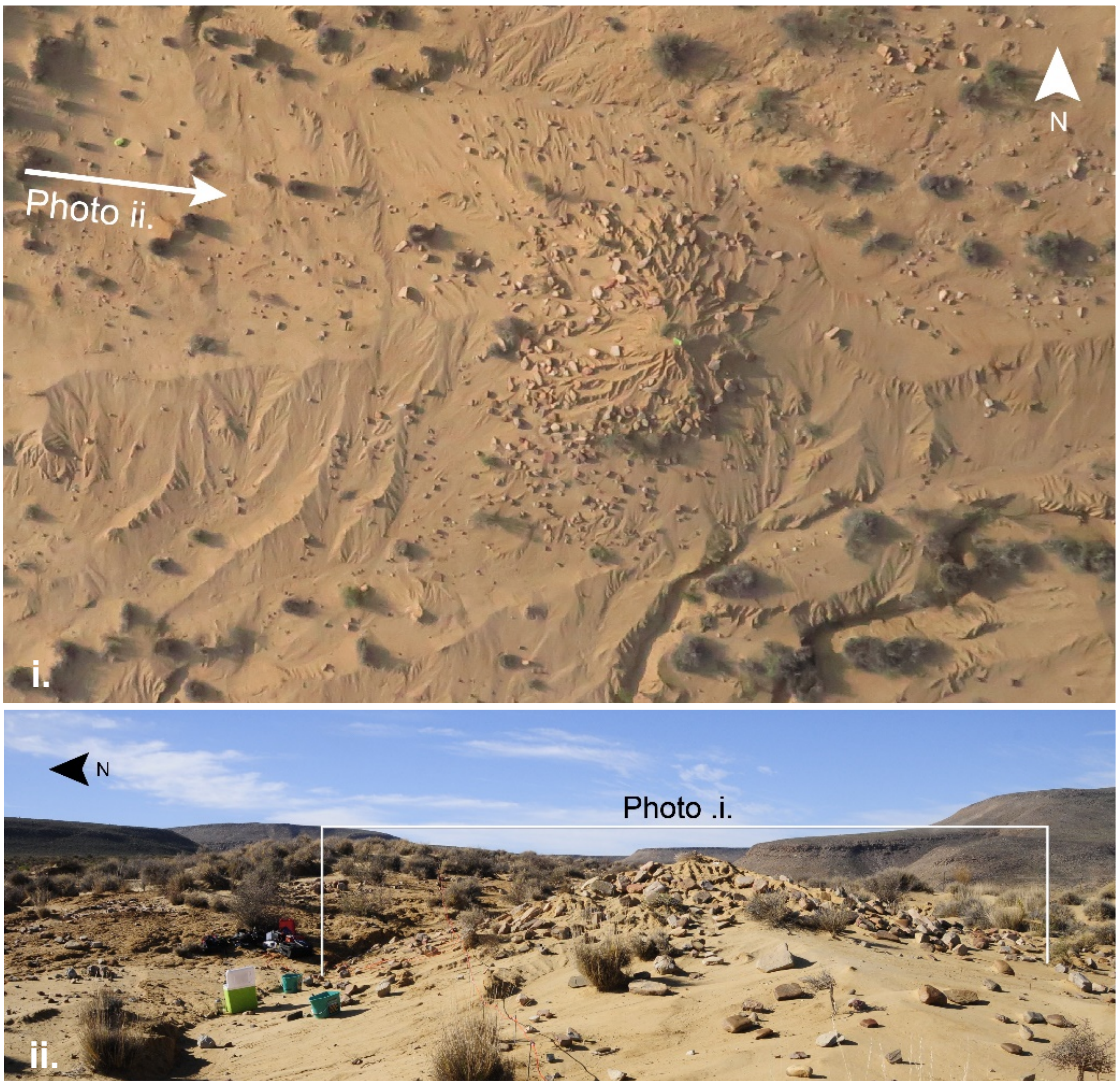

Figure 6.2. Photographs of an eroding sediment mound in the south-western slope (Exposure 1a) of UPK7 (see Figure 6.1, inset 'i'), depicting two views: The aerial (top, north at top of frame) and ground (bottom, facing east).

Figure 6.3. Circular stone ruins to the immediate east of the eastern tributary and at UPK9 (see Figure 6.1 'circular stone features' for the area in which they are located). These are possible deflated remnants of historic herder huts or small kraal, called 'lammerhok', used in the nineteenth and early twentieth century before the widespread use of fencing and the Fencing Act 1883. The length of the red field notebook is ~190 mm.

Figure 6.4. Historic stone buildings at UPK9 (see Figure 5.1a).

6.2.2 Bedrock

The Ceres Subgroup (Bokkeveld Group [485 – 330 Ma], Cape Supergroup) forms the dominant lithostratigraphy in the study area (see Chapter 3.2.2) and is observed beneath UPK7's sand mantle and paleochannel deposits (Tables 6.1 and 6.2A-B). The Ceres Subgroup is made up of three sandstone and three shale units. Its resistant sandstone bedding forms the northern cliff of the river channel north-west of UPK7 and outcrops in the bed of the western tributary and again in the upper eastern fringe of UPK7's colluvial hillslope. From this point it disappears beneath dune sand before reappearing at the base of the eastern tributary (Figure 5.1 & 6.5; Tables 6.1 and 6.2A-B). Accordingly, UPK7's exposed bedrock comprises well sorted quartz dominated, sandstone that alternates in structure from massive to layered and ranges in colour from reddish to light grey (Table 6.2A).

6.2.3 Tributaries

The bounding tributaries on the eastern and western side of UPK7 are active. The steep angle of descent, and the highly compacted state of sandstone cobbles and bedrock slabs observed in each tributary indicate intermittent, high-energy flows (Figure 6.5). Leeside dune sand was observed avalanching down into each channel from the west. However, the exposed bedrock observed at the base of both tributaries indicates active removal of these sands during rainfall events (Figure 6.5).

Figure 6.5. Photos of the exposed western bank of the eastern tributary showing the Palaeoterrace and a close up of its profile, exposed above bedrock and below the vegetated sands of the sediment stack. Photo taken in the eastern tributary looking north-west; west of the circular stone structures shown in Figure 6.1.

Compared to the eastern tributary, the western tributary cuts a steeper, more direct passage from the top of the northern plateau to the river below (Figure 5.1). It is shorter (~0.7 km) than the eastern tributary (~3.8 km), with outcropping bedrock exposed midway down the hillslope, creating a resistant surface before arcing west towards its outlet, away from the main sediment stack of UPK7 (see Figure 5.1). Fed by seven minor channels, the eastern tributary has a larger catchment than the western tributary and takes a meandering route from the top of the plateau to its outlet in the Doring River channel (see Figure 5.1).

As the eastern tributary reaches the lower hillslope, it is fed by two minor tributaries. One cuts a north-west to south-east route behind the colluvium slope of UPK7. The other runs from UPK9 in the east before joining the eastern tributary in the south-west, 170 m from the current eastern tributary outlet position (Figure 5.1). Together with debris flows from the hillslope, the load of these tributaries has contributed sediment and colluvium to UPK7, while also assisting in down-cutting bedrock as they joined the Doring River channel. This is suggested by the presence of alluvium, river cobble and cobble-sized slabs of bedrock exposed in several places along the eastern and western sides of both tributaries (i.e., Figure 6.5), which indicated the presence of a palaeoterrace and possible alluvial fan that underlies the sediment stack of UPK7.

6.2.4 Palaeoterrace

A bench of coarse water worn sandstone gravels crop out from beneath the sand mantle in the north-west, forming the eastern bank and outlet of UPK7's western tributary (Figure 6.1 and Figure 6.6A-B). It forms the westernmost part of the palaeoterrace that underlies the sand mantle of UPK7 (Figure 6.1). It was also observed cropping out from the western side of the eastern tributary, below the sand mantle and above bedrock (Table 6.1). Its profile in Figure 6.5 (inset) grades from clast to matrix supported. From the base of the hammer upwards the deposit is clast supported and is composed of imbricated water-warn sandstone gravels and pebbles that are angular to subrounded. Their clast size, orientation and imbrication are indicative of a high-energy fluvial system from up channel. The finer detritus between clasts is indicative of the intermittent nature of these flows (Figure 6.5).

This bench represents the exposed surface of a gravel-dominated attached bar that runs parallel to the modern terrace and is indicative of high energy transport that can only be achieved in flowing channels, distinguishing the palaeoterrace from the colluvial hillslope to the north. It possibly formed from the combined accretion of alluvium from the tributaries and the south-west downcutting and migration of the Doring River (Figure 5.1). Based on the difference in elevation observed from outcropping river boulders, the maximum thickness of the exposed palaeoterrace is ~5 m (Figure 6.1b).

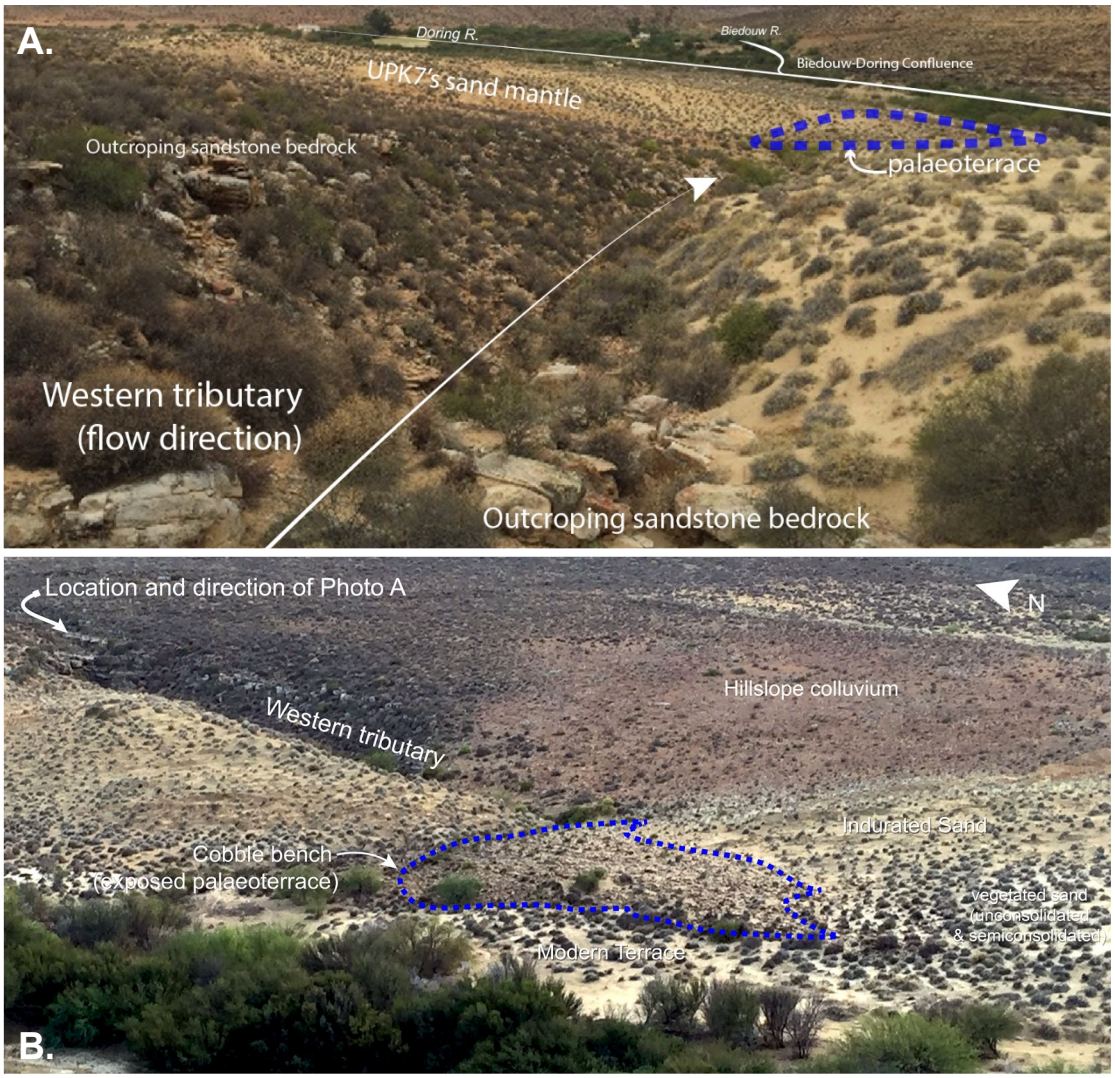

Figure 6.6. UPK7 western tributary and palaeoterrace. A. shows the western tributary from the north, looking towards UPK7's sand mantle and Doring-Biedouw River confluence, with the colluvial hillslope to its east, aeolian sand to its west, and the palaeoterrace to the west (blue dashed line). B. was taken from the southern cliff road facing north-east and shows the Doring river channel in the foreground and the western tributary outlet with the palaeoterrace (blue dash line) cropping out from beneath UPK7's sand mantle on the right.

6.2.5 Sand mantle

UPK7's mantle of sandy sediment drapes across the palaeoterrace and hillslope, rising from the modern terrace in the south-west towards the north-east (Figure 6.1b), with its highest point ('B' in Figure 6.1) located where the ridges of two dunes intersect. The ridge of the 'northern' dune extends from the south-east to the north-west—separating the colluvium in the north (the leeward side) from consolidated sediment, modern terrace, and river channel in the south (Figures 6.1). The second, 'eastern' dune delineates the eastern side of the sediment stack. It extends from the north to the south, with its slip face (leeward side) feeding into the eastern tributary and its windward side contributing to the stoss slope of the 'northern dune' and the colluvium in the north (Figure 6.1). Highly consolidated sediment appears to be recently exposed on all slopes by wind and water erosion that has deflated and stripped away overlying unconsolidated sand and vegetation (Figure 6.1, e.g., see Figure 5.1). A possible heuweltjie is exposed as a flat bench in the

middle of a south-eastern exposure of consolidated sediment providing a more resistent surface to these erosional processes compared to its surrounding (Figures 6.7 & 6.1).

Water erosion is indicated by the network of rills and gullies that have incised the middle to lower zones of the windward slopes (e.g., Figure 6.7). Rills begin in the upper hillslope zones of the sand mantle's consolidated sediment, with nick points developing into wide, shallow channels across this zone. As the network of rills travel down each hillslope, they have narrowed and deepened, becoming 'moderately developed' channels (Strahler 2-3 in Figure 6.1). In the lower zones of the south-facing exposure rills have developed into gullies (Strahler 4), forming a single deeply incised channel that feeds runoff from the surrounding surface to the base of the sediment stack and tributaries (Strahler 5 & 6, Figure 6.1).

Water erosion has also cut into the northern side of the sediment stack, possibly from hillslope runoff as well as an overflowing eastern tributary. This has removed consolidated and loose sand from the northern dune's slip face and the western side of the eastern dune's windward slope. It has also scoured and separated an island of residual consolidated sediment from the main stack (Figure 6.8). This residual mound of sediment overlies and is now surrounded on all except its south side by colluvium (Figure 6.1, Exposure 6).

To help delineate between hillslopes of consolidated sediment with different aspects or that are separated by unconsolidated sand/colluvium (i.e., the north facing hillslopes), they were given an area ID and termed 'Exposure' (see Table 6.3 and Figure 6.1). The south facing hillslope was subdivided into three parts due to its extensive surface area: Exposure 1a, 1b, and 1c, from west to east (Figure 6.1 and Table 6.3). Exposure 2 is the same area as 'Area of Analysis' 3 (AoA 3) in Low et al. (2017) (see Figure 5.3).

Table 6.3. List of Exposure names and their average aspect. See Figure 6.1 for locations.

Exposure	Hillslope aspect
1	south
a	south-west
b	south-west
c	south-east
2	east
3	west
4	north
5	north
6	north-east-south-west

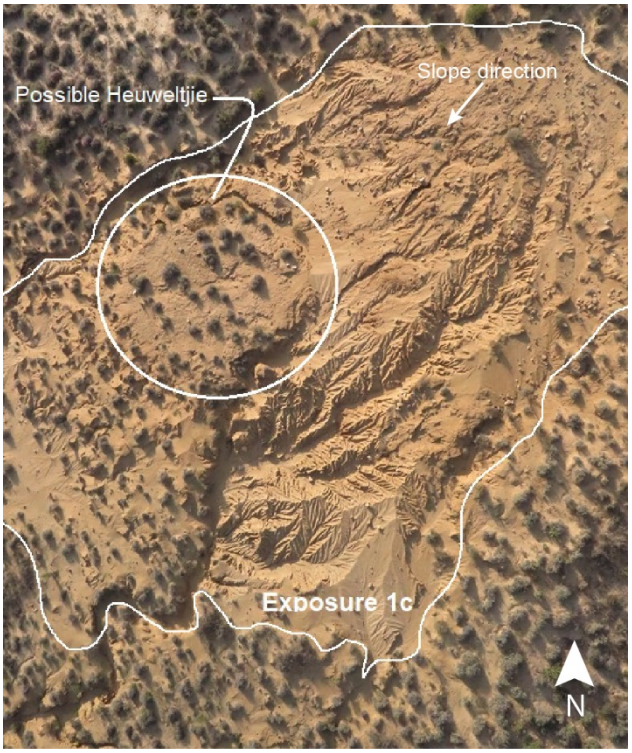

Figure 6.7. A possible heuweltjie is exposed on the consolidated sediment.

Figure 6.8. North-east facing photograph of Exposure 6, a residual island of consolidated sediment separated from the main sand mantle and surrounded on all but its south side by colluvium (see Figure 6.1). Note the heuweltjie in the background (dashed line). Aurore Val (height: 1.65 m) stands to the left of three OSL sample locations (see Appendix 4.1.4 and Figure A4.1.17 for details).

6.2.5.1 Lower Red without (LR) and with $CaCO_3$ (LRcc)

The oldest consolidated sediment unit at UPK7 is a yellowish brown, indurated sandy loam to loamy sand (Table 6.2A). It appears highly weathered and underlies the UY, IS and U-SCS units. Despite its dominant Munsell colour (10 YR 5/6; Table 6.2A), this unit appeared redder than its overlying units when observed in the field. As a result of this distinction, it was labelled the 'Lower Red' (LR) unit. The LR unit also occurs with and without calcium carbonate (cc), in the form of small calcrete nodules or the carbonate infilling of desiccation cracks. Its sedimentary structure varies from structureless (massive) to being comprised of blocky-angular and subangular aggregates (Table 6.2A).

Together, the exposed surface of the LR and LRcc measures a total of 3942 m^2. It is exposed as a residual mound of sediment in Exposure 6, above the colluvium in the north (Figures 6.1 & 6.8). The Lower Red unit was also observed as an exposed surface at the mid-zone of UPK7's southern slope where erosion and transportation are likely to be at their most intense (i.e., the transport slope; Figure 6.9). Its exposed extent on the southern slope extends from the north-west to south-east, across the main Exposures 1b and 1c (Figure 6.1). The LR occurs at the top of the slope, from underneath overlying UY sediment, while the LRcc appears at lower elevations, farther down the slope, before being covered by the IS (Figure 6.1a,b). On the north side of the sediment stack, from the top of Exposure 3's hillslope to the colluvium at its footslope, the sedimentary profile transitions from the UCS and UY to the LR (Figure 6.1). To the west, the steep residual mound of Exposure 6 shows the LR capped by UY sediment. LR is exposed between the top and mid-section of the slope, with a deposit of cumulic soil on the footslope overlying surrounding colluvium (Figures 6.8 & 6.9).

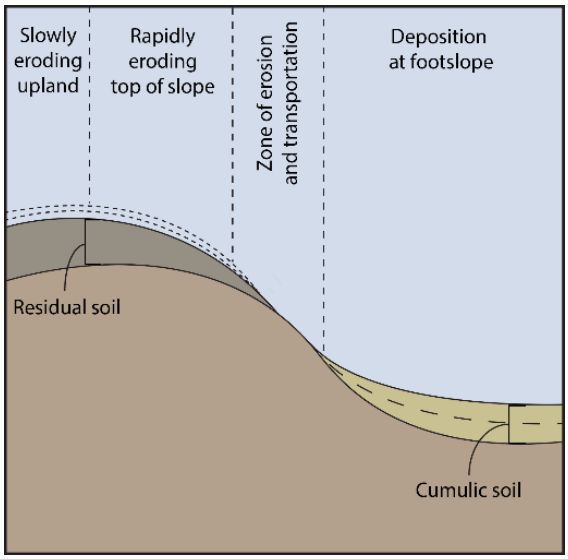

Figure 6.9. Diagram of soil catena, illustrating different erosion and deposition zones on a hillslope. Redrawn from Bierman et al. (2013, fig 3.12).

6.2.5.1.1 Samples and surface description

A total of 14 LR and LRcc surface and sediment descriptions were made from rSSQ (see Appendix 4.2.4). Three capture LR, while eleven record the surface composition of LRcc—four of which are possible heuweltjies. Recurring observations note a rough, uneven surface of yellowish brown sediment (10 YR 5/6), with frequent rilling that becomes more defined, narrower, and deeper downslope (Table 6.1 and Figure 6.1a). At higher elevations, the surface of LR is highly consolidated, moderately rough, and void of vegetation, with sparsely distributed calcrete nodules appearing downslope, at lower elevations. The presence of calcium carbonate within LR occurs in the lower sections of this unit (see also Figure A4.2.1a,b). This is indicated in surface Exposure 1b, where the deposit appears to grade downwards from LR into LRcc. Calcium carbonate is rare in the local geology and usually only occurs in low quantities from a secondary source such as rainfall or channel alluvium, in this case transported as fine lithic grains through aeolian processes. Therefore, the calcium carbonates observed in LR either derive from a secondary source, forming through repeated cycles of calcite evaporation in LR over a very long time or are from a concentrating agent (i.e., termites or roots, e.g., heuweltjies; McAuliffe et al. 2019).

UPK7's surface becomes highly weathered, transitioning from nodules to veins of calcrete that fill desiccation cracks, apparent across the top and middle of the southern hillslopes (Exposure 1a-c; Table 6.1). Calcrete nodules appear to overlie the LR sediment above veined LRcc—similar to UY—ranging in size and form (50 to < 5 mm, angular with low sphericity to sub-rounded with high sphericity; Table 6.2B). Surface artefacts vary from dense to sparse in coverage, which could indicate variation in artefact accumulation as a result of occupation duration and the distribution and scale of artefact discard or hillslope erosion. The latter is suggested by the channelling of artefacts into UPK7's network of rills across the mid-slope of Exposures 1b (i.e., Figure 6.10) and 1c (see Chapter 7 for artefact analysis).

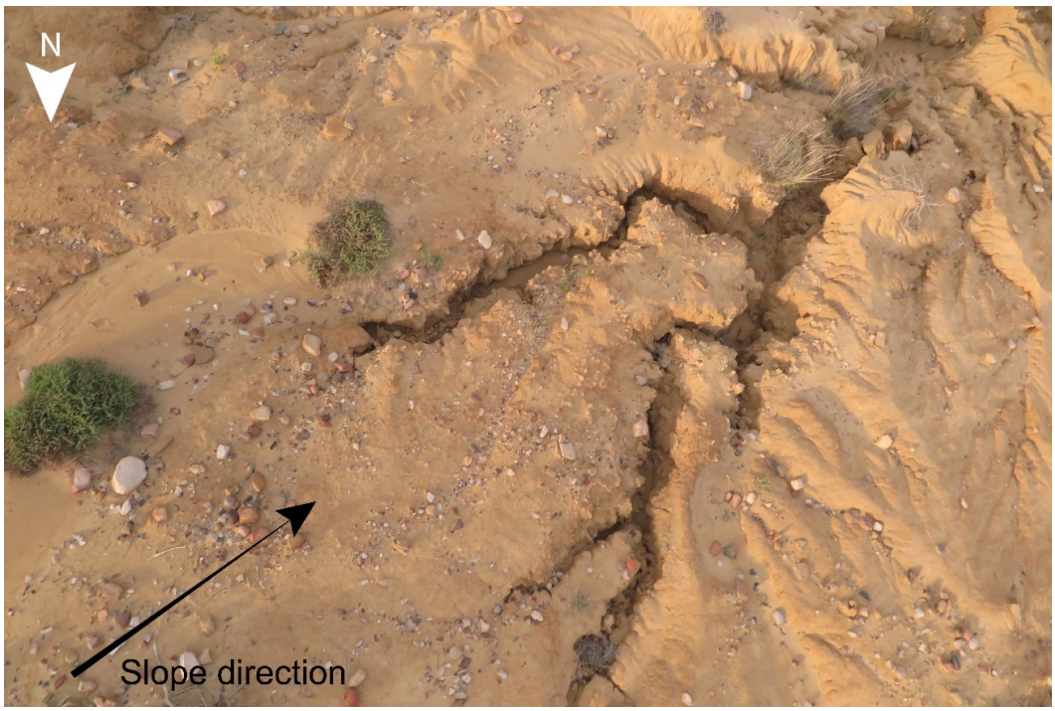

Figure 6.10. Aerial photo from 2016 UAV survey footage of Exposure 1b's middle zone, showing channelling of artefacts into a network of shallow to deeply incised rills.

A total of seven OSL cuts exposed the LR and LRcc in profile, from which eight sediment samples were collected for particle size, XRD and OSL analysis (Table A4.0.1 & Figure A4.0.1). Four samples were collected near and from below surface archaeology (see Appendix 4.1.4). Additional samples were collected from the side of the donga wall of Exposure 1b and three samples were taken from the LR unit of the residual mound of Exposure 6, isolated above the northern colluvium: OSL Cut 1 Upper (U) (91153/UOW-2012) and Lower (L) (91155/UOW-2013), and OSL Cut 2 (91157/UOW-2014). Calcium carbonate ($CaCO_3$) occurs as nodulated calcareous inclusions in OSL Cuts 4, 7, and 9, and as moderately to well-defined calcrete veins in OSL Cuts 6, 8, and 11 (see Appendix 4.1). The presence of $CaCO_3$ suggests the secondary formation of calcite in the LR as a possible outcome of the frequent wetting and drying of overlying sediments.

Field observations suggest LR has a higher silt and clay content than the overlying Upper Yellow unit (UY), and is more cohesive, holding its form when wet (see Appendix descriptions in 4.1 and 4.2; Table 6.2B). Lower Red sediments are also more porous on the surface of areas where it is found directly overlying colluvium, suggesting possible bioturbation. Bioturbation (i.e., termite frass) and salt precipitates were observed at the base of the eastern wall of OSL Cut 1L (Figure 6. 11).

Figure 6.11. Photograph of OSL Cut 1L and detail of salt mineralisation (white specks) and termite frass (dark sediment) at the base of the section's eastern wall, close to the surface.

In sandier portions of LR, grains are less cohesive and therefore more likely to disaggregate. As a result, the form of the hill of sediment in Exposure 6 and the apparent juncture between its upper and lower deposits possibly resulted from the displacement of residual upslope material, settling at the footslope before fanning out over the colluvium. Its highly rilled form suggests this (Figure A4.1.18b). To understand the relationship between the original deposits described from OSL Cut 1 Upper and Lower, and the surrounding colluvium, excavation into this deposit from the colluvial base beyond the slumped deposit of OSL Cut 2 is still needed. As it stands, the sediment sampled from OSL Cut 2 appears to overlie and post-date the surrounding colluvium.

6.2.5.1.2 Grain size and mineralogy

The grain size modes of the LR and LRcc are relatively bimodal compared to overlying unconsolidated and indurated sediment, with minimal variation between samples, showing a primary peak of 158-187 μm and a secondary peak of 14-23 μm (see Figure 6.12d and Appendix 4.3 – Table A4.3.1). The only minor outlier is sample 91057/UOW-2014, with a lower primary peak of 145 μm and a secondary peak of 10 μm reflecting its lower sand (57%), and higher combined silt (37%) and clay (7%) content compared to the other samples. The OSL samples collected from the IS and UY have more in common with the LR grain size modes than they do with Section Cut 1 IS samples.

Table A4.4.1 shows the mineral content of samples taken from the LR, LRcc and their transitional units (i.e., the LR to Colluvium unit sample 91064). Quartz is the dominant mineral in all LR and Exposure 6 sediments (72.5-86%; see Figure 6.13 & Table A4.4.2). Chlorite and iron minerals are also present throughout the LR and LRcc sediment, with minor traces of goethite present in all samples (0.5-1.2%), followed by traces of siderite (0.1-0.6%). As with LRcc, iron and clay minerals typically found in highly weathered soils (i.e., goethite, hematite, kaolinite and illite) occur in each sample. The detrital clay illite forms the dominant clay mineral in the LR sediments, while kaolinite occurs in the top and base sediments of Exposure 6 and in OSL Cut 4 (90022/UOW-1803). Hematite is absent from the LRcc samples, which suggests slightly different weathering conditions/processes involved in the formation of these sediment bodies. Chlorite also consistently contributes to the LR mineralogy, ranging from 0.9 to 1.3% for most samples. The LR-colluvium sample 91064 differs slightly from this range with a higher chlorite content of 2.7%.

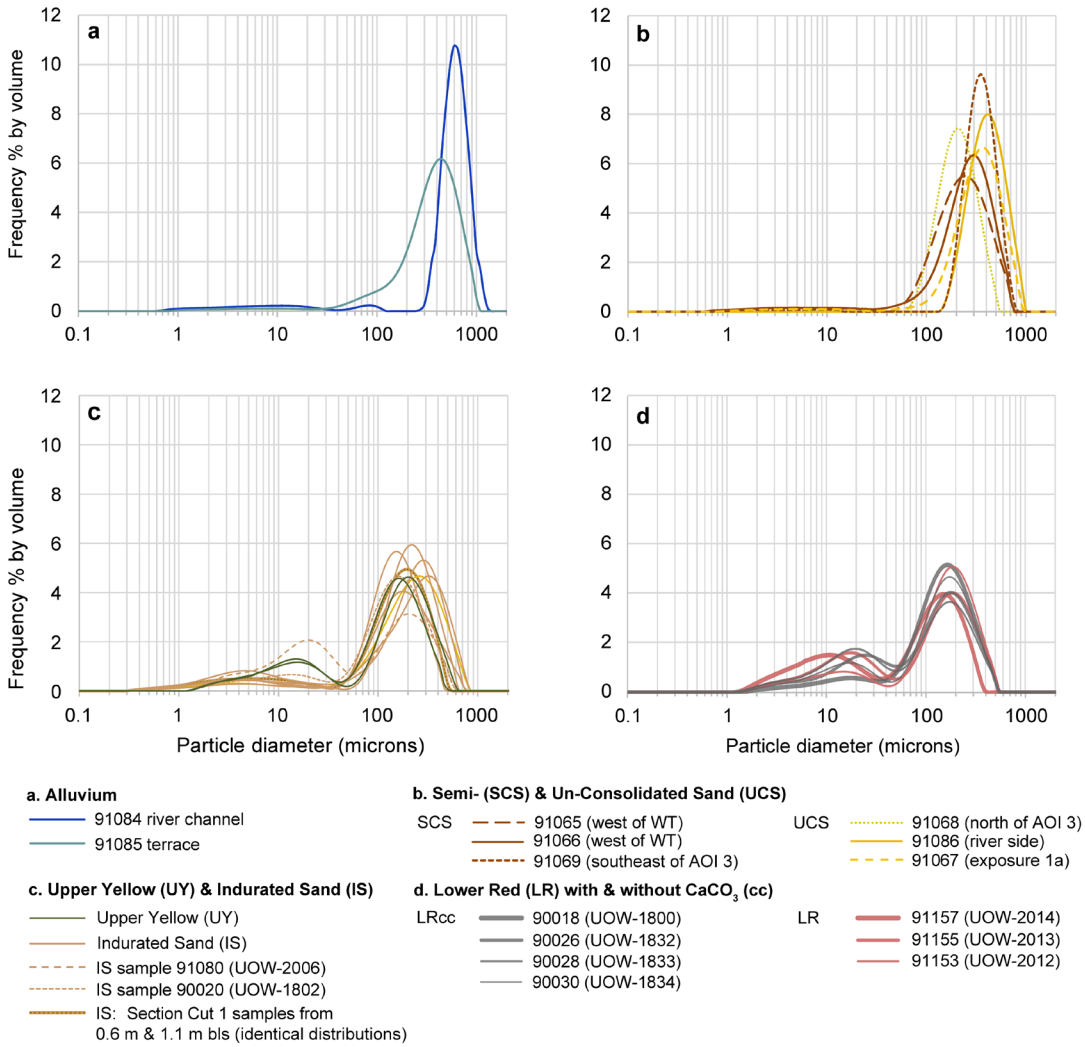

Figure 6.12. Grain size distributions for alluvium (a), semi- and unconsolidated sand samples (b), upper yellow and indurated sand (c), and lower red sediment samples (d) collected at or adjacent to UPK7.

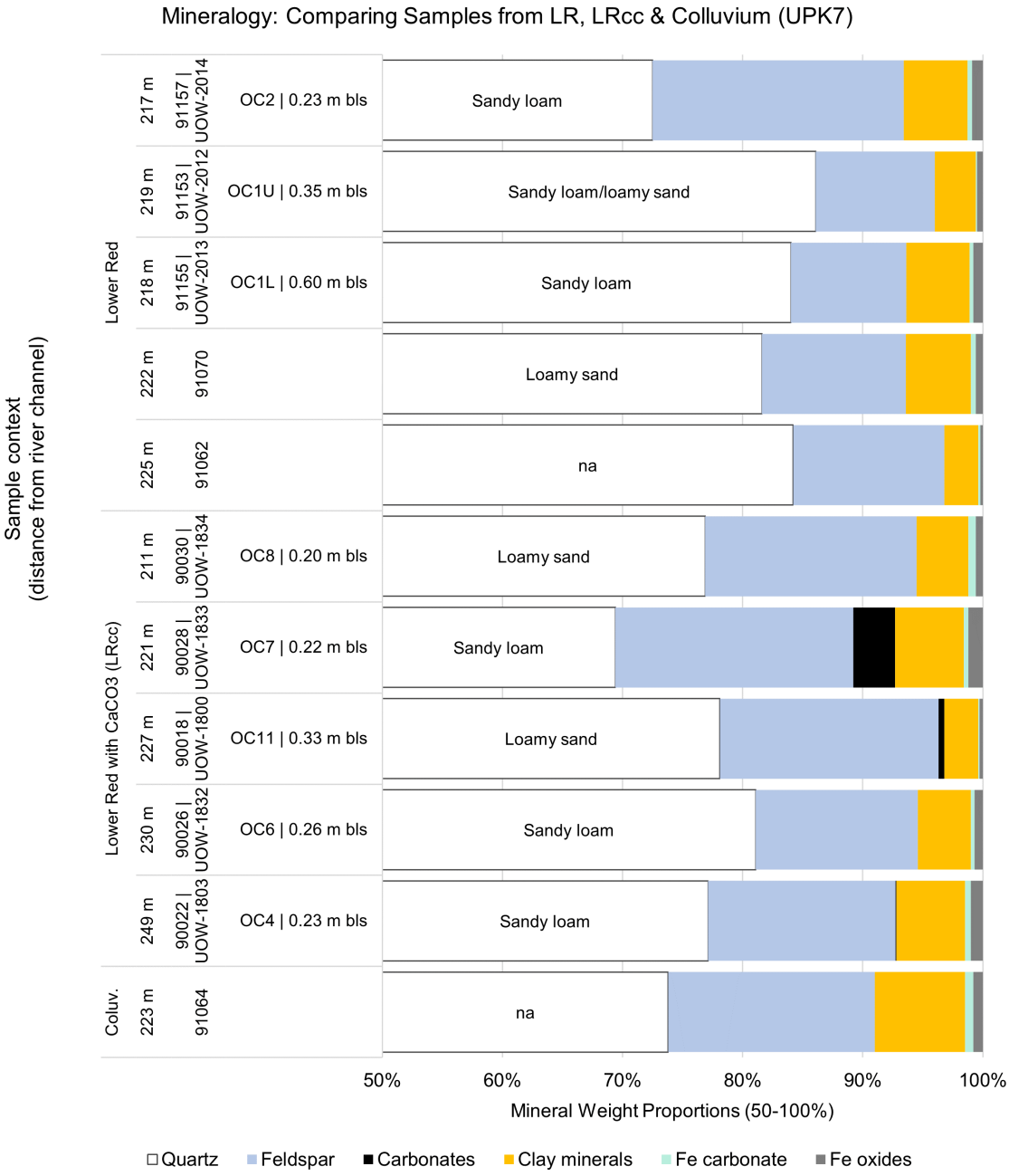

Figure 6.13. Mineral composition from XRD analysis of inferred LR, LRcc, and Colluvium samples, collected from OSL cuts and surface sediment across UPK7, showing additional minerals that form <50% of each (quartz dominated) sample.

Similarities in mineral composition between 91157/UOW-2014 and 91064 suggests that the surrounding colluvium may have contributed to OSL Cut 2 sediments during its deposition (Figure 6.13). Both samples were collected from the lower, base-level of the Exposure 6's sediment mound, with the latter sampled at the juncture between the overlying sediment unit and the colluvium surface of UPK7 (Figure A4.0.1). Their quartz content is also lower than most LRcc sediments, with the exception of sample 90028/UOW-1833, located in Exposure 1b. Samples 91157/UOW-2014 and 91064 include more K-feldspars, in the form of orthoclase and microcline, than any other LR or LRcc sample (Figure 6.13 & Table A4.4.1). Microcline is limited to the two LR samples as well as the LRcc sample 90030/UOW-1834 (Table A4.4.1).

The LRcc samples are composed of a similar – albeit slightly smaller – amount of quartz (69-82%) than the LR samples (72.5-86%) (Figure 6.13). Of the additional minerals, the LRcc have less K-feldspars (0.9-2.4%) and more Na-feldspars (12.6-17.4%) than the LR sediment (0.3-6.9% and 7.6-14.6%, respectively), with albite contributing > 10% of the LRcc mineral content (Table A4.4.1). All samples contain detrital clays, with illite (1.7-3.5%) as the dominant mineral and minor traces of kaolinite in all the LRcc samples, except 90026 (UOW-1832). Calcite is absent from the LR samples, which is consistent with field observations (Table A4.4.1). In contrast, calcite is present in two of the four LRcc samples, forming 3.5% of the mineral content of 90028/UOW-1833 and 0.5% in 90018/UOW-1800. Although, calcite is absent in LRcc samples 90030/UOW-1834 and 90026/UOW-1832, field observation, testing with HCl and Figures 6.14a & b indicate its presence as isolated features that were not captured during sampling.

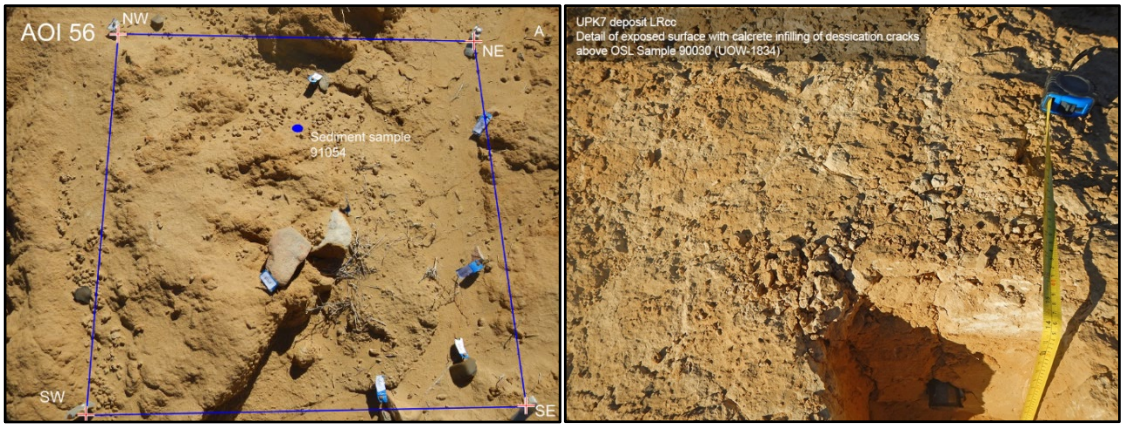

Figure 6.14a & b. CaCO3 occurs as either nodules in rSSQ 56 or veins in LRcc OSL Cut 8, as examples

6.2.5.2 Upper Yellow (UY)

The UY unit is the least exposed and possibly the most eroded of the consolidated deposits at UPK7. It occurs as 'patches' of small exposures at the top of slopes before transitioning down into older sediments such as LR and LRcc. It also occurs in isolation, as the low gradient Exposure 2 ('AoA 3' in Low et al. 2017), which is surrounded by overlying dune sand (UCS; Figure 6.15). Together, these differentially distributed patches of UY sediment cover a total of ~632 m^2, less than 10% of the extent of IS (Figure 6.1a).

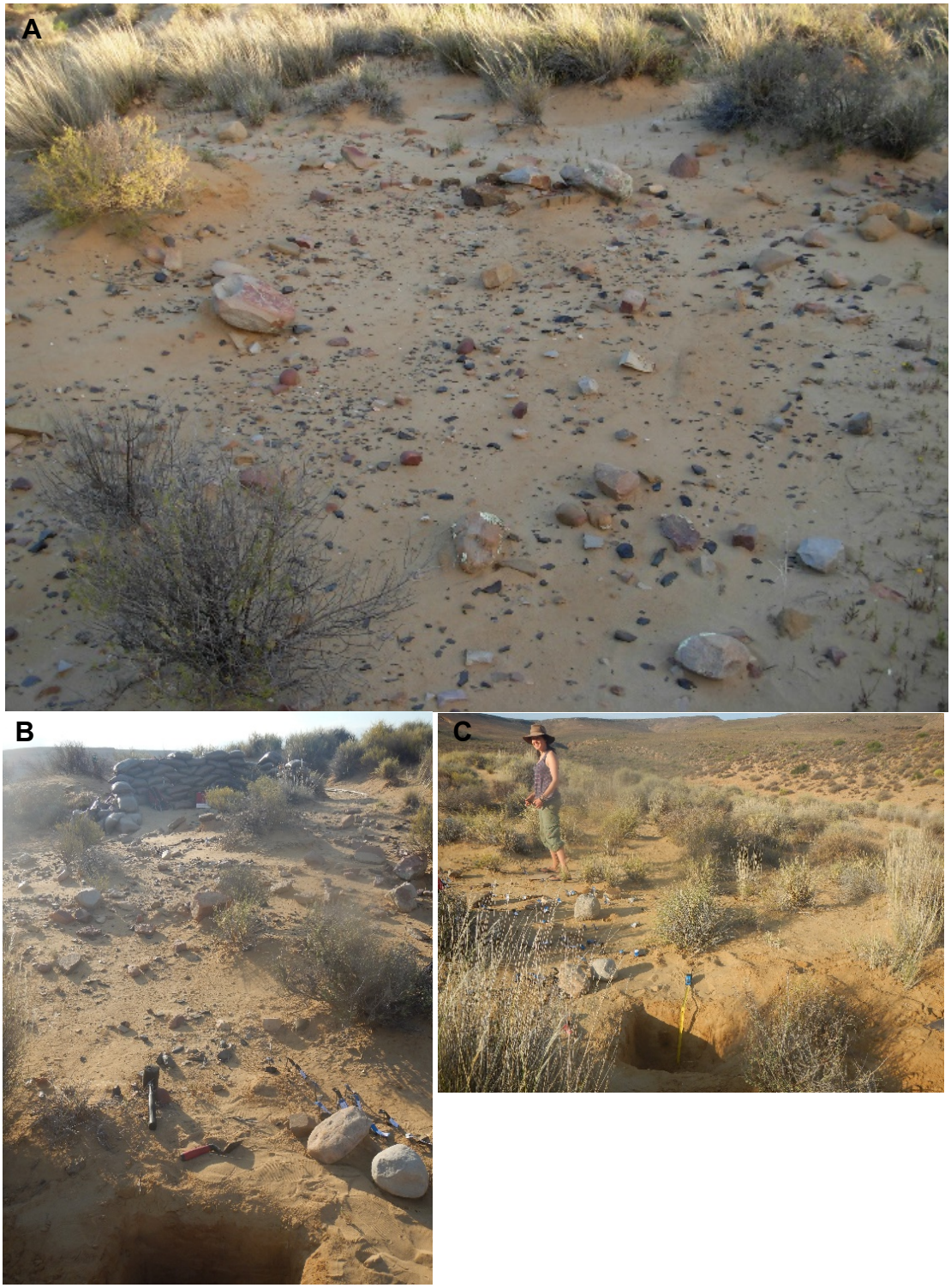

Figure 6.15. Photo showing the consolidated surface of Exposure 2 sparsely covered by vegetation, densely covered by artefacts, and surrounded by the slip face of UCS. Facing: a) south-east, b) north-west with OSL Cut 10 in foreground, c) north with the eastern tributary cutting across the midground with OSL Cut 10 in foreground.

6.2.5.2.1 Samples and surface description

Upper Yellow was randomly sampled across two exposures (rSSQ 20 in Exposure 1b and rSSQ 90 in Exposure 3; see Appendix 4.2 – Figures A4.2.15 & A4.2.17). The Early LSA artefact cluster occurs within Exposure 2 (see Low et al. 2017). Surface descriptions and fabric analysis were conducted by Low et al. (2017) and will be referred to in the Discussion chapter (Chapter 8). Recurring surface observations include the sparse presence of small, hard calcrete nodules of calcified roots (rhizoliths), on a 10 to 20 mm thick surface crust that overlies a highly indurated subsurface (Table 6.2A; Table A4.2.1 & Figure A4.2.35). This sediment is firm upon finger compression, followed by its breakdown into fine sandy loam that can leave the skin yellowish brown (10 YR 5/6; Table 6.2A). In addition to its siltier consistency, fine pores are present throughout its crust (Table 6.2A). Vegetation is rarely observed directly on this unit. When it is observed, it occurs as a mound of vegetation, pedestaled above UY, in UCS and SCS sediment (e.g., Figure 6.15a-c). Knick points and very shallow rilling occurs on UY at the top of the windward slopes of Exposures 1b, c and 3 (Figure 6.1a). This suggests that sheet wash erosion is progressively exposing and eroding back the top of the windward slopes (Figure 6.1a). Beneath its crusted surface UY is a highly indurated, fine yellowish brown (10YR 5/6), sandy loam to loam sediment that proved difficult to excavate with spade and trowel (see Table 6.2A,B and descriptions in Appendix 4.1.3).

6.2.5.2.2 Grain size and mineralogy

Two subsurface samples were collected from UY sediment for OSL, particle size, and XRD analysis: 90016 (UOW-1801), and 90024 (UOW-1804) (Appendix 4.1.4 & Table A4.0.1). The grain size distributions of the UY are compared to the IS, to determine if there is a compositional difference between the two sediment units (Figure 12c). Both units are predominantly fine sand, dominated by mode 1 grains. However, the UY samples have a higher silt content, showing a more pronounced secondary peak at ~14 μm, representing 23-27% of silt (Table A4.3.1). This difference is clearest when comparing the UY samples against the upper strata of Section Cut 1 (0.1 to 2.7 m bls), in which IS sand sized grains are more abundant and silt content is low. However, the IS OSL samples also show similarly high silt content, with OSL Cut 9 having a higher silt content than sediment from the UY and LR (see Table A4.3.1).

The mineral composition of UY is similar in both samples and to the IS units from Section Cut 1 and OSL Cut 9 (Figure 6.13). Quartz dominates (70-80%), followed by feldspar (15-25%), and less than 6% is composed of clay minerals, iron oxides and iron carbonate as well as the sheet silicate, chlorite (1.2-1.3%; Appendix 4.4 – Table A4.4.1).

6.2.5.3 Indurated Sand (IS)

IS is the uppermost and most extensive consolidated sediment unit observed beneath the UCS (Table 6.1), with a visible surface approximating 7200 m^2 (as of 2014, Figure 6.1a). This unit is observed overlying the gravel bench of the palaeoterrace in the north-west. From here it extends upslope across most of Exposure 1a and the southern extent of Exposures 1b and 1c (Figure 6.1a).

6.2.5.3.1 Samples and surface description

All rSSQ surface observations describe IS as a hard, smooth, indurated sandy surface, that is crusted, heavily rilled, and sparsely vegetated (Appendix 4.1.2, 4.2.2; Figures A4.2.1a,b; Table 6.1). This unit is often found partially covered by SCS and UCS (Table 6.2A). Surface clasts mostly consist of non-flaked gravel-sized material, including the recurring presence of small quartz clasts. A thin crust of varying thickness (~10-20 mm) forms the uppermost layer of exposed IS (Table 6.2A). When broken, small casts of trapped air (pores) are observed throughout (Table 6.2A), indicating moderate cohesion and rapid drying of wet sediment. This was also observed for UY, LR, LRcc, and Colluvium surface sediment (see Figure A4.2.1a,b). Pores form during the wetting and rapid drying of accumulated fine wind-blown particles, which are often observed as part of aridosols in semi-arid and arid environments (Bierman et al. 2013). Sediment cohesivity and the rapid drying and crustal formation of a deposit's surface was found to increase artefact adherence to an exposed surface, providing temporary artefact stability and has possibly led to the imbrication or pedestaling of smaller clasts, observed in rSSQ for UY, LR and LRcc (Figure A4.2.1a,b), that would otherwise fall within the size threshold for clasts most susceptible to movement (i.e., < 20 mm).

Twelve subsurface sediment samples were collected from locations that, at the time, were interpreted as IS based on deposit characteristics and stratigraphic position. Two OSL cuts were excavated into IS during the 2013 reconnaissance surveys, including UPK7-2 (UNL3809) and UPK7-3 (UNL3810) and two from OSL Cut 3 (90020 [UOW-1802]) and OSL Cut 9 (91080 [UOW-2006]) (see Figure A4.0.1 & Table A4.0.1). A further eight sediment samples were collected from the profile of Section Cut 1 and its associated auger hole (Figure 6.16; Appendix 4.1.2 – Table A4.1.1 & Figure A4.1.7). Section Cut 1 was excavated to a depth of 7 m below surface (bls) into the eastern wall of the deeply incised donga that runs south from Exposure 1b (Figure 6.16 & 91072 on Figure A4.0.1). The section was made just before the donga arcs south-east to its outlet in the eastern tributary, 62 m north-west of its outlet (see sample locations in Figure A4.0.1 & Profile in Figure 6.1).

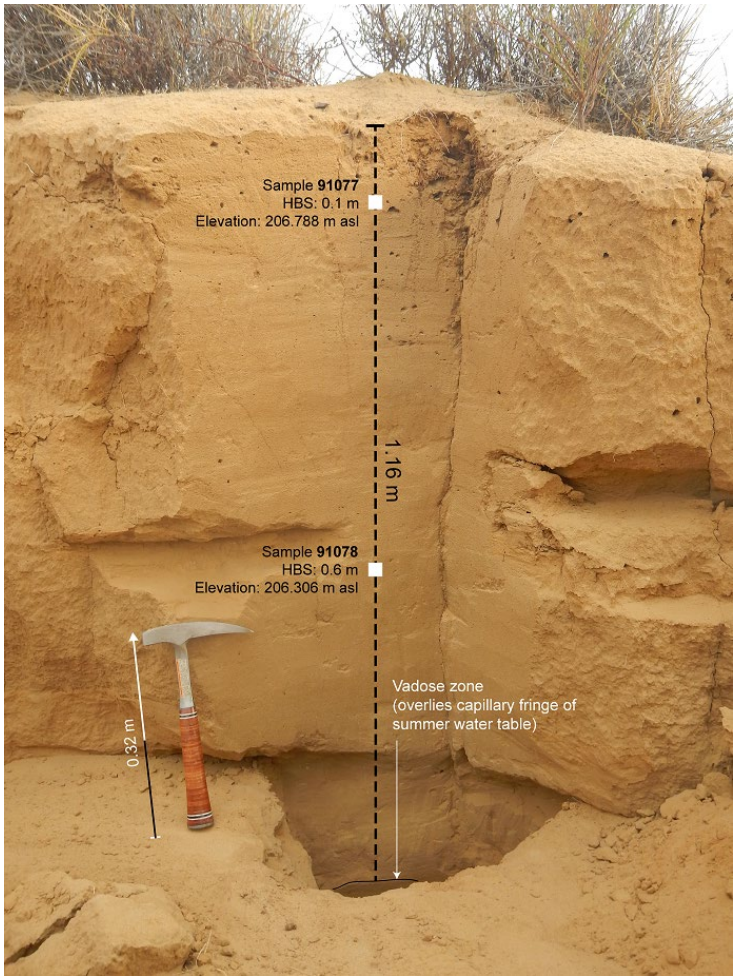

Figure 6.16. Profile photo of Section Cut 1, showing visible sampling locations. Eight samples were collected from 0.1-3.5 m below surface (bls) in 0.5 m intervals. The auger was used to sample from the surface pictured in the foreground (see Figure A4.1.7).

The sedimentary unit exposed by OSL Cut 9 is highly indurated with fine roots dispersed throughout its matrix. With respect to the relative depositional age of IS, OSL Cut 9 (sample 91080/UOW-2006) shows the IS unit overlying a surface of rubified, desiccated, and calcium carbonate rich LRcc sediment (Figure 6.17), with their compositional and structural differences supporting the stratigraphically younger depositional position for IS relative to LRcc. The sampled sediment of OSL Cut 9 possibly represents an older unit than IS, reworked by slope wash prior to IS formation. This cut also suggests that any sediment overlying LRcc in this area was removed prior to IS deposition. Both 90020 (UOW-1802) and 91080 (UOW-2006) indicate aqueous reworking of older deposits. While sediment exposed in OSL Cut 9 lacks clear indications of bedding, small calcrete nodules (~60 mm in diameter) are distributed throughout the section, as well as haphazardly orientated and loosely distributed stone artefacts, suggesting high energy reworking of older sediment and archaeological material from upslope.

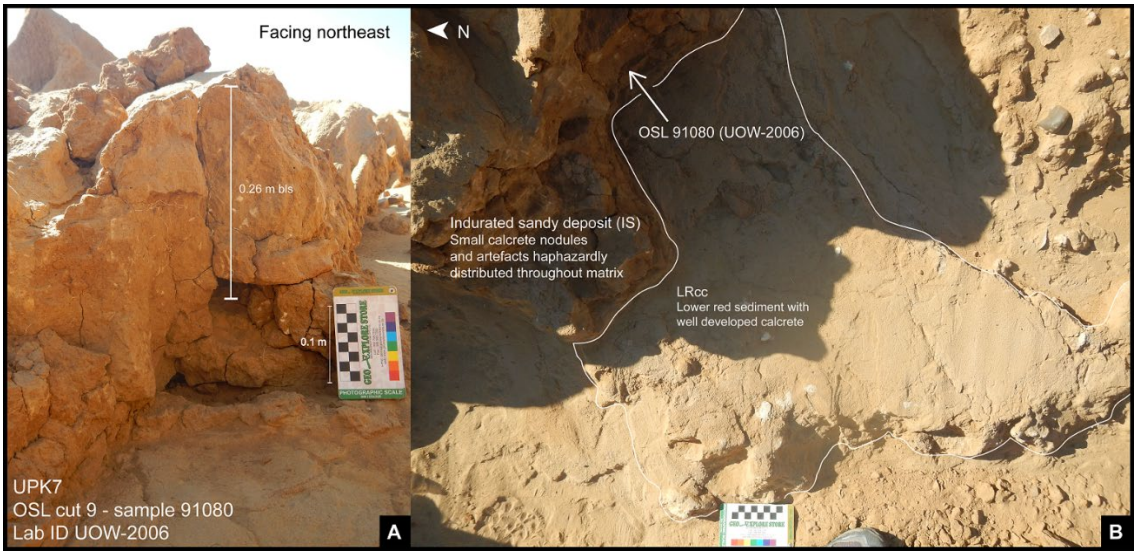

Figure 6.17. OSL cut 9 profile (A) and base (B) showing location of OSL sample tube 91080/UOW-2006, 0.26 m below the exposed surface (bls) of Exposure 1b's southern donga.

In contrast, OSL Cut 3 reveals the transition from a weathered, highly indurated surface layer that lacks obvious bedding, to finely laminated sand, ~10-15 cm bls (Figure 6.18). The surface condition above this cut is smooth, exposed and is largely void of clasts >20 mm in diameter. Figure 6.18a shows the presence of vegetated UCS and SCS in the background that overlies the IS sediment. The common characteristic between 91080 (UOW-2006) and 90020 (UOW-1802) is the indication of sediment movement or reworking probably by slope wash from upslope deposits. The finely laminated bedding of sands in OSL Cut 3 suggest that low-energy slope wash was involved in the deposition of the lower sediments (Figure 6.18b), sampled in 90020 (UOW-1802), while the overlying deposit lacks structure, suggesting weathering and bioturbation of input from aeolian processes. OSL Cut 9 on the other hand, indicates deposition of more pedogenic material from upslope, whilst producing enough energy to move artefacts of > 20 mm in maximum dimension.

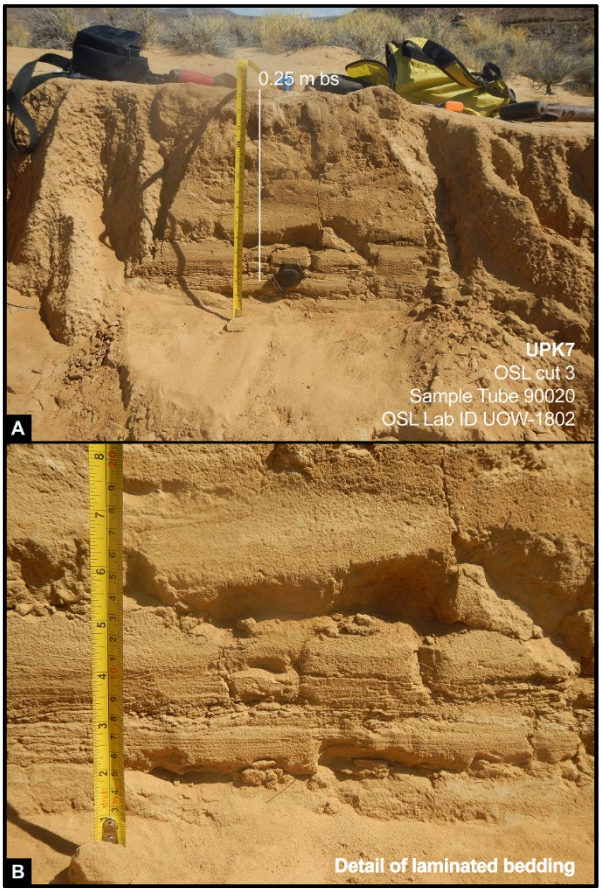

Figure 6.18. OSL Cut 3 profile (A) showing location of OSL sample tube 90020/UOW-1802, 0.25 m below the exposed surface of Exposure 1b's southern donga, and (B) detail of fine lamination sampled by tube 90020.

6.2.5.3.2 Grain size and mineralogy

Indurated Sand samples from Section Cut 1 and OSL Cut 3 are negatively skewed with mean particle diameters that range from 87-181 µm and grain size primary modes that peak between 146 and 308 µm (Figures 6.12c & 6.19, Appendix A4.3 – Table A4.3.1). Sand sized clasts dominate each sample (72-90%). However, OSL Cut 3 Sample 90020 (UOW-1802) indicates a higher silt component (19%) than in all Section Cut 1 samples (6-13%) except for the bottom (3.5 m bls) sample, 91076. Sampled sediment from OSL Cut 9 deviates from both Section Cut 1 and OSL Cut 3, with a bimodal distribution showing a primary peak that falls within the range of the other IS samples (194 µm) and a secondary peak around 19 µm, with 52% of grains being sand sized and 42% composed of silt. Despite the variation between cuts, there are consistently fewer sand sized particles in IS sediment (51-90%) than in the unconsolidated sediments (90-100%; cf. Figure 6.12b & c).

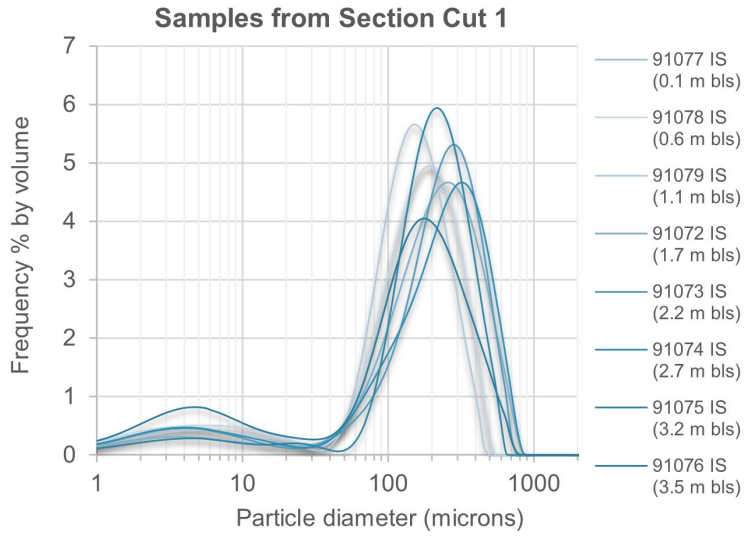

Figure 6.19. Grain size distributions of IS samples collected in 50 cm intervals from Section cut 1 and associated auger hole. bls = below surface.

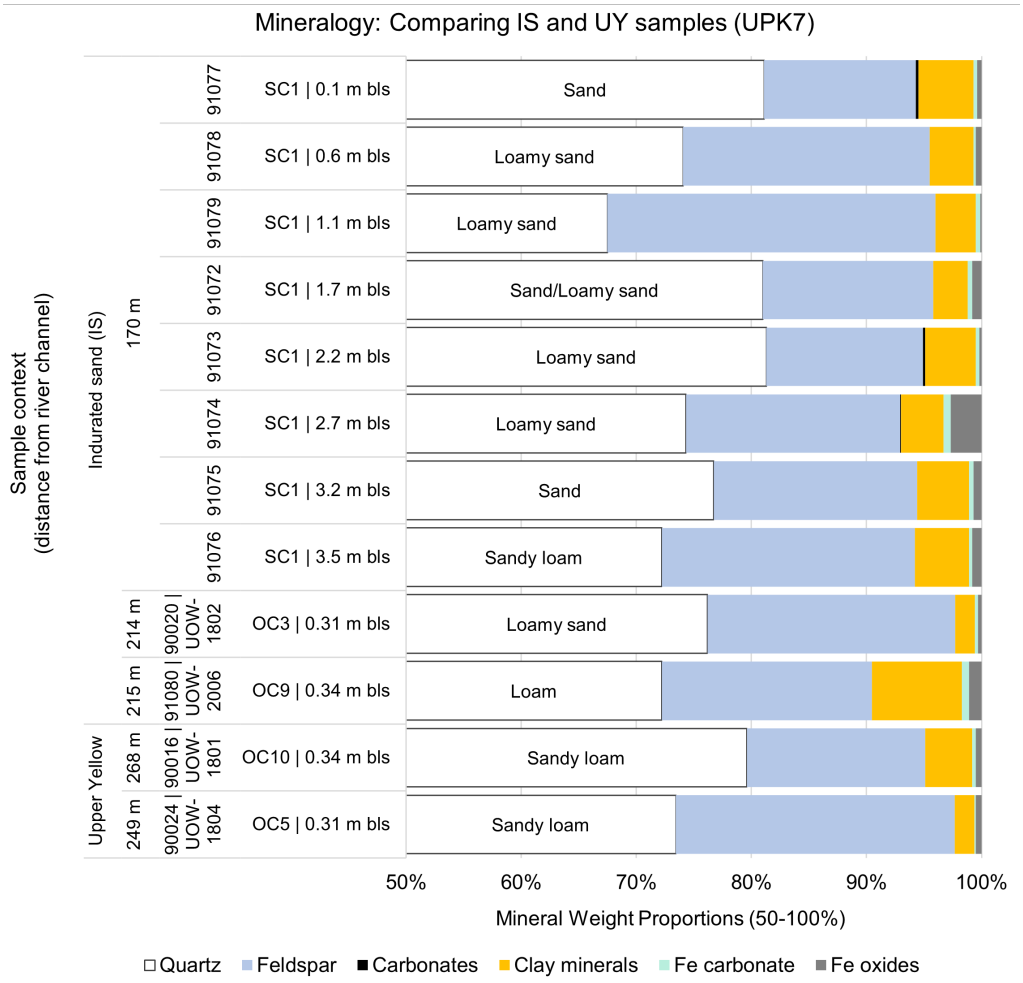

Figure 6.20. Mineral composition from XRD analysis of inferred IS samples, collected from OSL and section cuts at UPK7, showing additional minerals that form <50% of each (quartz dominated) sample

Na-feldspar (albite = 9-26%) forms the largest component of the additional minerals in the IS (Figure 6.20, Table A4.4.2). In most cases, there is more albite in the IS samples (8.9-26.4%) than there is in the UCS and SCS units (0.7-11.4%). Moreover, input of clay and iron minerals derived from highly weathered material (i.e., illite, chlorite, haematite, and goethite) is evident throughout each IS sample. This is most pronounced in OSL Cut 9 and the three lowest samples collected from 2.7 to 3.5 m bls of Section Cut 1. Samples collected below 2.2 m in Section Cut 1 also show an increase in K-feldspar, with the appearance of microcline at 2.7 m bls (6.5%) and 3.5 m bls (2.9%), similar to the channel alluvium (sample 91084).

The presence of chlorite in all samples except two from Section Cut 1's lower deposits 2.7 m bls and 3.5 m bls, indicate semi-arid to arid conditions where annual precipitation is too low to induce mineral leaching. If the fine lithic grains contributing to the addition mineral content of the IS derive from the deflation of river alluvium, then fluctuation in mineral frequencies between IS samples may indicate oscillating wind strengths from the river source over time. Although minor, calcite also fluctuates at several depths in Section Cut 1 (0.1% at 0.1 m bls, 0.2% at 2.2 m bls, and 0.2% at 2.7 m bls). An increase in calcium carbonate was noted during augering of the lower strata and suggests pedogenesis, typical of a B horizon, from ~2-3 m bls (apparent in Table A4.1.1). The presence of hematite in the lowest sample of Section Cut 1 (91076; 3.5 m bls) and the absence of chlorite suggests increased weathering and that the associated deposit was subjected to repeated transitions between wet and dry conditions, possibly during periods of higher annual precipitation. However, the presence of haematite and chlorite in sample 91072, from 1.7 m bls, suggests that while oscillating wet-dry conditions were actively weathering these sediments, the amount of precipitation was potentially lower allowing the preservation of chlorite in shallower units such as these.

Discerning a difference between the IS and UY in the field depends on a clear understanding of their stratigraphic and topographic context, making it difficult to differentiate between these two units in isolated instances without particle size measurements, a vertical perspective, or chronometric data. Despite this, the IS and UY appear to differ in macro-composition, colour, and particle size, as well as the presence of secondary features such as rhizoliths in the UY (Table 6.2A,B).

In IS sample units, lamination is evident in OSL Cut 3 (90020/UOW-1802, Figure 6.18) and the haphazard reworking of sediment, calcrete nodules, and artefacts in OSL Cut 9 (91080/UOW-2006, Figure 6.17) that suggests the deposition of slope washed sediments from upslope. The UY, on the other hand, is consistently located at high elevations or at the head of a slope and has more silt than the IS (Table A4.3.1). Silt content may indicate lower wind strengths during the UY accumulation or reflect their greater distance from the river channel compared to the IS samples. Difficulty in distinguishing between these two deposits—beyond the subtle difference in colour, texture, and occasional bedding structure—suggests that the deposits have the same source. Once again, the sediment unit exposed in OSL Cut 9 has the highest silt content (Figure 12c & Table A4.3.1) as well as felspar and clay mineralogy (Figure 6.20 and Table A4.4.1) suggesting that it derives from the erosion of older sediment than the IS, possibly occurring as a reworked unit of an older calcrete and loamy sand deposit such as the UY and/or LR.

6.2.5.4 Unconsolidated & Semi-Consolidated Sands compared to alluvium

The unconsolidated sandy deposit that extends across the toe of UPK7's hillslope (described in section

6.2.1) is the uppermost deposit identified at this locality and thus interpreted as the youngest. It is also the most recent example of a source-bordering dune and sand sheet at UPK7 (Table 6.1, see Figure 6.1), with unconsolidated sand migrating towards the north-east and east from the seasonally exposed channel sands of the Doring River. This is evident in the direction of the cross-bedding observed on the leeside of the eastern dune, which forms its steepest slip face feeding into the eastern tributary from the west (Figure 6.29).

6.2.5.4.1 Samples and surface description

The unconsolidated sandy deposits of UPK7 were subdivided into unconsolidated and semi-consolidated sand (UCS and SCS, respectively). SCS is associated with frequent vegetation growth, root presence, fine laminations of windblown sand, and, like UCS, varies in thickness across UPK7 (Tables A4.2.1 and 6.1). Artefacts are rare, but occasionally observed protruding out of this deposit, e.g., midway down a mound of pedestalled vegetation (see Figure A4.1.2., middle left of frame). UCS is composed of very poorly to moderately sorted, medium grained sand found overlying all of UPK7's sedimentary units (Tables 6.1 and 6.2A,B). It appears vegetated due to the presence of underlying SCS where enough water retention and stability occur for root growth. Artefacts observed within this unit occur only when UCS is thinly distributed over harder, underlying sediment.

Samples of river sediment (91084), terrace alluvium (91085), and UCS (91086) were collected along a surface profile for grain size and XRD analysis (see Figures 6.1a,b & A4.0.1). Additional UCS and SCS samples were then collected from surface and vegetated dune sand overlying IS sediment in Exposure 1a (91067; see Appendix 4.1.1 for sample details, Figure A4.1.2), on the leeward side of the western tributary's west bank (91065 and 91066; Figure A4.1.1), and to the north and south-east of Exposure 2 ('AoA 3' in Low et al. 2017; samples 91068 and 91069; see Figure A4.1.3).

6.2.5.4.2 Grain size and mineralogy

The unconsolidated sediment samples indicate the dominance of sand sized grains (90-100%), with silt and clay forming a minor component of each sample (<6% in each case; Appendix 4.3 – Table A4.3.1; Figure 6.12b). Alluvium sampled from the river channel and modern terrace (the thalweg) has some of the largest average particle diameters (374-559 μm; Table 6.2B). Modern terrace and aeolian sediment samples have smaller grain size averages than river alluvium and vary between samples, with a mean particle size of 203-417 μm (Figure 6.12b; Tables A4.3.1 and 6.2B). In accordance with source-bordering dune formation, they share a similar size mode, with their primary peaks ranging between 236-396 μm (Table A4.3.1). Moreover, average grain size decreases as distance from the river channel source increases (Appendix 4 – Figures A4.0.2 & A4.3). Deviation from the mean grain size also decreases with distance from the alluvial source (see map Figure A4.0.2). However, it should also be noted that distance between sample and river channel was calculated from the centre of the channel (see channel line in Figures 6.1 & A4.0.1) by measuring the nearest Euclidean distance values between the two locations. Moreover, the sample location of the river alluvium was upriver (south-east) of the proposed source location for the adjacent dunes (91084 in Figure A4.0.1). These factors may affect grain size comparison as the size of alluvium particles will also vary depending on flow velocity and the proximity of transported alluvium to riffles, which can introduce larger

particles into the sampled sediment.

UCS samples show the most variability in average grain size between samples (Figure 6.12b; see Table A4.3.1). This may reflect sample location and the local input of sand sized aggregates from the erosion of sediment units composed of more clay or weathering of silica-rich sandstone. For example, surface sediment on the southern slope of UPK7 is represented by UCS sample 91086, which is composed entirely of sand (100%) and has one of the highest quartz frequencies (96%) at UPK7 (Figures 6.12b & 6.21; Appendix 4.4 – Table A4.4.1), suggestive of the recent reworking of sandy sediment, possibly from the saltation or suspension of terrace sands during strong winds (e.g., Figure 6.28a).

While all unconsolidated and semi-consolidated sand samples show a dominance of quartz (80-96%), they vary in the types and proportions of additional minerals (Figure 6.21; Tables A4.4.1 & A4.4.2). River and terrace alluvium have mineral compositions that reflect their catchment of highly weathered products, including minerals derived from the long-term physical and chemical weathering of feldspars and iron oxides in the wider landscape (Table A4.4.1), with feldspars being the principle additional mineral (4.9%). Iron minerals are present at higher quantities in river sediment (1.2%) compared to terrace alluvium (0.7%), while clay minerals are more prominent in the modern terrace sample (2.6%) than in the river channel alluvium (0.8%). This is consistent with the modern terrace being less mobile, retaining more detrital grains than the seasonally flowing river. River channel and modern terrace sediments also contain carbonate minerals, calcite, or dolomite (both 0.3%; Table A4.4.2). The geology of the Doring River catchment is not calcareous (see Chapter 3), which suggests that the introduction of carbonates into the channel bed possibly derives from alternative sources such as precipitation and/or the degradation of organic matter from the surrounding hillslopes (McAuliffe et al. 2019). Moreover, the presence of the feldspar minerals in the river sediment may come from the weathering of diamictite clasts and Karoo dolerites in the wider catchment. The increase in feldspar content with distance from the river source may indicate preferential transport of the more platy feldspar grains which have a slightly larger surface area to volume compared to quartz.

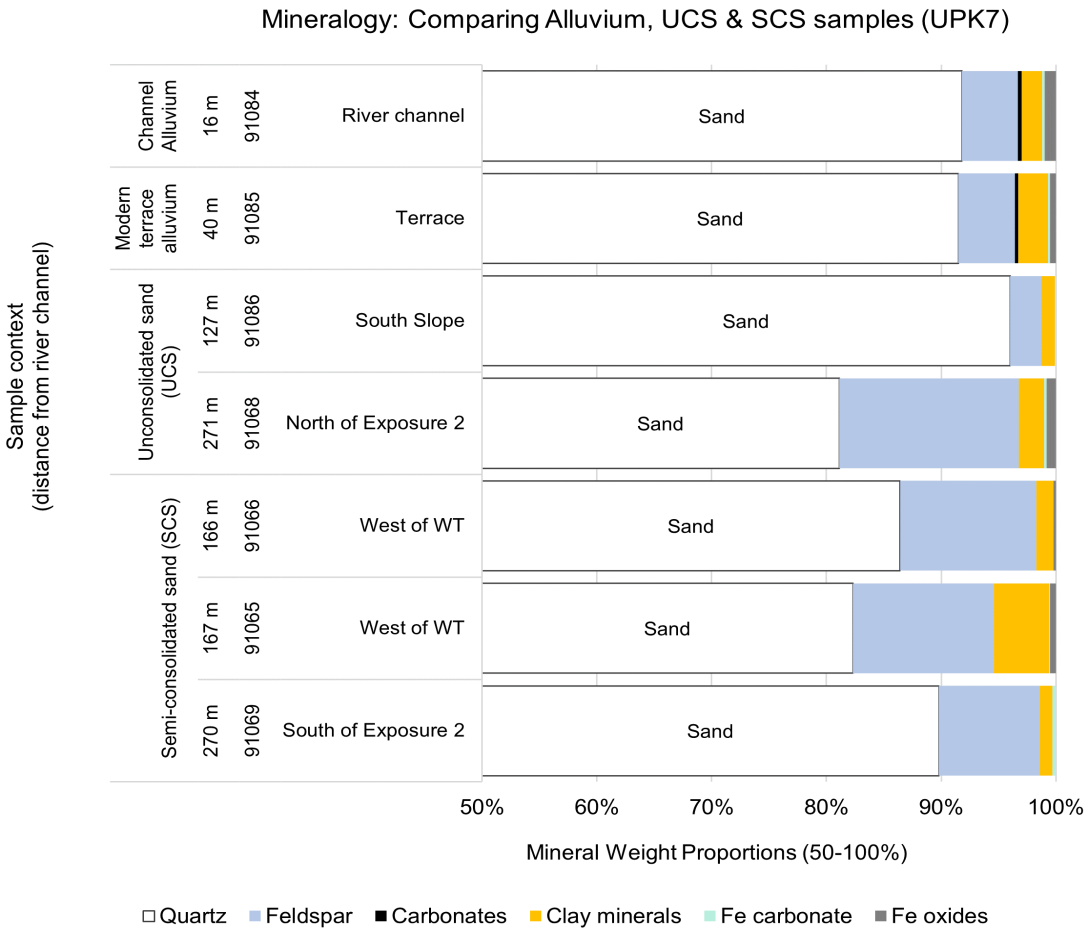

Figure 6.21. Mineral composition from XRD analysis of UCS, SCS and Alluvial samples collected from or adjacent to UPK7, showing additional minerals that form <50% of each quartz-dominated sample.

UCS and SCS vary in mineral composition across UPK7 (Figure 6.21). After quartz, these samples are dominated by the sodium feldspar albite. Albite (2.7-11.4%) is more common than labradorite (0-5.3%) in all sediment UCS and SCS samples at UPK7, which exceed the plagioclase contents in the river and terrace alluvium that also contain more potassium feldspars (orthoclase and microcline; Table A4.4.2). Clay mineral content is mainly contained in lithic grains (as seen in 91067). The closest UCS sample to the river channel has the smallest amount of albite (2.7%) and detrital clay (1.2 %) as well as minor traces of iron carbonate and oxides. The small contribution of additional minerals to the surface sand of the southern slope—together with its well sorted, mode 1-dominated grain size—suggests aeolian reworking from an existing sand deposit (Figure 6.21 & Table A4.4.2).

6.2.5.4.3 Summary

Subtle differences between samples can be attributed to the minor input of finer sediments from local sources, possibly through the breakdown of very fine lithic grains, the introduction of pedogenic material from sheetwash erosion of older deposits, and/or increased distance from the river channel. Kaolinite in these samples possibly represents weathered feldspar, while the presence of goethite may represent weathered dolerite. Despite the apparent variability in the proportion of additional minerals within and between the unconsolidated and semi-consolidated sand units (Figure 6.21), the modes and shape of UCS and SCS size distributions are similar to the alluvium samples (Figure 12a & b), with a moderate decrease

in average grain size as distance from river increases (Figure A4.0.2 & Table A4.3.1). UCS and SCS also show an increase in silt content (Mode 2) closer to exposures of consolidated deposits, together with the immediate presence of vegetation, reflecting the highly localised influence on their mineralogical variability.

The mineralogy and semi-consolidated state of some dune sands suggest older ages for SCS units that have yet to be investigated using OSL (see Sections 5.2 [Chapter 5] and 6.2 this Chapter), while active UCS were deposited as recently as the last century and are still actively moving under the present conditions (as seen by the rapid burial of permanent survey markers). These findings suggest that aeolian deposition is an active process in the formation of unconsolidated and semi-consolidated sands at UPK7. It is possible that this has been the main process of deposition in the study area since the Late Pleistocene, with changes in meteorological conditions influencing the stability of these units and their associated archaeology throughout this time.

6.2.5.5 Main trends in particle size and mineralogy

Several trends are apparent in the particle size distributions between each sediment unit. Firstly, silt content increases and sand content decreases as you move down through the stratigraphic sequence, from youngest to oldest deposit (Figure 6.22a). This is reflected in the decrease in mean and first modal grain size going down through the sequence (Figure 6.22b; Table 6.2B) and is evident in the change in sorting from moderately sorted to poorly, and very poorly sorted (Figure 6.23a; Table 6.2B). The increase in silt lower in the sequence is accompanied by an increase in the modal silt size (Mode 2) in the older units (Figure 6.23b; Table A4.3.1). The increase in Mode 2 size may reflect the weathering, and partial breakdown and comminution of lithic grains and feldspar, characteristic of paleosols. In which case this could be a function of the breakdown of lithic grains or the result of finer dust which has been progressively washed down through the profiles of porous, unconsolidated sand during repeated long-term cycles of wetting and drying. The contrast in sorting is particularly evident when compared to the modern river sand (stratigraphic levels 1 and 2; Figure 6.23a).

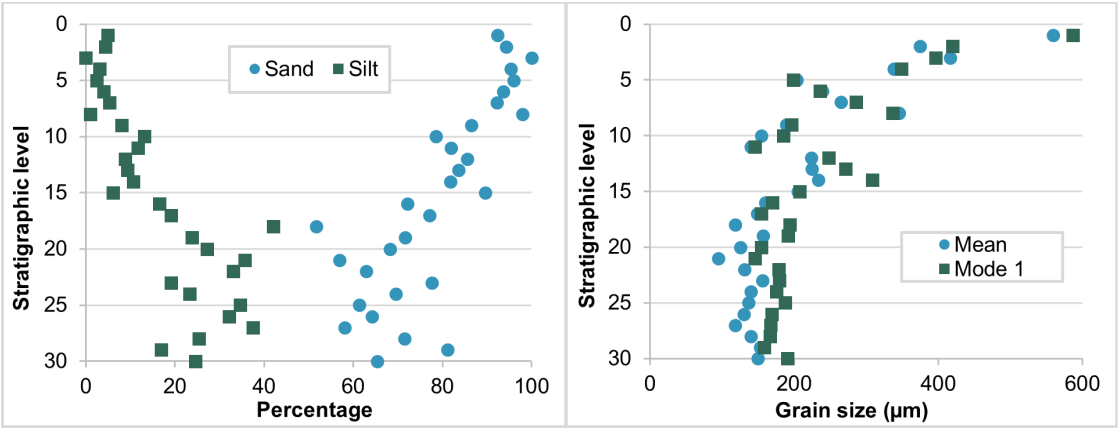

Figure 6.22. (a) Scatter plot of the percentages of sand (blue circles) and silt (green squares) plotted as a function of stratigraphic level. (b) Scatter plot of mean (blue circles) and mode 1 (green squares) grain size (µm) plotted as a function of stratigraphic level. The stratigraphic levels pertain to the youngest to oldest stratigraphic unit as defined in this thesis, i.e., Alluvium, UCS, SCS, IS, UY, LR-LRcc and colluvium (see Table 6.2B).

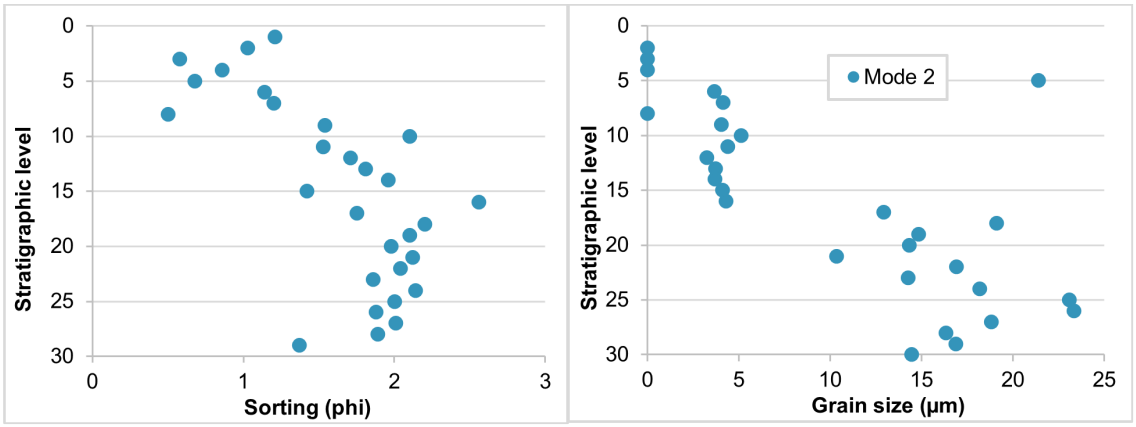

Figure 6.23. (a) Scatter plot of sorting (phi) and (b) mode 2 grain size (µm) plotted as a function of stratigraphic level. The stratigraphic levels pertain to the youngest to oldest stratigraphic unit as defined in this thesis, i.e., Alluvium, UCS, SCS, IS, UY, LR-LRcc and colluvium (see Table 6.2B).

An alternative possible explanation for the change in particle size through the sequence is that grain size has increased with time as conditions have become drier and wind strength has increased. For instance, the size of mode 1 grains of the older units is moderately-well sorted and mainly range from 150 to 200 microns with no coarse tail (Table A4.3.1)—well within the size range readily moved by aeolian activity. However, modal size increases to 400 microns (medium sand size) in the semi- and unconsolidated sands suggesting possibly higher average wind velocities (Table A4.3.1).

Trends in mineralogy are not as clear within and between sediment units. In accordance with the trend in weathering, there is a slight increase in clay mineral content with depth. However, the feldspar content shows a poorly defined increase with depth, while the quartz content decreases (Figure 6.24). Feldspar is predominantly much finer than quartz and is progressively washed down through the sequence, increasing the silt content and Mode 2 size as it accumulates in lower layers.

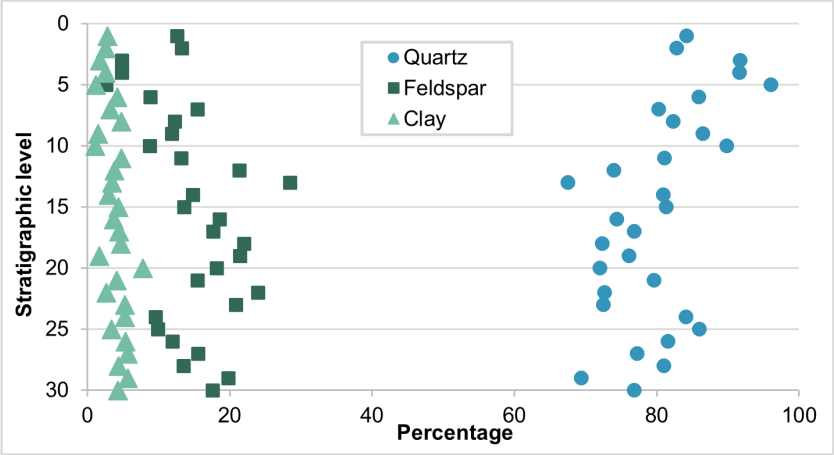

Figure 6.24. Scatter plot of the percentage of quartz (blue circles), feldspar (green squares) and clay (green triangles) minerals plotted as a function of stratigraphic level. The stratigraphic levels pertain to the youngest to oldest stratigraphic unit as defined in this thesis, i.e., Alluvium, UCS, SCS, IS, UY, LR-LRcc and colluvium (see Table 6.2B).

6.2.6 ERT subsurface stratigraphy

Subsurface evidence was obtained from geophysical surveys along two transects (labelled Line 1 and Line 2, see Figure 6.1a) using electrical resistivity tomography (ERT, see Chapter 5.5.3). ERT was employed to determine where bedrock and palaeoterrace extend beneath the exposed deposits of UPK7 and to identify the location, depth, and extent of subsurface contact between these basal units and the sediment units forming the sand mantle. The sand mantle does not appear to have been deposited in horizontal layers. Rather they seem to broadly follow the modern topography as a draped stratigraphy. Based on the ERT results the documented units have a combined thickness of 10 m to bedrock with an additional 4 m of bedrock or alluvial fan detected beneath these units (Figure 6.25). The stratigraphy shown in the ERT profiles suggests that "bedrock" influences the surface geomorphology of UPK7 (Figure 6.1a). This unit manifests as a distinct bench-like anomaly of moderate resistivity (~100 to 300 ohm.m) at the base of the subsurface profile of Line 1 (Figure 6.25), and as irregular areas of moderate to high resistivity at the base of Line 2's profile (Figure 6.25). The latter possibly represents the combined input of tributary and hillslope debris. The morphological irregularity and steep dip (~40º) of this geological unit suggests that it is unconsolidated sediment of an alluvial fan or debris flow.

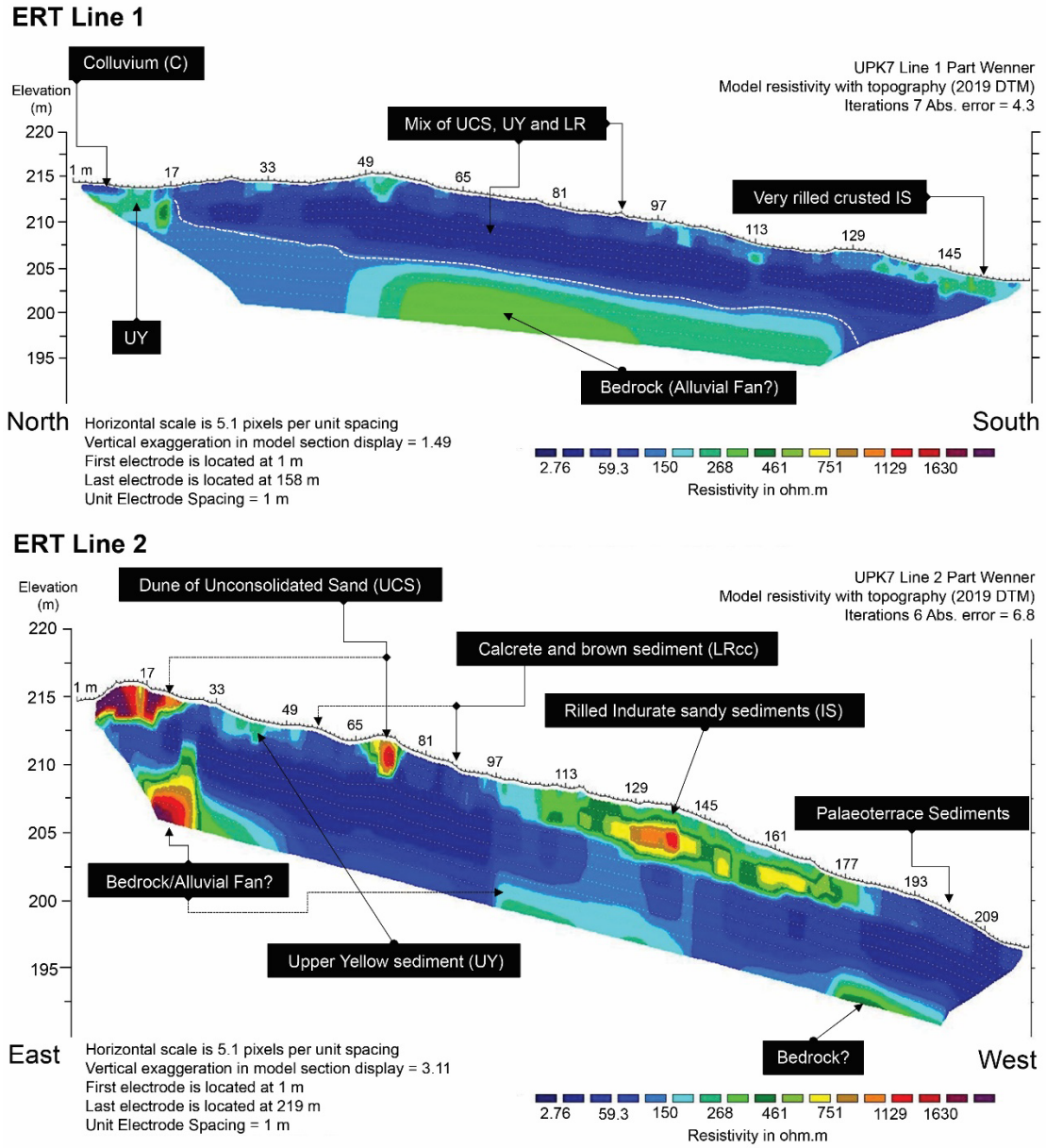

Figure 6.25. Stratigraphic results of two ERT profiles, Lines 1 and 2. Figures by Ian Moffat with updated geological labels by the author. See Figure 6.1a for the location and orientation of each ERT line across UPK7. The surface topography is based on the 2019 DTM (see details on DTM creation in Chapter 5.5.1 and Appendix 4.10).

The Indurated Sand is well distinguished in the ERT, with its high resistivity (268-1129 ohm.m) possibly reflecting the dominance of sand-sized particles and quartz compared to the more water retentive sandy loam and loamy sands of the Lower Red deposit (Figure 6.25 – Line 2). Line 2's profile also shows a marked difference between the resistivity of the Unconsolidated Sand dunes and their surrounding substrate (Figure 6.25). The Upper Yellow in Line 2 appears to have a similar moderate level of resistivity compared to Indurated Sand. However, the Indurated Sand appears thicker, suggesting that the Upper Yellow unit is truncated. The Upper Yellow can be distinguished from Lower Red in some cases. However, these units have relatively similar resistivity values, typical of geological units that are composed of similar source material and have formed through similar processes. Their low resistivity possibly reflects greater water retention, higher silt content and/or pedogenesis.

6.2.7 Proposed scenario for UPK7's depositional history

It is proposed here that the sand mantle overlying the palaeoterrace and hillslope are source-bordering dune and sand-sheet deposits. The orientation and morphology of UPK7's unconsolidated sands and the overall topography of the sediment stack suggest that aeolian sand is transported and deposited across the toe of the hillslope from the Doring River. While source-bordering dunes lack a formal definition, they can be described as dunes that form proximal to and on the leeside of their source (May 2014). The formation of source-bordering dunes requires 'a regular source of sand from a seasonally flowing sand-bed channel' (Bullard & McTainsh 2003). This is available during the dry season when the channel bed of the Doring River has stopped flowing, exposing stretches of alternating riffles and alluvium (Figure 6.26). During dry months, when the Doring River has ceased to flow, it exposes a channel floor that alternates between high energy flow-zones, exposing bedrock and river boulders or 'riffles' (i.e., the Doring channel at the Biedouw-Doring confluence), to thick alluvial sand deposits in slower flow-zones (Figure 6.26, see also Chapter 3.2.2). High winds redistribute source sediments from the river channel and surrounding hillslopes upslope and across the valley during the dry season. Dominant wind directions in the study area depend on the season and occur as westerlies and south-south-westerlies during the dry summer season (November to March) and north-north-easterlies during the wet season in winter (i.e., March to October; see Chapter 3.3.2.3). Westerly winds tend to persist all year; however, they occur more often and at higher speeds during the dry season.

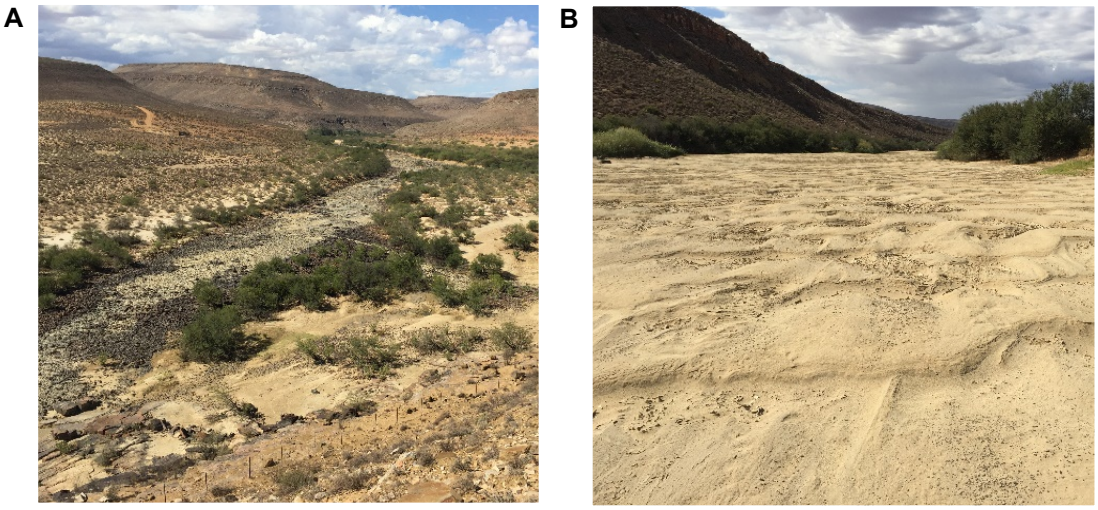

Figure 6.26. Examples of a) Riffle zone from UPK7 to the Doring-Biedouw confluence (photo faces upriver with UPK9 and the northern bank to the left of the channel and the Biedouw River outlet, UPK8 and the Pretorius home to the back right within the frame; UPK7 is out of shot to the left of the frame) and b) sand dominated channel that occurs between UPK1 and UPK7— a source for UPK7 sand during the summer westerlies.

Source-bordering dunes also depend on topographic position relative the source (Figure 6.1a). Hillslopes close to the Doring River channel that are dominated by colluvium and heuweltjie formations (e.g., Appleboskraal) and/or are only minimally covered by unconsolidated sand (UPK9) are often located where riffles and water holes dominate the dry channel bed, and/or when they are blocked from windblown sand due to their surrounding topography (e.g., Figure 6.27a & 29b). Where channel sand is exposed to the

dominant wind the sand can be blown well above river level (e.g., the winter easterlies in Figure 6.27). Figure 6.28a shows fine sand being transported eastward by dry season winds from exposed, highly eroded valley surfaces and the fluvial sand bed of the dry Doring River channel. When exposed and dry, alluvium will be carried by dominant westerly winds from the river channel north-east of UPK1 to UPK7, and eventually onto the toe of the hillslope that is UPK9. UPK9's location to the east UPK7 means that sand is deposited onto UPK7 before reaching UPK9 during the dry season (see Figure 5.1a).

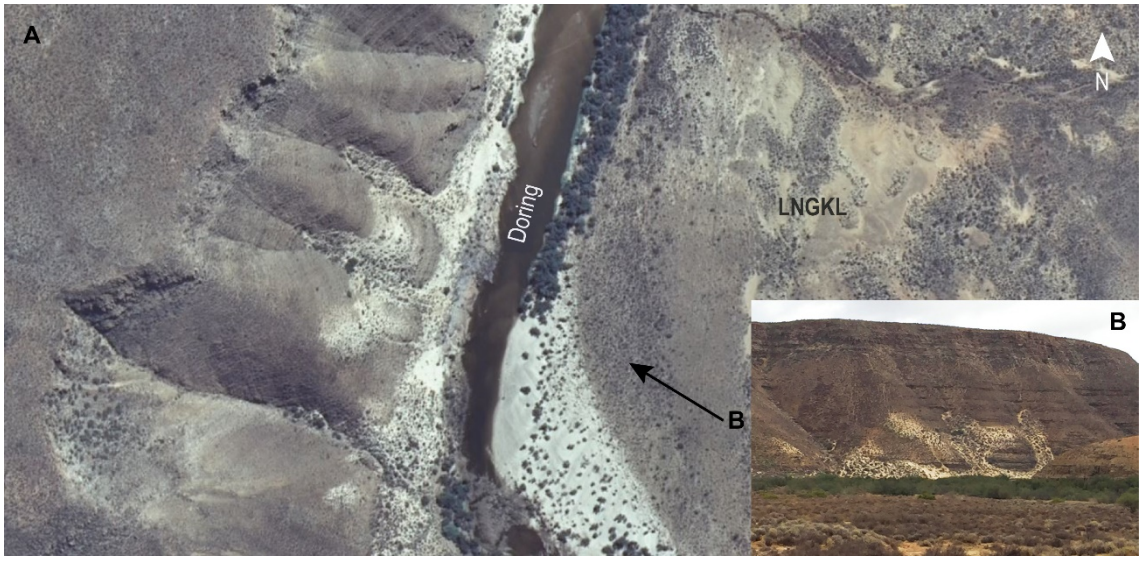

Figure 6.27 a-b. Aerial (a) and field view from Appleboskraal (b), showing the absence of unconsolidated sand across Lungkaal (LNGKL), juxtaposed against an abundance of windblown sand on the steep western flank of the Doring River. The arrow in 'a' indicates the direction of view shown in 'b' and the dominant winter wind direction which carries exposed modern terrace sand from the bank-attached bar at Lungkaal across the Doring River (when dry) to the western hillslopes. This cliff blocks the summer westerlies, limiting sand sheet and dune formation to the east at Appleboskraal (ABK).

Figure 6.28 a-b. Aeolian activity in the Doring River valley: a) View north-west from UPK9 depicting high westerly winds entraining sand from the channel and surrounding hillslope across UPK1 towards the study area. The unconsolidated sand on the east side of UPK7 forms the first ridge. b) Colluvium at UPK9 is separated by the Western Tributary from the unconsolidated sand dune farther west. It demonstrates the strength of the wind in this valley and the importance of topographic position, source availability, and timing of the source's exposure relative to the dominant wind regime. Photographs by Brian Jones, April 2016.

Where channel sediment is available, proximate, and unconstrained by topographic features, deposition tends to occur transverse to the dominant wind direction and downwind from the river source

(Bullard & McTainsh 2003). In accordance with this, the north-west to south-east bearing of UPK7's northern dune and the north to south bearing of the eastern dune are oriented transverse to the dominant summer wind regime of westerlies and south-westerlies (Figure 6.29a,b). They also align with the river's channel morphology and the valley's topography. The river runs north-west before bending to the west and opening to ploughed terraces on the southern bank and a high bedrock cliff on the northern side (Figure 5.1a). During the dry season, the dominant westerlies and south-westerlies are directed through and across both the channel and the terraces, carrying entrained sand to UPK7. This is further indicated by the cross-bedding of leeside dune sands, exposed on the western bank of UPK7's eastern tributary (Figure 6.29). Considering source and dominant wind direction at the time of its exposure, the most recent source of alluvium for UPK7 is located south-west and down river (Figure 6.26b). During the dry season, the thinning of vegetation cover, exposure of dry-channel river alluvium, and the drying of sediment units across the landscape provides the optimal conditions for the transport of fine sand onto UPK7.

Sediment units located close to their source are also typically composed of coarser, sand-sized material (63–500 μm), indicative of short transport distances involving saltation and surface creep that occur close to the ground's surface (Bullard & McTainsh 2003). That the sandy consolidated and unconsolidated sediment mantling the palaeoterrace and southern toe of the hillslope shows an inverse relationship between particle size and distance from the river channel suggests that the Doring River's channel bed is the dominant sediment source for sand mantle accumulation. This scenario is also supported by a decrease in mineralogical similarities as distance from the river channel increases.

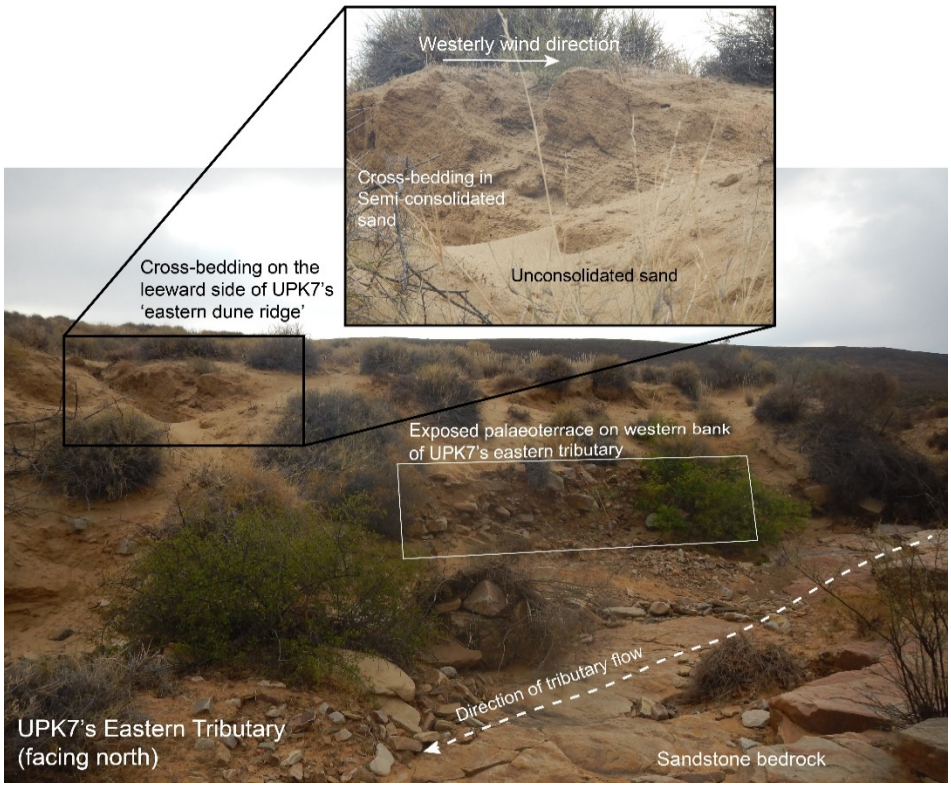

Figure 6.29. North facing photograph and inset of semi-consolidated and unconsolidated dune sand, palaeoterrace and sandstone bedrock exposed in UPK7's eastern tributary. The inset shows a close up of crossbedding, indicating that westerlies drive dune formation.

6.2.8 Summary

Over time the south-western migration of the main Doring River channel and hillslope erosion from both the eastern tributary and western tributary likely contributed to the continued incision of bedrock and the fanning out of debris from UPK7's northern hillslope. This produced a palaeoterrace—now located ~5 m above the modern terrace—upon which a mantle of sand has accumulated, stabilised, and destabilised. It is suggested that the main process involved in the formation of this sand mantle is aeolian transportation of sediment from the seasonally dry Doring River channel bed. The following section presents the OSL analysis carried out on sediment samples that were collected from each of the sand mantle's consolidated sediment units.

6.3 Substrate Age

6.3.1 OSL samples

Twelve sediment samples were collected for OSL analysis at UPK7 (Figure 6.30). A list of each sample's context and a brief description (OSL cut number, sampled sediment unit, depth of collection, and elevation in metres above sea level (m asl)) is provided in Appendix 4.6 (Table A4.6.1). Each sample is organised by context (i.e., deposit and exposure). A photographic and descriptive record of individual samples and their OSL cuts is provided in Appendix 4.1. A brief outline of sample preparation and the equipment used for each OSL sample was provided in Chapter 5.5.1. The following results and analysis are presented in conjunction with a more detailed outline of the methods used to measure and analysis UPK7's OSL samples, with only minor repetition for clarity.

Equivalent dose (D_e) estimates were calculated from quartz grains ~200 µm in diameter using standard single grain aluminium discs, employing the SAR procedure (Murray & Wintle 2000). Measurement of between 900 and 1900 individual quartz grains was carried out for each sample and any anomalous grains were removed from the final D_e determination following standard rejection criteria (e.g., Jacobs et al. 2006). The subsequent sections present the grain characteristics of each sample set and their performance using the SAR protocol to reduce error and refine each sample for D_e estimation. This is followed by the analysis and modelling of each sample's D_e and dose rate for age calculation.

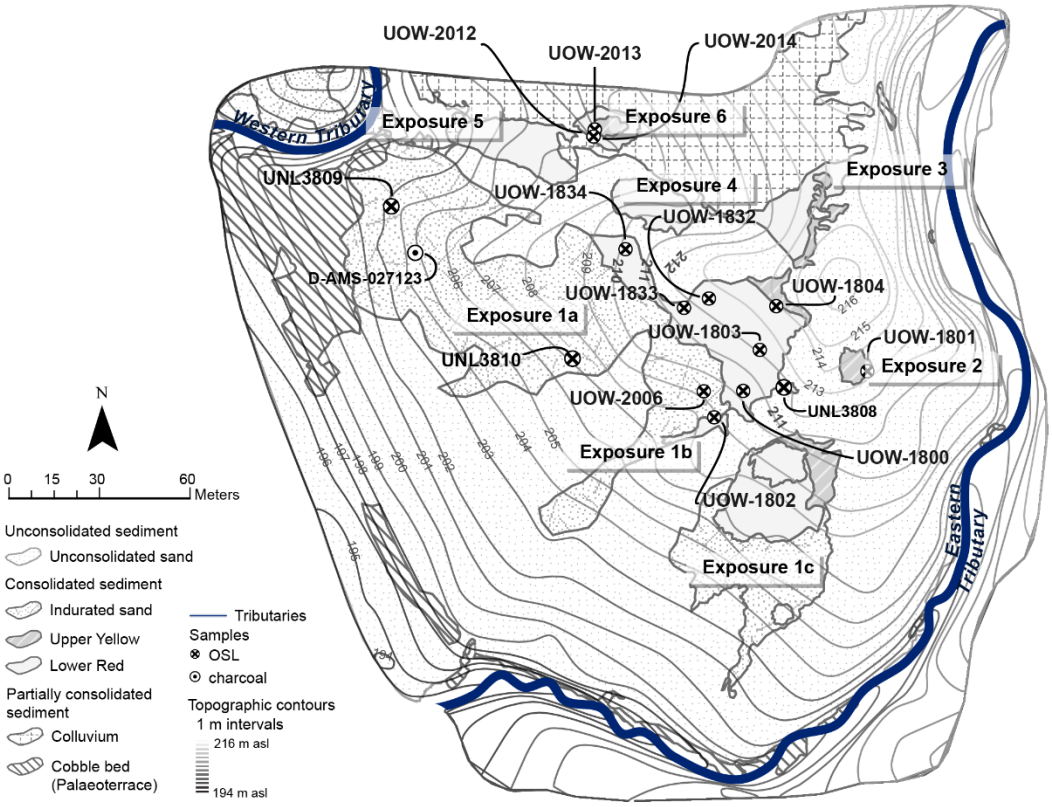

Figure 6.30. Map of UPK7 showing the locations of OSL samples collected from consolidated and unconsolidated sediment, including the locations of OSL samples processed at the UNL laboratory (see Shaw et al. 2019b). One charcoal rich sediment sample (D-AMS-027123) was also collected from a combustion feature on the indurated sediment surface and its location depicted here and in Figure A4.0.1. Topographic contours are drawn at 1 m intervals based on the 2019 UPK7 DTM.

6.3.2 Single grain characteristics

6.3.2.1 Dose recovery tests

A series of dose recovery tests were performed on a representative subsample from UPK7 to establish the optimum combination of preheat (PH) temperatures (Tables 6.4 and 6.5) needed in each SAR dose cycle. If the sample fails to return a measured dose consistent with unity (to within 2σ) then it is unlikely to produce a reliable D_e when the same preheat temperatures are used for measurement of a natural sample. Based on the sedimentological assessment in Section 6.2 and the geological setting of the Doring River's quaternary (E24J) catchment, it is assumed that the source geology of all quartz in the catchment is the same and that its depositional context is aeolian. Sample UoW-1803 was selected as the representative sample for all dose recovery tests. Sample 90022/UOW-1803 was collected from the LRcc deposit in Exposure 1b (Figures 6.30 & A4.0.1), which is expected to be one of the oldest consolidated sand deposits at this locality (Appendix 4.6 – Table A4.6.1). Grains were exposed to blue LEDs for 100,000s before they were given a known laboratory dose of 600 sß (~60 Gy). Dose response curves (DRC) were then constructed for individual grains using the single aliquot regenerative (SAR) procedure and five different combinations of preheat (PH) temperatures (PH_1 and PH_2) applied prior to each measurement of regenerative dose and test dose, respectively (Table 6.4).

Table 6.4. Preheat combinations applied to five sets of 300 single grains.

Set	Measured grains	PH_1 (°C/s)	Time (s)	PH_2 (°C/s)	Time (s)
A	300	160	10	160	5
B	300	180	10	180	5
C	300	240	10	160	5
D	300	260	10	160	5
E	300	260	10	220	5

Only sets A and C gave measured/given dose ratios consistent with unit at 2σ, while set C has the smallest OD (Table 6.5 & Figure 6.31). The distribution of measured/given dose ratios for set C are presented in Figure 6.32. Set C enables the accurate recovery of a known dose and is thus the most appropriate temperature combination for use in the SAR procedure. Thus, Set C's preheat combination of PH_1 240°C and PH_2 160°C (set C) was selected for the OSL dating of UPK7's deposits.

Table 6.5. Dose recovery test results for sample 90022/UOW-1803. Five different preheat combinations were tested (A-E). Grains were held constant at the chosen temperature for 10s (PH1) and 5s (PH2). The final preheat combination selected for OSL dating is highlighted in grey.

Preheat temperature combinations	Given dose	Grains accepted	Measured/ Given dose ratio^	Over-dispersion
Set	(~sß)	(n)		(%)
A (160/160)	1600	44	1.08 ± 0.05	11.2 ± 3.8
B (180/180)	600	23	1.19 ± 0.05	0
C (240/160)	600	84	0.99 ± 0.02	8.8 ± 2.3
D (260/160)	600	27	0.87 ± 0.05	24.4 ± 5.0
E (260/220)	600	29	0.82 ± 0.03	12.4 ± 4.5

^1σ uncertainties

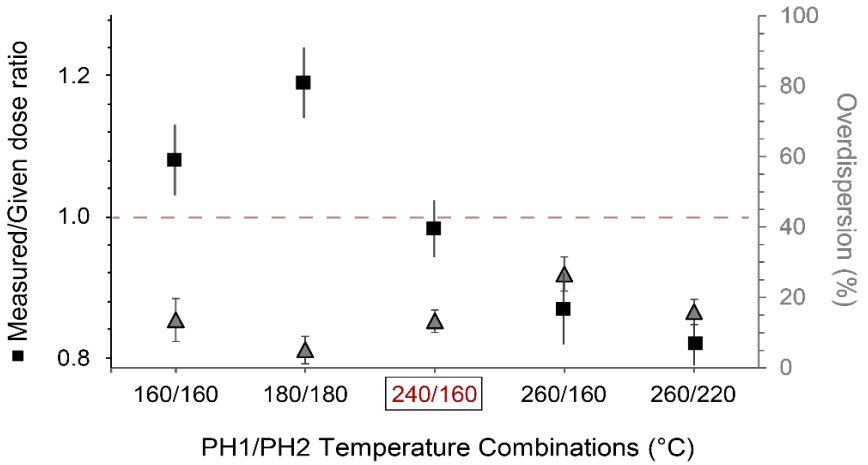

Figure 6.31. Dose recovery test results for sample 90022/UOW-1803, plotting the weighted mean measured/given dose ratios and overdispersion values (%) along with the respective standard errors (1σ). Triangles represent overdispersion values and the squares represent the weighted mean measured/given dose ratios.

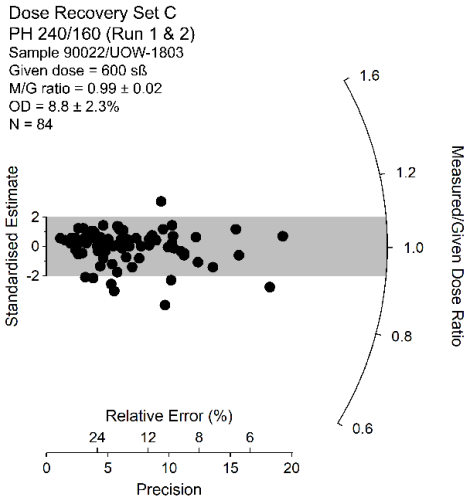

Figure 6.32. Radial plot of dose recovery test results for sample 90022/UOW1803 for the selected preheat combination C, outlined above and shown in Tables 6.4 and 6.5. The values for the given dose, weighted mean measured/given dose ratios, over-dispersion and accepted grain count are also provided. Grey band is centred on unity.

6.3.3 Grain rejection

Of the 12 OSL samples collected from UPK7, a total of 13,400 individual grains were measured. The inclusion of aberrant grains can result in inaccurate D_e estimates (e.g., see Jacobs et al. 2006; Jacobs et al. 2013; Thomsen et al. 2005). Before determining the D_e values for each sample, aberrant grains were rejected depending on their inherent brightness, level of recuperation, recycling ratio (RR), dose saturation, and OSL-IR depletion ratio (IRD) due to feldspar contamination. Table 6.6 provides details for the number of accepted and rejected grains, and the reasons for their rejection.

6.3.3.1 Dim OSL signal

Of the 14,300 grains measured, 96% (n = 13,779) failed criteria 1 and 2 (Table 6.6). Most (n = 11,376; 80%) had natural test dose (T_n) signals that were less than 3 sigma times the background signal (Table 6.6[1]). The rest (n = 1,568; 11%) had T_n signals with errors >20% (Table 6.6[2]). The decay curves for a typical

'dim' grain following a 210 Gy test dose and a 275 Gy regenerative dose are displayed in Figure 6.33. The OSL signal is indeterminable from instrumental background, regardless of size of dose. This suggests that 'dim' grains are not the result of using a test dose that is too small. After removing dim grains from each sample, 1,356 (9%) grains remain. The sizable rejection of grains due to weak signal is in accordance with OSL studies of South African material (see Jacobs et al. 2006; Jacobs et al. 2013; e.g., Jacobs et al. 2008).

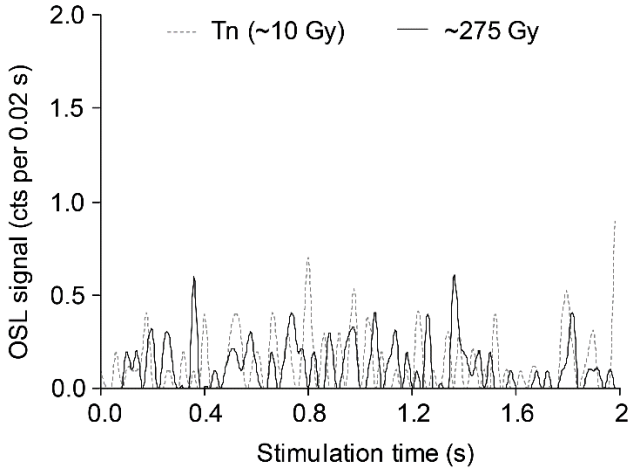

Figure 6.33. Representative example of decay curves for a grain with OSL signals after test dose stimulation and regenerative dose.

Table 6.6. The total number of single-grains measured, accepted, and rejected for each sample at UPK7. Grain rejection counts are further organised into eight criteria-specific columns.

	Sedimentary unit	Indurated Sediment (IS)		Upper Yellow (UY)		Lower Red (LR)			Lower Red with $CaCO_3$ (LRcc)				
	Texture	Loamy sand		Sandy loam		Sandy loam			Loamy sand				
	UoW OSL Lab ID	2006	1802	1801	1804	2012	2013	2014	1800	1803	1832	1833	1834
	Measured grains (n)	1900	1500	1000	1500	1000	1000	1000	1000	1000	1500	900	1000
Rejection criteria	1. Tn signal <3 sigma*BG	1500	1213	785	1235	785	815	776	744	747	1227	744	805
	2. Tn error >20%	304	145	102	131	133	97	108	117	129	132	88	82
	Grains with signal (n)	96	142	113	134	82	88	116	139	124	141	68	113
	3. Poor recycling ratio (RR)	4	5	17	30	11	10	13	15	13	7	15	17
	4. IR Depletion test	4	5	7	8	4	2	3	11	5	4	5	1
	5. 0 Gy dose >5% of Ln/Tn	0	0	0	0	0	0	0	0	0	1	0	0
	6. FOM* of growth curve exceeds 10%	26	24	16	21	15	19	13	34	26	27	13	24
	7. D_e not calculated by Interpolation	5	0	2	8	18	14	24	12	9	18	7	17
	8. Saturated in Ln/Tn	10	7	10	18	14	17	22	26	20	41	14	27
	Total number of accepted grains	47	101	61	49	20	26	41	41	51	43	14	27
	Total number of rejected grains	1853	1399	939	1451	980	974	959	959	949	1457	886	973

1. T_n is the OSL signal measured in response to the test dose given after measurement of the natural OSL signal, where the first 0.22 s of the T_N signal is <3 sigma of the BG signal (last 0.3 s); **2**. The natural test dose signal (T_n) error is greater than 20%; **3.** Recycling ratio is the ratio of the sensitivity-corrected OSL signals measured from duplicate doses to test the efficacy of the test dose correction used in the SAR procedure. Grains were rejected if the recycling ratio is more than 2σ away from unity; **4**. IR depletion of sensitivity-corrected OSL signal (L/T) after IRSL stimulation to remove and detect IR-sensitive grains (e.g., feldspars). Failure of grains to return an OSL-IR depletion ratio less than 2σ from unity resulted in grain exclusion; **5**. Tests if zero dose (Gy) sensitivity-corrected signal is within 5% of the sensitivity-corrected natural dose signal, if not then the grain is rejected; **6.** Figure of merit (FOM) of the growth curve exceeds 10%; **7**. The sensitivity-corrected natural OSL signal (L_n/T_n) interpolates with the DRC beyond the last regenerative dose resulting in an extrapolated D_e; **8**. Grains were rejected if DRC is saturated.

6.3.3.2 *Recycling ratio*

The recycling ratio assesses the efficacy of the test dose correction during the SAR procedure (Murray & Wintle 2000). To calculate the recycling ratio the first given dose (L_1) at the end of the SAR procedure was repeated (L_2) and the sensitivity-corrected OSL signals of these duplicate doses were divided ($(L_1/T_1)/(L_2/T_2)$). Grains that returned ratios more than 2σ from unity were rejected. Figure 6.34 shows the typical decay (a and b) and dose response (c) curve behaviour of a single grain with a poor recycling ratio. The normalised decay curves of the L_n and L_1 and L_2 are similar in shape, showing rapid signal decay in each case. However, the sensitivity-corrected doses (L_x/T_x) in the DRC indicate a poor recycling ratio suggesting that sensitivity occurred and that the T_n signals did not correct for this change appropriately (Figure 6.34). A total of 157 grains (12%) were rejected due to poor recycling ratios.

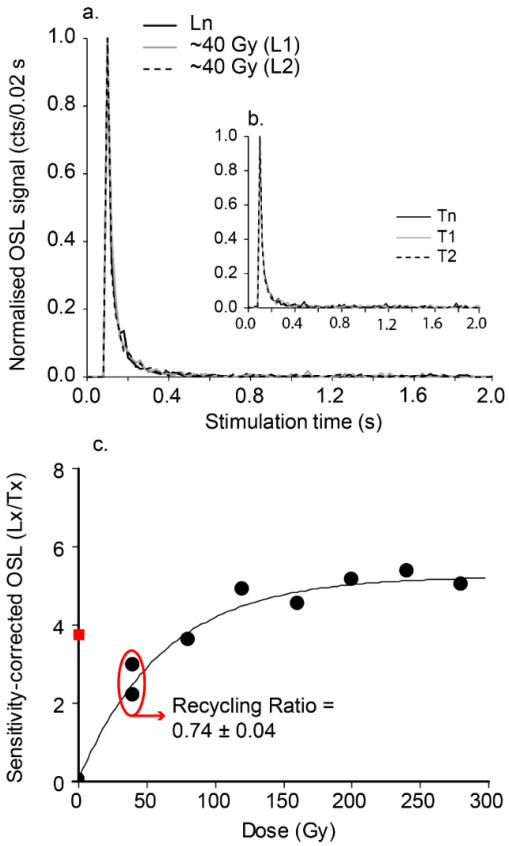

Figure 6.34. Normalised decay curves for the regenerative (a) and test dose (b) and the DRC (c) of one grain with a poor recycling ratio

6.3.3.3 *OSL-IR depletion ratio*

Not all quartz grains are pure and can contain inclusions of other types of minerals, such as feldspar (outlined in Chapter 5; Baril 2004). To test for potential contamination, each grain is exposed to an infrared (IR) laser diode at the end of the SAR procedure(Duller 2003). The OSL signal before and after IR-exposure is compared to calculate an OSL-IR depletion ratio (see Duller 2003). If a grain's OSL-IR depletion ratio is <2σ from unity, it is rejected.

An example of a quartz grain that was rejected on the basis of returning an OSL-IR depletion ratio

<2σ from unity is presented in Figure 6.35. Its decay curve shows a marked reduction in signal (red line) after IR exposure at room temperature (Figure 6.35a). Figure 6.35c shows the corresponding DRC, together with the two repeat points at ~40 Gy, used for calculation of the recycling and OSL-IR depletion ratios. The repeat point after exposure to IR (red dot) is inconsistent with the first, producing an OSL-IR depletion ratio significantly lower than 2σ from unity. Only 4% of grains (n = 59) from UPK7's OSL dataset showed significant loss of OSL signal due to feldspar contamination (Table 6.6).

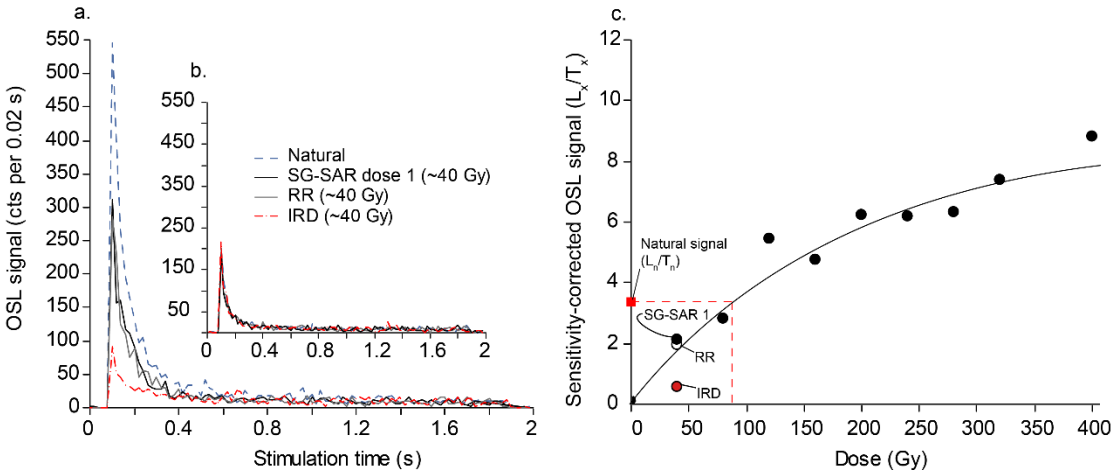

Figure 6.35. Example of an IR sensitive grain. a) shows a typical decay curve of the natural OSL signal (Ln, blue dashed line) compared to the first given dose of ~40 Gy (black line) in the SAR sequence, followed by the well-matched duplicated signal of ~40 Gy, applied to assess the grain's recycled ratio ('RR', light grey line), and the depleted IR stimulated signal of the same grain (red dash-dot line). b) is the associated test dose decay curve for each signal and shows similar signal strength and curve form between each measurement. c) is a DRC of the same grain showing the position of the sensitivity-corrected natural (Ln/Tn, red square), SG-SAR 1 (~40 Gy, black labelled circle), RR (white circle) and IRD (red circle) OSL signals. Unlike the SG-SAR 1 and RR points, the position of the IRD is more than 2σ from unity.

6.3.3.4 Recuperation

Recuperation is detected by comparing a grain's zero-dose sensitivity-corrected OSL signal to its sensitivity-corrected natural OSL signal (Wintle & Murray 2006). If a grain's zero-dose signal is more than 5% of the natural it is rejected (Murray & Wintle 2000). Recuperation levels for UPK7 samples were extremely low in all measured grains (<1%) (Table 6.6). Only one grain from sample 90026/UOW-1832 was rejected under this criterion.

6.3.3.5 L_n/T_n Interpolation and dose saturation

Some grains continue beyond the final regenerative dose resulting in the extrapolation of a D_e value (Figure 6.36a), while others plateau ('saturate') before interpolation with the L_n/T_n (e.g., Figure 6.36b). Grains with extrapolated D_e values or that exhibit dose saturation were rejected. However, samples with a high number of grains that have saturated DRCs or extrapolated D_e values can result in a truncated D_e distribution and thus an underestimated D_e for age calculation (Duller 2012; Li et al. 2017). As a conservative measure, the calculated age for these samples will be treated as minimum ages. The D_e values of 134 grains were calculated by extrapolation of the DRC. While the DRC of 226 grains saturated before interpolation with

the L_n/T_n. As a result, these grains were excluded from further analysis. Most of these grains occur in samples that come from the older units LR and LRcc, suggesting that their D_e distributions could be truncated (see below, Table 6.6).

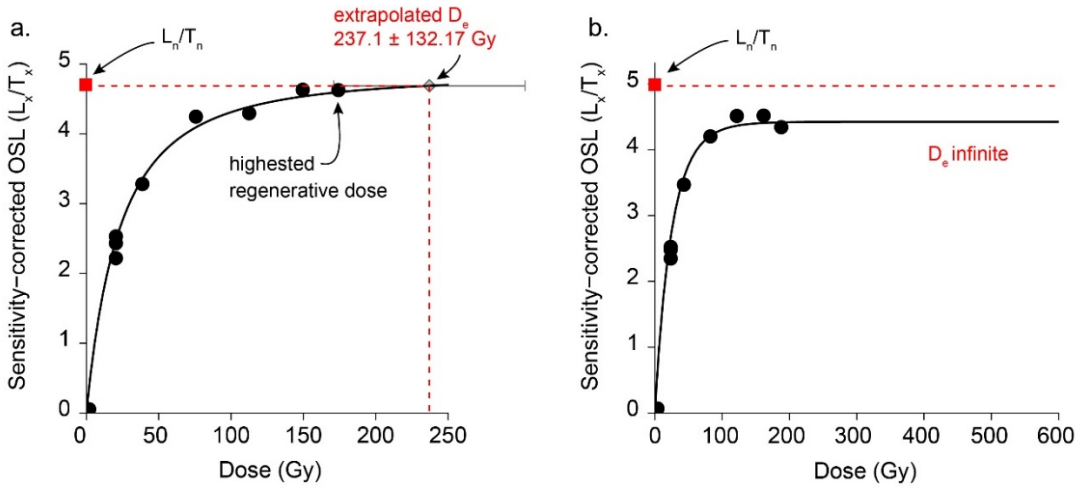

Figure 6.36. Example DRCs from sample UoW-1832 showing two grains rejected under criterion 7 (a) and 8 (b). A. Interpolation of the Ln/Tn (Red line) with a saturating exponential curve (black line) beyond the last regenerative dose (black circles), obtaining a De value by extrapolation (grey diamond, see criterion 7 in Table 6.6). B. Interpolation was not possible due to saturation (see criterion 8 in Table 6.6).

6.3.4 Accepted grains: decay and DRC characteristics

A total of 521 grains were accepted for all 12 samples from UPK7, representing 4% of the measured total and 38% of grains with signal (Tables 6.5 & 6.6). The D_e values of all accepted grains were determined by subtracting an average of the final 0.3 s from the first 0.22 s of OSL decay. The decay curves of accepted grains for one representative sample in each sediment unit are depicted in Figure 6.37.

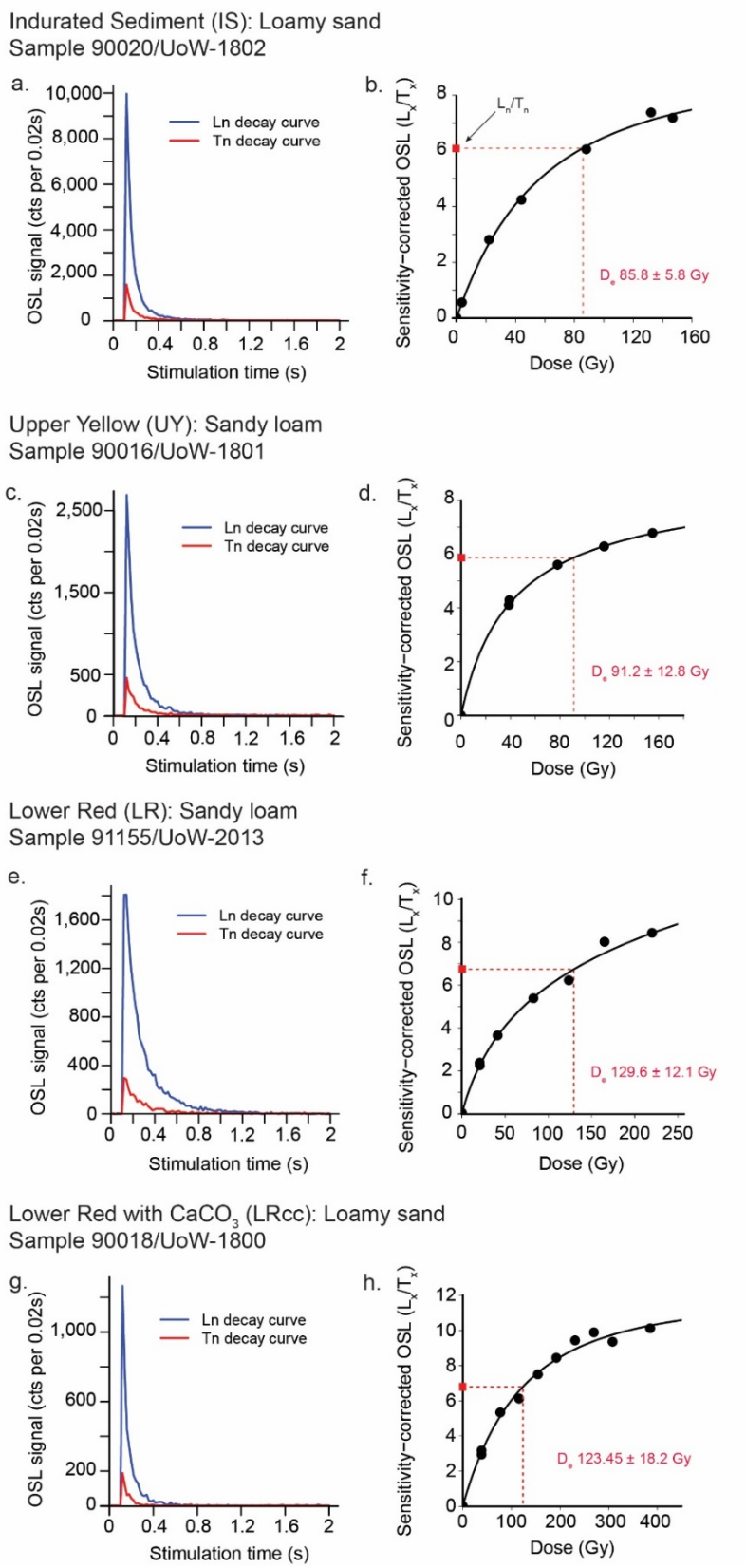

Figure 6.37. Typical OSL Ln and Tn decay curves (a, c, e, g) and DRCs (b, d, f, h) of single grains from one representative sample of each sediment unit. DRCs show the series of regenerative doses (black circles) given to each sample's grain. These are fitted with a single saturating exponential function. The Ln/Tn (red square) is projected onto the DRC and a De value is obtained by interpolation with the dose axis.

6.3.4.1 Interpreting D_e distributions for age calculation

D_e values for each sample were plotted using radial plots to assess the shape of each sample's D_e distribution for possible partial bleaching/mixing of grains prior to age calculation (Galbraith 1988; Galbraith et al. 1999). Radial plots of D_e values for each sample are presented in Appendix 4.7 with a description of the shape and interpretation of their distributions and the model chosen for estimating their D_e for age calculation. Radial plots show the distribution of accepted grains for a given sample with precision increasing from left to right of the graph. To obtain a consistent D_e value, 95% of points are expected to fall within a standardised estimate of ± 2 units of a central D_e value. The axis for the standardised estimate is located to the right of the plot and is represented by a grey band that spans ± 2 units either side of the central D_e, extending from left to right of the plotted area. The more dispersed the D_e values are the greater the standard error will be.

The D_e values of accepted grains for nearly all samples show significant overdispersion (OD; >30%; see Appendix 4.7). High OD results from multiple intrinsic and extrinsic factors, including differences in OSL behaviour from grain-to-grain, the introduction of younger intrusive grains through bioturbation (i.e., from roots and microfauna and possible small-scale variation in the beta dose rate on individual grains as a result of pedogenesis (Duller et al. 2000; Murray & Roberts 1997; Olley et al. 1999; Roberts et al. 1999).

Given that samples from the UY and LR/LRcc deposits that are considered aeolian in origin, it is assumed that their grains were well bleached prior to burial. However, indications of pedogenesis (i.e., downward percolation of feldspar minerals, evaporation of secondary carbonates and desiccation cracking) and bioturbation (i.e., root intrusion and possible termite activity) were observed for LR and LRcc samples. Under these conditions grains from older or younger units may have been introduced into their samples or coated during translocation (Appendix 4.6 – Table A4.6.1; (Bateman et al. 2007). Indications of slope and sheet wash deposition were also observed in the OSL cuts of UoW-1802 and 2006 (respectively), which can result in partial bleaching of grains (Table A4.6.1). However, sample UOW-1802, was collected below a finely bedded deposit from sediment that showed minimal structure. In either case, the samples were treated with caution.

6.3.4.2 Scattered distributions: Identifying outliers with nMAD

To systematically identify and exclude outliers in scattered distributions the normalised median absolute deviation (nMAD) of each sample was calculated and then remodelled using CAM (Rousseeuw et al. 2006). This involved calculating the median of all grain absolute distances from the sample's median, giving equal weight to the negative and positive deviations from this medium. D_e values were first converted from Gy to natural logarithms and then corrected for a normal distribution using the correction factor of 1.4826 (Galbraith & Roberts 2012; Wood et al. 2016). Once corrected, D_e values (log) greater than 2.0 were rejected and the remaining grains were modelled using CAM (Table 6.7).

Radial plots with CAM values rejecting nMAD outliers are shown in Appendix 4.7. Figures A4.7.1- A4.7.12, with outliers depicted as triangles. After applying nMAD and removing outliers, OD values of every sample, except UoW-1833, decreased markedly, increasing the precision and central D_e

value in each case (Table 6.7 & Appendix 4.7). Applying nMAD to 90028/UOW-1833's already low accepted grain count (n = 14) reduced its sample size to 12 grains, resulting the smallest OD in the sample set (<1%). However, with or without the exclusion of outliers, the number of accepted grains in this sample is too small to produce a reliable central D_e value and will require additional grains measurements to obtain a reliable sample age.

6.3.4.3 Mixed distributions: Identifying multiple components with FMM

Sample 90020/UOW-1802 was fitted with a finite mixture model (FMM; (Roberts et al. 2000) due to the clear presence of multiple populations depicted in its D_e distribution. Employing the methods used in Jacobs et al. (2008), the smallest Bayesian Information Criterion (BIC) and maximum log likelihood was used to isolate out and fit each identified component. Two components were identified, with 75% D_e values falling within 2 standardised estimates of ~64 Gy, while the remaining 25% of grains centre around 0.84 Gy (e.g., Figure A4.7.1). Such pronounced bimodality could indicate the cross-sampling of deposits with different depositional histories or the intrusion of younger grains into an older deposit through bioturbation. The former case is plausible given that this sample was collected from a finely laminated section in OSL Cut 3, immediately below a structureless unit that was likely deposited more recently (see Appendix 4.6 – Table A4.6.1 and Figure A4.1.5). However, the presence of roots throughout the deposit suggests that the downward migration of younger sediment is more likely. Both components were selected for age calculation, with the assumption that the larger of the two is representative of the sampled deposit, prior to mixing.

Table 6.7. Single-grain OSL results for samples collected from UPK7, organised by sedimentary context. Each sample is listed with their location, depth (m), total accepted versus measured grains, equivalent dose (De), overdispersion (OD) values, and ages (ka) and Age model used to calculate said age.

Sample ID		OC	Depth (m bls)	Grain count (n)		Before nMAD[a]		After nMAD	
						De	OD	D_e	OD
Field	OSL Lab		Current	Measured	Accepted (*)	(Gy 1σ)	(%)	(Gy 1σ)	(%)
Indurated Sediment (IS): Loamy sand - slope wash									
90020	UOW 1802	3	0.25	1500	83 (60)	23.5 ± 5.1	183.8 ± 15.8	66.3 ± 3.5	32.4 ± 4.6
91080	UOW 2006	9	0.26	1900	46 (45)	97.4 ± 9.5	52.5 ± 8.3	103.8 ± 7.2	28.3 ± 6.7
Upper Yellow (UY): Sandy loam - aeolian									
90016	UOW 1801	10	0.24	1000	60 (56)	78.6 ± 4.7	37.4 ± 5.3	78.6 ±4.7	34.4 ± 5.1
90024	UOW 1804	5	0.23	1500	49 (48)	97.6 ± 5.9	30.8 ± 5.3	100.3 ± 5.2	23.7 ± 5
Lower Red (LR): Sandy loam - aeolian									
91153	UOW 2012	1U	0.35	1000	20 (18)	118.6 ± 10.5	25.1 ± 9	128.5 ± 9.4	13.4 ± 9.6
91155	UOW 2013	1L	0.6	1000	26 (24)	128.4 ± 11.1	31.5 ± 7.7	139.8 ± 6.9	6.1 ± 9.4
91157	UOW 2014	2	0.23	1000	40 (38)	124.5 ± 7.6	20.6 ± 6.7	128.4 ± 7.4	17.2 ± 6.6
Lower Red with $CaCO_3$ (LRcc): Loamy sand - aeolian									
90018	UOW 1800	11	0.33	1000	41 (39)	116.4 ± 23.5	119.2 ± 15.4	151.1 ± 13.9	37.8 ± 8.9
90022	UOW 1803	4	0.23	1000	51 (45)	90.4 ± 12.1	87.7 ± 10.3	120.9 ± 6.9	20.7 ± 6.7
90026	UOW 1832	6	0.26	1500	43 (33)	81.7 ± 13	81.7 ± 13.0	127.2 ± 8.9	24.7 ± 7
90028	UOW 1833	7	0.22	900	14 (12)	137.2 ± 10.6	10.9 ± 9.1	152.5 ± 8.1	0
90030	UOW 1834	8	0.2	1000	27 (25)	88.9 ± 9.3	34.2 ± 8.2	94.0 ± 7.4	24.4 ± 7.5

[a] OD Values attained prior to nMAD outlier exclusion are listed for each sample.
* Accepted grain count after the removal of nMAD outliers and calculated using CAM = central age model (logged) (Galbraith et al. 1999)

6.3.4.4 Truncated D_e distributions

Another issue that can influence an estimate of a sample's central D_e value is the rejection of a large number of 'saturated' grains. As described above, this can truncate a sample's D_e distribution resulting in an underestimated D_e (see Duller, 2012; Li et al., 2016). A large proportion of grains were rejected on the basis of dose saturation and the extrapolation of D_e values for samples collected from LR and LRcc (see Table 6.6). Therefore, the higher end of their D_e distributions are interpreted as truncated (see Appendix 4.7). For this reason, the central D_e of each sample—modelled using CAM and nMAD—will be used for age calculation and interpreted as minimum depositional ages.

6.3.5 Dosimetry

Calculation of a sample's burial age requires the dose rate (DR) denominator in the age equation (age = D_e/DR). The DR (Gy/ka) is the rate at which a quartz grain, receives ionising radiation in the form of alpha (α) particles (internal and external), and beta (ß), gamma (γ) and cosmic radiation. Ionising radiation is primarily the result of the decay of uranium (U) and thorium (Th) and their daughter products, as well as potassium (K), which occur external to and within the sampled grains (Aitken 1985). Ionising radiation moves electrons into irregularities within the crystal lattice of a quartz grain, trapping them until further stimulation. Trapped electrons accumulate at a predictable rate through time because the rate of electron entrapment is proportional to the rate of a grain's absorption of ionising radiation. With half-lives in the order of 10^9 years, the natural abundance of ^{40}K and the parent isotopes of U and Th are considered constant for the time range being studied (Jacobs 2004).

A grain's internal dose rate occurs as a result of very small concentrations of U, Th and K decay chains in the form of α particles (Aitken 1998). Approximately 5 μm of the alpha-irradiated rinds of all quartz grains were etched using concentrated hydrofluoric (HF) acid (40%) to reduce their external α-concentration (U and Th decay chains) to a negligible state prior to measurement. The internal α dose rate was calculated using an alpha efficiency of 0.04 ± 0.01 (Rees-Jones 1995), resulting in an attenuated internal alpha DR of 0.032 ± 0.011 Gy/ka. The total combined alpha contribution of U and Th decay chain estimates were measured by emission counting using a thick-source alpha counter (TSAC; (Aitken 1985: Appendix J).

Beta dose rates (U, Th, K and Rb) were determined by low level ß counting the dosimetry of a powdered subsample in a Geiger Müller Beta Counter (GMBC) (Bøtter-Jensen & Mejdahl 1988), following methods outlined in Jacobs & Roberts (2015). Attenuation of the ß dose—potentially resulting from variance in moisture content, grain size and HF acid etching—was also accounted for during ß dose calculation (Brennan 2003; Mejdahl 1979).

Gamma (γ) dose rates was counted directly by emission counting using a thick-source alpha counter (TSAC; (Aitken 1985: Appendix J). This was performed in the UOW OSL laboratory using finely milled subsamples taken from the immediate vicinity (< 0.3 m) of the OSL sediment sample used to obtain a D_e. ß and γ dose rates were converted by adjusting for water content (Aitken 1985; Nathan & Mauz 2008) and employing the conversion factors set out in Guérin et al. (2011).

Long-term water content of 5.0 ± 1.3 % was also incorporated in the ß and γ dose rates. This value

is higher than the water content measured for each sample, to account for potential wetter paleoclimatic conditions in the WRZ and study area during the Late Pleistocene (see Chapter 3). A sample's measured DR is calculated under the assumption that the (dis)equilibrium of U and Th decay chains have undergone minimal change throughout the duration of sediment burial (Olley et al. 1998; Readhead 1987).

6.3.6 Cosmic-rays and burial depth estimates

The cosmic-ray contribution to the environmental DR was determined based on the altitude, geometric latitude, sediment density, and the depth below surface of each sample (Prescott & Hutton 1994). Because erosion and deposition are active processes in the ongoing formation of the study area, it is assumed that the current depth of a sample represents the minimum thickness of overburden protecting it since its initial burial. The thickness of sample overburden likely varied from its current amount throughout a sample's burial history. For this reason, three 'cosmic depth scenarios' were developed to assess the influence of plausible, yet conservative, sample depths on cosmic-ray dose rate calculations: S1. Current, S2. Historic, and S3. Stratified (Appendix 4.8 – Table A4.8.1). Table A4.8.2a,b presents a range of estimated and averaged burial depths for each OSL sample collected at UPK 7. These values are based on the proposed depositional sequence of a deposit, outlined in Chapter 6.1.4 (Table 6.1), and the three plausible scenarios (S1-S3) for their past burial depth below surface (Table A4.8.1).

Scenario 1 is based on a sample's depth below the current surface (at the time of collection). Scenario 2 accounts for the historic deflation of overburden above the current surface. The term 'historic' represents the last 300 years of deflation related to intensive farming practices in the catchment area. Historic deflation was deduced from the pedestalling of historic features identified throughout the wider-valley system. This provides a standard depth for predicting the amount of deflation that has taken place over the last 300 years, resulting in the exposures observed throughout the Doring River valley (see Chapter 6.1.6).

The height above the modern surface (0.4 m) and the calibrated radiocarbon age of a pedestalled historic stone hearth at LNGKL 5f (see below) is used to establish the minimum historic deflation value in the study area. Scenario 3 accounts for the removal of overlying deposits due to historic erosion (~0.4 m) in addition to a deposit-wide overburden of active unconsolidated sand (UCS, ~1 m in thickness). S3 assumes the repeated aeolian deposition, removal, and movement of UCS during the more arid conditions of the Holocene. Each scenario had negligible impact on the total cosmic-ray contribution of a sample, with only minimal difference observed in optical age for each sample. Even so, the historic scenario (S2) is considered the most plausible of the three as an enduring overburden thickness for the sampled surface of UPK7, with the stratified and current scenarios considered maximum and minimum burial depths, respectively. For this reason, S2 was used to calculate the cosmic-ray dose depths of each OSL sample (Table A4.8.2).

6.3.7 Measured dose rates

Table 6.8 presents the radionuclide concentrations, ß, γ, cosmic-ray and total dose rates as well as their field and standard water contents for all samples in the study area. Total dose rate uncertainties were calculated by adding, in quadrature, all systematic and random errors of the three dose rate contributors. Total dose rates range from ~2.6 to 1.7 Gy/ka for all samples. These vary markedly between samples in each sedimentary unit, indicating geochemical variance within and between sedimentary units. Variance may result from radionuclide disequilibrium between the more soluble ^{238}U and the more stable ^{232}Th elements within the same deposit depending on its more localised conditions across the study area or heterogenous micro dosimetry of ß dose emission from the immediate vicinity of the sampled grains.

6.3.8 Optical age estimates

Table 6.9 lists all final single-grain OSL ages along with their associated D_e values and dose rate estimates. The uncertainty for burial ages is shown as 1 se on the mean, obtained from the quadratic sum of all random and systematic errors from all known estimated sources. Finite age estimates were obtained for five samples. Three ages derive from CAM after nMAD grain exclusion. The age of one sample, UOW-2006, was obtained using the CAM without excluding outliers (see Appendix 4.7 – Figure A4.7.2). UOW-1833 is excluded as a valid age determination as the dataset is too small (n = 14) to produce a reliable burial age.

The larger portion of D_e values (75%) from the FMM output of sample UOW-1802 were used to calculate its age (highlighted in bold in Table 6.9). The intrusive grains identified in sample UOW-1802 formed 25% of the FMM output and date to ~420 ± 70 years. This suggests that grain intrusion occurred close to the timeframe connected with the onset of historic farming activity. It would be worth sampling sediments closer to the surface to determine the source of these younger grains and attain a larger sample size, thereby increasing the precision of its estimated burial age and the deposit composition from which it possibly derives.

Table 6.8. Environmental dose rate results for OSL samples collected from UPK7, organised by sedimentary context.

Sample ID		Water Content (%)		Radionuclide concentrations[a]			Dose rate (Gy/ka)[a & ^]			
Field	OSL Lab	Field	Standard	U (ppm)	Th (ppm)	K (%)	Beta*	Gamma*	Cosmic^	Total
Indurated Sediment (IS): Loamy sand - slope wash and aeolian deposition										
91080	UOW-2006	2.3	5 ± 1	2.57 ± 0.13	7.92 ± 1.09	1.38 ± 0.07	1.38 ± 0.05	0.96 ± 0.06	0.19 ± 0.03	2.57 ± 0.08
90020	UOW-1802	0.3	5 ± 1	1.87 ± 0.09	5.54 ± 0.80	1.11 ± 0.05	1.07 ± 0.04	0.71 ± 0.04	0.20 ± 0.03	2.01 ± 0.07
Upper Yellow (UY): Sandy loam - aeolian										
90016	UOW-1801	1.6	5 ± 1	1.90 ± 0.09	4.58 ± 0.69	1.14 ± 0.05	1.07 ± 0.04	0.68 ± 0.04	0.20 ± 0.03	1.97 ± 0.06
90024	UOW-1804	1.2	5 ± 1	2.34 ± 0.10	6.11 ± 0.81	1.08 ± 0.06	1.12 ± 0.04	0.78 ± 0.04	0.20 ± 0.03	2.13 ± 0.07
Lower Red (LR): Sandy loam - aeolian										
91153	UOW-2012	0.6	5 ± 1	2.32 ± 0.09	3.80 ± 0.65	0.82 ± 0.05	0.89 ± 0.03	0.61 ± 0.04	0.19 ± 0.03	1.73 ± 0.06
91155	UOW-2013	1.7	5 ± 1	1.63 ± 0.05	6.65 ± 0.85	1.10 ± 0.05	1.06 ± 0.04	0.73 ± 0.05	0.19 ± 0.03	2.01 ± 0.07
91157	UOW-2014	2.6	5 ± 1	2.76 ± 0.11	5.51 ± 0.85	1.27 ± 0.06	1.28 ± 0.04	0.84 ± 0.05	0.20 ± 0.03	2.35 ± 0.07
Lower Red with $CaCO_3$ (LRcc): Loamy sand - aeolian										
90018	UOW-1800	0.5	5 ± 1	1.95 ± 0.08	4.58 ± 0.63	1.02 ± 0.05	1.00 ± 0.04	0.66 ± 0.04	0.19 ± 0.03	1.88 ± 0.06
90022	UOW-1803	2	5 ± 1	2.04 ± 0.09	5.54 ± 0.78	1.23 ± 0.06	1.17 ± 0.04	0.76 ± 0.04	0.20 ± 0.03	2.15 ± 0.07
90026	UOW-1832	2.4	5 ± 1	2.01 ± 0.11	7.66 ± 1.00	1.15 ± 0.06	1.16 ± 0.04	0.83 ± 0.05	0.19 ± 0.03	2.21 ± 0.07
90028	UOW-1833	2.6	5 ± 1	2.33 ± 0.10	5.48 ± 0.77	1.12 ± 0.05	1.13 ± 0.04	0.76 ± 0.04	0.20 ± 0.03	2.12 ± 0.07
90030	UOW-1834	1.2	5 ± 1	1.66 ± 0.08	5.31 ± 0.71	0.96 ± 0.05	0.94 ± 0.03	0.64 ± 0.04	0.20 ± 0.03	1.81 ± 0.06

* se includes moisture content

^Cosmic-ray dose rate (se excludes moisture content) assumes an open-air context *without* rock overburden (Prescott and Hutton 1994). Overburden thickness accounts for current depth below surface and the minimum predicted historical overburden of ~0.4 m (see Appendix 4.8 – Tables A4.8.1 & A4.8.2).

[a] Using Thick Source α Counting (TSAC, for ^{238}U and ^{232}Th) + Geiger Müller ß Counting (GMBC) (for ^{40}K) for γ DR and GMBC for ß DR

Table 6.9. Single-grain OSL results for samples collected from UPK7, organised by sedimentary context. Each sample is listed with their location, depth (m), total accepted versus measured grains, equivalent dose (De), overdispersion (OD) values, and ages (ka) and Age model used to calculate said age.

Sample ID		OC	Depth (m bls)		Grain count (n)		De	OD	Total dose rate	Age[b]	Model[c]
Field	OSL Lab		Current	Historic	Measured	Accepted (*)	(Gy 1σ)	(%)	(Gy ka^{-1})	(ka)	
Indurated Sediment (IS): Loamy sand - slope wash											
91080	UOW 2006	9	0.26	0.66	1900	47 (45)	103.8 ± 7.2	28.3 ± 6.7	2.57 ± 0.08	40.4 ± 3.2	CAM
90020	UOW 1802	3	0.25	0.65	1500	101 (60)	64.3 ± 2.2 Gy (75%) 0.84 ± 0.14 Gy (25%)	183.8 ± 15.8	2.01 ± 0.07	32.1 ± 1.6 (75%) 0.42 ± 0.07 (25%)	FMM
Upper Yellow (UY): Sandy loam - aeolian											
90016	UOW 1801	10	0.24	0.64	1000	60	78.6 ± 4.7	34.4 ± 5.1	1.97 ± 0.06	39.9 ± 2.8	CAM + nMAD
90024	UOW 1804	5	0.23	0.63	1500	49 (48)	100.3 ± 5.2	23.7 ± 5	2.13 ± 0.07	47.2 ± 3	CAM + nMAD
Lower Red (LR): Sandy loam - aeolian											
91153	UOW 2012	1U	0.35	0.75	1000	20 (20)	128.5 ± 9.4	13.4 ± 9.6	1.73 ± 0.06	74.4 + inf./- 6.2	CAM + nMAD
91155	UOW 2013	1L	0.6	1	1000	26 (24)	139.8 ± 6.9	6.1 ± 9.4	2.01 ± 0.07	69.6 + inf./- 4.2	CAM + nMAD
91157	UOW 2014	2	0.23	0.63	1000	41 (38)	128.4 ± 7.4	17.2 ± 6.6	2.35 ± 0.07	54.7 + inf./- 3.7	CAM + nMAD
Lower Red with $CaCO_3$ (LRcc): Loamy sand - aeolian											
90018	UOW 1800	11	0.33	0.73	1000	41 (39)	151.1 ± 13.9	37.8 ± 8.9	1.88 ± 0.06	>80.4 + inf./- 8	CAM + nMAD
90022	UOW 1803	4	0.23	0.63	1000	51 (45)	120.9 ± 6.9	20.7 ± 6.7	2.15 ± 0.07	>56.2 + inf./- 3.8	CAM + nMAD
90026	UOW 1832	6	0.26	0.66	1500	43 (33)	127.2 ± 8.9	24.7 ± 7	2.21 ± 0.07	>57.5 + inf./- 4.6	CAM + nMAD
90028	UOW 1833	7	0.22	0.62	900	14	137.2 ± 10.6	0	2.12 ± 0.07	>64.9 + inf./- 5.5	CAM
90030	UOW 1834	8	0.2	0.6	1000	27 (25)	94.0 ± 7.4	24.4 ± 7.5	1.81 ± 0.06	>51.8 + inf./- 4.5	CAM + nMAD

[b] Assuming historic cosmic dose burial depth scenario (S2, see Appendix 4.8 – Tables A4.8.1 & A4.8.2).

[c] Age models by: CAM = central age model (logged) (Galbraith et al. 1999); FMM = finite mixture model (Roberts et al. 2000, Jacobs et al. 2008)

*Counts in parentheses represent the total number of grains modelled using the CAM following the identification and exclusion of outliers with the application of nMAD.

Sample UOW-1802 was collected from sediment exposed in a rill-cutting on the lower hillslopes of Exposure 1b and provides a burial age of 32.1 ± 1.6 ka for the Indurated Sand (Figures 6.38 & 6.39). This supports the OSL ages obtained from samples UNL3809 and UNL3810 (30.3 ± 1.3 ka and 30.5 ± 1.4 ka respectively), which were collected from Indurated Sands to the west of sample UOW-1802, from the middle and lower hillslope of Exposure 1a (Figure 6.38; (Shaw et al. 2019a). Although both samples UOW-2006 and UOW-1802 were grouped under indurated sediment in the field, subsequent field observations and analysis of the macro-structure of their section cuts (OSL cuts 9 and 3, respectively) suggest that the mechanics of their initial formation were different. The different sedimentary compositions and the processes involved in the deposition of samples UOW-2006 and UOW-1802 supports the sequential timing of their mean burial ages, with the aeolian deposition and burial of UOW-1802 post-dating the slope wash deposition of UOW-2006 (40.4 ± 3.2 ka) by at least 3.3 ka (Figure 6.40). Together, their deposition suggests a period of slope wash erosion of older, upslope deposits on the southern slope of Exposure 1b, followed by aeolian deposition and deposit stabilisation. During survey, their substrate grouping was based more on their proximity and similar elevations than sedimentary composition making this a good example of why future research at this locality would benefit from trench excavation and sampling.

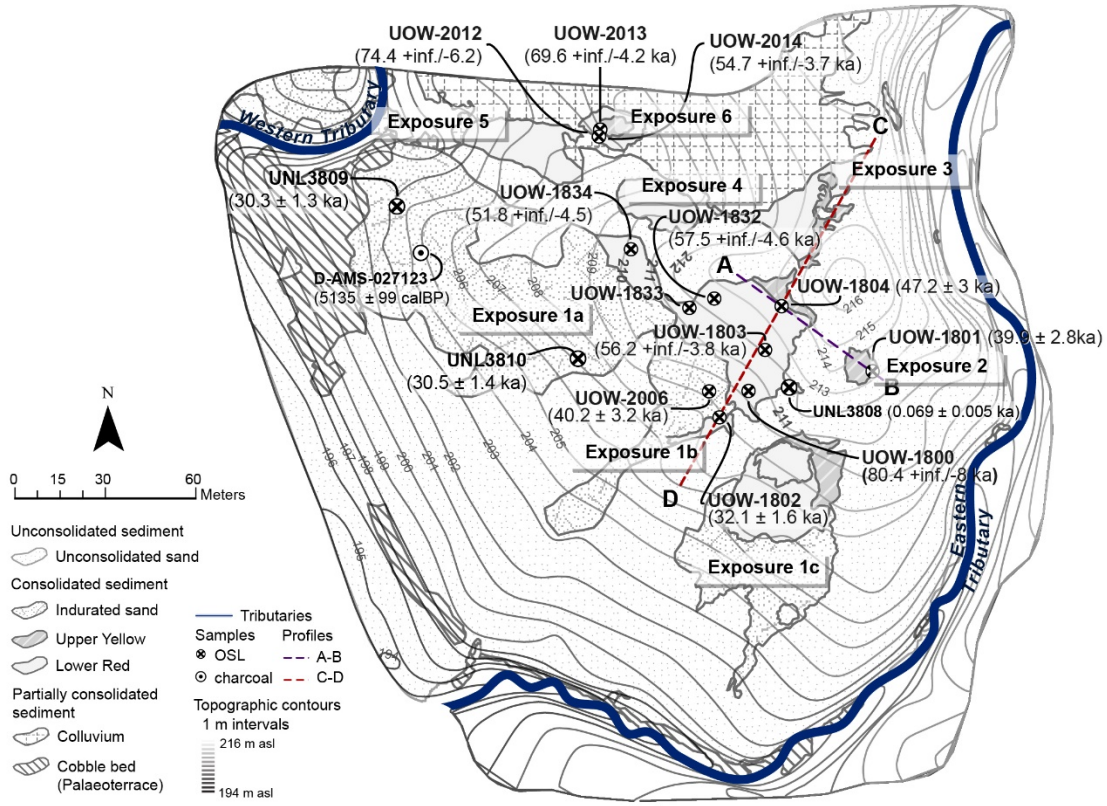

Figure 6.38. Map of UPK7 showing the locations of OSL samples collected from consolidated and unconsolidated sediment, including the locations of OSL samples processed at the UNL laboratory (see Shaw et al. 2019b). One charcoal rich sediment sample (D-AMS-027123) was also collected from a combustion feature on the indurated sediment surface and its location depicted here and in Figure A4.0.1. Topographic contours are drawn at 1 m intervals based on the 2019 UPK7 DTM. Profile lines 'A-B', and 'C-D' pertain to surface profiles presented in Figure 6.39 (below).

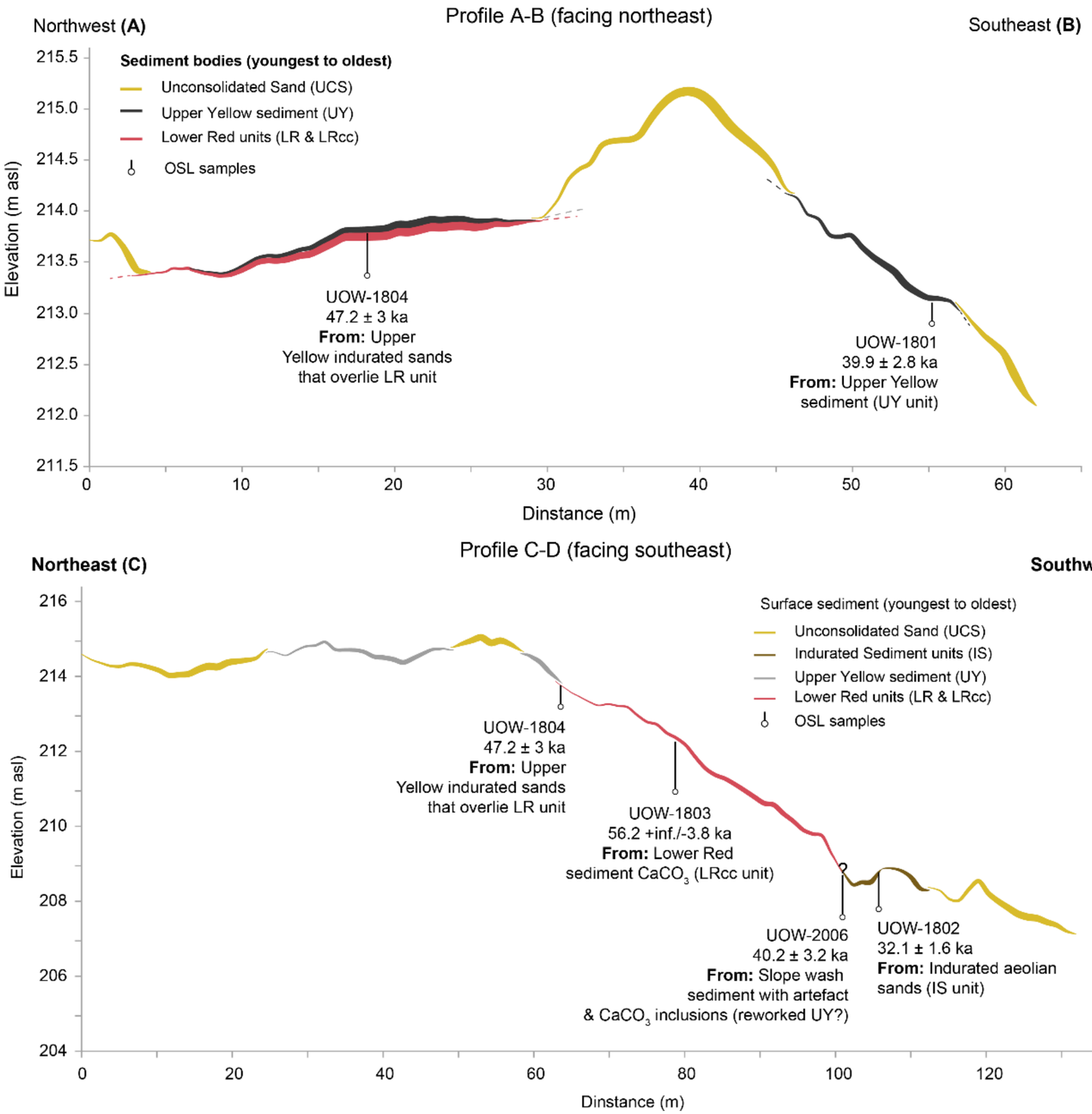

Figure 6.39. Surface profiles A-B (above) and C-D (below) showing the location and results of OSL samples and the surface distribution of the four main sediment units that form UPK7's sand mantle (listed in stratigraphic order): Unconsolidated Sand (UCS, yellow line), Indurated Sand (IS, brown line), Upper Yellow (UY, grey line), Lower Red (LR & LRcc, pink line). Profile line locations are depicted in Figure 6.38.

The slope wash sample UOW-2006 was also deposited around the time of UOW-1801's Upper Yellow formation (Figure 6.40). The ages for these samples and their errors overlap entirely, with a burial age of 40.4 ± 3.2 ka for UOW-2006 compared to 39.9 ± 2.8 ka UOW-1801 (Figure 6.40). However, they were taken from different slopes and differ in sediment composition (Figures 6.38 & 6.39). UOW-2006 was collected from OSL cut 9 that was cut into the side of a deeply incised rill at the bottom of the exposed south-facing slope (Appendix 4 – Figure A4.1.6). The exposed sedimentary structure of OSL cut 9 suggests that sample UOW-2006 formed as a result of slope wash erosion from higher up the southern slope, resulting in mass movement and deposition of older sediments and their associated archaeology downslope. In contrast, UOW-1801 appears to have formed through aeolian deposition. These samples support the idea that the local conditions in the study area oscillated between aeolian deposition and rainfall driven erosion ~40 ka.

Samples collected from the consolidated sediments of the Upper Yellow unit were deposited at different times, without overlap (Figure 6.40, Figures 6.38 & 6.39). A minimum gap of ~1.5 ka separates their deposition, with sample UOW-1804 (47.2 ± 3 ka) deposited prior to UOW-1801 (39.9 ± 2.8 ka; Figure 6.40). This is unsurprising given the contexts from which these samples were collected. UOW-1804 was sampled at the top of the southern slope at the juncture between indurated Upper Yellow and Lower Red sediment, providing a maximum depositional age for Upper Yellow on this slope (see Figures 6.39, Profile C-D). Sample UOW-1801, on the other hand, was collected from the leeward slope of the eastern dune crest (Figure A4.1.8, see Figures 6.39, Profile A-B). The Lower Red unit was not found during excavation of UoW-1801's OSL section (OSL cut 10) and its composition appeared less weathered than that of the older Upper Yellow sample 90024/UOW-1804 from the south facing slope. While differential weathering between the southern and eastern slopes could explain these differences, the younger age for 90016/UOW-1801 also indicates that differences in the timing of deposit formation could relate to different environmental conditions. Additional sampling is required to investigate these possibilities further. Considered together, the age determination for each sample from both IS and UY units overlap whilst maintaining their temporal order (Table 6.9 & Figure 6.40). This suggests a potentially continuous history of deposition with intermittent, localised erosion and redeposition of upslope sediments.

All samples collected from the highly weathered Lower Red sediments—with and without inclusions of calcium carbonates—have a relatively high percentage of saturated grains (>17%) compared to samples from the deposits of Upper Yellow and Indurated Sand. The ages for these samples are considered truncated and are treated in the following sections as minimum ages for the timing of sediment burial (see Table 6.9). This means that their deposition occurred no later than the given age estimate. However, sediment accumulation could have occurred at any point prior to this date. All samples with minimum depositional ages formed no later than ~47 ka (Figure 6.40). The oldest minimum age was obtained from sample 90018/UOW-1800, which was deposited no later than 72.4 ka (80.4 +inf./-8; Figure 6.40 & Table 6.9).

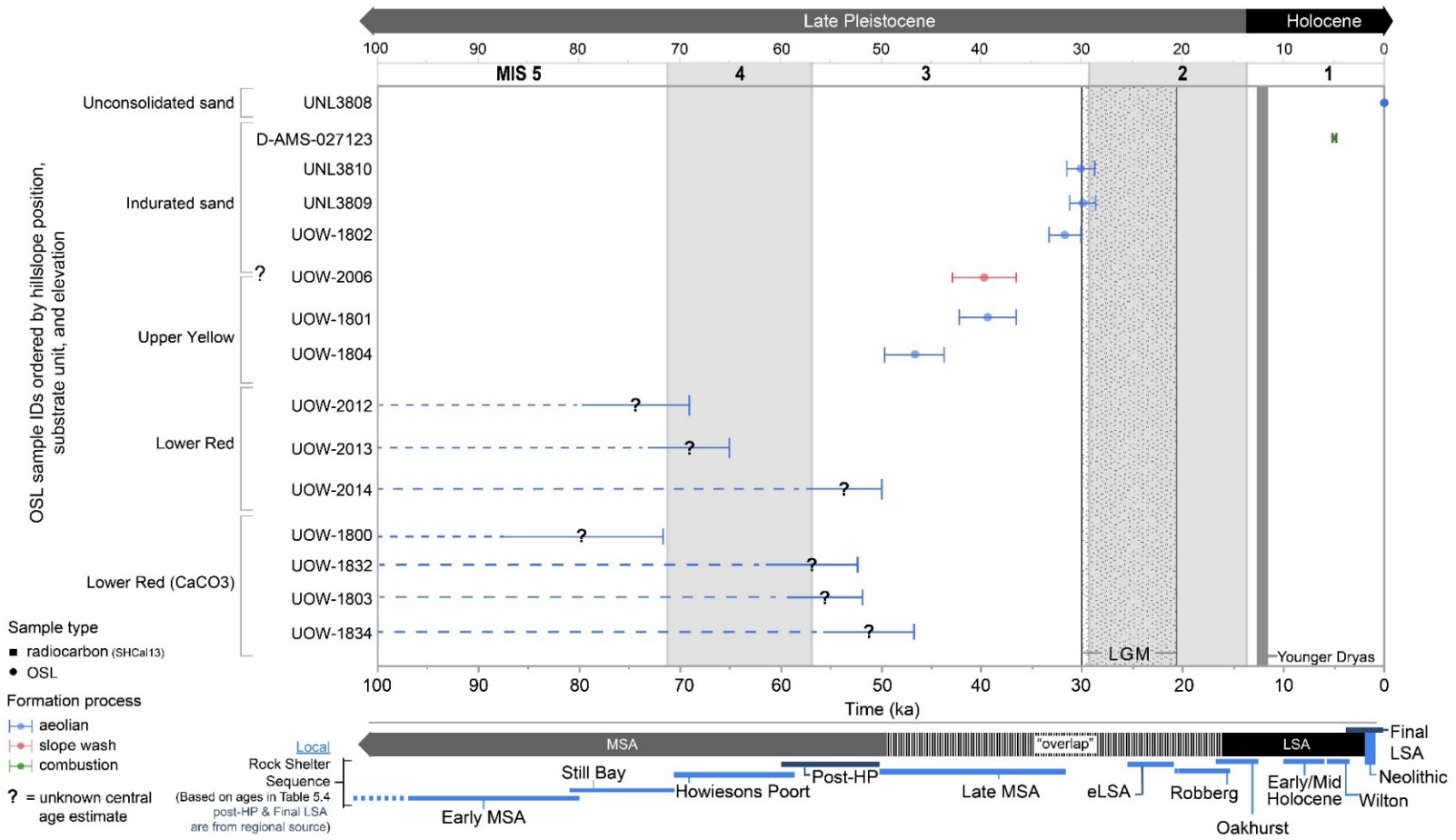

Figure 6.40. Distribution of OSL ages for UPK7 relative to a single, calibrated radiocarbon determination, and four different chronological systems: Epoch and Marine Isotope stages (MIS) at the top of the graph, and Stone Age and Industry sequence at the base of graph. Minimum burial ages are signified by a dashed line and question mark to show their potential truncation and latest possible age of deposition. MIS 1: 0-14 ka; MIS 2: 14-~29 ka; MIS 3: 29-57 ka; MIS 4: 57-71 ka; MIS 5: 71-130 ka (based on Stewart & Jones (2016, figure 1.1) and results from the LR04 stack analysis presented in Lisiecki & Raymo (2005)). Stone Age Industries are based on the local and regional rock shelter sequence presented in Chapter 5 – Table 5.4.

6.4 The Potential Impact of UPK7's Formation on Artefact Visibility and Movement

6.4.1 Introduction

Identifying the dominant processes involved in the formation of each deposit is not only essential for determining the potential age of sediment exposure, it also helps to determine the environmental and sedimentary conditions that promote or inhibit the post-depositional preservation and exposure of UPK7's archaeology. The formation and degredation of UPK7's sediment units results from the interaction between wind and rainfall. The deposition of sediment by wind is the inferred deposit-building process—its rate and amount controlled by surface roughness (i.e., vegetation cover; Figure 6.41), sediment source availability, and wind strength and direction (Bullard & McTainsh 2003). The accumulation of sediment helps to bury and preserve discarded artefacts and consequently inhibit their visibility. Moreover, irregularities in unconsolidated and semi-consolidated sand occur in areas where vegetation mounds or possible coppice dunes have formed. Not only do these features further indicate the simultaneous processes of sand accumulation, water retention and vegetation growth, they also signal conditions of deflation of the surrounding sediment by wind and rainfall overtime—the shift in topography and associated variation in the rates of saturation between vegetation mounds, thick UCS and crusted surfaces can channel runoff and increase deflation between mounds (Dougill & Thomas 2002; Langford 2000; Ravi et al. 2010).

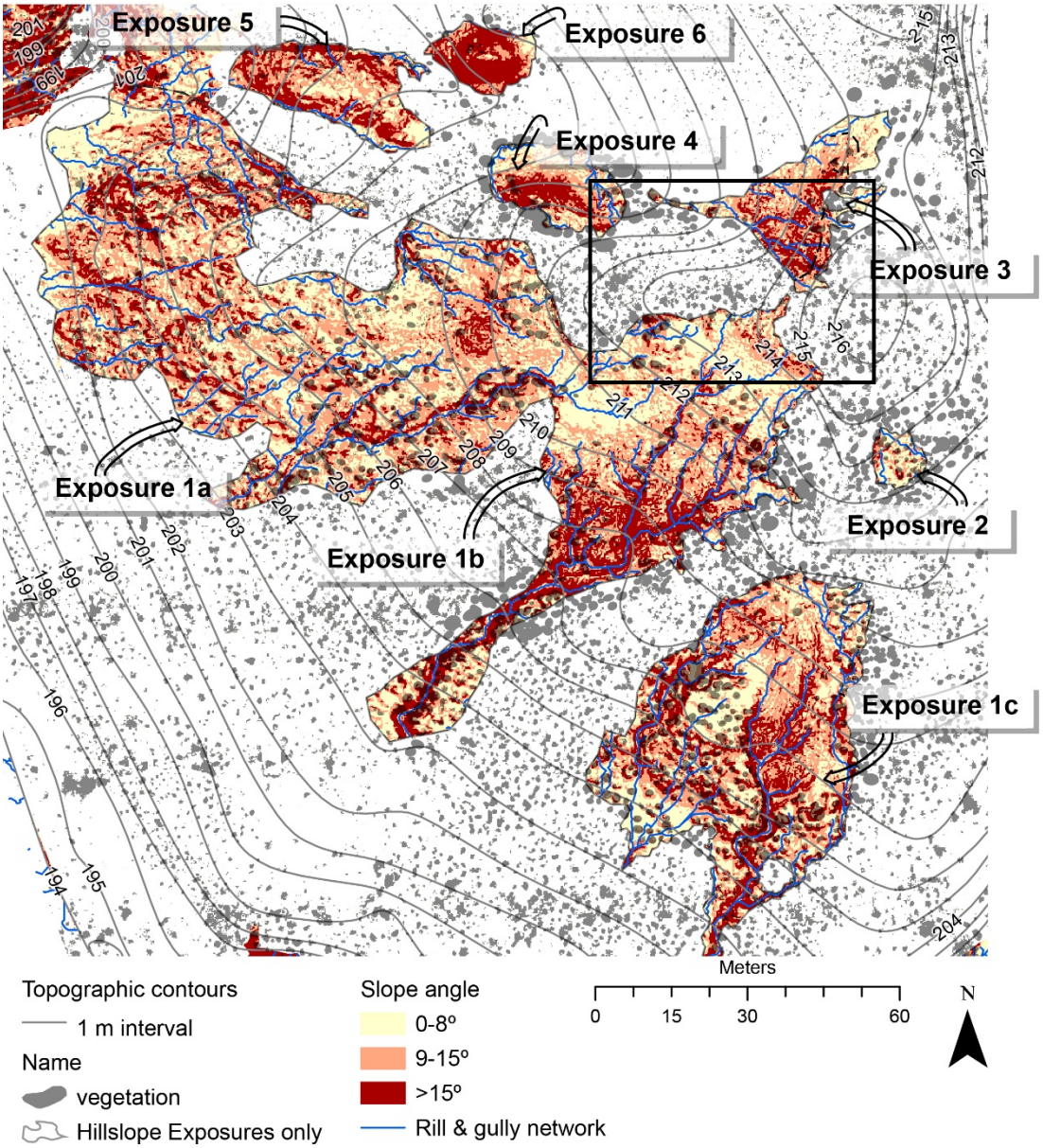

Figure 6.41. Topographic map of UPK7 showing crown height raster (based of filtered canopy cover from the 2019 DSM, see Figure 5.8d) and manually traced vegetation as well as slope angles (0-8°, 9-15°, > 15°) within each exposure calculated from the hydrologically corrected 2019 DTM (for details on DSM & DTM creation see Chapter 5.6 & Appendix 3). These features are depicted against 1 m interval topographic contours. The black frame marks that area captured in detail in Figure 6.43. Rills are only represented by Strahler classes 2 to 5 within exposures to reduce surface noise and isolate out shallow, moderate, and well-developed rills within each area. Class 1 is indicative of micro-topographic features that do not adequately represent rill locations, while class 5 and 6 channels occur downslope of exposures and include the western and eastern tributaries.

6.4.2 Deposition and erosion

The dynamic between wind and rainfall on UPK7' s slopes present a complex history of sediment accumulation, deflation and overland flow. The main processes contributing to the formation of UPK7's sediment stack is aeolian sand accumulation and hillslope erosion. However, erosion is outpacing deposition. Physical weathering appears to be more important than chemical weathering, with low levels of mineral leaching evident in the consolidated sediments. The LRcc and LR appear more resistant to both water and wind erosion compared to the Upper Yellow and Indurated Sand. However, this might have more to do with the duration of exposure of each deposit rather than the compositional differences between units. The sand mantle shows a clear relationship between the thinning or absence of vegetation and the location and extent of consolidated sediments that are crusted, rilled, and have moderate to steep slopes (e.g., Figure 6.42 & 43, Marzen et al. 2019; Ravi et al. 2010). Figure 6.42a is an example of the dual action of wind as it migrates in a leeward direction, removing sand from the stoss side and adding it to the lee side or slip face of the dune crest. In contrast, Figure 6.42b illustrates the different zones of susceptibility to downslope erosion on a hillslope. Erosion is at its slowest in the topmost upper hillslope zone—often marked by a residual body of sediment. Just below this area, the middle zone is most prone to erosion and the greatest degree of particle transport. The footslope or lower hillslope zone represents the cumulic zone where transported particles are deposited. While aeolian deposition and surface sand movement are likely to be more gradual forces of deposition and deflation in the study area, rainfall erosion—in the form of sheet wash and debris flows—has the potential to rapidly and effectively entrain both coarse and fine particles in a downslope direction.

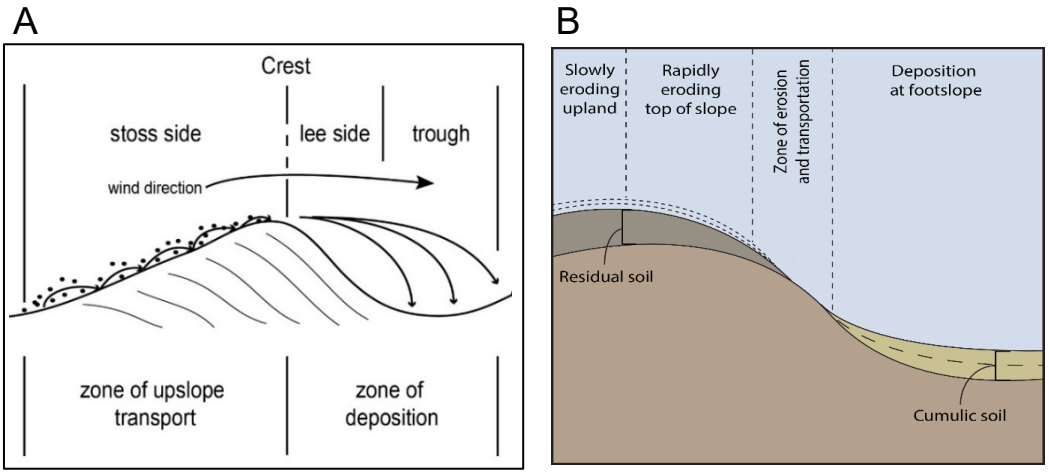

Figure 6.42. Examples of the basic processes and structure of dune formation (a) and slope erosion (b). 'B' is redrawn from Bierman et al. (2013, figure 3.12).

Given that hillslope position is an important predictor of sediment erosion, it is used as one of the main variables during analysis of artefact condition and movement in the subsequent Chapter 7. Hillslope positions were divided into three zones: upper, middle, and lower (Table 6.10). The upper zone accounts for the top 20% of a hillslope's elevation range, the lower zone accounts for the lower 40% of a hillslope's range, and the middle zone accounts for the middle 40% of a hillslope's range—between the upper and lower zones. The topmost elevation limit of the upper hillslope zone is defined by the maximum elevation

of the hillslope in question. The middle zone's topmost elevation limit is the lowest elevation of the upper zone, minus 0.1. Similarly, the lower zone's topmost elevation limit is the lowest elevation of the middle zone, minus 0.1. The lower limits of each zone were calculated by subtracting the given zone's percentage of the hillslope's total difference in elevation from the zone's topmost elevation.

Table 6.10. UPK7 Hillslope zones and their elevation ranges for each exposure.

Exposure	Hillslope zones & elevation ranges		
	Upper (20%)	Middle (40%)	Lower (40%)
1a	211.5-209.8	209.7-206.3	206.2-202.8
1b	215-213.4	213.3-210.1	210-206.8
1c	211-209.4	209.3-206.1	206-202.8
2	214.4-214.1	214.0-213.5	213.4-212.8
3	215.3-214.4	214.3-212.6	212.5-210.8
4	210.8-210.1	210.0-208.7	208.6-207.3

Based on the basic principles of dune formation and hillslope erosion, middle hillslope zones are most susceptible to sediment entrainment. Relocation of sediment during wind erosion would catalyse movement of sand toward the leeside of the dune crest, increasing sediment build-up and elevation at the crest of the dune before avalanching down the slip-face to either build-up or exit into the tributary below. Rainfall and rain splash erosion on the southern slope can relocate sediment downslope. On long, low gradient slopes, relocation might be more localised, with sediment lagging into a cumulic zone at the base of the slope. However, increased aridity, and flash flooding have formed deeply cut rills that can channel fine and coarse particles from the exposed slope direct to the river and adjacent terraces.

6.4.2.1 Wind, sand & vegetation

The formation and morphology of UPK7's unconsolidated deposits in relation to the surface condition and spatial arrangement of the exposed consolidated surfaces provides insight into the history of, and ongoing susceptibility to, deposition and erosion at this locality. Wind alters the location, spread, and form of deposited sand across a surface and has a propensity to accumulate in well-vegetated areas. Unconsolidated and semi-consolidated sands form a variable surface topography, with multiple dune crests observed across the locality as a result of dominant winds shifting during the dry season between south-westerlies and westerlies. The slip face of the eastern crest is expected to receive the greatest build-up of sand and have the lowest levels of artefact visibility as a result of artefacts and substrate burial. The north side of the northern crest forms another slip face and trough zone. Its slope dips steeply into the colluvium hillslope, which is largely devoid of unconsolidated or semi-consolidated sand. This indicates that the southward, downslope direction of overland and debris flow from the colluvium hillslope actively cuts into the back of the slip face and trough zone of the northern crest, removing sediment in a south-west direction, eventually evacuating into the western tributary (Figure 6.43).

The southern slope is the windward, stoss face of the northern dune crest. Its slope is more gradual, reducing the velocity of overland flow and impact of sheet wash erosion on the southern side compared to the northern side of the crest (cf. Exposure 3 to Exposure 1 in Figure 6.43). However, there are several less

pronounced dune crests visibly separating Exposure 1a, b and c. Their lee sides are all located east of their crests, similar to the eastern crest. Because of their more gradual slope angle and stoss position, Exposures 1a, b, and c are more likely to be vulnerable to erosion than the slip face sides of UPK7, in the north and east, which possibly promoted the relatively large areas of exposure on the south compared to the north and east sides of UPK7's crests. However, the presence of vegetation cover and the shallow nick points of rill channels at the top of the south side Exposures 1a-c, suggests that erosion in the upslope and mid-zones of their slope's is fairly recent.

Figure 6.43. Zones of erosion and deposition on the northern side of UPK7 where rills mainly drain into the Western Tributary. See Figure 6.41 for reference location.

6.4.2.2 Rainfall & rill development

Rainfall is one of the main erosional processes occurring in the study area. The strength and impact of spring flash-flooding was observed during the August field season in 2014 at Uitspankraal 1, located on the south side of the Doring River channel, 1.5-2 km down-river from UPK7 (Figure 6.1a). The exposed, highly consolidated, and sandy loam sediment at UPK1 was rapidly saturated, resulting in surface runoff (Figure 6.44a) that was either channelled into rills across and at the base of exposed hillslopes (Figure 6.44d) or water pooled in shallow depressions (Figure 6.44c). The rapid drying and contraction of exposed sediment after rainfall, formed hard, finely cracked crusts, between 5 and 20-mm thick. Small pores of trapped air were observed throughout this crust as well as the underside of exposed artefacts, where it contacted the substrate's surface. Sediment contraction and pore formation helped to increase the adhesion of surface artefacts to their underlying substrate. Paradoxically, this possibly increases their future resistance to slope wash. Pedestalled and imbricated capping stones were also observed protruding from exposed, crusted sediment (Figure 6.44b), providing another indicator of erosion caused by runoff. Figure 6.44b shows

several large (>100 mm in max dimension) imbricated sandstone cobbles acting as capping stones to an underlying pedestal of sediment. Behind these stones are the remnants of pedestalled sediment with missing capping stones, indicating recent slope wash removal (Figure 6.44b).

Figure 6.44. Flash flooding at UPK1, August 2014 (a, c, and d), and the remnants of sheet wash erosion in the form of imbricated sandstone slabs. Note the remnants of pedestalled sediment in the background of b without their capping stones.

In the case of UPK7, the impact of slope wash on slope morphology and sediment exposure is marked. The upper, middle, and lower slopes of exposed sediment are cut through by a network of rills (see Figures 6.43 & 6.44c) indicating extensive rainfall and slope wash erosion. High rates of artefact dispersal have been shown to increase close to channels (Schick 1987). For this reason, artefact size-sorting and abundance are examined relative to their proximity to rills and rill catchment size—as a result of slope angle and represented by rill depth. The hierarchical order of surface flow across UPK7 was assigned using the Strahler method, shown in Figure 6.43. Moderate to deeply incised rills have Strahler classes of 4 to 5, while shallow and fine rills feeding into these from upslope are classed from 2 to 3 (Figure 6.43). Rilled, steeply sloping areas on Exposure 1b are concentrated below 210 m asl (Figure 6.43) and below 208 m asl on the eastern and western side of Exposure 1c's hillslope.

Slope angle is highest (> 15º) in the well-rilled areas of Exposure 1a-c—particularly below 210 m asl on Exposure 1b—and on the exposed slopes north-west of Exposure 1 (i.e., Exposures 3, 4, 5, and 6;

see Figure 6.41). Object rolling occurs on slopes with angles > 32° (Ozán 2017). While artefacts below this angle require an increasing amount of additional, catalysing force to induce entrainment (i.e., debris and overland flow; Lenoble & Bertran 2004; Ozán 2017). Hillslopes with consolidated sediment are mostly low to moderately steep in gradient, with a median slope angle for all exposures of ~10.3º. Slope angles greater than 15º are often related to rilling and, to a lesser degree, vegetation. It is assumed here that slope angles >15 º that are proximate to rills will increase runoff velocity during periods of rainfall, and so the probability that heavier/larger artefacts will move with lighter/smaller artefacts is expected to increase in these contexts. In contrast, slope angles >15º that are associated with vegetation are expected to act as movement inhibitors (Behm 1985). To a lesser degree, steep hillslope angles are also apparent on both Exposure 1a and 1c in association with vegetation mounds (Figure 6.41).

6.4.2.3 Trampling

A fourth factor that can increase the impact of rainfall and wind erosion is surface trampling by stock farming. While trampling can compress and consolidate sediment, it can also break up surface crusts, destabilising the surface of the sediment body thereby making it more prone to wind and water entrainment (Marzen et al. 2019; Ries et al. 2014). Within the last 300 years, grazing has increased erosion rates across the Doring River valley (see below, and DirectAMS report in Appendix 4.9). This is most apparent where historic stone buildings are found, as well as areas close to more permanent water supply. Pedestalled stone structures are found throughout the valley, often in association with areas of erosion and highly exposed archaeological surfaces (i.e., Figure 6.45a,b). Their use over time likely intensified erosion within their immediate vicinity. Stone foundations cap underlying sediments, resulting in their characteristic pedestalling, and erosion of the remaining outer structure and underlying deposit (e.g., Figure 6.45). Deflation ranges from ~0.4 m at Lungkaal (see Figure 6.45B) to 1.6 m at UPK9. The maximum end of this range is used to calculate a conservative cosmic dose for deposits sampled for OSL analysis (see section 6.2.7).

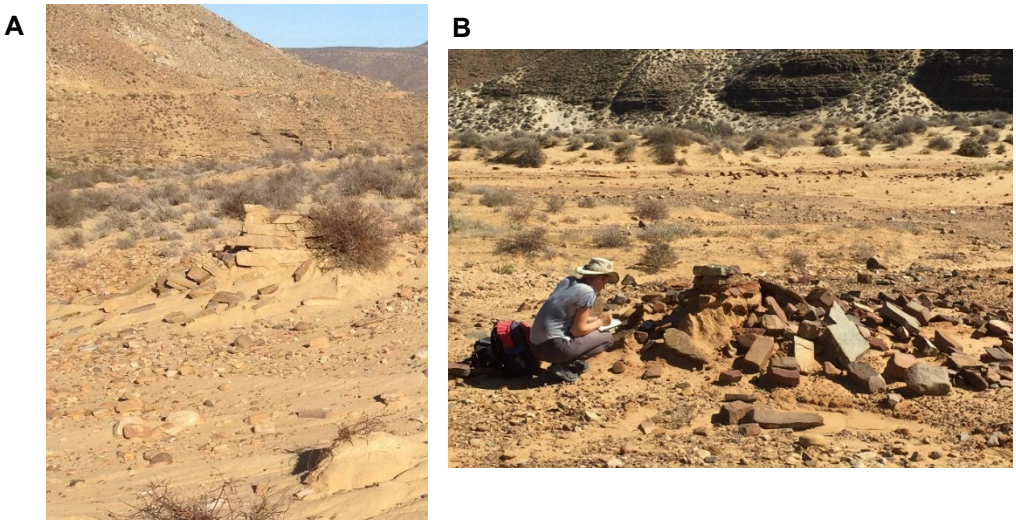

Figure 6.45. Photograph (facing south-west) of an historic stone hearth at UPK9 built on the Indurated Orange Sand (~27 ka) that has eroded down to expose an underlying colluvium (a), and the pedestalled foundations of an historic stone hearth at Lungkaal (facing west, b).

The absence of stone structures or anthropogenic modification suggests that UPK7 was less impacted by historic activity than other localities (i.e., UPK9). However, the northern side of the river channel was used for grazing until the 2016 purchase of UPK7 and UPK9 by the Pretorius family. It is also possible that domesticated ungulates were grazed by pastoralists in the valley from the earlier part of the Late Holocene until European contact. Therefore, trampling could still have had an impact on the stability and preservation of UPK7's sediment units and the archaeology discarded on them. Thus, the possible impact of trampling at this locality is investigated by analysing the fragmentation of surface clasts in the subsequent Chapter 7.

6.4.2.4 Rate and timing of erosion

Rate of erosion at UPK7 is unknown and it is unclear how much sediment and archaeological material has been removed as a result. As at UPK1, the height of pedestalled stone at UPK7 is no more than 100 mm above a given surface, while the pedestalled height of historic structures was recorded to between 400 and 600 mm at Lungkaal and UPK9, respectively (Figure 6.45b, see Appendix 4.9 for details). The conventional radiocarbon age obtained for the pedestalled stone hearth at Lungkaal (D-AMS 027125) is 135 ± 22 uncal BP (standard error to 1σ). Calibration was not possible due to the wiggle of the calibration curve (SHCal13, Hogg et al. (2016)) which resulted in multiple intercepts (see Appendix 4.9 for sample descriptions and the report for all conventional radiocarbon age determinations; Stuiver & Polach 1977, p.362). However, this sample indicates that sometime within the last 300 years ~600 mm of deflation occurred. Given the potential amount of sediment that has eroded from these localities—even in the last few centuries—it is surprising that surface artefacts persist on exposed surfaces such as UPK7. Their presence, density and inferred age raises the question of what mechanisms are enabling their preservation and to what degree has surface runoff impacted their organisation and technological composition.

CHAPTER 7.
RESULTS: SURFACE ARCHAEOLOGY

7.1. Introduction

This chapter investigates the influence of post-depositional processes on UPK7's surface archaeology following the structure outlined in Chapter 5.7.2. The main objective is to determine if UPK7's spatio-temporal patterning is the result of chance, post-depositional modification, and/or a reflection of human discard behaviour/occupation duration. Artefact spatial structure—density and diversity—is examined in relation to sedimentary context (i.e., surrounding geomorphology, surface condition), deposit age, and artefact composition (i.e., typo-technological composition, morphology, and condition [physical and/or chemical weathering]).

7.2. How is UPK7's Surface Archaeology Spatially Distributed and is it Random?

Published interpretations of UPK7's archaeology have repeatedly identified and targeted clustered areas of time-sensitive artefacts from phases within the MSA, LSA and Neolithic (Low et al. 2017; Will et al. 2015). In these studies, clusters were isolated based on the perceived temporal coherence and density of artefacts interpreted as typo-technologically diagnostic of the same Industry. The main assumption in each study was that the spatial distribution of UPK7's surface archaeology is not randomly distributed nor the result of chance. It is necessary to test this baseline assumption before investigating this spatio-temporal patterning further. The following examines the point-pattern of RNG-recorded artefacts at the global scale, looking at where and how artefacts are spatially distributed and testing if their point-pattern is the result of Complete Spatial Randomness (CSR).

7.2.1. The spatial distribution of all artefacts

Figure 7.1 shows the distribution of all 4,285 visible artefacts mapped during the 2019 RNG survey across UPK7 (survey limits defined by orange, dashed line). The visual impression, and hypothesis, is that these artefacts have a non-random distribution. Their visibility appears to coincide with the type of surface they occur on, with higher artefact densities on consolidated surfaces than unconsolidated sands. Artefacts also appear to concentrate in the north-east, in Exposure 1b, 2, and 3—where the consolidated sediments of the Upper Yellow and Lower Red deposits are exposed (Figure 7.1). The density of artefacts visibly decreases to the south and west as distance increases. Change in artefact density appears to coincide with a decrease in elevation and the transition from the exposed surface of Lower Red/Upper Yellow sediment to Indurated Sand—especially on Exposure 1a-c (Figure 7.1).

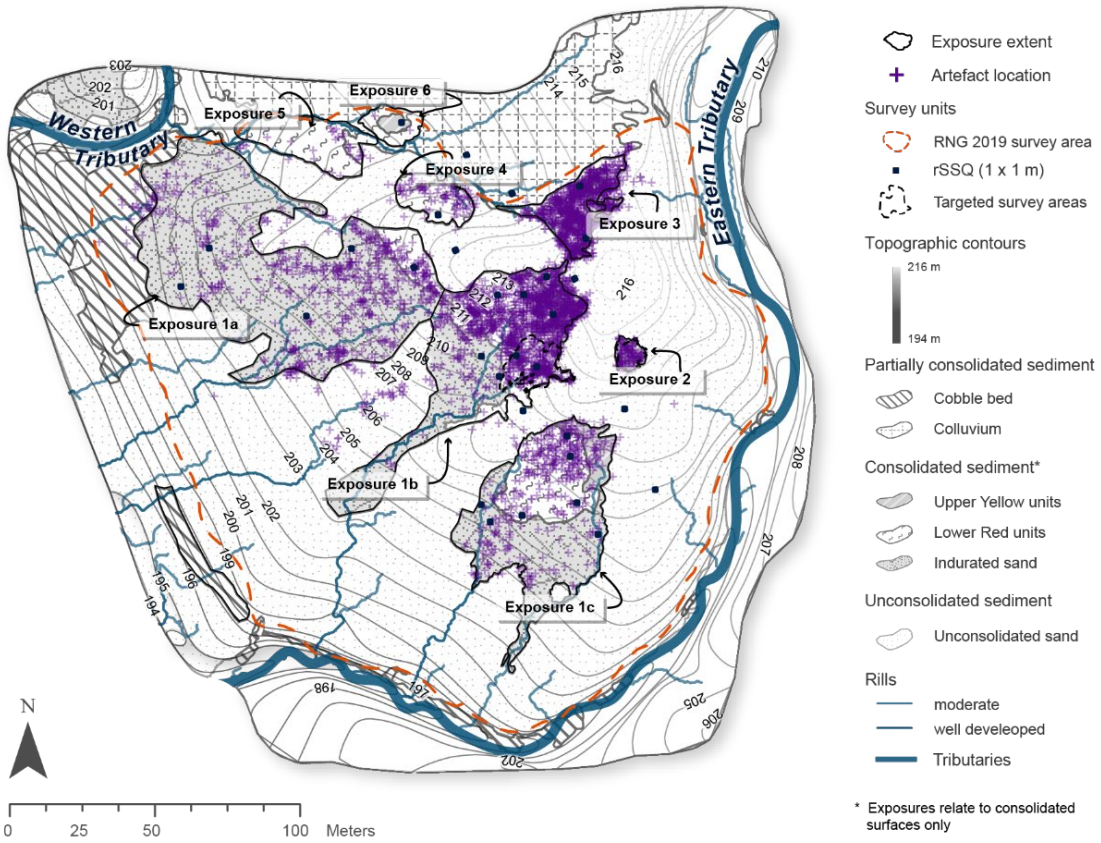

Figure 7.1. Distribution of individual artefact point locations recorded within the RNG survey boundary (orange dashed line). Recorded in 2019 during phase 1 of DRAP data collection. Artefact types exclude flakes and are shown in the context of UPK7's surface hydrology (Strahler classes 4 to 6 only, with 4 defined as moderate rilling, 5 as well developed rilling and 6 as tributaries), sediment type and substrate units, and surface elevation. Areas of exposure are outlined (solid black line) and labelled, from Exposure 1 to 6.

7.2.1.1. Testing for Complete Spatial Randomness

To test if artefacts are spatially distributed randomly at the global (locality-wide) scale a spatial Kolmogorov-Smirnov goodness-of-fit test (KS-test) for Complete Spatial Randomness (CSR) was performed. A KS-test compares the observed locations of all artefacts—irrespective of type—to a uniform Poisson distribution of CSR using their individually recorded x and y coordinates (Figure 7.2). The null hypothesis is that the point-pattern, depicted in Figure 7.1, represents CSR. The resulting output supports visual interpretation, showing poor fit between the observed distribution of artefact x and y coordinates and the expected CSR distribution (see Figure 7.2a and b), returning a p-value well below 0.05 for both x and y (x = D = 0.38391, p-value < 0.000*, y = D = 0.37891, p-value < 0.000*). Thus, the chances of surface artefact spatial distributions being random is extremely low.

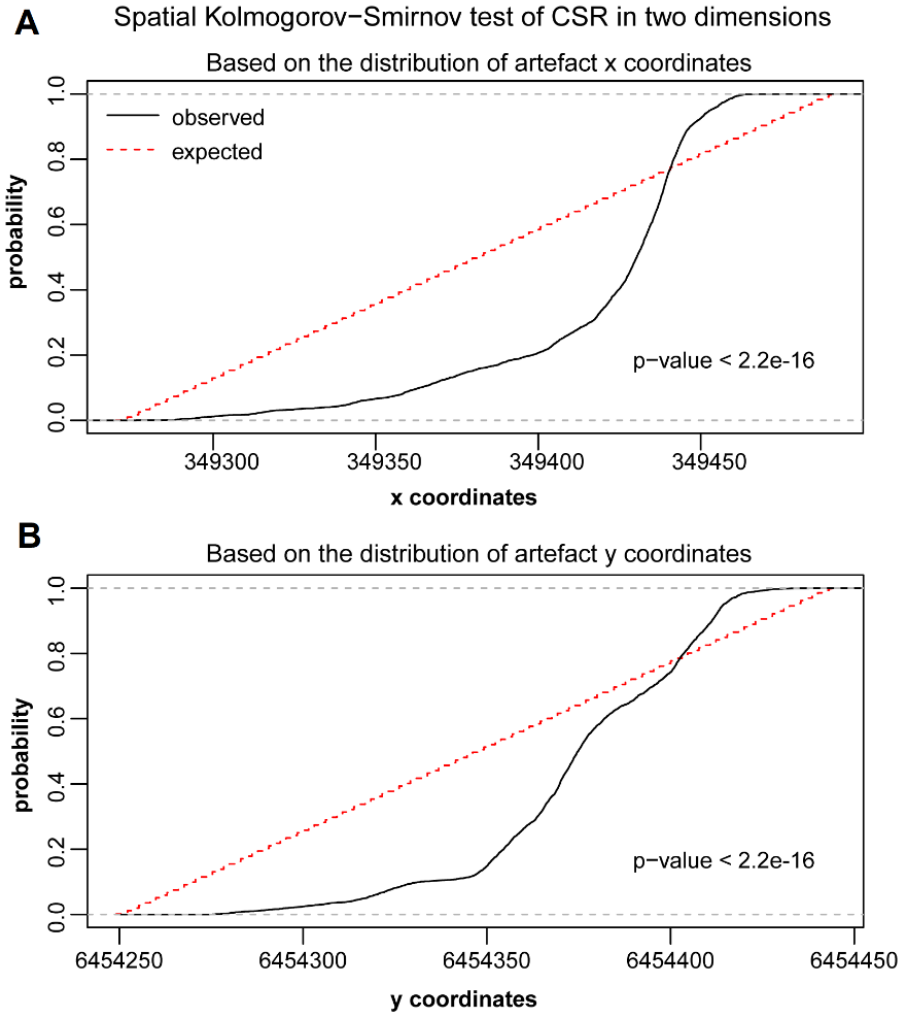

Figure 7.2. Two-dimension spatial Kolmogorov-Smirnov goodness-of-fit test for Complete Spatial Randomness (CSR, red dashed line) in the x (A) and y (B) coordinates of UPK7's RNG-surveyed surface archaeology (solid black lines). Both coordinate distributions show a significantly poor fit with CSR, well below the 5% alpha level (p-values <2.2e-16).

7.2.1.2. Artefact density

To determine how and where artefact density changes across the locality, an Optimized Getis-Ord Gi* Hot spot analysis was performed in ArcGIS Pro and mapped against UPK7's topography and the extent of its substrate units (Figure 7.3). A search radius of 14 m was chosen based on the average distance to 30 nearest neighbours. An incident weight of aggregated artefact counts was used in the analysis, with incident density defined by a mesh of hexagons—each 3.5 m wide and 3 m high. Only hexagons (n = 1157) containing at least 1 artefact were included in Hot Spot analysis.

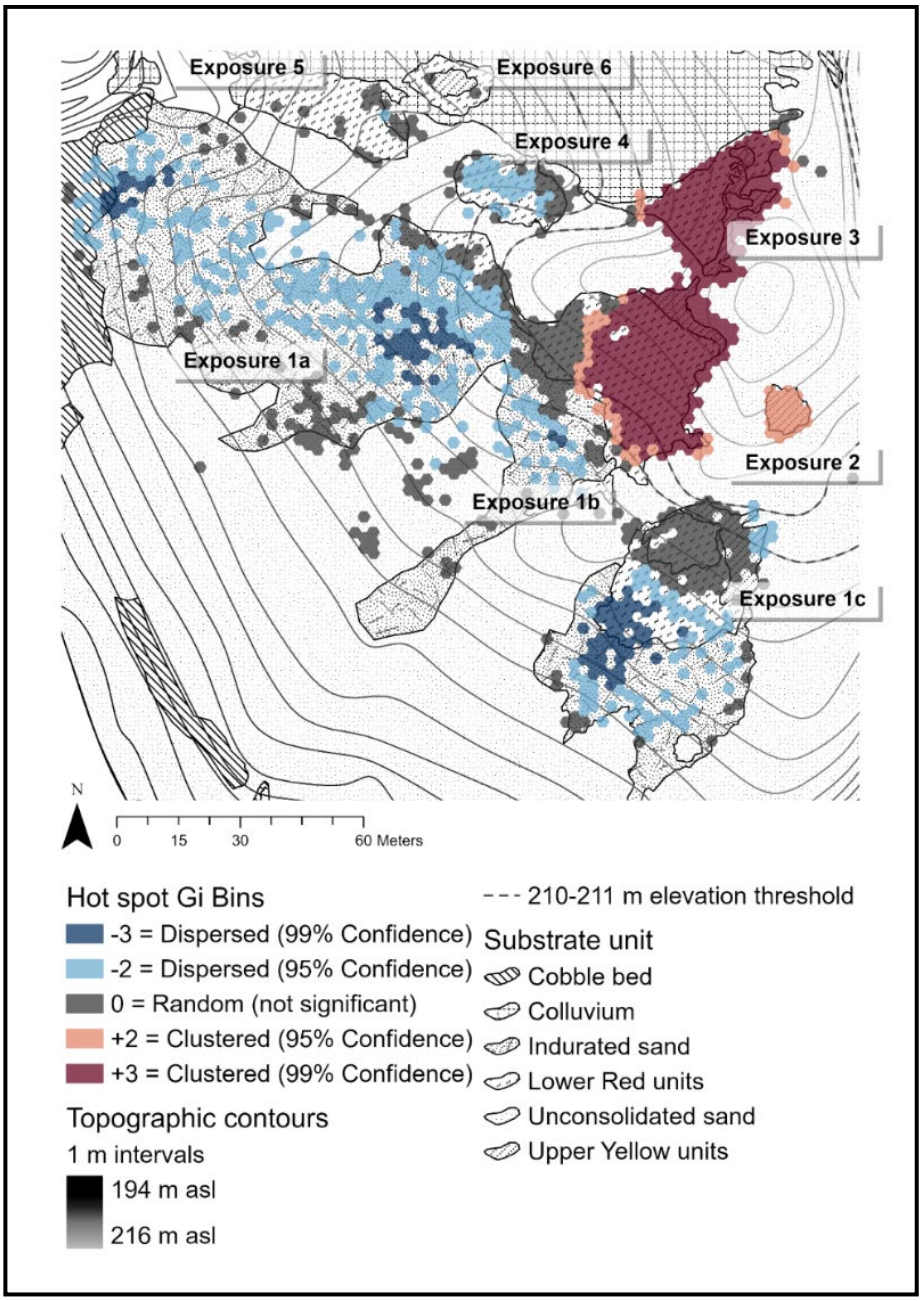

Figure 7.3. Hot-cold spot Geti-Ord Gi* map showing areas of significant (95-99%) high (hot coloured) and low (cold coloured) artefact counts as well as areas with no significantly structured pattern (grey hexagons) to artefact distributions.

The heat map in Figure 7.3 depicts the location and extent of high (hot) and low (cold) artefact densities against base layers of substrate type and surface topography. The Gi statistic identifies z-score bins of high (+) and low (-) density to different levels of statistical significance (99 and 95%). A bin value with a Gi statistic of +/- 3 indicates a significantly high/low artefact count at the 99% confidence level (p-value of 0.01), while +/- 2 equates to a confidence threshold of 95% (p-value of 0.05). Bin values of 0 indicate areas of random distribution that are neither significantly high nor low in artefact count. The resulting output (Figure 7.3) shows a highly polarised hot-cold pattern across UPK7's consolidated substrate units, with localised areas of randomly distributed artefacts. The polarity between areas of high and low densities supports visual impression of the mapped point distribution depicted in Figure 7.1—

identifying the highest artefact densities in the north-east—and the shift in artefact intensity above 210 m asl evident in Figure 7.2a,b.

Three areas of high density (hot spots) are evident at 95% confidence. These areas occur at high elevations—above 210 m asl—at the top of Exposure 1b's slope, and across all of Exposures 2 and 3. The substrate units that coincide with high density areas include Upper Yellow and Lower Red sediment. In some cases, high density zones extend into areas designated as Unconsolidated Sand at the juncture where consolidated sediment is covered be a veneer of loose sand. In contrast to high density zones, dispersed artefacts generally occur below 210 m (asl), with the largest surface of artefact dispersion covering the lower half of the southern slope of Exposure 1a-b, on the Indurated Sand. Surfaces with artefacts that lack statistically significant patterns in density or dispersion (coloured grey in Figure 7.3) are apparent as flattened zones in the intensity graph of Figure 7.2. These areas occur at the base of the southern slope and between high density and dispersed zones on all consolidated substrate units on the southern slopes of Exposure 1a to c (Figure 7.3). They are located in what appear to be transitional zones between high and low artefact densities that are possibly responding to a shift in elevation, slope angle, surface roughness where rill density increases—and/or substrate unit.

7.3. What is UPK7's Surface Archaeology Composed of and How is it Distributed?

The following subsections describe the archaeological composition and spatial distribution of UPK7's surface archaeology. Figure 7.4 presents a map series that compares the spatial distribution of each archaeological component found across UPK7's sand mantle. These are divided into five archaeological subcategories: 1. material type, 2. artefact type and lithic class, 3. implement types, 4. archaeological epoch, and 5. Industry. Presented in this way, spatial structure appears to vary depending on the categories chosen for visualisation and analysis. Material types (Figure 7.4a) and Artefact types & lithic class (Figure 7.4b) closely reflect the general point pattern assessed above as it was possible to allocate the entire artifact population to one of the types defined in each category. A large number of artefacts were also associated with a specific implement type and their overall point pattern broadly reflects the spatial patterning of the entire population (Figure 4c). Fewer artefacts could be allocated an inferred age, with areas of high artefact density (i.e., higher elevations, older deposits) over-represented compared with more dispersed areas (i.e., lower elevations/hillslope positions; Figure 7.4d,e). The following deals with the composition and spatial distribution of each component separately.

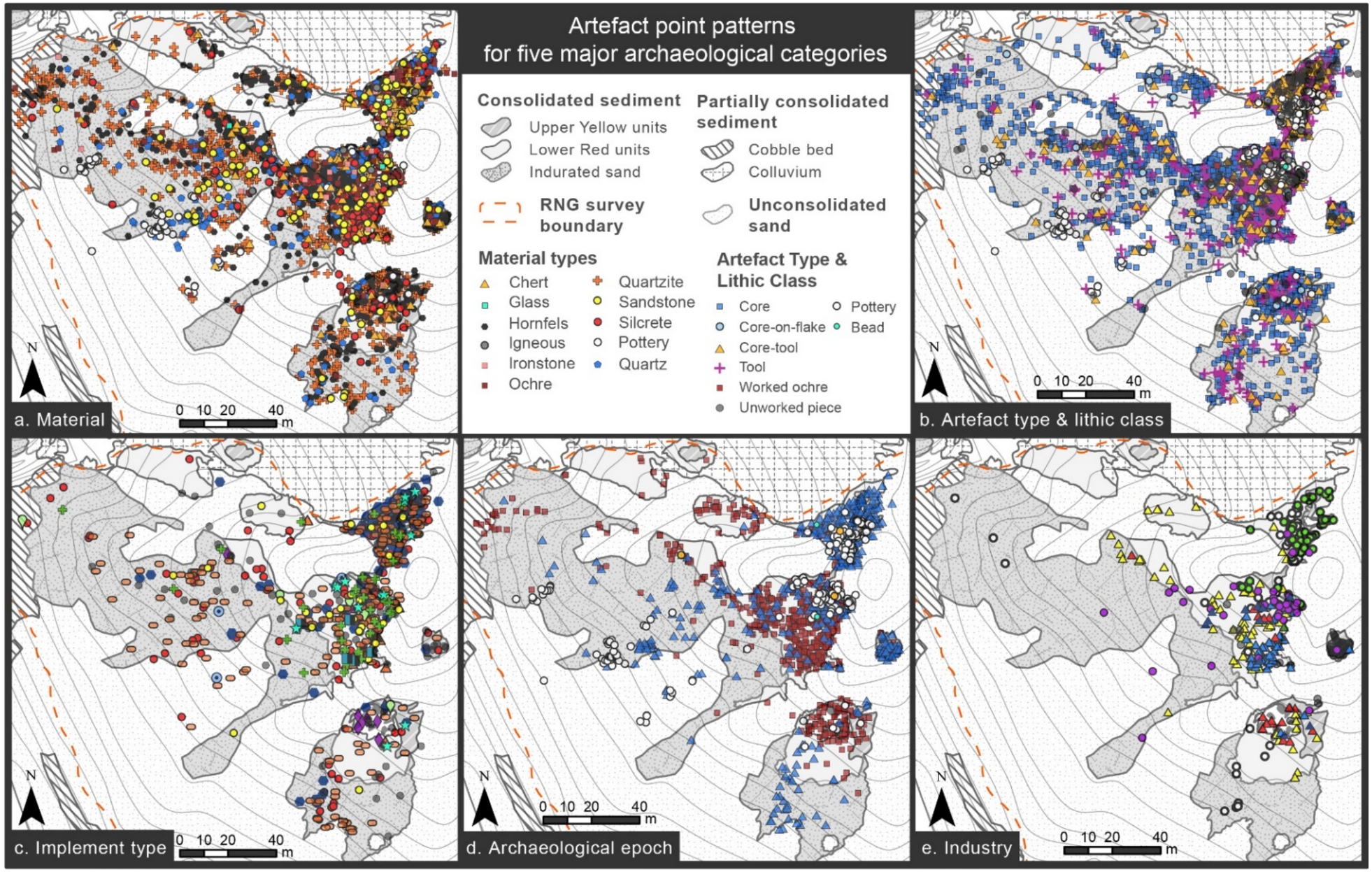

Figure 7.4. Map series comparing the artefact point patterns of five major archaeological components: (a) Material types, (b) Artefact types and lithic classes, (c) implement types, (d) archaeological epochs, and (e) Industries. The base layers of each map present the exposed extent of consolidated sediment (Indurated Sand, Upper Yellow, and Lower Red) and part of the unconsolidated sand unit, cobble bed and colluvium. Contour lines (grey) are spaced at 1 m intervals (refer to Figure 7.1 for further details). The 2019 survey area is outlined as a dashed orange line. Exposures are also given in Figure 7.1 and pertain to the bare-earth surfaces only.

7.3.1. Artefacts by material type

Of the 4,285 surface artefacts identified across UPK7's sand mantle, lithic, ochre, pottery, and glass represent the major artefacts materials, with lithics accounting for most of the dataset (92%, including quartz; Figure 7.4a). Pottery fragments only account for 4% of artefacts, while a single glass bead and a single piece of worked ochre were identified. Small, highly weathered splinters of bone occur towards the top of the stack on the Upper Yellow, but these were not recorded. No bone or other artefacts made from organic materials were observed.

Eight types of rocks and minerals were recorded (Figure 7.5 and Table 7.1). Of these, 35% are quartzite, which were likely sourced from local outcrops and river gravels. A similar proportion of hornfels artefacts (34%) was also identified and are also available from the Doring River as river-worn cobbles. Artefacts manufactured using quartz (8%), silcrete (6%), and chert (4%) occur at considerably lower frequencies than locally available materials, consistent with their availability in the local river gravels (Low & Mackay 2018), though silcrete is readily available in outcrops at Swartvlei, 5 km east of UPK7.

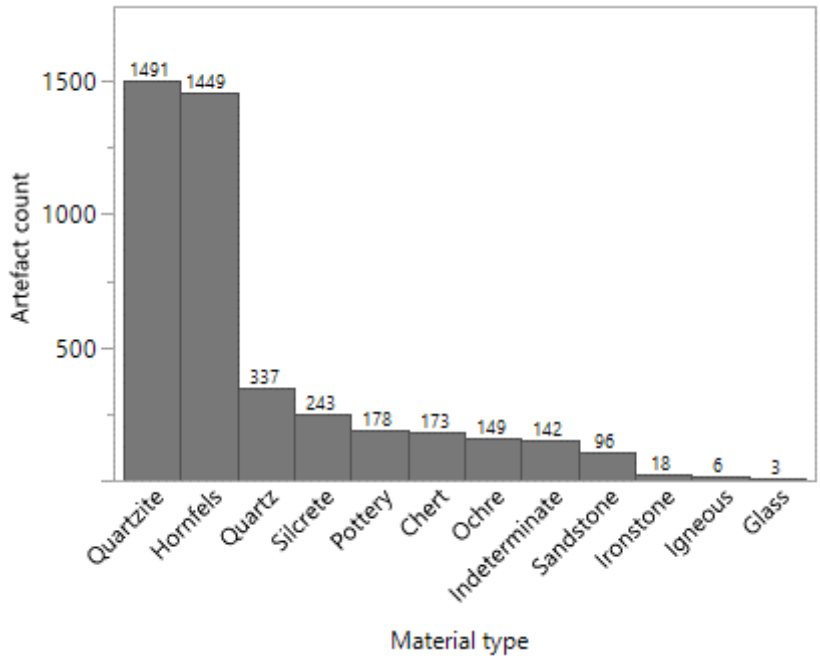

Figure 7.5. Artefact counts by material type, presented in descending order by artefact count.

Table 7.1. Material type counts and percentages for artefacts recorded within the RNG survey area at UPK7.

Material	Count	%
Quartzite	1491	35%
Hornfels	1449	34%
Quartz	337	8%
Silcrete	243	6%
Pottery	178	4%
Chert	173	4%
Ochre	146	3%
Sandstone	96	2%
Ironstone	21	<1%
Igneous	6	<1%
Glass	3	<1%
Indeterminate	142	4%
Total	4285	100%

The dominance of quartzite and hornfels is apparent in Figure 7.6. Both material types reflect the change in artefact density observed for the entire assemblage—high densities on the north-eastern slopes of the Upper Yellow and Lower Red and low densities across the Indurated Sand. Silcrete appears to be clustered in the high-density zone of the Lower Red, particularly at the highest elevations, along the north-western fringe where consolidated sediment shifts to unconsolidated sands (Figure 7.6). Although lower in frequency, a similar pattern is apparent for all other material classes except for pottery, which occur as small clusters at the top of the sand mantle overlying the Upper Yellow and the fringe of Lower Red, and at the footslope of the Indurated Sand (Figure 7.6). Its position at the top of the sand mantle coincides with a dense and diverse concentration of other material types, while it only coincides with a dispersed assortment of materials on IS's footslope (i.e., quartz, quartzite, sandstone, hornfels and ochre; Figure 7.4a and 7.6).

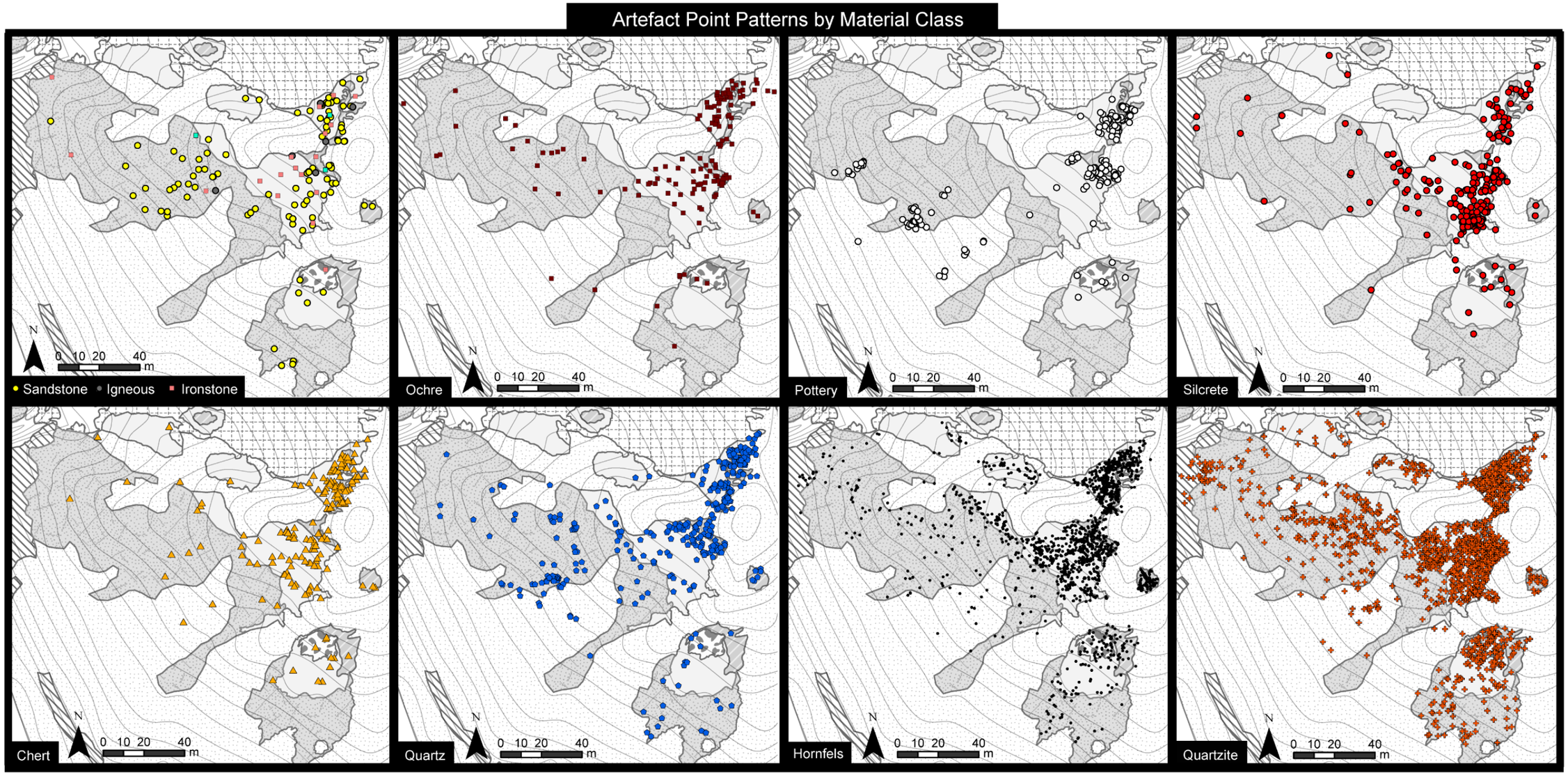

Figure 7.6. Map series comparing the artefact point patterns of eleven different material types identified for clasts >10 mm in maximum dimension during the 2019 RNG survey: Sandstone (yellow circles), igneous rock (grey circles), ironstone (pink squares), ochre (dark red squares), pottery (white circles), silcrete (bright red circles), chert (yellow triangles), quartz (blue circles), hornfels (black dots), and quartzite (orange crosses). The base layers of each map present the exposed extent of consolidated sediment (Indurated Sand, Upper Yellow, and Lower Red) and part of the unconsolidated sand unit, cobble bed and colluvium. Contour lines (grey) are spaced at 1 m intervals (refer to Figure 6.1 for further details). The 2019 survey area is outlined as a dashed orange line.

7.3.2. Artefacts by type and lithic class

UPK7's surface archaeology yields a broad range of stone artefact classes, excluding flakes (see Figure 7.4b). Cores dominate, accounting for 73% (n = 3117) of the RNG record (Table 7.2 and Figure 7.7). Tools (e.g., retouched pieces, grindstones, anvils, hammerstones) are the second largest class of stone artefacts, accounting for 12% of the record. Artefacts recorded as Core-tool—including pieces esquillees and cores with evidence of retouch—account for the third largest class (7%, n = 300). Only 21 core-on-flakes were identified, forming <1% of the assemblage. Fire cracked stone was also only recorded during the rSSQ survey and contributes 0.6% (n = 14) of the total random subsample. Although their relative frequency is low, the existence of fire cracked stone as possible heat retainers strengthen evidence for the use of hearth-related combustion at this locality.

The grouped category of artefact type and stone artefact class shares a similar spatial pattern to materials, with only minor variation from the general trend between types (Figure 7.8). Cores dominate both high- and low-density areas, followed by tools and core-tools (Figure 7.8). However, tools appear to decrease in frequency at higher elevations more than cores as distance from dense areas increases and elevation decreases. Again, diversity in artefact type and lithic class is highest in dense areas (Figure 7.4b).

Table 7.2. The counts and percentage of artefact types and lithic classes recorded within the RNG survey area at Exposure 1b. The sizable number of clasts identified as 'NA' are largely due to the recording of unworked ochre as part of the RNG Phase 1 data collection objectives (see material type counts in Table 7.1 above).

Artefact type & lithic class	Count	%
Stone Artefact	3932	92%
Core	3116	73%
Tool	494	12%
Core-tool	301	7%
Core-on-flake	21	<1%
Pottery	178	4%
Glass bead	1	<1%
Worked Ochre	1	<1%
Unworked piece	173	4%
Total	4285	100%

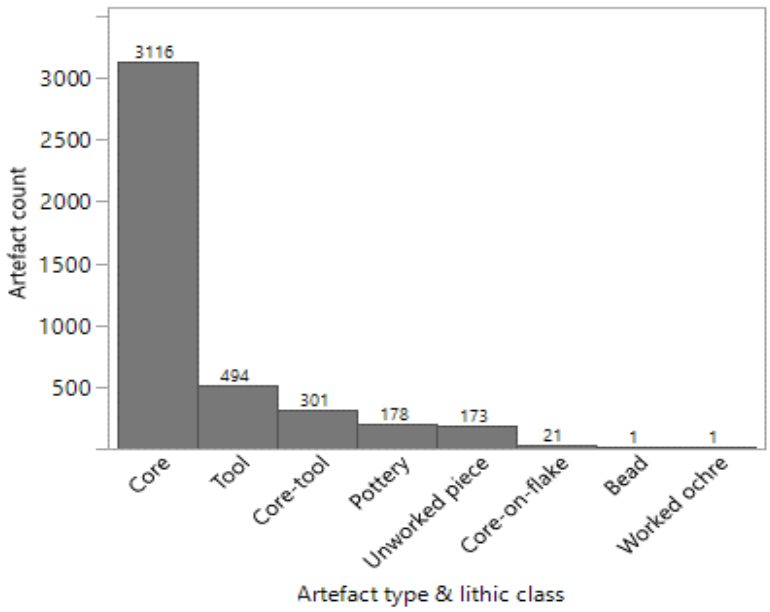

Figure 7.7. Frequency of artefact types and lithic classes in the RNG dataset Exposure 1bUPK7, presented in descending order of artefact count.

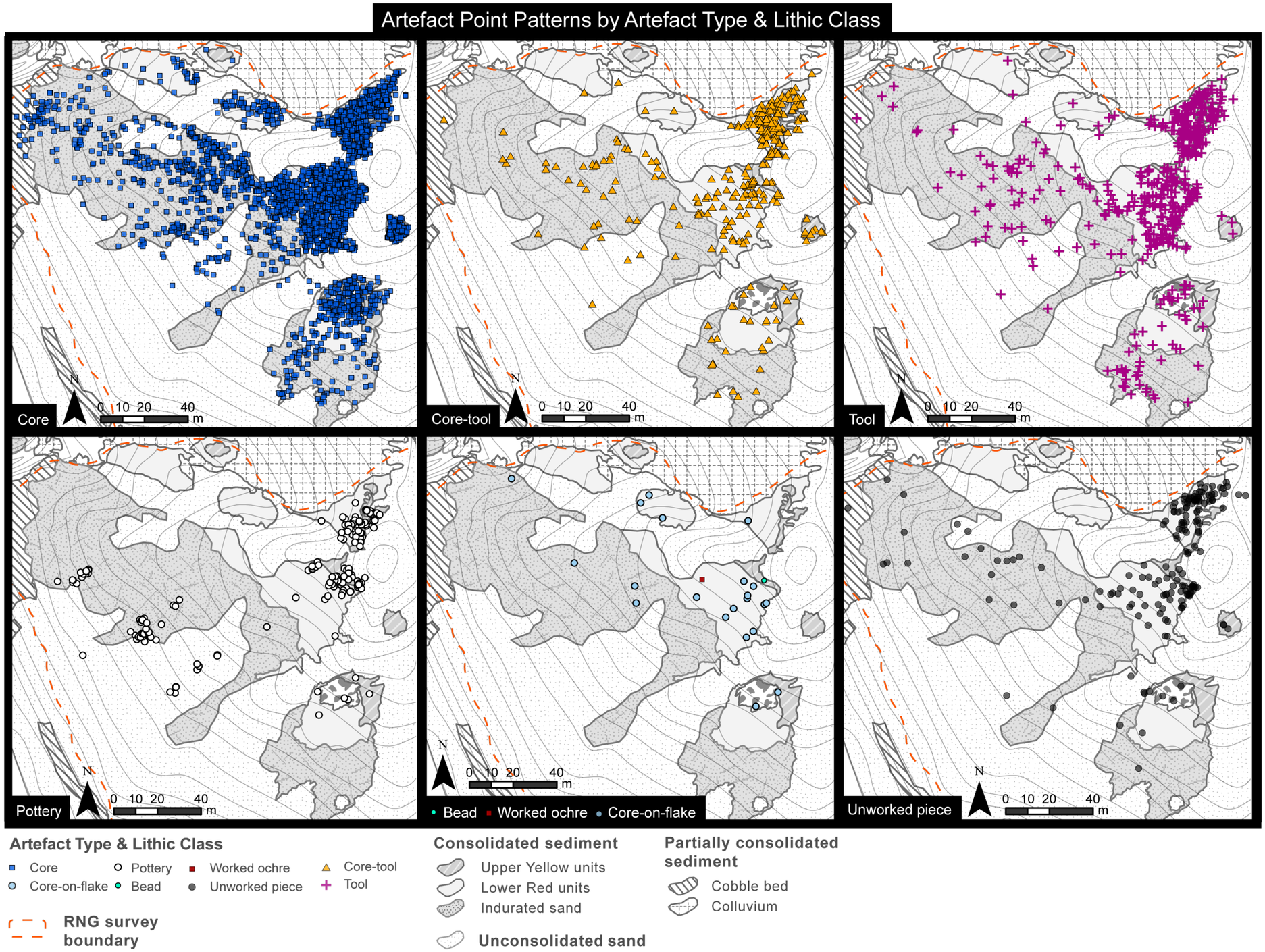

Figure 7.8. Map series comparing the artefact point patterns of eight artefact types and lithic classes that were identified for clasts ≥ 10 mm in maximum dimension during the 2019 RNG survey: Cores (blue squares), core-tools (yellow triangles), tools (pink crosses), pottery (white circles), beads (fluorescent blue dot), core-on-flake (pastel blue circles), worked ochre (red squares), and unworked piece (dark grey circles). The base layers of each map present the exposed extent of consolidated sediment (Indurated Sand, Upper Yellow, and Lower Red) and part of the unconsolidated sand unit, cobble bed and colluvium. Contour lines (grey) are spaced at 1 m intervals. The 2019 survey area is outlined as a dashed orange line.

7.3.3. Artefacts by implement

The RNG survey identified 22 tool types (Figure 7.4c), eight of which are a variant of scraper (see Table 7.3 and Figure 7.9). These account for 18% (n = 780) of the entire RNG dataset. Of these 22% were not characteristic of a specific implement type and were allocated the labelled 'Other'. The catch-all scraper "other" accounts for over 16% of the RNG dataset, followed by anvils (~14%), and pieces esquillees (~14%). Implements that form ≥2% or more of the entire assemblage include hammerstones (~7%), denticulates (~4%), notched pieces (~3%), grindstones (~3%), unifacial points (~2%), and thumbnail scrapers (~2%). There are similar, but low frequencies of backed pieces (~1.5%, n = 12), naturally backed knives (~1.7%, n = 13), and bifacial points (~1.5%, n = 12). The least common implements (≤1% of the total population) are burins and continuous, end, lateral, adze and other scraper variants (see Table 7.3).

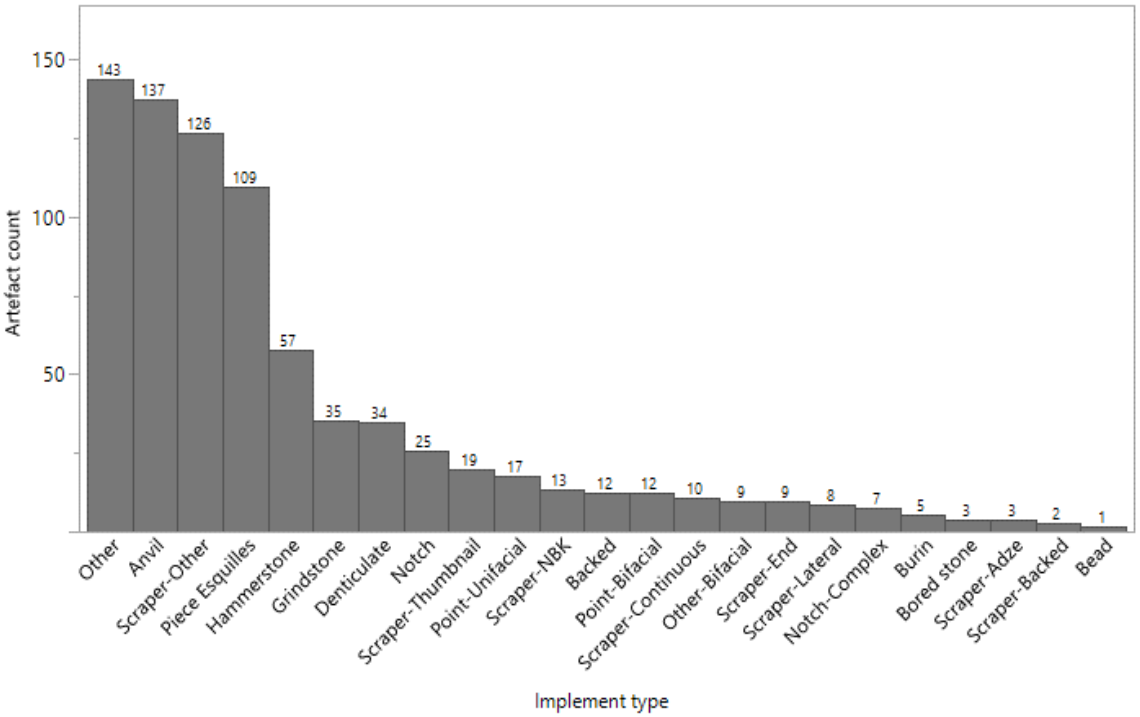

Figure 7.9. Bar graph showing implement types identified during RNG suExposure 1b at UPK7, presented in descending order of artefact count.

Table 7.3. Implement type counts and percentages, listed from largest to smallest counts.

Tool Type	Count	%
Other	168	22
Scraper-Other	126	16
Anvil	111	14
Pieces Esquillees	109	14
Hammerstone	56	7
Denticulate	34	4
Notch	25	3
Grindstone	24	3
Scraper-Thumbnail	19	2
Point-Unifacial	17	2
Scraper-NBK*	13	2
Backed	12	2
Point-Bifacial	12	2
Scraper-Continuous	10	1
Other-Bifacial	9	1
Scraper-End	9	1
Scraper-Lateral	8	1
Notch-Complex	7	1
Burin	5	1
Scraper-Adze	3	<1
Scraper-Backed	2	<1
Bead	1	<1
Total	780	100

*naturally backed knife (NBK)

Implement types are the most diverse and densest at the top of the sand mantle (Exposure 1b and 3) (Figure 7.4c and Figure 7.10). There also appears to be more burins, denticulates and notched pieces in this area—particularly on the LR—compared to the lower slopes of the IS. Diversity in implement type is low on the more dispersed surfaces of the IS, with hammerstones, grindstones, anvils, and scarpers dominating this surface compared to the high diversity and density of implements on the upslope deposits (Figure 7. 10). The upper hillslope sediment units of Exposure 1c appears to have fewer implements, lower density and less diversity compared to the top of Exposure 1b and 3. The dominant implement types are the grouped class, hammerstone, grindstone and anvils, and bifacial points, the latter inferred to be a Still Bay cluster (see Figure 5.2). The footslopes of Exposure 1c are similar in implement diversity (low) and type (scrapers, hammerstone, grindstone and anvils) on the IS to Exposure 1a-b (Figure 7.4c and 7.10). However, these implements appear to cluster at Exposure 1c's footslope. There is also similar number of pieces esquillees in this area to the exposed IS to the north-west. Pieces esquillees also occur as a dominant implement type on the UY and LR substrates of Exposure 3 along with grindstones, hammerstones and anvils (Figure 7.10). Denticulates occur more often on the LR at the top of Exposure 1b. There are few implements on the north and east facing LR and UY Exposures 4, 5 and 2 (Figure 7.10).

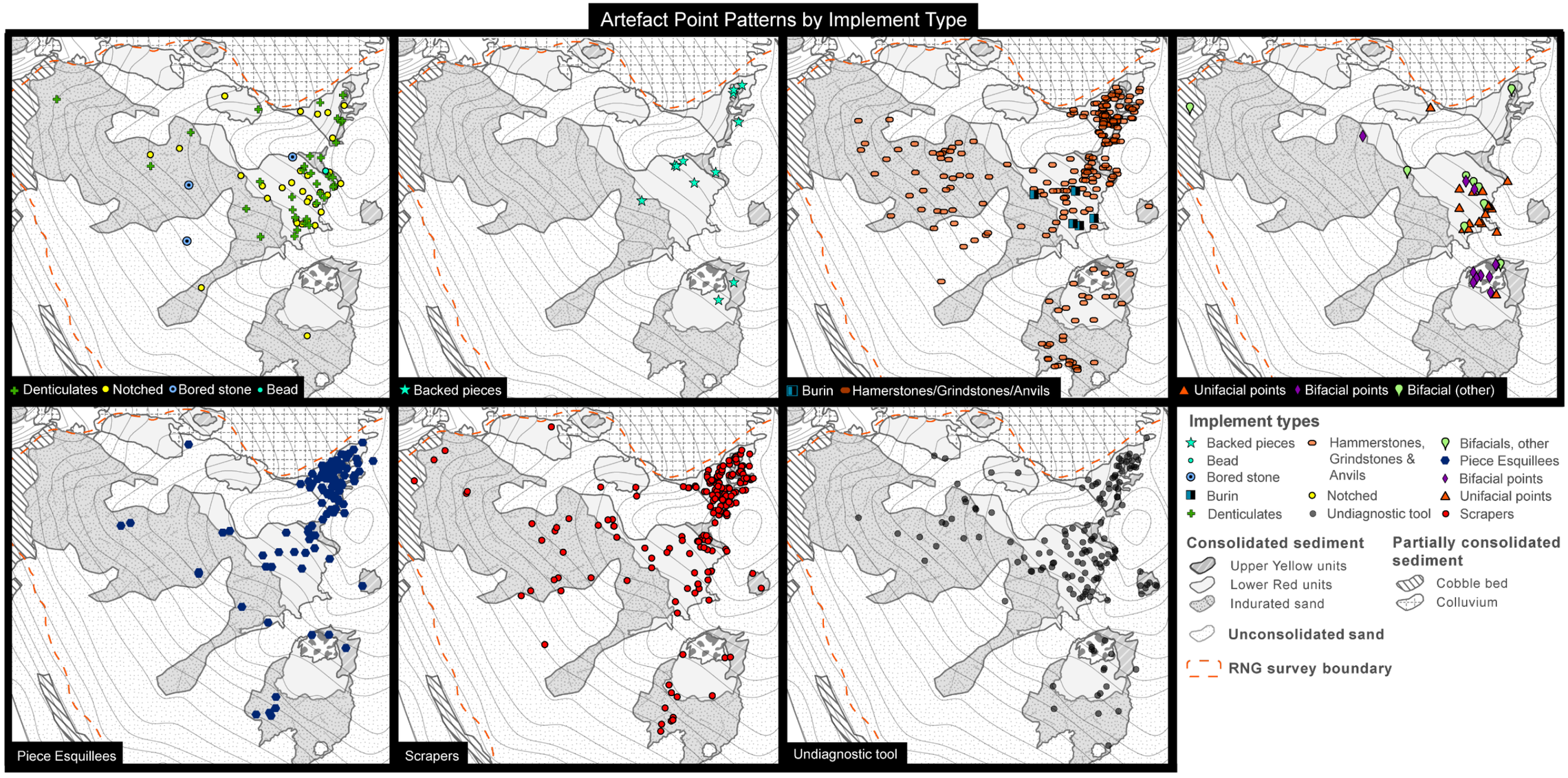

Figure 7.10. Map series comparing the artefact point patterns of thirteen different implement types that were identified for clasts ≥ 10 mm in maximum dimension during the 2019 RNG survey: Denticulates (green crosses), notched pieces (yellow circles), bored stone (black dotted blue circles), beads (fluorescent blue dot), backed pieces (fluorescent blue stars), burin (black and blue square), hammerstones, grindstones and/or anvils (pale pink ovals), unifacial points (orange triangles), bifacial points (purple diamonds), other bifacial pieces (lime green markers), pieces esquillees (blue circles), scrapers (red circles), and undiagnostic tools (dark grey circles). The base layers of each map present the exposed extent of consolidated sediment (Indurated Sand, Upper Yellow, and Lower Red) and part of the unconsolidated sand unit, cobble bed and colluvium. Contour lines (grey) are spaced at 1 m intervals. The 2019 survey area is outlined as a dashed orange line.

7.3.4. Artefacts by archaeological epoch

Archaeological epochs were identified for ~35% (1508) of RNG artefacts across UPK7, with 25% of all diagnostic artefacts associated with the MSA or LSA (Figure 7.4d). Of the artefacts at UPK7 that can be associated with a specific archaeological epoch, MSA artefacts dominate, forming ~52% (n= 783) of the sample, followed by 36% (n = 542) of artefacts associated with the LSA, 12% from the Neolithic (n = 178), and less than 1% from the ESA (n = 2) and Historic periods (n = 3; Table 7.4, Figure 7.11).

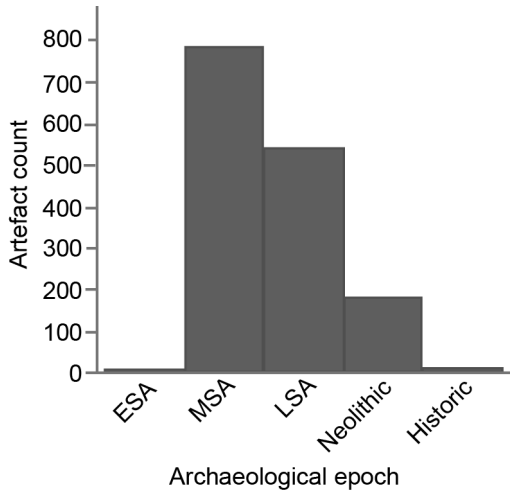

Figure 7.11. Bar graph of artefact frequencies by Archaeological epoch. Excludes temporally undiagnostic artefacts.

Table 7.4. Summary of time-diagnostic artefacts recorded during 2019 RNG-survey at UPK7, grouped by archaeological epoch and presented in chronological order from oldest to youngest

Archaeological epoch*	Count	%
ESA	2	<1
MSA	783	52
LSA	542	36
Neolithic	178	12
Historic	3	<1
Total	1508	100

*2777 artefacts were recorded as 'indeterminate' (65% of the RNG population)

Artefacts identified as diagnostic of an archaeological epoch show marked variation within the locality-wide pattern (Figure 7.12 compared to Figure 7.1). Each archaeological epoch shows a distinct point pattern within and between temporal groups which appears constrained by sediment unit and thus depositional age (see Figure 7.12). MSA artefacts largely occur as dense patches across the upper and middle extent of the northern and southern slopes. These patches appear to rest on the Lower Red consolidated sediment units. However, more dispersed instances of MSA artefacts are also evident at the base of the Indurated Sand unit in the north-west (Figure 7.12). Small concentrations of MSA artefacts also occur across the southern and northern exposures. LSA artefacts concentrate at the top of the northern, southern, and south-eastern slopes, covering Indurated Sand and Upper Yellow sediments. Neolithic artefacts overlap LSA material in the uppermost areas of the southern slope, north-eastern slope, and as smaller clusters on the lower southern slope. LSA artefacts also show a dispersed point pattern on the lower half of the southern slope.

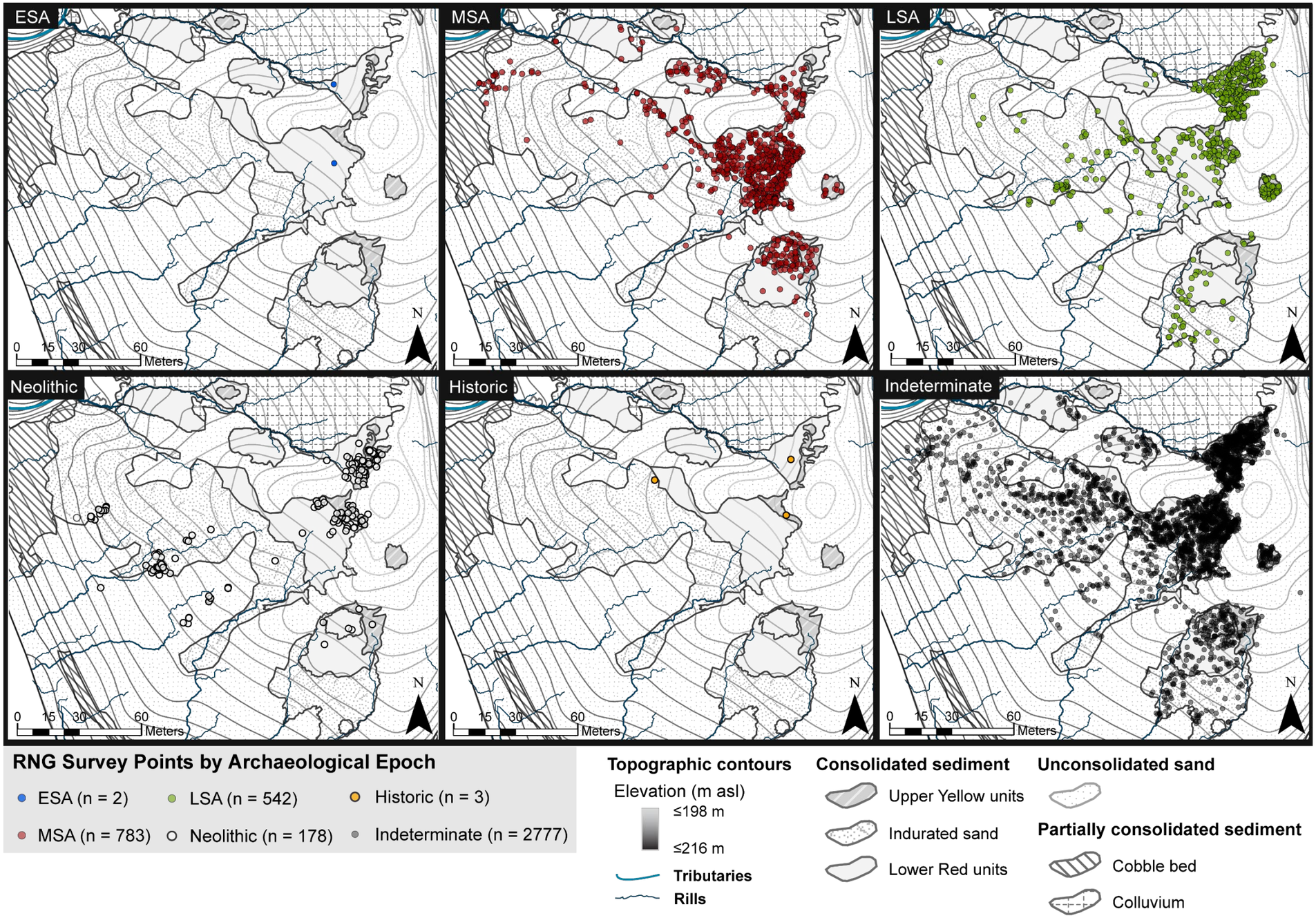

Figure 7.12. Map of the location and pattern of artefacts associated with a specific archaeological epoch: ESA (blue markers), MSA (red marker), LSA (green marker), Neolithic (white marker), Historic artefacts (yellow marker) and all other artefact locations with indeterminable temporal association (grey marker). These are presented against a series of physical conditions (base layers), including substrate type, topography (black [low] to light grey [high] elevation contour lines drawn in five-meter intervals), and hydrology (blue lines), with line thickness indicating channel type and degree of development (i.e., rills are narrower and darker than tributaries).

Visual inspection of low- and high-density areas suggests that each area yields artefacts from multiple epochs, suggesting temporal overlap. However, some areas show a greater diversity of epochs than others (Figure 7.12). This is most evident for the top of the south and north slopes. In contrast, the Lower Red unit at the top of the south-eastern slope, across the middle of central southern slope and on the Lower Red surfaces of the three exposed north-western slopes show a dominant MSA signal with some LSA and an absence of diagnostic ESA, Neolithic, and Historic artefacts. This patterning suggests removal of overlying Upper Yellow and possibly Indurated Sand deposits, leaving some lag of younger MSA and LSA material on Lower Red sediment. This is further suggested by the dispersed arrangement of Late MSA and Robberg artefacts across this surface in contrast to more clustered post-HP artefacts (see below).

7.3.5. Artefacts by archaeological Industry

When inferred artefact age is further broken down into Industries, the number of artefacts drops substantially, to 9% (n = 375) of the RNG dataset (Table 7.5 & Figure 7.4e). Artefacts assigned to the Late MSA have the highest frequencies, accounting for 25% of the total (Figure 7.13). This is followed by similar frequencies for the Oakhurst (16%), Early LSA (15%), Post-Howiesons Poort (14%), and Wilton (13%) (Table 7. 5). The Early MSA, Still Bay and Howiesons Poort have the smallest number of artefacts in the dataset (≤5%; Table 7.5 & Figure 7.13). However, due to the similar technological characteristics and the lack of clear diagnostic forms for the Early and Late MSA, it is possible that some artefacts were misassigned to the latter Industry.

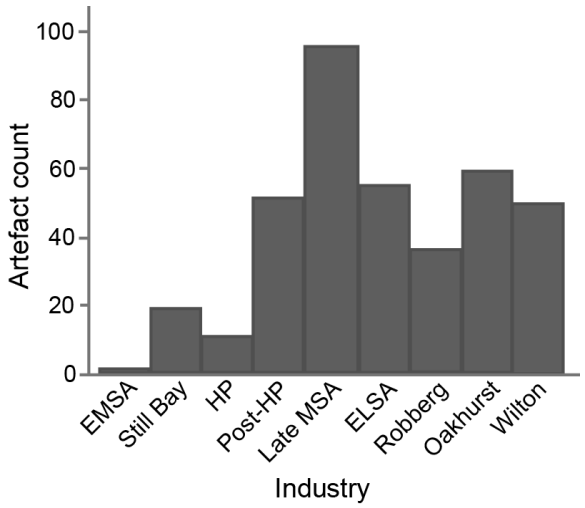

Figure 7.13. Bar graph of artefact frequencies by typo-technological Industry. Excludes undiagnostic artefacts.

Table 7.5. Summary of time-diagnostic artefacts recorded during 2019 RNG-survey at UPK7, grouped by archaeological Industry and presented in chronological order from oldest to youngest.

Industry*	Count	%
MSA		
Early MSA	1	<1
Still Bay	19	5
HP	11	3
Post-HP	51	14
Late MSA	95	25
LSA		
Early LSA	55	15
Robberg	36	10
Oakhurst	59	16
Wilton	49	13
Total	376	100

*3909 artefacts were recorded as 'indeterminate' (91% of the RNG population)

Figure 7.14 presents industry specific artefacts from the MSA and LSA. A spatio-temporal difference between diagnostic artefacts from different Industries is also apparent between the north-east slope and top of the south slope, with a dominance of Wilton and Oakhurst on the north-east slope (Exposure 3) and northern fringe of the southern slope compared to the dominance of artefacts from the Robberg (Figure 7.14). The more dispersed arrangement of Still Bay artefacts at the top of the south-east slope of Exposure 1c suggests a longer duration or multiple periods of exposure for these artefacts than the MSA artefacts at the top of the slope of the central southern slope (Exposure 1b). However, they still appear to cluster. Artefacts on the easternmost exposed slope (Exposure 2) are almost exclusively Early LSA (Figure 7.14). Such a time specific signal suggests short-term exposure on the eastern slope of UPK7, consistent with its slip-face position.

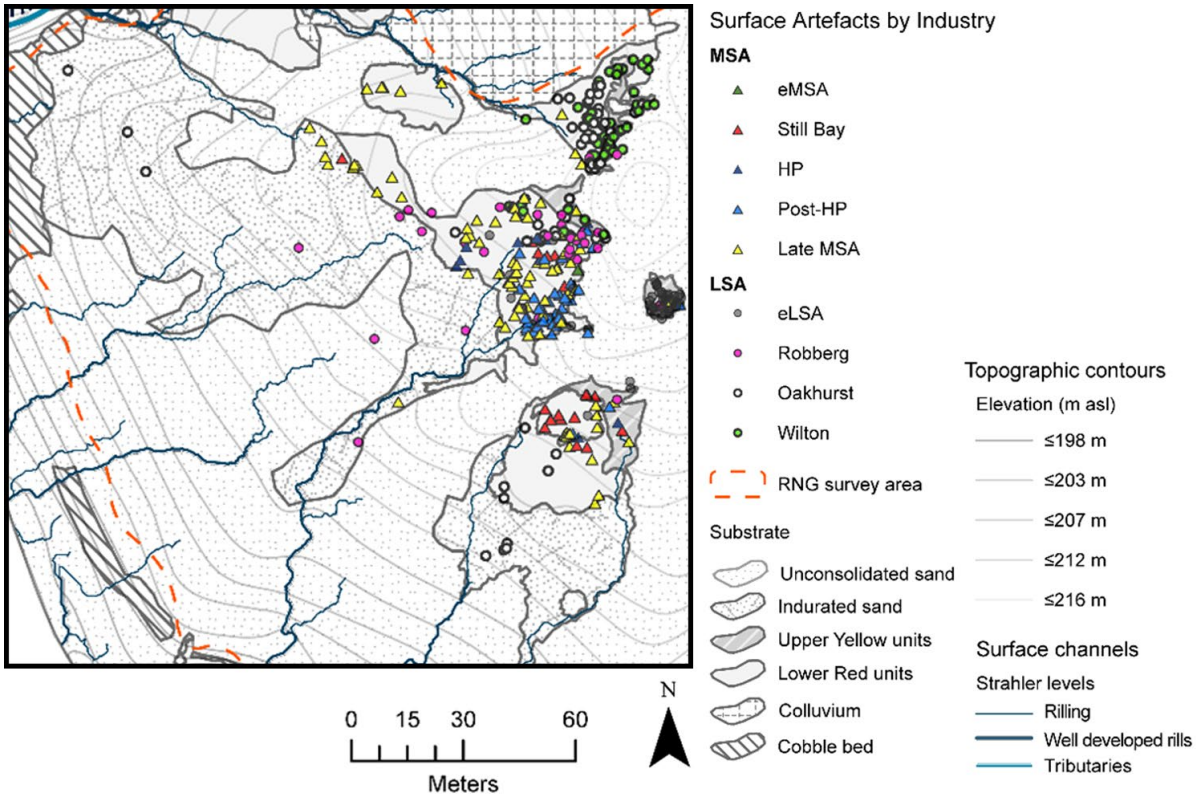

Figure 7.14. Point location and pattern of artefacts associated with a specific archaeological Industry: eMSA (green triangles), Still Bay (red triangles), Howiesons Poort (dark blue triangles), post-HP (light blue triangles), Late MSA (yellow triangles). eLSA (grey circles), Robberg (pink circles), Oakhurst (white circles), and Wilton artefacts (green circles). Artefacts without an Industry level association are excluded for visual clarity. These are presented against a series of physical conditions (base layers), including substrate type, topography (dark grey [low] to light grey [high] elevation contour lines drawn in five-meter increments), and hydrology (blue lines), with line thickness indicating channel type and degree of development (i.e., rills are narrower and darker than gullies and tributaries).

As previously mentioned, field observation and the published visual assessment of UPK7's surface archaeology (Will et al. 2015; Low et al. 2017) suggests that several clusters exist as dense patches (i.e., post-Howiesons Poort, early LSA, Wilton, and Neolithic) and dispersed scatters (i.e., Late MSA, Still Bay) of temporally diagnostic artefacts on consolidated deposits, older than 30 ka. The common thread between the Still Bay, post-HP, and Late MSA Industries is that they are mostly constrained to the northern end of the southern slopes (Exposure 1a-c). In contrast, LSA Industries are frequently found at every hillslope position (top, middle, and lower, see Figure 7.14) as high-density clusters and more dispersed scatters across multiple substrates.

A dense cluster of Early LSA artefacts occurs as a blow-out on exposed consolidated Upper Yellow sediment on the current slip-face of the eastern slope, which is separated from all other Industries. Robberg artefacts overlap LSA and MSA Industries at varying densities, at the northern end of the southern slope and across the lower half of the southern slope. Only a small number of Oakhurst and Robberg artefacts appear on the lower slopes of Indurated Sand (Figure 7.14). LSA Industries that post-date the Robberg (i.e., Oakhurst and Wilton) dominate the north-eastern exposure (Exposure 3) and show a dense spatial arrangement corresponding to the Upper Yellow sediments at the top of the north (Exposure 3) and south (Exposure 1b) slopes. Moreover, Neolithic artefacts are present as small patches of dense pieces of fragmented pottery at the top of the southern and northern slope and the base of the southern slope.

These patterns appear to partly correspond with the location and extent of the underlying substrate type and topography. The sparse occurrence of Robberg and Oakhurst artefacts on the lower southern slope could also result from the removal of smaller artefacts, characteristic of these industries, compared to their (mostly) larger MSA counterparts—though this does not account for patterning in the Wilton where small artefacts also dominate. Clustering of post-HP and Still Bay artefacts mid-slope of Exposure 1b suggests a higher level of spatial integrity on these surfaces than downslope. The same can be suggested for the top of the northern slope and the dense clustering of Wilton artefacts (Figure 7.14).

7.3.6 Conclusion

The contrast in spatial patterning between each of these archaeological categories suggests that processes influencing artefact organisation—be they behavioural and/or taphonomic—do not affect all artefacts equally. Visual assessment of each archaeological component suggests that diversity appears to be the dominant pattern and the main distinguishing factor between areas of high and low artefact density; areas of high artefact density appear to have a greater diversity of artefact types for all categories, thinning in more dispersed zones. The following section examines the spatial association between artefacts within each archaeological component—testing for spatial randomness and relatedness—followed by an assessment of artefact density and diversity.

7.4 Spatial Analysis by Archaeological Component: Relatedness, Density, and Diversity

7.4.1 Spatial autocorrelation

The Moran's I Global Spatial Autocorrelation tool in ArcGIS Pro was used to investigate spatial relatedness and test for CSR in the point-pattern of the five assemblage categories introduced above (i.e., material type, artefact, and lithic class, implement type, archaeological epoch, and Industry). Spatial autocorrelation follows the principle and expectation of Tobler's First Law, where "everything is related to everything else, but near things are more related than distant things" (Tobler 1970, p.236; cf. Waters 2017). In saying this it should be kept in mind that spatial relatedness should not be conflated with the concept of archaeological 'association'. The spatial relationship between artefacts was defined using the K-nearest neighbour and Euclidean distance parameters, in which the closest neighbours (or artefacts) of number k are included in the analysis. Here, k was determined by calculating the square root of the total point count in the RNG artefact dataset ($k = \sqrt{4285}$), thus $k = 65$.

Moran's Index indicates if the location of artefacts cluster with like values/attributes (positive Moran's I values for correlation), if dissimilar values are near to each other (negative Moran's I values for correlation), or if there is no discernible pattern and artefact values are randomly spatially organised, independent of the attribute being tested (Moran's Index = zero). The expected index is the expected Moran's I value if there is no spatial autocorrelation. Z-scores and p-values determine the statistical significance of the Moran's I value. The difference between z-score values is predicated on the size of the population tested. If the same parameters are used for each variable—as in this case—the z-score can be used to compare the strength of significantly autocorrelated variables.

Table 7.6 presents the results for the spatial autocorrelation of artefact location in relation to its class, material type, implement type and inferred age. All five categories returned significant values for clustered patterning (z-scores >2.58, p-values <0.01). This indicates that there is less than 1% likelihood that the proximity of artefact attributes is the result of chance, rejecting the null hypothesis for CSR or a lack of spatial autocorrelation in every case. Thus, artefacts located close together are very likely to have similar attributes (e.g., a core is more likely to occur near another core than a tool, or MSA artefacts are more likely to be proximate to other MSA artefacts than they are with LSA artefacts and so on).

Table 7.6. Results from Moran's I Global Spatial Autocorrelation test, using K-nearest neighbour (k = 65) to assess spatial autocorrelation of artefact locations in relation to a series of intrinsic factors: material type, artefact type and lithic class, implement type, archaeological epoch, and Industry. Organised from lowest to highest autocorrelation.

Categories	Moran's Index	expected index	variance	z-score	p-value	outcome
Artefact type & lithic class	0.09	-0.00023	0.000006	33.8	0.00	clustered
Epoch	0.08	-0.00023	0.000006	30.4	0.00	clustered
Industry	0.05	-0.00023	0.000006	21.6	0.00	clustered
Material type	0.05	-0.00023	0.000006	19.8	0.00	clustered
Implement type	0.01	-0.00023	0.000006	6.0	0.00	clustered

Comparison of the z-scores between each category indicates that spatial autocorrelation is strongest for artefact type/lithic class and archaeological epoch, and weakest for implement types (Table 7.6). A low Moran's I and z-score for implement type suggests that implement diversity is more of a factor in artefact spatial organisation than any other category. The propensity for artefacts diagnostic of the same Industries to occur close together supports published accounts of Industry defined clusters at the locality (Low et al. 2017; Shaw et al. 2019; Will et al. 2015). However, using Moran's I to assess spatial relatedness is limited to the detection of global patterns. It is unable to demonstrate how this pattern manifests across the locality, in which more localised variation between artefacts and context are possible. To understand how spatial relatedness manifests across the locality, artefact density and diversity are examined in the following sections at the scale of the archaeological population and by archaeological component. Each area of analysis has the potential to reflect a shift in the processes controlling artefact location and composition (i.e., anthropogenic and/or post-depositional).

7.4.2 Artefact density

7.4.2.4. Density by inferred artefact age

Using the same methods outlined above, Hot-spot analysis was performed on MSA, LSA, and Neolithic artefacts to test the visual interpretation of their spatio-temporal organisation (Figure 7.15). Figure 7.15a shows considerable overlap between artefacts from these three epochs in Exposure 3 (north slope) and at the top of Exposure 1b. Although some separation is evident between MSA artefacts and other archaeological epochs on the southern slope.

MSA artefacts (Figure 7.15b) cluster on Lower Red sediment at the top of the south slope, and form more dispersed distributions at the top of Exposures 1a and 1c on the south slope and at the base of slopes on Exposures 3, 4, and 5 (in the north) and 1a (in the north-west). In contrast, LSA artefacts show significant clustering (>95% confidence) on Lower Red and Upper Yellow sediment on the north slope, and on the east slope in Exposure 2. The distribution of LSA artefacts across the middle of the southern slope show a significantly dispersed pattern, while artefacts from this epoch at the top and base of the south slope are randomly distributed (Figure 7.15c). Random distributions of LSA artefacts overlap with randomly distributed artefacts from the Neolithic. Neolithic artefacts only show random distributions, at the top of the north and south slopes and the base of the south slope, suggesting that artefact counts are too low to show a significant pattern in these areas (Figure 7.15d).

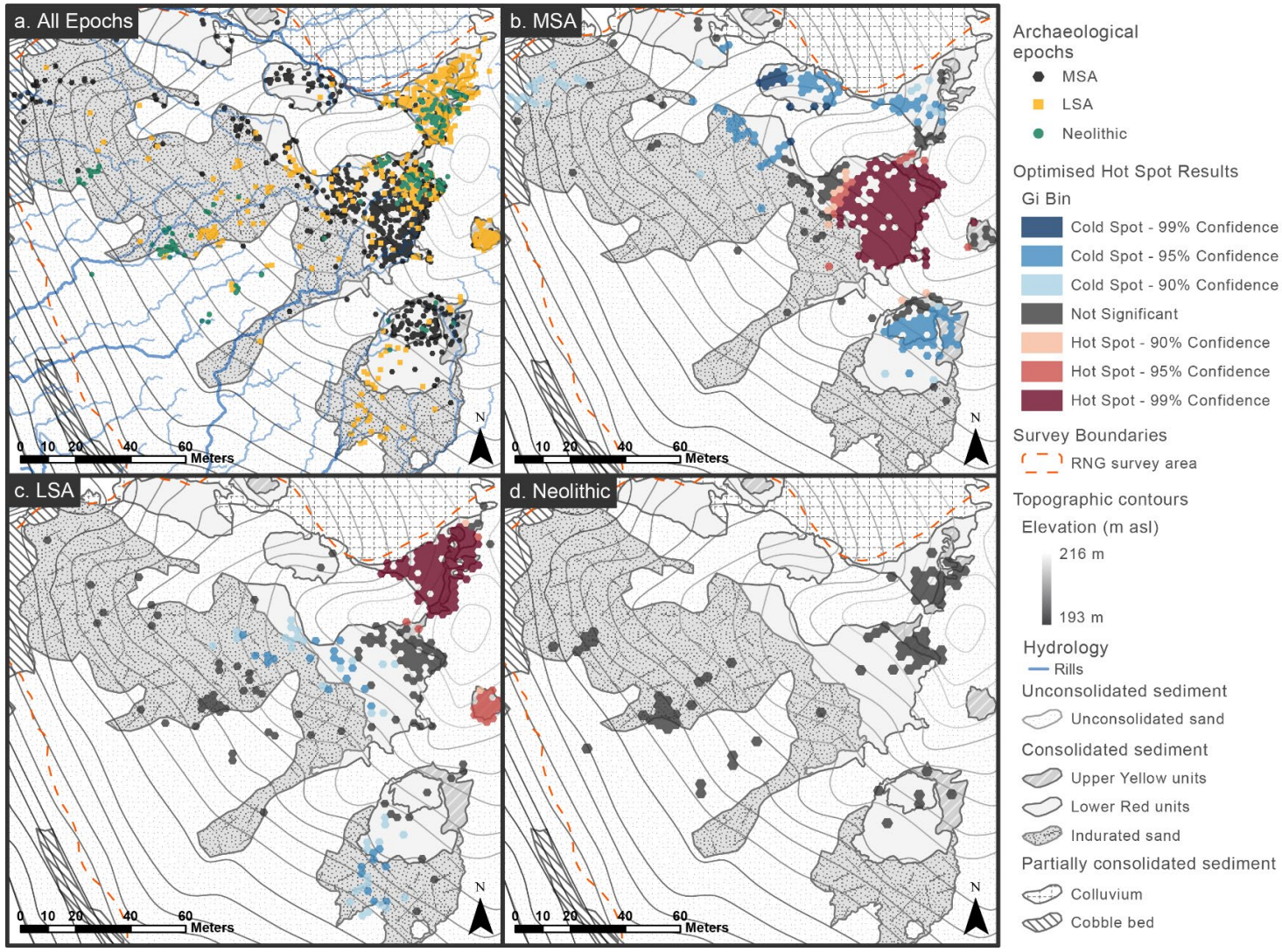

Figure 7.15. The distribution and density of MSA, LSA, and Neolithic artefacts at UPK7. Frame A presents the general point pattern of all three archaeological epochs (MSA = black hexagons, LSA = yellow squares, Neolithic = green circles) in relation to UPK7's topography, substrate and sediment types, and rill locations. Frames b to d present Hot-cold spot density maps for artefacts associated with the MSA, LSA, and Neolithic, respectively. Blue signifies dispersed (cold) artefacts, black signifies random distributions, and red indicates dense (hot) distributions.

Analysis of artefact density by Industry was not possible using Hot-Cold Spot analysis due the low frequencies in each Industry— most have less than 60 artefacts. An analysis of spatial autocorrelation (presented in section 7.4.1) has already shown that clustering does occur for UPK7's Industries. However, this test does not specify if clustering varies between or applies to all Industries. To test for clustering between Industries, nearest neighbour distance analysis was employed using ArcGIS Pro.

Counter to published and visual interpretation, the Still Bay is randomly distributed (Table 7.7). The same applies to the Howiesons Poort and the Robberg. The low frequencies for Still Bay and Howiesons Poort artefacts are a limiting factor in quantifying their spatial patterning with confidence. However, after the Wilton, Still Bay and Howiesons Poort artefacts cover the smallest proportion of the total area surveyed (6 and 4% respectively, Table 7.7), which is limited to the LR and transitional areas between LR and UY in the middle and upper hillslope zones. Robberg artefacts are randomly spread over a larger area (13%, Table 7.7), occurring on all three consolidated sediment units (LR, UY, and IS) and holding upper, middle, and lower hillslope positions. This suggests Still Bay and Howiesons Poort artefacts remain constrained by sediment unit and thus age, while Robberg artefacts have either been discarded across sediment units that were all exposed at similar times during MIS2 or Robberg artefacts have been dispersed by other means from upslope and onto the IS after initial discard. All other Industries, from the MSA (Late MSA) and LSA (Early LSA, Oakhurst, and Wilton), show significant clustering (p-value = <0.05, Table 7.7). Artefacts assigned to the Early LSA, Post-Howiesons Poort and Wilton cover the smallest area that was surveyed (Table 7.7). In contrast, the Late MSA and Oakhurst clusters show the largest spread across the survey area.

Table 7.7. Artefact abundance and nearest neighbour results for artefacts classified by Industry.

Industry*	n	Mean distance~	Expected mean distance	Nearest Neighbour Index^	Z-score	P-value	Pattern	Area of analysis"
SB	19	5.6	6.4	0.8	-1.06	0.29	random	3085 (6%)
HP	11	6.8	6.8	1.0	-0.03	0.98	random	2046 (4%)
P-HP	51	2.6	3.1	0.8	-2.27	<0.05	clustered	1999 (4%)
LMSA	95	2.8	5.1	0.6	-8.13	<0.01	clustered	9683 (20%)
ELSA	55	1.6	3.1	0.5	-6.85	<0.01	clustered	2107 (4%)
Robberg	36	7.3	6.7	1.1	1.05	0.30	random	6453 (13%)
Oakhurst	59	3.4	9.1	0.4	-9.13	<0.01	clustered	19352 (40%)
Wilton	49	2.3	2.8	0.8	-2.64	<0.01	clustered	1561 (3%)

*Historic artefacts excluded: <5 artefacts; ~Distance measure is Euclidean; ^The ratio of the observed and expected mean distances; "Minimum enclosing rectangle in m^2 and % of total survey area; Industry abbreviations: SB = Still Bay, HP = Howiesons Poort; p-HP = post-Howiesons Poort; LMSA = Late MSA; Early LSA = Early LSA.

7.4.3. Artefact density and diversity

Every archaeological component analysed above showed a common trend of high artefact density at high elevations, on the upper and middle hillslope zones of the sand mantle, where the UY and LR are exposed. In contrast, artefacts categorised by material type, artefact type and lithic class, and implement type show highly dispersed distributions across the lower elevations of middle to lower hillslopes zones, which is most notable on the southern hillslopes that expose the IS. Time-diagnostic artefacts show the most extreme pattern where they are dense at the top of the sand mantle and infrequent and highly dispersed or absent at lower elevations. The main compositional factor that distinguishes high and low densities for each archaeological component is diversity. To demonstrate the relationship between artefact diversity and

artefact density the diversity indices of material type, artefact type and lithic class, and implement type from the rSSQ dataset were plotted as a function of the natural log transformed density (log) using linear regression (Figure 7.16).

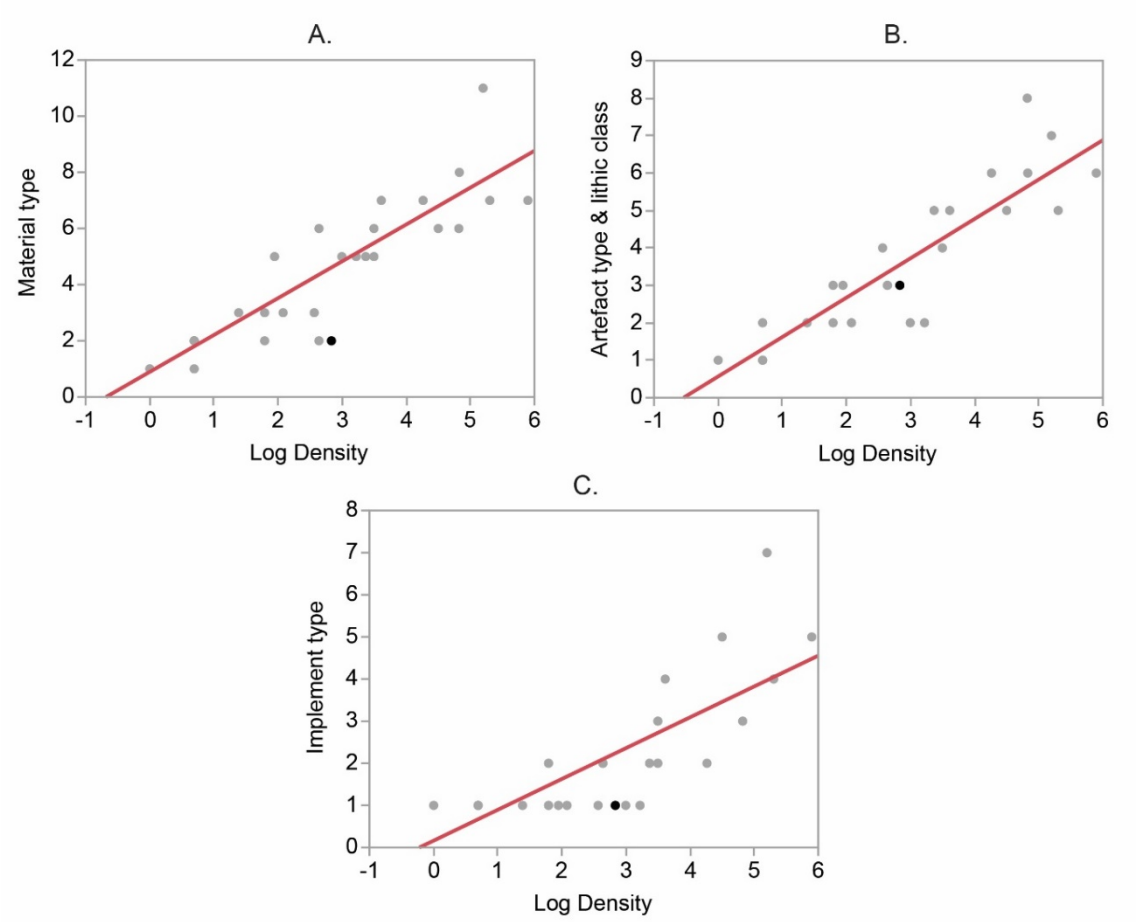

Figure 7.16. Linear regression of the number of artefact types within the archaeological categories material type, artefact type/lithic class and implement type, using the rSSQ dataset, and plotted as a function of log transformed artefact density: A) Material types: $p < 0.0001$, Adjusted $R2 = 0.77$, B) Artefact type/lithic class: $p < 0.0001$, Adjusted $R2 = 0.78$, C) Implement type: $p < 0.0001$, Adjusted $R2 = 0.58$.

All three categories show a positive linear relationship between artefact diversity and density (Figure 7.16), supporting visual interpretation that artefact diversity increases with artefact density. An unsurprising result given that diversity and density are not independent variables. Diversity indices are traditionally used to test for occupation duration/intensity (Schiffer 1987; Schlanger 1990)—the assumption being that long term or more intensive place use or repeated unrelated activity in the same place over a long time ('time-dependent accumulation') will result in the accumulation of a greater variety of artefact types as well as an increased likelihood of rarer items being introduced into an assemblage (the 'Clarke effect', Davies & Holdaway 2017; Schiffer 1987). However, artefact diversity and density may also reflect sediment availability and preservation bias, where long term discard activity is differentially preserved due to periodicity in sediment aggradation and erosion. Thus, it is imperative that the relationship between UPK7's surface archaeology—its composition and condition—and its physical environment are understood before interpreting this pattern as a behavioural trend.

7.5. Artefact Spatial Patterning in Relation to Geomorphic Setting and Artefact Condition

The preceding sections examined the general spatial patterning and composition of artefacts across UPK7, supporting the observations of clustering in diagnostic artefacts presented in Will et al. (2015) and Low et al. (2017). Interpreting the observed point pattern without consideration of the sedimentary system would suggest that artefact density, diversity and spread is indicative of the duration and/or intensity of place use over time. However, this assumes that artefact accumulation occurred without removal and/or was unaffected by post-depositional modification. Given the depositional history and geomorphology of this locality—the increasing aridity and fluctuations between wet and dry conditions, and the highly weathered, rilled condition of UPK7's consolidated sediments—it is unlikely that artefact and sediment accumulation happened in a stable and unchanging setting or that artefacts were immune to such an active and long history of landform development. The following sections investigate the relationship between the spatio-temporal patterning of surface artefacts and their physical environment (i.e., elevation, slope angle, hillslope position and substrate unit). If a relationship is found, further enquiry is made into the possible processes promoting/inhibiting this relationship. For instance, taphonomic markers are considered that could influence the relative intensity of artefacts (i.e., movement and visibility) through loss in one area (e.g., sheet wash entrainment and/or burial) and increase in another (e.g., exposure and/or fragmentation).

7.5.1. Artefact density and elevation

In the preceding sections it was noted that change in artefact density appeared to coincide with several possible topographic and/or depositional features across UPK7. One of the main topographic features of the locality is elevation, with artefacts appearing to shift from high to low density between 210 and 211 m asl. To test the association between density and elevation, the dependence of artefact point pattern intensity was modelled as a function of elevation (Figure 7.17a) using the rhohat function[1] in the Spatstat package in R (Baddeley & Turner 2004; R Core Team 2015).

There is a marked increase in artefact density above 210 m asl (Figure 7.17a). However, minor oscillations in artefact densities are evident below this threshold, between 208 and 209 m asl, and to a lesser degree around 205 m asl—that relates to the lower zone of the southern hillslope (Exposures 1a to c). A sharp drop in density is also evident at elevations above 215 m asl (Figure 7.17a). This is the point at which consolidated sediment shifts to unconsolidated sand on the upper hillslopes of Exposure 1b and 3 and suggests that unconsolidated sand is inhibiting artefact visibility.

[1] The object of class "rhohat" is a kernel-smoothed intensity estimate of a point process (i.e., artefact density), as a function of a given spatial covariate (i.e., elevation). Thus, 'Rho' or 'ρ' represents the rate at which artefact intensity changes relative to a change in elevation. It is a nonparametric estimator and thus does not assume a particular form for the relationship between the spatial point pattern and its covariate (Baddeley & Turner 2004).

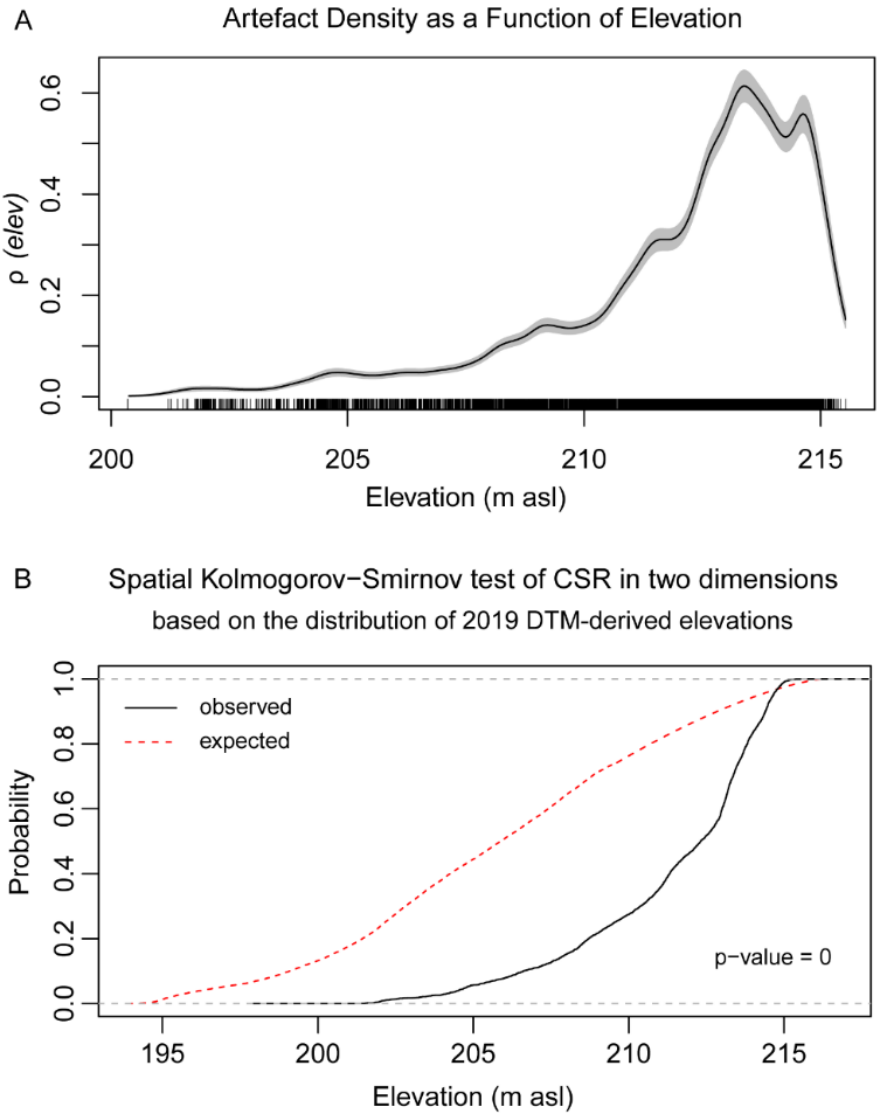

Figure 7.17. (a) Artefact density as a function of elevation. (b) Spatial Kolmogorov-Smirnov test of complete spatial randomness in two dimensions based on the distribution of 2019 DTM-derived elevations.

To test the significance between artefact intensity and elevation, the spatial Kolmogorov-Smirnov test (KS-test) of Complete Spatial Randomness (CSR) was performed (Figure 7.17b). Figure 7.17b shows artefact intensity to be well below its expected probability until the very top of the sediment stack, ~214.5 m asl. With a p-value of <0.05 (D = 0.096, p = < 2.2e-16) there is an extremely low probability that this pattern is the result of chance. However, elevation in itself does not explain what factors are influencing the spatio-temporal patterning in surface archaeology across UPK7. Rather, it demonstrates that an association exists between the spatial distribution of artefacts and UPK7's physiological setting. This could be due to a number of processes that change depending on elevation, such as the hillslope dynamics of deposition, stabilisation and removal of sediment, and/or where people preferred to carry-out their activities across the locality. Both cases can influence artefact density by catalysing and inhibiting its visibility and movement.

7.5.2. Artefact visibility and sediment composition

To determine if the inhomogeneous pattern in artefact location is the result of sediment composition inhibiting/heightening artefact visibility, their frequencies are compared and tested for significant differences between unconsolidated, fully, and partially consolidated surfaces. Based on initial visual impression, artefact visibility is expected to be high on consolidated sediment, moderate on partially consolidated sediment, and low on unconsolidated sediment. The null hypothesis is that there is no difference in visibility between surfaces. If the association between artefact location and sediment type is the result of chance, then the null hypothesis is that the proportion of artefacts in each context is the same as the proportion of surface area each sediment type covers within the surveyed area. Thus, under the null hypothesis a greater proportion of artefacts are expected to occur on unconsolidated than consolidated surfaces given their relative areas (see Table 7.8).

Table 7.8 and Figure 7.18 show the proportion of artefacts visible on each sediment type. The highest artefact frequencies occur on consolidated sediment (88%), while artefacts found on unconsolidated and partially consolidated sediment contribute less than 10% to the total surveyed area (see Table 7.8). Based on the size of their exposure, the proportion of artefacts in each context are significantly different from their expected counts (Chi-squared Goodness-of-Fit Test = 6014.7, df = 2, p-value = 0), rejecting the null hypothesis of independence between variables (Table 7.8 and Figure 7.18). Of note, are the standardised residuals of the fully consolidated (77.5) and unconsolidated surfaces (-71.6). While both are large, the direction of this difference is polarised, with consolidated sediment yielding more artefacts than expected, and unconsolidated sediment yielding less. This strongly suggests that artefact visibility is related to the composition (hard or soft) of UPK7's deposits, with their depositional history, timing, and duration of exposure all potentially impacting artefact spatio-temporal organisation.

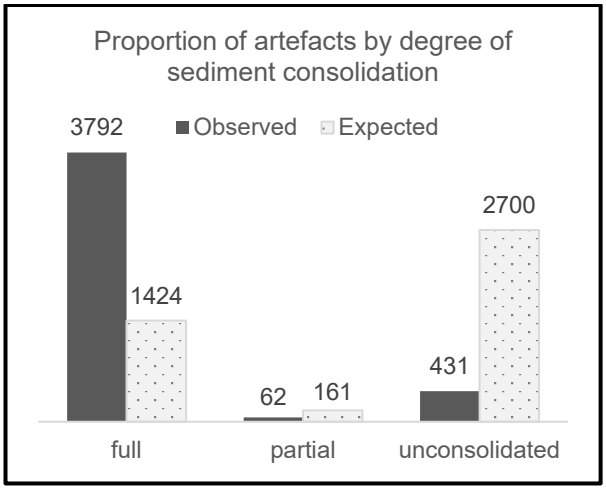

Figure 7.18. Proportion of artefacts on units with different degrees of sediment compaction.

Table 7.8. Artefact count by sediment type and the proportion of each within the survey area

	Surveyed area		Artefacts			
Substrate Composition	m^2	Proportion	Count	Proportion	Expected	Standardised residuals
Fully consolidated	11467	0.33	3792	0.88	1424	77.5
Unconsolidated	21735	0.63	431	0.10	2700	-71.6
Partially consolidated	1297	0.04	62	0.01	161	-9.8
Total	34499	1.00	4285	1.00	4285	

To understand how artefact exposure has affected the spatial distribution of surface artefacts on UPK7's consolidated sediment, artefact density, size and condition is assessed in the following sections against a topographic setting (i.e., slope angle, hillslope position) and substrate age to detect artefact movement and weathering due to exposure to repeated rainfall events, wet-dry cycles, and trampling.

7.5.2.1. Artefact density and movement

The shift in artefact spatial distribution from high density above 210 m asl to low density below this elevation could reflect the dominant slope angles at these elevations either as a response to rainfall erosion or the presence of vegetation (see Chapter 6.4). If sheetwash has influenced the organisation of surface artefacts across the locality, artefact density is expected to decrease as slope angle increases, with a marked drop in artefact numbers on slope angles higher than 15º (Figure 6.41). It is hypothesised that sheet/slope wash has affected the spatial patterning of artefacts across UPK7. Therefore, the null is that there is no relationship between slope angle and artefact frequency on slopes < 15º and no difference between artefact density above and below 15º.

7.5.2.2. Artefact density and slope angle

To determine if sheetwash erosion is influencing change in artefact density and dispersion, artefact density was plotted as a function of artefact slope angle—also produced using the rhohat function in the R Spatstat package (Baddeley & Turner 2004). A relationship between artefact frequency and slope angle is evident, but weak (Figure 7.19a). Although artefact density shows a gradual decrease in density as slope increases, this relationship is not pronounced, with Figure 7.19a showing similar artefact densities maintained across a broad range of low to moderate (3-15°) and high (16-20°) gradients and only a gradual drop in densities from 20° and higher. However, in accordance with experimentally derived expectations (see above), there is a marked drop in artefact density above 30°, which suggests that in most cases this remains the threshold for static repose. The probability that the relationship between artefact density and slope angle is the result of chance is extremely low (KS-test statistic D = 0.096, p = < 2.2e-16) (Figure 7.19b). With an AUC value of 0.5, slope is not a strong predictor of artefact density.

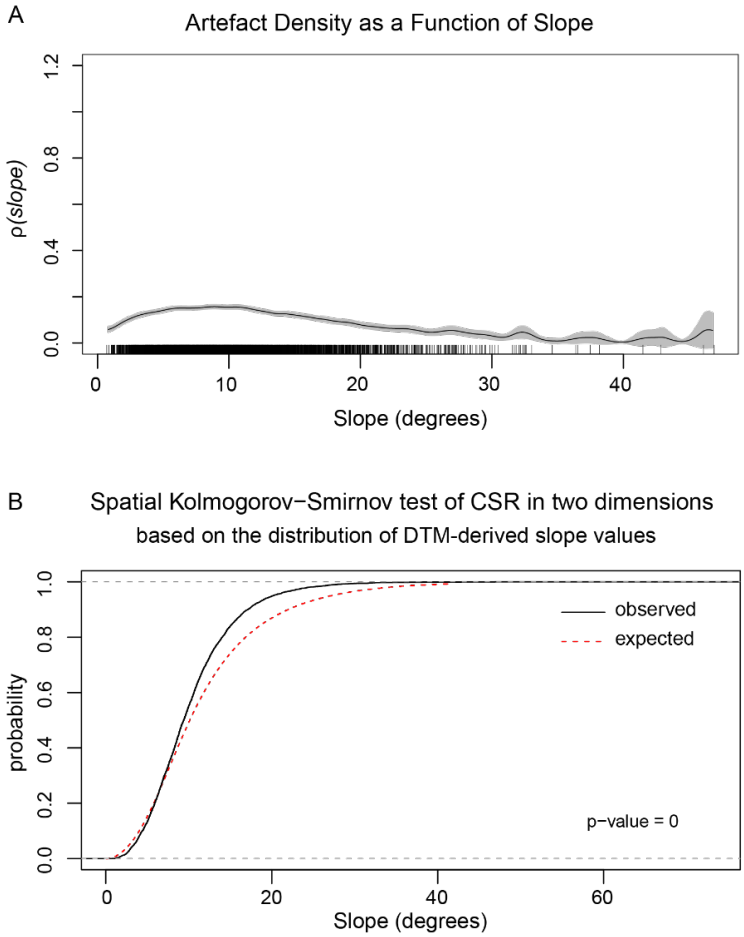

Figure 7.19. (a) Artefact density as a function of slope. (b) Spatial Kolmogorov-Smirnov test of complete spatial randomness in two dimensions based on the distribution of 2019 DTM-derived slope values.

7.5.2.3. Artefact size and topographic setting

The weak relationship between artefact density and slope angle suggests that other factors in addition to slope angle are influencing the spatial distribution of artefacts at this locality. Artefact movement can vary depending on artefact size (e.g., larger artefacts at low slope angles are less likely to move than smaller artefacts) and density (e.g., surface armouring adds resistance to object disaggregation and substrate erosion) and can be inhibited or catalysed by surface roughness (vegetation and rilling; see Chapter 6.4). The threshold size for surface clasts most susceptible to runoff is ≤ 20 mm (Schick 1986). Although Sheppard & Kleindienst (1996) have shown that flakes <30 mm in maximum dimension are most susceptible to entrainment.

Although the size distribution of artefacts in the RNG dataset are positively skewed (Figure 7.20), only 5% (n = 231) of RNG artefacts measure 20 mm or less in maximum dimension, with a median artefact size of 62 mm, and an IQR of 48 mm. This distribution could reflect the dominance of lightly reduced cores at this locality, with some cortex evident on ~87% of cores (n = 2,728), and 65% of cores with at least 25% cortical coverage (n = 2,036). However, without the inclusion of flakes in the RNG dataset it is uncertain whether artefact size and the minor effect of slope angle on the frequency of artefacts across exposures reflects a size bias, runoff-induced size-sorting, intensity of core reduction, discard behaviour, transportation into and out of the study area, or a combination of these factors (assessed below).

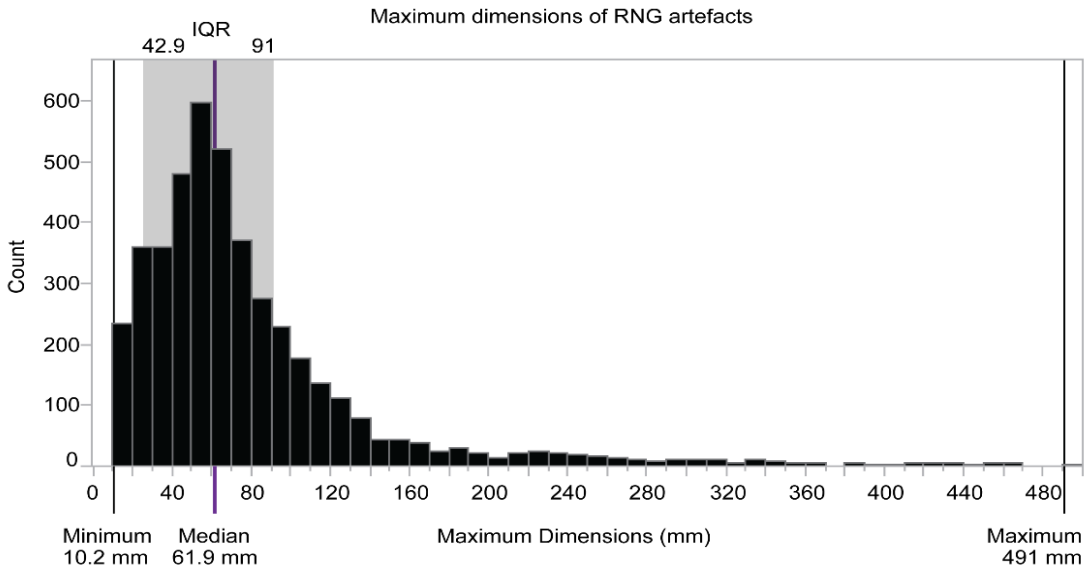

Figure 7.20. Distribution of RNG-survey-derived maximum artefact dimensions for UPK7. Interval sizes for bins are 10 mm.

7.5.2.3.1 rSSQ flake composition and size distributions

As mentioned in Chapter 5.7.1.3, flakes are typically smaller and lighter than other lithic classes. Consequently, flakes are less resistant to sheetwash entrainment at lower slope angles than other stone artefact classes, making them sensitive proxies for detecting sheetwash and trampling that could otherwise be masked by core-rich datasets (i.e., the RNG dataset). Although they were not recorded during RNG survey, flakes were randomly recorded across all substrate units and slope angles during the rSSQ survey. Of the 2,366 surface clasts recorded across 32 rSSQ, 26 squares captured archaeology with maximum dimensions above 10 mm. From these squares 1,088 flakes were identified, with flakes representing 79% of the total assemblage while cores represent 9%, and tools 4% (Table 7.9).

Flake proportions are similar to those observed by Low et al. (2015; 83%) who analysed all artefact classes >20 mm in maximum dimension within Exposure 2 (previously 'AOA3'), while their percentage of cores are marginally lower (7.8%) and tools lower still (1.1%) (Table 7.9). The median maximum dimensions (24 mm) for flakes considered 'intact' (i.e., complete, bipolar, and longitudinally split flakes) are smaller than the median maximum dimensions of both cores (58.5 mm) and tools (41.5 mm) in the same dataset (Figure 7.21). RSSQ flakes also have relative size distributions consistent with the typical composition of a stone artefact assemblage. Moreover, 30% of intact flakes (n = 219) have maximum dimensions below 20 mm, suggesting that rainfall has not completely removed these artefacts from the survey area. However, without a spatial understanding of these size distributions it is unclear if and where artefact movement has occurred. To determine if change in artefact density between upslope and downslope contexts is the result of slope/sheet wash, the maximum dimensions of flakes deemed—at a minimum—morphologically 'intact' (i.e., complete, longitudinally snapped and/or longitudinally cone split, and bipolar flakes) were assessed against hillslope position (Table 7.11). Flakes occurring on steep slopes, >15º, are examined separately from flakes that occur on moderate to low slope gradients, ≤15°, and their proximity to rilling and vegetation visually assessed throughout the analysis.

Table 7.9. rSSQ composition by artefact class and break type, showing the count and frequency of artefacts in each category.

Class*	Count	%
Flakes	1,088	79
complete, bipolar & longitudinally split flakes	720	52
broken flake, transverse	368	27
Cores	121	9
complete core	112	8
broken core	9	1
Tools	50	4
complete tool	40	3
broken tool	10	1
Other	18	1
pottery fragment	4	<1
heat shatter	14	1
broken, unclear	104	8
Total	1381	100%

*NA = 14 (1%)

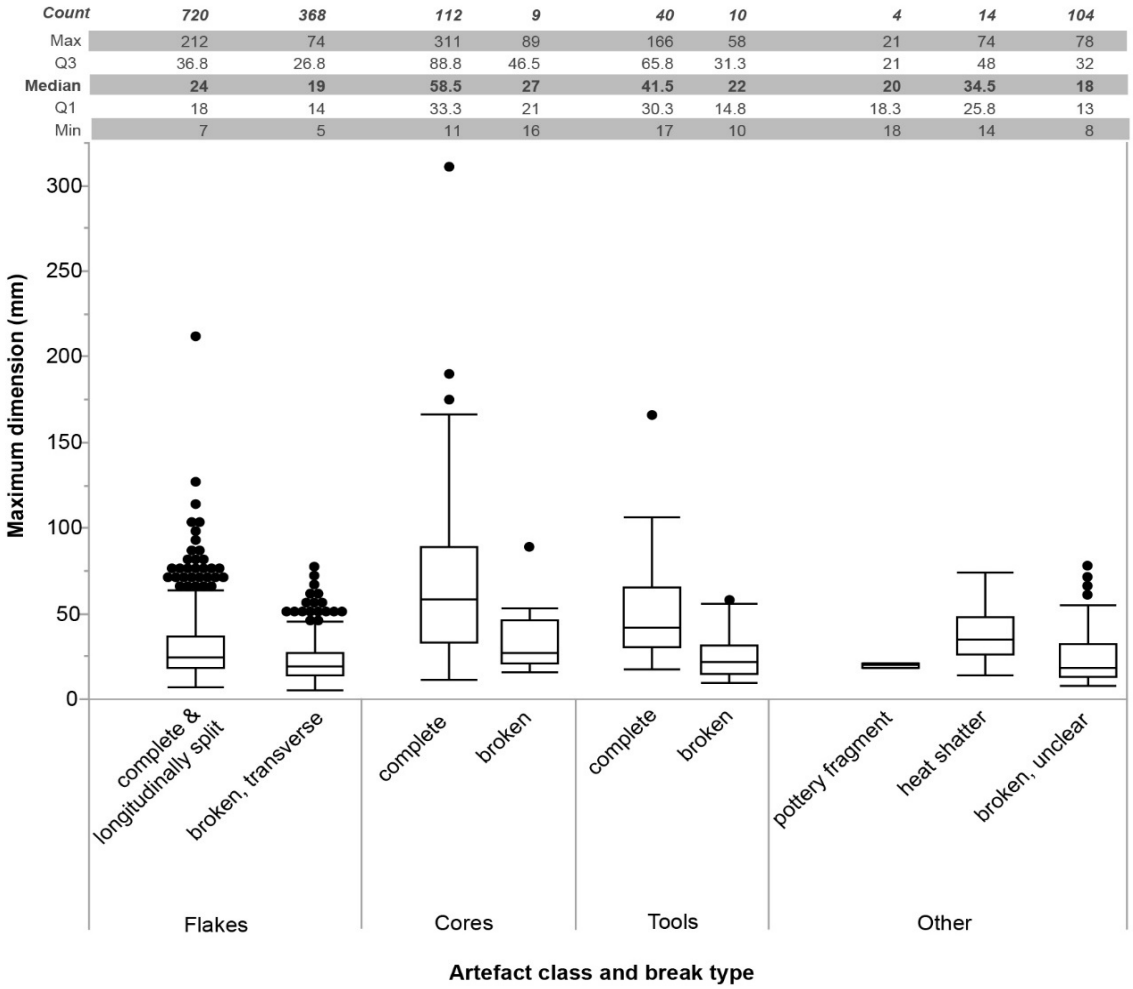

Figure 7.21. rSSQ composition by artefact class and break type, showing the distribution of maximum dimensions (mm) between each category.

7.5.2.3.2 Size-sorting across UPK7

The differences between the median maximum dimensions of intact flakes in each hillslope zone are compared across the locality (Table 7.11). Flake maximum dimensions are not normally distributed (Shapiro-Wilk test for normality: *W* statistic = 0.797, p <0.0001, see Figure 7.21), thus nonparametric comparisons of median artefact size between hillslope positions were performed using the Wilcoxon method, in JMP Pro (14.1.0). At a minimum, the presence of at least one rSSQ with more than 2 flakes is required in at least two hillslope zones to be included in statistical analysis. If this was not upheld, the data for that hillslope was excluded.

The rSSQ dataset is a random discontinuous sample of artefact surface conditions (i.e., artefact elevation and thus slope position). For this reason, not all hillslope positions were captured during rSSQ survey, with only the central southern slope Exposure 1b sampled across all three hillslope zones (Table 7.10). For example, the north-east slope Exposure 3 was randomly sampled twice, providing a relative record of artefact maximum dimensions within the bounds of rSSQ 25 and 90. The average artefact elevations for rSSQ 25 and rSSQ 90 are 213 and 214.6 m asl, respectively. Their average elevations provide ordinal categories to compare the distribution of artefact sizes between upper (i.e., rSSQ 90) and middle (i.e., rSSQ 25) hillslope conditions, but not the lower, foot slope of Exposure 3. If slope wash has impacted this exposure, then artefacts recorded at higher elevations—in the upper zone—are expected to have larger maximum dimensions than at lower elevations—with median sizes decreasing towards the base of the slope. Exposure 4 has a single intact flake on a low to moderate slope (≤15º) and was excluded from further analysis, while Exposures 2, 5, and 6 were either not captured in the random sample survey or in the case of 5 and 6, did not yield intact flakes.

Table 7.10. Flake* frequencies by slope angle, exposure, and hillslope position

Slope angle (°)	Exposure	rSSQ N	Frequency of flakes* by hillslope position/slope class			
			Total N	Upper	Middle	Lower
>15	1a	0	0	0	0	0
	1b	3	4	1	1	2
	1c	2	3	3	0	0
	3	1	12	12	0	0
≤15	1a	3	32	29	3	0
	1b	8	448	231	210	7
	1c	5	34	26	8	0
	3	2	153	84	69	0

Only a small number of rSSQ and intact flakes occurred on slope angles >15º (upper n = 16, middle n = 1, and lower n = 2; Table 7.10). Exposure 3 yielded the largest number of artefacts on gradients steeper than 15º (n = 12), albeit in a single rSSQ. These occur in the upper zone of the hillslope (214.6 m asl), with a positively skewed size distribution and a small median maximum flake size of 20 mm and a tightly constrained IQR of 30 (Table 7.11). In contrast only a few artefacts were recovered from multiple rSSQ for the same slope angle class (>15º) in Exposures 1b and 1c. Three or less flakes were held in repose for this slope class. In Exposure 1b these are spread between three rSSQ, each occurring in a different hillslope

zone. All of these flakes are larger than 60 mm, except for one flake in the lower zone (12 mm). A single rSSQ in Exposure 1c captured three artefacts on slopes >15º that range from 24 to 69 mm in maximum dimension. These sample sizes are too small to perform a reliable analysis and the p-value of each hillslope pair for slope angles >15º (Table 7.12). This is also why each pair comparison using the Wilcoxon method was not possible for flakes found on slope angles >15º for individual exposures.

Despite this, the upslope position in Exposure 3 and the number and small size of intact flakes held on its steeply angled slope, is unexpected. This result suggests that surface artefacts either have not been subjected to enough force (i.e., strong, or repeated sheetwash events) to cause downslope entrainment on Exposure 3's upper slopes or there is input due to progressive erosion of *in situ* artefacts. The hillslope position and slope angle at which these artefacts were recorded are influenced by vegetation mounds in this area—rather than a network of rills (see Figure 6.41)—which helps to increase localised resistance to erosion during rainfall events.

Table 7.11. The distribution of flake maximum dimensions by hillslope position for each exposure (grouped by slope angle bin)

Slope angle (°)	Exposure	rSSQ N	Hillslope position	Flake* N	Min	Median	Max	IQR
>15	1b	1	Upper	1	63	63	63	0
		1	Middle	1	93	93	93	0
		1	Lower	2	12	69.5	127	115
	1c	2	Upper	3	24	27	69	45
	3	1	Upper	12	10	20	49	30
≤15	1a	1	Upper	29	16	34	78	35
		2	Middle	3	42	46	114	72
	1b	2	Upper	231	7	21	103	16
		4	Middle	210	10	25	101	15
		2	Lower	7	12	13	13	9
	1c	2	Upper	26	12	26	212	20
		3	Middle	8	10	32.5	57	40
	3	1	Upper	84	12	24.5	72	16
		1	Middle	69	10	26	85	25

Table 7.12. Nonparametric Wilcoxon test of differences between the median maximum dimensions of flakes* randomly sampled on the upper, middle, and low hillslopes for the entire locality and by exposure.

Slope angle (°)	Hillslope Positions	Score Mean Difference	Std Error Difference	Z	*p*-value[a]
>15	Middle, Lower	0.000	1.225	0.000	1.000
	Upper, Lower	-0.563	3.998	-0.141	0.888
	Upper, Middle	-7.969	5.199	-1.533	0.125
≤15	Upper, Lower	92.72	41.55	2.231	< 0.05
	Middle, Lower	89.47	32.83	2.725	< 0.01
	Upper, Middle	-46.19	14.95	-3.090	< 0.01
Exposure					
3	Upper, Middle	-4.91	7.20	-0.682	0.495
1a	Upper, Middle	-8.46	5.69	-1.488	0.137
1b	Middle, Lower	65.84	24.11	2.731	< 0.05
	Upper, Lower	46.66	26.39	1.768	0.077
	Upper, Middle	-53.10	12.15	-4.372	< 0.0001
1c	Upper, Middle	0.25	4.02	0.061	0.951

*Complete, bipolar & longitudinally split (LS) flakes; [a]alpha = 0.05

The size distribution of Exposure 3's flakes found on low to moderate gradients (≤15º) are positively skewed in both upslope (214.6 m asl) and downslope (213 m asl) settings, with median maximum dimensions of 20 and 26 mm, respectively (Table 7.11). The downslope context shows a greater range of intact flake sizes, with a larger median maximum dimension than in the upslope zone. However, there is no significant difference between upslope and downslope medians (Mann-Whitney test: Sum of ranks = 5499.5, Z statistic = 0.68, p-value = 0.5, Table 7.12). In which case the null hypothesis that median flake sizes are similar irrespective of slope angle/position cannot be rejected for Exposure 3 (p-value is > 0.05, Table 7.12). Therefore, it is very unlikely that surface artefacts sampled on this slope have moved.

For Exposure 1a, three survey squares randomly subsampled intact flakes across a range of slope positions (upper = 210.5 m asl, middle = 208.2 m asl, and lower = 206.5 m asl). The upper slope rSSQ returned the largest flake counts (n = 29), with only 1 flake from the middle slope position and 2 from the lower position. Flakes at 210.5 m asl are positively skewed (Table 7.11) with a median maximum dimension of 34 mm (Table 7.11). The two lower squares (rSSQ elevation 208.2 m asl n = 1, 206.5 m asl n = 2) show larger size values (114 and 44 mm) than at the top of the slope. However, their sample sizes are very small and either lack or differ in their size distributions to the upslope rSSQ, rendering statistical comparison between each pair unreliable. However, the dramatic drop in artefact density below 210 m asl on this slope is in accordance with the shift in RNG artefact densities.

The hillslope of Exposure 1b was randomly sampled six times. The number of intact flakes recorded reflects the polarity in artefact density observed for the RNG dataset, with higher artefact frequencies per 1 m^2 above 210 m asl than downslope of this elevation (Table 7.10). The median maximum dimension of flakes on the lower hillslopes (below 210 m asl) are < 20 mm. Above 210.1 m asl median maximum flake dimensions are > 20 mm and < 30 mm. However, these values and their IQR vary between upper (214-213 m asl) and middle (212.9 – 210 m asl) hillslope position. At each elevation, flakes have an

approximately 50% probability of measuring below 30 mm in maximum dimension. With an approximately 10 mm difference in flake sizes between the highest elevation and lowest elevation (Table 7.11)—suggesting a shift to smaller artefacts from the upper to lower slope positions.

The Kruskal-Wallis test of ranked sums indicates that median artefact sizes are smaller than expected at the top of the slope, larger than expected across the middle zone, and smaller than expected at the base of the slope (Table 7.12), rejecting the null hypothesis that flake size does not change with slope position (Chi-square = 27.5, df 7, p-value <0.001). The spatial distribution and size-sorting of artefacts on this hillslope does not follow a clear linear trend of decreasing artefact size in a downslope direction for sheet wash entrainment. This suggests that sheet wash has impacted artefacts on the middle and lower zones of this hillslope more than its upslope area, indicating that other factors in addition to sheetwash processes are influencing the size distribution of artefacts across Exposure 1b. Exposure 1c captured low density subsamples of flakes in five rSSQ, all of which occur on slopes ≤15°. These squares randomly sampled elevations from upslope (210.3 m asl) to the exposure's foot slope (207 m asl), with higher artefact frequencies upslope than downslope (see Table 7.10). This is in line with the general trend of declining artefact numbers with decreasing elevation in Exposures 1a and 1b, to the west of this slope. There is a slight decrease in median flake sizes from 210.3 to 209.6 m asl. However, median artefact sizes oscillate at lower elevations and do not show a consistent trend in size-sorting nor a significant difference in medians between slope positions (Table 7.12, Chi-square 7.2, df = 4, p-value =0.13). In the case of Exposure 2, Low et al. (2017) tested for size-sorting in across the area and found that artefact size distributions were similar across this area, ruling out the possibility of artefact entrainment.

7.5.3 Summary of artefact movement

Artefact density is highest on upper and, in some cases, middle hillslopes (i.e., Exposure 1b), independent of slope angles <15-20º and > 40º, with higher artefact abundance than expected for slope angles between this range (20-40º). Exposure 3 accounts for the higher-than-expected persistence of artefacts in upper hillslope contexts on slope angles above 15º, while all other exposures suggest artefacts are being removed—irrespective of size. Hillslopes above 15º in the southern slope Exposures 1a, b, and c are often associated with well-developed, dense rilling, suggesting that artefacts are being channelled and removed in these areas when proximate to rills.

On low to moderate slopes (≤15º), median flake sizes vary independent of slope position on all hillslopes except Exposure 1b. Exposure 1b has an unexpected flake size distribution relative to hillslope position with the largest median and minimum sized intact flakes occurring on the middle hillslopes, while artefacts found at the top and very bottom of these hillslopes are, on average, smaller. This suggests that artefacts on Exposure 1b were affected by sheet wash processes from the middle zone. It is possible that greater retention of smaller artefacts in the upper zone reflects shorter term exposure to wet-dry cycles than middle zone artefacts. The potential for exposed slopes and hillslope zones to differ in the amount of time their current surfaces have been exposed may also explain why there are consistently lower flake frequencies below 211 m asl on Exposures 1a and 1c.

While visible artefacts principally occur on consolidated hillslopes, artefact density varies across the locality, where artefacts (irrespective of type) are densest at high elevations and more dispersed at low

elevations. There is also a distinctive pattern in the distribution of artefacts when categorised by inferred age, material type, artefact size and condition. This variation in spatial patterning suggests that other factors have influenced where an artefact is located. Slope angle holds a weak relationship with artefact density. However, slope angles >15º that are associated with surface rilling indicate that flakes are absent or rare—irrespective of size—implying that artefact movement and slope wash removal are more pronounced in areas with well-developed rilling (i.e., the middle to lower hillslope zones of Exposure 1b and 1c). Flakes are also smaller on upper hillslopes compared to middle hillslopes of low to moderate slope angle, suggesting that artefact movement is inhibited in the upper slope zone more so than it is from the middle to lower hillslope positions. Thus, the marked polarity in artefact density above and below 210 m asl cannot be explained by sheet wash processes and slope angle alone. To determine if differential exposure between hillslopes has impacted the condition and density of artefacts across UPK7, fragmentation and weathering of physiologically and morphologically sensitive artefacts are examined in the following section.

7.6. Exposure and Artefact Condition

7.6.1. Fragmentation

This section investigates fragmentation across UPK7's consolidated hillslopes in stone artefacts considered less resilient to the process of trampling (i.e., implements and flakes). Fragmentation can increase the relative number of artefacts in a given population and thus the perceivable density of artefacts in one area over another. Fragmentation can also reduce an artefact's size and increase its chances of entrainment—depending on the duration of artefact exposure.

With the hardness of exposed sediment at UPK7, artefact classes that are typically longer and thinner than they are wider and thicker would be expected to break under applied pressure during trampling events (Weitzel et al. 2014). Thus, fragmentation was recorded for implements during the RNG survey (Figure 7.23) and flakes during the rSSQ survey as they are the most susceptible to breakage out of the stone artefact classes defined above. Stone artefacts are also more resilient than other classes of artefact to short-term weathering (cf., pottery, which only occurs in a fragmented state at UPK7), enabling an examination of longer-term exposure and possible trampling trends across the locality. The median maximum dimension of both intact (69 mm) and broken (62.5 mm) implements is much larger than that of flakes (intact = 24 mm, broken = 19, Figure 7.22). With this in mind, the difference in the average size of intact implements compared to intact flakes is also expected to influence their susceptibility to breakage. The fragmentation of flakes can occur during manufacture, use and trampling (Holdaway & Stern 2004, pp.111-117). For this reason, complete, bipolar, and longitudinally split flakes are grouped as a minimum record of intact, unbroken flakes, while transversely broken flakes, with their platforms intact (proximal flakes), are treated as the minimum record of unintentional fragmentation.

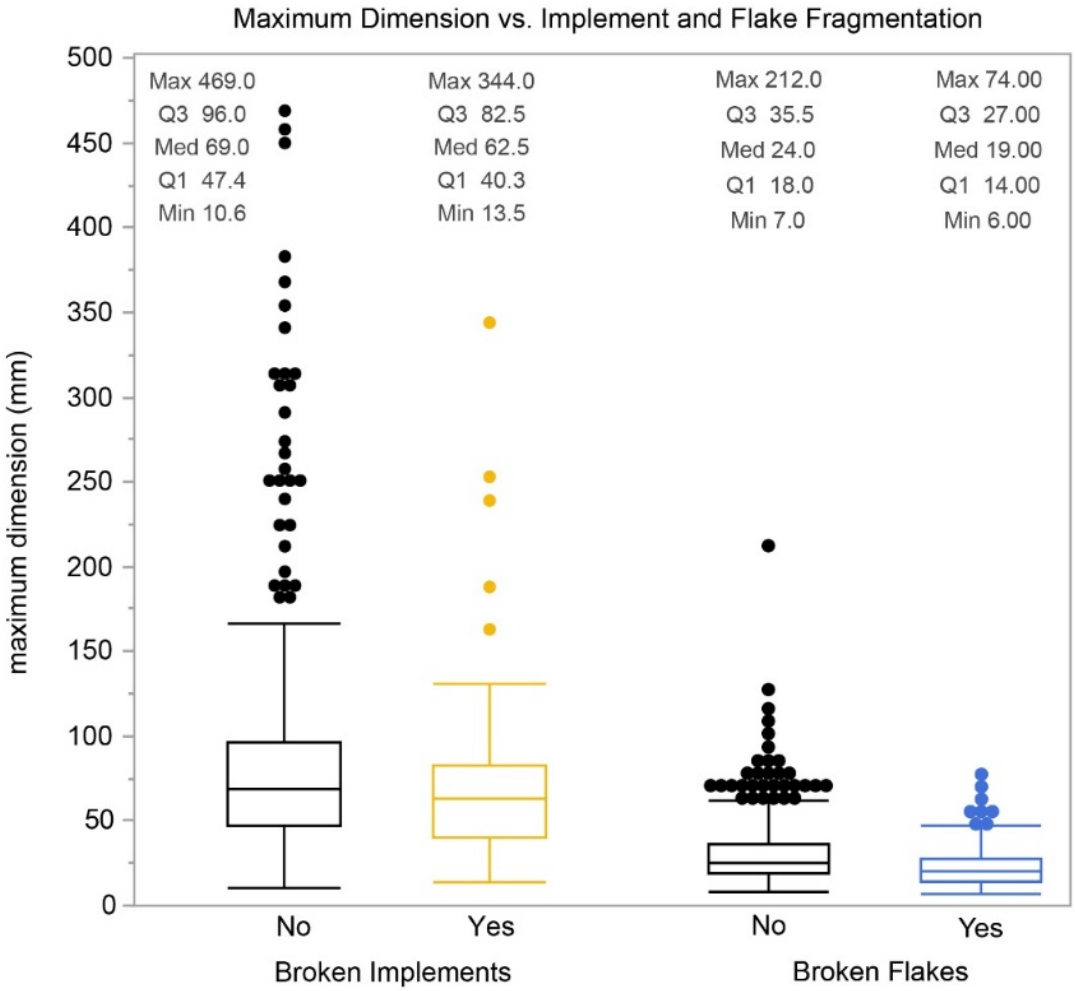

Figure 7.22. Maximum dimension (mm) distributions for intact and broken implements (RNG dataset) and flakes (rSSQ dataset) and their associated quantiles.

Overall, fragmentation is low across UPK7, with 23% of implements identified at UPK7 found in a broken state (Table 7.13). When plotted by exposure, all generally south-facing hillslopes (Exposure 1a to b) show the highest proportion of implement breakage (Figure 7.24; see also Figure 7.23) out of UPK7's eight areas of exposure, with the largest percentage of broken relative to intact implements occurring on the south-east slope, Exposure 1c (34%), deviating from the overall, locality-wide percentage of broken implements by 11%. There is less observable variance between broken and intact implements when grouped by hillslope zone and substrate, with similar proportions of breakage held between each context (Figure 7.24). However, there is very low probability that the relative proportions of complete and intact implements differ significantly across different exposures, hillslope zones, and substrates (see Table 7.14). Thus, the null hypothesis that fragmentation is independent of hillslope context (exposure, hillslope zone) cannot be rejected. Rather, these results suggest that implement breakage is equally as likely to occur on one hillslope as it is on another. The small percentage of implement breakage for the locality also suggests that post-depositional processes acting on implement condition did not lead to significant fragmentation overall.

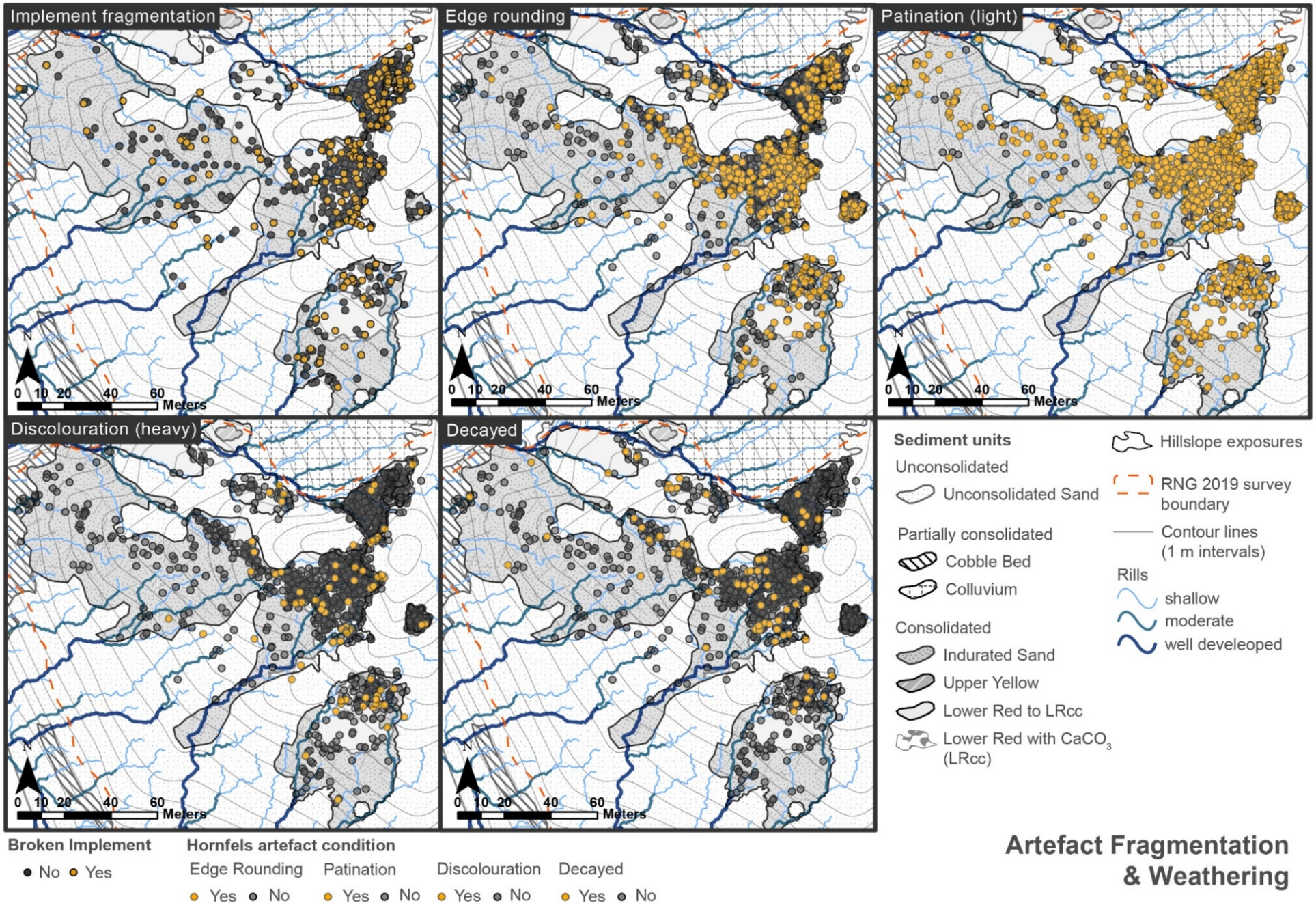

Figure 7.23. Comparative map series of artefact weathering (i.e., edge and surface condition). Edge condition represented by implement fragmentation and hornfels-specific edge rounding. Surface condition is organised into three stages of weathering: 1. Patination, 2. Discolouration, and 3. Decay.

Table 7.13. The total number and frequency of broken compared to intact implements recorded during RNG survey on UPK7's consolidated sediment units*.

Broken Implement	N	% of Total
No	495	77%
Yes	150	23%
Total	645	100%

*For implements found on Indurated sand, Lower Red units, Upper Yellow units only

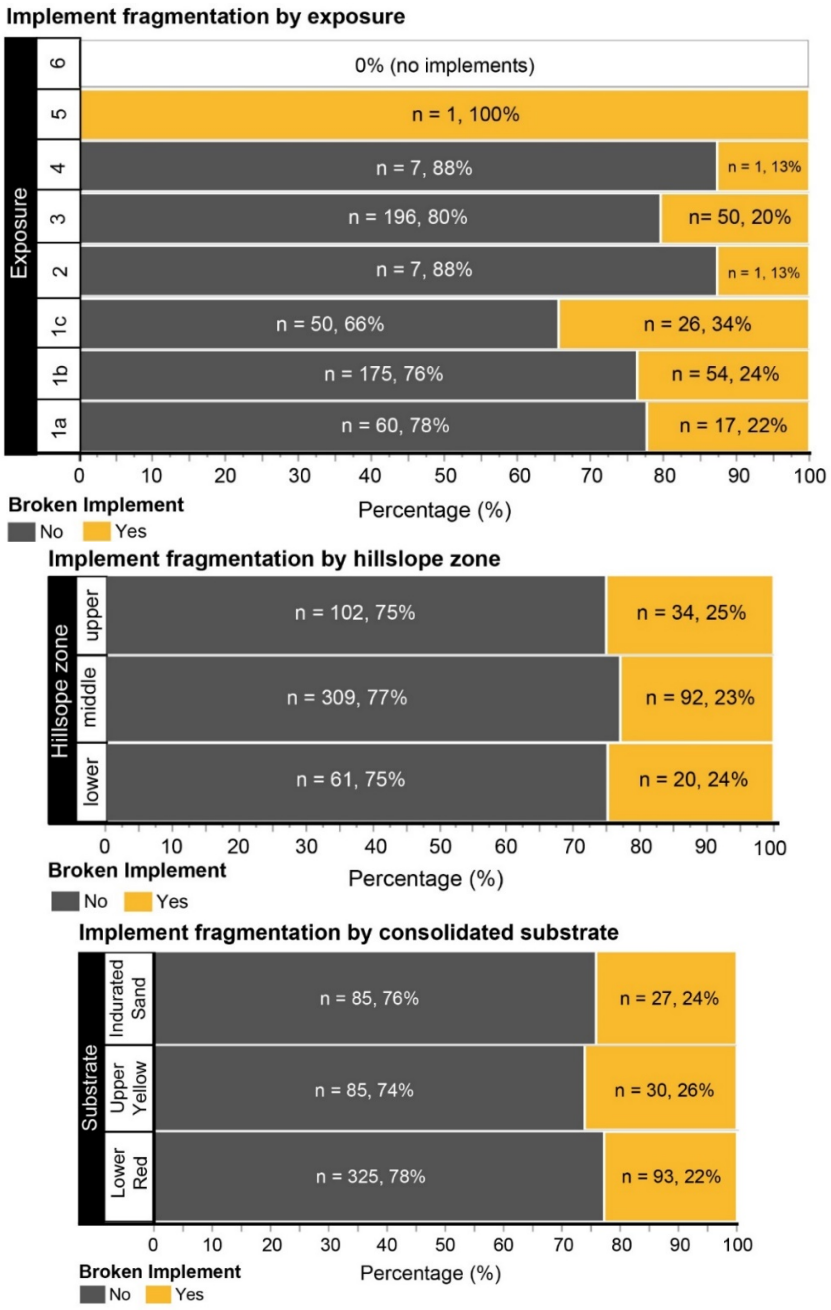

Figure 7.24. Stacked percentage graphs of the relative proportions of intact and broken implements by different hillslope settings (exposure, hillslope zone, substrate), recorded during RNG survey of UPK7.

Table 7.14. Pearson's Chi-square test for independence and significance for implement breakage when implements (n = 603) are considered across different hillslope contexts: exposure (the entire hillslope), hillslope zones (upper, middle, and lower), and substrate units (Indurated Sand, Upper Yellow, and Lower Red). Alpha = 0.05.

Pearson's Chi-Square test for comparing implement breakage by hillslope context

Hillslope context	Df	R^2	test statistic	*p*-value
Exposure 1a, 1b, 1c, 2, 3, 4^	5	0.0103	7.426	0.1908
Upper, middle, lower	2	0.0005	0.349	0.8400
Indurated Sand, Upper Yellow, Lower Red	2	0.0016	1.152	0.5623

^ Exposures with implement counts below 5 (i.e., Exposure 5, and 6) were excluded from analysis

The overall proportion of fragmented flakes (21%; Table 7.15) is similar to broken implements (23%). However, flake fragmentation is significantly different between different exposures (Pearson's Chi-Square: test statistic = 15.676, Df = 3, p-value < 0.001), different hillslope positions (Pearson's Chi-Square: test statistic = 7.938, Df = 2, p-value < 0.05) and different substrates (Pearson's Chi-Square: test statistic = 8.523, Df = 2, p-value < 0.05) (Table 7.16 and Figure 7.25a-c). This suggests that implements vary less in their response to factors causing breakage than flakes. When fragmentation is assessed at the scale of the exposure, the north-east Exposure 3 yields the smallest percentage of broken flakes (11%), showing 10% less fragmentation in this area than the locality-wide average (21%). While the south-west exposure, 1a, and south-east exposure, 1c, are lower than the average fragmentation percentage, but only by < 5%. In contrast, the southern central exposure, 1b, shows 3% more fragmentation than the average.

When examined at the scale of the hillslope zone (i.e., upper, middle, lower) and substrate, fragmentation is highest on lower hillslope zones (47%) and Indurated Sand (42%), than the overall percentage of fragmentation for the locality (21%). Similar proportions of flake breakage are expected between the Indurated Sand and lower zone hillslopes, given that lower hillslopes are largely composed of Indurated Sand (see preceding section and Chapter 6). This result suggests that post-depositional processes catalysing fragmentation were either more intensive on lower hillslopes or that broken artefacts were moved through sheet wash to this zone as a result of their smaller sizes. Furthermore, Upper Yellow fragmentation is 4% lower than the locality-wide percentage for breakage, reflecting Exposure 3's small fragmentation values. These results suggest that the archaeology on the Upper Yellow has been subjected to the least amount of trampling, while artefacts resting on the Indurated Sand and lower hillslopes generally have been subjected to the most fragmentation— particularly on hillslope Exposure 1b.

The south-eastern slope, Exposure 1c, presents the greatest contrast in fragmentation trends between flakes and implements. Implements show the highest percentage of fragmentation on this hillslope than any other. In contrast, there are less broken flakes on this hillslope than on the other exposures. One possibility is that the more pronounced size-sorting observed for this hillslope and the implied sheet wash processes that have impacted this surface have preferentially removed broken flakes more often than broken implements as a result of the larger size of implements (median maximum dimension = 62 mm) compared to broken flakes (median maximum dimension = 19 mm; Figure 7.25).

Table 7.15. The total number and frequency of broken compared to intact flakes^ recorded during rSSQ survey on UPK7's consolidated sediment units*.

Broken flakes^	N	% of Total
No	681	79%
Yes	180	21%
Total	861	100%

^ Intact flakes = complete, bipolar, longitudinal splits; broken flakes = proximal flakes
* For flakes found on Indurated sand, Lower Red units, Upper Yellow units only

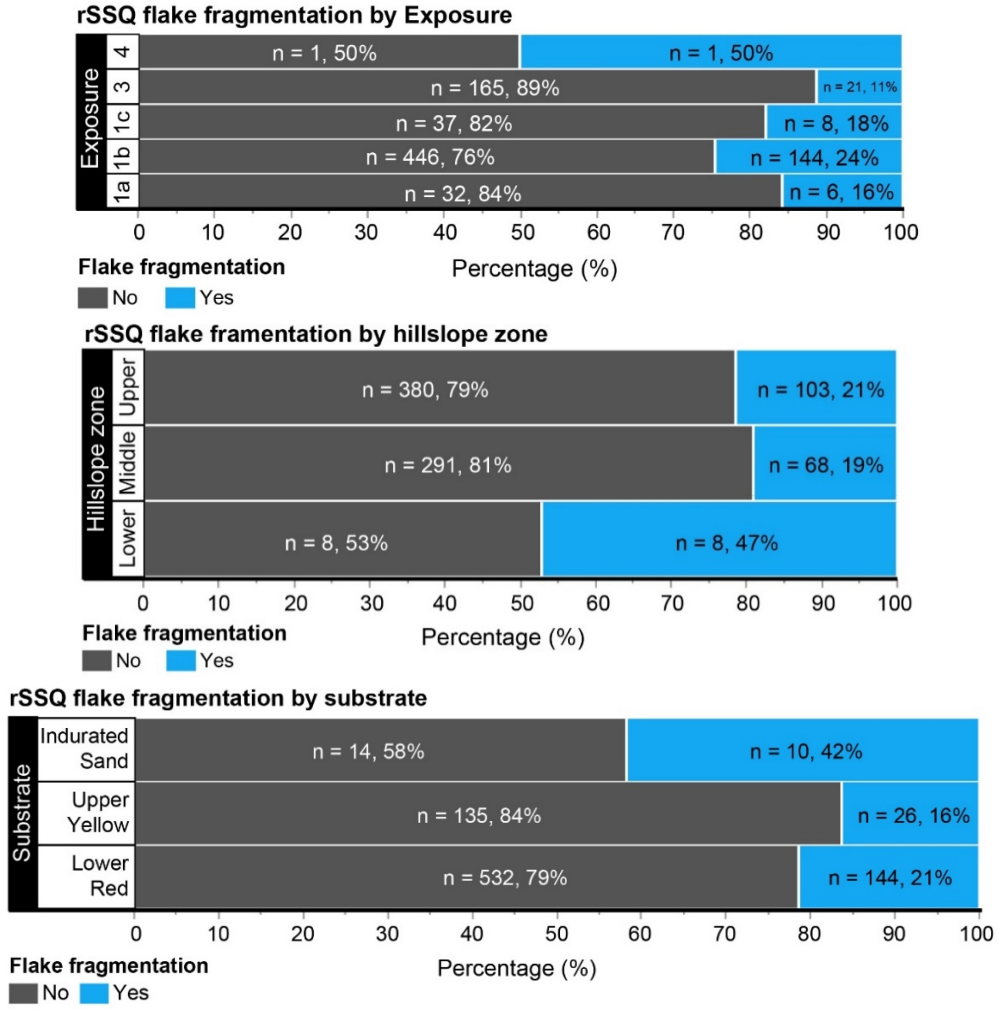

Figure 7.25. Stacked percentage graphs of the relative proportions of intact and broken flakes by different hillslope settings (exposure, hillslope zone, substrate), recorded during rSSQ survey of UPK7.

Table 7.16. Pearson's Chi-square test for independence and significance for flake breakage* when flakes (n = 861) are considered across different hillslope contexts: exposure (the entire hillslope), hillslope zones (upper, middle, and lower), and substrate units (Indurated Sand, Upper Yellow, and Lower Red). Alpha = 0.05. Significant contingency in bold.

Hillslope context	Df	R^2	test statistic	*p*-value
Exposure 1a, 1b, 1c, 2, 3, 4^	3	0.0195	15.676	0.0013
Upper, middle, lower	2	0.0076	7.938	0.0189
Indurated Sand, Upper Yellow, Lower Red	2	0.0087	8.523	0.0141

*intact flakes = complete, bipolar, longitudinal splits; broken flakes = proximal flakes
^Exposures with <5 flakes were excluded from analysis

7.6.2. Weathering

Hornfels artefacts were selected to examine weathering across the locality. Their dominance—second to quartzite—and their visually discernible sensitivity to weathering (Sandy & Cole 1982) make them a useful proxy for determining variation in the degree and relative duration of exposure across multiple hillslopes and substrate units. Table 7.17 shows that most hornfels artefacts are patinated (77%), while edge rounding was observed on 33% of hornfels artefacts. In contrast, only a small percentage of artefacts show heavy weathering, in the form of discolouration (5%) and decay (6%) (Table 7.17). To determine if each type of artefact weathering, and thus the relative duration of exposure, is spatially organised across the locality, the location of hornfels artefacts—with (yellow markers) and without (black markers) each type of weathering—are presented in the comparative map series of Figure 7.23 and Table 7.18. The dominance of patination is apparent for both high- and low-density areas—affecting hornfels artefacts across all areas of UPK7's exposed, consolidated sediment (i.e., exposure, hillslope position, substrate age).

Table 7.17. The number and percentage of hornfels artefacts that do or do not show signs of weathering. There are four categories of weathering: Edge rounding, patination, discolouration, and decay. Each type is presented separately. However, only the three different stages of surface condition are treated as mutually exclusive.

Weathering	No		Yes		Total	
	N	%	N	%	N	%
Edge condition						
Edge Rounding	871	67%	432	33%	1303	100%
Surface condition						
Patinated	298	23%	1005	77%	1303	100%
Discolouration	1237	95%	66	5%	1303	100%
Decayed	1230	94%	73	6%	1303	100%

Table 7.18. Comparison of the observed count and percentage of hornfels artefacts (n = 1299) with weathering for each hillslope context. Expected counts are shown in parentheses.

Exposure	Edge rounded (obs n, % [exp n])	Patinated (obs n, % [exp n])	Discoloured (obs n, % [exp n])	Decayed (obs n, % [exp n])
1a	43, 27% (52.9)	109, 69% (122.6)	4, 3% (8)	17, 11% (8.9)
1b	213, 40% (176)	423, 80% (408)	30, 6% (26.9)	38, 7% (29.7)
1c	56, 43% (43.2)	93, 72% (100)	19, 15% (6.6)	7, 5% (7.3)
2	44, 52% (27.9)	79, 94% (65)	2, 2% (4.3)	0, 0% (4.7)
3	67, 19% (119)	273, 76% (276)	7, 2% (18.2)	5, 1% (20.5)
4	9, 23% (13)	25, 64% (30)	4, 10% (2)	15%
Total observed (n, %)	432, 33%	1002, 77%	66, 5%	73, 6%
Hillslope zone				
Upper	105, 40% (86)	203, 77% (201.9)	18, 7% (13.2)	15, 6% (15.5)
Middle	250, 32% (255)	599, 77% (598)	37, 5% (39)	49, 6% (46)
Lower	49, 25% (63.1)	146, 76% (148)	7, 4% (10)	9, 5% (11.4)
Total observed (n, %)	404, 33%	948, 77%	62, 5%	73, 6%
Substrate				
Indurated Sand	47, 26% (60)	128, 71% (139.6)	8, 4% (9)	11, 6% (10.2)
Upper Yellow	96, 39% (82)	202, 82% (190.5)	13, 5% (12.5)	3, 1% (13.9)
Lower Red	289, 33% (289.6)	672, 77% (671.9)	45, 5% (44)	59, 7% (48.9)
Total observed (n, %)	432, 33%	1002, 77%	66, 5%	73, 6%

There is also a significant difference in the percentage of edge rounded artefacts between hillslope zones and substrate units (p-value <0.05), with hornfels artefacts showing more edge rounding in the high-density areas on the upper hillslope zones (40%), on the Upper Yellow (39%) and the Lower Red (33%), substrate than there are on middle and lower hillslopes, on surfaces of the Indurated Sand (Table 7.19). While hornfels artefacts with light patination dominate all areas relative to those without patination, there is significant variation in the percentage of patinated artefacts between different exposures and substrates. Hornfels artefacts in the easternmost exposure, 2, show the highest percentage of patination (94%), followed by the south central and south-east exposures, 1b (86%) and 1c (82%). While the northern Exposure 4 and south-west exposure, 1a, show the least amount of patination (67% and 70%, respectively) (Table 7.19).

Table 7.19. Chi-square tests for independence.

Chi-square test for independence between hillslope Exposures 1a, 1b, 1c, 2, 3, and 4 (Df = 5)

Artefact weathering	R^2	Pearson Chi-square	p-value*
Edge rounded	0.044	69.9	< 0.0001
Patinated	0.023	28.9	< 0.0001
Discoloured	0.062	37.7	< 0.0001
Decayed	0.071	34.2	< 0.0001

*Alpha = 0.05

Chi-square test for independence between upper, middle, and lower hillslope zones (DF = 2)

Artefact weathering	R^2	Pearson Chi-square	p-value*
Edge rounded	0.0071	11.053	0.004
Patinated	0.0001	0.168	0.919
Discoloured	0.0054	2.740	0.254
Decayed	0.0014	0.762	0.683

*Alpha = 0.05

Chi-square test for independence between Indurated Sand, Upper Yellow, Lower Red (Df = 2)

Artefact weathering	R^2	Pearson Chi-square	p-value*
Edge rounded	0.0048	7.838	0.020
Patinated	0.0051	7.249	0.027
Discoloured	0.0004	0.194	0.908
Decayed	0.027	11.296	0.004

*Alpha = 0.05

There are similar numbers of artefacts with discolouration and decay (Table 7.17). However, their point patterns are different for each hillslope (Table 7.18). The southern hillslopes of Exposure 1b and c show the highest frequencies of hornfels artefact discolouration and decay. However, there are more artefacts showing decay on the upper hillslopes of Exposure 1a than those that show discolouration. There are also more artefacts that show discolouration on the upper and middle zone of Exposure 1c than there are decayed artefacts. On Exposure 1b discoloured artefacts appear loosely scattered across the upper and middle hillslope zones, while decayed artefacts occur in greater numbers along the high-density middle hillslope zone of Exposure 1b, which extends westward into Exposure 1a, on the Lower Red.

Considered by substrate unit, Lower Red sediment shows a high number of discoloured and decayed artefacts across Exposures 1a, 1b, 1c, 4. The Upper Yellow sediment has similar, but low, numbers of discoloured and decayed artefacts across each hillslope, except Exposure 2, in which discoloured hornfels occurs, but not artefacts in a decayed condition (Figure 7.23d,e). These results suggest artefacts on hillslopes of the Indurated Sand have been exposed for the shortest duration. Artefacts that occur on Upper Yellow sediment, which also occupy the upper hillslope zones of Exposure 1b, 3 and all of Exposure 2, have undergone less exposure compared to artefacts on Lower Red sediment. However, the lack of decayed hornfels on the Upper Yellow sediments of Exposure 2 compared to 3, suggest that artefact decay is related to the different exposure and/burial of artefacts, rather than the collective maximum age of the underlying substrate. Considered together, differences in longer-term artefact weathering between exposures, hillslope zones, and substrate units suggest that artefacts on Lower Red sediment have been exposed to more wet-dry cycles than artefacts on the Upper Yellow and Indurated Sand. This suggests that

artefacts found on these substrate units are related to both the age of the deposit and the timing of its exposure.

7.7. Association Between Artefact Spatio-Temporal Patterning and Substrate Age

7.7.1. Artefact abundance and substrate unit

To determine if the spatial distribution and age of artefacts across UPK7's consolidated sediments are constrained by the age of their underlying deposit, artefact frequency and inferred artefact age are examined in relation to deposit type. Table 7.20 compares the relative proportions of artefacts to their expected proportions given the extent of each exposed substrate unit (Indurated Sand, Upper Yellow, and Lower Red). The expected proportion of artefacts on each substrate is determined by the proportion of the total consolidated surface area (11,467 m^2) a given substrate surface holds, e.g., Indurated Sand accounts for 63% of the total consolidated surface area at UPK7. Based on this proportion, 63% of the total artefact count is expected on this surface—assuming that artefacts are distributed evenly across consolidated sediment, irrespective of the underlying substrate unit (see Table 7.20).

Table 7.20. Expected proportions of artefacts on consolidated substrate units (chi-squared = 3300, df = 2, p-value <0.0001)

	Surveyed area		Artefacts			
Substrate unit	m^2	Proportion	Count	Proportion	Expected	Standardized Residuals
Indurated Sand	7192	0.63	729	0.19	2389	-55.83
Upper Yellow	576	0.05	587	0.15	190	29.61
Lower Red	3700	0.32	2476	0.65	1213	43.95
Total	11467	1.00	3792	1.00	3792	

Artefact frequencies are found to be significantly different between each substrate (chi-squared = 3300, df = 2, p-value <0.0001), rejecting the null hypothesis that variation in artefact frequency between substrate types is the product of chance (Table 7.20). Artefact frequencies on Indurated Sand are well below the value expected for this context, returning a standardized residual of -55.83 (Table 7.20). In contrast, Lower Red and Upper Yellow both return large positive residuals (43.95 and 29.61, respectively), indicating that artefact frequencies are much higher than expected if independent from substrate type. Lower Red sediment also yields a larger standardized residual compared to Upper Yellow, indicating a stronger positive association.

7.8. Inferred Age by Consolidated Substrate Unit

7.8.1. Association between archaeological epoch and substrate age

The following analysis assesses the location and frequency of diagnostic artefacts—at the temporal scale of the archaeological epoch—in relation to each substrate unit and the depositional age it represents. Table 7.21 and Figure 7.26 separates diagnostic artefacts into their associated archaeological epochs (MSA, LSA and Neolithic) and presents their proportional frequencies by substrate unit. The Pearson's chi-squared goodness-of-fit test was used to assess whether the inferred age of artefacts have a higher probability of being different between each consolidated substrate unit or if they are distributed equally across these surfaces. The null hypothesis is that artefact age is independent of substrate extent and will show similar frequencies across all substrate units. Artefacts identified as temporally undiagnostic or that have sample sizes under five artefacts (i.e., ESA and Historic period) were excluded from analysis (see Table 7.21).

Table 7.21. Comparison of artefact counts and conditional frequencies across each consolidated deposit (Lower Red, Upper Yellow, and Indurated Sand), by archaeological epoch (MSA, LSA, Neolithic). The values pertaining to n and its associated proportion for each archaeological epoch are observed values. The expected n is calculated by multiplying the total observed n for each archaeological epoch by the proportion of surface area each substrate unit covers within the RNG survey area (11467 m2): Lower Red (3700 m2) = 0.32; Upper Yellow (576 m2) = 0.05; Indurated Sand (7192 m2) = 0.63.

		Archaeological Epoch		
Substrate unit		MSA	LSA	Neolithic
Lower Red	Observed n (col %)	602 (83)	255 (55)	60 (47)
	Expected n[a.] (%)[b.]	233 (32)	148 (32)	41 (32)
	Standardised residual[c.]	24.17	8.80	2.78
Upper Yellow	Observed n (col %)	68 (9)	135 (29)	28 (22)
	Expected n[a.] (%)[b.]	36 (5)	23 (5)	6 (5)
	Standardised residual[c.]	5.33	23.35	8.98
Indurated Sand	Observed n (col %)	57 (8)	74 (16)	41 (32)
	Expected n[a.] (%)[b.]	458 (63)	292 (63)	81 (63)
	Standardised residual[c.]	-18.74	-12.76	-4.44
Epoch Total	Observed n (col %)	727 (100)	464 (100)	129 (100)
	Chi-squared (df = 2)	965.09	778.23	100.44
	p-value	< 0.001	< 0.001	< 0.001

[a.] Expected n = total artefact count for an archaeological epoch multiplied by the proportion of a substrate's surface area
[b.] Expected % = proportion of a substrate's surface area
[c.] Standardized residual = (observed count – expected count) / √expected count.

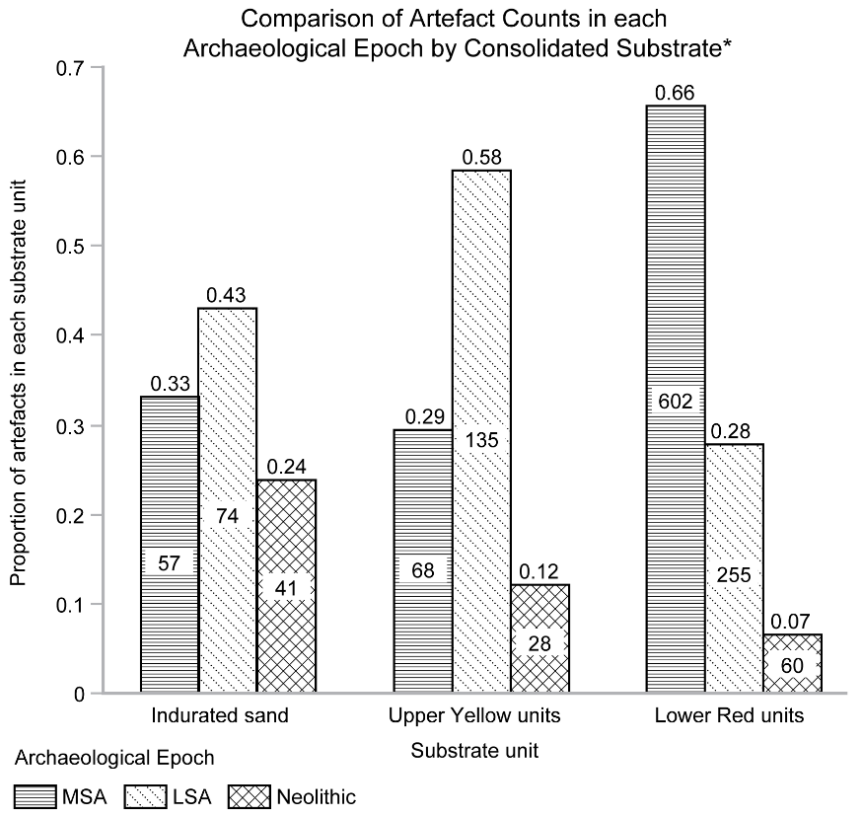

Figure 7.26. Comparison of artefact frequencies between archaeological epochs within each consolidated substrate. *Artefacts excluded from this graph include undiagnostic artefacts ('indeterminates') and artefacts associated with the ESA and Historic period. ESA and Historic artefact samples sizes are too low to be visually informative.

All three archaeological epochs returned statistically significant (p-values <0.05) chi-squared statistics (MSA: chi-squared = 965.09, df = 2, p-value < 0.000*; LSA: chi-squared = 778.23, df = 2, p-value < 0.000*; Neolithic: chi-squared = 100.44, df = 2, p-value < 0.000*), rejecting the null hypothesis. This indicates that there is a high probability (>95% confidence) that an artefact's archaeological epoch is associated with the substrate it occurs on.

All archaeological epochs occur on the Lower Red and Upper Yellow units with higher-than-expected proportional frequencies than if there was independence between artefact and substrate unit. There is a stronger positive association between the Lower Red unit and MSA artefacts (standardized residual = 24.2), than there is for LSA (standardized residual = 8.8) and Neolithic artefacts (standardized residual = 2.78; Table 7.21). In contrast, there is a stronger positive association between the Upper Yellow unit and LSA artefacts (standardized residual = 23.35) than there is for MSA and Neolithic artefacts (Table 7.21). In every case, the observed count of MSA, LSA, and Neolithic artefacts on the IS fell well below the expected amount given the large, exposed area that this substrate covers (Table 7.21), resulting in strong negative association between archaeological epoch and sediment unit. The strength of their standardised residuals also increases with the age of the epoch—Neolithic artefacts have the weakest association with IS while MSA artefacts have the strongest negative association with this unit. A pattern that is in line with the age of the sediment unit relative to the inferred age of the artefacts.

7.8.1.1. MSA artefacts

The relationship between the discard age of UPK7's surface archaeology and the depositional age of an underlying substrate unit follow the law of superposition. MSA artefacts have a strong association with the oldest consolidated deposit at the locality (Lower Red unit, >47 ka; Table 7.21 & Figure 7.26). Moreover, the percentage of MSA artefacts and the size of their standardized residuals is substantially lower on the younger substrates of Upper Yellow and Indurated Sand (see Table 7.21). Overall, the positive association between MSA artefacts and the Lower Red and Upper Yellow units suggest that depositional order influences the spatial organisation of MSA archaeology across this locality. This is further supported by the strong negative association between MSA artefacts and the Indurated Sand unit (see Table 7.21). The small number of MSA artefacts that do occur on the Indurated Sand unit (n = 57, 8%) are at odds with this pattern and could be the outcome of relocation, either by anthropogenic or environmental factors. This reasoning also applies to the small number of MSA artefacts found on the Upper Yellow unit.

7.8.1.2. LSA artefacts

All three substrate units were deposited during or prior to the LSA (> 30 ka) and thus are expected to yield LSA archaeology, provided that each unit was exposed during this time and not removed wholesale. This pattern is evident in Table 7.21, with LSA artefacts occurring on all three units (Figure 7.26). The proportion of LSA artefacts increases with substrate age, with 55% occurring on the Lower Red, 29% on the Upper Yellow, and 16% on the Indurated sand unit (Table 7.21). However, the proportion of artefacts relative to the size of its underlying substrate shows that the Upper Yellow unit yields more than double the expected amount of LSA artefacts compared to the Lower Red unit. This suggests that a stronger relationship exists between LSA artefacts and the Upper Yellow sediment than it does for the older Lower Red deposit.

Moreover, the distribution of LSA artefacts across each surface suggests differential exposure and erosion in relation to topographic position. For example, the density of LSA artefacts is highest at the top of the slope of Exposures 1b and 3 where the Upper Yellow sediment immediately overlies the Lower Red sediment (Figure 7.26). This suggests that LSA artefacts are eroding out of the Upper Yellow deposit and onto the Lower Red unit, thus increasing their frequency on the older deposit.

7.8.1.3. Neolithic artefacts

The highest observed frequency of Neolithic artefacts occurs on the oldest and youngest consolidated substrate units (Table 7.21, Figure 7.26). However, when considered as proportional frequencies of each substrate's relative surface area, Table 7.21 indicates that the highest proportional frequency of Neolithic artefacts is associated with the Upper Yellow unit, with less than expected frequencies on the Indurated Sand. High proportional frequencies on the Upper Yellow unit suggests that this surface was exposed during the Neolithic period (sometime in the last 1.7 to 0.2 ka). Once, again, the standardised residuals for each substrate unit suggest a stronger association between Neolithic artefacts and the Upper Yellow unit, and possibly reflect indirect occurrence on the oldest and youngest units by way of deflation and runoff.

7.9. Association Between Industries and Substrate Age

The following investigates whether there is an association between the location of artefacts assigned to the MSA and LSA Industries and the age/location of each consolidated sediment unit. Based on the inferred age of each Industry (see Table 5.4), the burial ages of the Indurated Sand and Upper Yellow, and the minimum burial ages for the Lower Red (see Table 6.9), a series of expectations are posed (all inferred age ranges quote local sequences unless unavailable, see Table 5.4):

1. The Early MSA, Still Bay, Howiesons Poort and post-Howiesons Poort accumulated on sediment prior to the formation of the oldest burial age for the Upper Yellow (47.2 ± 3 ka). Therefore, they are expected to have a stronger association with the LR, than the UY and IS.
2. The accumulation of artefacts assigned to the Late MSA (~33-50 ka, see Table 5.4) coincided with the formation of the UY (between ~37 and ~50 ka) and/or the IS (between ~34 and ~29 ka). If the former, then Late MSA artefacts are expected to be exposed on the LR through the erosion of the UY. If the latter, Late MSA artefacts are expected to have a stronger association with the UY, through the erosion of the IS.
3. The accumulation of artefacts assigned to the Early LSA (~22-25 ka), Robberg (~16-22 ka), Oakhurst (13-17 ka) and Wilton (~4-6 ka) occurred after the formation of the IS. Therefore, LSA Industries are expected to have a stronger association with the IS than the UY and LR.

Based on these expectations, it is hypothesised that the location of exposed artefacts assigned to a specific Industry are associated with sediment units that predate their discard. The null is that the location of Industry-diagnostic artefacts is independent of substrate type and age.

When presented as a contingency table and graph (Table 7.22 and Figure 7.27), the IS shows the lowest artefact counts across all Industries and was excluded from further significance tests due to its low values (<5 in most cases). The low frequencies for all Industries on the IS is expected for artefacts assigned to Industries that predate the IS (i.e., Still Bay, Howiesons Poort, and post-Howiesons Poort). The rare occurrence of these Industries on the IS suggests relocation from older sediment unit's upslope of their current positions. Based on the preceding analyses of hillslope size-sorting and condition, their displacement likely occurred as a result of horizontal movement from runoff.

In contrast, the low frequencies of LSA Industries on the IS compared to their high positive association on the UY and LR is unexpected given that they post-date the formation of the IS. However, their stronger spatial association with the older sediment units occurs in the upper zones of the sand mantle's hillslopes, where horizontal dispersion is less pronounced than on the IS, and mid to lower hillslope zones generally. Moreover, the vertical displacement of younger artefacts onto more recently exposed, older units is actively taking place in the upslope areas as erosion cuts back into the leeside of the northern and eastern dunes—providing one explanation for the strong association between these Industries and the UY and LR.

Table 7.22. The number and frequencies (% in brackets) of artefacts assigned to each Industry listed by sediment unit.

Industry	Substrate			Total
	Indurated sand	Upper Yellow	Lower Red	
Early MSA	0	0	1 (100)	1
Still Bay	1 (5)	4 (21)	14 (74)	19 (100)
Howiesons Poort	0 (0)	2 (18)	9 (82)	11 (100)
Post-HP	0 (0)	3 (6)	46 (94)	49 (100)
Late MSA	7 (8)	7 (8)	78 (85)	92 (100)
Early LSA	0 (0)	41 (84)	8 (16)	49 (100)
Robberg	5 (16)	5 (16)	22 (69)	32 (100)
Oakhurst	7 (12)	14 (24)	38 (64)	59 (100)
Wilton	0 (0)	17 (44)	22 (56)	39 (100)
Total	20 (5)	93 (25)	238 (64)	351 (100)

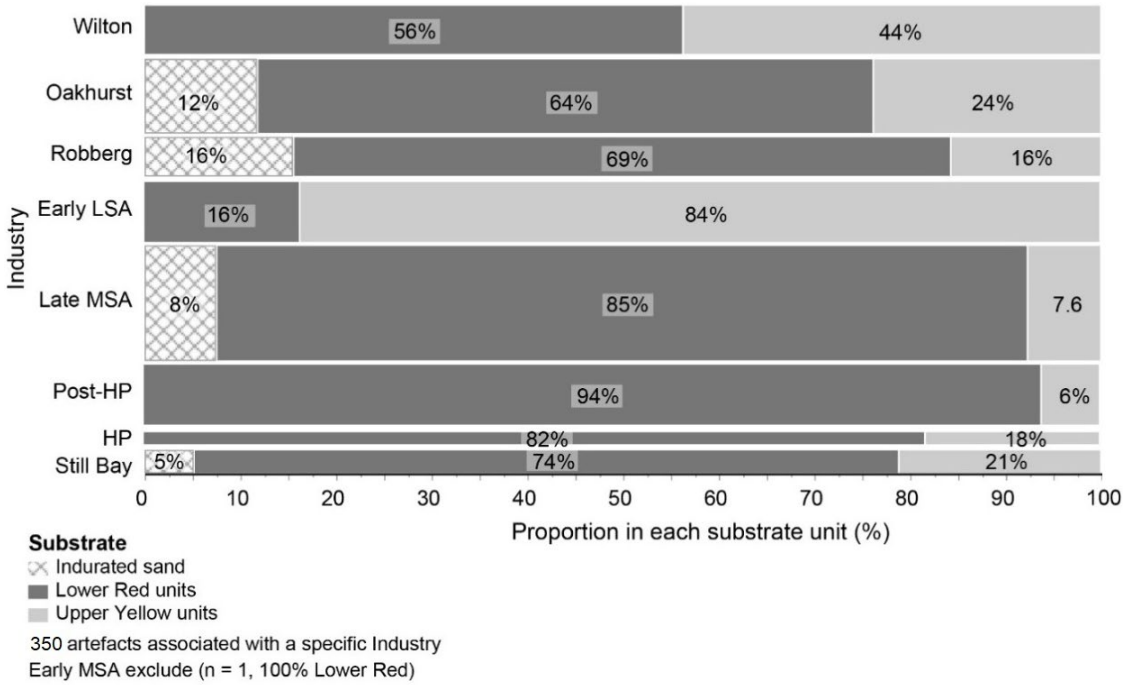

Figure 7.27. The proportion of artefacts identified on each consolidated sediment unit, grouped by Industry.

Contingency analysis was performed for all archaeological Industries with more than one artefact in each sediment unit to determine if there is a significant and/or strong association between each Industry and the underlying sediment units UY and LR (see Table 7.23). There is a significant difference in the spatial occurrence of Industries between these two sediment units (Pearson $\chi^2 = 109.76$, df = 7, $p < 0.0001$), indicating that the location of Industry-specific artefacts depends on the location and possible age of the underlying deposit—rejecting the null hypothesis for independence. Adjusted Residuals were also calculated to provide further insight into the main Industries influencing this significant result and to assess the strength of association between each Industry and the sediment units UY and LR. According to

Agresti(2003) an adjusted residual that is greater than ± 2 indicates an association between variables, while values less than ± 2 will lack distinction between variables.

Industries with random spatial distributions—the Still Bay, Howiesons Poort, and Robberg (see above)—are no more or less associated with the UY or LR (Table 7.23). For the Still Bay and Howiesons Poort this is unexpected given their inferred ages. However, this result coupled with their random point pattern further supports the inference that both Industries have been subjected to post-depositional disaggregation.

Table 7.23. Contingency analysis of Archaeological Industries by Sediment Unit (Pearson $\chi 2 = 109.76$, df = 7, $p < 0.0001$). Adjusted Residuals that show a lack of fit with the null (> ± 2, Agresti 2013) are presented in bold.

		Archaeological Industry								
Substrate		**SB**	**HP**	**PHP**	**LMSA**	**ELSA**	**R**	**O**	**W**	**Marginals**
Upper Yellow	Obs	4	2	3	7	41	5	14	17	93
	Exp	5.1	3.1	13.8	24.0	13.8	7.6	14.7	11.0	
	Column %	22.2	18.2	6.1	8.2	83.7	18.5	26.9	43.6	
	Residual	-1.1	-1.1	-10.9	-17.0	27.2	-2.6	-0.7	6.0	
	Std. Res	-0.5	-0.6	-2.9	-3.5	7.3	-0.9	-0.2	1.8	
	Adj. Res	-0.6	-0.7	-3.7	-4.7	9.4	-1.2	-0.2	2.3	
Lower Red	Obs	14	9	46	78	8	22	38	22	237
	Exp	12.9	7.9	35.2	61.1	35.2	19.4	37.3	28.0	
	Column %	77.8	81.8	93.9	91.8	16.3	81.5	73.1	56.4	
	Residual	1.1	1.1	10.8	17.0	-27.2	2.6	0.7	-6.0	
	Std. Res	0.3	0.4	1.8	2.2	-4.6	0.6	0.1	-1.1	
	Adj. Res	0.6	0.7	3.7	4.7	-9.4	1.2	0.2	-2.3	
	Marginals	18	11	49	85	49	27	52	39	330

Adjusted standardised residuals >+/-2 indicates a lack of fit of the null hypothesis (in bold, (Agresti 2003)); Adjusted residuals in bold are those that exceed +/- 2. Industry Abbreviations: ELSA = Early LSA, EMSA = Early MSA, HP = Howiesons Poort, LMSA = Late MSA, O = Oakhurst, PHP = post-Howiesons Poort, R = Robberg, SB = Still Bay, W = Wilton; Adj. Res = (Obs - Exp) / SQRT(Exp*(1-RowMarginal/n)*(1-ColumnMarginal/n); Std. Res = (Obs - Exp) / SQRT of Exp

There is also no distinction between the UY and LR for artefacts assigned to the Oakhurst, despite their clustered spatial pattern at the top of the sediment (Table 7.23). Thus, the rarity of Oakhurst on IS and its lack of an association with any one sediment unit predating the IS further supports the inference that Oakhurst artefacts have relocated to the lower slopes of the IS after their initial discard onto exposed LR and UY, or a now deflated deposit that overlay both sediment units. In contrast, artefacts assigned to the MSA Industries, post-Howiesons Poort and Late MSA, have strong positive associations with the LR (*respective Adjusted residuals = 3.7 and 4*) and strong negative associations with the the UY (*respective Adjusted residuals = -3.7 and -4*, Table 7.23). The opposite is evident with the LSA Industries, Early LSA and Wilton that are positively associated with the UY and negatively associated with the LR. Moreover, artefacts assigned to the Early LSA show one of the strongest associations in the dataset (Table 7.23).

The positive association between post-Howiesons Poort artefacts and the LR is expected. The negative association between Late MSA artefacts and the UY suggests that these artefacts were discard during the accumulation of the UY or exposure of the LR, prior to the formation of the IS (Table 7.23). The strong positive association between Early LSA artefacts and the UY is unsurprising given the mostly

isolated occurrence of Early LSA artefacts on the eastern hillslope of Exposure 2. However, its lack of association with the IS and strong association with the UY suggests that Early LSA artefacts accumulated either on younger deflating sediment above the current surface of the UY or were discarded directly onto an exposed UY surface. The condition of these artefacts suggests they have been subjected to some abrasion and short-term cycles of wet and dry conditions while showing minimal effects from runoff. The lack of evidence for post-depositional movement, while showing signs of in situ weathering (i.e., edge rounding and patination), suggests that they have accumulated on the UY possibly through younger unconsolidated sediment. The rarity of younger Industries, including Neolithic artefacts, in this area also suggests that Early LSA artefacts were buried prior to the discard of Robberg or younger material and exposed to this surface level after the Neolithic.

The negative association between artefacts assigned to the Wilton and the LR is expected given the Holocene age of this Industry. However, again, the rarity of Wilton on the IS and its positive association with the UY suggest that processes other than deposit age are influencing the distribution of artefacts assigned to this Industry. Its clustered occurrence on the UY, at the top of the sand mantle and in its upper hillslope zones support the inference that artefacts in this area have retained horizontal integrity while their absence on the IS suggests that sediment and artefacts post-dating the IS have been removed from this area. The presence of Neolithic artefacts across the IS suggests that the removal of artefacts older than ~3.6 ka happened prior to the Late Holocene. It is also possible that the small size of Wilton artefacts made them more susceptible to runoff on the slopes of the IS. This is supported by the dominance of larger classes of stone artefacts across this sediment unit (i.e., cores, grindstones, anvils, hammerstones).

CHAPTER 8.
DISCUSSION

8.1. Introduction

The preceding chapters investigated the formation and geochronology of UPK7's sediment units, followed by an examination of the spatial distribution, composition, and condition of surface archaeology in relation to this depositional context. The objective of this chapter is to (1) bring together and explore the association between these three areas of study, (2) to address the published interpretations for UPK7 in light of these findings, and (3) to discuss UPK7's depositional history in relation to the history of regional and catchment scale palaeoenvironmental and anthropogenic change.

8.2. Depositional History of UPK7

The accumulation of UPK7's artefact-bearing sandy sediment spans at least 80 ka of seasonal aeolian deposition, differential stabilisation, exposure and erosion. The main processes of that catalyse or contribute to sediment and artefact movement identified for all deposits are sheet wash, trampling and winnowing. The impact of these processes on the archaeology varies depending on sediment consolidation, topographic setting, vegetation coverage and the amount of activity in a particular area at any given time. These processes have thus affected the distribution and condition of overlying archaeology to varying degrees over time and across the locality. The following depositional history is organised chronologically from the oldest to the youngest deposit, set heuristically at the scale of the Marine Isotope Stages. This enables subsequent discussion about UPK7's formation history in relation to its regional history of palaeoenvironmental change and human-environment interaction.

8.2.1. Potential conditions for artefact movement

Artefacts discarded onto loose or partially consolidated sand during the initial formation of the Lower Red, Upper Yellow and Indurated Sand units, may have experienced as much as ~200 mm of vertical displacement as a result of small and large mammal trampling (see Chapter 6; e.g., Eren et al. 2010). The continued accumulation of younger overlying sands or repeated trampling of artefacts would result in their burial, effectively reducing subsequent horizontal movement and the general disaggregation of an artefact scatter (Forssman & Pargeter 2014). Artefacts that settle on harder underlying sediment are likely to remain in their place of repose for longer than artefacts on or throughout loose and semi-consolidated sands, provided they remained buried (Phillips et al. 2019).

In their current exposed state, the consolidated sediment bodies of Indurated Sand, Upper Yellow and Lower Red are lithified, providing hard, weathered surfaces, with minimal vegetation cover that increases the visibility of overlying artefacts and their susceptibility to entrainment. These deposits are more resistant to runoff and wind deflation than the unconsolidated and semi-consolidated sands. Once exposed all consolidated deposits share similar responses to rainfall erosion (i.e., sheet and slope wash erosion and subsequent rill development)—with the Lower Red sediment possibly being more resilient than the sandy and sandy loam units of the Upper Yellow and Indurated Sand. Trampling can also break up the

crusted surface of these deposits, making them more vulnerable to both wind and rainfall erosion. Thus, while an exposed, crusted surface promotes artefact visibility, artefact exposure also increases their vulnerability to erosional forces.

Through experiment and simulation of artefact exposure and movement on the hillslopes of Indurated Sand, Phillips et al. (2019) found that more artefacts moved during a period immediately following the initial discard on consolidated sediment than in subsequent years, slowing to a steadier rate thereafter. One property of the crusted sediment that helped to slow this movement was the development of vesicles between the surface lithic and its underlying sediment creating temporary adhesion between the two surfaces—observed for all lithic classes. This suggests that after a wetting-event, artefacts exposed on consolidated sediment have an additional level of resistance to subsequent sheetwash events and wind erosion so long as their adhesion to the sediment directly beneath them remains intact. Trampling and heavy enough rainfall will undoubtedly dislodge this connection. However, sheetwash processes tend to pedestal these artefacts first before undercutting results in the artefacts imbrication, lag and further horizontal entrainment.

Phillips et al. (2019) also showed that crusted, bare-earth, consolidated surface conditions on slopes between 10 and 11° can catalyse assemblage entrainment resulting in the removal of ~47% of artefacts beyond 5 m of their original discard within the first 100 years of exposure. This nearly doubles to 86% within 1000 years of discard, followed by complete removal beyond 5 m of place of original discard, over a period of 10,000 years. Thus, it is reasonable to predict that, under similar surface conditions, clusters of diagnostic artefacts with inferred ages older than 10,000 years recorded on exposed substrate equivalent to, or older than this age were exposed recently or only intermittently over the many millennia following their initial discard.

With these factors in mind, artefacts currently exposed on consolidated sediment are expected to be younger than the consolidation of the sediment body, unless they were moved from an older deposit (e.g., through reuse, animal kicking and/or sheet wash entrainment). The latter scenario would be possible if the upslope deposit were older in age and exposed older artefacts than the downslope deposit. Any exposed sediment is prone to sheet wash erosion. Therefore, if artefacts were discarded directly onto an exposed, hardened sediment and remained exposed to multiple wet-dry seasonal cycles, their spatial patterning is expected to show:

- Size-sorting where slope angles are greater than 9° (i.e., the middle zone of the southern hillslope).
- Low densities where slope angles are greater than 15º (i.e., densely rilled areas or transition zones from residual often vegetated substrate to bare-earth).
- High rates of weathering (patination and discolouration).
- A general spatial pattern of disaggregation.

Thus, areas with high densities, low rates of weathering, and clustered distributions of diagnostic artefacts—particularly those containing artefacts more than 10 ka in age—will be interpreted as the result of both rapid burial and relatively recent exposure.

Given the history of substrate formation and exposure outlined in the preceding sections, Table 8.1 sets out four scenarios that could lead to the current state of substrate exposure at UPK7: Scenario 1.

Exposure between the formation and subsequent burial by a younger deposit; Scenario 2. Progressive erosion initiating from formation of the youngest unit the end of MIS 3 (~30 ka); Scenario 3. Exposure since the advent of indigenous pastoralism (post-2 ka); and Scenario 4. Exposure since the introduction of European farming methods (post-0.3 ka). While each scenario is a simplification of a more complex formation history, their purpose is to draw out differences and help to identify the most plausible scenario(s) for the sequential development of UPK7's geoarchaeological formation.

Table 8.1. Four scenarios that could lead to the current state of substrate exposure at UPK7.

Scenario 1.		Exposure between cessation of substrate formation and subsequent burial by a younger deposit				
Scenario description		The location of each substrate and the extent of their exposed surfaces has remained the same since their deposition and partial burial by a younger deposit.				
Substrate		Lower Red unit (LR)	Upper Yellow unit (UY)		Indurated Sand unit (IS)	Unconsolidated Sand unit (UCS)
Unit		4	3a	3b	2	1
Depositional history		The oldest consolidated sediment body. Deposited any time before the deposition of UY [unit 3a])	Deposited at 47 ka on south slope [unit 3a] and 40 ka on east slope [unit 3b]; after LR [unit 4a/b] and Before IS [unit 2]		Deposited 32-30 ka on south slope	Deposited at least 70 years ago
Scenario specific history		Exposure over large area from >47 ka to present	Exposure from 47 ka to present (from mid MIS3)	Exposure from 40 ka to present (from late-MIS3)	Exposure from 30 ka to present (from MIS 2)	Exposure from last century to present
Expectations	Artefact accumulation, density & clustering	Longest period of accumulation. Highest artefact density Dispersed and clustered material expected	Longer period of accumulation compared to IS and UCS. Higher density than IS and UCS. Similar density to LR due to less time for weathering and erosion, and 47-40 ka years of potential artefact accumulation.		Shortest period of accumulation.	

	Diagnostic artefact composition	Diagnostic artefacts from Late MSA, the LSA (early LSA, Robberg, Oakhurst, early to middle Holocene, Wilton), the Neolithic and historic period. No clustering of artefacts older than ~5 ka (i.e., no Wilton) due to the disaggregation of artefacts as a result of long-term exposure to overland flow.	Diagnostic artefacts from late MSA, the LSA (early LSA, Robberg, Oakhurst, early to middle Holocene, Wilton), the Neolithic and historic period.	Diagnostic artefacts from the LSA (early LSA, Robberg, Oakhurst, early to middle Holocene, Wilton), the Neolithic and historic period.	Artefacts from the historic period at the earliest.
	Taphonomic bias	Younger artefacts dominate as a result of longer-term removal of older material from the record.	Younger artefacts dominate as a result of progressive removal of older material from the record.	Taphonomic bias, where younger artefacts dominate as a result of progressive removal of older material from the record.	Least amount of time exposed or for sediment to accumulate; deposit with or without modern finds, including structures related to the last 70 years of use.
	Condition of artefact (weathering /size-sorting)	Evidence of artefact movement from overland flow, larger artefacts showing more weathering and possible fragmentation.	Evidence of artefact movement from overland flow, larger artefacts showings more weathering and possible fragmentation.	Some evidence of artefact movement, weathering, and fragmentation. Artefacts from the MSA expected to occur on the Indurated Sand unit through downslope movement or anthropogenic retrieval and placement of older artefacts from older deposits onto younger sediment.	Fragmentation (e.g., ceramics, glass) and chemical weathering (e.g., oxidation of metal objects).

Scenario 2		2. Progressive Erosion initiating from late-MIS 3 (~30 ka)				
Scenario description		In principle, the older the deposit the longer the duration of exposure. The location of each substrate and the extent of their exposed surfaces has remained the same since exposure and progressive erosion initiated after late MIS 3. Each substrate surface was buried by a younger deposit until all deposits began to be re-exposed from ~30 ka, after the formation and possible induration of the Indurated Sand unit.				
Substrate		Lower Red unit	Upper Yellow unit		Indurated Sand unit	Unconsolidated Sand unit
Unit		4	3a	3b	2	1
Depositional history		The oldest consolidated sediment body, deposited any time before the deposition of the UY [unit 3a])	Deposited 47 ka on south slope [unit 3a] and 40 ka on east slope [unit 3b]; after LR [unit 4a/b] and Before IS [unit 2]		Deposited 32-30 ka on south slope	Deposited at least 70 years ago
Scenario specific history		Exposure until burial 47 ka. Re-exposure from MIS 2 (post-30 ka). After the removal of overlying Upper Yellow and the Indurated Sand.	Exposure through late MIS3 (from 47 to 32 ka). Re-exposure from MIS 2 (post-30 ka) after the removal of overlying sands (possibly younger Upper Yellow and the Indurated Sand).	East slope formation ~40 ka. Initial exposure in the late MIS 3—Between 40 and 32 ka. Re-exposure from MIS 2 (post-30 ka) after the removal of overlying sands (possibly the Indurated Sand).	Exposure from 30 ka to present (from late MIS3 to MIS1)	Surface occupying current position within the last century.
Expectations	Artefact accumulation, density, & clustering	No artefacts discarded between 40 and 30 ka (i.e., late MSA artefacts). If present, they result from the downward lag of overlying material, resulting in a spatial pattern indicative of disaggregation and size sorting (due to a loss of smaller items).	Late MSA artefacts discarded in situ, but potentially disaggregated during extended periods of exposure after 30 ka. Artefacts discarded after 30 ka may show clustering – more likely for younger artefacts.	LSA artefacts may show clustering – more likely for younger artefacts.	LSA artefacts may show clustering – more likely for younger artefacts.	

		Any artefacts discarded in the area after 30 ka can occur on Lower Red. However only pre-47 ka and more recent material should show clustering – more likely for younger artefacts.				
	Diagnostic artefact composition	Diverse composition of inferred artefact ages, including possible ESA, MSA (possible early MSA, Still Bay, Howiesons Poort, post-Howiesons Poort) as well as LSA (early LSA, Robberg, Oakhurst, early to middle Holocene, Wilton), Neolithic and historic artefacts.	Diagnostic artefacts from Late MSA, the LSA (early LSA, Robberg, Oakhurst, early to middle Holocene, Wilton), the Neolithic and historic period.	Diagnostic artefacts from the LSA (early LSA, Robberg, Oakhurst, early to middle Holocene, Wilton), the Neolithic and historic period. Few Late MSA artefacts	Artefacts from the MSA expected to occur on the Indurated Sand unit through downslope movement or anthropogenic retrieval and (re)placement of older artefacts from older deposits onto younger sediment. Diagnostic artefacts from the LSA (early LSA, Robberg, Oakhurst, early to middle Holocene, Wilton), the Neolithic and historic period.	Artefacts from the historic period at the earliest.
	Taphonomic bias	Markers of taphonomy should correlate positively with age	Disaggregation and markers of taphonomy should correlate positively with age	disaggregation and markers of taphonomy should correlate positively with age	disaggregation and markers of taphonomy should correlate positively with age	
	Artefact condition (weathering/size-sorting)	Strong evidence for movement, weathering, and fragmentation on this surface.	Evidence of artefact movement, weathering, and fragmentation.	Evidence of artefact movement, weathering, and fragmentation.	Evidence of artefact movement, weathering, and fragmentation.	

Scenario 3		3. Exposure since the Neolithic (from 2 ka)				
Scenario description		Each substrate surface was buried by a younger deposit until all deposits were exposed 2 ka, with erosion catalysed by pastoralism.				
Substrate		Lower Red unit	Upper Yellow unit		Indurated Sand unit	Unconsolidated Sand unit
Unit		4	3a	3b	2	1
Depositional history		The oldest consolidated sediment body, deposited any time before the deposition of the UY [unit 3a])	Deposited 47 ka on south slope [unit 3a] and 40 ka on east slope [unit 3b]; after LR [unit 4a/b] and Before IS [unit 2]		Deposited 32-30 ka on the southern slope	Deposited at least 70 years ago
Scenario specific history		Surface exposure until ~47 ka (early to mid-MIS3) as a result of burial by Upper Yellow unit 3a and possible burial by Indurated Sand unit 2, ~32 ka. Surface was then exposed to potential artefact accumulation from 2 ka until present. Some vertical displacement of artefacts from Upper Yellow deposit (post-47 ka) is possible. Few artefacts are expected from the latter half of MIS3, until the Neolithic.	Surface was first exposed to potential artefact accumulation between ~47 and ~30 ka as a result of burial by Indurated Sand unit 2. Surface was then exposed to potential artefact accumulation from ~2 ka until present.		Surface was exposed to potential artefact accumulation and removal 32 to 30 ka and subsequently and intermittently covered by active sand dune until complete exposure from ~2 ka	Surface extent and morphology roughly the same since the Neolithic period.
Expectations	Artefact accumulation, density, & clustering	Greater diversity of artefact sizes and inferred ages, reflecting MSA land use	Some vertical displacement of artefacts from Indurated Sand unit 2 is possible–but few artefacts are expected from MIS 2 (the LGM) until the Neolithic.		Possible clustering of Early LSA, Robberg, Oakhurst, mid/late Holocene, Wilton	

			Any artefacts dating from MIS 2 to the Neolithic will not be clustered. Greater diversity of artefact sizes and the possible retention of artefact clustering from Late MSA. Lower artefact frequencies/densities than the Lower Red unit 4.		
	Diagnostic artefact composition	Industries that antedate early LSA. Spatial overlap of MSA Industries and with Neolithic artefacts. The retention of clustering observed for MSA Industries if artefacts pertaining to the same Industry were discarded in the same place over time. Diagnostic artefacts from Late MSA and earlier, the Neolithic and historic period. High artefact frequencies and densities, especially from the MSA. Low frequencies of LSA as a result of vertical displacement and post-exposure movement from upslope deposit.	Diagnostic artefacts no older than the Late MSA. Diagnostic artefacts from the Neolithic and historic period. Low frequencies of LSA as a result of some vertical displacement and minor movement (post-exposure) from upslope deposits.	Diagnostic artefacts from the LSA (i.e., early LSA, Robberg, Oakhurst, mid/late Holocene, Wilton), the Neolithic and historic period.	No diagnostic artefacts from the Neolithic or earlier.
	Taphonomic bias			younger artefacts dominate as a result of longer-term removal of older material from the record.	
	Artefact condition	Minimal evidence of chemical weathering due to short exposure times.	Minimal evidence of artefact movement, and more evidence of artefact fragmentation.	Evidence of artefact movement, weathering, and fragmentation.	

	(weathering /size-sorting)	Minimal artefact movement caused by overland flow Evidence of artefact fragmentation and minor horizontal disaggregation reflecting intensive trampling and kicking by humans and domesticated ungulates of artefacts exposed on hard surfaces.	Minimal chemical weathering of artefacts due to exposure.		

Scenario 4		4. Exposure since the advent of European farming methods (from 300 years ago)				
Scenario description		Each substrate surface was buried by a younger deposit until all deposits were exposed 0.3 ka, with erosion catalysed by the introduction of European farming methods.				
Substrate		Lower Red unit	Upper Yellow unit		Indurated Sand unit	Unconsolidated Sand unit
Unit		4	3a	3b	2	1
Depositional history		The oldest consolidated sediment body, deposited any time before the deposition of the UY [unit 3a])	Deposited 47 ka on south slope [unit 3a] and 40 ka on east slope [unit 3b]; after LR [unit 4a/b] and before IS [unit 2]		Deposited 32-30 ka on south slope	Deposited at least 70 years ago
Scenario specific history		Surface exposure until ~47 ka (early to mid-MIS3) as a result of burial by Upper Yellow unit 3a and possible burial by Indurated Sand unit 2, ~32 ka. Surface was then exposed to potential artefact accumulation from ~300 years ago. Some vertical displacement of artefacts from Upper Yellow deposit (post-47 ka) is possible.	Surface was first exposed to potential artefact accumulation between 47 and 32 ka as a result of burial by Indurated Sand unit 2. Surface was then exposed to potential artefact accumulation from ~300 years ago.		Surface was exposed to potential artefact accumulation and removal around 32 ka and subsequently covered by active sand dune until complete exposure from ~300 years ago.	Surface extent and morphology roughly the same since the Neolithic period.
Expectations	Artefact accumulation, density, & clustering	Greater diversity of artefact sizes, inferred ages and possibly higher artefacts densities.	Greater diversity of artefact sizes and possible artefact clustering. Lower artefact frequencies/densities than the Lower Red unit 4.			
	Diagnostic artefact composition	Diagnostic artefacts from Late MSA and earlier, and the historic period.	Few artefacts are expected from MIS 2 (the LGM) until the historic period. Diagnostic artefacts no older than the Late MSA.		Diagnostic artefacts from the LSA (i.e., early LSA, Robberg, Oakhurst, mid/late Holocene, Wilton), the Neolithic and historic period.	No diagnostic artefacts from the Neolithic or earlier.

		Younger artefacts from the LSA and Neolithic only occur on this unit as a result their post-depositional movement from upslope. High artefact frequencies and densities from the MSA.			
	Taphonomic bias	None. Highest artefact densities occur on this deposit, and these are associated with older, not younger, artefacts.	None. High artefact densities occur on these deposits, second to Lower Red, and these are associated with older, not younger, artefacts.	Younger artefacts dominate as a result of longer-term removal of older material from the record.	
	Artefact condition (weathering/ size-sorting)	Minimal evidence of artefact movement and chemical weathering. Evidence for fragmentation	Some vertical displacement of LSA artefacts from Indurated sand unit 2 is possible. Minimal evidence of artefact movement. Substantial evidence of artefact fragmentation. Minimal chemical weathering of artefacts due to short-term exposure.	Substantial evidence of artefact movement, weathering, and fragmentation.	

8.2.2. Prior to MIS 3: >58 ka

8.2.2.1. Formation of UPK7's palaeoterrace and colluvium foundation

The formation of a palaeoterrace against a bedrock and colluvial hillslope established a foundation on which a series of sandy sediment bodies and their associated archaeology have accumulated (see Figure 6.2 a,b). The basal Cobble Bed unit at UPK7 is exposed along the southern extent of the sediment stack, underlying modern Unconsolidated Sand upslope of the modern river terrace. Bedrock possibly acts as a barrier to its northern reach, where the river channel was unable to cut in farther before migrating and downcutting in a southward direction.

The results from Electrical Resistivity Tomography (ERT) suggest the palaeoterrace extends beneath the sediment stack to just south of the northern dune crest, south of the hillslope colluvium and Exposure 3. To the north of the sandy sediment stack, colluvium has formed through hillslope debris flows. Colluvium underlies the Unconsolidated Sand, Indurated Sand, Upper Yellow Sand and Lower Red (with (LRcc) and without (LR) calcium carbonate inclusions). It extends to the north of UPK7's northern dune crest and is assumed to be a continuation of hillslope erosion that initiated prior to the formation of the Lower Red.

The formation of the palaeoterrace and colluvium have not been dated. However, at nearby UPK9, the colluviated hillslope unit is underlain by a well-developed calcrete with U-Th ages of 226 ± 25 ka (S91090) and 202 ± 48 ka (S91091) (Shaw et al. 2019, see SOM table 3). This is consistent with the presence of Acheulian bifaces in the colluvium hillslope north of UPK7's sediment stack. Together, they suggest that the colluvium and overlying sandy units accumulated sometime after the start of MIS 6 (~191 ka, Lisiecki & Raymo 2005).

8.2.2.2. The Lower Red

8.2.2.2.1. History of sedimentation

The bulk of the sandy sediment overlying the palaeoterrace and bedrock foundation is aeolian sand that was transported onto UPK7's hillslope from the Doring River's seasonally-dry channel bed. The current hardness of this sediment suggests it transformed into a soil B-horizon beneath a thick sandy—now removed—A-horizon and possibly an E-horizon. For this reason, it is assumed that the timing of sediment consolidation postdates deposit burial age and antedates current surface exposure. Archaeology showing minimal signs of horizontal entrainment and disaggregation was either discarded directly onto these hardened surfaces well after deposit burial and consolidation, or they accumulated concurrently with the deposit followed by their vertical lag onto its B-horizon as the surrounding sediment was deflated. In the case of the former, the accumulation of artefacts onto an exposed hardened surface would have to occur rapidly in the Doring River valley under present-day conditions to maintain horizontal integrity. Depending on the rate of sedimentation and erosion, this would mean that the vertical and horizontal distribution of these artefacts represents a shorter period of discard behaviour than those that have lagged onto a single surface as a result of deflation

The oldest consolidated units are Lower Red and LRcc. There is no obvious stratigraphic relationship between them. The increased presence of calcium carbonate in the LRcc may imply that it is

older, and/or that it relates in some way to the middle Pleistocene calcretes at UPK9 and UPK1 (Bleed et al. 2017; Shaw et al. 2019; Watson et al. 2020). In either case, calcium carbonate veins in LRcc are post-depositional, forming after at least part of Lower Red had accumulated. Calcium is rare in the geology of the region and is often accumulated in sedimentary units by biological agents, such as plant matter and/or insects such as the southern harvester termites (McAuliffe et al. 2019). Thus, it is possible that post-depositional alteration explains the physical difference between the Lower Red and LRcc, and that their distinction is stratigraphically meaningless. The accretion of calcium carbonate in the desiccation cracks of the LRcc is at least indicative of strongly seasonal conditions when rapid drying of wet substrate repeatedly took place in the area. Similar conditions are currently observed throughout the valley system. Calcium carbonate nodules and veining are only observed in the Lower Red, and only small calcrete nodules were observed eroding out of the Upper Yellow in some areas.

Samples collected for OSL analysis from Lower Red sediment represent minimum ages due to the dominance of saturated quartz grains identified in their OSL samples. The minimum depositional age for the LR/LRcc varies substantially, from 51.8 -4.5/+inf ka to 80.4 -8/+inf. This restricts the timing for deposition of the Lower Red to no later than the first half of MIS 3 (51.8 -4.5/+inf ka) and, in some cases, to no later than MIS 5 (80.4 -8/+inf ka). Both are consistent with the oldest depositional age of overlying Upper Yellow (47.2 ± 3 ka). As noted earlier, the underlying colluvial hillslope constrains initiation of the accumulation of Lower Red sands to after the start of MIS 6 (<191 ka). The history of formation of the Lower Red over this time is currently unclear given the evidence and ages at hand. As the main process for the formation of these deposits is interpreted to be seasonal aeolian deposition, it is assumed that the formation of Lower Red sediment was continuous so long as this seasonal regime was active, and a source of channel sand was available. It is possible that sand accumulation occurred gradually from the start of MIS 6 until burial by Upper Yellow sands and subsequent Lower Red consolidation.

8.2.2.2.2. Artefact condition

Artefacts on the Lower Red show higher proportions of flake fragmentation than those on the Upper Yellow and lower fragmentation than flakes on IS. This suggests that the Lower Red artefacts were exposed to more wet-dry cycles and trampling than Upper Yellow artefacts and less than those on Indurated Sand. If trampling occurred over a single continuous period of exposure, artefacts would also be vulnerable to runoff erosion, resulting in extensive lateral movement, followed by attrition (Phillips et al. 2019). With this in mind and under the current conditions—hard, crusted surfaces, largely devoid of vegetation and densely rilled—Lower Red artefacts should show extensive size-sorting, artefact attrition or at least low artefact densities, as a result of sheet wash erosion. This is only observed on the highly eroded, steeply sloping (>15º) residual mounds to the north of the main sediment stack (i.e., Exposures 4 and 6), which are largely devoid of artefacts in their upper and middle zones. Thus, artefacts on the southern hillslopes of Lower Red were not exposed for long enough to induce size-sorting through sheet wash erosion.

Observations on artefact condition do not provide strong support for continuous exposure of Lower Red after the deposition of the Upper Yellow ~47 ka (Scenario 1), or within the last ~32-30 ka for that matter (Scenario 2). Simulated findings based on current semi-arid conditions at UPK7 show a significant reduction in artefact numbers within 100 years (47% loss), 1000 years (87% loss) and complete

artefact attrition within 10 ka (Phillips et al. 2019). Considered in relation to the southern hillslope, the high artefact densities, retention of smaller artefacts (<20 mm) in their middle and upper zones, moderate rates of weathering, and persistence of clustering among some Industries make it unlikely artefacts discarded on Lower Red were exposed for more than a few thousand years. This is considered further in the following subsection with reference to the inferred ages of the overlying archaeology, and with respect to their spatial distribution and density across the Lower Red.

8.2.2.2.3. Spatio-temporal dynamic between diagnostic artefacts and depositional context

Despite lacking a burial age for the surface of the Lower Red, 83% of diagnostic artefacts overlying this deposit are associated with the MSA (300-40 ka), consistent with the minimum age of 47 ka. MSA artefacts occur on every exposed surface of the Lower Red and LRcc, with lower proportions of MSA artefacts found on the Upper Yellow (9%) and the Indurated Sand (8%). Artefacts characteristic of the Still Bay Industry occur as low-density, non-clustered scatters on the upper and middle zones of the southern hillslope exposures (Exposure 1b and at the top of Exposure 1c). Their presence suggests that Lower Red sediments were present by the time Still Bay artefacts were in use in local rock shelter sequences at ~77-70 ka (Högberg 2014; Shaw et al. 2019). This is in line with the oldest minimum age obtained for the Lower Red deposition (80.4 -8/+inf ka). Similarly, the lack of Acheulian bifaces on the Lower Red, and the implied post MIS 7 age of the underlying colluvium suggests the onset of accumulation occurred between MIS 6 (191-130 ka) and MIS 5 (130-71 ka), i.e., 191 to 71 ka.

The rarity of MSA artefacts on the Indurated Sand is in sharp contrast to their dominance on the Lower Red. This, together with the downslope position of the Indurated Sand relative to the Lower Red, and the beginnings of sheet wash entrainment of material from the lower elevations of Lower Red, suggest that MSA artefacts have moved onto the Indurated Sand from the Lower Red, after 30 ka. Sheetwash size-sorting between the middle zone of Exposure 1b and its lower zone support this interpretation and implies contemporaneous exposure to rainfall erosion between the Lower Red and the current surface of the Indurated Sand. However, high frequencies and densities of MSA artefacts still remain on the middle zone of Exposure 1b's Lower Red, which suggests that artefact entrainment happened recently. This is in line with the proposed recent exposure of the current level of the Indurated Sand in the last 5 ka (Scenarios 3 and 4) and possibly more recently given the high frequency of material preserved on this deposit, despite its highly exposed surface conditions.

At UPK7 post-Howiesons Poort artefacts occur as a densely clustered area of artefacts on the eastern fringe of Exposure 1b, in the middle zone of this hillslope. This accounts for 94% of post-Howiesons Poort artefacts identified at UPK7. The remaining 6% occur on the Upper Yellow as isolated pieces, often in transitional zones between the Upper Yellow and Lower Red and where rill channels are cutting into the Upper Yellow to expose the underlying Lower Red. The temporal bracket for the use and discard of post-Howiesons Poort artefacts in the region predates the earliest date for the formation of the Upper Yellow. The broad age for the regional post-Howiesons Poort is 60-50 ka, however the presence of 'Nubian' Levallois cores in this cluster may allow refinement; such artefacts occur only at the Howiesons Poort/ post-Howiesons Poort transition at Klipfonteinrand 1 and Mertenhof. Therefore, the post-Howiesons Poort cluster on the Lower Red likely dates closer to 60 ka than to 50 ka—if the rock shelter sequences can be

used as a guide. These artefacts were thus discarded and buried, probably relatively rapidly, on a still-accumulating Lower Red sometime after 60 ka.

Exposure of the Lower Red on the southern hillslope after 50 ka is suggested by the abundance of Late MSA artefacts in Exposures 1a, 1b, and 1c. That this includes an opportunistic refit of final flake to core (Mackay, pers. comm. 2020) suggests limited movement of at least some pieces. Although Late MSA archaeology is dated to between ~50-33 ka at PL8, it is rarely found overlying the Upper Yellow sediment, suggesting that these artefacts were mostly discarded prior to the consolidation – if not necessarily the formation – of the Upper Yellow. Late MSA artefacts are also only found on the Indurated Sand as part of a rilled transitional zone between the Lower Red and Indurated Sand (i.e., the top of Exposure 1a). This may also apply to their occurrence on the Upper Yellow. However, two Late MSA artefacts were recorded in Exposure 2, which is now surrounded by younger overlying Unconsolidated Sand.

The absence of typo-technological Industries post-dating the Robberg (i.e., Oakhurst, Wilton, Neolithic and historic) from the middle zone of Lower Red in Exposure 1b suggest that the overlying Indurated Sand and younger sediment were removed from this area as recently as the Neolithic or the historic period. Another possibility is that during this time this part of UPK7 was not exposed to enough lithic discard behaviour to result in a detectible typological signal. It is also possible that LSA artefacts found dispersed across the partially deflated Indurated Sand in Exposure 1 are the combined result of artefacts transported downslope from the erosion of younger sediment upslope and the deflation of artefacts from overlying sediment onto the Indurated Sand.

8.2.2.2.4. Summary and scenario outcome

Across the locality, exposed Lower Red sediment shows differing degrees of erosion and archaeological preservation. As a result, no single scenario presented in Table 8.1 aligns with its archaeological state and formation at the locality-wide scale. That said, LSA artefacts are only common on the Lower Red in areas where LSA artefacts occur at high densities on younger sediment units immediately upslope (Figure 7.15). Almost no LSA artefacts were found on Lower Red where LSA artefacts are absent immediately upslope (i.e., in the northern hillslope Exposures 4 and 5). The same pattern holds even more strongly for Neolithic artefacts. Only near the transition zones between the Lower Red and Indurated Sand, where slope gradient steepens and rills become moderate to deeply incised (Figure 6.41), is there statistically significant evidence for size-sorting that could potentially explain this pattern in terms of the attrition of younger artefacts. Otherwise, clustering of post-Howiesons Poort artefacts, and the fact that hornfels artefacts on Lower Red are not appreciably more heavily weathered than those on the younger units is not consistent with an extended period of exposure of this unit. Thus, Scenario 1 cannot be supported, and Scenario 2, requiring that Lower Red became available to receive discarded artefacts sometime after 30 ka, is inconsistent with the lack of LSA artefacts across most of the unit. Only Scenarios 3 and 4 – whereby significant erosion and exposure initiates after 2 ka – seem consistent with the evidence from Lower Red.

8.2.3. MIS 3: 59 to 29 ka

The sandy substrate of the Upper Yellow and Indurated Sand accumulated through similar processes following the formation of Lower Red sediment, involving the aeolian transport of river alluvium onto UPK7's hillslope. With the possible exception of the Lower Red, all the burial ages measured from the sediment of the Upper Yellow and Indurated Sand relate to MIS 3 (57 to 29 kya, Lisiecki & Raymo 2005).

8.2.3.1. Formation of the Upper Yellow

8.2.3.1.1. History of sedimentation

Approximately 47 kya a substantial period of sand accumulation initiated, and at least partially overlaid the Lower Red with Upper Yellow sands. MIS 3 aeolian deposition and stabilisation of Upper Yellow sediments are suggested by the presence of sample 90024/UOW-1804 (47.2 ± 3 ka) and its overlying Upper Yellow sediment near the top of the southern slope of Exposure 1b. However, evidence of the continued accumulation of Upper Yellow after ~47 ka, well into the latter half of MIS 3, is preserved on the eastern side of UPK7, where a burial age of 39.9 ± 2.8 ka (90016/UOW-1801) was returned from sediment collected at Exposure 2. In the lower zone of the Exposure 1b hillslope, the slope wash deposit from which the Indurated Sand sample 91080/UOW-2006 (40.4 ± 3.2 ka) was collected suggests that by around 40 kya rainfall or wind erosion had removed the Upper Yellow sediment downslope of UOW-1804, along with any associated archaeology.

Sedimentological results, location and age suggest sample UOW-2006 derives from the slope-wash-erosion of upslope calcrete-containing sandy sediment and artefacts around the time of Upper Yellow deposition and possibly while it was still in its unconsolidated state. The amount of sediment and archaeology removed is unknown. However, the exposure of Lower Red and its associated archaeology (discussed in more detail below) suggest that only the Upper Yellow substrate and any artefacts contained therein were affected by this slope wash event.

The composition of the sampled deposit from which UOW-2006 was collected also indicates that calcrete was present in the eroded deposit of Upper Yellow by 40 ka—possibly the same inclusions observed in the Upper Yellow sediment in a few areas across UPK7. However, aeolian deposition was active during this time as indicated by the aeolian deposited sands of UOW-1801 collected on the eastern slope, which also dated to ~40 ka. The likelihood of deposit preservation on this side of the sediment stack is higher as a result of its leeward position on the slip-face of the dune, where deposition outweighs erosion and surface exposure.

A gap of at least 3.3 ka between slope-wash erosion and the stabilization of a large body of now loamy sand (Indurated Sand) across the southern slope suggests the accumulation of aeolian sand during this time remained unstable—potentially burying and exposing older underlying sediment between ~40 ka and ~32 ka. Therefore, while the eastern side of UPK7 was prone to sand accumulation that would promote artefact burial and preservation, its windward side was subjected to periodic conditions of sand accumulation, deflation, and substrate exposure.

8.2.3.1.2. Artefact condition

After the Lower Red, the Upper Yellow is the second oldest consolidated sandy unit at UPK7 and is associated with the second highest artefact densities. Artefacts are found on nearly every surface of exposed Upper Yellow sediment—including the eastern hillslope of Exposure 2, the upper zone of the northern hillslope of Exposure 3, and the upper hillslope zone of Exposures 1b and 1c. Artefacts on the Upper Yellow have low rates of fragmentation and limited size-sorting, with weathering rates that are similar to if generally slightly higher than Lower Red. The presence of a cluster of post-Howiesons Poort artefacts likely dating 58-55 ka on Lower Red suggests a maximum elapse of 8-11 kya for exposure of Lower Red before accumulation of Upper Yellow. In contrast, if Upper Yellow were not subsequently covered by another sediment unit, artefacts deposited on that surface would have been exposed for around 40 kya. That that difference is not supported by variation in rates of fragmentation, size-sorting, or weathering, suggests that, until recently, the consolidated surface of the Upper Yellow was buried by an overlying deposit of sand. The current presence of young Unconsolidated Sand immediately over the Upper Yellow implies that either the Indurated Sand, along with any associated archaeology, has been removed from above the Upper Yellow, and/or it never became a consolidated soil B-horizon in this area to form a stable body of sediment above the Upper Yellow unit. Alternatively, another unit post-dating MIS 3 formed in this area but was subsequently removed.

8.2.3.1.3. Spatio-temporal dynamic between diagnostic artefacts and depositional context

The rarity of Late MSA archaeology on the Upper Yellow is unexpected given that the Late MSA was in use during and after the accumulation of the Upper Yellow in the catchment. However, the composition of the Upper Yellow during its burial between 47 to 40 ka was probably more conducive to the burial of artefacts in this deposit and the intermittent exposure of the Lower Red, than accumulation of these as a time-averaged horizon on top of the Upper Yellow sediment. Thus, the Late MSA artefacts observed on the Lower Red today are more likely the result of lagged artefacts onto this deposit from downward movement through the overlying unconsolidated Upper Yellow sands or the direct accumulation of artefacts onto the Lower Red during intermittent and/or full exposure of its surface between ~40 and 32 ka. The rarity of Late MSA artefacts across the Upper Yellow generally and the eastern hillslope, Exposure 2, together with the concentrations of Early LSA , supports the scenario that the discard and accumulation of Late MSA artefacts across UPK7 had ceased by the time the Upper Yellow had consolidated at <40 ka. The dispersed distribution of Early LSA artefacts on the Lower Red surface of Exposures 1b and 1c add weight to this possibility.

Early LSA technology was dated between ~25-22 ka at PL8 (Mackay et al. 2019a) and ranges from 46-20 ka across different regions of southern Africa (Bousman & Brink 2018; Lombard et al. 2012). Thus, its dense clustering on the consolidated Upper Yellow in Exposure 2 corresponds with both local and continental shelter chronologies. Its clustered distribution, coupled with the good condition of these artefacts (i.e., low to insignificant amounts of weathering compared to the Lower Red, fragmentation, and size-sorting) compared to other UPK7 hillslopes suggests they were subjected to minimal wet-dry conditions, sheetwash erosion or trampling. The strongest indication that Exposure 2 remained buried until recently is the near-complete absence of artefacts associated with younger Industries in this area. The one

exception is a single artefact associated with the immediately subsequent Robberg, suggesting some overlap of younger material shortly after the Early LSA, possibly through vertical displacement. This is further supported by Exposure 2's geomorphic position on the eastern slip face of the N-S dune crest, which is prone to the accumulation of thick dune sand. Moreover, the complete absence of Early LSA artefacts on the Indurated Sand suggests that this part of UPK7's depositional history has been erased and/or that Early LSA technology was no longer discarded at UPK7 after consolidation of the Indurated Sand (post-30 ka). None of these observations can be reconciled with Scenarios 1 or 2; only recent loss of overlying sediment under Scenarios 3 and 4 is plausible.

8.2.3.2. Indurated Sand

8.2.3.2.1. History of sedimentation

Initial deposition of the Indurated Sand post-dated the Upper Yellow. Indurated Sand is the second largest exposed sediment body at UPK7, second to the Unconsolidated Sand. The time of deposition of the Indurated Sand was assessed from three sediment samples using OSL dating methods: 32.1 ± 1.6 ka (90020/UOW-1802), 30.3 ± 1.3 ka (UNL3809) and 30.5 ± 1.4 ka (UNL3810) (Shaw et al. 2019, SOMs). These were collected from the middle and lower zones of the southern side of UPK7's main hillslope, Exposures 1a-1b. These results provide a maximum age of ~30 ka for artefacts recorded on its current surface.

The Indurated Sand was not observed directly overlying Upper Yellow sediment. Rather, it is found on the lower zones of UPK7's southern hillslope, while the Upper Yellow is restricted to the upper hillslope zones of Exposures 1b, 1c, 3, 6, and possibly 5, and is the only substrate unit identified in Exposure 2. It is possible that the Indurated Sand represents the continued accumulation of Upper Yellow sand and that younger sediment was removed to expose Upper Yellow sands dated to ~47 and 40 ka at higher elevations (>210 m asl). However, both units are observed directly overlying Lower Red sediment. The older, Upper Yellow unit, which is dated to ~47 ka, directly overlaps the Lower Red on the upper hillslope zones of Exposures 1b and 1c.

In contrast, the Indurated Sand is found downslope of, but directly overlapping Lower Red sediment in Exposure 1a, suggesting that the older Upper Yellow sands were removed prior to the accumulation of the Indurated Sand at ~30-32 ka. The absence of Upper Yellow sediment in the middle zone of Exposures 1a, 1b and 1c suggests that the Upper Yellow has a history of differential erosion across the locality between 40 and 32 ka, supporting interpretation that the windward side of UPK7's sediment stack was susceptible to active sand accumulation and movement during this time. The absence of Indurated Sand from the eastern and northern exposures could indicate the removal of this unit from upper hillslope zones. However, its absence farther north suggests a limited northern reach of aeolian deposition—possibly the result of a change in dominant wind direction and strength during the dry months at the end of MIS 3, prior to the LGM.

8.2.3.2.2. Artefact condition

Artefacts overlying the Indurated Sand show a significantly dispersed non-random distribution across most of its surface except for randomly distributed artefacts found along its footslopes and where moderate to

well-developed rills cut into its sediment. Areas that show the most structure in their dispersion (>99% confidence) coincide with areas where geomorphic anomalies occur, departing from the hillslope trend of their surrounding topography (i.e., the heuweltjie-like sedimentary feature located midway down the hillslope of Exposure 1c, that forms a hard, highly weathered platform of LRcc; the large residual mound of Indurated Sand in the middle zone at the eastern end of Exposure 1a which is covered by sandstone cobbles, each similarly large in size). Its consolidated state suggests that—like the Lower Red and Upper Yellow—the area in which Indurated Sand currently occurs once formed a soil B-horizon below a thick deposit of unconsolidated A- or E-horizon sands. The presence of vegetated semi-consolidated sand and active Unconsolidated Sand overlying parts of this substrate are possible remnants of a more extensive body of overlying sand. However, the large extent of exposed Indurated Sand, the absence of consolidated sediment post-dating its formation ~32 to 30 kya, and the existence and exposure of the basal layer of a combustion feature, just below the surface of this substrate, implies that the current surface of this deposit was at least partially exposed 5,000 years ago. However, despite how dispersed its overlying archaeology is, the presence of artefacts across the Indurated Sand suggests that processes promoting artefact preservation and inhibiting sheetwash entrainment (i.e., burial beneath a sandy substrate and the aide of stabilising vegetation) have temporarily prevented or slowed the near-complete removal of these artefacts over the last 5 ka.

A scenario of long-term burial beneath a stable sand sheet followed by recent/short term exposure of artefacts that overlie the Indurated Sand is supported by the condition of these artefacts. They show relatively low frequencies of edge rounding, patination, and discoloration compared to those from the Upper Yellow and Lower Red, which suggests that wind-blown weathering was minimal and that the artefacts were exposed to relatively few wet-dry cycles. The significantly higher proportion of fragmented flakes on the Indurated Sand (42%), however, suggests these artefacts may have been subjected to more trampling than those on older units, though given the typical state of weathering, this may have occurred recently.

Size-sorting of artefacts between the middle zone and footslope of Exposure 1b—an area that transitions from the Lower Red to the overlying Indurated Sand—suggests that some artefacts on the Indurated Sand have moved from upslope as a result of sheetwash erosion when both deposits were exposed. With the relative condition of artefacts between substrate units in mind, this probably happened within the last 5 ka. The presence of pottery clusters further supports the contention that Indurated Sand was exposed in the last 2 ka.

8.2.3.2.3. Spatio-temporal dynamic between diagnostic artefacts and depositional context

The highest frequencies of Robberg (23-16 ka) artefacts were recorded in the upper zone of Exposure 1b across both the Upper Yellow and Lower Red. They were also identified as randomly distributed, isolated finds on the Indurated Sand, on the Upper Yellow sediment at Exposures 1c, 2 and 3 and the Lower Red in Exposures 1a and 3. In the case of the Indurated Sand, Robberg artefacts often occur in the context of transitional zones between deposits, or proximate to rills. However, this does not apply to their distribution on the Upper Yellow and Lower Red, which suggests that these artefacts were discarded after the consolidation and exposure of the Upper Yellow and Lower Red. This is expected given the age of the Upper Yellow in Exposure 1b (~47 ka) and the temporal bracket for the Robberg in the catchment's rock

shelter sequence (Mackay et al. 2019b). However, it also implies that these units were devoid of overlying consolidated sediment, or that the overlying sediment was not thick enough or stable enough to become indurated. Moreover, the rarity of Robberg artefacts on the Indurated Sand and the absence of Upper Yellow sediment below 213 m asl suggests that overlying archaeology and deposits have been removed.

This is also shown in the sparse scattering of Oakhurst artefacts on the Indurated Sand as well as the complete absence of Wilton artefacts. In contrast, both Industries occur above 213 m asl in Exposure 1b's Lower Red to Upper Yellow transitional zone—overlapping Robberg in this area. They also occur at higher frequencies on the Upper Yellow and Lower Red sediment in Exposure 3. Given the high level of integrity observed in the archaeological condition of the upper hillslope zones of both areas, the presence of Early LSA, Robberg, Oakhurst and Wilton Industries on the Upper Yellow indicate that this area was used throughout MIS 2 and 1, despite the absence of consolidated sediment dating to this time. Pottery also occurs in Exposure 3 and at the top of Exposure 1b, suggesting that these surfaces were occupied sometime within the last 2 ka. However, the absence of pottery across the middle zone of the southern slope and presence at the footslope of the Indurated Sand suggests that the exposure of this zone, and the exposure of both the Indurated Sand and Lower Red to their current surface, involved the removal of any Neolithic material and archaeology.

Deposition of the Indurated Sand at ~32-30 ka coincides with and antedates the appearance of the LSA in the catchment and WRZ generally. However, direct discard on this substrate is only evident in the occurrence of clustered diagnostic and non-diagnostic artefacts on the lower zones and southern fringe of Exposure 1a and—to a less structured degree—in Exposure 1c. Several clusters are composed of fragmented pottery that appears in the catchment at less than 1.7 ka (i.e., at Klipfonteinrand; Shaw et al. 2019) and less than 1 ka in the Putslaagte tributary (i.e., PL8; Shaw et al. 2019). One cluster is dominated by small quartz bipolar cores and three hornfels refits (i.e., complete core, flake, and cortical blade). The others are composed of scrapers and sandstone implements (i.e., grindstone, hammerstone/anvils). With the exception of the pottery, these clusters are not diagnostic of a particular archaeological epoch or Industry. However, their clustered composition and the presence of refits suggests that the duration of their exposure has not been long enough for sheet wash entrainment to impact horizontal integrity. The quartz cluster is also located near one of the pottery clusters suggesting that its discard and exposure are within the last 1.7 ka. Considered together and given the rapid attrition rates that are possible when the Indurated Sand is exposed, the clustered occurrences on the Indurated Sand appear to be recent Late Holocene (< 3 ka) additions. In contrast the dispersed, rare distribution of LSA artefacts across this substrate, together with the occasional Oakhurst artefact and the complete absence of Wilton, suggest that overlying sediment and artefacts post-dating the consolidation of the Indurated Sand and antedating the Late Holocene have been removed either through rainfall or wind erosion. Artefacts that do occur on this substrate have either lagged down onto this unit from up-slope or were discarded on its surface within the last 5 ka.

The low frequencies of significantly dispersed MSA artefacts at the westernmost footslope of the Indurated Sand are anomalous given the depositional history and inferred ages of the sedimentary system and archaeology presented above. One explanation is that this transitional zone between the palaeoterrace and the Indurated Sand yields MSA artefacts that were either discarded onto the underlying cobble bench or are eroding out from the Upper Yellow sediment misidentified as Indurated Sand.

8.2.3.2.4. Summary and scenario outcome

Consistent with the results for Lower Red, there is no evidence to support prolonged exposure of Upper Yellow and Indurated Sand to their current extent. Despite being the uppermost consolidated unit at the top of UPK7, evidence for weathering, winnowing, and fragmentation of artefacts on Upper Yellow is not much greater than for the underlying Lower Red. The spatial integrity implied by the cluster of early LSA artefacts likely to date 27-22 ka on Upper Yellow further implies that this unit was covered for an extended period of time after its deposition ceased. Despite this, however, there is an abundance of younger LSA artefacts dating from 22-2 ka on this sediment unit. Had there been an overlying unit to protect the Early LSA cluster, how did its removal not result in removal – or at least significant attrition – of artefacts assigned to the Robberg, Oakhurst, Wilton, and Neolithic? The most plausible answer, described in more detail below, is that the overlying sediments never became lithified, allowing artefacts discarded after MIS 3 to move down through the loose substrate onto the underlying lithified Upper Yellow surface without losing significant horizontal integrity. None of these possibilities support Scenario 1, though Scenarios 2-4 appear plausible. The combined evidence from Indurated Sand contributed significantly to this issue. The presence of a hearth dating to roughly 5 kya (see below) suggest the surface of that 30-ka unit was exposed in the mid Holocene. The presence of pottery clusters suggests it was available for discard in the last 2 ka. The former observation appears to support a possibility between Scenarios 2 and 3.

8.2.4. MIS 2 to MIS 1: 29 ka to present

After MIS 3 the history of deposition at UPK7 becomes more ephemeral, with conditions during MIS 2 and/or MIS 1 apparently unsuitable to the formation and/or preservation of consolidated sediment. Subsequent ages are limited to a single mid-Holocene ^{14}C age (5135 ± 99 cal BP) obtained from a combustion feature, with remnants of its base found cutting into the current surface level of the Indurated Sand, followed by a single Late Holocene OSL age for the Unconsolidated Sand (see below for sample details).

8.2.4.1. Absence of younger consolidated sands

The absence of OSL burial ages from MIS 2 and most of MIS 1 may be due to bias in restricting sampling to consolidated sediments. However, the lack of consolidated sediment with ages post-dating 30 ka and most of the Holocene (from MIS 2 and throughout MIS 1) suggests that dune sand was active or reactivated over this time, or younger consolidated sediment has been removed. In the case of the former scenario, instability may have prevented long-term subsurface consolidation and thus preservation of younger sediment. Induration usually occurs in the B-horizon of a soil. In unconsolidated sand this may be a few metres below the surface. It is therefore reasonable to assume that an extended phase of thick dune formation followed the burial of the Indurated Sand at ~30 ka. However, the absence of consolidated dune sand post-dating this unit suggests that the Indurated Sand was either the last fully consolidated deposit at UPK7 or overlying consolidated sediment has since been deflated. The latter is suggested by the existence and partial erosion of an indurated sandy unit at nearby UPK9, the Indurated Orange Sand, which was deposited at ~27 ka (see Watson et al. 2020). Deflation of the Indurate Orange Sand by ~400 mm to the current level of the underlying colluvium happened within the last few hundred years—evidenced by the

historic stone hearth that is now pedestalled above the colluvium (see Figure 8.1; Shaw et al. 2019, p.409). However, and as noted earlier, that would require an explanation of how such a unit was removed without significant loss of younger LSA archaeology; the evidence from Lower Red suggests that loss of significant overlying sediment generally resulted in loss of its related archaeology.

Figure 8.1. Photograph of Brian Jones (height: 1.72 m) at UPK9 standing to the north of an historic stone hearth, built on the Indurated Orange Sand (~27 ka) that has eroded down to expose an underlying colluvium. Photograph taken facing south-west, towards UPK7 (in the north-west) and UPK1 (beyond the midground hillslope and river channel bend).

8.2.4.2. Semi consolidated and Unconsolidated Sand

8.2.4.2.1. History of sedimentation

The youngest sediment body, the Unconsolidated Sands, is composed of active sand that is predominantly loose, overlying a more stable, semi-consolidated sand that is prone to vegetation growth and reactivation. Both units provide a surface context that is conducive to artefact burial through vertical displacement and/or deposition—conditions that effectively reduce artefact visibility. The Unconsolidated Sand and Semi-consolidated deposit underlying this are taken to be analogous to the initial stages of deposit formation for all preceding sediment bodies, during which time they formed soil A- or E-horizons to older, more deeply buried, fully consolidated B-horizons. Unconsolidated Sand is the largest sand unit on the UPK7 hillslope. It is actively accumulating and moving across the locality, periodically covering, and exposing underlying, crusted Pleistocene surfaces and their artefacts in the process. Dated to last century (~70 years ago, UNL3808: 0.069 ± 0.005, Figure 6.40 & 6.38; see Shaw et al. (2019, SOMs), the Unconsolidated Sand post-dates the burial age of its underlying consolidated sediment by ~30 ka—leaving a considerable temporal gap in the depositional history of the locality, not reflected in the archaeology. However, with only a single sediment sample providing a date for the extensive body of Unconsolidated Sand it is reasonable to assume that this deposit is the result of a much longer depositional history than its more recent age suggests.

Semi-consolidated Sands were not dated. However, this deposit accumulated either during the Holocene or as early as the terminal Pleistocene. The burial age of ~30-32 ka for the underlying unit, the Indurated Sand (Table 6.8), provides a maximum age for this unit. The occasional, haphazardly orientated stone artefacts observed in one exposed, vegetated section of Semi-consolidated Sand suggests that people were using and discarding stone tools as the sediment body formed. Its poorly consolidated state would promote the vertical displacement of artefacts throughout its matrix. Although rare, the presence of stone artefacts in this deposit suggests that they were in use during the formation of the Semi-consolidated Sand.

The rarity of Stone Age artefacts on the Unconsolidated Sand is in line with the timing of the deposit's formation and its composition. However, the general rarity of historic items (n = 3) and/or absence of structures across UPK7 is unexpected given the use of the Doring and Biedouw River valleys throughout the Late Holocene—particularly during the last century (see Chapter 4). Artefacts that are visible in the Unconsolidated Sands occur where loose sand is present as a fine veneer on an older, consolidated deposit, often at the juncture between an exposed, older, often rilled deposit and the overlying Unconsolidated Sand (i.e., at the edge of an exposed hillslope or rill). These artefacts either relate to the exposure of the underlying consolidated surface, or to the erosion of an overlying sediment body still covered by Unconsolidated Sands beyond this juncture. Possible factors limiting the accumulation and/or preservation of historic remains include the poor potential of the sedimentary unit's composition for preserving and exposing historic remains, a short timeframe, a land-use intensity too low to accumulate an historic record in this area, and/or restricted access to the hillslope from the Biedouw River valley and southern banks of the Doring River.

The loose composition of the Unconsolidated Sand and its propensity to shift and deflate across the study area promotes burial of objects and structures through sand accumulation, as well as winnowing, deflation and object trampling. It is therefore possible that historic material is present but buried within and beneath the Unconsolidated Sand. The occurrence of historic items in the upper hillslope zones of Exposures 1a, 1b, and 3—at the juncture between the Lower Red and Indurated Sand and on the Upper Yellow and Lower Red (see Figure 7.4)—suggest that these artefacts have undergone minimal lateral entrainment from sheetwash; it is unlikely that they have moved far from their discard-origin. However, it is possible that their current state of repose results from vertical displacement, lagging down from an overlying, loose sand onto a more consolidate surface below.

Another possibility is that the current surface level of the Upper Yellow and Lower Red were already exposed when these items were discarded. In either case, there are only three historic objects identified across this locality. This is in sharp contrast to the abundance of historic structures, hearths and items (i.e., glass, ceramics, metal, and a saddle badge dated to 1851; (Shaw et al. 2019, pp.405, 409) found at UPK9, which date to within the last few hundred years—a locality ~250 m to the east of UPK7 (Watson et al. 2020). This suggests that use of the less accessible, northern side of the Doring River was both possible and intensive enough to leave an archaeological record. Thus, the proximity of UPK9 to UPK7, the evident intensity of activity on UPK9's hillslope and its continued use for grazing, drainage and storage of farm equipment eliminates the possibility that UPK7's minimal historic record is due to a lack of historic activity on the northern side of the Doring River. It also rejects the possibility that the rarity of historic artefacts on

UPK7 are the result of the short window of time necessary to accumulate material residues from modern and historic activity.

However, lack of access to UPK7 by vehicle across the eastern tributary would reduce the kind of activities and material record left at this locality. UPK7 is accessible from the northern side of the Doring River, either from the direction of UPK9 or from the plateau north of UPK7. The steep cliff on the opposing side of the river reduces the ease of direct access to this locality from the south towards the north side of the river channel. Direct access from UPK9 involves traversing the sandy modern river terrace or crossing the eastern tributary. Unlike UPK9, this would likely reduce the ease of building stone structures and accessing the UPK7 hillslope by wagon or automobile. Therefore, restricted ease of access possibly limited activity on UPK7's surface to stock grazing and herding on foot or horseback, reducing opportunity for the accumulation of anthropogenic debris over the past century. However, grazing of this land has left an erosive signature, evinced by the timing of consolidated deposit exposure and the condition and inferred age of surface artefacts exposed on these deposits.

8.3. The Accumulation and Preservation of Archaeology at UPK7

The sedimentology and geochronology presented above provide a broad framework for the depositional history of UPK7 as well as an understanding of the main processes involved in the formation of its sediment stack. The following section discusses the condition, spatial structure and inferred age of the archaeology found exposed on these deposits and how they inform our understanding of this depositional history, the influence of topography, the timing of substrate exposure and interpretation of Late Pleistocene to Holocene occupation and place use.

8.3.1. Review of Scenarios based on UPK7's history of formation

8.3.1.1. Exposure

Although the Lower Red sediment is the oldest sandy sediment body in the study area, there is little evidence to suggest it was subject to prolong periods of exposure. Artefact weathering and fragmentation is not appreciably higher than on the younger units, despite the fact that some artefacts on Lower Red (those from the Still Bay, 77-70 ka) are more than twice as old as the LSA artefacts that dominate Upper Yellow. The post-Howiesons Poort cluster in Exposure 1b, with an inferred age of 55-58 kya, suggests that at least some parts of Lower Red were buried within 7 kya. Noting the earlier modelling work of Phillips et al (2019), exposure of the consolidated surface of Lower Red may well have been considerably briefer than this. Similar arguments can be made for the Upper Yellow and Indurated Sand, at least to the extent that weathering patterns indicate durations of exposure not more substantial than that experienced by Lower Red. The coherence of the Early LSA cluster on Upper Yellow appears further to reinforce that most of the archaeology at UPK7 did not experience prolonged exposure immediately following discard. The absence of any dated sediment younger than 30 kya then becomes a key issue. As argued earlier, either there was an MIS 2 unit analogous to the Indurated Orange Sand at UPK9, or the sands which covered Upper Yellow and Indurated Sand at UPK7 never became consolidated. For reasons discussed above, the latter argument is favoured.

These issue aside and returning to the initial Scenarios posited at the start of this Chapter,

none of the findings suggest extended periods of exposure as outlined in Scenarios 1 and 2. The mid Holocene radiocarbon age is currently perhaps the only evidence that supports a duration of exposure any longer than that posited in Scenario 3 (2 kya). While ultimately it may not be possible to disentangle the plausibility of Scenarios 3 and 4, the history of agropastoralism in the Doring River valley, its intensification following the arrival of Europeans, the persistent overstocking of goats in the region, and the evidence throughout the valley for undercutting of historical structures by up to 600 mm all favour Scenario 4—that erosion of the sediment stack at UPK7 has accelerated in the last 300 years.

8.3.1.2. Chronology

Typo-technologically defined culture historic units were employed in this thesis to provide a locally and regionally defined temporal signal to assess the depositional history of UPK7's aeolian derived sediment bodies as well as the potential timing and duration of their exposure—a history that involved the differential accumulation, movement, and removal of material culture for at least the last 80 ka. Through qualitative and quantitative analysis of their spatial organisation an intricate relationship was established between archaeological epochs, their associated technocomplexes, and the burial age of their underlying substrates. The majority of diagnostic artefacts follow the law of superposition relative to the burial age of their underlying substrate. The observed distribution of artefacts represents a complex history of discard, erosion, and preservation, with overlap of Industries in most areas and some areas where exposure and preservation have resulted in the accumulation and burial of a single Industry of artefacts (i.e., Early LSA archaeology in Exposure 2 on the eastern side of the modern north-south dune crest). However, even when treated in isolation, the accumulation of diagnostic artefacts could have potentially taken place over a substantial amount of time, thereby capturing a time-averaged record of discard and post-discard activities at varying scales of time.

The temporal scale of Lower Red deposition is less certain than for the Upper Yellow and Indurated Sand units. It is bound by a maximum uranium-thorium age of ~260 ka, inferred from stratigraphic and compositional similarities observed at UPK9. The oldest minimum age for the burial of Lower Red sediment is 80 ka, which is in accordance with the inferred age range for the Still Bay artefacts that directly overly the Lower Red unit on two hillslopes (Exposures 1b and 1c), based on the OSL-derived age estimate of ~87 to ~72 ka from Hollow Rock Shelter (Högberg 2014, pp.144-145; Högberg & Larsson 2011). It is likely that Lower Red sediment continued to accumulate after this, suggested by the younger minimum burial ages of ~57, ~54 and ~52 ka, and the cluster of post-Howiesons Poort artefacts likely dating 58-55 ka.

The Lower Red and its associated MSA archaeology were buried by Upper Yellow sands from ~47 ka. The tightly clustered, and weathered condition of post-Howiesons Poort antedates this burial age and suggests that these artefacts were deposited in the still-accumulating A-horizon of Lower Red, protecting them from disaggregation and erosion. Late MSA artefacts, with an inferred age of 50-33 ka are distributed across both the Lower Red and the Upper Yellow units, though are appreciably more common on the former. Their presence across both units, abundance on the Lower Red, and absence from the Indurated Sand suggests that discard of these artefacts occurred between 55 ka (youngest archaeologically-inferred age for the Lower Red) and before 32 ka (formation of the Indurated Sand). Though their dispersed

condition suggests disaggregation, three observations suggest a different explanation. First, regardless of burial scenario they are unlikely to have been exposed for longer than the strongly-clustered post-Howiesons Poort. Second, opportunistic refits were made during collection of the RNG data. Third, the Late MSA at Klein Hoek displays a comparable pattern of abundance and dispersal; the pattern may not be taphonomic. Given the persistence of quartzite-dominant post-Howiesons Poort archaeology until 50 kya at sites in the region, the most likely explanation for the Late MSA at UPK7 is that it was discarded during the accumulation of Upper Yellow, 47-40 ka, and subsequently lagged onto Lower Red during recent erosion of their host unit.

The scarcity of Early LSA artefacts on the Lower Red unit together with its abundance on the Upper Yellow sediment of the eastern hillslope dated to ~40 ka, supports the burial of the Lower Red unit beneath Upper Yellow over the duration of Early LSA artefact discard (27-22 ka). The preservation of Early LSA artefacts, their density, and the absence of a strong signal from other Industries in this location suggests they were discarded during the accumulation of the Indurated Sand and buried prior to the Robberg (22-16 ka). This may also suggest that the current dune crest separating the eastern leeward face from the northern and southern hillslopes did not exist in this position during or prior to the formation of Upper Yellow sediment. Rather, dominant wind directions may have shifted at 40 ka, to more like the current system. Under this scenario, the area of Exposure 2 captures a distinct record of discard between 40 and 32 ka. It would be interesting to know whether Late MSA archaeology occurs beneath this deposit.

In contrast to the Early LSA and all older Industries, artefacts from the Robberg onwards are invariably dispersed and spread across multiple substrates. The clustering evidence and integrity from the Early LSA implies the presence of MIS 2 sediments in the upper elevation areas of UPK7 that no longer exists. Any artefacts from the Robberg onwards would necessarily have been deposited on or within that substrate, and their subsequent dispersal reflects deposition during its erosion. This aside, however, there is a topographically controlled trend in which artefact density occurs more frequently and/or intensively at higher elevations, irrespective of substrate age. It is likely that, even allowing for extensive loss of sediment from the middle and lower slopes of UPK7, occupation was always concentrated towards the dune crest.

8.3.2. Considering scale and its implications for archaeological interpretation

When interpreting variability in the composition of surface archaeology across UPK7 an understanding of the temporal and spatial scale of artefact association is required. Artefacts within a particular substrate can represent the time-averaged accumulation of directly discarded, vertically and/or horizontally lagged artefacts over multiple temporal scales (i.e., 10-10^2 ka). For instance, the Lower Red clearly represents the longest duration of artefact accumulation, in which artefacts are mostly MIS 5 and MIS 4/3 in inferred age, whereas Indurated Sand artefacts are restricted to MIS 1 and mixed with some lag from upslope MIS 3 and 2 material.

We can discuss behaviour and occupation duration by cluster structure and spread, but if we are to present a more rounded account of behavioural variability then artefacts need to be considered at the coarsest scale of accumulation to be certain of the temporal scale that these artefacts represent.

8.3.2.1. Artefact density in relation to substrate deposition and exposure

The results of the previous chapter show that artefact density is associated with elevation and the age of their underlying substrate. This association runs counter to what would be expected of taphonomically biased surface archaeology. Artefact numbers are highest on the oldest substrate (i.e., Lower Red, followed by Upper Yellow), lower on younger deposits (i.e., Indurated Sand) and rare or absent from the youngest substrate, Unconsolidated Sand. There are several possible explanations for this pattern:

1. The discard of cultural materials happened more frequently in the deeper past than the more recent past, and prior to the consolidation of overlying sands.

2. Artefact discard occurred at a constant rate through time. However, the length of time that a consolidated deposit was able to 'receive' discarded artefacts—be it through discard directly onto its exposed surface or from the vertical displacement or lag of artefacts from overlying sediment—was longer for older deposits.

3. Artefact discard occurred at a similar rate for all deposits or more intensively on younger deposits. However, recent artefact removal—either through human transport or erosional forces—has preferentially depleted the frequency of archaeology on younger substrates.

The plausibility of Explanation 1 depends on a well-preserved archaeological record and the conducive state (consolidated) and development (buried or exposed) of each deposit for the accumulation and burial of artefacts over a similar length of time. This scenario suggests a change in landuse involving a decrease in artefact discard activity, possibly resulting from a decrease in occupation. It demands that the environmental and climatic conditions (i.e., seasonally driven wet-dry cycles involving winter rainfall, dry season channel exposure and wind transport of sediment) required for the formation of these deposits were held constant from at least the beginning of MIS 3 to present.

Explanation 2 requires the duration of exposure to be longer for older deposits and shorter for younger deposits and/or for overlying sediment to remain soft or partially consolidated for decreasing lengths of time, thereby reducing the amount of time a consolidated surface can accrue overlying archaeology. Under this scenario the accumulation of archaeology and the intensity of artefact discard remained reasonably constant from the MSA to present—despite evidence of increased behavioural variability in southern Africa's archaeological record coupled with rock shelter evidence for fluctuating occupation intensity throughout this time.

Explanation 3 depends on evidence for the non-cultural/cultural removal of surface archaeology on younger deposits relative to evidence for the retention of artefacts on older deposits. In the case of non-cultural depletion of younger archaeology, both the erosion and removal of younger artefacts and younger sediment are expected. This should also be evident in the frequency and location of diagnostic artefacts. Fewer artefacts diagnostic of more recent discard is expected than artefacts with older inferred ages. However, where younger artefacts and deposits of a similar age are rare or absent, artefacts of an equivalent age should still be present on the older substrates. In the case of cultural transforms—such as transportation of artefacts from younger substrate and/or the preferential use of areas where older substrate is exposed—younger deposits should be preserved with associated artefacts occurring on these, albeit at lower frequencies than on older substrates. This explanation would also result in higher artefact numbers on older deposits, thus presenting a similar outcome to the one proposed for Scenario 2.

8.4. Palaeoclimate and Landuse Impact on Preservation and Visibility

With the preceding formation history in mind, the following section presents a discussion on the relationship between UPK7's formation history and our current, regional-scale knowledge of environmental change over the last 100 ka. Particular attention is paid to the discontinuous history of UPK7's formation and archaeological exposure and what this tells us about the preservation of archaeology at the locality and the intensity and timing of land use in the study area. Similar to the preceding section, the following discussion is organised chronologically, by Marine Isotope Stage, from MIS 1 to >4. Covering 100 ka of environmental change in the Western Cape region.

The depositional history of UPK7's sediment stack indicates that source bordering sands have been deposited by way of aeolian transportation for at least 80 ka. The deposits of Lower Red, Upper Yellow, and Indurated Sand preserve at least partial records of periods when sand accumulation outpaced its erosion, possibly indicating times when conditions were more humid and thus more conducive to pedogenesis. Sand accumulation relies on the availability of dry channel alluvium and indicates repeated periods of extended dry seasons in which the riverbed was dry for long enough to enable aeolian transport and deposition, similar to the current seasonal regime observed today. Stabilisation of these deposits would also require soil building conditions such as increased moisture and vegetation growth. Their eventual consolidation would also require their preservation and conversion into a B-horizon beneath a thick A-horizon of sand. Together these conditions suggest that from at least 70 ka to 30 ka, the seasonal regime providing dry channel sands together with the wind conditions required to transport and deposit these sands onto UPK7 were active. It also suggests that their stabilisation and preservation resulted from more humid conditions than those of the Holocene, and possibly even the terminal Pleistocene. The absence of consolidated sediment after 30 ka suggests that conditions during this time were less conducive to promoting the stabilisation of overlying dune sands and sand sheets, though caution is required given implications from the distribution and state of artefacts that sediment units younger than 30 ka were at one time present but subsequently removed. To the extent that the conditions favouring sediment and accumulation are not hyper-local, the evidence for a ~27 ka sediment unit at UPK9, immediately east of UPK7, is germane.

Since the terminal Pleistocene, drier conditions in the study area would increase the impact of processes that catalyse erosion (i.e., more extreme rainfall events, increased animal, and anthropogenic activity and thus foot traffic) and increase the likelihood of reactivation of stable deposits across the locality. A broad range of evidence suggests that the exposure of older sediment bodies across UPK7 was relatively recent, most notably the distribution and clustering of pottery fragments on the lower zones of the Indurated Sand and on the upper zones of the Upper Yellow. The horizontal integrity of these clusters appears high, with limited winnowing of small artefacts. The stone artefacts associated with the lower cluster of pottery include evidence of refitting and are also in good condition relative to the archaeology on the Indurated Sand and Lower Red, at higher elevations. Likewise, the pottery clustered at the top of UPK7s sediment stack, on the Upper Yellow, is associated with stone artefacts that show minimal weathering, fragmentation and size-sorting compared to artefacts on the Lower Red and Indurated Sand. Their horizontal integrity coupled with their general absence from the middle zone of the southern hillslopes which expose both Lower Red and Indurated Sand sediment—albeit with some down-slope lag from Upper Yellow onto Lower

Red in Exposure 1b—suggests that pottery in the upper zone is related to discard that occurred prior to the extensive erosion and removal of sediment from these lower elevations, while the lower zone pottery cluster could relate to a later period of discard activity after the exposure of the current Indurated Sand and Lower Red surfaces. The earliest evidence of pottery found in the region dates to < 2 ka BP (Kaplan 1987; Nackerdien 1989; Parkington et al. 1980) and its use continued in the catchment until as recently as ~430 BP and ~230 BP (Parkington & Poggenpoel 1971; Sealy & Yates 1994)—constrains the contemporaneous timing of exposure of Lower Red and Indurated Sand to their current surface extents—to within the last 2 ka. The clustered pottery fragments in the lower zone of Indurated Sand were either transported to this position as a cluster during this time or has accumulated since the exposure of the Indurated Sand and Lower Red, possibly as recently as 200 years ago.

The introduction of pottery also postdates the arrival of Ovis and pastoralism at coastal sites in southern Africa (Sealy & Yates 1994). The connection between pottery and increase in concentrated ungulate activity in areas of grazing is indicated by the recent fragmentation of implements across the entire locality, irrespective of substrate age or hillslope zone. This indicates that extensive trampling occurred across the locality when all sediment units were exposed to their current surfaces at least within the last 2 ka. Significant differences in flake fragmentation between sediment units suggests that the Indurated Sand has experienced longer or more intensive trampling activity than the Upper Yellow and Lower Red. This suggests that the Indurated Sand deposit was exposed to foot traffic prior to the exposure of these older units within at least the last 2 ka. It also suggests that the archaeology on the older units was not subjected to as much trampling during their initial discard and exposure compared to the artefact's discarded onto the Indurated Sand unit, post-30ka. Overall, trampling has increased, be it due to longer periods of exposure of Indurated Sand or more intensive activity on this deposit when artefacts were being discarded or knapped for use elsewhere. While aridification since the LGM coupled with more acute oscillations between wet and dry conditions during the Holocene has most likely increased the rate of weathering and erosion at UPK 7, the introduction of pastoralism and European farming in the region has actively compounded these processes, as evidence by the striking fenceline effect at the locality Klein Hoek 1 (Ames et al. 2020). Together the interplay between environment and anthropogenic conditions has induced the Late Holocene deflation and exposure of Late Pleistocene sediment and archaeology. Under these conditions, topographic setting plays an important role in promoting or inhibiting the preservation and spatial integrity of this material.

8.5. Study Implications for the History of Landuse in the Doring River Catchment (Historic to Prehistoric)

The objective of this section is to bring together the archaeological findings (taphonomic and behavioural) of this study and those previously published for UPK7, the wider landscape of the Doring River catchment, and Western Cape region. This section links with the preceding palaeoenvironmental discussion to provide perspective on the kinds of knowledge we can expect to gain about the catchment's history of landuse—given the constraining factors promoting and inhibiting the preservation of archaeology at UPK7

UPK7 has been likened to a stone resource, wherein people in the past came to gear-up, discarding cores and end products in preference for larger flakes to use elsewhere (Low et al. 2017; Shaw et al. 2019).

If this is the case, the question is whether this behaviour prevailed throughout the Late Pleistocene and into the Holocene. If this activity depended on the availability of stone, it would have in turn depended on the continued availability of stone as both worked and unworked material as well as intermittent exposure of previously transported/worked material to increase its visibility for access and use. However, if these artefacts were visible and available for gearing-up and re-use they would also be vulnerable to processes of erosion and weathering that would result in their disaggregation within 1,000 years and eventual removal within 10,000 years. Thus, it is unlikely that the Pleistocene artefacts observed today would have remained in their current position without showing a greater degree of size-sorting and erosion than the results of this study show if they were exposed throughout the terminal Pleistocene and Holocene.

Added to this is the proximity of raw materials sourced from the river channel. Changes in the morphology of the river over the past 70 ka possibly influenced when, where and how often river-sourced material was discarded in the valley. One plausible explanation for the lower frequency of LSA material at UPK7 relative to the MSA and to the LSA found at UPK9 could be due to the position of exposed channel riffles in the river channel relative to UPK7. Prior to 25 ka the riffle zone may have extended down past UPK7 providing a local river source of core material and access to the water in the downstream pool. Since 25 ka headward erosion of the pool may have eliminated the riffle source from near UPK7 and replaced it with sand. The riffle source would have been nearer to UPK9, possibly accounting for the greater LSA archaeology in this area.

However, based on the depositional history of UPK7, the dominant condition influencing the frequency of LSA relative to MSA archaeology is hillslope erosion (i.e., slope angle and rill formation). Moreover, although UPK9 lacks the same degree of sand accumulation across its surface, its lower hillslope gradients have possibly enabled greater retention of LSA material compared to UPK7.

There are also notable absences and markedly lower frequencies of diagnostic artefacts for some Industries over others. The rarity of Howiesons Poort artefacts at UPK7 reflects the characteristic dynamic between a paucity of Howiesons Poort in open-air contexts compared to its artefact rich deposits in rock shelters—a trend that continues to confound researchers of both rock shelter and open-air contexts. One possible explanation is that Howiesons Poort backed and notched artefacts were less well preserved compared to Still Bay, post-Howiesons Poort and Late MSA archaeology. Although, diagnostic artefacts for the Still Bay, Howiesons Poort, post-Howiesons Poort and Late MSA Industries are located in high density areas largely representing MSA accumulation, the lower frequency and randomly distributed Still Bay and Howiesons Poort artefacts suggests some horizontal displacement and possibly even erosion of these artefacts prior to the accumulation of subsequent MSA Industries. Moreover, under conditions of exposure, the larger Still Bay bifacial points would also be more resistant to entrainment on slopes below 15º than the smaller backed and notched pieces of the Howiesons Poort (Chambers 2016), which would explain the high frequency of Still Bay artefacts compared to the Howiesons Poort, despite the Still Bay being older.

However, the propensity for sand accumulation and pedogenesis during the formation of the Lower Red and Upper Yellow suggests that the discard of artefacts between MIS 5 and 3 promoted artefact burial and preservation rather than long-term exposure. Under these conditions the spatial organisation and relative frequency of Still Bay and Howiesons Poort diagnostic artefacts could be considered less a

reflection of post-depositional attrition and more an indication of discard behaviour across the study area over time. However, a lesson learned from the presence of Late MSA archaeology across UPK7 and its occurrence at PL1 is that the absence of specific artefact types considered characteristic of a period or Industry in rock shelters is not necessarily representative of stone tool use, reduction, and discard across the wider landscape. Another key take-home from the Late MSA is that dispersed appearance on land-surfaces does not necessarily imply disaggregation. At UPK7, as at all other localities where is has been observed (Shaw et al., 2019), Late MSA artefacts are highly dispersed. However, their state of weathering, lack of size-sorting, and presence of refits suggests that this is not a consequence of horizontal deposition. It may simply be that Late MSA artefacts were discarded in a disaggregated pattern when compared to the preceding post-Howiesons Poort and subsequent Early LSA. The Howiesons Poort pattern may similarly be explained by land-use: that its discard in the open reflects short-term occupation by highly mobile groups, rather than any spatial variation in technological form.

CHAPTER 9.
CONCLUSIONS

The objective of this thesis was to understand the formation of Late Pleistocene open-air surface archaeology in relation to its sedimentary system. A geoarchaeological approach was taken, combining interdisciplinary field and analytical methods from the Earth and archaeological sciences (i.e., sedimentological, geomorphological, geochronological, archaeological, and geospatial methods). The study focused on one of 16 archaeologically abundant sediment stacks in the semi-arid landscape of the Doring River valley. Through this investigation the main depositional and erosional processes involved in the formation of UPK7's sand mantle were identified, and its depositional history reconstructed. This made it possible to assess how the spatial patterning, visibility and preservation of the locality's surface archaeology reflects the history of UPK7's formation as well as its history of occupation.

At the start of this study six questions were posed:

1. What is a 'sediment stack' in the sense the DRAP has used the term, and how did the one at Uitspankraal 7 form?
2. When did it form?
3. What are the main processes of deposition and erosion at UPK7?
4. How have these processes promoted or inhibited the visibility and movement of its associated archaeology over time?
5. How does this formation history relate to the inferred age of the archaeology? And what temporal scale(s) of archaeological formation are we working with?
6. How recently has surface exposure of UPK7's archaeology occurred, and what are the implications for its future?

Each of these were investigated and answered in-turn. The following summarises the main findings relating to each question:

1) The DRAP's use of the term sediment stack is intended as a generalisation. However, its valley-wide application to all archaeology-bearing landforms in the study area gives the impression that these landforms share similar formation histories. However, this study demonstrates the importance of local-scale conditions in the formation of UPK7 (i.e., the surrounding topography and position relative to river channel morphology and channel bed composition). The foundation of UPK7's sediment stack formed through bedrock-constrained hillslope erosion and point-bar terrace development from the southward migration of the Doring River. Within the last ~191 ka, source-bordering sand dune accumulated through aeolian transport of seasonally available channel alluvium over this foundation. This sand mantle continues to form under seasonal wet-dry conditions, largely from the dry-season erosion of channel alluvium by south-westerly winds. The sand mantle's overall morphology is roughly contiguous with the topography of the underlying palaeoterrace and hillslope. However, surface topography is also influenced by the direction and strength of the wind relative to the location and proximity of channel alluvium to the hillslope. The position of the most recent dune ridges indicates pivoting wind directions from westerlies to southwesterlies.

2) UPK7's sand mantle formed over more than 80 ka. This history involved the formation of at least four distinct sediment units, starting first with the aeolian accumulation of deflated channel alluvium, followed by stabilisation and consolidation, with pedogenesis evident in the oldest unit, Lower Red. Lower Red accumulated prior to the deposition of Upper Yellow,

at ~47 ka. The presence of calcium carbonates within the Lower Red unit indicates long term secondary processes of evaporation within the unit during strong seasonal conditions of repeated rapid drying of wet sediment. The initiation of Upper Yellow sand accumulation occurred between ~50 and 44 kya and continued until at least ~37 ka. During this time, at least one slope wash event resulted in the removal of mid slope sediment sometime between ~44 and ~37 kya. A gap of at least ~3 ka between this slope wash event and the stabilisation of Indurated Sand suggests a period of instability, during which time sand accumulated, but did not stabilise. Only topographically protected areas of the sand mantle (i.e., the leeside of the eastern dune ridge) were mostly protected from erosion and exposure. The accumulation and stabilisation of Indurated Sand across most of UPK7 occurred between ~34 and 29 kya. Sedimentation becomes more ephemeral during MIS2, with the absence of consolidated sediment post-dating Indurated Sand suggesting overlying deposits never stabilised and/or were deflated. The unconsolidated and semi-consolidated sand units are considered analogous of the initial formation of the older, now consolidated, sediment units—actively accumulating and shifting across the hillslope, while providing periodic coverage for underlying deposits. Until further dating programmes are carried-out for the semi-consolidated sediment, it remains unclear how old this deposit is, possible representing formation since the terminal Pleistocene.

3) The main erosional processes identified at UPK7 are wind and rainfall. Wind erosion slowly deflates surface sediment from the windward facing hillslope, exposing, and catalysing the vertical displacement of artefacts, while moving sand either to the leeside of the northern and eastern dune ridges or from the sediment stack altogether. Rainfall driven hillslope erosion destabilises and entrains sediment and artefacts through rain splash, sheet wash and slope wash. Rainfall has had the most impact on the southern hillslopes and northern hillslopes. Surface crusts and slope angle catalyse rill development from ~9°, and gully development from 15°. Rills and gullies are densest from the middle hillslope zone downwards. Lower Red is exposed in the middle hillslope zone where processes of weathering and transportation are active closest to rills. Upper Yellow sediment is exposed on both the fringe and at the top of the sand mantle, where sediment is actively eroding. This is exposing Upper Yellow beneath residual sand and above lagged artefacts and sediment. Slope angles are >15 in the fringe zone and below 9° at the very top of the sand mantle. The Indurated sand unit is a combination of lagged sediment and aeolian sand. It is located on the lower hillslope zones where it is thick, deeply incised by rills and gullies, and has a slope angle >9°. This deposit forms a surface where sheet wash and wind deflation dominate over most of its surface with slope wash entrainment occurring close to deeply incised rills and gullies.

4) The depositional and erosional processes of wind and rain. coupled with an artefact's topographic setting (i.e., slope angle & hillslope position) control archaeological visibility and movement. The topography of UPK7's sediment stack is largely the product of at least 80 ka of aeolian sand accumulation onto the cobble and bedrock hillslope in conjunction with rainfall and wind erosion. The growth and density of vegetation is highest where Unconsolidated Sand and Semi-consolidated Sand occurs, covering all but the central and northernmost hillslope of UPK7. These conditions inhibit artefact visibility, likely covering a substantial portion of the archaeological record of UPK7. The position of the two dune crests suggests that the dominant wind directions are from south-west to north-east and south to north. The position of both dune crests provides a degree of protection to the archaeology, with artefacts in Exposure 2 indicating long-term burial of Early LSA artefacts on the leeward side of the north-south dune crest. There are two potentially dominant windward sides of the locality that are thus prone to active movement of Unconsolidated Sand across its surface. These are the south and west facing slopes (Exposures 1 a-c and 3). The absence of the Unconsolidated Sand and Indurated Sand on the northernmost hillslopes (Exposures 4-6)

suggest that the sediment in these areas were and continue to be removed in this part of the study area. The condition of artefacts in the upper hillslope zones of UPK7 are also consistent with hillslope morphology and erosion, being subject to the least sediment entrainment—as evidenced in the retention of residual Upper Yellow sediment and Unconsolidated Sand in the north-east of the study area. However, from the middle zone downwards entrainment is evident in the size-sorting of artefacts, especially on the southern hillslopes (i.e., Exposure 1b). These areas are also extensively altered by moderate to well-developed rills, effective at stripping the surrounding surface of artefacts of all sizes on slopes greater than 15º. Overall, there is a topographically controlled pattern where the density of artefacts is highest at the top of the sand mantle, irrespective of substrate age, suggesting that human activity was often concentrated in this area.

5) When artefacts are assessed at the scale of archaeological epoch the spatial distribution of MSA artefacts are shown to have a significant association with the oldest deposit, Lower Red, whereas LSA artefacts have a significantly high proportional frequency with Upper Yellow sediment compared to the older Lower Red substrate and the younger Indurated Sand. When the temporal scale of inferred artefact age is constrained to the typo-technological Industry, this provides some insight into the dynamic between the timing of substrate and archaeological accumulation and exposure, in some cases indicating contemporaneous exposure of multiple deposits with different burial ages.

6) Substantial deflation of sediment post-dating the accumulation of Indurated Sand appears to have taken place sometime in the last 30 ka, increasing with intensity in the Holocene, supporting aspects of both Scenarios 3 and 4. This has culminated in the recent exposure of all three consolidated substrate units, the removal of overlying sediment dated to between 30 and 5 ka, and the exposure of an extensive archaeological record in the last 2 ka. Human activity in the area has perpetuated and, in some cases, accelerated both the sediment load available for deposition and the destabilisation and erosion of deposits in the study area, playing an antagonistic role in a system already dominated by erosional processes in an increasingly tumultuous climate.

9.1 Contribution and Implications

This study contributes to a resurgence in southern Africa's open-air research that has taken place over the last decade. However, of greater significance is its contribution to the rare number of geoarchaeologically driven open-air projects carried-out in the interior and subcontinent generally. The fact that the number of dedicated open-air geoarchaeological studies of southern Africa's open-air surface archaeology can be counted on one hand is a cause for serious concern, especially given that it is nearly a century since Goodwin and van Riet Lowe's seminal work on the southern African Stone Age, and over half a century since the introduction of radiometric techniques. Added to this is the fact that rock shelters are restricted to geologically conducive environments and few yield continuous chronostratigraphic sequences. This emphasises the need to continue to expand the geoarchaeological sample. It also highlights the need for a close working relationship between projects. This is particularly crucial if reconstructing human-environment interactions at a landscape and regional scale during southern Africa's Late Pleistocene is to become a fruitful undertaking.

This thesis also draws attention to a disconcerting lag in the development of methodological approaches tailored to the specific challenge of extracting data from open air contexts. This goes some way towards explaining why southern African research continues to underestimate, underexplore, and

underrepresent a potentially rich source of human behavioural information in models of Late Pleistocene human-environment interaction.

9.1.1 Studying the Doring River sediment stacks

At its most basic, this thesis demonstrates the necessity of investigating the local formation processes and depositional histories of an open-air context in order to determine how the condition, age and spatial distribution of surface archaeology is both influenced and constrained by its sedimentary system. The formation contained in a sediment stack is sensitive to local conditions and depends on a range of historical contingencies (i.e., river morphology, sediment supply, topography, and landuse practises and intensity during the late Holocene), as well as catchment and regional conditions relating to climate and geology. Likewise, the exposed archaeology at UPK7 also differs in amount, age and spatial distribution compared to other sediment stacks (Shaw *et al.* 2019). There should not be an expectation, therefore, that the catchall 'sediment stack' used to refer to archaeologically visible localities in the Doring River valley are the same or preserve equivalent formation histories. For this reason, a geoarchaeological assessment of the formation dynamics of each sediment body is recommended. Ideally, this would be carried out as part of a larger project dedicated to soil stratigraphic characterisation and analysis of alluvial, aeolian, and colluvial units at the regional, basin-wide scale. This will help to capture aspects of the landscape's history of formation not otherwise captured by UPK7 and to establish the stratigraphic relationship of all depositional units and soil events in the study area. If possible, all units should be dated, not just the consolidated deposits related to a sand mantle.

The DRAP's prioritisation of sediment stacks also tends to limit chronological discussion to the age of the deposits being studied, risking the exclusion of older (i.e., the ESA LCT associated with the colluvium of UPK7)—and in some cases younger—artefacts or discard patterns that occur outside of the confines of a specific landform (e.g., at a more disparate scale). Therefore, future research should also be directed at investigating the spatio-temporal distribution and formation context of artefacts beyond the exclusive sediment-stack-based focus that predominates to this day. Inclusion of low-visibility areas will provide a broader perspective on the environmental and behavioural patterns observed at high-visibility localities like UPK7.

9.1.2 Interpretation of visible archaeology

If this thesis could be said to have one overriding message, it is the degree to which the visibility, density, and diversity of time-diagnostic artefacts are largely dependent on the sedimentary system once they are discarded. Caution is therefore advised when undertaking research that seeks to track and compare the presence-absence of archaeology at the scale of the archaeological epoch and/or technological Industry—be it across a landscape, region, or the entire subcontinent. The combination of factors controlling the visibility of certain Industries include: 1) the morphology of the diagnostic artefacts characterising a specific Industry, 2) the stage of reduction at which artefacts are discarded, 3) where and how often discard occurs, and 4) the timing, duration, and composition of the sediment an artefact is discarded onto and/or incorporate into and/or eroded from. However, the depositional conditions of the latter most often preclude detection of the preceding conditions. Thus, studies that attempt to model landuse change based on the

presence-absence of certain time-diagnostic artefacts across a landscape, without first accounting for their formation history and the entire range of stone artefact classes (i.e., tools, cores, *and* flakes), run the risk of presenting spatio-temporal patterns that result from local scale processes of preservation and sediment composition rather than change in site function, occupation duration, or abandonment.

Caution is also advised when attempting to formulate site-based interpretations of the spatial organisation of the surface archaeology across UPK7. Interpretation of clustered versus dispersed archaeology should be carried out using both visual and spatial analyses, together with considerations of deposition and exposure durations, change in deposit composition over time, and the environmental and anthropogenic processes involved. Together, these factors can promote or inhibit the visibility of artefacts through their removal or burial, overemphasising the relative (local scale) density of archaeology in some areas while downplaying the density of artefacts in another.

9.1.3 Temporal control and the scale of interpretation

Open-air deposits are readily datable. The main limitation to this is the technique used and how this is associated with the accumulation and exposure of the archaeology and its sedimentary context. So, while the 'blanket dating' envisaged by Parkington (1990) over thirty years ago is not possible in open-air settings (or even stratified contexts for that matter), this study shows that it is possible to constrain the age of surface archaeology through a combination of inferred artefact age, spatial analysis, sedimentological analysis, and chronometric dating.

While it is difficult to temporally constrain UPK7 artefacts to the Industry-specific resolution often obtained in rock shelters, it is nonetheless possible to provide a coarse temporal scale for the archaeology without limiting technological investigations to diagnostic artefacts. Archaeology across the three main deposits at UPK7 yields a record of artefact accumulation prior to the LGM (in some areas between 40 and 30 ka) as well as archaeology that post-dates the LGM (in some areas after the use of pottery). Moreover, most of UPK7's deposits and a large component of its archaeology accumulated during MIS 3 or earlier. This provides an intriguing counterpoint to the rock shelter evidence, which suggests declining occupation in the region. It thus contributes to the emerging pattern that people continued to occupy the river valley rather than abandon this region—albeit more often in open settings than in rock shelters. The inclusion of this information into what is currently a rock shelter dominated narrative provides a multiscale-perspective on long- and short-term change in human-environment interaction across the wider region that is not otherwise captured by rock shelter deposits in the Western Cape.

9.1.4 Implications for palaeoenvironmental reconstruction

This study also highlights the deficit in knowledge of the palaeoenvironmental record in the eastern Cederberg when compared to the western Olifants-Doring Basin and Western Cape coast. Based on its current environmental conditions, it is clear that the Doring-Olifant catchment is composed of multiple microclimates, with the Doring River valley often receiving less rain as a result of its rain shadow position than its western tributaries and the Cederberg mountains. Therefore, this study highlights the necessity of additional palaeoenvironmental research both within and farther east of the valley to improve and supplement our understanding of UPK7's depositional history in both its own right and as part of the wider

landscape. One drawback to this endeavour is the limited organic archive. Thus, the depositional history of UPK7 and that of other localities in the valley provide a valuable record and rare insight into the palaeoenvironmental conditions of at least the last 50 ka.

9.2 Final Words

The interaction between humans and their environment continues to influence the formation and preservation of UPK7's archaeology. However, this has had an accelerating impact on the erosion of UPK7's archaeology within at least the last 2 ka. Thus, the findings in this study and elsewhere (Ames *et al.* 2020) reinforce the urgency and importance of investigating the surface and subsurface archaeology in the Doring River valley and open-air settings generally. By deliberately ignoring coarse-scale aggregates (both spatial and temporal), we run the risk of losing behavioural information and thus biasing spatial and chronological models of hunter-gatherer occupation duration and behavioural variability across an environmentally dynamic landscape. We also run the risk of inadvertently excluding environmental archives for the Late Pleistocene and Holocene that are otherwise poorly preserved in interior and open-air settings. Thus, this work contributes to the emerging consensus that the rock shelter narrative for human behavioural evolution is indeed biased and, as a consequence, fails to capture landscape scale behavioural trends during the Late Pleistocene. However, this cannot be confidently rectified unless conducted with the combined input of rock shelter and open-air evidence, obtained through geoarchaeological methods, and framed by their unique formation histories. Therefore, the future of southern African Late Pleistocene research depends on developing its approach to investigating the formation and spatio-temporal scale of open-air archaeology and the context that enables its existence as a proxy for past behaviour, irrespective of its perceived state of exposure and spatial integrity.

REFERENCES

1:1M SOTER for the GLADA partner countries Argentina, China, Cuba, South Africa, Senegal and The Gambia, and Tunisia (2008) [online database], available: http://www.fao.org/ag/agl/lwdms.stm

AgiSoft (2018) 'Agisoft PhotoScan User Manual, Professional Edition', Version 1.4.

Agresti, A (2003) *Categorical data analysis*, John Wiley & Sons.

Aitken, MJ (1985) *Thermoluminescence dating*, London: Academic Press Inc.

Aitken, MJ (1998) *Introduction to optical dating: the dating of Quaternary sediments by the use of photon-stimulated luminescence*, Clarendon Press.

Ambrose, Stanley H (2010) 'Coevolution of composite-tool technology, constructive memory, and language: Implications for the evolution of modern human behavior', *Current Anthropology*, 51(S1), S135-S147.

Ames, CJH, S Chambers, M Shaw, N Phillips, BG Jones & A Mackay (2020a) 'Evaluating erosional impacts on open-air archaeological sites along the Doring River, South Africa: methods and implications for research prioritization', *Archaeological and Anthropological Sciences*, 12(5), 103.

Ames, CJH, LA Gliganic, C Cordova, K Boyd, BG Jones, L Maher & B Collins (2020b) 'Chronostratigraphy, site formation, and palaeoenvironmental context of Late Pleistocene and Holocene occupations at Grassridge Rock Shelter (Eastern Cape, South Africa)'.

Ames, CJH, J Riel-Salvatore & BR Collins (2013) 'Why we need an alternative approach to the study of modern human behaviour', *Canadian Journal Of Archaeology*, 37, 21-47.

Ames, CJH, M Shaw, C O'Driscoll & A Mackay (2020c) 'A multi-user mobile GIS solution for documenting large surface scatters: an example from the Doring River, South Africa', *Journal of Field Archaeology*, 45(6), 394-412.

Amschwand, N (2003) 'Crossing the Doorn (Doring) River', *VASSA Journal*, 10, 26-30.

Anders, N, J Valente, R Masselink & S Keesstra (2019) 'Comparing Filtering Techniques for Removing Vegetation from UAV-Based Photogrammetric Point Clouds', *Drones*, 3(3), 61.

Anderson, G (1991) *Andriesgrond Revisited: Material Culture, Ideologies and Social Change*, unpublished thesis University of Cape Town.

Andrefsky, W (2005) *Lithics: Macroscopic Approaches to Analysis*, 2nd ed., Cambridge: Cambridge University Press.

Angulo, RJ, GC Lessa & MCd Souza (2006) 'A critical review of mid- to late-Holocene sea-level fluctuations on the eastern Brazilian coastline', *Quaternary Science Reviews*, 25(5), 486-506.

Araujo, AGM, AM Strauss, JK Feathers, JC Paisani & TJ Schrage (2013) 'Paleoindian open-air sites in tropical settings: A case study in formation processes, dating methods, and paleoenvironmental models in central Brazil', *Geoarchaeology*, 28(3), 195-220.

Archer, W (2017) *What is Still Bay? Human Behavioural Variability and Biogeography Reflected in Southern African Middle Stone Age Bifacial Points*, unpublished thesis.

Arnold, JR & WF Libby (1949) 'Age determinations by radiocarbon content: checks with samples of known age', *Science*, 110(2869), 678-680.

Backwell, LR, F d'Errico & WE Banks (2018) 'New Excavations at Border Cave, KwaZulu-Natal, South Africa'.

Baddeley, AJ & R Turner (2004) 'Spatstat: An R package for analyzing spatial point pattens'.

Bailey, GN (2008) 'Time perspectivism: Origins and consequences' in Holdaway, S. & Wandsnider, L., eds., *Time in Archaeology: Time Perspectivism Revisted*, Salt Lake City: The University of Utah Press.

Bar-Yosef, O (1998) 'On the nature of transitions: the Middle to Upper Palaeolithic and the Neolithic Revolution', *Cambridge Archaeological Journal*.

Barich, BE, EA Garcea & C Giraudi (2006) 'Between the Mediterranean and the Sahara: geoarchaeological reconnaissance in the Jebel Gharbi, Libya', *Antiquity*, 80(309), 567-582.

Baril, MR (2004) 'Emission and excitation spectra of feldspar inclusions within quartz', *Radiation Measurements*, 38(1), 87-90.

Bateman, M, C Boulter, A Carr, C Frederick, D Peter & M Wilder (2007) 'Preserving the palaeoenvironmental record in drylands: bioturbation and its significance for luminescence-derived chronologies', *Sedimentary Geology*, 195(1-2), 5-19.

Baxter, A (1996) *Late quaternary palaeoenvironments of the Sandveld* [PhD], unpublished thesis University of Cape Town.

Beaumont, PB, AB Smith & JC Vogel (1995) 'Before the Einiqua: the archaeology of the frontier zone'.

Beaumont, PB & JC Vogel (1972) 'On a new radiocarbon chronology for Africa south of the Equator: Part 2', *African Studies*, 31(3), 155-182.

Behar, DM, R Villems, H Soodyall, J Blue-Smith, L Pereira, Ene Metspalu, R Scozzari, H Makkan, S Tzur, D Comas, J Bertranpetit, L Quintana-Murci, C Tyler-Smith, RS Wells & S Rosset (2008) 'The Dawn of Human Matrilineal Diversity', *American Journal Of Human Genetics*, 82(5), 1130–1140.

Behm, JA (1985) 'An Examination of the Effects of Slope Wash on Primary Deposits of Chipping Debris: A Reply to Baumler', *Lithic Technology*, 14(3), 126-129.

Bernard, ÉA (1962) *Théorie astronomique des pluviaux et interpluviaux du Quaternaire africain: fluctuations séculaires du régime d'insolation des latitudes tropicales et leurs effets sur les régimes thermiques et pluviométriques*, Inst. belge pour l'encouragement de la recherche scientifique outre-mer.

Bierman, PR, D Montgomery & C Massey (2013) 'Key concepts in geomorphology; a future-looking community-based textbook that builds on our past', *Abstracts with Programs - Geological Society of America*, 45(7), 577-577.

Binford, LR (1981) 'Behavioral archaeology and the "Pompeii premise"', *Journal Of Anthropological Research*, 37(3), 195-208.

Binford, LR (1985) 'Human ancestors: changing views of their behavior', *Journal of Anthropological Archaeology*, 4(4), 292-327.

Binford, LR (2001) *Constructing Frames of Reference: An Analytical Method for Archaeological Theory Building Using Ethnographic and Environmental Data Sets*, Berkeley, CA: University of California Press.

Binford, SR & LR Binford eds. (1968) *New Perspectives in Archeology*, Chicago,: Aldine Pub. Co.

Bleed, P, M Douglass, A Sumner, M Behrendt & A Mackay (2017) 'Photogrammetrical Assessment of Procedural Patterns and Sequential Structure in “Handaxe” Manufacture: A Case Study along the Doring River of South Africa', *Lithic Technology*, 42(1), 3-12.

Blome, MW, AS Cohen, CA Tryon, AS Brooks & J Russell (2012) 'The environmental context for the origins of modern human diversity: A synthesis of regional variability in African climate 150,000–30,000 years ago', *Journal Of Human Evolution*, 62(5), 563-592.

Bluff, KCP (2017) *The Terminal Pleistocene of Klipfonteinrand Rock Shelter in the Cederberg*, unpublished thesis, University of Cape Town.

Bøtter-Jensen, L, E Bulur, G Duller & A Murray (2000) 'Advances in luminescence instrument systems', *Radiation Measurements*, 32(5-6), 523-528.

Bøtter-Jensen, L & V Mejdahl (1988) 'Assessment of beta dose-rate using a GM multicounter system', *International Journal of Radiation Applications and Instrumentation, Part D, Nuclear Tracks and Radiation Measurements*, 14(1-2), 187–191.

Bouzouggar, A, N Barton, M Vanhaeren, F d'Errico, S Collcutt, T Higham, E Hodge, S Parfitt, E Rhodes & J-L Schwenninger (2007) '82,000-year-old shell beads from North Africa and implications for the origins of modern human behavior', *Proceedings of the National Academy of Sciences*, 104(24), 9964-9969.

Braun, DR, NE Levin, D Stynder, AIR Herries, W Archer, F Forrest, DL Roberts, LC Bishop, T Matthews, SB Lehmann, R Pickering & KE Fitzsimmons (2013) 'Mid-Pleistocene Hominin occupation at Elandsfontein, Western Cape, South Africa', *Quaternary Science Reviews*, 82(0), 145-166.

Brennan, BJ (2003) 'Beta doses to spherical grains', *Radiation Measurements*, 37(4), 299-303.

Breuil, AH (1945) 'A preliminary survey of work in South Africa', *The South African Archaeological Bulletin*, 1(1), 5-7.

Brown, FH, I McDougall & JG Fleagle (2012) 'Correlation of the KHS Tuff of the Kibish Formation to volcanic ash layers at other sites, and the age of early *Homo sapiens* (Omo I and Omo II)', *Journal Of Human Evolution*, 63(4), 577-585.

Brown, KS, CW Marean, AIR Herries, Z Jacobs, C Tribolo, D Braun, DL Roberts, MC Meyer & J Bernatchez (2009) 'Fire as an engineering tool of early modern humans', *Science*, 325(5942), 859-862.

Bräuer, G (1984) 'A craniological approach to the origin of anatomically modern Homo sapiens in Africa and implications for the appearance of modern Europeans' in *The origins of modern humans: a world survey of the fossil evidence*410.

Bullard, JE & GH McTainsh (2003) 'Aeolian-fluvial interactions in dryland environments: Examples, concepts and Australia case study', *Progress in Physical Geography*, 27(4), 471-501.

Burkitt, MC (1928) *South Africa's Past in Stone and Paint*, Cambridge University Press.

Butzer, KW (1971) 'Fine alluvial fills in the Orange and Vaal basins of South Africa', *Proceedings of the Association of American Geographers*, 3.

Butzer, KW (1984) 'Late quaternary environments in South Africa', in *Late Cainozic palaeoclimates of the Southern Hemisphere. International symposium held by the South African Society for Quaternary*

Research; Swaziland, 235-264.
Butzer, KW (2008) 'Challenges for a cross-disciplinary geoarchaeology: The intersection between environmental history and geomorphology', *Geomorphology*, 101(1-2), 402-411.
Cann, RL (1988) 'DNA and human origins', *Annual Review Of Anthropology*, 17, 127-143.
Cann, RL, M Stoneking & AC Wilson (1987) 'Mitochondrial DNA and human evolution', *Nature*, 325(6099), 31-36.
CapeFarmMapper (2018) *CapeFarmMapper (version 2)* [online], available: https://gis.elsenburg.com/apps/cfm/ [accessed February 2018].
Carr, AS, A Boom, BM Chase, ME Meadows & HL Grimes (2015) 'Holocene sea level and environmental change on the west coast of South Africa: evidence from plant biomarkers, stable isotopes and pollen', *Journal of Paleolimnology*, 53(4), 415-432.
Carr, AS, BM Chase & A Mackay (2016) 'Mid to Late Quaternary Landscape and Environmental Dynamics in the Middle Stone Age of Southern South Africa' in Jones, C. S. & Stewart, A. B., eds., *Africa from MIS 6-2: Population Dynamics and Paleoenvironments*, Dordrecht: Springer Netherlands, 23-47.
Cartwright, C & J Parkington (1997) 'The wood charcoal assemblages from Elands Bay Cave, southwestern Cape: principles, procedures and preliminary interpretation', *The South African Archaeological Bulletin*, 59-72.
Chambers, J (2016) 'Like a rolling stone? The identification of fluvial transportation damage signatures on secondary context bifaces', *Lithics–The Journal of the Lithic Studies Society*, (24), 66.
Chambers, SJ-R (2019) *Modelling Erosional Sensitivities of Archaeological Sites Using DEM's from Low Altitude UAV Imagery* [Honours Dissertation], unpublished thesis (BSc (Hons)), University of Wollongong.
Chandler, G & C Merry (2010) 'The South African geoid 2010: SAGEOID10', *Position IT*, 29-33.
Chase, BM, JT Faith, A Mackay, M Chevalier, AS Carr, A Boom, S Lim & PJ Reimer (2018) 'Climatic controls on Later Stone Age human adaptation in Africa's southern Cape', *Journal Of Human Evolution*, 114 (Supplement C), 35-44.
Chase, BM & ME Meadows (2007) 'Late Quaternary dynamics of southern Africa's winter rainfall zone', *Earth-Science Reviews*, 84(3), 103-138.
Chase, BM, EM Niedermeyer, A Boom, AS Carr, M Chevalier, F He, ME Meadows, N Ogle & PJ Reimer (2019) 'Orbital controls on Namib Desert hydroclimate over the past 50,000 years', *Geology*.
Chase, BM & LJ Quick (2018) 'Influence of Agulhas forcing of Holocene climate change in South Africa's southern Cape', *Quaternary Research*, 08/13, 1-7.
Chase, BM, LJ Quick, ME Meadows, L Scott, DS Thomas & PJ Reimer (2011) 'Late glacial interhemispheric climate dynamics revealed in South African hyrax middens', *Geology*, 39(1), 19-22.
Clark, JD (1950) 'The newly discovered Nachikufu culture of Northern Rhodesia and the possible origin of certain elements of the South African Smithfield culture: Presidential address', *The South African Archaeological Bulletin*, 5(19), 86-98.
Clark, JD (1957) *3rd Pan-African Congress on Prehistory: Livingstone 1955*, Chatto & Windus.
Clark, JD (1959) *The Prehistory of Southern Africa*.
Clark, JD (1975) 'Africa in prehistory: peripheral or paramount?', *Man*, 175-198.
Clark, JD, GH Cole, GL Isaac & MR Kleindienst (1966) 'Precision and definition in african archaeology', *The South African Archaeological Bulletin*, 21(83), 114-121.
Coe, AL (2011) *Geological Field Techniques*, Wiley.
Cohen, AL, JE Parkington, GB Brundrit & NJ van der Merwe (2017) 'A Holocene Marine Climate Record in Mollusc Shells from the Southwest African Coast', *Quaternary Research*, 38(3), 379-385.
Compton, JS (2011) 'Pleistocene sea-level fluctuations and human evolution on the southern coastal plain of South Africa', *Quaternary Science Reviews*, 30(5), 506-527.
Conard, NJ, TJ Prindiville & AW Kandel (1999) 'The 1998 fieldwork on the stone age archaeology and palaeoecology of the Geelbek Dunes, West Coast National Park, South Africa', *South African Field Archaeology*, 8, 35-45.
Conrad, J, M Carstens & C Lasher (2012) *Olifants-Doorn WMA Classification Phase 3A - Groundwater Technical report, Department of Water Affairs, South Africa*.
Cooke, HBS (1957) 'Observations relating to Quaternary environments in East and Southern Africa', in *Geological Society of South Africa*.
Cooper, J, A Green & J Compton (2018) 'Sea-level change in southern Africa since the Last Glacial Maximum', *Quaternary Science Reviews*, 201, 303-318.
Cowling, R, K Esler & P Rundel (1999) 'Namaqualand, South Africa–an overview of a unique winter-

rainfall desert ecosystem', *Plant Ecology*, 142(1), 3-21.
Cramer, MD, J von Holdt, L Khomo & JJ Midgley (2016) 'Evidence for aeolian origins of heuweltjies from buried gravel layers', *South African Journal of Science*, 112, 01-10.
Cruz-Uribe, K, RG Klein, G Avery, M Avery, D Halkett, T Hart, RG Milo, C Garth Sampson & TP Volman (2003) 'Excavation of buried Late Acheulean (Mid-Quaternary) land surfaces at Duinefontein 2, Western Cape Province, South Africa', *Journal of Archaeological Science*, 30(5), 559-575.
d'Errico, F & CS Henshilwood (2007) 'Additional evidence for bone technology in the southern African Middle Stone Age', *Journal Of Human Evolution*, 52(2), 142-163.
d'Errico, F, A Pitarch Martí, C Shipton, E Le Vraux, E Ndiema, S Goldstein, MD Petraglia & N Boivin (2020) 'Trajectories of cultural innovation from the Middle to Later Stone Age in Eastern Africa: Personal ornaments, bone artifacts, and ocher from Panga ya Saidi, Kenya', *Journal Of Human Evolution*, 141, 102737.
Davies, B & SJ Holdaway (2017) 'Windows on the Past? Perspectives on Accumulation, Formation, and Significance from an Australian Holocene Lithic Landscape', *Mitteilungen der Gesellschaft für Urgeschichte*, 26, 125.
Davies, B, SJ Holdaway & PC Fanning (2016) 'Modelling the palimpsest: An exploratory agent-based model of surface archaeological deposit formation in a fluvial arid Australian landscape', *The Holocene*, 26(3), 450-463.
Deacon, HJ (1976) 'Where hunters gathered: a study of Holocene Stone Age people in the Eastern Cape', *South African Archaeological Society*.
Deacon, HJ (1979) 'Excavations at Boomplaas cave - a sequence through the upper Pleistocene and Holocene in South Africa', *World Archaeology*, 10(3), 241-257.
Deacon, HJ (1989) 'Late Pleistocene palaeoecology and archaeology in the Southern Cape, South Africa' in Mellars, P. & Stringer, C. B., eds., *The Human Revolution*, Edinburgh: Edinburgh University Press, 547-564.
Deacon, HJ & J Deacon (1999) *Human Beginnings in South Africa: Uncovering the Secrets of the Stone Age*, Walnut Creek, CA: Altamira Press.
Deacon, HJ & J Thackeray (1984) 'Late Pleistocene environmental changes and implications for the archaeological record in southern Africa', *Late Cainozoic Palaeoclimates of the Southern Hemisphere*, 375-390.
Deacon, J (1984) *The Later Stone Age of Southernmost Africa*, BAR.
Deacon, J & N Lancaster (1988) *Late Quaternary Palaeoenvironments of Southern Africa*, Oxford University Press, USA.
Dibble, H, V Aldeias, Z Jacobs, D Olszewski, Z Rezek, S Lin, E Álvarez Fernandez, C Barshay-Szmidt, E Hallett-Desguez, D Reed, K Reed, D Richter, T Steele, A Skinner, B Blackwell, E Doronicheva & M El-Hajraoui (2013) 'On the industrial attributions of the Aterian and Mousterian of the Maghreb', *Journal Of Human Evolution*, 64, 194-210.
Dietl, H, AW Kandel & NJ Conard (2005) 'Middle Stone Age settlement and land use at the open-air sites of Geelbek and Anyskop, South Africa', *Journal of African Archaeology*, 3(2), 231-242.
Dietrich, J (2015) 'Agisoft Photoscan Crash Course (updated for version 1.1.6)', *Advanced Geographic Research: Studying Environmental Geography with Fun Remote Sensing Tools* [online], available: https://adv-geo-research.blogspot.com/2015/06/photoscan-crash-course-v1-1.html.
Dijkshoorn, J, V van Engelen & J Huting (2008) *Soil and landform properties for LADA partner countries (Argentina, China, Cuba, Senegal and The Gambia, South Africa and Tunisia)*, Wageningen: ISRIC - World Soil Information and FAO.
Dougill, AJ & AD Thomas (2002) 'Nebkha dunes in the Molopo Basin, South Africa and Botswana: formation controls and their validity as indicators of soil degradation', *Journal of Arid Environments*, 50(3), 413-428.
Duller, G, L Bøtter-Jensen & A Murray (2000) 'Optical dating of single sand-sized grains of quartz: sources of variability', *Radiation Measurements*, 32(5-6), 453-457.
Duller, GAT (2003) 'Distinguishing quartz and feldspar in single grain luminescence measurements', *Radiation Measurements*, 37(2), 161-165.
Duller, GAT (2012) 'Improving the accuracy and precision of equivalent doses determined using the optically stimulated luminescence signal from single grains of quartz', *Radiation Measurements*, 47(9), 770-777.
Duller, GAT (2015) 'Luminescence dating', *Encyclopedia of Scientific Dating Methods*, 390-404.
Dunnell, RC (1992) 'The Notion Site' in Rossignol, J. & Wandsnider, L., eds., *Space, Time, and Archaeological Landscapes*, Boston, MA: Springer US, 21-41.
Endicott, P, SY Ho & C Stringer (2010) 'Using genetic evidence to evaluate four palaeoanthropological

hypotheses for the timing of Neanderthal and modern human origins', *Journal Of Human Evolution*, 59(1), 87-95.
Enloe, JG (2006) 'Geological processes and site structure: Assessing integrity at a Late Paleolithic open-air site in northern France', *Geoarchaeology*, 21(6), 523-540.
Eren, MI, A Durant, C Neudorf, M Haslam, C Shipton, J Bora, R Korisettar & M Petraglia (2010) 'Experimental examination of animal trampling effects on artifact movement in dry and water saturated substrates: a test case from South India', *Journal of Archaeological Science*, 37(12), 3010-3021.
Evans, U (1994) 'Hollow Rock Shelter, A Middle Stone Age site in the Cederberg', *Southern African Field Archaeology*, 3(2), 63-73.
Fanning, PC & SJ Holdaway (2001) 'Temporal limits to the archaeological record in arid western NSW, Australia: lessons from OSL and radiocarbon dating of hearths and sediments', in *Australasian Connections and New Directions: Proceedings of the 7th Australasian Archaeometry Conference*.
Farmer, EC, PB Demenocal & TM Marchitto (2005) 'Holocene and deglacial ocean temperature variability in the Benguela upwelling region: Implications for low-latitude atmospheric circulation', *Paleoceanography*, 20(2).
Feathers, J (2015) 'Luminescence dating at Diepkloof Rock Shelter – New dates from single-grain quartz', *Journal of Archaeological Science*, 63, 164-174.
Feathers, JK & DA Bush (2000) 'Luminescence dating of middle stone age deposits at Die Kelders', *Journal Of Human Evolution*, 38(1), 91-119.
Felix-Henningsen, P, AW Kandel & NJ Conard (2003) 'The significance of calcretes and paleosols on ancient dunes of the Western Cape, South Africa, as stratigraphic markers and paleoenvironmental indicators', *BAR International Series*, 1163, 45-52.
Fisher, E, R-M Albert, GA Botha, H Cawthra, I Esteban, JW Harris, Z Jacobs, A Jerardino, CW Marean, FH Neumann, J Pargeter, M Poupart & J Venter (2013) 'Archaeological reconnaissance for Middle Stone Age sites along the Pondoland Coast, South Africa', *Paleoanthropology*, 2013, 104-137.
Fitzsimmons, KE, N Stern & CV Murray-Wallace (2014) 'Depositional history and archaeology of the central Lake Mungo lunette, Willandra Lakes, southeast Australia', *Journal of Archaeological Science*, 41, 349-364.
Flint, RF (1959) 'Pleistocene climates in eastern and southern Africa', *Geological Society of America Bulletin*, 70(3), 343-374.
Foley, E, C Spry & N Stern (2017) 'Establishing the integrity and stratigraphic origin of stone artefact scatters on the surface of the Lake Mungo lunette in south-eastern Australia', *Journal of Archaeological Science: Reports*, 13, 547-557.
Foley, R & MM Lahr (2003) 'On stony ground: lithic technology, human evolution, and the emergence of culture', *Evolutionary Anthropology: Issues, News, and Reviews: Issues, News, and Reviews*, 12(3), 109-122.
Forssman, T & J Pargeter (2014) 'Assessing surface movement at Stone Age open-air sites: first impressions from a pilot experiment in northeastern Botswana', *Southern African Humanities*, 26, 157–76.
Fortuin, M & AC Woodford (2006) *Groundwater Reserve Determination Study for the Olifants/Doorn Catchment (SRK Project Number 348965),* Department of Water Affairs & Forestry.
Fuchs, M, A Kandel, N Conard, S Walker & P Felix-Henningsen (2008) 'Geoarchaeological and chronostratigraphical investigations of open-air sites in the Geelbek Dunes, South Africa', *Geoarchaeology: An International Journal*, 23(4), 425-449.
Galbraith, RF (1988) 'Graphical display of estimates having differing standard errors', *Technometrics*, 30(3), 271-281.
Galbraith, RF & RG Roberts (2012) 'Statistical aspects of equivalent dose and error calculation and display in OSL dating: an overview and some recommendations', *Quaternary Geochronology*, 11, 1-27.
Galbraith, RF, RG Roberts, GM Laslett, H Yoshida & JM Olley (1999) 'Optical dating of single and multiple grains of quartz from Jinmium rock shelter, northern Australia: Part I, experimental design and statistical models', *Archaeometry*, 41(2), 339-364.
Gasse, F, F Chalié, A Vincens, MA Williams & D Williamson (2008) 'Climatic patterns in equatorial and southern Africa from 30,000 to 10,000 years ago reconstructed from terrestrial and near-shore proxy data', *Quaternary Science Reviews*, 27(25-26), 2316-2340.
Goldberg, P, CE Miller, S Schiegl, B Ligouis, F Berna, NJ Conard & L Wadley (2009) 'Bedding, hearths, and site maintenance in the Middle Stone age of Sibudu cave, KwaZulu-Natal, South Africa', *Archaeological and Anthropological Sciences*, 1(2), 95-122.
Gómez-Robles, A (2019) 'Dental evolutionary rates and its implications for the Neanderthal–modern human divergence', *Science Advances*, 5(5), 1268.

Goodwin, AJH (1931) '25. South African Archaeology', *Man*, 31, 25-26.
Goodwin, AJH & BD Malan (1935) 'Archaeology of the Cape St. Blaize cave and raised beach, Mossel Bay', *Annals of the South African Museum*, 24, 111-140.
Goodwin, AJH & C Van Riet Lowe (1929) 'The Stone Age cultures of South Africa', *Annals of the South African Museum*, 27.
Grab, S (2015) 'Sandstone landforms of the Karoo Basin: Naturally sculptured rock' in Grab, S. & Knight, J., eds., *Landscapes and Landforms of South Africa*, 1 ed., Online: Springer International Publishing, XIII, 187.
Grab, S & J Knight eds. (2015) *Landscapes and Landforms of South Africa*, 1 ed., online: Springer International Publishing.
Green, RE, J Krause, AW Briggs, T Maricic, U Stenzel, M Kircher, N Patterson, H Li, W Zhai & MH-Y Fritz (2010) 'A draft sequence of the Neandertal genome', *Science*, 328(5979), 710-722.
Grün, R, JS Brink, NA Spooner, L Taylor, CB Stringer, RG Franciscus & AS Murray (1996) 'Direct dating of Florisbad hominid', *Nature (London)*, 382(6591), 500-501.
Guérin, G, N Mercier & G Adamiec (2011) 'Dose-rate conversion factors: update', *Ancient TL*, 29(1), 5-8.
Guérin, G, AS Murray, M Jain, KJ Thomsen & N Mercier (2013) 'How confident are we in the chronology of the transition between Howieson's Poort and Still Bay', *Journal Of Human Evolution*, 64(4), 314-317.
Hallinan, E (2013) *Stone Age Landscape Use in the Olifants River Valley, Western Cape* [Thesis], unpublished thesis (Master of Philosophy), University of Cape Town.
Hallinan, E & JE Parkington (2017) 'Stone Age landscape use in the Olifants River Valley, Clanwilliam, Western Cape, South Africa', *Azania: Archaeological Research in Africa*, 1-49.
Hallinan, E & M Shaw (2015) 'A new Middle Stone Age industry in the Tankwa Karoo, Northern Cape Province, South Africa', *Antiquity*, 89(344), f1-f6.
Hays, JD, J Imbrie & NJ Shackleton (1976) 'Variations in the Earth's orbit: pacemaker of the ice ages', in American Association for the Advancement of Science Washington, DC.
Hendriks, H & JN Rossouw (2009) *Adopt-a-River Programme Phase II: Development of an Implementation Plan (Project Number WP 9583),* Department of Water Affairs (DWA), South Africa.
Henshilwood, CS, F d'Errico, M Vanhaeren, K Van Niekerk & Z Jacobs (2004) 'Middle stone age shell beads from South Africa', *Science*, 304(5669), 404-404.
Henshilwood, CS, F d'Errico & I Watts (2009) 'Engraved ochres from the Middle Stone Age levels at Blombos Cave, South Africa', *Journal Of Human Evolution*, 57(1), 27-47.
Henshilwood, CS, F d'Errico, CS Henshilwood & F d'Errico (2011) *Homo Symbolicus: The Dawn of Language, Imagination and Spirituality*.
Henshilwood, CS & B Dubreuil (2011) 'The Still Bay and Howiesons Poort, 77–59 ka: Symbolic material culture and the evolution of the mind during the African Middle Stone Age', *Current Anthropology*, 52(3), 361-400.
Henshilwood, CS & CW Marean (2003) 'The origin of modern human behavior: Critique of the models and their test implications', *Current Anthropology*, 44(5), 627-651.
Henshilwood, CS & J Sealy (1997) 'Bone artefacts from the Middle Stone Age at Blombos Cave, Southern Cape, South Africa', *Current Anthropology*, 38(5), 890-895.
Henshilwood, CS, JC Sealy, R Yates, K Cruz-Uribe, P Goldberg, FE Grine, RG Klein, C Poggenpoel, K Van Niekerk & I Watts (2001) 'Blombos Cave, southern Cape, South Africa: preliminary report on the 1992–1999 excavations of the Middle Stone Age levels', *Journal of Archaeological Science*, 28(4), 421-448.
Henshilwood, CS, KL van Niekerk, S Wurz, A Delagnes, SJ Armitage, RF Rifkin, K Douze, P Keene, MM Haaland & J Reynard (2014) 'Klipdrift shelter, southern Cape, South Africa: preliminary report on the Howiesons Poort layers', *Journal of Archaeological Science*, 45, 284-303.
Högberg, A (2014) 'Chronology, stratigraphy and spatial distribution of artefacts at Hollow Rock Shelter, Cape Province, South Africa', *The South African Archaeological Bulletin*, 69(200), 142-151.
Högberg, A (2016) 'A Lithic Attribute Analysis on Blades from the Middle Stone Age Site, Hollow Rock Shelter, Western Cape Province, South Africa', *Lithic Technology*, 41(2), 93-113.
Högberg, A & L Larsson (2011) 'Lithic technology and behavioural modernity: New results from the Still Bay site, Hollow Rock Shelter, Western Cape Province, South Africa', *Journal Of Human Evolution*, 61(2), 133-155.
Högberg, A & M Lombard (2016) 'Still Bay Point-Production Strategies at Hollow Rock Shelter and Umhlatuzana Rock Shelter and Knowledge-Transfer Systems in Southern Africa at about 80-70 Thousand Years Ago', *PLoS ONE*, 11(12), e0168012.

Hogg, AG, Q Hua, PG Blackwell, M Niu, CE Buck, TP Guilderson, TJ Heaton, JG Palmer, PJ Reimer, RW Reimer, CSM Turney & SRH Zimmerman (2016) 'SHCal13 Southern Hemisphere Calibration, 0–50,000 Years cal BP', *Radiocarbon*, 55(4), 1889-1903.
Holdaway, SJ & PC Fanning (2014) *Geoarchaeology of Aboriginal Landscapes in Semi-Arid Australia*, CSIRO Publishing.
Holdaway, SJ & N Stern (2004) *A Record in Stone: The Study of Australia's Flaked Stone Artefacts*, Canberra: Aboriginal Studies Press.
Holmgren, K, JA Lee-Thorp, GRJ Cooper, K Lundblad, TC Partridge, L Scott, R Sithaldeen, A Siep Talma & PD Tyson (2003) 'Persistent millennial-scale climatic variability over the past 25,000 years in Southern Africa', *Quaternary Science Reviews*, 22(21), 2311-2326.
Hublin, J-J, A Ben-Ncer, SE Bailey, SE Freidline, S Neubauer, MM Skinner, I Bergmann, A Le Cabec, S Benazzi, K Harvati & P Gunz (2017) 'New fossils from Jebel Irhoud, Morocco and the pan-African origin of *Homo sapiens*', *Nature*, 546(7657), 289-292.
Humphreys, AJB & AI Thackeray (1983) *Ghaap and Gariep: Later Stone Age Studies in the Northern Cape*, South African Archaeological Society.
Imbrie, J (1980) 'Modeling the Climatic Response to Orbital Variations', *Science*, 207(4434), 943-953.
Imbrie, J, JD Hays, DG Martinson, A McIntyre, AC Mix, JJ Morley, NG Pisias, WL Prell & NJ Shackleton (1984) The Orbital Theory of Pleistocene Climate: Support From a Revised Chronology of the Marine d18O Record'.
Imbrie, J & K Palmer (1986) *Ice Ages: Solving the Mystery*, Harvard University Press.
Inglis, RH, PC Fanning, A Stone, DN Barfod, A Sinclair, H-C Chang, AM Alsharekh & G Bailey (2019) 'Paleolithic artifact deposits at Wadi Dabsa, Saudi Arabia: A multiscalar geoarchaeological approach to building an interpretative framework', *Geoarchaeology*, 34(3), 272-294.
Inskeep, RR (1967) 'The Late Stone Age' in Bishop, W. W. & Clark, J. D., eds., *Background to Evolution in Africa*, Chicago: University of Chicago Press, 557–582.
Inskeep, RR (1978) 'The Bushmen in prehistory', *The Bushmen: San Hunters and Herders of Southern Africa*, 33-56.
Isenburg, M (2019) LAStools - Efficient LiDAR Processing Software (Version 191018).
Isla, FI (1989) 'Holocene sea-level fluctuation in the southern hemisphere', *Quaternary Science Reviews*, 8(4), 359-368.
Jacobs, Z (2004) *Development of Luminescence Techniques for Dating Middle Stone Age Sites in South Africa* [Monograph], unpublished thesis (PhD), University of Wales Aberystwyth.
Jacobs, Z (2010) 'An OSL chronology for the sedimentary deposits from Pinnacle Point Cave 13B—A punctuated presence', *Journal Of Human Evolution*, 59(3–4), 289-305.
Jacobs, Z, GA Duller & AG Wintle (2006) 'Interpretation of single grain De distributions and calculation of De', *Radiation Measurements*, 41(3), 264-277.
Jacobs, Z, EH Hayes, RG Roberts, RF Galbraith & CS Henshilwood (2013) 'An improved OSL chronology for the Still Bay layers at Blombos Cave, South Africa: further tests of single-grain dating procedures and a re-evaluation of the timing of the Still Bay industry across southern Africa', *Journal of Archaeological Science*, 40(1), 579-594.
Jacobs, Z, B Li, N Jankowski & M Soressi (2015) 'Testing of a single grain OSL chronology across the Middle to Upper Palaeolithic transition at Les Cottés (France)', *Journal of Archaeological Science*, 54, 110-122.
Jacobs, Z & RG Roberts (2008) 'Testing times: old and new chronologies for the Howieson's Poort and Still Bay industries in environmental context', *Goodwin Series*, 9-34.
Jacobs, Z & RG Roberts (2015) 'An improved single grain OSL chronology for the sedimentary deposits from Diepkloof Rockshelter, Western Cape, South Africa', *Journal of Archaeological Science*, 63, 175-192.
Jacobs, Z & RG Roberts (2017) 'Single-grain OSL chronologies for the Still Bay and Howieson's Poort industries and the transition between them: Further analyses and statistical modelling', *Journal Of Human Evolution*, 107, 1-13.
Jacobs, Z, RG Roberts, RF Galbraith, HJ Deacon, R Grün, A Mackay, P Mitchell, R Vogelsang & L Wadley (2008a) 'Ages for the Middle Stone Age of southern Africa: implications for human behavior and dispersal', *Science*, 322(5902), 733-735.
Jacobs, Z, AG Wintle, GAT Duller, RG Roberts & L Wadley (2008b) 'New ages for the post-Howiesons Poort, late and final Middle Stone Age at Sibudu, South Africa', *Journal of Archaeological Science*, 35(7), 1790-1807.
Jahn, R, H Blume, V Asio, O Spaargaren & P Schad (2006) *Guidelines for soil description*, FAO.
Jarvis, A, HI Reuter, A Nelson & E Guevara (2008) *Hole-filled Seamless SRTM data V4* [map], sheet

International Centre for Tropical Agriculture (CIAT).
Jerardino, A (1995) 'Late Holocene Neoglacial episodes in southern South America and southern Africa: a comparison', *The Holocene*, 5(3), 361-368.
Jerardino, A (2012) 'Large Shell Middens and Hunter-Gatherer Resource Intensification Along the West Coast of South Africa: The Elands Bay Case Study', *The Journal of Island and Coastal Archaeology*, 7(1), 76-101.
Johnson, JP (1907) *The Stone Impliments of South Africa*, London: Longmans, Green & Co.
Johnson, RT (1959) *Rock-paintings of the south-west Cape*, Nasionale Boekhandel.
Johnson, T & H Rabinowitz (1955) 'Citrusdal Rock-Paintings', *The South African Archaeological Bulletin*, 122-123.
Kandel, AW, M Bolus, K Bretzke, AA Bruch, MN Haidle, C Hertler & M Märker (2015) 'Increasing behavioural flexibility? An intergrative macro-scale approach to understanding the Middle Stone Age of Southern Africa', *Journal of Archaeological Method and Theory*, 1-46.
Kandel, AW & N Conard (2012) 'Settlement patterns during the Earlier and Middle Stone Age around Langebaan Lagoon, Western Cape (South Africa)', *Quaternary International*, 270, 15-29.
Kandel, AW, P Felix-Henningsen & NJ Conard (2003) 'An overview of the spatial archaeology of the Geelbek Dunes, Western Cape, South Africa', *BAR International Series*, 1163, 37-44.
Kaplan, J (1987) 'Settlement and subsistence at Renbaan Cave', *Papers in the Prehistory of the Western Cape, South Africa*, 332, 350-72.
Keller, CM (1969) 'Mossel Bay: A redescription', *The South African Archaeological Bulletin*, 23(92), 131-140.
Kelly, RL (1995) *The foraging spectrum: Diversity in hunter-gatherer lifeways*, Smithsonian Inst Press.
Khan, NS, E Ashe, TA Shaw, M Vacchi, J Walker, WR Peltier, RE Kopp & BP Horton (2015) 'Holocene Relative Sea-Level Changes from Near-, Intermediate-, and Far-Field Locations', *Current Climate Change Reports*, 1(4), 247-262.
Klein, RG (1989) 'Biological and behavioural perspectives on modern human origins in southern Africa' in Mellars, P. & Stringer, C. B., eds., *The Human Revolution: Behavioral and Biological Perspectives on the Origins of Modern Humans*, Edinburgh: Edinburgh University Press, 529-546.
Klein, RG (2000) 'Archeology and the evolution of human behavior', *Evolutionary Anthropology: Issues, News, and Reviews*, 9(1), 17-36.
Klein, RG (2008) 'Out of Africa and the evolution of human behavior', *Evolutionary Anthropology: Issues, News, and Reviews*, 17(6), 267-281.
Klein, RG, G Avery, K Cruz-Uribe, D Halkett, JE Parkington, T Steele, TP Volman & R Yates (2004) 'The Ysterfontein 1 Middle Stone Age site, South Africa, and early human exploitation of coastal resources', *Proceedings of the National Academy of Sciences of the United States of America*, 101(16), 5708-5715.
Klein, RG & K Cruz-Uribe (1987) 'Large mammal and tortoise bones from Eland's Bay Cave and nearby sites, Western Cape Province, South Africa', *Papers in the prehistory of the western Cape, South Africa*, 1, 132-163.
Klein, RG & K Cruz-Uribe (2000) 'Middle and later stone age large mammal and tortoise remains from Die Kelders Cave 1, Western Cape Province, South Africa', *Journal Of Human Evolution*, 38(1), 169-195.
Klein, RG, K Cruz-Uribe, D Halkett, T Hart & JE Parkington (1999) 'Paleoenvironmental and human behavioral implications of the Boegoeberg 1 late Pleistocene hyena den, Northern Cape Province, South Africa', *Quaternary Research*, 52(3), 393-403.
Knight, J & D Stratford (2020) 'Investigating lithic scatters in arid environments: The Early and Middle Stone Age in Namibia', *Proceedings of the Geologists' Association*.
Koopman, A, S Kluiving, SJ Holdaway & W Wendrich (2016) 'The effects of Holocene landscape changes on the formation of the archaeological record in the Fayum Basin, Egypt', *Geoarchaeology*, 31(1), 17-33.
Korn, H & H Martin (1957) 'The Pleistocene in South West Africa', in *Proceedings of the 3rd Pan-African Congress on Prehistory*, Chatto and Windus London, 14-22.
Kuman, K (1989) *Florisbad and =/Gi: The Contribution of Open-Air Sites to Study of the Middle Stone Age in Southern Africa* [Ph.D. Thesis], unpublished thesis University of Pennsylvania.
Kuman, K, M Inbar & R Clarke (1999) 'Palaeoenvironments and cultural sequence of the Florisbad Middle Stone Age hominid site, South Africa', *Journal of Archaeological Science*, 26(12), 1409-1425.
Kuzmin, YV, S Keates & C Shen (2007) 'Geoarchaeological aspects of the origin and spread of microblade technology in northern and central Asia'.
Lambeck, K, H Rouby, A Purcell, Y Sun & M Sambridge (2014) 'Sea level and global ice volumes from

the Last Glacial Maximum to the Holocene', *Proceedings of the National Academy of Sciences*, 111(43), 15296-15303.
Lancaster, N (2002) 'How dry was dry?—Late Pleistocene palaeoclimates in the Namib Desert', *Quaternary Science Reviews*, 21(7), 769-782.
Lane, SN & KS Richards (1997) 'Linking river channel form and process: time, space and causality revisited', *Earth Surface Processes and Landforms: The Journal of the British Geomorphological Group*, 22(3), 249-260.
Langford, RP (2000) 'Nabkha (coppice dune) fields of south-central New Mexico, U.S.A', *Journal of Arid Environments*, 46(1), 25-41.
Larsson, L (2010a) 'Report on the Archaeological Excavation of Hollow Rock Shelter, Sevilla 48, Pakhuis Pass, Clanwilliam District, Western Cape', *Unpublished report. Department of Archaeology, University of Cape Town and at the Archaeological Department at Lund University*.
Larsson, L (2010b) 'What Can Be Found in a Hollow Rock? A site from the Middle Stone Age in Western Cape, South Africa', *Understanding the Past. Papers offered to Stefan K. Kozlowski*, 199-206.
Leakey, LSB & JD Solomon (1929) 'East African archaeology', *Nature*, 124(9).
Lenoble, A & P Bertran (2004) 'Fabric of Palaeolithic levels: Methods and implications for site formation processes', *Journal of Archaeological Science*, 31(4), 457-469.
Li, B, Z Jacobs, RG Roberts, R Galbraith & J Peng (2017) 'Variability in quartz OSL signals caused by measurement uncertainties: Problems and solutions', *Quaternary Geochronology*, 41, 11-25.
Libby, WF, EC Anderson & JR Arnold (1949) 'Age determination by radiocarbon content: world-wide assay of natural radiocarbon', *Science*, 109(2827), 227-228.
Lin, SC, MJ Douglass & A Mackay (2016) 'Interpreting MIS3 artefact transport patterns in southern Africa using cortex ratios: an example from the Putslaagte valley, Western Cape', *South African Archaeological Bulletin*, 71(204), 173.
Lisiecki, LE & ME Raymo (2005) 'A Pliocene-Pleistocene stack of 57 globally distributed benthic δ18O records', *Paleoceanography*, 20(1).
Loftus, E, P Mitchell & C Ramsey (2019) 'An archaeological radiocarbon database for southern Africa', *Antiquity*, 93(370).
Loftus, E, J Sealy & J Lee-Thorp (2016) 'New radiocarbon dates and Bayesian models for Nelson Bay Cave and Byneskranskop 1: Implications for the South African later stone age sequence', *Radiocarbon*, 58(2).
Lombard, M (2012) 'Thinking through the Middle Stone Age of sub-Saharan Africa', *Quaternary International*, 270, 140-155.
Lombard, M, L Wadley, J Deacon, S Wurz, I Parsons, M Mohapi, J Swart & P Mitchell (2012) 'South African and Lesotho Stone Age sequence updated', *The South African Archaeological Bulletin*, 67(195), 123-144.
Lombard, M, L Wadley, Z Jacobs, M Mohapi & RG Roberts (2010) 'Still Bay and serrated points from Umhlatuzana rock shelter, Kwazulu-Natal, South Africa', *Journal of Archaeological Science*, 37(7), 1773-1784.
Lotter, MG, RJ Gibbon, K Kuman, GM Leader, T Forssman & DE Granger (2016) 'A Geoarchaeological Study of the Middle and Upper Pleistocene Levels at Canteen Kopje, Northern Cape Province, South Africa', *Geoarchaeology*, 31(4), 304-323.
Lotter, MG & K Kuman (2018) 'The Acheulean in South Africa, with announcement of a new site (Penhill Farm) in the lower Sundays River Valley, Eastern Cape Province, South Africa', *Quaternary International*, 480, 43–65.
Low, MA (2018) *Understanding the Character and Organisation of Early Microlithic Systems During the Last Glacial Peak (~29–12 ka) in the Western Cape, South Africa* [Thesis], unpublished thesis (Doctor of Philosophy), University of Wollongong, available: https://ro.uow.edu.au/theses1/484.
Low, MA (2019) 'Continuity, Variability and the Nature of Technological Change During the Late Pleistocene at Klipfonteinrand Rockshelter in the Western Cape, South Africa', *African Archaeological Review*, 1-22.
Low, MA & A Mackay (2016) 'The late Pleistocene microlithic at Putslaagte 8 rockshelter in the Western Cape, South Africa', *South African Archaeological Bulletin*, 71(204), 146.
Low, MA & A Mackay (2018) 'The Organisation of Late Pleistocene Robberg Blade Technology in the Doring River Catchment, South Africa', *Journal of African Archaeology*, 16(2), 168-192.
Low, MA, A Mackay & N Phillips (2017) 'Understanding Early Later Stone Age technology at a landscape-scale: evidence from the open-air locality Uitspankraal 7 (UPK7) in the Western Cape, South Africa', *Azania: Archaeological Research in Africa*, 1-34.
Lukich, V, S Cowling & M Chazan (2020) 'Palaeoenvironmental reconstruction of Kathu Pan, South Africa,

based on sedimentological data', *Quaternary Science Reviews*, 230, 106153.
Mabbutt, J (1957) 'Some Quaternary events in the winter rainfall area of the Cape Province', in *Third Pan-African Congress on Prehistory: Livingstone*, 6-13.
Mackay, A (2012) *Report on Excavations at Klipfonteinrand 2011/12, V2*, Australian National University, Canberra.
Mackay, A (2016a) 'Technological Change and the Importance of Variability: The Western Cape of South Africa from MIS 6-2' in Jones, C. S. & Stewart, A. B., eds., *Africa from MIS 6-2: Population Dynamics and Paleoenvironments*, Dordrecht: Springer Netherlands, 49-63.
Mackay, A (2016b) 'Three arcs: observations on the archaeology of the Elands Bay and northern Cederberg landscapes', *Southern African Humanities*, 29(1), 1-15.
Mackay, A, CR Cartwright, S Heinrich, MA Low, MC Stahlschmidt & TE Steele (2019) 'Excavations at Klipfonteinrand Reveal Local and Regional Patterns of Adaptation and Interaction Through MIS 2 in Southern Africa', *Journal of Paleolithic Archaeology*.
Mackay, A, E Hallinan & TE Steele (2018) 'Provisioning Responses to Environmental Change in South Africa's Winter Rainfall Zone: MIS 5-2' in Robinson, E. & Sellet, F., eds., *Lithic Technological Organization and Paleoenvironmental Change: Global and Diachronic Perspectives*, Cham: Springer International Publishing, 13-36.
Mackay, A, Z Jacobs & TE Steele (2015) 'Pleistocene archaeology and chronology of Putslaagte 8 (PL8) rockshelter, Western Cape, South Africa', *Journal of African Archaeology*, 13(1).
Mackay, A, BA Stewart & BM Chase (2014a) 'Coalescence and fragmentation in the late Pleistocene archaeology of southernmost Africa', *Journal Of Human Evolution*, 72, 26-51.
Mackay, A, A Sumner, Z Jacobs, B Marwick, K Bluff & M Shaw (2014b) 'Putslaagte 1 (PL1), the Doring River, and the later Middle Stone Age in southern Africa's Winter Rainfall Zone', *Quaternary International*, 350, 43-58.
Mackay, A & A Welz (2008) 'Engraved ochre from a Middle Stone Age context at Klein Kliphuis in the Western Cape of South Africa', *Journal of Archaeological Science*, 35(6), 1521-1532.
Maggs, T (1967) 'A quantitative analysis of the rock art from a sample area in the western Cape', *South African Journal of Science*, 63(3), 100.
Maherry, A, M Horan, L Smith-Adao, Hv Deventer, J Nel, R Schulze & R Kunz (2013) *Delineating River Network Quinary Catchments for South Africa and Allocating Associated Daily Hydrological Information (WRC Report No. 2020/1/12)* Water Research Commission (WRC) www.wrc.org.za [accessed March 2015].
Malan, BD (1970) 'Remarks and reminiscences on the history of archaeology in South Africa', *The South African Archaeological Bulletin*, 25(99/100), 88-92.
Manhire, AH, JE Parkington, AD Mazel & OCM TM (1986) 'Cattle, sheep and horses: a review of domestic animals in the rock art of southern Africa', *Goodwin Series*, 22-30.
Manhire, A (1987) *Later Stone Age settlement patterns in the Sandveld of the south-western Cape Province, South Africa*, British Archaeological Reports Limited.
Manhire, A (1993) 'A report on the excavations at Faraoskop Rock Shelter in the Graafwater district of the south-western Cape', *Southern African Field Archaeology*, 2, 3-23.
Marean, CW (2010) 'Pinnacle Point Cave 13B (Western Cape Province, South Africa) in context: The Cape Floral kingdom, shellfish, and modern human origins', *Journal Of Human Evolution*, 59(3–4), 425-443.
Marean, CW, M Bar-Matthews, J Bernatchez, E Fisher, P Goldberg, AI Herries, Z Jacobs, A Jerardino, P Karkanas & T Minichillo (2007) 'Early human use of marine resources and pigment in South Africa during the Middle Pleistocene', *Nature*, 449(7164), 905-908.
Marean, CW, RM Cowling & J Franklin (2020) 'The Palaeo-Agulhas Plain: Temporal and spatial variation in an extraordinary extinct ecosystem of the Pleistocene of the Cape Floristic Region', *Quaternary Science Reviews*, 106161.
Marzen, M, T Iserloh, W Fister, M Seeger, J Rodrigo-Comino & JB Ries (2019) 'On-site water and wind erosion experiments reveal relative impact on total soil erosion', *Geosciences*, 9(11), 478.
Mason, R, M Klapwijk, R Welbourne, B Sandelowsky & T Maggs (1973) 'Early Iron Age settlement of southern Africa', *South African Journal of Science*, 69, 324-326.
Mason, RJ (1962) *Prehistory of the Transvaal*.
May, J-H (2014) 'Source-Bordering Dune' in *Encyclopedia of Planetary Landforms*, New York, NY: Springer New York, 1-4.
McAuliffe, JR, MT Hoffman, LD McFadden, W Bell, S Jack, MP King & V Nixon (2019) 'Landscape patterning created by the southern harvester termite, Microhodotermes viator: Spatial dispersion of colonies and alteration of soils', *Journal of Arid Environments*, 162, 26-34.

McBrearty, S & AS Brooks (2000) 'The revolution that wasn't: a new interpretation of the origin of modern human behavior', *Journal Of Human Evolution*, 39(5), 453-563.
McBurney, CB (1967) *The Haua Fteah (Cyrenaica) and the Stone Age of the South-East Mediterranean*, CUP Archive.
McDougall, I, FH Brown & JG Fleagle (2005) 'Stratigraphic placement and age of modern humans from Kibish, Ethiopia', *Nature*, 433(7027), 733-736.
McNabb, J & P Beaumont (2012) 'Excavations in the Acheulean Levels at the Earlier Stone Age Site of Canteen Koppie, Northern Province, South Africa', in *Proceedings of the Prehistoric Society*, Cambridge University Press, 51-71.
McPherron, SJP & HL Dibble (2009) *E4 (Version 4.5)* [online], available: http://www.oldstoneage.com/software/e4.shtml.
Meadows, M & J Sugden (1990) 'Late Quaternary vegetation history of the Cederberg, south-western Cape Province', *Palaeoecology of Africa*, 21, 269-282.
Meadows, M & J Sugden (1991) 'The application of multiple discriminant analysis to the reconstruction of the vegetation history of Fynbos, southern Africa', *Grana*, 30(2), 325-336.
Meadows, ME & AJ Baxter (1999) 'Late Quaternary palaeoenvironments of the southwestern Cape, South Africa: a regional synthesis', *Quaternary International*, 57, 193-206.
Meadows, ME & JM Sugden (1993) 'The late quaternary palaeoecology of a floristic kingdom: the southwestern Cape South Africa', *Palaeogeography, Palaeoclimatology, Palaeoecology*, 101(3), 271-281.
Mejdahl, V (1979) 'Thermoluminescence dating: beta-dose attenuation in quartz grains', *Archaeometry*, 21(1), 61-72.
Mellars, P (1996) 'The Emergence of Biologically Modern Populations in Europe: A Social and Cognitive Revolution', in *Proceedings-British Academy*, Oxford University Press Inc., 179-202.
Meteoblue (2017a) 'Climate 32.03°S 19.4°E', [online], 2006-2017available: [accessed 7th November 2017].
Meteoblue (2017b) *Wind rose for 32.03°S 19.4°E* [image online], available: https://www.meteoblue.com/en/weather/forecast/modelclimate/-32.034N19.402E202_Africa%2FJohannesburg [accessed 7th November 2017].
Meteoblue (2017c) *Windspeed chart for 32.03°S 19.4°E* [image online], available: https://www.meteoblue.com/en/weather/forecast/modelclimate/-32.034N19.402E202_Africa%2FJohannesburg [accessed 7th November 2017].
Meyer, M, J-L Arsuaga, C de Filippo, S Nagel, A Aximu-Petri, B Nickel, I Martínez, A Gracia, JMB de Castro & E Carbonell (2016) 'Nuclear DNA sequences from the Middle Pleistocene Sima de los Huesos hominins', *Nature*, 531(7595), 504-507.
Midgley, J, C Harris, A Harington & A Potts (2012) *Geochemical Perspective on Origins and Consequences of Heuweltjie Formation in the Southwestern Cape, South Africa* [online database].
Miller, CE, P Goldberg & F Berna (2013) 'Geoarchaeological investigations at Diepkloof Rock Shelter, Western Cape, South Africa', *Journal of Archaeological Science*, 40(9), 3432-3452.
Miller, JM & PR Willoughby (2014) 'Radiometrically dated ostrich eggshell beads from the Middle and Later Stone Age of Magubike Rockshelter, southern Tanzania', *Journal Of Human Evolution*, 74, 118-122.
Mitchell, LJ (2009) *Belongings: property, family, and identity in colonial South Africa (an exploration of frontiers, 1725-c. 1830)* [online], available: https://quod-lib-umich-edu.ezproxy.uow.edu.au/cgi/t/text/text-idx?c=acls;idno=heb99030.0001.001.
Mitchell, P (1988) 'The late Pleistocene early microlithic assemblages of southern Africa', *World Archaeology*, 20(1), 27-39.
Mitchell, P (2002) *The Archaeology of Southern Africa*, Cambridge, UK: Cambridge University Press.
Mitchell, P (2008) 'Developing the archaeology of marine isotope stage 3', *Goodwin Series*, 52-65.
Moore, A, T Blenkinsop & F Cotterill (2009) 'Southern African topography and erosion history: plumes or plate tectonics?', *Terra Nova*, 21, 310-315.
Mounier, A & M Mirazón Lahr (2019) 'Deciphering African late middle Pleistocene hominin diversity and the origin of our species', *Nature Communications*, 10(1), 3406.
Mourre, V, P Villa & CS Henshilwood (2010) 'Early use of pressure flaking on lithic artifacts at Blombos Cave, South Africa', *Science*, 330(6004), 659-662.
Murray, AS & RG Roberts (1997) 'Determining the burial time of single grains of quartz using optically stimulated luminescence', *Earth and Planetary Science Letters*, 152(1-4), 163-180.
Murray, AS & AG Wintle (2000) 'Luminescence dating of quartz using an improved single-aliquot regenerative-dose protocol', *Radiation Measurements*, 32, 57-73.

Nackerdien, R (1989) *Klipfonteinrand 2: A Sign of the Times*, unpublished thesis, University of Cape Town.
Nathan, RP & B Mauz (2008) 'On the dose-rate estimate of carbonate-rich sediments for trapped charge dating', *Radiation Measurements*, 43(1), 14-25.
Neumark, SD (1957) *Economic Influences on the South African Frontier 1652-1836*, Standford, California: Standford University Press.
Noble, W & I Davidson (1991) 'The evolutionary emergence of modern human behaviour: Language and its archaeology', *Man*, 223-253.
O'Driscoll, CA & A Mackay (2020) 'On the Operation of Retouch in Southern Africa's Early Middle Stone Age', *Journal of Paleolithic Archaeology*.
Oestmo, S, BJ Schoville, J Wilkins & Curtis W. Marean (2014) 'A Middle Stone Age Paleoscape near the Pinnacle Point caves, Vleesbaai, South Africa', *Quaternary International*, 350, 147-168.
Olley, J, G Caitcheon & A Murray (1998) 'The distribution of apparent dose as determined by optically stimulated luminescence in small aliquots of fluvial quartz: Implications for dating young sediments', *Quaternary Science Reviews*, 17, 1033-1040.
Olley, J, GG Caitcheon & R Roberts (1999) 'The origin of dose distributions in fluvial sediments, and the prospect of dating single grains from fluvial deposits using optically stimulated luminescence', *Radiation Measurements*, 30(2), 207-217.
Orton, J (2014) 'SALSA: The Holocene technocomplexes, a reply to Lombard and colleagues', *The South African Archaeological Bulletin*, 69(199), 110-112.
Ozán, IL (2017) 'Gravity and the formation of the archaeological record: Main concepts and methodological tools', *Geoarchaeology*, (00), 1–16.
Pargeter, J (2016) 'Lithic miniaturization in Late Pleistocene southern Africa', *Journal of Archaeological Science: Reports*, 10, 221-236.
Pargeter, J, E Loftus & P Mitchell (2017) 'New ages from Sehonghong rock shelter: Implications for the late Pleistocene occupation of highland Lesotho', *Journal of Archaeological Science: Reports*, 12, 307-315.
Pargeter, J & M Low (2018) 'Lithic miniaturization and behavioral variability 18-11 kcal. BP in southernmost Africa'.
Parkington, J (1976a) 'Coastal Settlement between the Mouths of the Berg and Olifants Rivers, Cape Province', *The South African Archaeological Bulletin*, 31(123/124), 127-140.
Parkington, J (1976b) *Follow the San: An Analysis of Seasonality in the Prehistory of the South Western Cape*, unpublished thesis (PhD), University of Cambridge.
Parkington, J (1978) 'The Pleistocene/Holocene Transition in the Western Cape', *BAR International Series*, (405-407).
Parkington, J (2000) 'Palaeovegetation at the Last Glacial Maximum in the Western Cape, South Africa: Wood charcoal and pollen evidence from Elands Bay Cave', *South African Journal of Science*, 96(11-12), 543-546.
Parkington, J (2010) 'Coastal diet, encephalization, and innovative behaviors in the late Middle Stone Age of southern Africa', *Human Brain Evolution: The Influence of Freshwater and Marine Food Resources. Wiley-Blackwell, NY*, 189-202.
Parkington, J, C Charles, PL Carter, HJ Deacon, J Deacon, AJB Humphreys, RR Inskeep, G Isaac, L Jacobson, ML Brooker, A Mazel, PT Robertshaw, CG Sampson, AI Thackeray & TP Volman (1980) 'Time and Place: Some Observations on Spatial and Temporal Patterning in the Later Stone Age Sequence in Southern Africa [with Comments and Reply]', *The South African Archaeological Bulletin*, 35(132), 73-112.
Parkington, J, R Yates, A Manhire & D Halkett (1986) 'The social impact of pastoralism in the southwestern Cape', *Journal of Anthropological Archaeology*, 5(4), 313-329.
Parkington, J, P Nilssen, C Reeler & C Henshilwood (1992) 'Making sense of space at Dunefield Midden campsite, Western Cape, South Africa', *Southern African Field Archaeology*, 1(2), 63-70.
Parkington, J & C Poggenpoel (1971) 'A Late Stone Age Burial from Clanwilliam', *The South African Archaeological Bulletin*, 26(101/102), 82-84.
Parkington, JE (1972) 'Seasonal mobility in the late stone age', *African Studies*, 31(4), 223-244.
Parkington, JE (1990) 'A view from the South: southern Africa before, during and after the Last Glacial Maximum' in Gamble, C. & Soffer, O., eds., *The World at 18,000 BP*, London: Unwin Hyman, 214-228.
Parkington, JE & PA Mellars (1990) *The Emergence of Modern Humans*.
Parkington, JE, R Yates, A Manhire & D Halkett (1986) 'The social impact of pastoralism in the southwestern Cape', *Journal of Anthropological Archaeology*, 5(4), 313-329.
Paxton, BR (2008) *The Influence of Hydraulics, Hydrology and Temperature on the Distribution, Habitat*

Use and Recruitment of Threatened Cyprinids in a Western Cape River, South Africa, unpublished thesis University of Cape Town.
Paxton, BR & J King (2009) *The Influence of Hydraulics, Hydrology and Temperature on the Distribution, Habitat Use and Recruitment of Threatened Cyprinids in a Western Cape River, South Africa, WRC Report No. 1483/1/09*Water Research Commission.
Péringuey, L (1911) 'The Stone Ages of South Africa', *Annals of the South African Museum*, 8, 1–218.
Phillips, N, J Pargeter, M Low & A Mackay (2019) 'Open-air preservation of miniaturised lithics: experimental research in the Cederberg Mountains, southern Africa', *Archaeological and Anthropological Sciences*, 11(11), 5851-5877.
Plaskett, J (2012) 'The Stone Artefacts of Putslaagte 8: Exploring Variation in Stone Artefact Assemblages of the Western Cape', *Unpublished BA Honours, University of Cape Town*.
Porraz, G, M Igreja, P Schmidt & JE Parkington (2016a) 'A shape to the microlithic Robberg from Elands Bay Cave (South Africa)', *Southern African Humanities*, 29(1), 203-247.
Porraz, G, J Parkington, J-P Rigaud, CE Miller, C Poggenpoel & C Tribolo (2013) 'The MSA sequence of Diepkloof and the history of southern African Late Pleistocene populations', *Journal of Archaeological Science*, 40(9), 3542-3552.
Porraz, G, VC Schmid, CE Miller, C Tribolo, C Cartwright, A Charrié-Duhaut, M Igreja, S Mentzer, N Mercier & P Schmidt (2016b) 'Update on the 2011 excavation at Elands Bay Cave (South Africa) and the Verlorenvlei stone age', *Southern African Humanities*, 29, 33.
Porraz, G, A Val, L Dayet, P De La Pena, K Douze, CE Miller, ML Murungi, C Tribolo, VC Schmid & C Sievers (2015) 'Bushman Rock Shelter (Limpopo, South Africa): a perspective from the edge of the Highveld', *The South African Archaeological Bulletin*, 166-179.
Potts, AJ, JJ Midgley & C Harris (2009) 'Stable isotope and 14C study of biogenic calcrete in a termite mound, Western Cape, South Africa, and its palaeoenvironmental significance', *Quaternary Research*, 72(2), 258-264.
Prescott, JR & JT Hutton (1994) 'Cosmic ray contributions to dose rates for luminescence and ESR dating: large depths and long-term time variations', *Radiation Measurements*, 23(2-3), 497-500.
Prüfer, K, F Racimo, N Patterson, F Jay, S Sankararaman, S Sawyer, A Heinze, G Renaud, PH Sudmant & C De Filippo (2014) 'The complete genome sequence of a Neanderthal from the Altai Mountains', *Nature*, 505(7481), 43-49.
Quick, L (2009) *Late Quaternary Vegetation History and Palaeoenvironments of the Cederberg Mountains, South Africa: Evidence from Hyrax (Procavia capensis) Middens* [Masters Thesis], unpublished thesis.
Quick, LJ & FD Eckardt (2015) 'The Cederberg: A Rugged Sandstone Topography' in Grab, S. & Knight, J., eds., *Landscapes and Landforms of South Africa*, Switzerland: Springer International Publishing.
R Core Team (2015) *R: A Language and Environment for Statistical Computing* [online], available: https://www.R-project.org/.
Railsback, LB, PL Gibbard, MJ Head, NRG Voarintsoa & S Toucanne (2015) 'An optimized scheme of lettered marine isotope substages for the last 1.0 million years, and the climatostratigraphic nature of isotope stages and substages', *Quaternary Science Reviews*, 111(Supplement C), 94-106.
Rapp, GR & CL Hill (2006) *Geoarchaeology: The Earth-Science Approach to Archaeological Interpretation*, 2nd ed., Yale University Press.
Ravi, S, DD Breshears, TE Huxman & P D'Odorico (2010) 'Land degradation in drylands: Interactions among hydrologic–aeolian erosion and vegetation dynamics', *Geomorphology*, 116(3-4), 236-245.
Readhead, M (1987) 'Thermoluminescence dose rate data and dating equations for the case of disequilibrium in the decay series', *International Journal of Radiation Applications and Instrumentation. Part D. Nuclear Tracks and Radiation Measurements*, 13(4), 197-207.
Rees-Jones, J (1995) 'Optical dating of young sediments using fine-grain quartz', *Ancient TL*, 13(2), 9-14.
Reich, D, RE Green, M Kircher, J Krause, N Patterson, EY Durand, B Viola, AW Briggs, U Stenzel & PL Johnson (2010) 'Genetic history of an archaic hominin group from Denisova Cave in Siberia', *Nature*, 468(7327), 1053-1060.
Rezek, Z, SJ Holdaway, DI Olszewski, SC Lin, M Douglass, S McPherron, R Iovita, DR Braun & D Sandgathe (2020) 'Aggregates, Formational Emergence, and the Focus on Practice in Stone Artifact Archaeology', *Journal of Archaeological Method and Theory*.
Richter, D, R Grün, R Joannes-Boyau, TE Steele, F Amani, M Rué, P Fernandes, J-P Raynal, D Geraads, A Ben-Ncer, J-J Hublin & SP McPherron (2017) 'The age of the hominin fossils from Jebel Irhoud, Morocco, and the origins of the Middle Stone Age', *Nature*, 546(7657), 293-296.
Ries, J, K Andres, S Wirtz, J Tumbrink, T Wilms, K Peter, M Burczyk, V Butzen & M Seeger (2014)

'Sheep and goat erosion–experimental geomorphology as an approach for the quantification of underestimated processes', *Zeitschrift für Geomorphologie*, 58(3), 023-045.
Rigaud, JP, PJ Texier, J Parkington & C Poggenpoel (2006) 'Le mobilier Stillbay et Howiesons Poort de l'abri Diepkloof', *Comptes Rendus Palevol*, 5, 839-849.
Rijssen, WJJV (1984) 'South-Western Cape Rock Art: Who Painted What?', *The South African Archaeological Bulletin*, 39(140), 125-129.
Roberts, RG, RF Galbraith, JM Olley, H Yoshida & GM Laslett (1999) 'Optical dating of single and multiple grains of quartz from Jinmium rock shelter, northern Australia: part II, results and implications', *Archaeometry*, 41(2), 365-395.
Roberts, RG, RF Galbraith, H Yoshida, GM Laslett & JM Olley (2000) 'Distinguishing dose populations in sediment mixtures: a test of single-grain optical dating procedures using mixtures of laboratory-dosed quartz', *Radiation Measurements*, 32(5), 459-465.
Rousseeuw, PJ, M Debruyne, S Engelen & M Hubert (2006) 'Robustness and Outlier Detection in Chemometrics', *Critical Reviews in Analytical Chemistry*, 36(3-4), 221-242.
Sahle, Y, LE Morgan, DR Braun, B Atnafu & WK Hutchings (2014) 'Chronological and behavioral contexts of the earliest Middle Stone Age in the Gademotta formation, main Ethiopian rift', *Quaternary International*, 331, 6-19.
Sampson, CG (1968) *The Middle Stone Age industries of the Orange River scheme area*, National Museum.
Sampson, CG (1974) *The Stone Age Archaeology of Southern Africa*.
Sampson, CG (1984) 'Site Clusters in the Smithfield Settlement Pattern', *The South African Archaeological Bulletin*, 39(139), 5-23.
Sampson, C & B Bousman (1985) 'Variations in the size of archaeological surface sites attributed to the Seacow River Bushmen', *South African Journal of Science*, 81(6), 321-323.
Sampson, CG, V Moore, CB Bousman, B Stafford, A Giordano & M Willis (2015) 'A GIS analysis of the Zeekoe Valley Stone Age archaeological record in South Africa', *Journal of African Archaeology*, 13(2), 167-185.
Sandy, MJ & WF Cole (1982) 'The influence of the degree of weathering of hornfels rock on its physical properties and durability', in *Proceedings of the Eleventh Australian Road Research Board Conference*, University of Melbourne, , August 23-27, 1982, Australian Road Research Board (ARRB), 80-89.
Scerri, EM (2017) 'The North African Middle Stone Age and its place in recent human evolution', *Evolutionary Anthropology: Issues, News, and Reviews*, 26(3), 119-135.
Schalke, HJWG (1973) 'The upper quaternary of the cape flats area (Cape Province, South Africa)', *Scripta Geologica*, 15, 1-67.
Schick, KD (1986) *Stone Age Sites in the Making: Experiments in the Formation and Transformation of Archaeological Occurrences*, Oxford, England: British Archaeological Reports Ltd.
Schick, KD (1987) 'Modeling the formation of Early Stone Age artifact concentrations', *Journal Of Human Evolution*, 16(7–8), 789-807.
Schiffer, MB (1987) 'Formation processes of the archaeological record'. Albuquerque, New Mexico: University of New Mexico Press.
Schlanger, SH (1990) 'Artifact assemblage composition and site occupation duration', *Perspectives on Southwestern Prehistory*, 103-121.
Schmidt, I, G Ossendorf, A Bolten & O Bubenzer (2016) 'Human occupation in southern Namibia during the Late Pleistocene-A geoarchaeological approach', *Quaternary International*, 404, 186-187.
Schmidt, P & A Högberg (2018) 'Heat treatment in the Still Bay - A case study on Hollow Rock Shelter, South Africa', *Journal of Archaeological Science: Reports*, 21, 712-720.
Schmidt, P & A Mackay (2016) 'Why Was Silcrete Heat-Treated in the Middle Stone Age? An Early Transformative Technology in the Context of Raw Material Use at Mertenhof Rock Shelter, South Africa', *PLoS ONE*, 11(2), e0149243.
Schmidt, P, D Stynder, NJ Conard & JE Parkington (2020) 'When was silcrete heat treatment invented in South Africa?', *Palgrave Communications*, 6(1), 73.
Schoeneberger, PJ, DA Wysocki & EC Benham (2012) *Field Book for Describing and Sampling Soils*, Government Printing Office.
Schrire, C (2010) 'Hilary John Deacon: Archaeologist (1936–2010)', *South African Journal of Science*, 106(11/12), 2.
Schuller, I, L Belz, H Wilkes & A Wehrmann (2018) 'Late Quaternary shift in southern African rainfall zones: sedimentary and geochemical data from Kalahari pans', *Zeitschrift für Geomorphologie*, 61(4), 339-362.
Schwarcz, H & W Rink (2000) 'ESR dating of the Die Kelders Cave 1 site, South Africa', *Journal Of*

Human Evolution, 38(1), 121-128.
Scott, L (1994) 'Palynology of late Pleistocene hyrax middens, southwestern Cape Province, South Africa: A preliminary report', *Historical Biology*, 9(1-2), 71-81.
Scott, L, E Marais & GA Brook (2004) 'Fossil hyrax dung and evidence of Late Pleistocene and Holocene vegetation types in the Namib Desert', *Journal of Quaternary Science*, 19(8), 829-832.
Scott, L & S Woodborne (2007a) 'Pollen analysis and dating of Late Quaternary faecal deposits (hyraceum) in the Cederberg, Western Cape, South Africa', *Review of Palaeobotany and Palynology*, 144(3-4), 123-134.
Scott, L & S Woodborne (2007b) 'Vegetation history inferred from pollen in Late Quaternary faecal deposits (hyraceum) in the Cape winter-rain region and its bearing on past climates in South Africa', *Quaternary Science Reviews*, 26(7-8), 941-953.
Sealy, J & R Yates (1994) 'The chronology of the introduction of pastoralism to the Cape, South Africa', *Antiquity*, 68(258), 58.
Sealy, JC, NJvd Merwe, KA Hobson, DR Horton, RB Lewis, J Parkington, P Robertshaw & HP Schwarcz (1986) 'Isotope Assessment and the Seasonal-Mobility Hypothesis in the Southwestern Cape of South Africa [and Comments and Replies]', *Current Anthropology*, 27(2), 135-150.
Shahack-Gross, R (2017) 'Archaeological formation theory and geoarchaeology: State-of-the-art in 2016', *Journal of Archaeological Science*, 79, 36-43.
Shaw, M (2017) *A Landscape Approach to the Surface Archaeology of the Bos River, Tankwa Karoo, Northern Cape*, unpublished thesis University of Cape Town.
Shaw, M, CJ Ames, N Phillips, S Chambers, A Dosseto, M Douglas, R Goble, Z Jacobs, B Jones, SC-H Lin, MA Low, J-L McNeil, S Nasoordeen, CA O'Driscoll, RB Saktura, TA Sumner, S Watson, M Will & A Mackay (2019a) 'The Doring River Archaeology Project: Approaching the Evolution of Human Land Use Patterns in the Western Cape, South Africa', *Paleoanthropology*, 400, 422.
Shaw, M, CJH Ames, N Phillips, S Chambers, A Dosseto, M Douglass, R Goble, Z Jacobs, B Jones, SC-H Lin, MA Low, J-L McNeil, S Nasoordeen, CA O'Driscoll, RB Saktura, TA Sumner, S Watson, M Will & A Mackay (2019b) 'The Doring River Archaeology Project: Approaching the evolution of human land use patterns in the Western Cape, South Africa', *PalaeoAnthropology*, 400-422.
Shea, JJ (2011) 'Homo sapiens Is as Homo sapiens Was', *Current Anthropology*, 52(1), 1-35.
Shea, JJ (2014) 'Sink the Mousterian? Named stone tool industries (NASTIES) as obstacles to investigating hominin evolutionary relationships in the Later Middle Paleolithic Levant', *Quaternary International*, 350, 169-179.
Shea, JJ (2019) 'European Upper Palaeolithic cultural taxa: better off without them?', *Antiquity*, 93(371), 1359-1361.
Sheppard, PJ & MR Kleindienst (1996) 'Technological change in the earlier and middle stone Age of Kalambo Falls (Zambia)', *African Archaeological Review*, 13(3), 171-196.
Shreve, R (1972) 'Movement of water in glaciers', *Journal of Glaciology*, 11(62), 205-214.
Singer, R & J Wymer (1982) *The Middle Stone Age at Klasies River Mouth in South Africa*.
Smith, AB & MR Ripp (1978) 'An archaeological reconnaissance of the Doorn/Tanqua Karoo', *The South African Archaeological Bulletin*, 118-133.
Smuts, JC (1932) *Climate and man in Africa*.
Söhnge, PG, DJL Visser & C Van Riet Lowe (1937) 'The geology and archaeology of the Vaal River Basin', *South African Geological Survey Memoir*, 35, 1–184.
Stahlschmidt, MC, N Nir, N Greenbaum, T Zilberman, O Barzilai, R Ekshtain, A Malinsky-Buller, E Hovers & R Shahack-Gross (2018) 'Geoarchaeological Investigation of Site Formation and Depositional Environments at the Middle Palaeolithic Open-Air Site of 'Ein Qashish, Israel', *Journal of Paleolithic Archaeology*.
Steele, T, A Mackay, K Fitzsimmons, M Igreja, B Marwick, J Orton, S Schwortz & M Stahlschmidt (2016) 'Varsche Rivier 003: A Middle and Later Stone Age Site with Still Bay and Howiesons Poort Assemblages in Southern Namaqualand, South Africa', *PaleoAnthropology*.
Steele, TE, E Álvarez-Fernández & E Hallet-Desguez (2019) 'Personal ornaments in early prehistory a review of shells as personal ornamentation during the African Middle Stone Age', *Paleoanthropology*, 24, 24-51.
Stern, N (1994) 'The implications of time-averaging for reconstructing the land-use patterns of early tool-using hominids', *Journal Of Human Evolution*, 27(1-3), 89-105.
Stewart, B, AG Parker, G Dewar, M Morley, L Allott, S Jones & BA Stewart (2016) *Africa from MIS6-2: Population Dynamics and Paleoenvironments*.
Stewart, BA & SC Jones (2016) 'Africa from MIS 6-2: The Florescence of Modern Humans' in *Africa from MIS 6-2,* Springer, 1-20.

Stringer, C (2016) 'The origin and evolution of Homo sapiens', *Philosophical Transactions of the Royal Society B: Biological Sciences*, 371(1698), 20150237.
Stringer, CB & P Andrews (1988) 'Genetic and fossil evidence for the origin of modern humans', *Science*, 239(4845), 1263-1268.
Stuiver, M & HA Polach (1977) 'Discussion: Reporting of 14C data', *Radiocarbon*, 19(3), 355-363.
Stuut, J-BW, MA Prins, RR Schneider, GJ Weltje, JF Jansen & G Postma (2002) 'A 300-kyr record of aridity and wind strength in southwestern Africa: inferences from grain-size distributions of sediments on Walvis Ridge, SE Atlantic', *Marine Geology*, 180(1), 221-233.
Sugden, JM & ME Meadows (1989) 'The use of multiple discriminant analysis in reconstructing recent vegetation changes on the Nuwelveldverg, South Africa', *Review of Palaeobotany and Palynology*, 60(1-2), 131-147.
Tattersall, I (1995) *The Fossil Trail: How We Know What We Think We Know About Human Evolution*, Oxford University Press, USA.
Taylor, J (1991) 'Computer programs for standardless quantitative analysis of minerals using the full powder diffraction profile', *Powder Diffraction*, 6(1), 2-9.
Taylor, RE (1997) 'Radiocarbon dating', *Chronometric Dating in Archaeology*, 65-96.
Taylor, RE (2018) 'Radiocarbon Dating in Archaeology' in Smith, C., ed., *Encyclopedia of Global Archaeology*, Cham: Springer International Publishing, 1-11.
Taylor, RE & O Bar-Yosef (2014) *Radiocarbon Dating: An Archaeological Perspective*, 2nd ed., Routledge.
Texier, P-J, G Porraz, J Parkington, J-P Rigaud, C Poggenpoel, C Miller, C Tribolo, C Cartwright, A Coudenneau, R Klein, T Steele, C Verna & O Bar-Yosef (2010) 'A Howiesons Poort tradition of engraving ostrich eggshell containers dated to 60,000 years ago at Diepkloof Rock Shelter, South Africa', *Proceedings of the National Academy of Sciences of the United States of America*, 107(14), 6180-6185.
Thackeray, AI (1977) *Stone Artefacts from Klipfonteinrand*, unpublished thesis (B.A. (Hons)), University of Cape Town.
Thackeray, AI (1992) 'The middle stone age south of the Limpopo River', *Journal of World Prehistory*, 6(4), 385-440.
Thompson, JC, A Mackay, V de Moor & E Gomani-Chindebvu (2014) 'Catchment survey in the Karonga District: A landscape-scale analysis of provisioning and core reduction strategies during the Middle Stone Age of northern Malawi', *African Archaeological Review*, 31(3), 447-478.
Thomsen, KJ, A Murray & L Bøtter-Jensen (2005) 'Sources of variability in OSL dose measurements using single grains of quartz', *Radiation Measurements*, 39(1), 47-61.
Tishkoff, SA, FA Reed, FR Friedlaender, C Ehret, A Ranciaro, A Froment, JB Hirbo, AA Awomoyi, J-M Bodo, O Doumbo, M Ibrahim, AT Juma, MJ Kotze, G Lema, JH Moore, H Mortensen, TB Nyambo, SA Omar, K Powell, GS Pretorius, MW Smith, MA Thera, C Wambebe, JL Weber & SM Williams (2009) 'The Genetic Structure and History of Africans and African Americans', *Science*, 324(5930), 1035-1044.
Tobler, WR (1970) 'A computer movie simulating urban growth in the Detroit region', *Economic geography*, 46(sup1), 234-240.
Toffolo, MB, JS Brink, C van Huyssteen & F Berna (2017) 'A microstratigraphic reevaluation of the Florisbad spring site, Free State Province, South Africa: Formation processes and paleoenvironment', *Geoarchaeology*, 32(4), 456-478.
Tribolo, C, N Mercier, E Douville, JL Joron, JL Reyss, D Rufer, N Cantin, Y Lefrais, CE Miller, G Porraz, J Parkington, JP Rigaud & PJ Texier (2013) 'OSL and TL dating of the Middle Stone Age sequence at Diepkloof Rock Shelter (South Africa): a clarification', *Journal of Archaeological Science*, 40(9), 3401-3411.
Tribolo, C, N Mercier, H Valladas, JL Joron, P Guibert, Y Lefrais, M Selo, PJ Texier, JP Rigaud, G Porraz, C Poggenpoel, J Parkington, JP Texier & A Lenoble (2009) 'Thermoluminescence dating of a Stillbay–Howiesons Poort sequence at Diepkloof Rock Shelter (Western Cape, South Africa)', *Journal of Archaeological Science*, 36(3), 730-739.
Tyson, P (1999) 'Late-Quaternary and Holocene palaeoclimates of southern Africa: a synthesis', *South African Journal of Geology*, 102(4), 335-349.
Underhill, D (2011) 'A History of Stone Age Archaeological Study in South Africa', *South African Archaeological Bulletin*, 66(193), 3-14.
Van Aardt, AC, CB Bousman, JS Brink, GA Brook, Z Jacobs, PJ du Preez, L Rossouw & L Scott (2015) 'First chronological, palaeoenvironmental, and archaeological data from the Baden-Baden fossil spring complex in the western Free State, South Africa' in Runge, J., ed., *Changing Climates,*

Ecosystems and Environments within Arid Southern Africa and Adjoining Regions, CRC Pree, Taylor & Francis Group, 117.
Van Hoepen, ECN (1932) 'Die Suid-Afrikaanse klipwerktuie in internasionale verband', *Argeologiese Navorsinge van die Nasionale Museum*, 1(2), 17–25.
Van Riet Lowe, C (1929) 'Fresh light on the prehistoric archaeology of South Africa', *Banthu Studies*, (3), 388–389.
Van Sittert, L (2002) 'Holding the Line: The Rural Enclosure Movement in the Cape Colony, c. 1865–1910', *The Journal of African History*, 43(1), 95-118.
Vanhaeren, M, F d'Errico, KL Van Niekerk, CS Henshilwood & RM Erasmus (2013) 'Thinking strings: additional evidence for personal ornament use in the Middle Stone Age at Blombos Cave, South Africa', *Journal Of Human Evolution*, 64(6), 500-517.
Vigilant, L, M Stoneking, H Harpending, K Hawkes & AC Wilson (1991) 'African populations and the evolution of human mitochondrial DNA', *Science*, 253(5027), 1503-1507.
Villa, P, M Soressi, CS Henshilwood & V Mourre (2009) 'The Still Bay points of Blombos Cave (South Africa)', *Journal of Archaeological Science*, 36(2), 441-460.
Villa, P, S Soriano, N Teyssandier & S Wurz (2010) 'The Howiesons Poort and MSA III at Klasies River main site, Cave 1A', *Journal of Archaeological Science*, 37(3), 630-655.
Vogel, J & P Beaumont (1972) 'Revised radiocarbon chronology for the Stone Age in South Africa', *Nature*, 237(5349), 50-51.
Volman, TP (1978) 'Early archeological evidence for shellfish collecting', *Science*, 201(4359), 911-913.
Volman, TP (1981) *The Middle Stone Age in the Southern Cape*, unpublished thesis University of Chicago, Department of Anthropology.
Volman, TP (1984) 'Early prehistory of southern Africa' in Klein, R. G., ed., *Southern African Prehistory and Palaeoenvironments*, Rotterdam: Balkema, 169-220.
Wadley, L (1993) 'The Pleistocene Later Stone Age south of the Limpopo River', *Journal of World Prehistory*, 7(3), 243-296.
Wadley, L (2007) 'Announcing a Still Bay industry at Sibudu Cave, South Africa', *Journal Of Human Evolution*, 52(6), 681-689.
Wadley, L (2013) 'Recognizing Complex Cognition through Innovative Technology in Stone Age and Palaeolithic Sites', *Cambridge Archaeological Journal*, 23(2), 163-183.
Wadley, L (2015) 'Those marvellous millennia: the Middle Stone Age of Southern Africa', *Azania: Archaeological Research in Africa*, 50(2), 155-226.
Wadley, L, T Hodgskiss & M Grant (2009) 'Implications for complex cognition from the hafting of tools with compound adhesives in the Middle Stone Age, South Africa', *Proceedings of the National Academy of Sciences*, 106(24), 9590-9594.
Wadley, L & LC Prinsloo (2014) 'Experimental heat treatment of silcrete implies analogical reasoning in the Middle Stone Age', *Journal Of Human Evolution*, 70, 49-60.
Waelbroeck, C, L Labeyrie, E Michel, JC Duplessy, J McManus, K Lambeck, E Balbon & M Labracherie (2002) 'Sea-level and deep water temperature changes derived from benthic foraminifera isotopic records', *Quaternary Science Reviews*, 21(1), 295-305.
Wainscoat, JS, AV Hill, A Boyce, J Flint, M Hernandez, SL Thein, JM Old, J Lynch, AG Falusi & DJ Weatherall (1986) 'Evolutionary relationships of human populations from an analysis of nuclear DNA polymorphisms', *Nature*, 319(6053), 491-493.
Walker, EA (1930) 'Relief and the European settlement of South Africa', *Scottish Geographical Magazine*, 46(1), 1-9.
Walker, M, S Johnsen, SO Rasmussen, T Popp, JP Steffensen, P Gibbard, W Hoek, J Lowe, J Andrews & S Björck (2009) 'Formal definition and dating of the GSSP (Global Stratotype Section and Point) for the base of the Holocene using the Greenland NGRIP ice core, and selected auxiliary records', *Journal of Quaternary Science*, 24(1), 3-17.
Walter, RC, RT Buffler, JH Bruggemann, MM Guillaume, SM Berhe, B Negassi, Y Libsekal, H Cheng, RL Edwards & R Von Cosel (2000) 'Early human occupation of the Red Sea coast of Eritrea during the last interglacial', *Nature*, 405(6782), 65-69.
Waters, N (2017) 'Tobler's First Law of Geography' in Richardson, D., Castree, N., Goodchild, M. F., Kobayashi, A., Liu, W. & Marston, R. A., eds., *International Encyclopedia of Geography*John Wiley & Sons, Ltd.
Watson, S, M Low, N Phillips, C O'Driscoll, M Shaw, C Ames, Z Jacobs & A Mackay (2020) 'Robberg Material Procurement and Transport in the Doring River Catchment: Evidence from the Open-Air Locality of Uitspankraal 9, Western Cape, South Africa', *Journal of African Archaeology*, 18(2), 209-228.

Wayland, E (1934) 'Rifts, rivers, rains and early man in Uganda', *The Journal of the Royal Anthropological Institute of Great Britain and Ireland*, 64, 333-352.
Weitzel, MC, KB Borrazzo, A Ceraso & C Balirán (2014) 'Trampling fragmentation potential of lithic artifacts: an experimental approach', *Intersecciones en Antropología*, 15.
Wilkins, J (2020) 'Is it Time to Retire NASTIES in Southern African? Moving Beyond the Culture-historical Framework for Middle Stone Age Lithic Assemblage Variability', *Lithic Technology*, 1-13.
Wilkins, J, KS Brown, S Oestmo, T Pereira, KL Ranhorn, BJ Schoville & CW Marean (2017) 'Lithic technological responses to Late Pleistocene glacial cycling at Pinnacle Point Site 5-6, South Africa', *PLoS ONE*, 12(3), e0174051.
Wilkins, J & M Chazan (2012) 'Blade production ~500 thousand years ago at Kathu Pan 1, South Africa: support for a multiple origins hypothesis for early Middle Pleistocene blade technologies', *Journal of Archaeological Science*, 39, 1883-1900.
Wilkins, J, BJ Schoville, KS Brown & M Chazan (2012) 'Evidence for early hafted hunting technology', *Science*, 338(6109), 942-946.
Will, M, A Mackay & N Phillips (2015) 'Implications of Nubian-Like Core Reduction Systems in Southern Africa for the Identification of Early Modern Human Dispersals', *PLoS ONE*, 10(6), e0131824.
Williams, M (2017) 'Formation processes and context of complex stratigraphic features at the MSA archaeological sites of Pinnacle Point Site 5-6 and Mertenhof during MIS 3 in southern Africa'.
Willoughby, PR (1993) 'The middle stone age in East Africa and modern human origins', *African Archaeological Review*, 11(1), 3-20.
Willoughby, PR (2006) *The Evolution of Modern Humans in Africa: A Comprehensive Guide*, Rowman Altamira.
Willoughby, PR (2020) 'Modern human behavior', *Oxford Research Encyclopedia of Anthropology*.
Wiltshire, N (2011) *Spatial Analysis of Archaeological Sites in the Western Cape Using an Integrated Digital Archive* [Master's thesis], unpublished thesis (MS), University of Cape Town.
Wintle, AG (1997) 'Luminescence dating: laboratory procedures and protocols', *Radiation Measurements*, 27(5-6), 769-817.
Wintle, AG & AS Murray (2006) 'A review of quartz optically stimulated luminescence characteristics and their relevance in single-aliquot regeneration dating protocols', *Radiation Measurements*, 41(4), 369-391.
Wood, B, D Doherty & E Boyle (2020) 'Hominin Taxic Diversity' in *Oxford Research Encyclopedia of Anthropology*.
Wood, R, Z Jacobs, D Vannieuwenhuyse, J Balme, S O'Connor & R Whitau (2016) 'Towards an accurate and precise chronology for the colonization of Australia: The example of Riwi, Kimberley, Western Australia', *PLoS ONE*, 11(9), e0160123.
Wurz, S (2013) 'Technological trends in the Middle Stone Age of South Africa between MIS 7 and MIS 3', *Current Anthropology*, 54(S8), S305-S319.
Wurz, S (2019) 'Human evolution, archaeology and the South African Stone Age landscape during the last 100,000 years' in *The Geography of South Africa,* Springer, 125-132.

APPENDIX 1.

STUDY AREA: LAND TENURE

1.1 Possible Indications of Recent Anthropogenic Modification at Uitspankraal

Within the last century, anthropogenic modifications in the area of the Doring-Biedouw confluence are suggested by the topographic map series for grid 3219AB. There are three map editions in this series: 1960, 1986 and 2003 (Figure A1.1). The dates for each map represent the year they were surveyed and often postdate the aerial photography they were based on by a year. For topographic map 3219AB 1960, air photographs were taken in 1959 and survey was completed in 1960. Together they were drawn up in 1964. The second edition was published in 1987 and is based on 1986 aerial imagery. The third edition was published in 2006, although it was drawn up in 2003. What is clear from all three maps is that the Biedouw-Doring confluence has been divided into several farmstead locations for the better part of the 20th Century. Three main homesteads are recorded on the 1960s map, together with the presence of cultivated wetlands on either side of the Biedouw channel, before it joins with the Doring River. The road leading to this drif (R355) is accessed from Pakhuis Pass, making it at least as old as the development of this pass in 1877 (see Chapter 4.2.2; Amschwand 2003).

Between 1986 and 2003, UPK1 and the farmland immediately surrounding the present-day exposures appears to have undergone marked changes in its use and access. The first is the addition of a dirt track running north and then west from the Hough family homestead, which cuts along UPK1's southern side (the same track used to drive to the locality) and eventually leads to Appleboskraal. This track was first recorded in the second map edition of 1987, appearing in aerial photographs between 1959 and 1986 (Figure A1.1). By the third edition, this road is more defined, two buildings and a dam to the east of UPK1 have been added, as well as extensive cultivation fields on the terraces north of UPK1, parallel to the Doring River. These features were either not clearly seen or did not exist during the production of the 1986 and 1959 maps. These buildings and the delineation of "cultivated land" across what was originally terrace, suggests that the ploughed fields at UPK1 and the highly eroded dirt road that runs along its back, were only identified in aerial photographs within the last 30-50 years. Reviewing the aerial imagery that was available over this time by comparing these with the features drawn in each map edition suggests that their accuracy in representing the presence of buildings, cultivated land, and dirt roads was dependent on the quality and resolution of the aerial imagery available at the time. This is evident after enhancing aerial photographs taken in 1959, from which the two buildings identified in the 2003 edition are apparent in the photo (Figure A1.1). However, the dam and presence of field cultivation remains unclear.

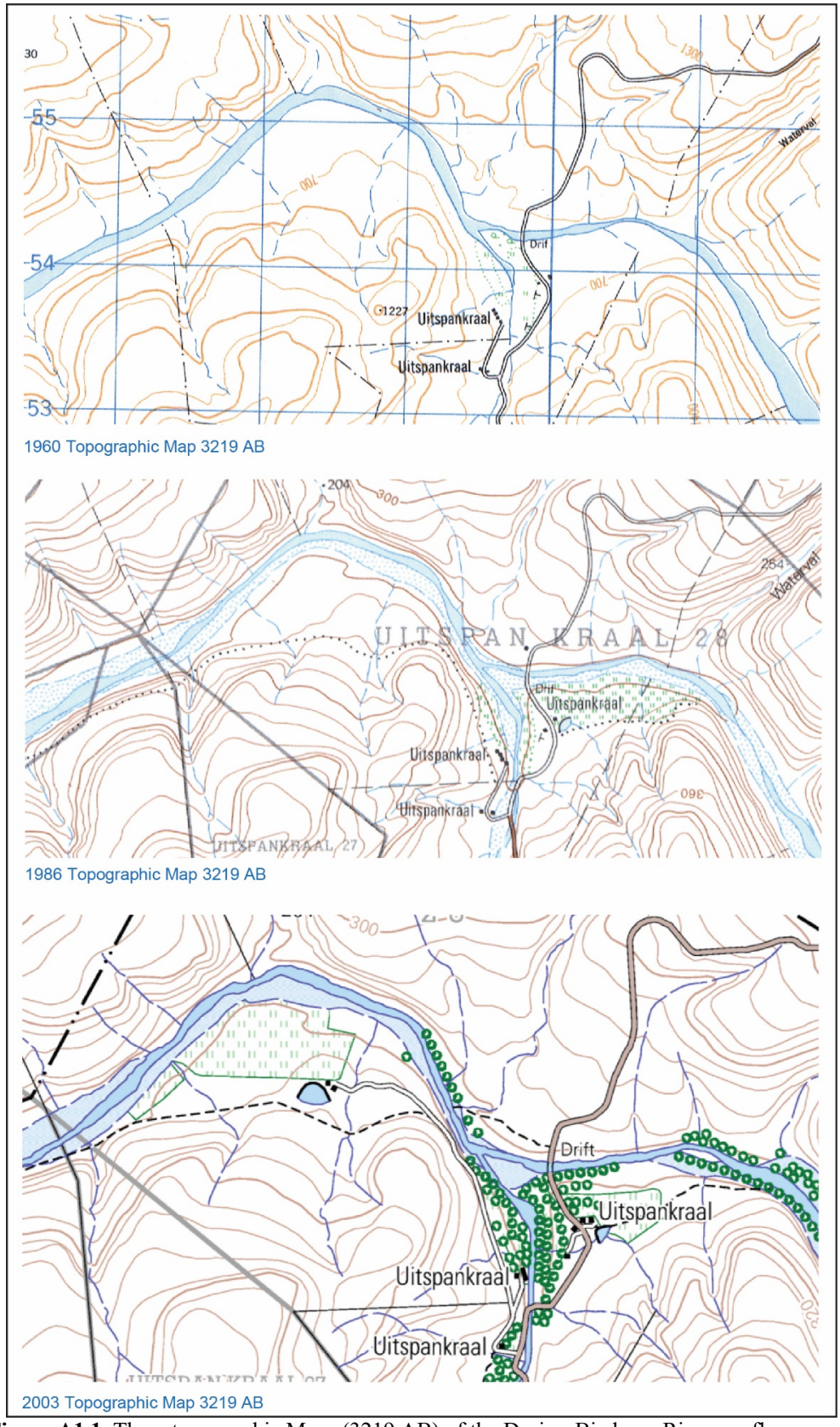

Figure A1.1. Three topographic Maps (3219 AB) of the Doring-Biedouw River confluence and surrounding farmland of Uitspankraal, comparing farm and road development from 1960, 1986 and 2003.

1.2 Eighteenth Century Loan Farm Tenure Near the Doring River Valley

The first recorded colonial use of the Doring River's catchment were two loan farms located close to the Doring River's outlet into the Olifants River, Brakkefontein and Pakhuis (Figure A1.2). From their initial purchase, both farms continued to be tenured throughout the 18th Century and were held by at least one claimant for at least three decades before transfer to another farmer. Their use probably followed the seasonal trekking tradition of grazing and lambing sheep between the Karroo in the winter, and the Cederberg mountains in the drier summer months (Van der Merwe 1945). This strategy aimed to maximize and conserve the veld available between ecozones by employing seasonal rotation throughout the year (Parkington 1972).

Brakkefontein was claimed in 1727 by prominent burgher Daniel Pfeil, who owned this land for 31 years before transferring it in 1752 to Barend Lubbe. Brakkefontein, like many other farms in the region, was not the main residence of the claimant. For example, Daniel Pfeil's primary residence was in the Cape district (Mitchell 2009:para. 128). Moreover, Barend Lubbe's primary residence was at the loan farm Groot Valleij, located on the east side of the Olifants River, which he held from 1736, until his death in 1785. It is likely that they had herders maintaining and grazing the land in the catchment on their behalf. As was an ongoing tradition in the region, Brakkefontein was transferred to Barend's son Barend Fredrik Lubbe in 1758, where he and his wife, Johanna Maria Keyser, established their home. The early death of B.F. Lubbe saw the transfer of Brakkefontein to his son Paul Willem Lubbe in c.1791. Paul held this farm until 1810.

To the south of Brakkefontein, west of the Cederberg mountains, the Pakhuis loan farm was claimed by Christiaan Liebenburg in 1743 and then transferred to Cornelis Koopman in 1744. Cornelius held this land for 50 years before it was transferred to Jacobus Redelinghuizen in 1794 and then to Johannes Jacobus Botha in 1800. Cornelis Koopman was one of few mixed-race farmers who, along with Khoisan, held land claims in the region. Cornelis also tenured the DoringBos (DoornBoshe) (Figure A1.2; (Mitchell 2002, 2009). However, it is not possible to say which loan farm he occupied year-round, nor the duration of his tenure of the Doringbos (Mitchell 2009, figure 3.9). There are also frequent discrepancies between land hold records in the Doring River valley. Matthys Scheffer is listed by Mitchell (2009, fig 3.9) as either a mixed-race or Khoisan claimant of Onrust (Figure A1.2) in 1777, despite the Lubbe family being recorded as holding this land from 1750 to 1791 (Table A1.1).

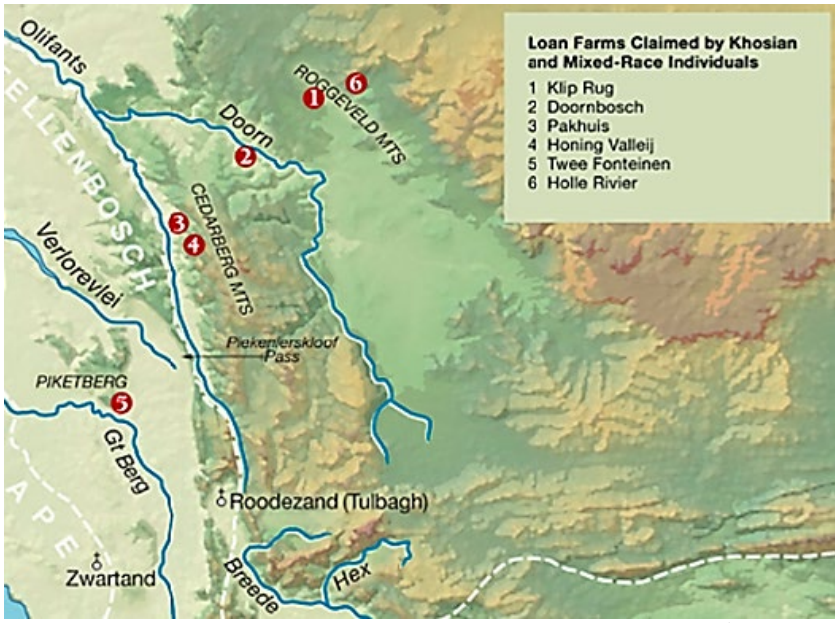

Figure A1.2. Loan farms tenured by mixed-race and Khoisan farmers in the 18th Century. Detail from Mitchell (2009, fig. 3.10).

1.2.1 Lubbe Family and land tenure along the Doring/Biedouw Rivers

As part of a bigger estate of loan farms in the Olifants-Doring Catchment, Barend Lubbe and his decedents farmed the land in and around the Doring River for 270 years, from the 1750s to present day. Barnand Lubbe and his brother Henrik first owned land within the Olifants-Doring Catchment from as early as 1725 (Mitchell 2009). In addition to Brakkefontein, their loan farms in the Doring Catchment included Bloemfontein (1776-17851), Onrust (1750-1791) and Brandewijns Rivier (1777-1778) west of the Doring River (see Figure A1.3 and Table A1.1, Mitchell, 2009). Thereafter, Bloemfontein and Onrust were taken on by Barend's son Frans Lubbe adding to his loan farm, Zandrift, which was in the Biedouw River valley and likely settled by Frans from 1780 (see Figure A1.3 and Table A1.1, Mitchell, 2009). Frans' purchase of an opstal at Bloemfontein during Barend Lubbe's auction suggests that structural modification, albeit modest (based on the price of purchase), was already in place in the valley by the late 1700s (Mitchell, 2009).

[1] previously owned by brother Jan Hendrik Lubbe between 1770-1773

Table A1.1. Lubbe Family land tenure in the Doring River Catchment during the 18th Century. Source: after Mitchell (2009, figure 7.6).

Farm name	Claimant	Dates of tenure	Reference
Onrust	Barend Lubbe	1750–1785	CA: RLR 12:143
	Frans Lubbe	1786–1791	CA: RLR 35:44.4
Brakkefontein	Barend Lubbe	1752–1762	CA: RLR 13:58
	Barend Frederik Lubbe	1758–1791	CA: RLR 15:62
	Paul Willem Lubbe	–1810	CA: MOOC 8/58.36a
Bloemfontein	Jan Hendrik Lubbe	1770–1773	CA: RLR 21:83
	Barend Lubbe d'oud	1776–1785	CA: RLR 24:190
	Frans Lubbe	1787–1791	CA: RLR 36:116.1 CA: MOOC 10/15.6
Brandewijns Rivier	Hendrik Lubbe	1777–1778	CA: RLR 25:102
Zanddrift	Frans Lubbe	1780–1793	CA: RLR 27:130

Figure A1.3. Location map of the Lubbe family farms between 1725-1830. Sourced from Mitchell (2009, figure 7.4).

APPENDIX 2.

FIELD SEASON DATA COLLECTION: FOCUS AND ASSISTANCE

The following is an outline of the research focus and data collection approach for each field season carried-out specifically for this doctorate. This would not have been possible without the few, yet vital, people who were available to assist me with survey, sampling, and data collection between 2014 and 2017.

2014

The main researchers who formed the UPK7 survey team in 2014 were Marika Low (lithic attribute recording and data entry in the ELSA zone AoA3 [PhD data collection, including Low *et al.* (2017)]), Alex Mackay (season and project director, lithic attribute data entry design [AoA 1 and 2], attribute logging [AoA 1], spatial data collection), Manuel Will (lithic attribute data logging in p-HP AoA 2, Nubian data collection design and recording (see Will *et al.* 2015), and myself (lithic data entry in AoA 1 and UPK9, spatial data collection, data management, OSL and sediment sampling characterisation [PhD data collection]). Regular data loggers and field assistants included Wesley Flear and Cede Bryne (AoA1), who also carried out the 2014 silcrete source survey from the Doring River to Swartvlei using handheld GPS units (Trimble Junos). Brian Jones attended part of this season to assist with survey and provide advice on and supervision of the initial identification, mapping, description, and sampling of exposed geomorphological units at UPK1, UPK7, and Appleboskraal (ABK).

2015

March

Joint season with Marika Low. One month at UPK7, involved piloting the random sample square (rSSQ) survey protocol, and involved rSSQ sediment sampling and descriptions, and topographic survey and modelling. Assisted by Matthew Shaw and Benjamin Marais.

May

Involved continuation of rSSQ survey at UPK7, with the assistance of Blair McPhee.

August

Two weeks at UPK1 involved sample square data collection, sediment sampling, and topographic survey and modelling. Assisted by Brigette E. Cohen.

2016

March

One month at UPK 7, involved sample square data collection, sediment sampling and valley-wide survey and topographic survey and modelling. Assisted by Blair McPhee.

April

Two weeks, involved sediment sampling and valley-wide survey and characterisation of the Doring's geomorphology, including localities PL1, LNGKL, KH1, ABK, UPK 1 to 9. Assisted and advised by Brian Jones.

August

The August 2016 field season was divided into three parts:

- Part one: two weeks of rSSQ survey and sediment sampling at UPK1. The author was assisted by Gizelle Kotze, Morne Valentyn, and Chris Thornhill.
- Part two: one week of drone survey of UPK1 and UPK 7. This was made possible with assistance from Dominic Stratford (drone owner and pilot), Aurore Val (survey and sampling assistance).
- Part three: 1.5 weeks, involving rSSQ data collection (assisted by Aurore Val, Alex Blackwood, Alex Mackay) and OSL sampling (assisted by Aurore Val) at UPK7.

2017

June

UPK7 geophysical survey (Electrical Resistivity) by Ian Moffatt (assisted by me), and my final assessment of the exposed chronostratigraphic sequence (0.5-1 week), with advice from Ian Moffatt.

APPENDIX 3.
SUPPLEMENTARY INFORMATION FOR CHAPTER 5:
SURFACE MODELLING & E4 CODING

The following provides supplementary information to Chapter 5, including the steps involved in modelling Uitspankraal 7's bare-earth morphology (Chapter 5.6, see Figure 5.9 for workflow) and the coding used in E4 for the in-field collection of artefact and non-flaked stone attribute data.

3.1 Stage 1. Image Processing in Photogrammetry

Photos taken during the 2019 UAV-flyover of UPK7 were first checked for distortion, file corruption, and duplication during an initial dataset sweep. Any photos found to be poor in quality were removed prior to PhotoScan processing. In PhotoScan, the quality of each photo was automatically assessed using the *Estimate of Image Quality* tool in PhotoScan. This produced quality values, in which 1 is the highest quality and anything below this value indicates a decrease in image quality. The user manual suggests an exclusion threshold of ≤ 0.5, while Dietrich (2015) suggests a higher threshold of 0.6. However, over half of the photo-set has image quality values below 0.5, ranging between 0.82 and 0.29 with a median of 0.46 and a standard deviation of 0.17. Even the exclusion of images with the poorest quality readings (below 0.3) resulted in sizable gaps in point cloud coverage. For this reason, the entire photo-set was used.

Cleaned, geotagged images were automatically aligned in PhotoScan with fixed camera calibration, preventing adjustments to the images. The quality of photo alignment is shown in Figure 5.7, where blue frames represent high quality alignment and orange represents low quality image alignment. Improvement of poorly aligned cameras was not possible using the in-built features in PhotoScan. One way to correct this issue is to use images from previous seasons to increase the number of cameras in order to fill the areas with gaps. However, even though this option would help to provide a DSM of higher quality and complete coverage, it is not ideal for tracking erosion and deposition between seasons which depends on isolating each photo series by their year of capture. To maintain temporal integrity between seasons the dataset was limited to 2019 imagery, producing gaps of up to 80 cm in the north-eastern and central eastern side of the locality, in areas of unconsolidated sand dune (Figure A3.1).

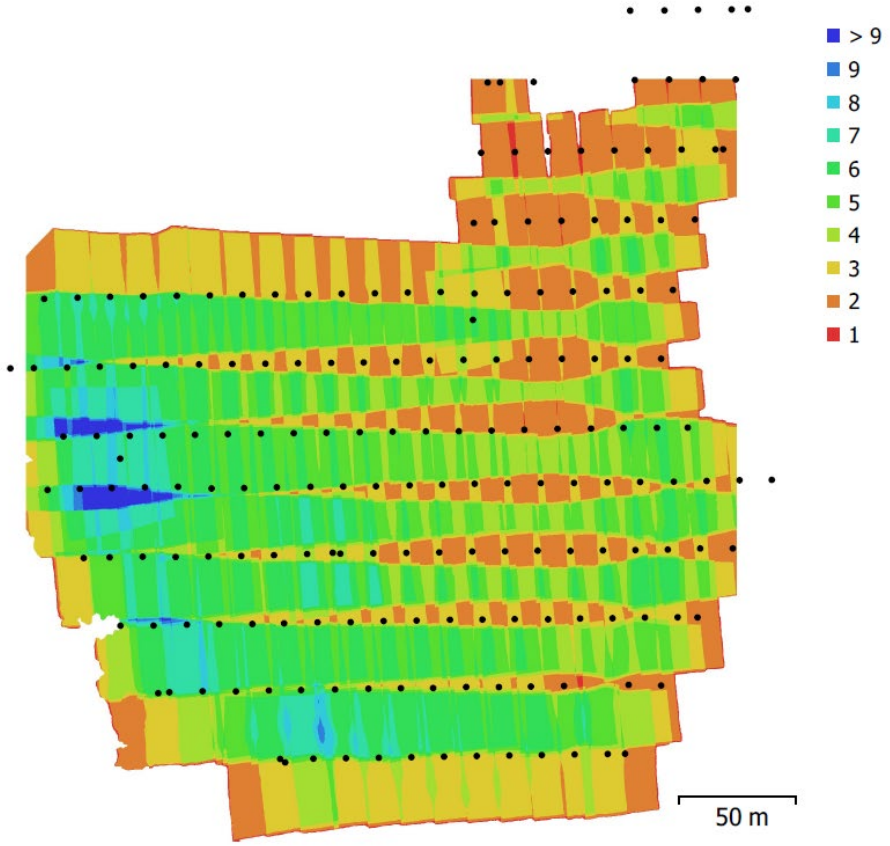

Figure A3.1. Agisoft PhotoScan reported figure of camera locations and image overlap.

Aligned photos were georeferenced using 10 RTK-recorded and post-field corrected ground control points (GCPS) rather than the in-built coordinate data recorded by the UAV camera. A base of linking nodes or markers that reference a series of in-field ground control points (GCPs) were established and their positions manually aligned for spatial reference throughout model building. GCP markers were represented by bright yellow crosses set out across the ground of the survey area, together with pre-established survey marks used for the total station survey at the site. Each GCP provides a corrected coordinate reference for rectifying the elevations of the UAV model. The accuracy of the georeferenced model was assessed based on the individual GCP and total Root Mean Square Error (RMSE). GCPs that showed RMSEs substantially higher than other GCPs and increased the total RMSE were excluded to increase the accuracy of the georeferenced dataset. Figure 5.8 shows the locations of each control point and their estimated errors (summarized in Tables A3.1 and A3.2). The total RMSE for all GCPs was 2.38 cm (Table A3.2), and 2 cm or less for individual point positions (Figure A3.2 and Table A3.1). This amount of error is sufficiently low for producing a 20 cm resolution DTM.

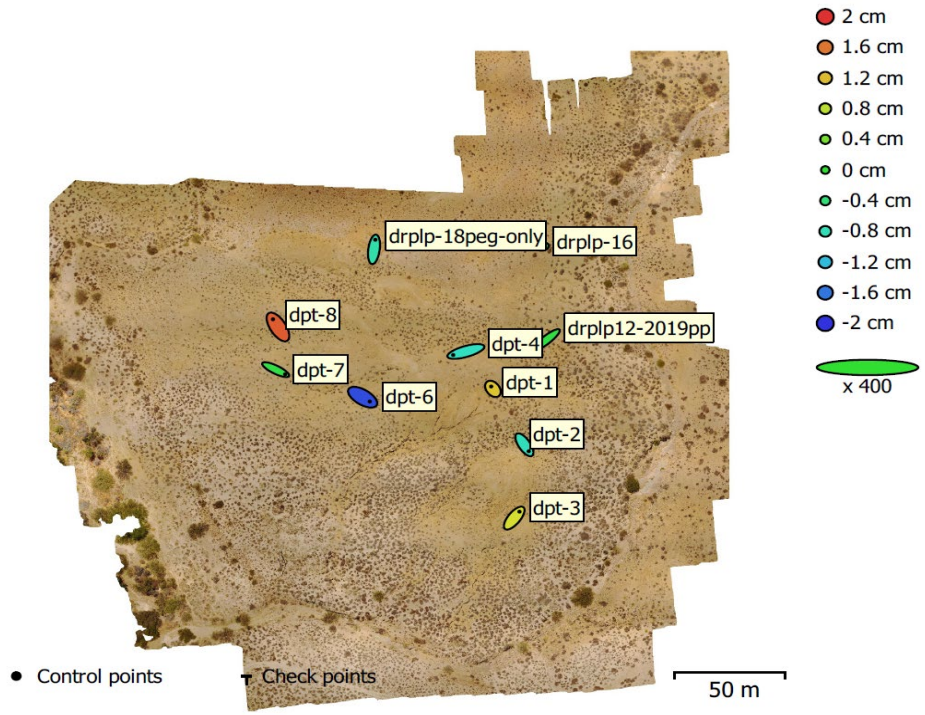

Figure A3.2. Locations of UPK7 2019 UAV ground control points (GCP) and their associated error estimates.

Table A3.1. Control point RMSE (x, y, z = easting, northing, altitude, respectively)

GCP no.	X error (cm)	Y error (cm)	Z error (cm)	Total (cm)	Image (pix)
dpt-1	-0.40	0.60	1.15	1.36	0.08 (4)
dpt-2	0.99	-1.62	-0.80	2.06	0.39 (2)
dpt-3	1.19	1.59	0.96	2.21	0.60 (3)
dpt-4	-2.85	-0.89	-0.83	3.10	0.03 (2)
dpt-6	1.6	-1.05	-1.84	2.66	0.17 (4)
dpt-7	2.13	-1.15	-0.11	2.42	0.26 (6)
dpt-8	-1.12	1.91	1.76	2.83	0.10 (6)
drplp12-2019pp	-2.22	-1.92	-0.10	2.94	0.07 (2)
drplp-16	0.43	0.11	-0.04	0.44	0.04 (2)
drplp-18peg-only	0.29	2.39	-0.69	2.51	0.24 (2)
Total RMSE	1.56	1.48	1.03	2.38	0.26

Table A3.2. Total Control point RMSE (x, y, z = easting, northing, altitude, respectively)

Count	X error (cm)	Y error (cm)	Z error (cm)	XY error (cm)	Total (cm)
10	1.56	1.48	1.03	2.15	2.38

3.2 Stage 2. Vegetation Filtering & Bare-earth Interpolation

The following presents the process and results of vegetation filtering and interpolation of UPK7's 2019 imagery. The methods and materials used for capturing and processing the aerial imagery is outlined here and supplement details given in Chapter 5.6.2.

3.2.1 TIN Densification in LAStools (via Purpose-built GUIs)

Traditionally used for LIDAR processing, LAStools (under the GNU Lesser General Public License [LGPL] v2.1 1999) provides an automated TIN densification algorithm using 'lasground_new.exe' (an updated version of lasground.exe) for modelling complex terrains (http://lastools.org). LAStools can be used through a series of GUIs that represent tool-specific modules or as part of a larger software package such as ArcGIS desktop and QGIS. Here, the LAStools program and GUI files were downloaded and used under the conditions set out by the LGPL.

3.2.1.1. Filtering mode parameters

A dense point cloud (DCP) in LAS file format was exported from PhotoScan for use in LAStools. The following steps/modules and their parameters were taken in LAStools and ArcGIS Pro to filter vegetation and to perform bare-earth interpolation:

1. Lastile
    1. Import raw DCP las file
    2. Tiles of 50 with 5 m buffers
    3. Filename: "UPK7_2019_DSM_[tileID]"
    4. Name suffix: tile.laz
2. Lasthin1 (lasnoise not needed after this)
    1. Thin 0.1 m grid
    2. Class 8
    3. 50 percentile (central selection between upward and downward outliers)
    4. Suffix output as *thin*
3. Las2las
    1. Run thinned tiles through las2las, dropping class 0 and keeping class 8 points only (a within-licence measure)
4. Lasground1
    1. Classify thinned points (classed as 8) to ground (class 2) vs vegetation (class 1)
    2. Produce three las files: one for each filtering mode, dropping buffers ('flagged as withheld' during tiling stage) and merging tiles into a single file each time.
    3. Four parameter sets used (output file name: "UPK7_2019*_[mode]*_merged":
        i. Nature (6,147,948 of 7,421,614 as ground)

        lasground_new -cpu64 -v -lof file_list.2432.txt -merged -drop_withheld -nature -odir "H:\PhD_South_Africa\Doring_Paleo_Landscape_Project\DTM\UPK7_DroneDSM_2019\LAStools_filtering\Trial 11_finalisedmethods\FilterMode_testfiles" -o "UPK7_2019_nature_merged.las"

        ii. Wilderness (6,700,019 of 7,421,614 as ground)

        lasground_new -cpu64 -v -lof file_list.5124.txt -merged -drop_withheld -wilderness -ignore_class 0 -odir "H:\PhD_South_Africa\Doring_Paleo_Landscape_Project\DTM\UPK7_DroneDSM_2019\LAStools_filtering\Trial 11_finalisedmethods\FilterMode_testfiles" -o "UPK7_2019_wild_merged.las"

        iii. Nature4step

        lasground_new -cpu64 -v -lof file_list.2432.txt -merged -drop_withheld -step 4 -sub 3 -bulge 1 -offset 0.05 -odir "H:\PhD_South_Africa\Doring_Paleo_Landscape_Project\DTM\UPK7_DroneD

SM_2019\LAStools_filtering\Trial 11_finalisedmethods\FilterMode_testfiles" -olas

iv. Aggressive (3,986,171 of 7,421,614 as ground)
lasground_new -cpu64 -v -lof file_list.2432.txt -merged -drop_withheld -step 4 -bulge 0.5 -spike 0.1 -down_spike 0.5 -offset 0.01 -odir "H:\PhD_South_Africa\Doring_Paleo_Landscape_Project\DTM\UPK7_DroneDSM_2019\LAStools_filtering\Trial 11_finalisedmethods\FilterMode_testfiles" -o "UPK7_2019_aggressive_merged.las"

Table A3.3. Four modes of filtering using LAStools, together with their associated parameters. Nature and wilderness modes are built-in filter options in LAStools' module lasground_new (v190927). Nature4step and aggressive mode are both custom filters. Colours coordinate with profile graph lines in Figure A3.4.

Filter mode	Step (m)	Sub (m)	Bulge (m)	Spike (m)	Down spike (m)	Offset (m)	Search intensity
nature	5	3	1	1	1	0.05	default
wilderness	3	6	1	1	1	0.05	default
nature4step	4	3	1	1	1	0.05	default
aggressive	4	na	0.5	0.1	0.05	0.01	default

5. classified las files, each produced using a different set of filtering parameters, were imported into ArcGIS Pro and statistics run.

Table A3.4. Classification results for filtered and unfiltered las point clouds using nature, wilderness, nature4step, and aggressive filtering modes along with the minimum and maximum elevations for each.

Filter mode	Classification	point count	%	Z min	Z max	Point spacing
Unfiltered	0 unclassified	7,421,614	100	192.65	219.09	0.101
nature	1 object	1,273,666	17.16	192.96	219.05	0.101
	2 bare-earth	6,147,948	82.84	192.66	219.10	0.101
wilderness	1 object	721,595	9.72	192.85	219.09	0.101
	2 bare-earth	6,700,019	90.28	192.65	218.72	0.101
nature4step	1 object	1,023,168	13.79	192.85	219.09	0.101
	2 bare-earth	6,398,446	86.21	192.66	218.73	0.101
aggressive	1 object	3,435,443	46.29	192.97	219.09	0.101
	2 bare-earth	3,986,171	53.71	192.66	218.13	0.101

3.2.2 Qualitative comparison of filtering parameters

Multiple parameters were trialled and qualitatively assessed for their reliability to correctly classify terrain and non-terrain surfaces (Table A3.7). Comparative assessment involved visual examination of four different parameter-sets using LASview (filtered between RGB and classification as a point cloud and also in tin mode) and profile graphs in ArcGIS Pro (post-DTM creation), rating each set following Sithole & Vosselman (2004) (see Tables A3.6 and A3.7).

3.2.2.1 Visual assessment of filtering quality

Step one: Interpolation

Two interpolation methods were used to produce a 2.5D surface of bare-earth elevations for UPK7:

i. Interpolation 1:
   - Value: elevation
   - Interpolation type: Binning
   - Cell assignment method for points: Nearest neighbour
   - Void filling method: Linear assignment from triangulated area
   - Output value type: float
   - Sampling Type: cell size
   - Sampling value: 0.2 m

ii. Interpolation 2:
   - Value: elevation
   - Interpolation type: TIN
   - Cell definition: Triangulation
   - Cell value assignment: Natural neighbour
   - Output value type: float
   - Sampling Type: cell size
   - Sampling value: 0.2 m

Table A3.5. Two Interpolation methods and the parameters selected for each to digitally model the terrain of UPT7's nature filtered DSM.

Interpolation method	Type	Cell definition	Cell value assignment	Void filling	Sampling value (m)
1	Binning	binning	nearest neighbour	linear	0.2
2	TIN	triangulation	natural neighbour	natural neighbour	0.2

The first model (Interpolation 1) employed binning interpolation, assigning cells with points using Inverse Distance Weighted (IDW) and natural neighbour to identify and fill cells without points, and the second (Interpolation 2) involved Natural neighbour TIN interpolation. The sampling resolution for both model outputs was set to 0.2 m. Interpolation 1 was used to visually compare the difference in surface filtering and morphological representation between each filtering mode.

Step two

Profile stacks produced across a range of surface complexities

Step three

A series of line graphs were produced to visually compare a DTMs using the different filtering modes and unfiltered DSM (attained by interpolating any of the three las files in unfiltered mode)

Step four

The preferred filtering mode was selected based on point cloud and stacked profile visual assessment (after Sithole and Vosselman 2004).

3.2.3 Filtering results

Results were evaluated in LASview and ArcGIS Pro (after DTM creation). Table A3.6 presents the qualitative rating for vegetation and ground discontinuity for each mode of filtering. To evaluate each condition, a series of profile lines were laid out in ArcGIS Pro that covered a variety of surface types depicted in Figures A3.3 (also see Figure A3.4), including high and low vegetation (Figure A3.4E), clustered and standalone vegetation (Figure A3.4B), deep and narrow rilling (Figure A3.4A and B), steep slopes and high mounds (Figure A3.4C, D, and F), and vegetated slopes (Figure A3.4C and F). Line colours relate to parameter-set colours shown in Tables A3.7 & A3.8).

***Table A3.6.** Meaning of good (g), fair (f) and poor (p) (used in Table A3.7)

Rating	Item filter rating	Influence rating
Good	Item filtered most of the time (>90%)	No influence
Fair	Item not filtered a few times	Small influence on filtering of neighbouring points
Poor	Item not filtered most of the time (< 50%)	Large influence on filtering of neighbouring points

*Source: Sithole and Vosselman (2004)

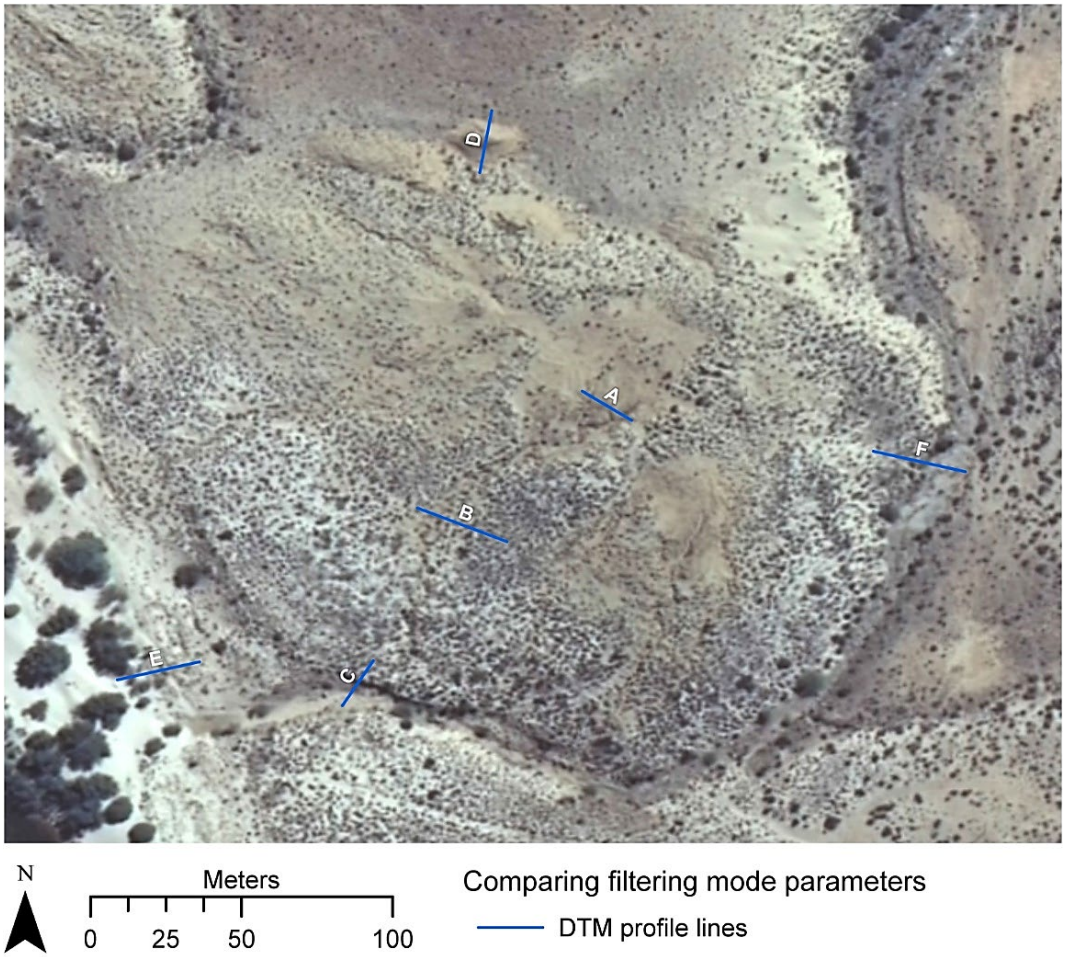

Figure A3.3. Profile line location map. Profile lines in a range of topographic and vegetation settings to assess how well each filter mode represents different surface types across UPK7. All profiles were interpolated using the same method: Binning, Linear, Nearest Neighbour (Interpolation 1, see methods for details). The labels associated with each profile line relate to the profile figure labels in Figure A3.4.

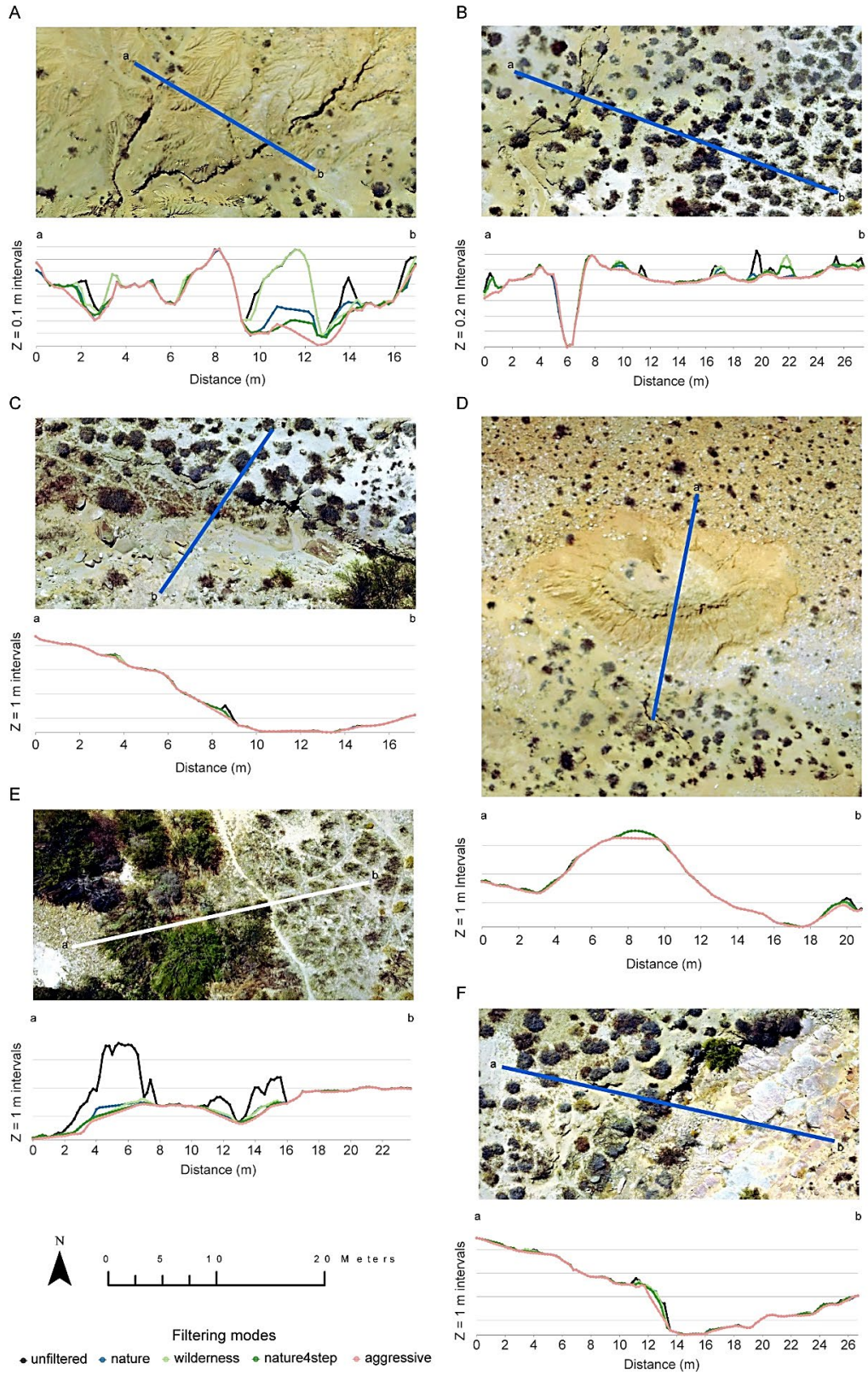

Figure A3.4. Comparing filter modes in profile for a range of topographic and vegetation scenarios of varying complexities across UPK7. All profiles were interpolated using the same method: Binning, Linear, Nearest Neighbour (Interpolation 1, see methods for details). Profile line colours relate to tabulated filter modes in Tables A3.7 and A3.8. See Figure A3.3 for profile line location map.

Classification of high isolated and clustered vegetation was fair to good for all four filter modes (Figure A3.4e & Table A3.7). However, each mode varied in success when classifying low lying vegetation and preserving bare-earth discontinuities (Table A3.7). Wilderness has the smallest step size (3 m), which helped to maintain the morphology of rilled exposures (i.e., Figure A3.4a), producing the lowest frequency of type I errors out of the four filtering modes (Figure A3.4a and Table A3.8). However, it was less effective in identifying low, isolated vegetation compared to the other filtering modes (Figure A3.4b), committing Type II errors more frequently (Tables A3.7 and A3.8). At the other extreme, the aggressive mode successfully filtered clustered and isolated low-lying vegetation, producing fewer Type II errors (Figure A3.4e and Figure A3.4b, Table A3.8). However, this mode also returned the most Type I errors, with bare-earth often misidentified as vegetated surface. Added to this, the aggressive mode obtained the poorest result for preserving discontinuities and maintaining sharp edges (e.g., Figure A3.4c,f, Table A3.7). In the case of profile Figure A3.4a, this mode almost entirely removed the highly rilled, unvegetated sediment body that occurs between 9 and 13 m along the profile line, while in Figure A3.4d it flattens the top of a large mound of residual sediment.

The custom filter, nature4step, has a step of 4 m, 1 m less than nature and 1 m more than wilderness mode. However, it shows the poorest performance compared to both filter modes in rilled settings (Figure A3.4a) and only showed minor improvements in its identification of low-lying shrubs compared to wilderness (e.g., Figure A3.4b). Overall, the nature mode produced the best results. With the largest step size (5 m) it reduced the frequency of Type II and Type I errors observed for wilderness and aggressive modes respectively (Table A3.8). However, wilderness still outperforms nature mode with respect to sharp edge detection and preservation of discontinuities (e.g., Figure A3.4a,c). Nature mode was selected for surface classification and manually edited to reduce type I errors in areas with rilling.

Table A3.7. Qualitative comparison of filters. Colours coordinate with profile graph lines**.**

	Nature	Wilderness	Nature4step	Aggressive
Vegetation				
low isolated	f	p	f	g
low clustered	f	f	f	g
high isolated	f	f	f	g
high clustered	g	g	g	g
vegetation on slopes	g	f	f	p
Discontinuity				
preservation	p	f	p	p
sharp ridges	p	p	p	p
Overall rating	**fair-good**	**fair**	**fair**	**poor**

*after Sithole and Vosselman (2004)

Table A3.8. Qualitative assessment of Type I and II errors for each filter mode. Colours coordinate with profile graph lines.

	Nature	Wilderness	Nature4step	Aggressive
Type I error (bare-earth as object)	moderate	moderate-low	moderate-low	high
Type II error (object as bare-earth)	moderate	high	moderate-high	low

3.3 Stage 3. DTM Creation and Accuracy Assessment

A thinned point cloud sample was produced using nature mode in LAStools to compare the accuracy the two interpolations methods presented above (Table A3.5) in ArcGIS Pro:

1. Lasground2
    a. Classify thinned points, classed as 8, as ground (class 2) or vegetation (class 1) using selected filtering mode
    b. Output remains tiled with buffers flagged and suffix as 'NatFilt'
    lasground_new -cpu64 -v -lof file_list.14956.txt -cores 7 -nature -odir "H:\PhD_South_Africa\Doring_Paleo_Landscape_Project\DTM\UPK7_DroneDSM_2019\LAStools_filtering\Trial 11_finalisedmethods\tiles\thin\class8output\Nature_filtered" -odix "_nature" -olaz
2. Lasthin2
    a. Input: nature filtered tiles
    b. Randomly classify ground points (class 2) within each 0.3 x 0.3 m area as class 7 ("noise") (selects ~10% of the point dataset) ignore unclassified '1'
    c. Output: merge tiles and drop_withheld (buffer points) (of use *lasmerge*)
    d. File name: UPK7_2019_NatureClassifiedDSM
    lasthin -cpu64 -v -lof file_list.12860.txt -merged -drop_withheld -ignore_class 1 -step 0.3 -random -classify_as 7 -odir "H:\PhD_South_Africa\Doring_Paleo_Landscape_Project\DTM\UPK7_DroneDSM_2019\LAStools_filtering\Trial 11_finalisedmethods\ClassifiedDSM" -o "UPK7_2019_NatureClassifiedDSM.las"
3. Import into ArcGIS Pro to assess interpolation accuracy
    a. Convert the class 7 points into a separate feature class
        i. *LAS to multipoint*: average point spacing 0.101, class code 7
        ii. multipart (mp) to singlepart (sp)
        iii. add a new field to the output attribute table that is populated with each point's elevation using *calculate geometry*

    N.B. Use this file in place of the randomly plotted points file

    b. Create two DTMs of the original classified las file using interpolation methods 1 and 2 (parameters listed in Table A3.5 above):
        i. Interpolation 1 output: UPK7_2019_NatureClassifiedDTM_int1BIN_partial
        ii. Interpolation 2 output: UPK7_2019_NatureClassifiedDTM_int2TIN_partial
    c. Derive elevations in the class 7-point file from each interpolated surface
        i. Use the *Extract Multi Values to Points* to extract surface elevations from the two interpolated surfaces into new fields titled after each interpolation method (i.e., 'ZBIN' and 'ZTIN')
    d. Create two new fields that will be populated with the z-difference between class 7 elevations and the elevation of a given surface (e.g., 'Zdiff_BIN' and 'Zdiff_TIN')
    e. Use *Calculate Field* for each field and perform the following calculations:
        i. Zdiff_BIN = !Zclass7! - !ZBIN!

ii. Zdiff_TIN = !Zclass7! - !ZTIN!

f. Produce histograms showing the distribution of z-value differences for each interpolation method (see Figures A3.5 A & B)

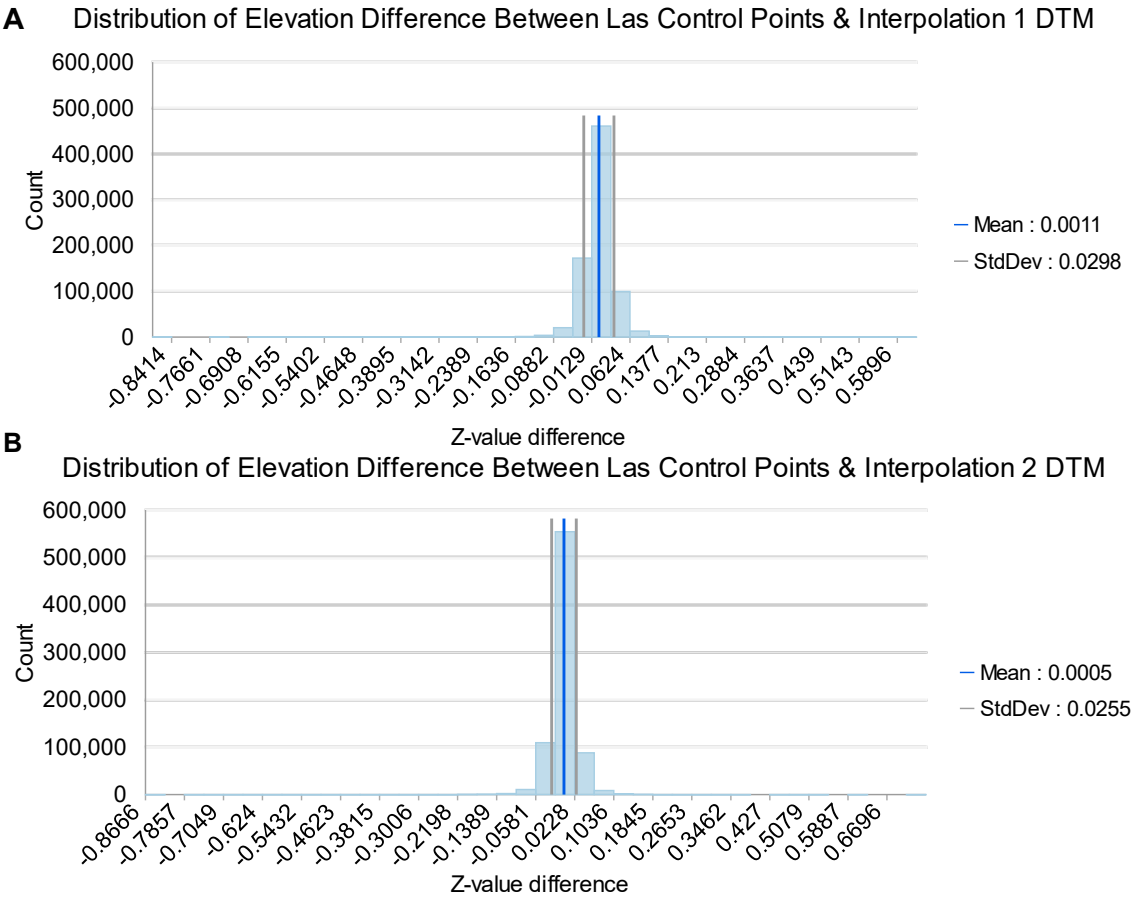

Figure A3.5. Histogram distributions showing the elevation difference between las control points and two interpolation methods together with their respective mean and standard deviations (1 σ). A) shows this difference for Interpolation 1, and B) shows it for interpolation 2.

Both interpolation methods have very low mean differences in elevation from las control point elevations (~1 mm), and less than 0.5 mm difference in mean values between the two interpolation methods (see Table A3.10, cf. Figure A3.5A and B). Note that the difference in count (y-axis) between the two methods is due to the number of null values returned after interpolation (Figure A3.5A and B, see also Table A3.9). This results from edge effect and the different ways in which each interpolation method deals with this. Interpolation 1 has a lower count than Interpolation 1, suggesting that the second method is better at dealing with edge effect. Edge effect is reduced by using a clipping mask during final interpolation.

Table A3.9. Unfiltered and filtered (nature mode) classification point counts, percentages, and the minimum and maximum elevations for each.

Year	Filter mode	Classification	point count	%	Z min	Z max	Point spacing
2019	Unfiltered	0 unclassified	7,421,614	100	192.65	219.09	0.101
	Nature	2 bare-earth	5,375,064	72.42	192.85	218.99	0.101
		1 vegetation	1,270,811	17.12	193.04	219.09	0.101
		7 control sample 'noise'	775,739	10.45	192.65	218.97	0.101

Table A3.10. Mean difference in elevation between interpolated surfaces and LAS subsampled points

Year	Interpolation method	mean difference	SD of mean difference
2019	BIN (1)	0.0011	0.0297
2019	TIN (2)	0.0005	0.0255

Figure A3.6a and b present profile views of both types of interpolation for filtered (DTM) and unfiltered (DSM) surfaces in contexts with low-lying vegetation and pronounced rilling. In both cases, only minor differences are apparent between the two types of interpolation, supporting and visually demonstrating the mean z-difference and standard deviations for each method presented in Figure A3.5a and b. Because the two methods return similar mean accuracies and show minor differences in how they model the surface of UPK7 it becomes arbitrary as to which method is selected for final DTM creation. However, to maintain consistency between sediment stacks, Interpolation method 2 was selected for final DTM creation, which is in line with the type of interpolation used elsewhere in the study area.

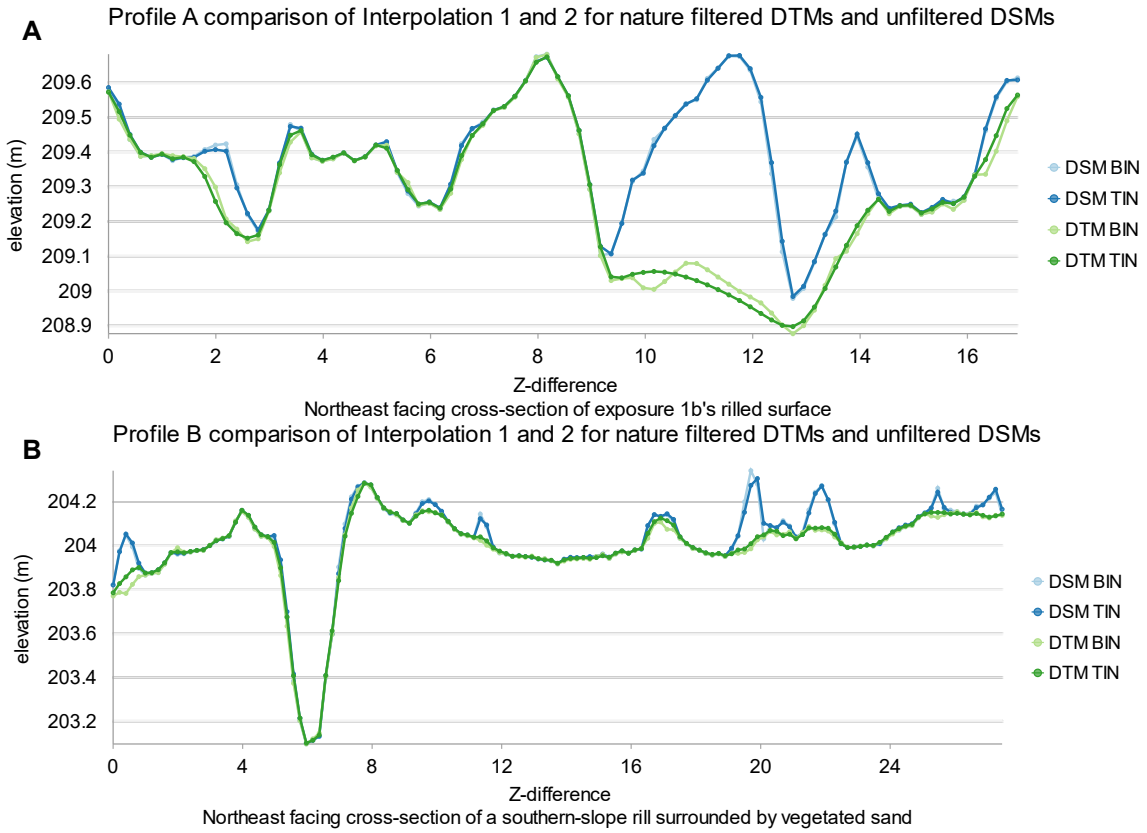

Figure A3.6. Profile stacks interpolated using two different interpolation methods (1 or BIN and 2 or TIN) showing elevation and surface modelling results for bare-earth (DSM, blue) and unfiltered (DSM, green) models.

4. After selecting a preferred interpolation method, two models were produced with manually edited rilled zones (reclassed as 2):
    i. a DTM of class 2 and 7 points
    ii. a DSM of all points to use in the canopy height model (CHM)
5. Point error checking was performed for DTM clipping and edge effect was checked to designate clipping extent

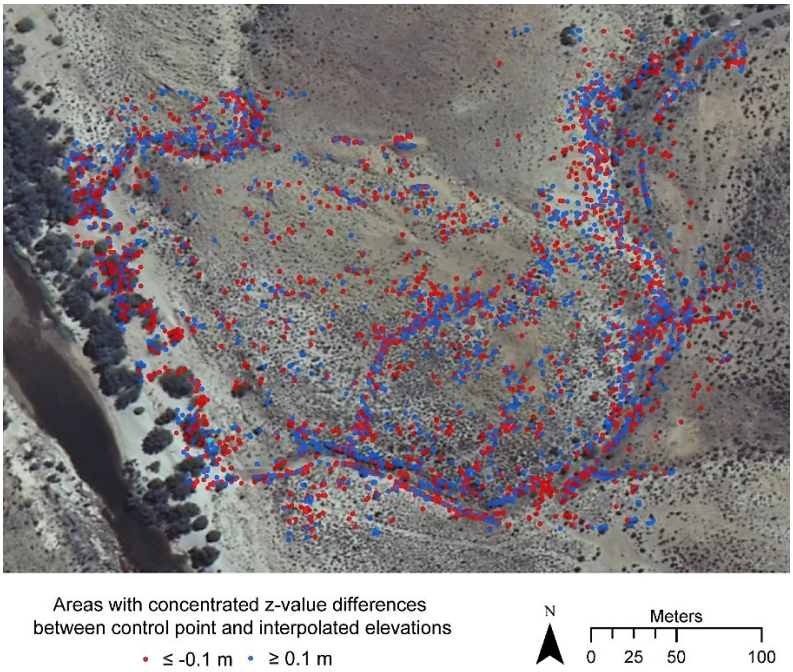

Figure A3.7. Map showing areas where large z-value differences occur between the interpolated surface and the subset of control las points < -10 cm and >10 cm.

Figure A3.7 shows areas where the greatest degree of inaccuracy occurs in an interpolated surface for UPK7. Unsurprisingly, areas of discontinuity (i.e., steep slope, high canopy, rilling, and tributaries) result in the greatest discrepancy in interpolated terrain. To improve the accuracy of rill representation, manual reclassification of rilled areas - misclassified using nature mode (see above assessment) – was performed by isolating-out these areas using polygons and manually classifying these areas as ground (class 2) using the reassign classification tool in ArcGIS Pro. Edge effect also influences interpolation accuracy (Figure A3.6). This was reduced by creating a clipping mask 3-4 m inside the raw extent of the DSM to which the terrain model is limited during interpolation.

3.4 Hydrological Conditioning

An iterative approach was taken to identify and fill sinks through the repeated use of flow direction, sink, and fill tools in ArcGIS Pro, trialling fill z limits with the average sink depth used as the starting z limit value. Flow direction is assigned to the steepest downslope neighbour using the 'D8' method (the default in ArcGIS Pro). The *Sink* tool draws from this information to compute the location of sinks in the study area. To attain a plausible filling range the average depth of each sink was determined from the unconditioned DTM with map algebra using zonal statistics (after Mark 1988), implementing the following steps:

1. Produce a raster record of sinks (sinks = Sink(flowdir))
2. Compute and produce a raster of sink areas (sink_areas = Watershed(flowdir, sinks)
3. Calculate minimum fill values in each sink area (sink_min = ZonalStatistics(sink_areas, "Value", elevation, "Minimum")
4. Calculate maximum fill values in each sink area (sink_max = ZonalFill(sink_areas, elevation)
5. In Raster Calculator, subtract sink max and mins to get sink depth: *sink_depth = Minus(sink_max, sink_min)*
6. Sample sink_depth for sink locations using the sample tool

The mean sink depth for UPK7's 2019 dataset is 0.73 ± 1 m with a median of 0.36 m. Employing the iterative process outlined above, sinks filled to a maximum of 0.54 m returned a depressionless DEM for 2019. After producing a depressionless DTM, a stream network was created by computing both flow direction and accumulation. A minimum cell accumulation threshold of 100 was used to produce a stream network, implemented using *Con* evaluation in ArcGIS Pro. The output of the orthophoto, final DTM, Hillshade and the crown height of filtered surface vegetation are presented in Figure 5.8 (in Chapter 5).

3.5 E4 Script for RSSQ Clast Data Collection

[E4]

Filename=DRPLPsamplesquares1x1m.mdb

Delaytime=1

Table=LithicAnalysis_DATEHERE

BackColor=16777215

[entrydate]

Type=Numeric

Prompt=enter date of data entry:

Length=10

Carry=True

[project]

Type=Text

Prompt=Enter the Project name:

Length=20

Carry=True

[poi]

Type=Text

Prompt=Enter name for Place of Interest (POI):

Length=20

Carry=True

[aoi_no]

Type=Text

Prompt=Enter 'areas of interest' (AOI) ID number:

Length=20

Carry=True

[aoi_type]

Type=Text

Prompt=Enter AOI type:

Length=20

Carry=True

[substrate]

Type=Menu

Prompt=Select the substrate type:

Menu=calcrete nodules, sandy sediment, sand, calcrete seams, NBS, NBS_cal, colluvium, bedrock, cobble layer, nd

Length=20

Carry=True

[clast_id]

Type=Text

Prompt=Enter clast's unique ID:

Length=20

Unique=True

Autoinc=True

[orientaxis]

Type=Menu

Prompt=Select presense or absence of orientation axis:

Menu=y, n, VOID

Length=4

[orientation_mn]

Type=Numeric

Prompt=Enter applicable object orientation (in magnetic north):

Length=10

Condition1=orientaxis y AND

Condition2=orientaxis NOT VOID

[buried]

Type=Menu

Prompt=Is the object buried or imbricated above ground?

Menu=y, n, imbricated, pedastal

Length=10

Condition1=orientaxis NOT VOID

[buriedpc]

Type=Menu

Prompt=Select the percentage of object buried:

Menu=0, 1-25%, 26-50%, 51-75%, 76-99%, 100%

Length=10

Condition1=buried y AND

Condition2=orientaxis NOT VOID

[buriedaxis]

Type=Menu

Prompt=How is the object buried?

Menu=na , lat-thick , long-thick , long-length , long-width , long-length-thick , long-width-thick , long-length-width , Long-L-W-T

Length=17

Condition1=buried y AND

Condition2=orientaxis NOT VOID

[material]

Type=Menu

Prompt=Select the raw material type:

Menu=silcrete, quartzite, quartz, clearquartz, hornfels, CCS, ochre, ironstone, shale, dolerite, sandstone, other

Length=11

Condition1=orientaxis NOT VOID

[maxlength]

Type=Numeric

Prompt=Enter max length:

Length=10

Condition1=orientaxis NOT VOID

[maxwidth]

Type=Numeric

Prompt=Enter max width:

Length=10

Condition1=orientaxis NOT VOID

[maxthick]

Type=Numeric

Prompt=Enter max thickness:

Length=10

Condition1=orientaxis NOT VOID

[weight]

Type=Numeric

Prompt=Enter object's weight:

Length=10

Condition1=orientaxis NOT VOID

[cortextpc]

Type=Menu

Prompt=Select the percentage of cortex:

Menu=0, 1-25%, 26-50%, 51-75%, 76-99%, 100%

Length=10

Condition1=orientaxis NOT VOID

[cortextype]

Type=Menu

Prompt=Select cortex surface type:

Menu=fluvial, aeolian, outcrop, crystal, nd

Length=20

Condition1=cortextpc NOT 0 AND

Condition2=orientaxis NOT VOID

[weathering]

Type=Menu

Prompt=Select type of weathering:

Menu=patinated, decayed, none

Length=20

Condition1=orientaxis NOT VOID

[object_condition]

Type=Menu

Prompt=Select the condition of object:

Menu=angular, subangular, subrounded, rounded, unknown

Length=20

Condition1=orientaxis NOT VOID

[find_type]

Type=Menu

Prompt=Select the find type:

Menu=artefact, nonflakedstone, bone, other

Length=20

Condition1=orientaxis NOT VOID

[artefactclass]

Type=Menu

Prompt=Select the artefact type:

Menu=na angfrag bipolarflake brokeflake broketool compflake compsplit compsplittool comptool core corefrag coretool distflake distsplit distsplittool disttool flakecore flakedp heatshatter LCS medflake medsplit medtool proxflake proxsplit proxsplittool proxtool pottery workedochre

Length=20

Condition1=find_type NOT nonflakedstone AND

Condition2=orientaxis NOT VOID

[edge_condition]

Type=Menu

Prompt=Select the condition of the artefact's edges:

Menu=fresh, fracture, stepped, edgerounding, chattering, pseudoretouch, pseudonotch, unknown

Length=20

Condition1=find_type NOT nonflakedstone AND

Condition2=artefactclass na compflake compsplit proxflake proxsplit medflake medsplit distsplittool distflake distsplit brokeflake comptool compsplittool broketool proxtool proxsplittool disttool distsplittool medtool LCS coretool core corefrag flakecore angfrag flakedp bipolarflake heatshatter pottery workedochre AND

Condition3=orientaxis NOT VOID

[flakeform]

Type=Menu

Prompt=Select flake form:

Menu=expanding, converging, intermediate, point, blade, block, na

Length=20

Condition1=find_type NOT nonflakedstone AND

Condition2=artefactclass compflake LCS comptool broketool proxtool disttool distsplittool flakecore bipolarflake AND

Condition3=orientaxis NOT VOID

[termination]

Type=Menu

Prompt=Select flake termination:

Menu=feather, step, plunge, hinge, abrupt, na

Length=20

Condition1=find_type NOT nonflakedstone AND

Condition2=artefactclass compflake compsplit LCS distflake distsplit distsplittool comptool compsplittool disttool flakecore bipolarflake AND

Condition3=orientaxis NOT VOID

[platsurf]

Type=Menu

Prompt=Select platform suface:

Menu=na, plain, cortical, marginal, missing, crushed, faceted, dihedral, punti, trimmed, abraded

Length=10

Condition1=find_type NOT nonflakedstone AND

Condition2=artefactclass compflake compsplit LCS proxflake proxsplit comptool compsplittool proxtool proxsplittool distsplittool core flakecore bipolarflake AND

Condition3=orientaxis NOT VOID

[extplatmod]

Type=Menu

Prompt=Select exterior platform modification:

Menu=scar, cortical, trimmed, na

Length=10

Condition1=find_type NOT nonflakedstone AND

Condition2=artefactclass compflake compsplit LCS proxflake proxsplit comptool compsplittool proxtool proxsplittool distsplittool core flakecore AND

Condition3=orientaxis NOT VOID

[dorsalscarno]

Type=Numeric

Prompt=Enter number of flake scars:

Length=10

Condition1=find_type NOT nonflakedstone AND

Condition2=artefactclass compflake AND

Condition3=cortextpc NOT 100% AND

Condition4=orientaxis NOT VOID

[scardirect]

Type=Menu

Prompt=Enter flake scar direction:

Menu=na, 1, 2, 3, 4, 12, 13, 14, 23, 24, 34, 123, 124, 134, 234, 1234

Length=10

Condition1=find_type NOT nonflakedstone AND

Condition2=artefactclass compflake AND

Condition3=cortextpc NOT 100% AND

Condition4=orientaxis NOT VOID

[flakelength]

Type=Numeric

Prompt=Enter flake length:

Length=10

Condition1=find_type NOT nonflakedstone AND

Condition2=artefactclass compflake compsplit LCS bipolarflake comptool compsplittool proxsplittool distsplittool coretool AND

Condition3=orientaxis NOT VOID

[flakewidth]

Type=Numeric

Prompt=Enter flake width:

Length=10

Condition1=find_type NOT nonflakedstone AND

Condition2=artefactclass compflake distflake proxflake bipolarflake comptool proxtool medtool disttool distsplittool coretool AND

Condition3=orientaxis NOT VOID

[flakethick]

Type=Numeric

Prompt=Enter flake thickness:

Length=10

Condition1=find_type NOT nonflakedstone AND

Condition2=artefactclass compflake compsplit distflake proxflake bipolarflake comptool compsplittool broketool proxtool proxsplittool medtool distsplittool disttool coretool AND

Condition3=orientaxis NOT VOID

[platwidth]

Type=Numeric

Prompt=Enter platform width:

Length=10

Condition1=find_type NOT nonflakedstone AND

Condition2=artefactclass compflake proxflake comptool proxtool AND

Condition3=orientaxis NOT VOID AND

Condition4=platsurf NOT missing

[platthick]

Type=Numeric

Prompt=Enter platform thickness:

Length=10

Condition1=find_type NOT nonflakedstone AND

Condition2=artefactclass compflake compsplit LCS proxflake comptool proxtool AND

Condition3=orientaxis NOT VOID AND

Condition4=platsurf NOT crushed missing

[corscardir]

Type=Menu

Prompt=Select core scar direction:

Menu=na , unidirectional , bidirectional , orthogonal , centripetal , uni-bidirectional , uni-centripetal , bi-centripetal , multidirectional

Length=20

Condition1=find_type NOT nonflakedstone AND

Condition2=artefactclass coretool core corefrag flakecore AND

Condition3=orientaxis NOT VOID

[coreface_n]

Type=Numeric

Prompt=Enter number of core surfaces:

Length=10

Condition1=find_type NOT nonflakedstone AND

Condition2=artefactclass coretool core corefrag flakecore AND

Condition3=orientaxis NOT VOID

[surftouching]

Type=Numeric

Prompt=Enter number of core surfaces touching:

Length=10

Condition1=find_type NOT nonflakedstone AND

Condition2=artefactclass coretool core corefrag flakecore AND

Condition3=orientaxis NOT VOID

[coreflakes]

Type=Menu

Prompt=Select the core products:

Menu=na , normal , points , blades , normal+points , normal+blades , points+blades , multiple , nd

Length=74

Condition1=find_type NOT nonflakedstone AND

Condition2=artefactclass coretool core testcore corefrag flakecore AND

Condition3=orientaxis NOT VOID

[coretyp]

Type=Menu

Prompt=Select a value for core type:

Menu=na , testcore , singleplat , oppoplat , bifacial , unifacial , discoid , radial , nuclear , lev-pref , lev-recur , amorphous , bipolar

Length=20

Condition1=find_type NOT nonflakedstone AND

Condition2=artefactclass coretool core corefrag testcore flakecore AND

Condition3=orientaxis NOT VOID

[longcorescar]

Type=Numeric

Prompt=Enter the length of the longest complete core scar:

Length=10

Condition1=find_type NOT nonflakedstone AND

Condition2=artefactclass coretool core testcore corefrag flakecore AND

Condition3=orientaxis NOT VOID

[corelength]

Type=Numeric

Prompt=Enter core length (measure along the longest complete scar):

Length=10

Condition1=find_type NOT nonflakedstone AND

Condition2=artefactclass core flakecore AND

Condition3=orientaxis NOT VOID

[corewidth]

Type=Numeric

Prompt=Enter core width (measure perpendicular from the mid-point of core length):

Length=10

Condition1=find_type NOT nonflakedstone AND

Condition2=artefactclass core flakecore AND

Condition3=orientaxis NOT VOID

[corethick]

Type=Numeric

Prompt=Enter core thickness (measure perpendicular to core width at mid-point of core length):

Length=10

Condition1=find_type NOT nonflakedstone AND

Condition2=artefactclass core flakecore AND

Condition3=orientaxis NOT VOID

[ret_class]

Type=Menu

Prompt=Select the retouch class:

Menu=na, denticulate, notch, scraper, backed, bifacial, unifacial, utilized, other

Length=20

Condition1=find_type NOT nonflakedstone AND

Condition2=artefactclass comptool compsplittool broketool proxtool proxsplittool medtool distsplittool disttool coretool AND

Condition3=orientaxis NOT VOID

[ret_type]

Type=Menu

Prompt=Select retouch scar type:

Menu=fine, coarse, irregular, nd

Length=20

Condition1=find_type NOT nonflakedstone AND

Condition2=artefactclass comptool compsplittool broketool proxtool proxsplittool medtool disttool coretool AND

Condition3=ret_class NOT na AND

Condition4=orientaxis NOT VOID

[ret_quad1D]

Type=Menu

Prompt=Select retouch form initiated from dorsal onto ventral surface for quad 1:

Menu=none, denticulate, notch, scalar, stepped, invasive

Length=20

Condition1=find_type NOT nonflakedstone AND

Condition2=artefactclass comptool compsplittool broketool proxtool proxsplittool medtool disttool distsplittool coretool AND

Condition3=ret_class NOT na AND

Condition4=orientaxis NOT VOID

[ret_quad1V]

Type=Menu

Prompt=Select retouch form initiated from ventral onto dorsal surface for quad 1:

Menu=none, denticulate, notch, scalar, stepped, invasive

Length=20

Condition1=find_type NOT nonflakedstone AND

Condition2=artefactclass comptool compsplittool broketool proxtool proxsplittool medtool disttool distsplittool coretool AND

Condition3=ret_class NOT na AND

Condition4=orientaxis NOT VOID

[ret_quad2D]

Type=Menu

Prompt=Select retouch form initiated from dorsal onto ventral surface for quad 2:

Menu=none, denticulate, notch, scalar, stepped, invasive

Length=20

Condition1=find_type NOT nonflakedstone AND

Condition2=artefactclass comptool compsplittool broketool proxtool proxsplittool medtool

disttool distsplittool coretool AND

Condition3=ret_class NOT na AND

Condition4=orientaxis NOT VOID

[ret_quad2V]

Type=Menu

Prompt=Select retouch form initiated from ventral onto dorsal surface for quad 2:

Menu=none, denticulate, notch, scalar, stepped, invasive

Length=20

Condition1=find_type NOT nonflakedstone AND

Condition2=artefactclass comptool compsplittool broketool proxtool proxsplittool medtool disttool distsplittool coretool AND

Condition3=ret_class NOT na AND

Condition4=orientaxis NOT VOID

[ret_quad3D]

Type=Menu

Prompt=Select retouch form initiated from dorsal onto ventral surface for quad 3:

Menu=none, denticulate, notch, scalar, stepped, invasive

Length=20

Condition1=find_type NOT nonflakedstone AND

Condition2=artefactclass comptool compsplittool broketool proxtool proxsplittool medtool disttool distsplittool coretool AND

Condition3=ret_class NOT na AND

Condition4=orientaxis NOT VOID

[ret_quad3V]

Type=Menu

Prompt=Select retouch form initiated from ventral onto dorsal surface for quad 3:

Menu=none, denticulate, notch, scalar, stepped, invasive

Length=20

Condition1=find_type NOT nonflakedstone AND

Condition2=artefactclass comptool compsplittool broketool proxtool proxsplittool medtool disttool distsplittool coretool AND

Condition3=ret_class NOT na AND

Condition4=orientaxis NOT VOID

[ret_quad4D]

Type=Menu

Prompt=Select retouch form initiated from dorsal onto ventral surface for quad 4:

Menu=none, denticulate, notch, scalar, stepped, invasive

Length=20

Condition1=find_type NOT nonflakedstone AND

Condition2=artefactclass comptool compsplittool broketool proxtool proxsplittool medtool disttool distsplittool coretool AND

Condition3=ret_class NOT na AND

Condition4=orientaxis NOT VOID

[ret_quad4V]

Type=Menu

Prompt=Select retouch form initiated from ventral onto dorsal surface for quad 4:

Menu=none, denticulate, notch, scalar, stepped, invasive

Length=20

Condition1=find_type NOT nonflakedstone AND

Condition2=artefactclass comptool compsplittool broketool proxtool proxsplittool medtool disttool distsplittool coretool AND

Condition3=ret_class NOT na AND

Condition4=orientaxis NOT VOID

[ret_scar_no]

Type=Numeric

Prompt=Enter number of retouch scars:

Length=10

Condition1=find_type NOT nonflakedstone AND

Condition2=artefactclass comptool compsplittool broketool proxtool proxsplittool medtool disttool distsplittool coretool AND

Condition3=ret_class NOT na AND

Condition4=orientaxis NOT VOID

[technique]

Type=Menu

Prompt=Select technology:

Menu=none , lev-p , lev-r , nubian , backed , bfp , bfo , ufp , pbp , se , so , adze , nbk , outils_ecailles , scaled-p , flake_as_core , burin , denticulate , discoid , kombewa , handaxe , cleaver , hammer , anvil , grinder-top , grinder-base

Length=98

Condition1=find_type NOT nonflakedstone AND

Condition2=artefactclass NOT compsplit proxflake proxsplit medflake medsplit distflake distsplit brokeflake angfrag flakedp AND

Condition3=coretyp NOT testcore AND

Condition4=orientaxis NOT VOID

[epoch]

Type=Menu

Prompt=Select potential Epoch:

Menu= NA, nd, LSA, MSA, ESA

Length=20

Condition1=find_type NOT nonflakedstone

Condition1=find_type NOT nonflakedstone AND

Condition2=artefactclass NOT compsplit proxflake proxsplit medflake medsplit distflake distsplit distsplittool brokeflake angfrag flakedp AND

Condition3=coretyp NOT testcore AND

Condition4=orientaxis NOT VOID

[industry]

Type=Menu

Prompt=Select potential industry association:

Menu= NA, nd, Wilton, Oakhurst, Robberg, eLSA, LateMSA, Post-HP, HP, SB, Fauresmith, eMSA, Acheulean

Length=20

Condition1=find_type NOT nonflakedstone

Condition1=find_type NOT nonflakedstone AND

Condition2=artefactclass NOT compsplit proxflake proxsplit medflake medsplit distflake distsplit distsplittool brokeflake angfrag flakedp AND

Condition3=coretyp NOT testcore AND

Condition4=orientaxis NOT VOID

[photo_count]

Type=Numeric

Prompt=Enter number of photos taken:

Length=10

Condition1=find_type NOT nonflakedstone AND

Condition2=artefactclass comptool compsplittool broketool proxtool proxsplittool disttool distsplittool medtool coretool core corefrag flakecore nuclearcore heatshatter pottery workedochre AND

Condition3=coretyp NOT testcore AND

Condition4=orientaxis NOT VOID

[camera]

Type=Menu

Prompt=Select camera model:

Menu=na, coolpix silver, coolpixblack, cannon 400D

Length=20

Condition1=find_type NOT nonflakedstone AND

Condition2=artefactclass comptool compsplittool broketool proxtool proxsplittool disttool distsplittool medtool coretool core corefrag flakecore nuclearcore heatshatter pottery workedochre AND

Condition3=photo_count NOT 0 AND

Condition4=coretyp NOT testcore AND

Condition5=orientaxis NOT VOID

[photo_no]

Type=Text

Prompt=Enter photo number series (e.g., DMS1234-1238):

Length=20

Condition1=find_type NOT nonflakedstone AND

Condition2=artefactclass comptool compsplittool broketool proxtool proxsplittool disttool distsplittool medtool coretool core corefrag flakecore nuclearcore heatshatter pottery workedochre AND

Condition3=photo_count NOT 0 AND

Condition4=coretyp NOT testcore AND

Condition5=orientaxis NOT VOID

[comments]

Type=Text

Prompt=Enter any additional observations:

Length=150

APPENDIX 4.

SUPPLEMENTARY RESULTS FOR CHAPTER 6

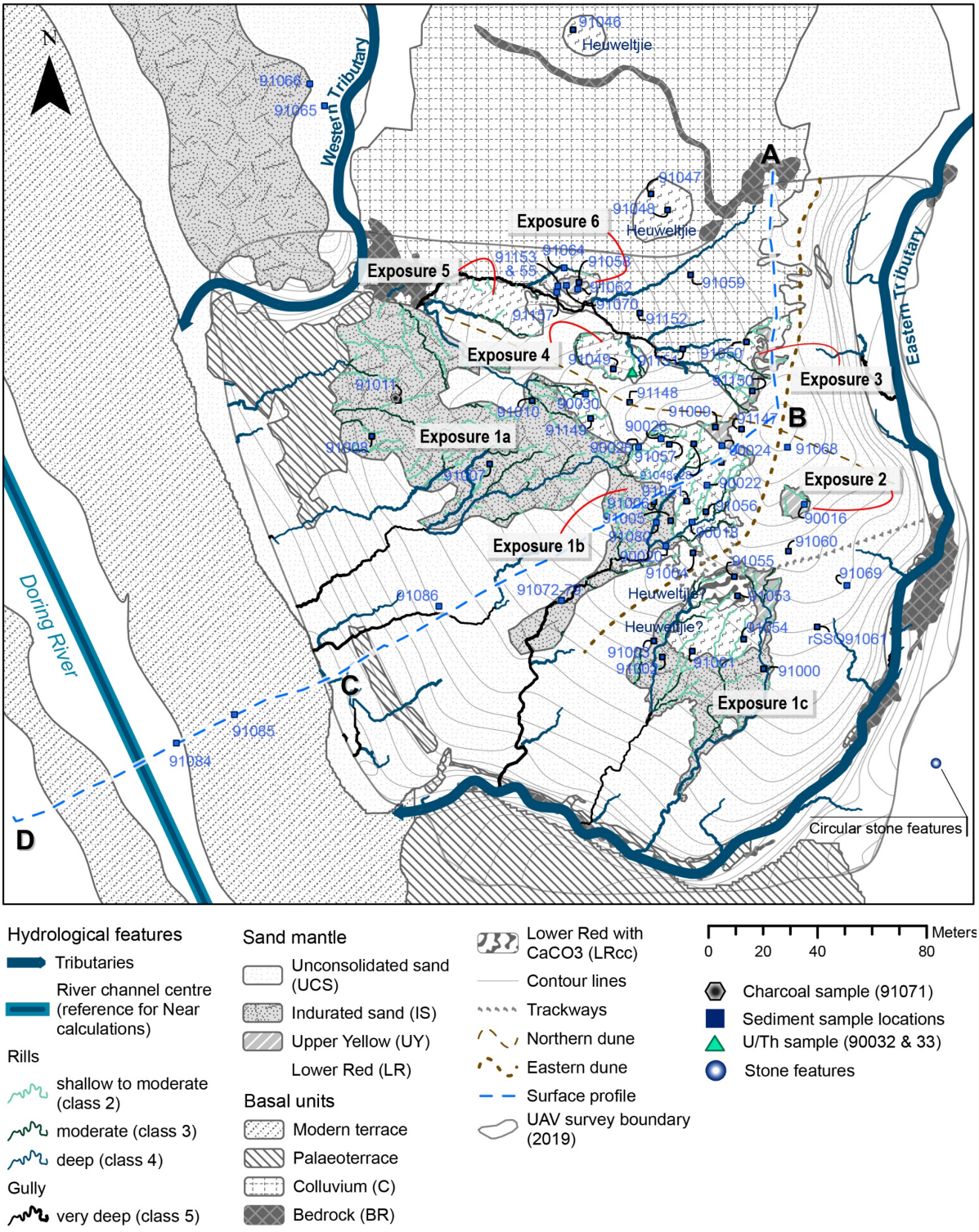

Figure A4.0.1. Map of UPK7 and its immediate surrounds showing the location of all sediment samples listed in Table 1 (below) against the unconsolidated and consolidated sediment units introduced in Chapter 6. Base layers include a 2010 aerial and SRTM 3 arc DEM and the 2019 UPK7 DTM. The results of the surface profile line (blue dash line) and its associated labels are depicted in Figure 6.2.

Table A4.0.1. Sediment sample index listing all samples, their sample context unit, depth below surface

(bls), elevation above sea level (asl), distance from centre of river channel and whether they were subjected to particle size analysis (PSA) and/or XRD analysis. Samples are grouped by sediment unit and ordered by proximity to river.

Field ID	OSL Lab ID	Sample unit	Depth (m bls)	Elevation m asl	Distance from river m	PSA (y/n)	XRD (y/n)
Alluvium							
91084		-	0-0.05	191	16	y	y
91085		-	0-0.05	194	40	y	y
Unconsolidated sand							
91086		-	0-0.05	202	127	y	y
91008		rSSQ 19	0-0.05	202.6	128	n	n
91003		rSSQ 14	0-0.05	205.9	190	n	n
91004		rSSQ 15	0-0.05	210	216	n	n
91148		rSSQ 93	0-0.05	211.6	219	n	n
91061		rSSQ 61	0-0.05	208.4	246	n	n
91060		rSSQ 60	0-0.05	211.1	248	n	n
91147		rSSQ 89	0-0.05	215.4	252	n	n
91068		-	0-0.05	-	271	y	y
Semi-consolidated sand							
91066		-	0-0.05	-	166	y	y
91065		-	0-0.05	-	167	y	y
91077		SC1	0.1	205	170	y	y
91078		SC1	0.6	204.5	170	y	y
91069		-	0-0.05	-	270	y	y
IS, Indurated sand							
91079		SC1	1.1	204	170	y	y
91072		SC1	1.7	203.4	170	y	y
91073		SC1	2.2	202.9	170	y	y
91011		rSSQ 22	0-0.05	204.4	142	n	n
91007		rSSQ 18	0-0.05	206.5	162.5	n	n
91010		rSSQ 21	0-0.05	208.2	186	n	n
91002		rSSQ 6	0-0.05	205.7	190	n	n
91006		rSSQ 17	0-0.05	210.1	211	n	n
91005		rSSQ 16	0-0.05	209.7	214	n	n
90020	UOW 1802	OC3	0.31	210.47	214	y	y
91000		rSSQ 5	0-0.05	207	222	n	n
UY, consolidated sand							
91080	UOW 2006	OC9	0.22	210.47	215	y	y
91009		rSSQ 20	0-0.05	214	243	n	n
90024	UOW 1804	OC5	0.23	215.31	249	y	y
91150		rSSQ 90	0-0.05	214.6	261	n	n
90016	UOW 1801	OC10	0.24	214.12	268	y	y
LR, consolidated loamy sand							
91001		rSSQ 7	0-0.05	207.3	201	n	n
91153	UOW 2012	OC1U	0.35	209.02	218.5	y	y
91155	UOW 2013	OC1L	0.6	208.76	218.5	y	y
91058		rSSQ 64	0-0.05	209	220	n	n
91051		rSSQ 53	0-0.05	210.9	222	n	n
91070		-	0-0.05	209	222	y	y
91062		-	0-0.05	209	225	n	y
91056		rSSQ 58	0-0.05	211.2	227	n	n
91157	UOW 2014	OC2	0.23	207.9	231	y	y
LRcc, consolidated loamy sand, CaCO3 inclusions							
91074		SC1	2.7	202.4	170	y	y
91075		SC1	3.2	201.9	170	y	y

91076		SC1	3.5	201.6	170	y	y
91149		rSSQ 94	0-0.05	210.5	203	n	n
90030	UOW 1834	OC8	0.2	211.98	211	y	y
91049		rSSQ 26	0-0.05	210.3	218	n	n
91054		rSSQ 56	0-0.05	208	220	n	n
90028	UOW 1833	OC7	0.22	212.68	220.5	y	y
91053		rSSQ 55	0-0.05	209.5	225	n	n
91057		rSSQ 59	0-0.05	212.6	225	n	n
91055		rSSQ 57	0-0.05	210.3	226.5	n	n
90018	UOW 1800	OC11	0.33	211.55	227	y	y
90026	UOW 1832	OC6	0.26	213.68	229.5	y	y
91048s28		rSSQ 28	0-0.05	213	233.5	n	n
90022	UOW 1803	OC4	0.23	213.83	238	y	y
91050		rSSQ 25	0-0.05	213	267	n	n
Heuweltjie, consolidated loamy sand, CaCO3 inclusions							
91046		rSSQ 23	0-0.05	218.3	257	n	n
91047		rSSQ 27	0-0.05	212.9	258	n	n
91048		rSSQ 24	0-0.05	213.6	261	n	n
Colluvium							
91152		rSSQ 92	0-0.05	208.9	236	n	n
91151		rSSQ 91	0-0.05	210.3	244.5	n	n
91059		rSSQ 62	0-0.05	212	259	n	n
91064		-	0-0.05	207	223	n	y

Table A4.0.2. Soil descriptions for all samples and their associated unit-wide summaries. Not determined = '-'.

Unit & Sample IDs	Basal Contact	Upper Contact	Observed Thickness (m)	ERT* Derived Thickness	Matrix Colour	Particle Size Range (vol. weighted mean [μm]	Particle Size Class^	Sorting (Std Dev phi Φ)*	Texture Class^	Rounding	Consistence (dry)	Sedimentary Structures	Mottles	Inclusions
Modern Terrace/ Alluvium (T0)	PT; BR	None	-	-	-	374-559 μm	Medium sand	Poorly sorted (1.03-1.21)	Sand	-	Loose	Structureless-single grain (weak)	None	None
91084 (river channel)	BR	None	Surface sample	-	-	559	Medium sand	Poorly sorted (1.21)	Sand	-	Loose	Structureless-single grain	none	None
91085 (T0)	PT; BR	None	Surface sample	-	-	374	Medium sand	Poorly sorted (1.03)	Sand	-	Loose	Structureless-single grain	none	None
UCS/SCS	SCS; IS; LRcc	None	0.6-1.4	5 m	10 YR 6/4, light yellowish brown	203-417 μm	Medium sand	Moderately to poorly sorted (0.50-1.20)	Sand	Medium sphericity; subangular to subrounded	Loose	Structureless-single grain and layered (thin laminations; weak)	None	Fine roots; insect burrows
91086	Not visible	None	Surface sample	-	-	417	Medium sand	Moderately sorted (0.58)	Sand	-	Loose	Structureless-single grain	-	-
91008	-	None	Surface sample	-	-	-	-	-	-	-	Loose	Structureless-single grain	-	-
91003	IS	None	Surface sample	-	-	-	-	-	-	-	Loose	Structureless-single grain	-	None
91004	IS	None	Surface sample	-	-	-	-	-	-	-	Loose	Structureless-single grain	-	-

91148	SCS	None	Surface sample	-	2.5 YR 6/4 (light yellowish brown)	-	Medium sand	Moderately sorted	Sand	Medium sphericity; subangular	Loose	Structureless-single grain	-	Fine roots
rSSQ 91061	SCS	None	Surface sample	-	10 YR 7/4 (very pale brown)	<1000 µm (375-500 µm; using 10x)	-	Moderately to well sorted (using 10x)	-	Low sphericity; subangular to subrounded	Loose	Structureless-single grain	-	Fine roots
91060	LRcc	None	Surface sample	-	10 YR 6/4 (light yellowish brown)	500-100 µm (using 10x)	-	Poorly sorted (using 10x)	-	Moderate sphericity; subrounded and subangular	Soft	Structureless-single grain	-	Fine roots
91147	SCS	None	Surface sample	-	Between 10 YR 7/6 (yellow) and 10 YR 6/6 (brownish yellow)	≤750 µm (250 and 180 µm; using 10x)	Medium to fine sand	Moderately to poorly sorted (using 10x)	Sand	Moderate to low sphericity; angular to subangular	Loose	Structureless-single grain	-	Fine roots
91068	SCS	None	Surface sample	-	-	203	Medium sand	Moderately sorted (0.68)	Sand	-	Loose	Structureless-single grain	-	None
91066 (SCS)	Not visible	UCS	1.39	-	-	265	Medium sand	Poorly sorted (1.20)	Sand	-	Soft	Layered (thin laminations) to blocky angular (weak)	-	Medium roots
91065 (SCS)	Not visible	UCS	0.85	-	-	240	Medium sand	Poorly sorted (1.14)	Sand	-	Soft	Layered (thin laminations) to blocky subangular (weak)	-	Fine roots
91069 (SCS)	Not visible	UCS	0.75	-	-	346	Medium sand	Well-moderately sorted (0.50)	Sand	-	Soft	Layered (weak; thin laminations)	-	Fine roots; insect and animal burrows

IS	UY?; LRcc	UCS; SCS	0.1-3.7	4 m	Yellowish brown	140-225 µm	Fine to medium sand	Poorly to very poorly sorted (1.53-2.10)	Loamy Sand	-	Indurated; hard; smooth	Massive and Layered (weak, thin laminations); fine surface cracking; crusted surface of varying thicknesses (10-20 mm); porous	None	Small calcrete nodules; fine roots; insect burrows
91077 (SCS)	SCS	UCS	0.6	-	-	189	Fine sand	Poorly sorted (1.54)	Sand	-	-	Single grain (moderate)	None	Fine roots; insect burrows
91078 (SCS)	IS	SCS	0.6	-	-	154	Fine sand	Very poorly sorted (2.10)	Loamy sand	-	-	Single grain (moderate)	None	-
91079	IS	IS	3.7	-	-	140	Fine sand	Poorly sorted (1.53)	Loamy sand	-	Indurated	Massive (moderate)	None	-
91072	IS	IS	3.7	-	-	224	Medium sand	Poorly sorted (1.71)	Sand/Loamy sand	-	Indurated	Massive (moderate)	None	-
91073	LRcc	IS	3.7	-	-	225	Medium sand	Poorly sorted (1.81)	Loamy sand	-	Indurated	Massive (moderate)	None	-
91011	Not visible	None	Surface sample	-	-	-	-	-	-	-	Indurated	Crusted	None	-
91007	Not visible	UCS (veneer)	Surface sample	-	-	-	-	Poorly sorted	-	-	Hard, indurated, smooth	Massive	None	-
91010	Not visible	None	Surface sample	-	Yellowish brown	-	-	-	-	-	-	-	None	Small calcrete nodules on surface (eroding out from sediment?)

91002	Not visible	None	Surface sample	-	-	-	-	-	-	-	Hard, indurated	Crusted	None	Small calcrete nodules on surface (eroding out from sediment?)
91006	Not visible	Thin layer of UCS	Surface sample	-	Yellowish brown	-	Fine sand	Poorly sorted	Loamy sand	-	Indurated	Crusted; porous	None	-
91005	Not visible	None	Surface sample	-	Yellowish brown	-	Fine sand	Poorly sorted	Loamy sand	-	Hard, smooth, indurated	Massive; crusted; porous	None	-
90020	UY?	25 cm of cemented massive IS or younger unit	0.12	-	-	149	Fine sand	Poorly sorted (1.75)	Loamy sand	-	Hard, Indurated	Layered (coherent)	None	-
91000	Not visible	UCS	Surface sample	-	-	-	Fine sand	Poorly sorted	-	-	Indurated	Very fine surface cracks; thin weak crust	None	-
UY	LR; LRcc	UCS; SCS	0.28-0.32	2-5 m	10 YR 5/6, yellowish brown	119-157 µm	Very fine to fine sand	Poorly to very poorly sorted (1.98-2.20)	Sandy loam to loam	-	Indurated; slightly hard to hard	Massive and blocky subangular; crusted surface, porous	None	Effervescent; calcrete nodules (≤60 mm ⌀); fine roots; stone artefacts
91009	Not visible	UCS (veneer)	Surface sample	-	-	-	Fine sand	-	-	-	Indurated	Massive	None	Flaked and non-flaked stone on surface
90024	LRcc	SCS	0.28	-	-	125	Very fine sand	Poorly sorted (1.98)	Sandy loam	-	Slightly hard	Massive; crusted	None	Flaked and non-flaked stone on surface; fine roots first 150 mm
91150	LRcc	UCS (Veneer)	Surface sample	-	10 YR 5/6 (yellowish brown)	≤ 250 (using 10x)	Medium sand	Well sorted (using 10x)	Loamy sand (using 10x)	-	Hard; Indurated	Surface thickly crusted (2 cm)	None	Effervescent; calcrete nodules; root casts; coated single grains
90016	Not visible	UCS (1-5 cm thick)	0.3	-	-	157	Fine sand	Very poorly sorted (2.10)	Sandy loam	-	Consolidate; indurated; slightly hard	Massive	None	Fine roots

91080 (originally listed under IS)	LR	None	0.32	-	-	119	Very fine sand	Very poorly sorted (2.20)	Loam	-	Indurated	Blocky subangular	None	Small soft calcrete nodules (~60 mm ⌀); fine roots; stone artefacts
LR/LRcc	LRcc; C	LR; UY; IS; UCS	0.3-0.8	3-7 m	Yellowish to reddish brown	95-500 µm	Very fine to medium sand	Poorly to very poorly sorted (1.37-2.56)	Sandy loam to loamy sand	Moderate to high sphericity; subrounded and subangular	Indurated; slightly hard to very hard	Structureless-massive (cemented) and blocky-subangular/ angular; desiccation cracks and carbonate infilling; crusted surface; porous	None	Insect burrows/casts; hard small calcrete nodules (≤55 mm ⌀); salt crystallisation; fine roots; pores; rugose biocrusts
91074 (UY/ LRcc)	LRcc	IS	0.8 (BOE)	-	-	234	Medium sand	Poorly sorted (1.96)	Loamy sand	-	Indurated	-	None	Calcrete nodules
91075 (LRcc)	LRcc	LRcc	0.8 (BOE)	-	-	205	Medium sand	Poorly sorted (1.42)	Sand	-	Indurated	-	None	Calcrete nodules
91076 (LRcc)	Not visible	LRcc	0.8 (BOE)	-	-	160	Fine sand	Very poorly sorted (2.56)	Loamy sand	-	Indurated	-	None	Calcrete nodules
91001	Not visible	None	Surface sample	-	-	-	Fine sand	-	Loamy sand	-	Indurated; slightly hard	Crusted	None	Roots; many small calcrete nodules
91153	Not visible	UY	0.7 (BOE)	-	Yellowish brown	156	Fine sand	Poorly sorted (1.86)	Sandy loam/loamy sand	-	Consolidated; slightly hard	Massive	None	Fine roots/insect burrows
91155	Not visible	LR	0.7 (BOE)	-	Yellowish brown	131	Fine sand	Very poorly sorted (2.04)	Sandy loam	-	Indurated; hard	Massive	None	Speckling of white precipitates (salt?); insect burrows; fine white chalky calcareous inclusions; no roots

91058 (UY or LR?)	Not visible	None	Surface sample	-	10 YR 6/6 (brownish yellow)	100-250 (using 10x)	-	Well-sorted fine fraction (using 10x)	Loamy sand (using 10x)	Moderate to high sphericity; subrounded	Slightly hard; very friable	-	None	Medium to small calcrete nodules (5-55 mm ⌀)
91051	Not visible	None	Surface sample	-	10 YR 5/6 (yellowish brown)	<500 (using 10x)	Fine to medium sand (using 10x)	Moderately sorted (using 10x)	Loamy sand (using 10x)	High sphericity, sub rounded grains (larger grains); low sphericity, subangular grains (smaller grains)	Compacted; slightly hard; friable	Thin surface crust (0.1-0.05 cm thick)	None	Calcrete nodules
91056	LRcc	None	Surface sample	-	10 YR 5/6 (yellowish brown)	<500 (using 10x)	Fine to medium sand (using 10x)	Poorly sorted	Sandy loam (using 10x)	Low sphericity and subangular (larger grains); high sphericity and subrounded (smaller grains)	Indurated; firm	Massive; smooth; thinly crusted surface with fine surface cracks	None	Fine; white speckled concentrations of salt crystals
91062	Not visible	None	Surface sample	-	-	134	Fine sand	Poorly sorted (1.81)	Loamy sand	-	-	-	None	-
91070	Not visible	None	Surface sample	-	-	140	Very fine sand	Very poorly sorted (2.14)	Loamy sand	-	-	-	None	-
91157	LRcc/C	None	0.3 (BOE)	-	Reddish brown	95	Very fine sand	Very poorly sorted (2.12)	Sandy loam	-	Indurated; hard	Massive	None	Speckling of white precipitates (salt?)
91149	LRcc	UCS	Surface sample	-	10 YR 5/6 (yellowish brown)	≤ 250 (using 10x)	Medium sand	Well to moderately sorted (10x)	Sandy loam	Moderate to high sphericity; subrounded	Indurated; very hard	Crusted (5-10 mm thick); surface cracks (moderate to fine)	None	Calcrete-veined; surface of dispersed subangular calcrete nodules; surface artefacts and non-flaked stone; fine roots

90030	LRcc	None	0.3	-	-	140	Fine sand	Poorly sorted (1.89)	Loamy sand	-	Indurated	Massive	None	Calcrete veining (not well defined; extends 100 mm bls); calcrete nodules; fine roots; artefacts not present (surface nor in matrix)
91049	LRcc	None	Surface sample	-	10 YR 5/6 (yellowish brown)	<375 (using 10x)	Fine to medium sand (using 10x)	Poorly to moderately sorted (10x)	Loamy sand	High sphericity; subangular	Indurated; very hard	Massive; crusted	None	Calcrete nodules (25-3 mm ⌀); root casts
91054	LRcc	None	Surface sample	-	10 YR 5/6 (yellowish brown)	100-500 (using 10x)	Fine to medium sand (using 10x)	Poorly sorted (10x)	Sand	Low sphericity; moderately rounded to subangular	Consolidated; slightly hard	Moderate to fine cracks; crusted; porous	None	Calcrete nodules (<30 mm ⌀, pebbles to granules low sphericity, subangular); pores; root casts
90028	LRcc	None	0.3	-	Brown	118	Very fine sand	Very poorly sorted (2.01)	Sandy loam	-	Indurated; very hard	Blocky angular or lumpy	None	Calcrete nodules; medium to fine roots
91053	LRcc	None	Surface sample	-	10 YR 5/6 (yellowish brown)	≤ 250 (using 10x)	Medium sand	Well sorted (using 10x)	Sand	Low sphericity; subangular	Indurated; slightly hard	Crusted (5-15 mm thickness); cracks	None	Calcrete nodules; some calcrete veining
91057	LRcc	None	Surface sample	-	10 YR 6/6 (brownish yellow)	≤ 250 (using 10x), 750 max	Fine to medium sand (using 10x)	Moderately sorted (using 10x)	Sand	Moderate to high sphericity; subrounded	Indurated; very hard	-	None	Fine calcrete veining
91055	LRcc (Heuweltjie ?)	None	Surface sample	-	10 YR 5/6 (yellowish brown)	<500 (using 10x)	Medium sand (using 10x)	Moderately sorted (using 10x)	Loam	Moderate to low sphericity; angular to subrounded	Indurated; very hard	-	None	Calcrete nodules (≤ 35 mm ⌀); calcrete veining; rugose biocrust
90018	LRcc	LR	0.46	-	-	153	Fine sand	Poorly sorted (1.37)	Loamy sand	-	Indurated	Thinly crusted; massive	None	Large calcrete nodules; roots (upper 100 mm)
90026	LRcc	None	0.3	-	-	131	Fine sand	Poorly sorted (1.88)	Sandy loam	-	Indurated; very hard	Blocky subangular	None	Fine calcrete veining

91048s28	Not visible	None	Surface sample	-	10 YR 5/6 (yellowish brown)	≤ 250 (using 10x)	Medium sand	Moderately to well sorted (using 10x)	Sandy loam	High sphericity; angular to subangular	Indurated; very hard	Cracks; thick crust (15-30 mm)	None	Small calcrete nodules (20 mm ⌀, low sphericity, subangular-subrounded); root casts
90022	LRcc	UY	0.31	-	-	137	Fine sand	Very poorly sorted (2.00)	Sandy loam	-	Indurated; very hard	Massive	None	Calcrete nodules; root casts
91050	C	UCS	Surface sample	-	10 YR 5/4 (yellowish brown)	≤ 250 (using 10x)	Medium sand	Well sorted (10x)	Sandy loam	Medium sphericity; subrounded	Indurated; hard	Smooth, crusted surface.	None	Small calcrete nodules on surface (5-25 mm ⌀)
91046	Not visible	None	Surface sample	-	10 YR 6/4 (light yellowish brown)	≤ 250 (using 10x)	Medium sand	Moderately sorted (10x)	Loam	high sphericity; subangular	Indurated; hard	Crusted (5-7 mm thick)	None	Calcrete nodules (20 mm ⌀); fine root holes; rugose biocrust on surface
91047	Not visible	None	Surface sample	-	10 YR 5/6 (yellowish brown)	≤ 250 (using 10x)	Medium sand	Moderately to well sorted (10x)	Loamy sand	high sphericity; subangular	Indurated; hard	-	None	Calcrete nodules (5-10 mm ⌀); rugose biocrust on surface
91048	Not visible	None	Surface sample	-	10YR between 6/4 and 6/6 (light yellowish brown to brownish yellow)	≤ 250 (using 10x)	Medium sand	Moderately sorted (10x)	Sandy loam	high sphericity; subrounded	Indurated; hard	Crusted (10-15 mm thick)	None	Calcrete nodules (25 - <50 mm ⌀); fine roots; rugose biocrust on surface
Palaeoterrace	BR	LR; UY; IS; UCS	2.6	8 m	-	-	-	-	-	-	-	Granular	None	-
Colluvium	BR	LR; UCS	-	1.5 m	7.5 YR 7/6 to 7.5YR 5/6, reddish yellow to strong brown	100-750 µm	Fine to medium sand	Very poorly sorted (2.47)	Sandy loam to loam	Moderate sphericity; subrounded	Compacted; hard	Granular; fine desiccation cracking; crusted	None	Stoney (5-300 mm max. dimensions), clay coating on quartz grains

91152	Light grey sandstone bedrock	UCS (veneer)	Surface sample	-	From 7.5 YR 7/6 (reddish yellow) to 10 YR 5/6 (yellowish brown)	≤ 150 (using 10x)	Fine sand	Very poorly sorted (10x)	Loam	high to moderate sphericity; subrounded	Compacted; slightly hard	Poorly developed fine desiccation cracks; crusted	None	Stoney (5-200 mm max dimension)
91151	Light grey sandstone bedrock	UCS	Surface sample	-	10 YR 5/4 (yellowish brown)	<100-500 (10x)	Fine to medium sand (using 10x)	Poorly to moderately sorted (10x)	Loam	moderate to high sphericity; subangular	Heterogenous (indurated and very hard to firm)	-	None	Stoney (10-300 mm max dimension); pores (small to large); quartz grains finely coated
91059	Not visible	UCS	Surface sample	-	Surface: 10 YR 6/4 (light yellowish brown); substrate: 7.5YR 5/6 (strong brown)	250-750 (10x)	Medium sand	Well sorted (10x)	Loam	Moderate to low sphericity; subrounded (substrate)	Well consolidated	Crusted	None	Stoney (10-300 mm max. dimension); pores (small to large); quartz grains finely coated
91064	-	-	Surface sample	-	-	150	Fine sand	Very poorly sorted (2.47)	Sandy loam	-	-	-	None	-
Bedrock	Not visible	C; PT	-	-	Reddish to light grey	-	-	Well sorted	Sand	-	Lithified; extremely hard; cemented	Massive; layered	None	Quartz grains

^Source: FAO (1990)
*Source: Folk et al. (1957)

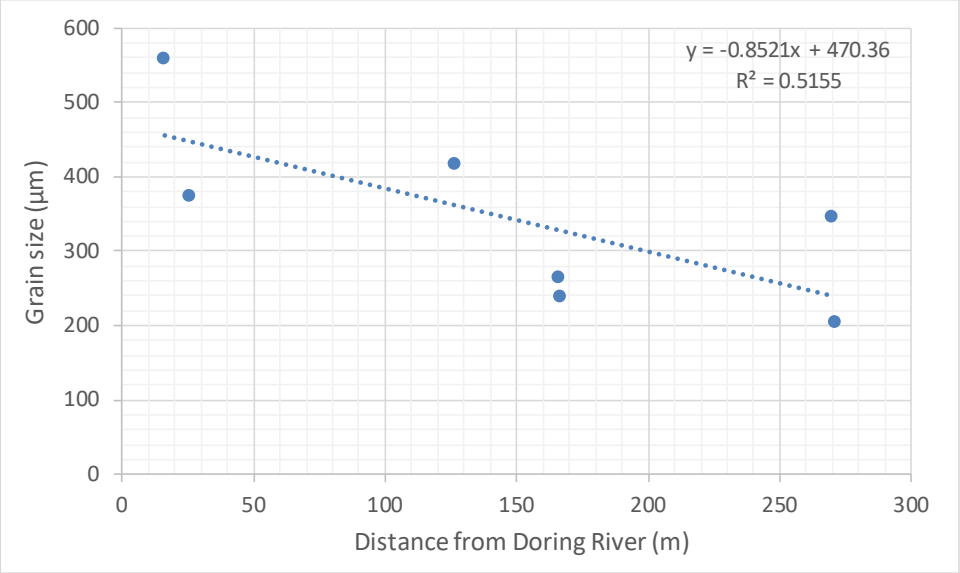

Figure A4.2. Plot of mean grain size versus distance from the Doring River for unconsolidated sediment samples at UPK7.

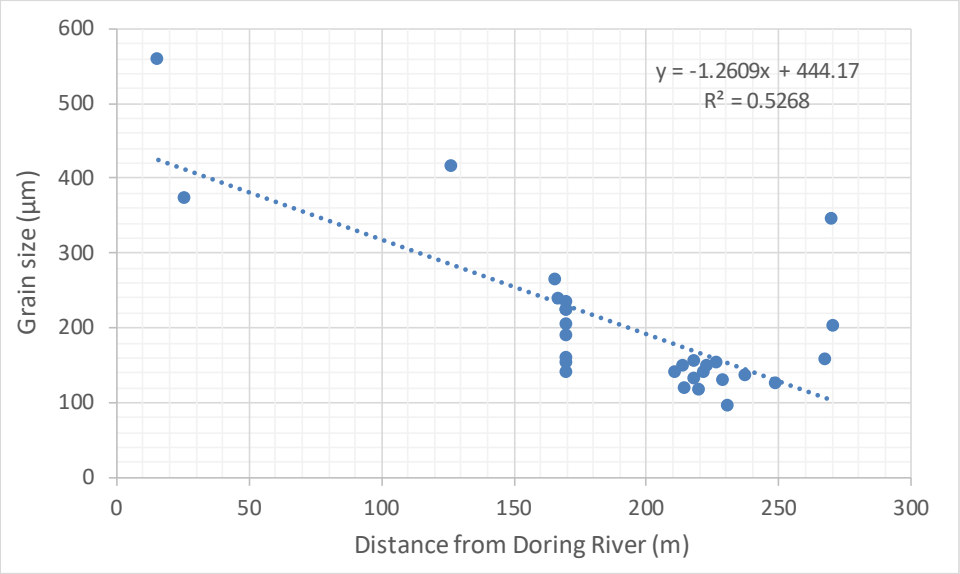

Figure A4.3. Plot of grain size versus distance from the Doring River for all sediment samples at UPK7. While showing a similar trend to Figure A4.2 the older samples are finer grained than the younger samples.

4.1 Sediment Sample Field Notes (Excluding RSSQs)

The following content lists and describes each OSL sediment sample collected across UPK7, grouped by substrate unit, and presented in stratigraphic order.

4.1.1 Unconsolidated Sand (UCS) and Semi-Consolidated Sand (SCS)

Sample 91065 to 91068 and 91086

SCS sample 91066 was collected ~10 m upslope of SCS sample 91065 (see panorama in Figure A4.1.1, bottom) and appears sandier and less consolidated in composition. Both sample locations are composed of finely laminated, sandy sediments directly below pedestalled vegetation and labelled SCS as a result.

Figure A4.1.1. SCS sampling locations for sediment samples 91065 and 91066. Top: Photos of SCS samples 91065 (left) and 91066 (right) are depicted with 100 mm scale. Bottom: sample positions are shown relative to UPK7's western tributary. Note Brian Jones in the panoramic scene for scale as he collects sample 91065.

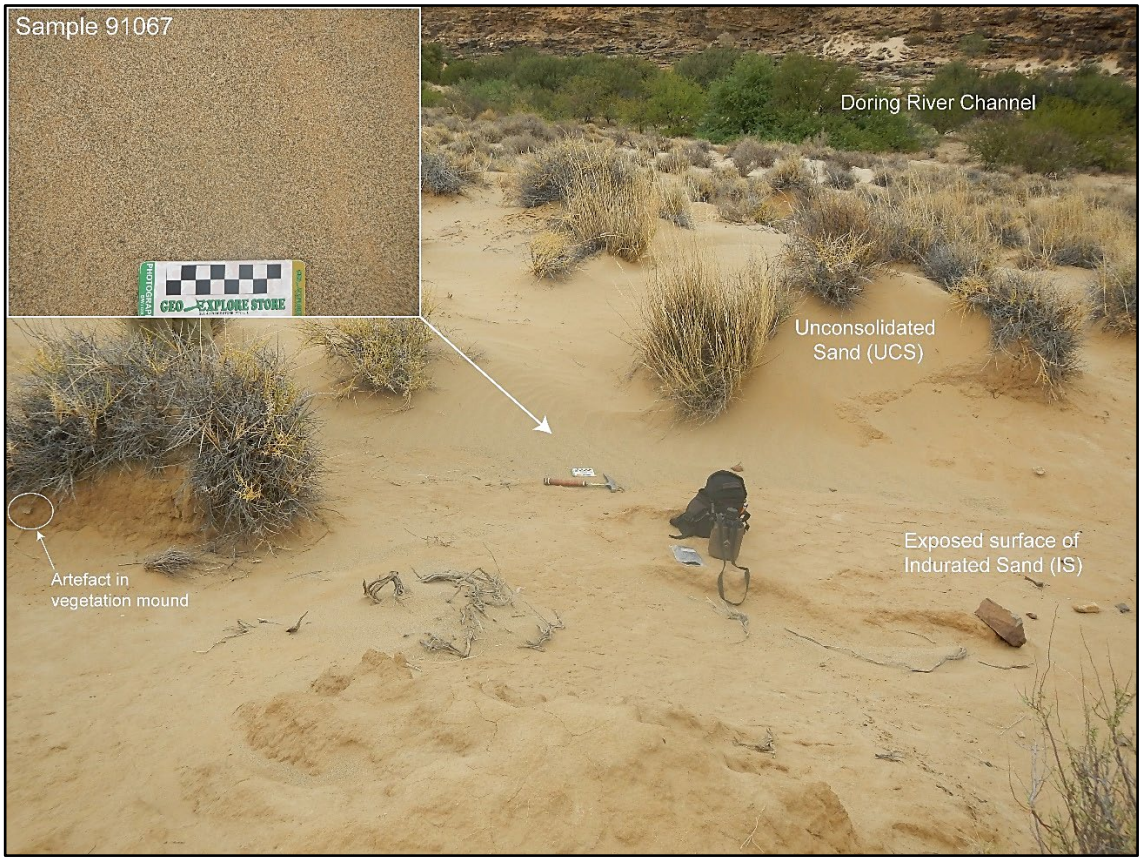

Figure A4.1.2. UCS sampling location. The surface detail of UCS sample 91067 is inset into the sample's context photo at the top of the figure.

Samples 91068 was collected from loose surface sand (or UCS) on the leeward (slip) side of UPK7's eastern sand bank, ~14 m north of AOI 3/Exposure 2 and ~11 m east of Exposure 1b (Figure A4.1.3). Sample 91069 occurred ~55 m southeast of 91068, ~28 m east of Exposure 1c, and ~17 m upslope of the eastern tributary. It was collected from a vegetation mound of semi-consolidated, finely laminated sand (or SCS). Samples 91086, 91067, and 91068 were interpreted as UCS. All three samples derive from loose sand close to vegetation (see Figures 6.3c, 6.11a-b, A4.1.2 and A4.1.3b). However, 91067 and 68 are closer to consolidated sediment in Exposures 1 and 2 than sample 91086 which is surrounded by a large deposit of unconsolidated aeolian sediment and directly upslope of the river terrace.

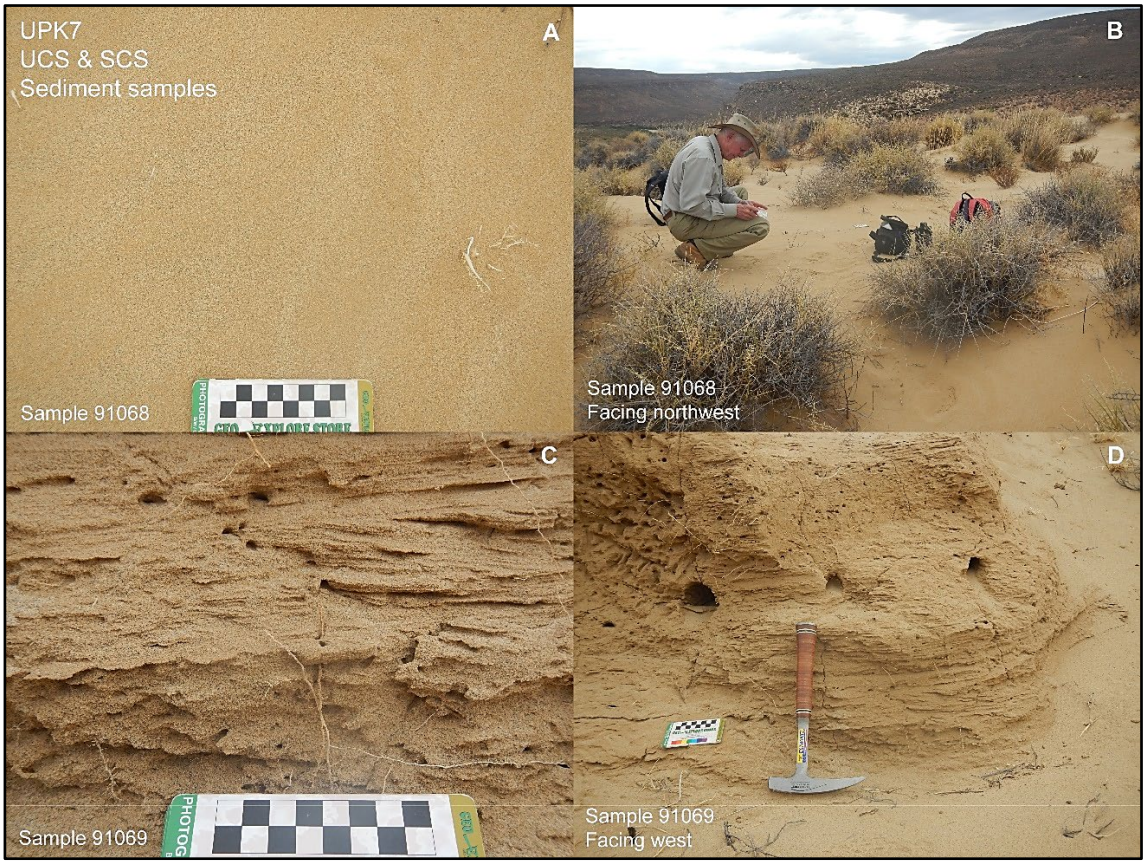

Figure A4.1.3. Photographs of UCS and SCS sampling surface details and settings for 91068 (A-B) and 91069 (C-D).

OSL cut [NA]: Sample tube UPK7-1

Lab ID (OSL/XRD):	UNL-3808
Elevation (asl):	213.5 m
Bls:	0.30 m
Unit:	UCS

Description:

OSL cut made in 2013 by AM (Figure A4.1.4). Originally recorded with Juno and later mapped using a total station and returning an elevation of 213.478 m asl. The sediment sampled was described as a loose sandy, vegetated dune deposit. It immediately overlies the p-HP surface of silcrete rich archaeology and the LR-LRcc sedimentary unit.

Osl samples. Except for UPK 7-1 (UNL3808), which was collected in 2013 and analysed by Ronald Goble at the University of Nebraska (see Shaw *et al.* 2019, SOM), returning an age of ~70 years (UPK 7-1 [UNL3808]: 0.069 ± 0.005 ka, using MAM). There were no other OSL samples taken from UPK7's UCS unit.

Figure A4.1.4. Photos showing the location of OSL sample UNL-3808. Left: sample context, Right: Detail of section sediment and sample hole.

4.1.2 Indurated sandy deposit (IS)

OSL cut 3: Sample tube 90020

Lab ID (OSL/XRD): UOW-1802/X11562
Elevation: 210.5
Sample depth (bls): ~0.31 m
Unit: IS

Description:

Sample 90020 was collected from OSL cut 3, which was cut into the southeast wall of Exposure 1b's southern slope donga (Figure A4.1). The exposed unvegetated surface appears weathered (see rSSQ 16, Section 4.2.2), is hard to excavate, indurated, and smooth. From 0 to 25 cm bls the section is comprised of an upper, overlying deposit of highly indurated sandy sediment that lacks structure (massive). From 25 to 37 cm bls, sediment structure abruptly and smoothly changes into a finely laminated, indurated loamy sand, with a thickness of 12 cm to the base of excavation. The OSL sample 90020/UOW-1802 was collected from the finely laminated, loamy sand at ~0.31 m bls. Calcrete inclusions are absent from the entire section.

Figure A4.1.5. IS sampling location for sediment sample 90020. Tape measures 0.39 m below surface (bls).

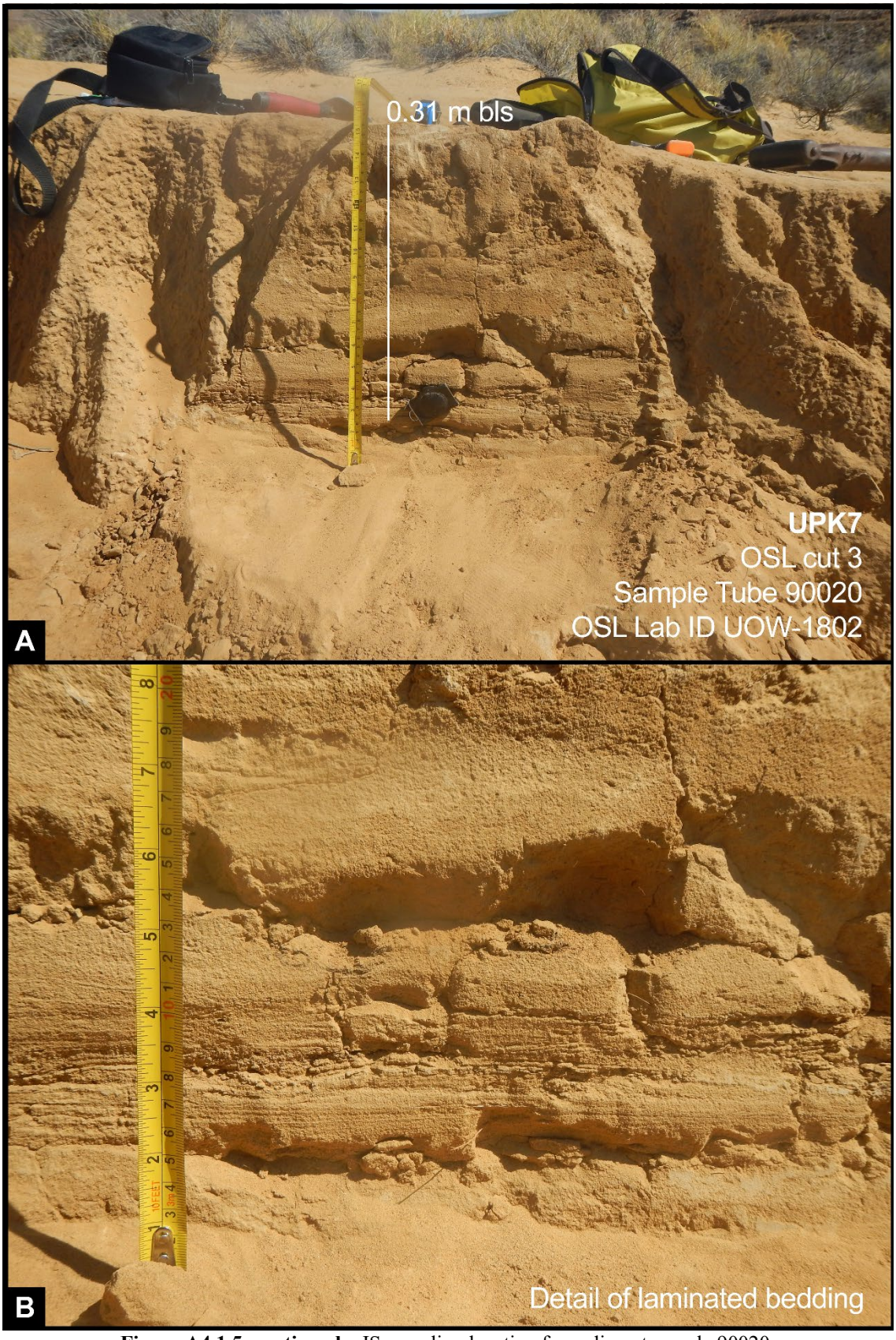

Figure A4.1.5. continued... IS sampling location for sediment sample 90020.

OSL cut 9: Sample tube 91080 (UOW-2006)

Lab ID (OSL/XRD):	UOW-2006/X11614
Elevation:	210.5 m
Sample depth (bls):	0.23 m
Unit:	UY or LR

Description:

OSL cut made into the southern face of a donga, located south of EXP1b's slope. Characterised as indurated sandy sediment showing a blocky sub-angular structure with inclusions of small secondary calcrete nodules that are dispersed throughout the matrix and several artefacts orientated along the same plane and at the same level, 20 cm bls. The base of this deposit exposes a moderately well-developed surface etched by desiccation cracks with inclusions of larger, hard calcrete nodules. The thickness of the sampled deposit from donga surface to base of excavation (BOE) is 32 cm.

In-field examination placed this deposit in the IS unit based on location, tracking of similar sediment exposed in the donga, and its surface characteristics . However, its matrix is harder, appears to contain more clay and silt than the sandier sediments of other IS samples, and holds nodules of calcrete that are also not typical of IS. Its matrix appears closer to that of UY or LR, particularly when its characteristics are compared to the upslope surface of LR, observed beneath the survey area RNG1/2. Thus, the sediment exposed in this section may relate to the deposit underlying RNG 1/2, which is notable for the rough calcareous surface caused by the deflation and exposure of small secondary inclusions of calcrete nodules observed in OSL cut 9's profile, and interpreted in the field as LR grading into LRcc.

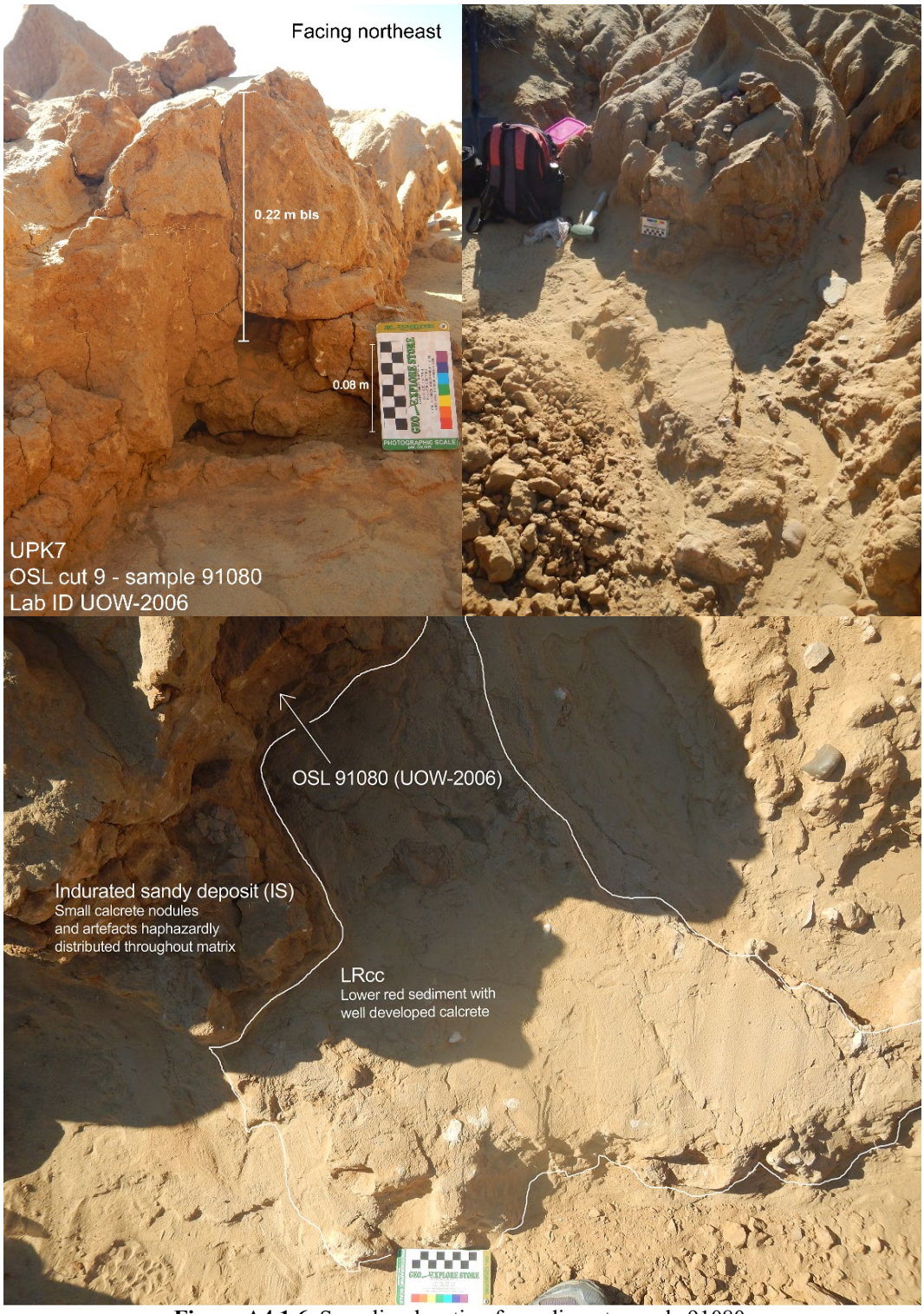

Figure A4.1.6. Sampling location for sediment sample 91080.

Section Cut 1: Samples 90072 to 90079 (n = 8)

Elevation (asl): 207 - 203 m

bls: 0.1 - 3.5 m (0.5 m sampling intervals)

Unit: Semi-consolidated sand to IS to LRcc

Description:

Section cut 1 (SC1) was excavated into the eastern wall of the deeply incised donga that runs south from Exposure 1b. The section was made just before the donga arcs southeast to its outlet in the eastern tributary, about 52 m south of RNG1/2 and 62 m northwest of its outlet. Eight samples were collected at 0.5m intervals starting from 0.1 m below the surface (bls) of the spade cut section and ending at 3.5 m bls, at the base of the auger hole (Table A4.1.1). Sediment becomes more indurated with depth from 0.1-0.6 m bls and calcareous from 2.7 m bls. The surface is covered in unconsolidated sand and vegetation and the first 0.1 m are bioturbated (Figure A4.1.7).

Table A4.1.1. Log of sediment samples from Section Cut 1 into Exposure 1b that were subjected to XRD analysis. Includes sediment sampling descriptions and substrate notation.

Sample ID	XRD	Elevation (m asl)	Depth (m bsl)	Substrate notes	Description	Substrate
91077	X11587	207	0.1	Semi-consolidated sand with roots. Surface covered by unconsolidated sand.	Geosample, Excavated as a section, then augered	SCS
91078	X11588	206	0.6	Transitioning into more indurated sandy sediment.	Geosample, Excavated as a section, then augered	SCS
91079	X11584	206	1.1	Indurated sandy sediment.	Geosample, Excavated as a section, then augered	IS
91072	NA	205	1.7	Indurated sandy sediment.	Geosample, Excavated as a section, then augered	IS
91073	X11626	204.5	2.2	Indurated sandy sediment.	Geosample, Excavated as a section, then augered	IS
91074	X11625	204	2.7	Indurated sandy sediment with carbonates.	Geosample, Excavated as a section, then augered	LR
91075	X11634	203.5	3.2	Indurated sandy sediment with carbonates.	Geosample, Excavated as a section, then augered	LR
91076	X11639	203	3.5	Indurated sandy sediment with carbonates.	Geosample, Excavated as a section, then augered	LR

Figure A4.1.7. Section cut 1 (SC1) showing profile of spade cut section and auger hole in foreground (A), Brian standing with the full-length Auger (3 m) next to SC1 (B), and the height (C), and base of the spade cut section (D).

4.1.3 Upper Yellow unit (UY)

Sample 90016 (UOW-1801) was collected from the very poorly sorted, consolidated, sandy loam sediment of OSL Cut 10, from below Exposure 2's archaeological surface. The second UY sample, 90024 (UOW-1804) was collected from the lower section of OSL Cut 5, sampling a deposit of sandy loam that underlies the semi-consolidated sediment of a vegetation mound. OSL Cut 5 was made directly below an exposed archaeological surface, typically dominated by quartzite, yet abundant in hornfels and late LSA material, including pottery. Both samples were collected at 0.24-0.23 m below the exposed surface of their respective cuts.

OSL cut 10: Sample tube 90016

Lab ID (OSL/XRD):	UOW-1801/X11560
Elevation:	214.117
bls:	0.24 m
Unit:	UY

Description:

Thin cover (~1-5 cm) of overlying loose sand of UCS. Substrate of well consolidated sandy loam sediment increasing in induration with depth. Fine roots observed in profile. No clear structure - deposit lacks obvious bedding planes. Below ELSA surface archaeology, sampled as RNG 3.

Figure A4.1.8. UY sampling location for sediment sample 90016.

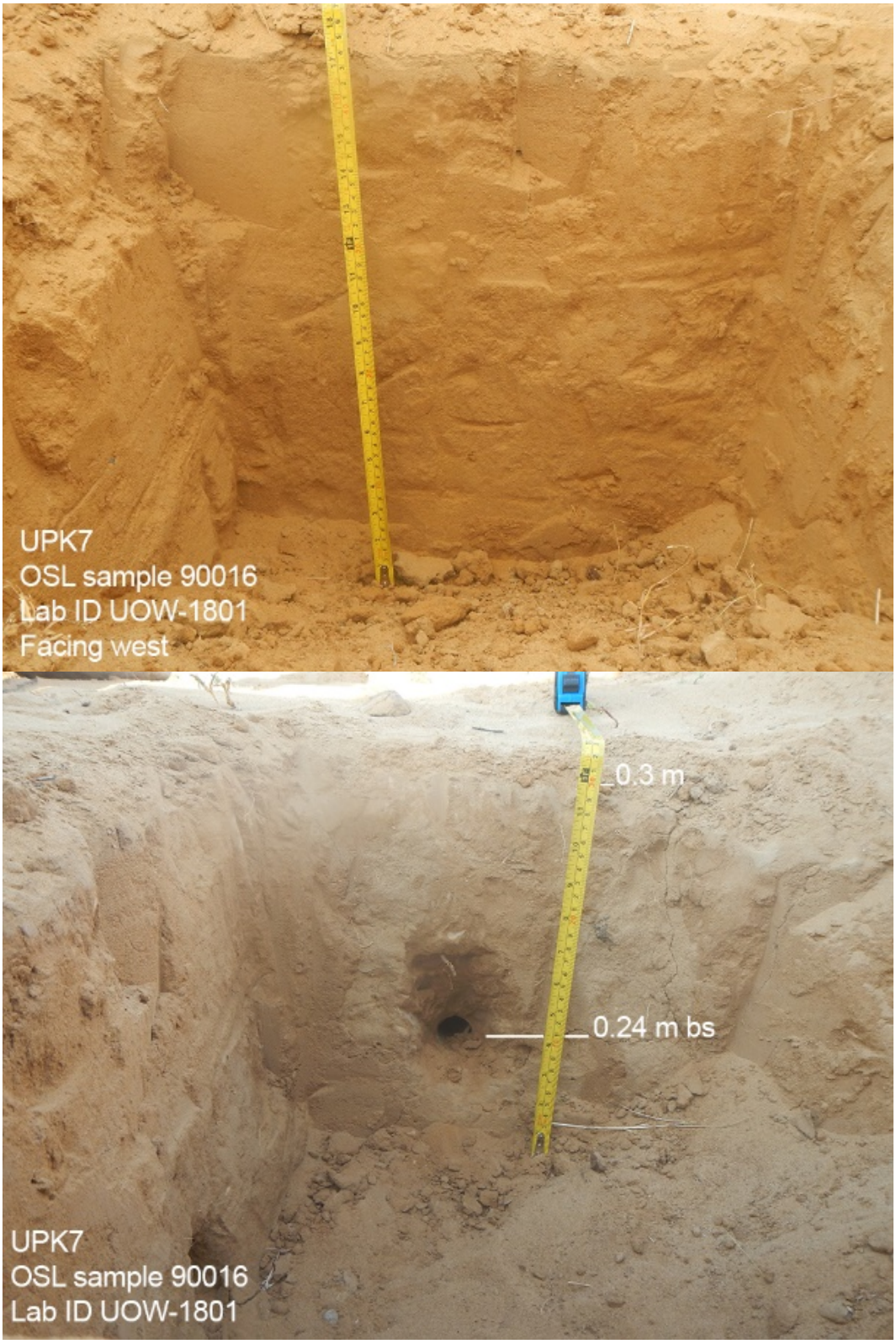

Figure A4.1.8. Continued

OSL cut 5: Sample tube 90024 (UOW-1804)

Lab ID (OSL/XRD): UOW-1802/X11562
Elevation: 215 m
bls: 0.23 m
Unit: UY

Description:

Cut into side of vegetation mound and underlying semi-consolidated sand; sampled sandy loam, no calcrete present; hard but breaks up between and fingers into fine sediment. Approximately 4 meters WNW of surface profile, presented in Figure 6.1b. Directly below exposed archaeological surface of late LSA material, including pottery, and rich in hornfels. Younger deposition than 90022/23 (UOW-1803).

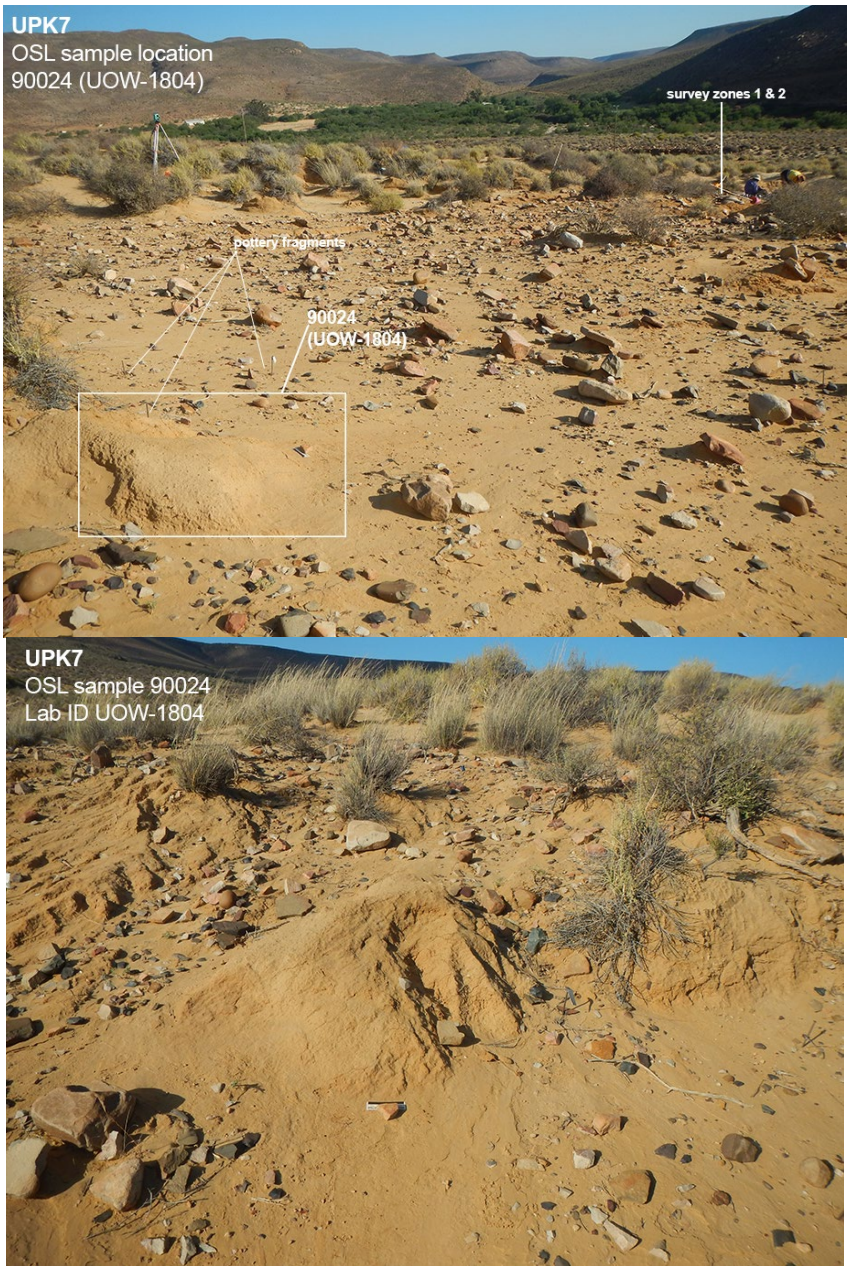

Figure A4.1.9. UY sampling location for sediment sample 90024.

Figure A4.1.10. UY sampling location for sediment sample 90024.

4.1.4 Lower Red sediment with and without calcium carbonates (LRcc & LR)

OSL Cut 11: Sample tube 90018

Lab ID (OSL/XRD): UOW-1800

Elevation: 210 m

bls: 0.33 m

Unit: LRcc

Description:

Located in the southern half of UPK7's central exposure (EXP1b), OSL sample 90018 was taken from the southern wall of a deeply incised gully (donga), OC 11. OSL 90018 derives from LRcc sediment, below and south of RNG 1 and 2 (see Figure 6.38). The surface of this cut is smooth, washed, and thinly crusted. Slope wash erosion is indicated by pedestalled and imbricated archaeological and non-flaked clasts that range in size from pebbles to cobbles. Underlying this, to a depth of ~10 cm, the substrate is weathered with roots observed throughout and no obvious signs of lamination. This grades into indurated sandy sediment with large masses of carbonate observed throughout substrate. Bedding structure was not observed. The sediment sample 90018 was collected below the large calcareous inclusions, in highly indurated sand, for OSL, XRD and grain size analysis.

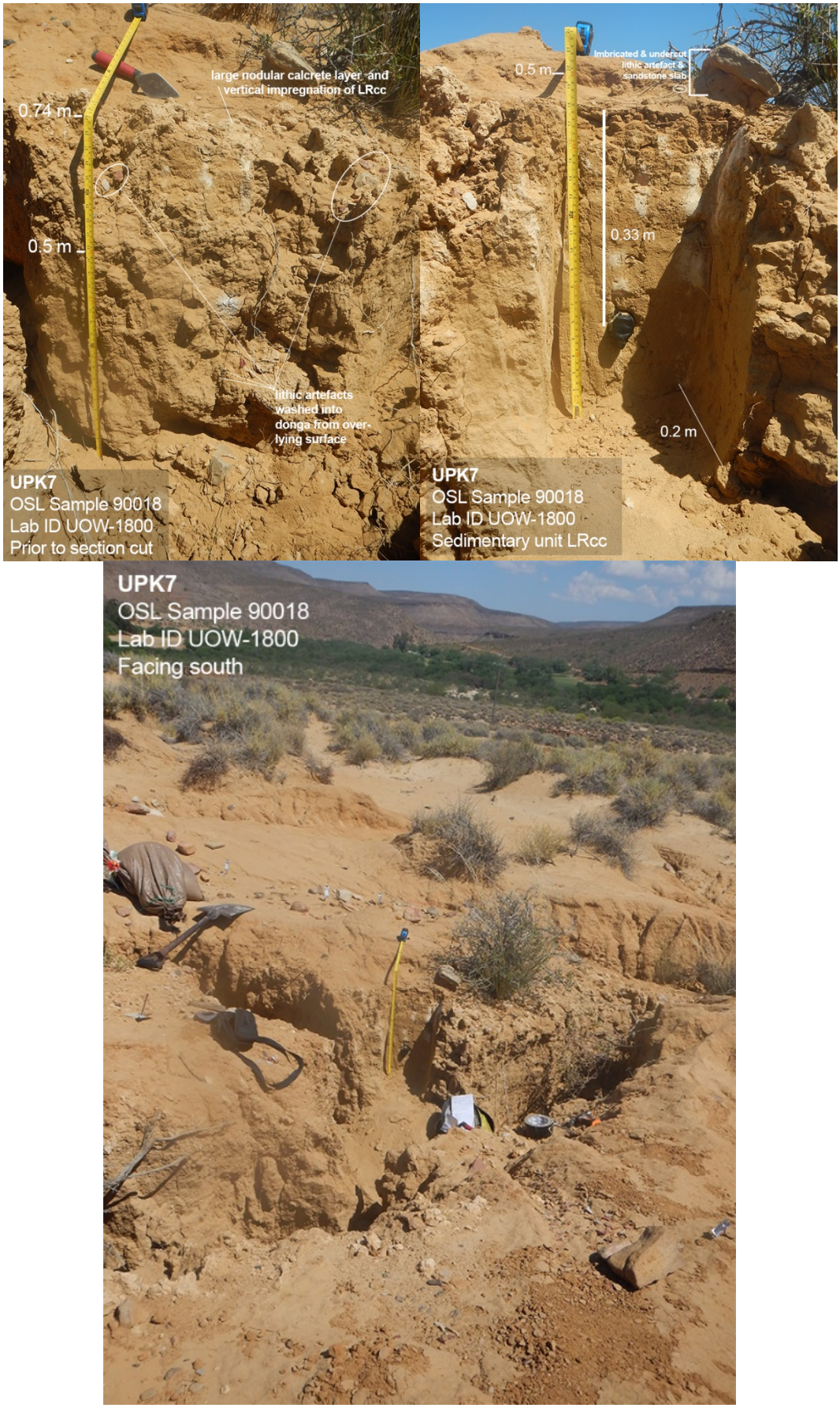

Figure A4.1.11. LRcc sampling location for sediment sample 90018.

OSL cut 6: Sample tube 90026

Lab ID (OSL/XRD): UOW-1832

Elevation: 212 m

bls: 0.26 m

Unit: LRcc

Description:

OSL sample 90026 was collected from LRcc sediment 26 cm below surface. Due to the concreted nature of the deposit, additional depth could not be attained. The first 1.5 cm of exposed section was prone to cracking during sampling. Despite this, the sample appeared to remain intact within the tube. Fine veins of calcrete run vertically through the sampled deposit. Upslope and potentially overlying this osl cut is a hornfels-dominated archaeological surface, possibly LSA. Downslope and west, artefacts are more reminiscent of MSA technology, dominated by convergent blades and local grey quartzite.

Figure A4.1.12. LRcc sampling location for sediment sample 90026.

OSL cut 4: Sample tube 90028

Lab ID (OSL/XRD):	UOW-1833
Elevation:	211 m
bls:	0.22 m
Unit:	LRcc

Description:

OSL sample 90028 was collected southwest and downslope of OC6, sample 90026 (UOW-1832). The sampled sediment was interpreted in-field to be LRcc. It is more concreted than the 90026 matrix, suggesting a lower depositional position and the erosion of less indurated, overlying sediments. There is no visible calcrete veining, only the minor presence of isolated calcrete nodules. Its sedimentary composition appears well sorted under handlens (x10).

Overlying archaeology is dominated by convergent blades and quartzite raw material, suggesting MSA association. However, a hornfels naturally back knife (NBK) was found in this scatter, suggesting a younger LSA (i.e., Wilton) admixture. This may suggest that the overlying surface was re-exposed during use of the Wilton industry, or that the NBK was moved to its current position by either cultural or non-cultural processes, since UPK7's more recent exposure.

Figure A4.1.13. LRcc sampling location for sediment sample 90028.

OSL cut 8: Sample tube 90030

Lab ID (OSL/XRD):	UOW-1834
Elevation:	210.5 m
bls:	0.20 m
Unit:	LRcc

Description:

Collected from a remnant mound of lower red sediment with veined calcrete running throughout its matrix (see Figure A4.1.14), OSL 90030 (UOW-1834) derives from the section cut OC8, located northwest of both OSL 90026 and 90028. The overlying surface of this residual mound is devoid of archaeology. The surface is well formed with veins of calcrete within an indurated sandy sediment. Sample 90030 was taken from beneath a veined calcrete surface (see Figure A4.1.14). Figure A4.1.14 shows veins of calcrete are not well defined and only appear to extend ~100 mm below the surface of the section cut (Figure A4.1.14). The remaining substrate yields nodulated carbonates and fine roots.

The sampled area is a pedestaled remnant of the lower deposit that surrounds it at ground level and is veined with calcrete (see Figure A4.1.14). This lower surface is overlain by artefacts, sampled in rSSQ 94 (Figure A4.2.28). The pedestaled state of the residual mound sampled by 90030 indicates intensive weathering of this deposit. The continuation of calcrete veining in the surrounding lower surface suggests that these deposits were once a continuation of a sloped unit, increasing in elevation to the northeast.

Figure A4.1.14. continued.. LRcc sampling location for sediment sample 90030.

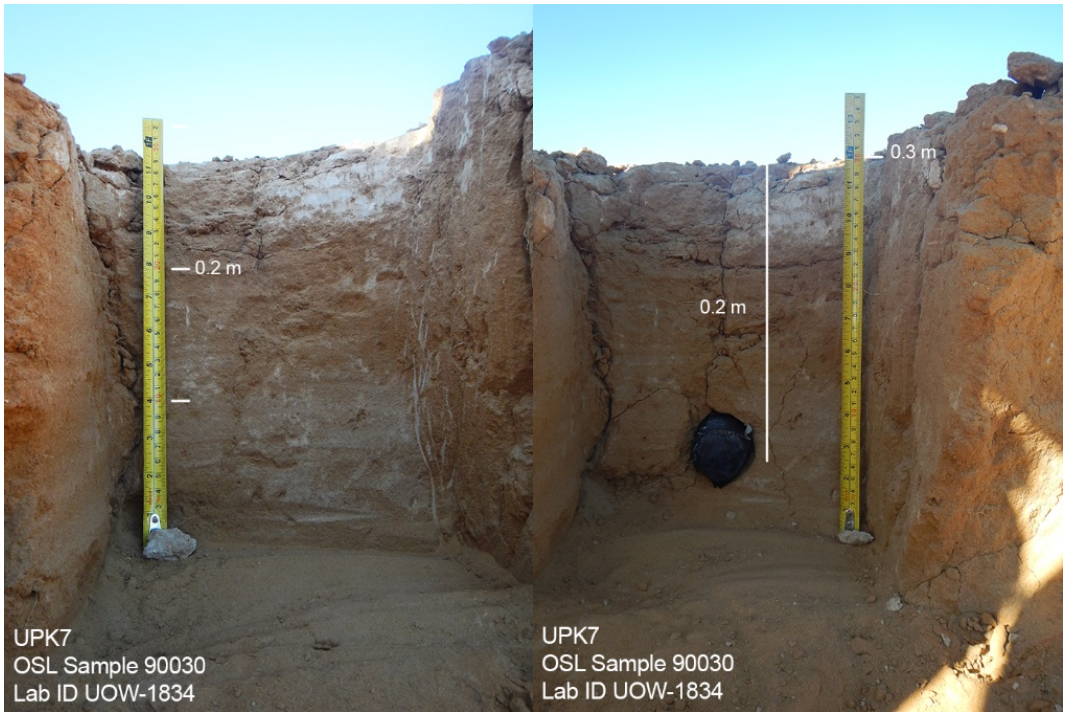

Figure A4.1.14. continued.. LRcc sampling location for sediment sample 90030.

OSL cut 4, sediment sample 90022

Lab ID (OSL/XRD): UOW-1803
Elevation: 212 m
bls: 0.23 m
Unit: LR

Description:

Cut exposes sparse nodules of calcium carbonate within an indurated sediment. The section was cut into the side of the semi-consolidated sediment of a vegetation mound. A lens of artefacts and nonflaked stone separate overlying sediment that is finely laminated, bioturbated (roots), and sandy (similar to 90018 or 90020) from underlying very hard sediment. The latter was sampled. This OSL cut was made ~5.5 m southeast of the surface profile line (Figure 6.1 a-b & 6.39).

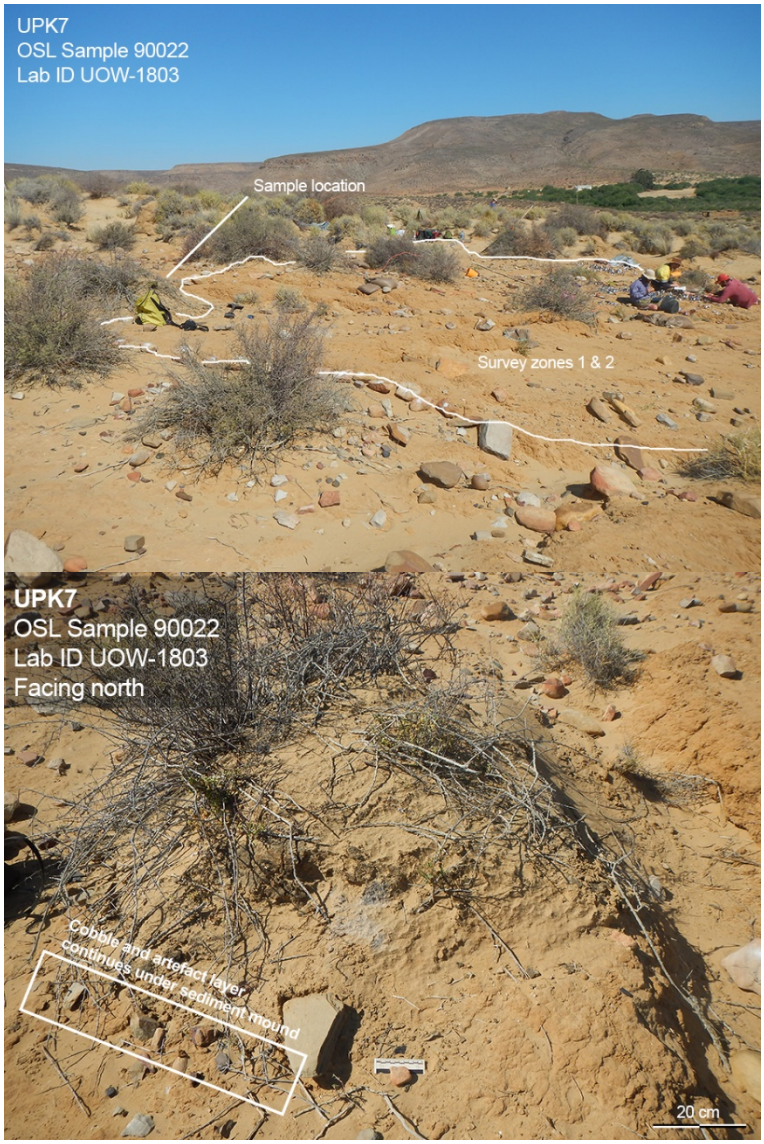

Figure A4.1.15. LR sampling location and context for sediment sample 90022.

Figure A4.1.16. LR sampling context and section detail for sediment sample 90022, before and after sampling.

OSL cut 1U: sediment sample 91153

Lab ID (OSL/XRD):	UOW-2012
Elevation:	207.5 m
bls:	0.35 m
Unit:	Lower Red

OSL cut 1L: sediment sample 91155

Lab ID (OSL/XRD):	UOW-2013
Elevation:	207 m
bls:	0.60 m
Unit:	Lower Red

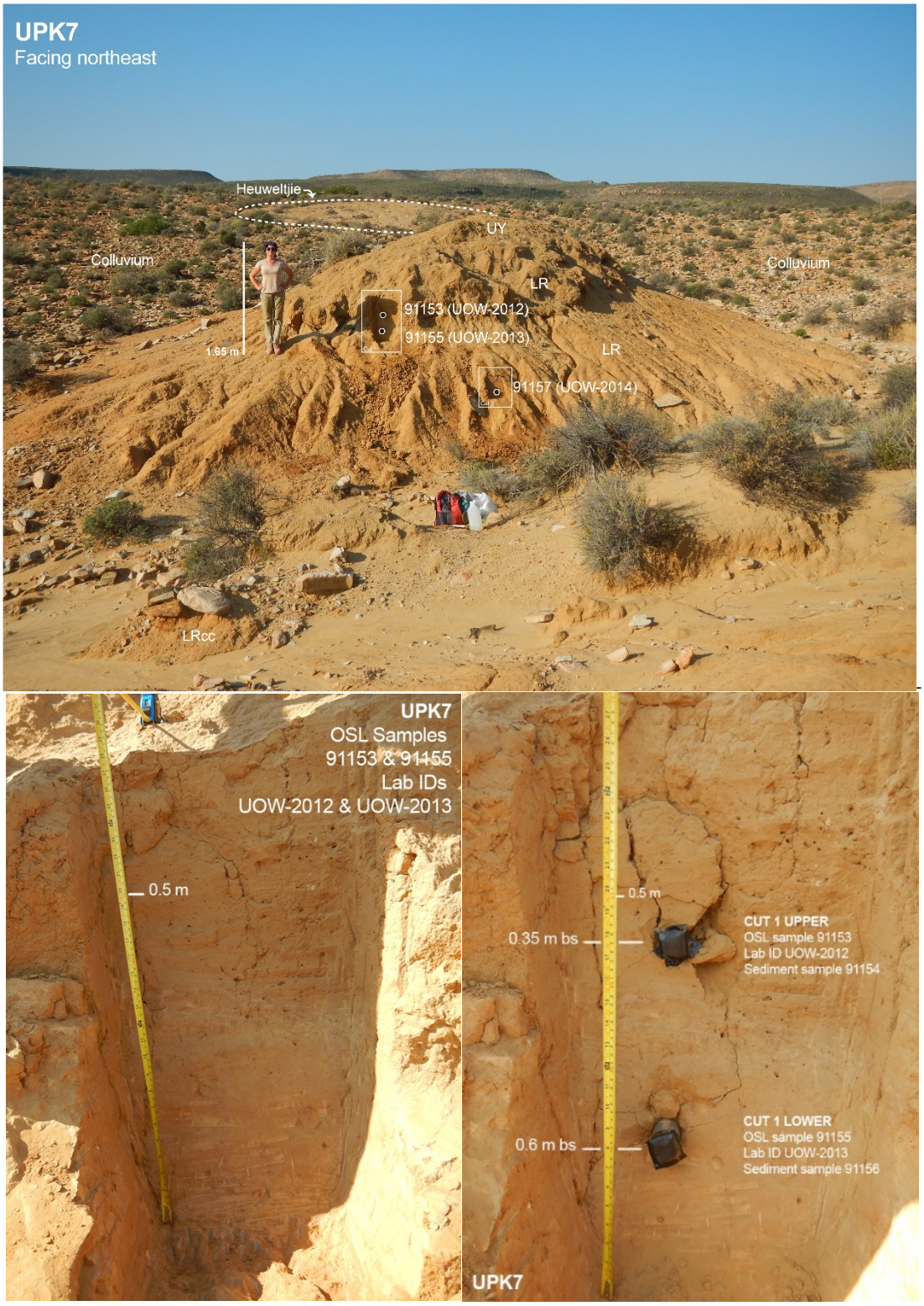

Figure A4.1.17. LR sampling locations for sediment samples 91153 and 91155. Aurore Val stands at a height of 1.65 m.

OSL cut 2: Sample tube 91157

Lab ID (OSL/XRD):	UOW-2014
Elevation:	206 m
bls:	0.23 m
Unit:	LR

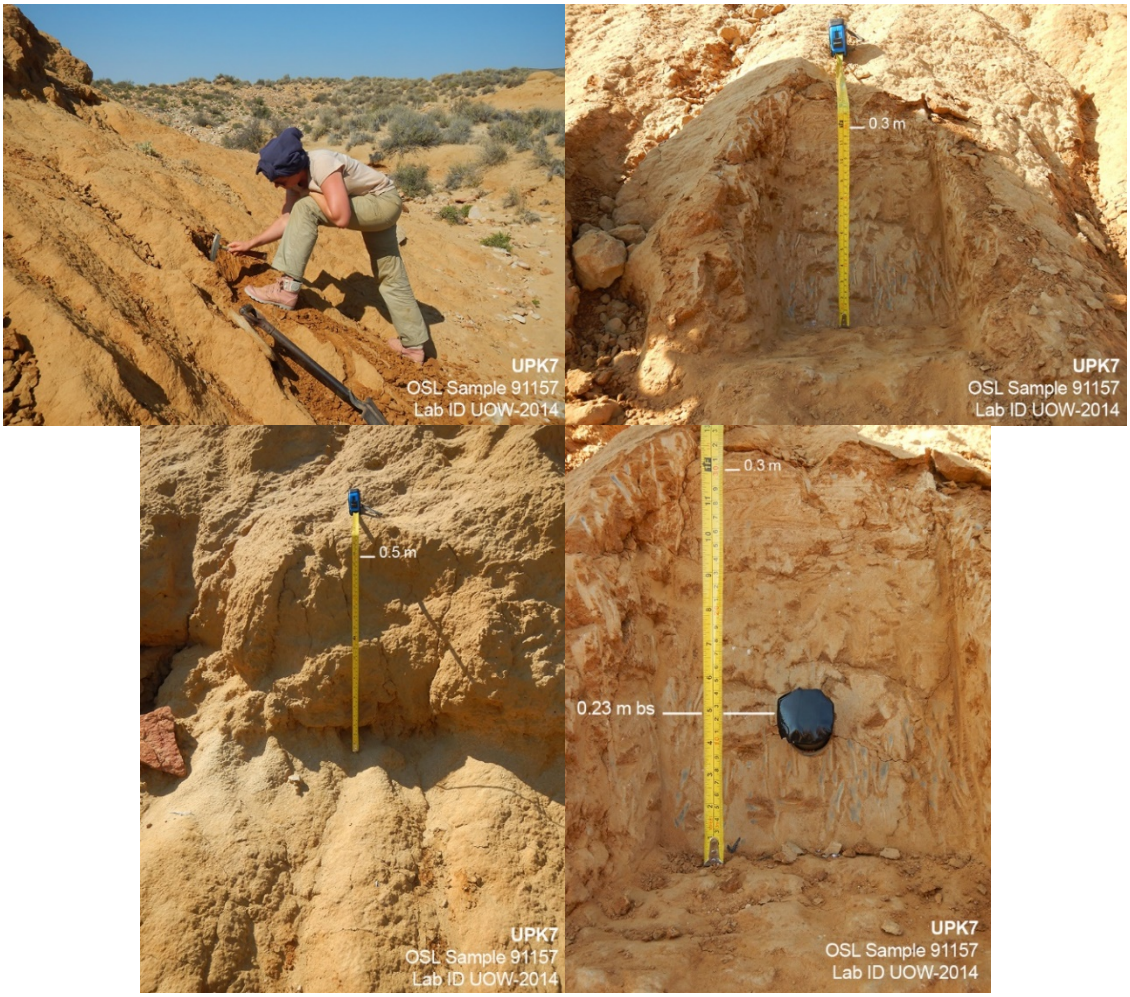

Figure A4.1.18. LR sampling location for sediment sample 91157.

4.2 RSSQ Surface and Sediment Sample Field Notes

Surface and sediment descriptions of each rSSQ are provided below. These are grouped by sediment unit and listed in numerical order within each context. 'AOI' stands for Area of Interest and is used interchangeably with 'rSSQ' throughout this appendix.

4.2.1 Unconsolidated Sand

rSSQ 14 - 91003

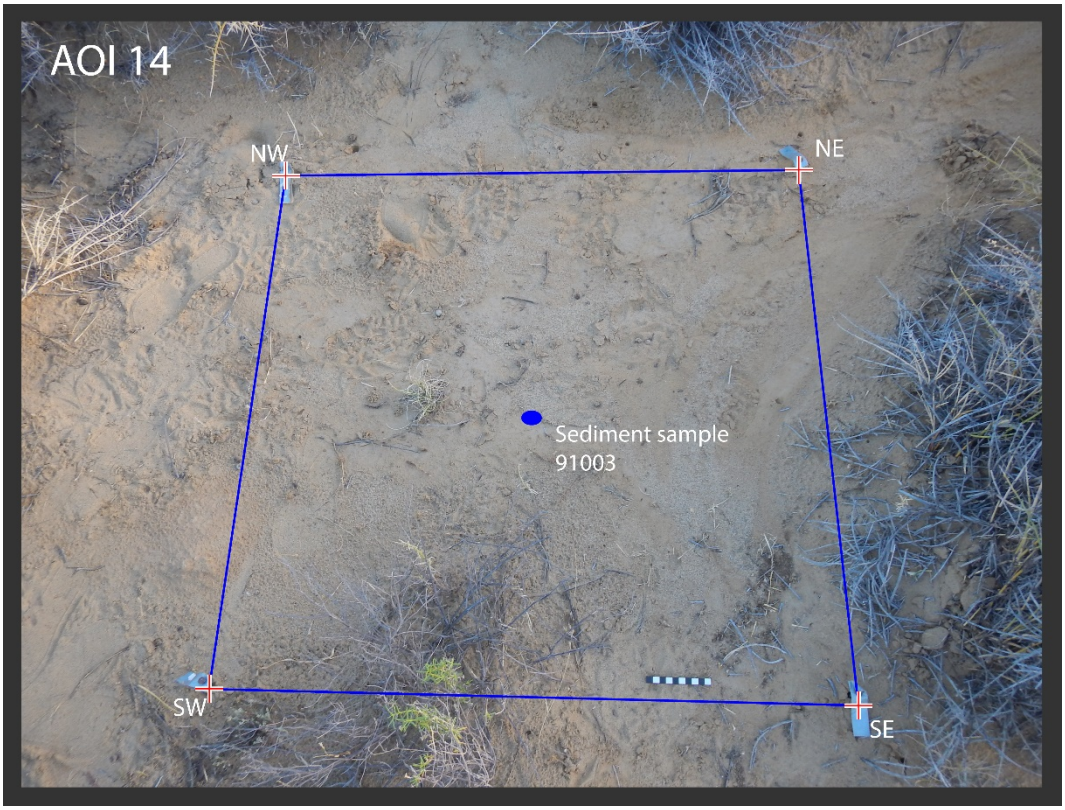

Figure A4.2.1. UCS sampling location for sediment sample 91003.

Immediate area is well vegetated with a thick layer of recent Aeolian sand dune covering underlying fluvial sediment (too deep to be included in sample). Animal scat and vegetation debris observed scattered across this square's surface. No lithic remains (artefact or non-flaked stone) visible above 5mm.

Sample ID 91003

Equipment	Geo-pick and metal scoop
Position	Centre of square
Photo no.	DSCN 2653
Camera	CoolPix Silver

rSSQ 15 - 91004

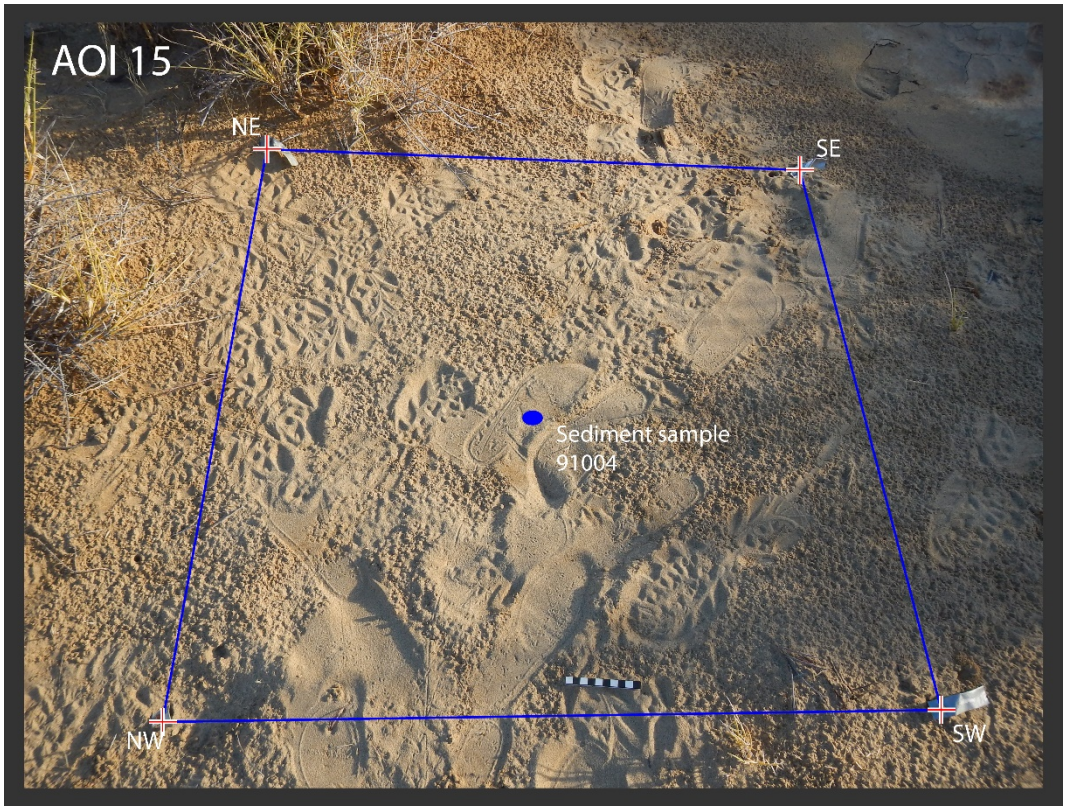

Figure A4.2.2. UCS sampling location for sediment sample 91004.

Aeolian sand dune thickly draped over fluvial sediment.

Sample ID 91004

Equipment	Geo-pick and metal scoop
Position	Centre of square
Photo no.	DSCN 2654
Camera	CoolPix Silver

rSSQ 19 – 91008

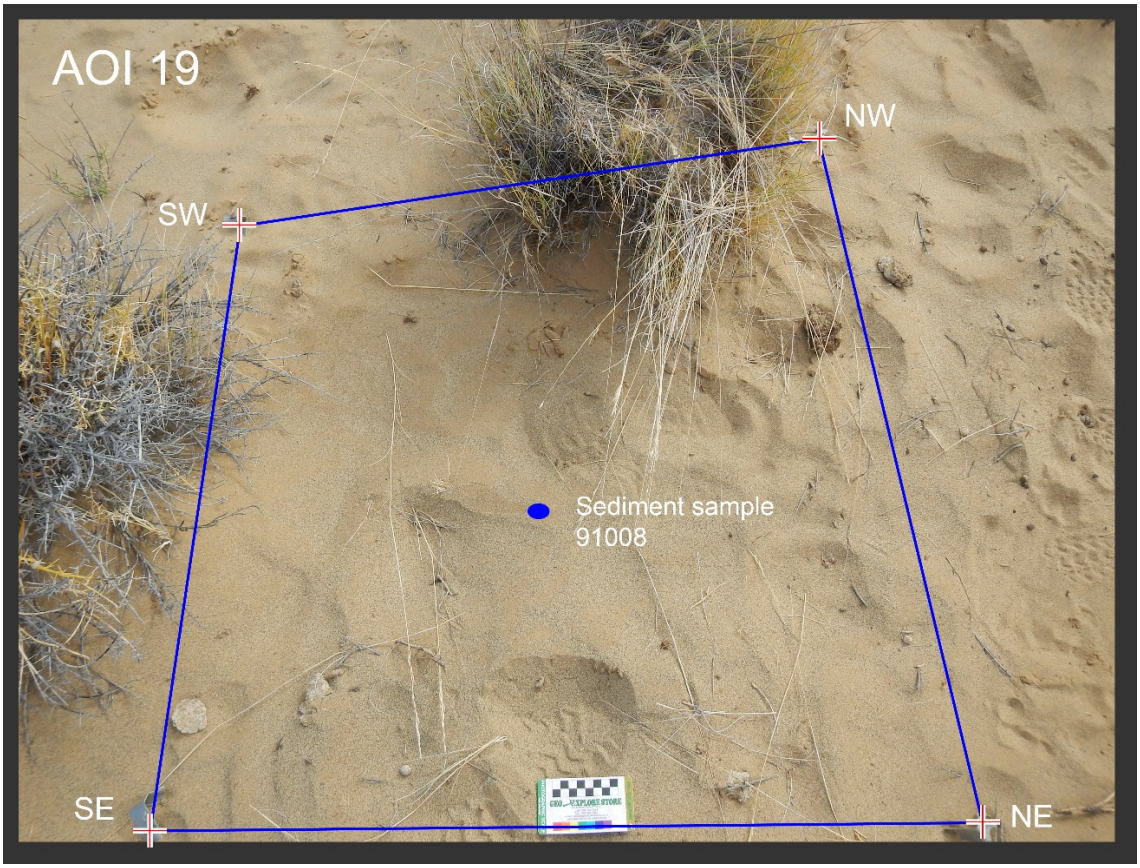

Figure A4.2.3. UCS sampling location for sediment sample 91008.

Aeolian sand and vegetation underlying a sparse cover of organic debris (i.e., skat). No lithic clast material.

Sample ID 91008

Equipment	Sample bag and hand as scoop
Position	Centre of square
Photo no.	DSCN 2843, DSCN2844
Camera	CoolPix Silver

rSSQ 60 - 91060

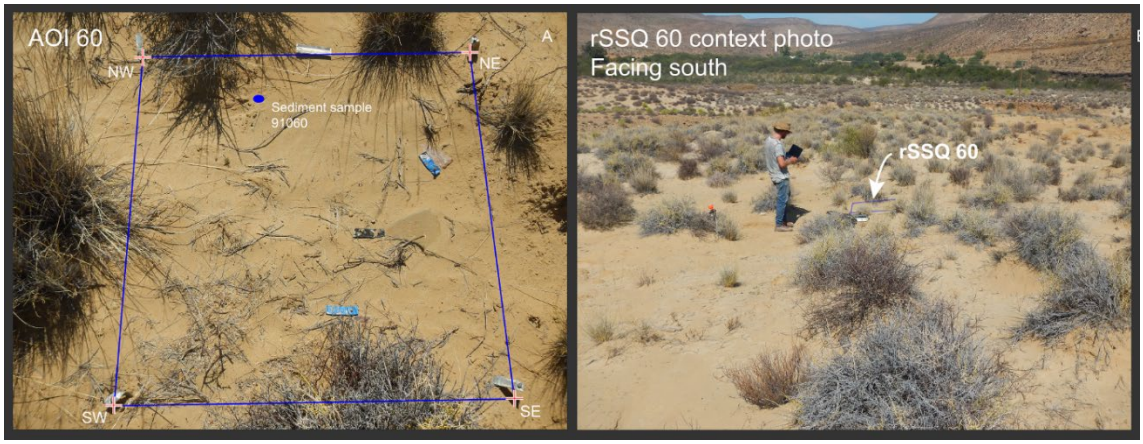

Figure A4.2.4. UCS sampling location for sediment sample 91060.

Sampled surface fairly level with immediate vicinity surrounding square relatively well vegetated. Square consists of sandy sediment mixed with vegetation debris and three large lithic clasts – no other obvious clasts. However, a meter south of square a small 2 x 2-meter exposure of calcareous sediment is present with a range of artefacts distributed across its surface. This exposure is only slightly down slope of square 60, the latter potentially overlying a similar surface.

Sample ID 91060

Equipment	Trowel
Position	Along northern boundary – west of centre.
Photo no.	DSCN 3888
Camera	CoolPix Silver

Munsell Chart Colour (dry)

Colour not completely homogeneous, 6/4 10YR

Grain size

Size ranges from less than 500 to 100 micrometres.

Grain roundedness

Moderate sphericity – subrounded and subangular.

Sorting

Poorly sorted.

Consistency

Sandy with absence of balling potential. Slight silty presence.

rSSQ 61 - rSSQ91061

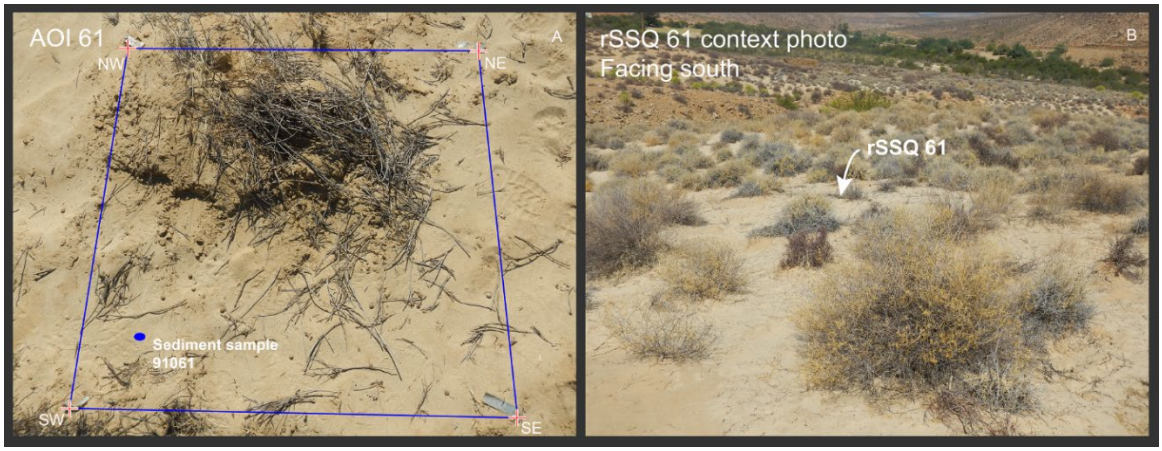

Figure A4.2.5. UCS sampling location for sediment sample 91061.

Surface fairly level with immediate vicinity surrounding square relatively well vegetated. There is a large remnant mound of vegetation in the centre of square. Square consists of sandy sediment mixed with vegetation debris – no obvious clasts present. Both underlying and overlying sediment is relatively uniform, consisting of semi-consolidated sand.

Sample ID 91061

Equipment Trowel

Position SW corner of square

Photo no. DSCN 3889

Camera CoolPix Silver

Munsell Chart Colour (dry)

Colour not completely homogeneous. 7/4 10YR

Grain size

On average 375-500 µm in size. However, overall range 1000 or less.

Grain roundedness

Low sphericity, subangular-subrounded

Sorting

Moderately sorted

Consistency

Sandy. Holds form poorly when wet.

rSSQ 89 – 91147

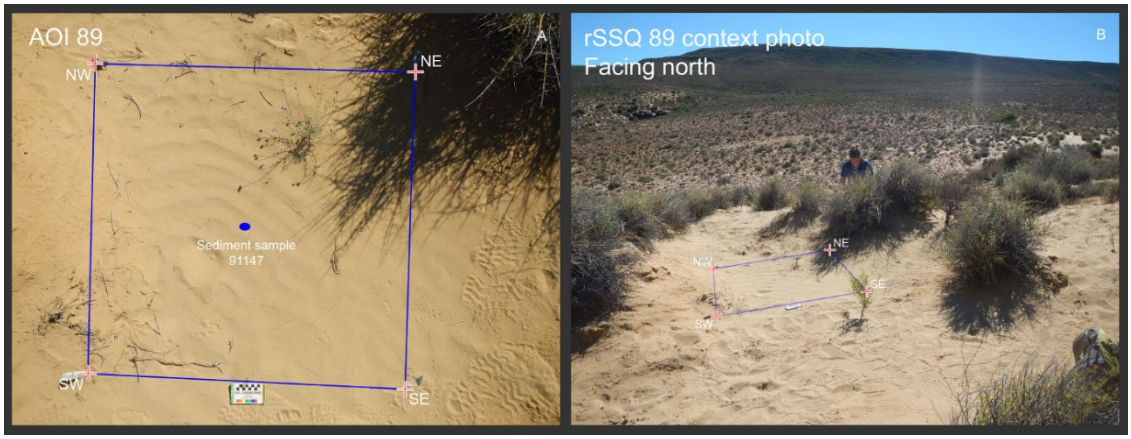

Figure A4.2.6. UCS sampling location for sediment sample 91147.

Within the modern sand dune, dated within the last 60 years. Surrounding context is moderately vegetated. Small vegetation within the square. Positioned between archaeologically rich calcareous surface in the south and colluvial surface in the north. No clasts. Little organic material in the south-west corner. Loose and easy to excavate with the trowel. Slightly consolidated underneath, probably due to recent rain. About 10 mm below surface, the sand is more consistently indurated but still very easy to break up with fingers. Consists of fine root system.

Sample ID 91147

Equipment	Trowel
Position	Center of square
Photo no.	DSCN 4930 (sunlight), top magnetic north; 4931 (without sun)
Camera	CoolPix Silver

Munsell Chart Colour (dry)

Between 7/6 on the 10YR (yellow) and 6/6 on the 10YR (brownish yellow)

Grain size

Equal 2 and less than 750 µm; the majority of grains however are between 250 and 180 µm. Between fine and medium sand

Grain roundedness

Moderate to low sphericity; angular to sub-angular

Sorting

Moderately to poorly sorted

Consistency

Milky and clear quartz grains. Fine grained shale clasts. Form does not hold when wet.

rSSQ 93 – 91148

Figure A4.2.7. UCS sampling location for sediment sample 91148.

Located in the central dune between the colluvium in the north and the archaeological surface in the south; surrounded by moderate vegetation. Square contains early-stage vegetation - fairly organic rich. Very little slope difference. No clasts.

Sample ID 91148

Equipment	Trowel
Position	Southern corner of the square (middle between eastern and western corners)
Photo no.	DSCN 4932 (sunlight)
Camera	CoolPix Silver

Munsell Chart Colour (dry)

6/4 on the 2.5YR (light yellowish brown)

Grain size

Range between equal 2 and less than 750 µm; the majority are between 250 and 180 µm.

Grain roundedness

Medium sphericity; sub-angular.

Sorting

Moderately sorted; medium-sized sand grains.

Consistency

Includes milky clear quartz grains and fine-grained shale. Form does not hold when wet.

4.2.2 Indurated Sand

rSSQ 5 – 91000

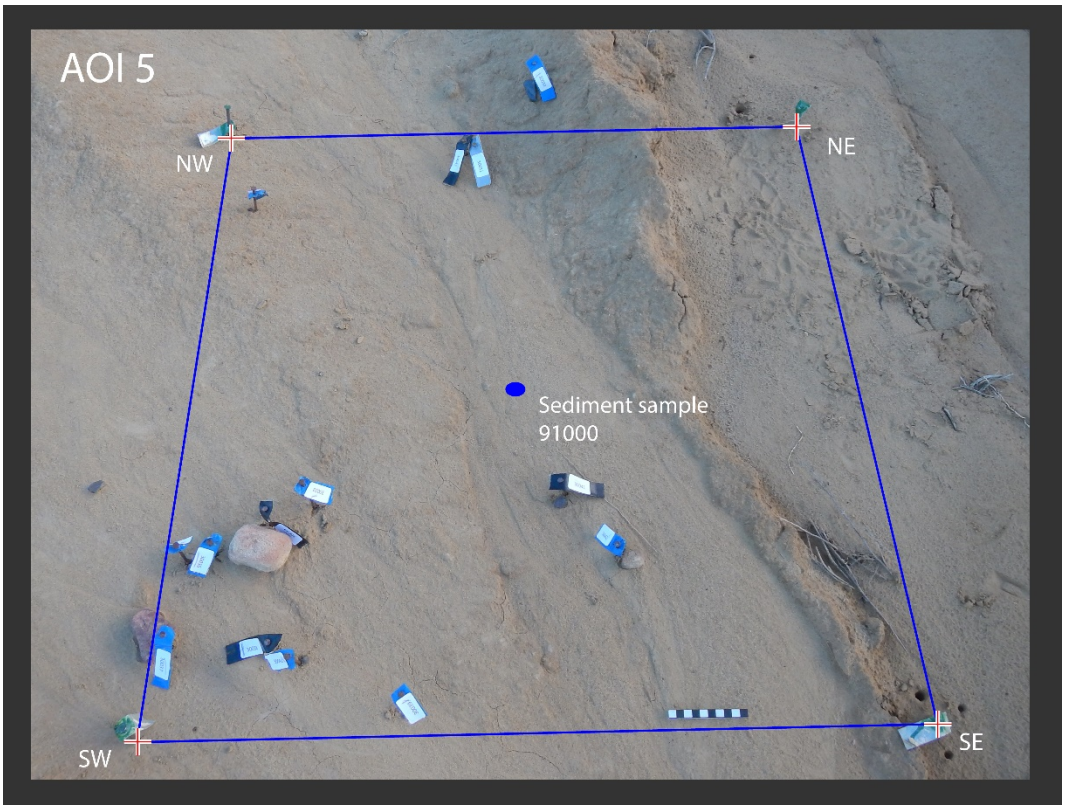

Figure A4.2.8. IS sampling location for sediment sample 91000**.**

Surface of fine grained indurated sand, consisting of quartz and gravel grain sized clasts. Sand filled rill. Overlying sediment is a thin veneer of both rain and wind deposited unconsolidated sand, visible in the centre and to the east of the sample square.

Sample ID 91000

Equipment	Geo-pick and metal scoop
Position	Centre of square
Photo no.	DSCN 2650
Camera	CoolPix Silver

rSSQ 6 – 91002

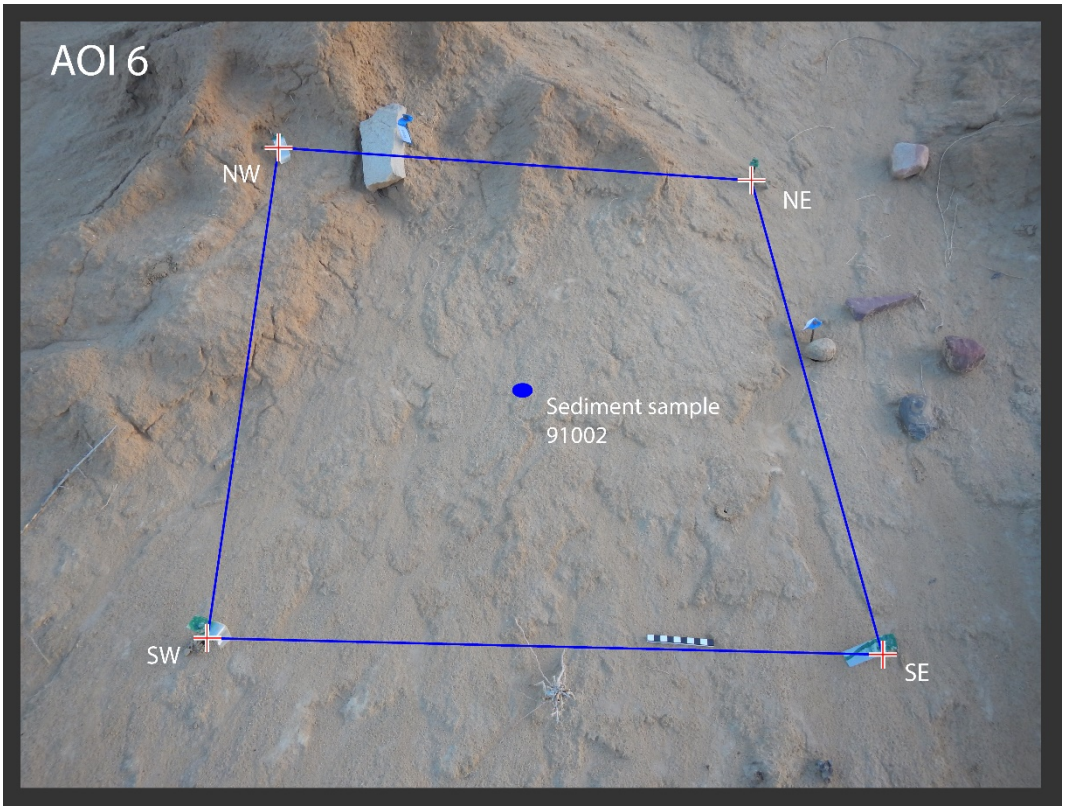

Figure A4.2.9. IS sampling location for sediment sample 91002.

Surface is a hard crust of indurated sediment consisting of fine grains of quartz, poorly sorted. Lighter patches of sediment apparent, but not dominant. Some surface cracking. Sparse stone coverage: One large, angular sandstone block intersecting northern boundary of sample square and another well-rounded stone on the eastern boundary.

Sample ID 91002

Equipment	Geo-pick and metal scoop
Position	Centre of square
Photo no.	DSCN 2652
Camera	CoolPix Silver

rSSQ 16 – 91005

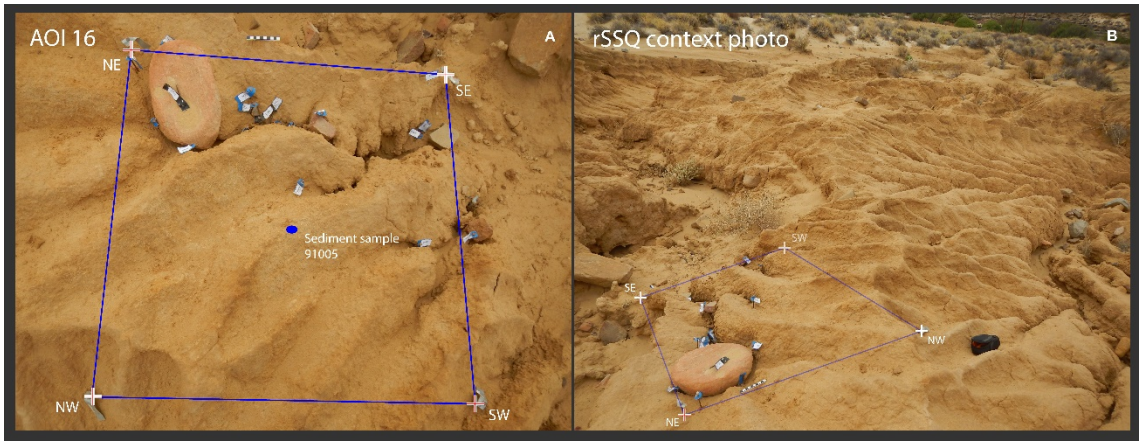

Figure A4.2.10. IS sampling location for sediment sample 91005.

Heavily rilled area. Minimal vegetation. Highly washed erosional surface. Hard sediment is indurated. Poorly sorted.

Sample ID 91005

Equipment	Geo-pick and metal scoop
Position	Centre of square
Photo no.	DSCN 2656
Camera	CoolPix Silver

rSSQ 17 – 91006

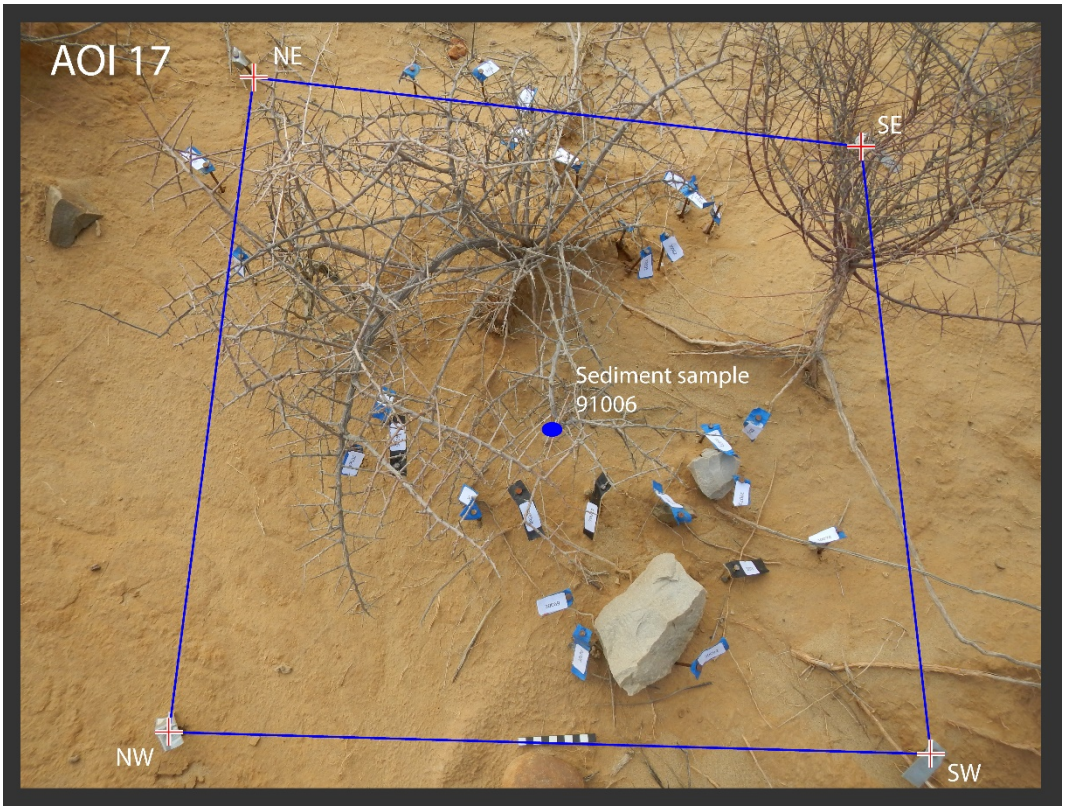

Figure A4.2.11. IS sampling location for sediment sample 91006.

Very thin layer of sand covering a highly indurated surface. Well rooted from vegetation located inside and adjacent to sample square. Crusted surface consists of casts of air pockets. Sediment is sandy with grains of quartz, gravel, and silt (smears between fingers when wet, staining fingers yellow brown).

Sample ID 91006

Equipment	Geo-pick and metal scoop
Position	Centre of square
Photo no.	DSCN 2655
Camera	CoolPix Silver

rSSQ 18 – 91007

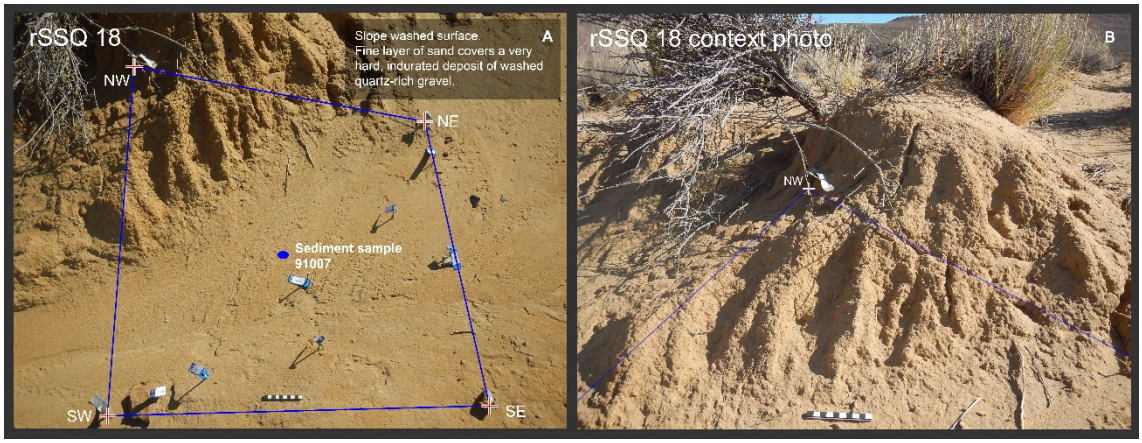

Figure A4.2.12. IS sampling location for sediment sample 91007.

Slope washed aeolian deposit. Fine layer of sand covers a very hard, indurated deposit of washed fine quartz and gravel grains.

Sample ID 91007

Equipment	Geo-pick and metal scoop
Position	Centre of square
Photo no.	DSCN 2657
Camera	CoolPix Silver

rSSQ 21 – 91010

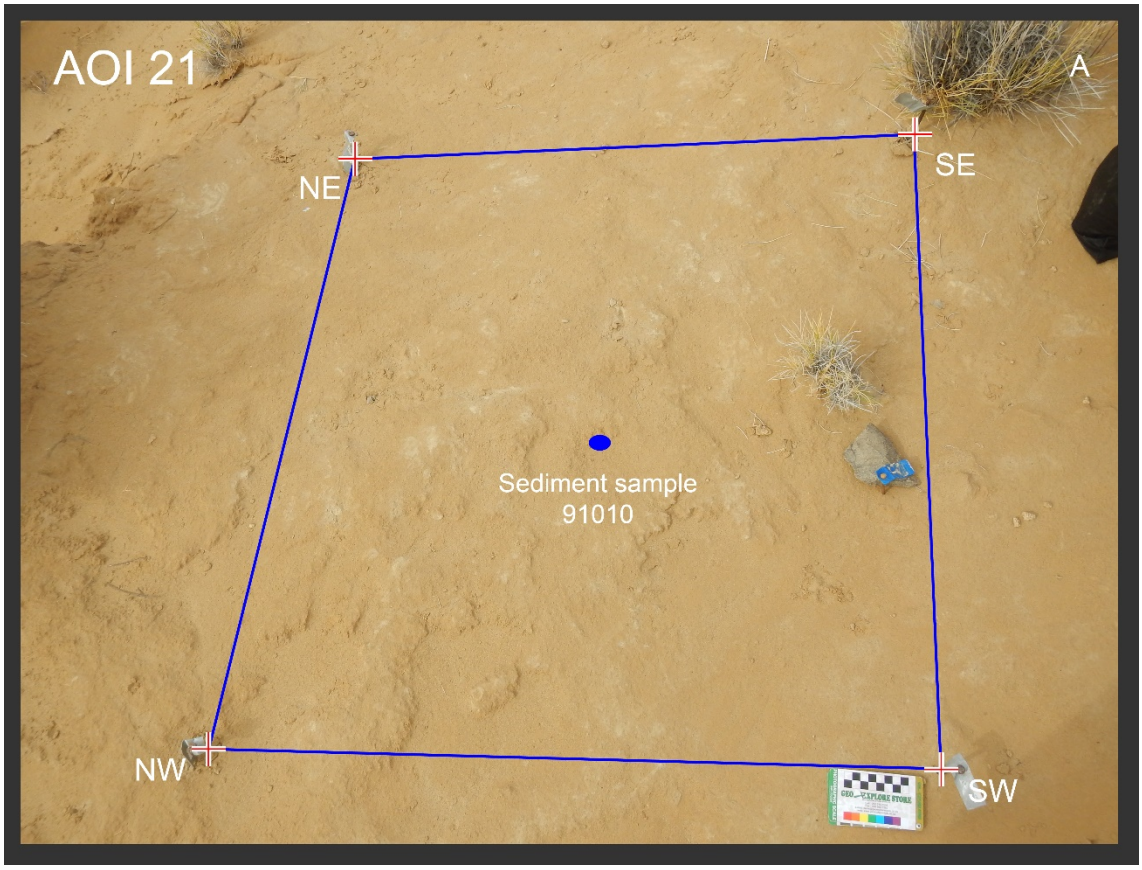

Figure A4.2.13. IS sampling location for sediment sample 91010.

Indurated sand with patches of lighter sediment (carbonates or precipitates?). One clast identified (large complete flake [ID: 30230]). Small calcrete nodules observed on surrounding surface.

Sample ID 91010

Equipment	Geopick and trowel
Position	Centre of square
Photo no.	DSCN 2888-91
Camera	CoolPix Silver

rSSQ 22 – 91011

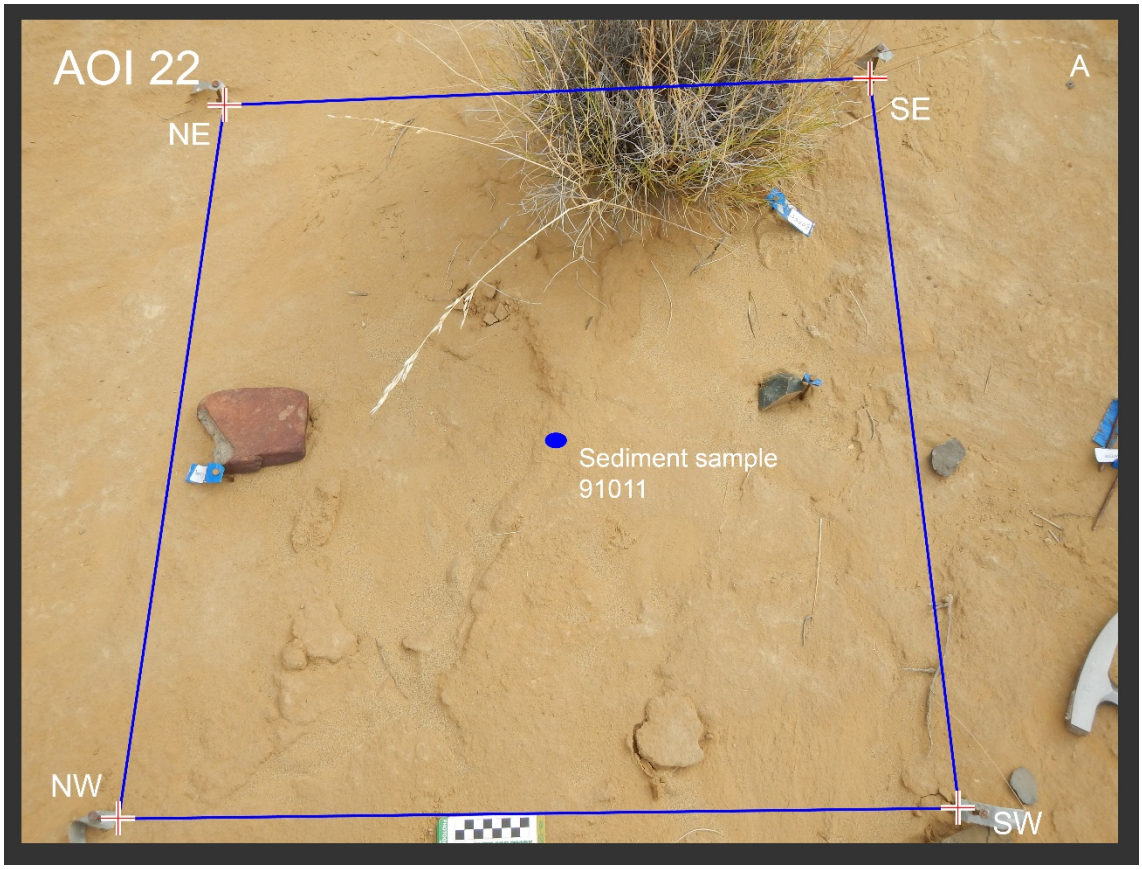

Figure A4.2.14. IS sampling location for sediment sample 91011.

Indurated Aeolian sand. Three clasts identified (Two cores).

Sample ID 91011

Equipment	Geopick and trowel
Position	Centre of square
Photo no.	DSCN 2892, 2899
Camera	CoolPix Silver

4.2.3 Upper Yellow

rSSQ 20 – 91009

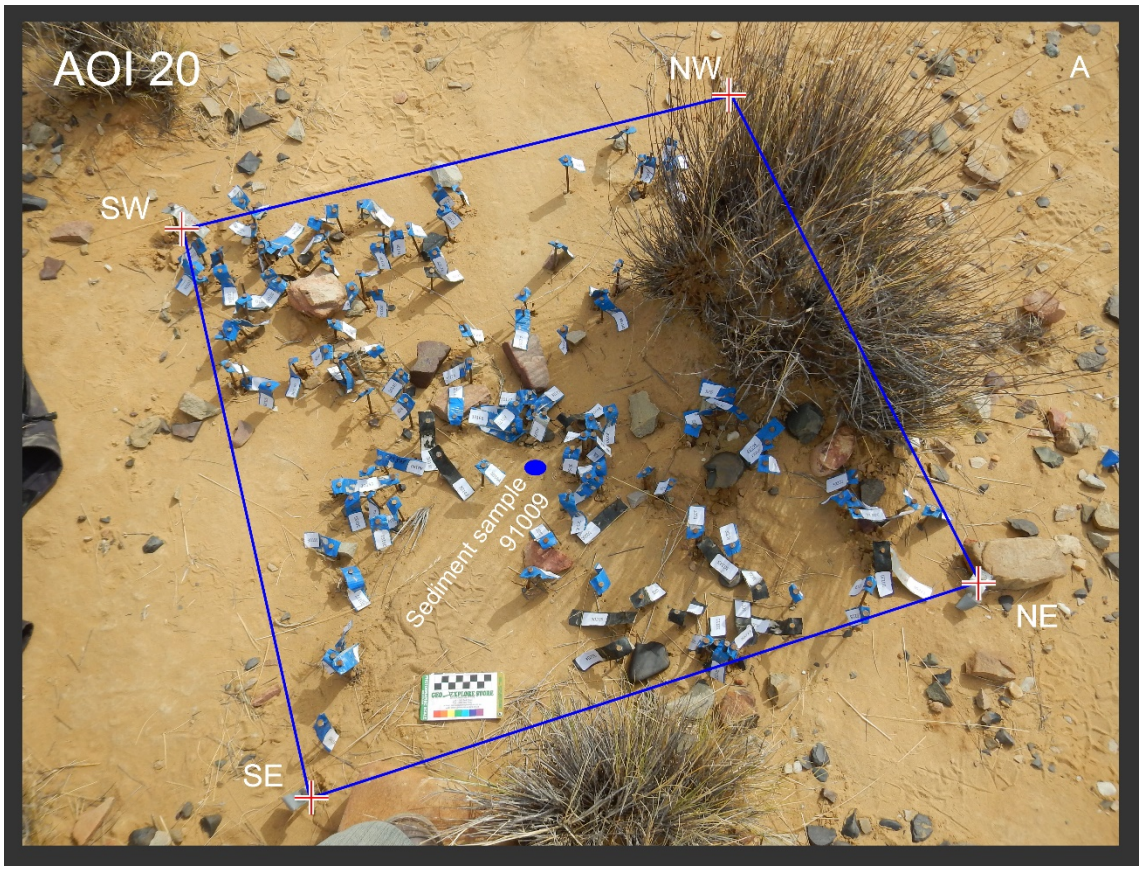

Figure A4.2.15. UY sampling location for sediment sample 91009.

Indurated fine grained sand. Covered by a thin veneer of UCS. About 152 stone clasts (flaked and non-flaked) identified >5mm (point IDs: 30100-30252) within the square's boundaries.

Sample ID 91009

Equipment	Geopick and trowel
Position	Centre of square
Photo no.	DSCN 2845, 2845, 2887
Camera	CoolPix Silver

rSSQ 90 – 91150

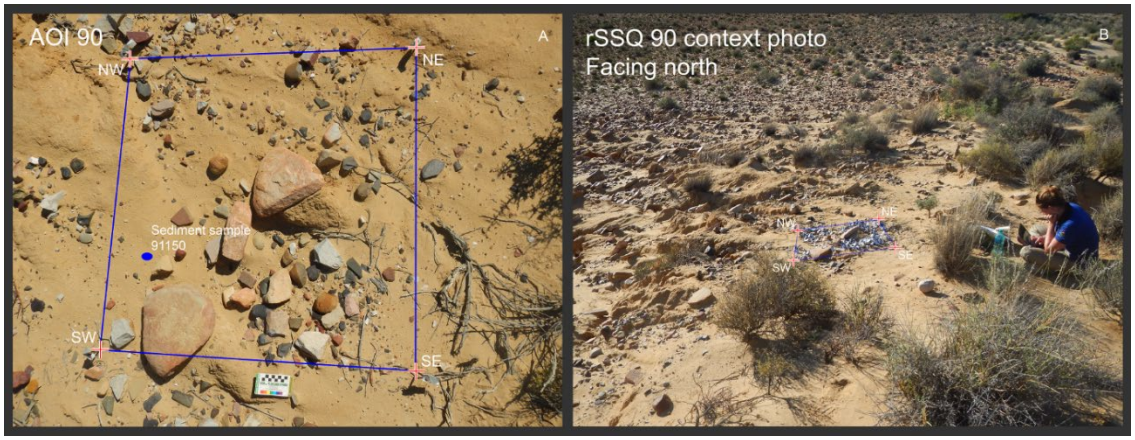

Figure A4.2.16. UY sampling location for sediment sample 91150, rSSQ 90.

RSSQ 90 is located on the younger deposit, within nodular calcrete sediment. Calcrete nodules seem to increase in visibility down slope to the west. Square positioned at the top of a donga. Rilling here is under-developed as it is quite shallow. Winnowing occurs in the square. No vegetation inside the sample square. Moderate surrounding vegetation (in the east and in the south of it). Slope of 10 degrees. Surface is irregular with heterogeneous topography across the square. Dense archaeological remains and blocks of sandstone across the square with the highest density and greater variety of class sizes in the south-east corner (upslope). The large (ca. 200-300 mm) tabular sandstones are all imbricated. STA's size range is from less than 5 mm to 180 mm. The material type is highly variable, from fine-grained to coarse-grained material. There are no calcrete nodules exposed inside the square (only present to the east, down slope). Fine veneer of sand covering the surface coming from the eastern side, up slope. Sediment is highly indurated. Absence of desiccation cracking. Thick surface crust from about 15 to 20 mm in thickness. Root casts present throughout it but few actual roots visible. Consistently hard underneath. Most of the quartz grains seem coated in an even finer layer of sediment.

Sample ID 91150

Equipment Trowel

Position South-west corner of the square

Photo no. DSCN 4966; 4967 (close-up)

Camera CoolPix Silver

Munsell Chart Colour (dry)

5/6 in the 10YR (yellowish brown)

Grain size

≤ 250 µm

Sorting

Well sorted

Consistency

Form holds when wet: moderate. Silty sand. Slight reaction to the HCl in the sediment (contains calcrete) and turns yellow upon reaction.

4.2.4 Lower Red

rSSQ 7 – 91001

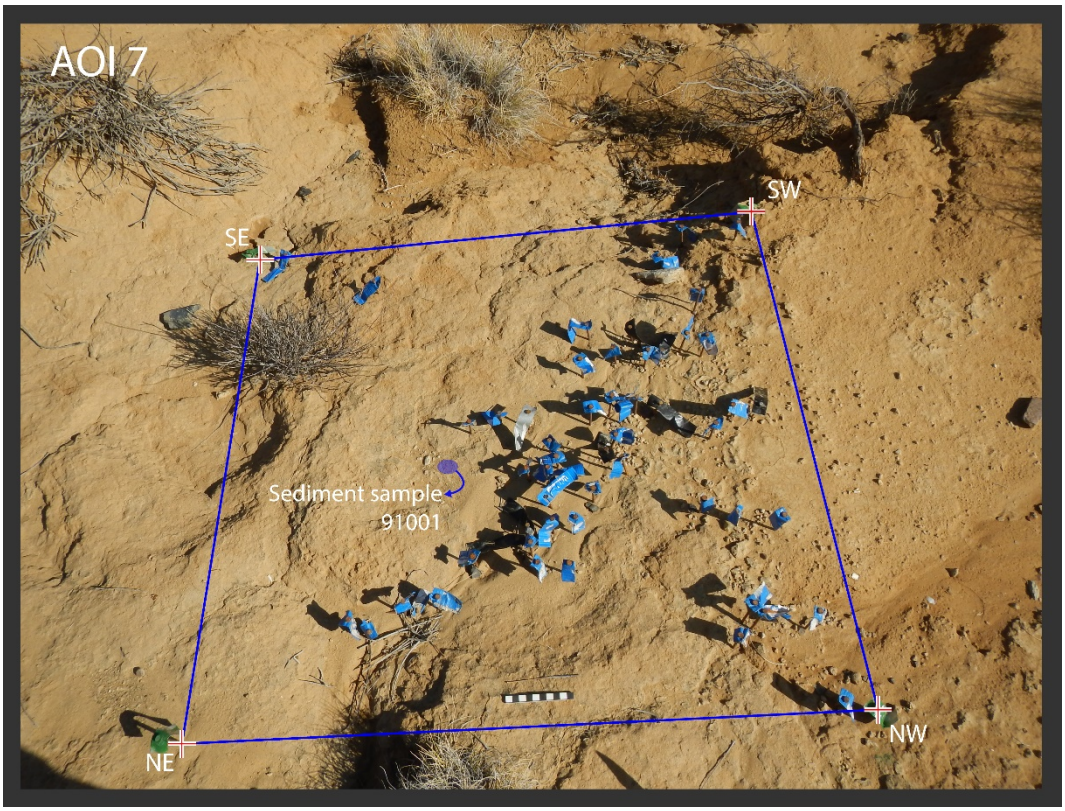

Figure A4.2.17. LR sampling location for sediment sample 91001.

Sediment easier to break up compared to rSSQ 5 sample 91000. Artefacts occur in low areas of surface topography. Small calcrete nodules are eroding out of a loamy sandy matrix. More vegetation in this immediate area compared to rSSQ 5. Beneath the indurated crust sediment is fine and easily broken-up. Appears to be many tiny clasts of both lithic and calcrete.

Sample ID 91001

Equipment	Geo-pick and metal scoop
Position	Centre of square
Photo no.	DSCN 2651
Camera	CoolPix Silver

rSSQ 53 – 91051

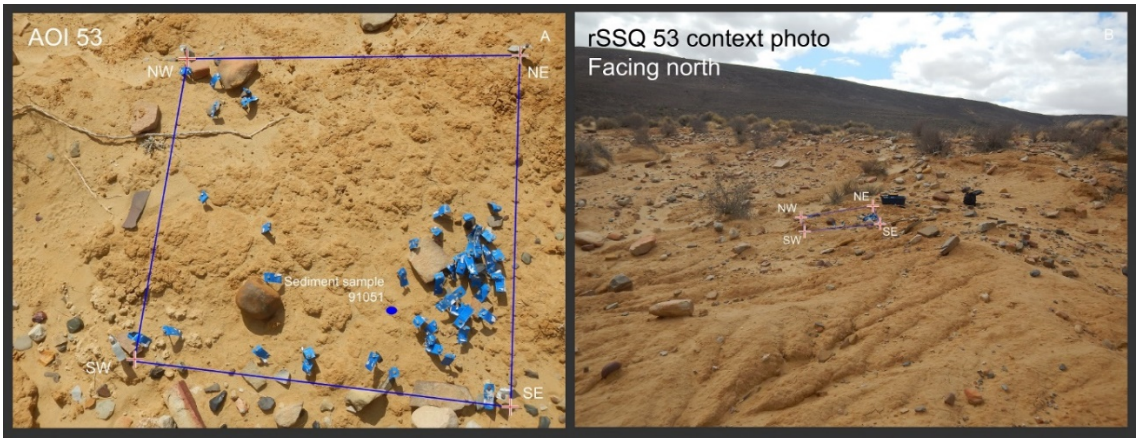

Figure A4.2.18. LRcc sampling location for sediment sample 91051.

Square positioned on weathered surface, sloping downward from east to west (Figure A4.2.18 Right). Nodular calcrete is visibly eroding out of substrate (see southwest corner of Figure A4.2.18 Left). Southern side of square fringes an archaeologically dense area, RNG 1, recorded in Oct 2014as. A rill cuts the southern margin of the square that is relatively dense with artefacts of varying dimension and material (see Figure A4.2.18 Left). In contrast, non-flaked stone clasts >5 mm in maximum dimension are sparsely distributed throughout square and mostly concentrated in SE corner. Fine roots observed throughout sampled deposit and vegetation debris covers the sample square's surface. Sediment was moderately difficult to excavate with trowel.

Sample ID 91051

Equipment	Trowel
Position	Off centre, southwest corner
Photo no.	DSCN 3676-7
Camera	CoolPix Silver

Munsell Chart Colour (dry)

10YR 5/6 (Yellowish brown)

Grain size

Less than 500 µm. Consists of quartz and shale.

Grain roundedness

Variable in form: high sphericity and sub rounded grains, as well as low sphericity, sub angular grains.

Sorting

Moderately sorted

Consistency

Holds form poorly when wet, mostly sandy with small amount of silt. Deposit varies between compacted sediment (fairly friable, easily crushed between fingers) and calcrete nodular clumps. Surface crust 5-10mm thick.

rSSQ 58 – 91056

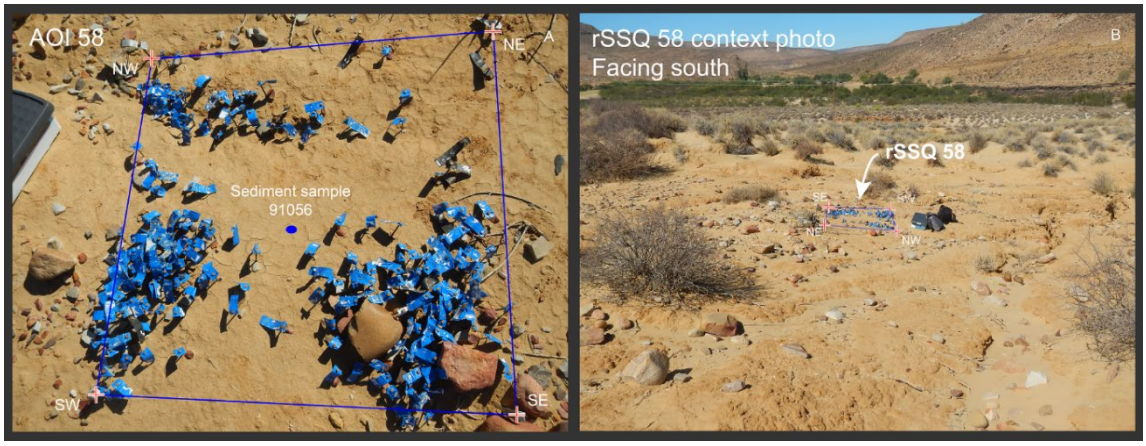

Figure A4.2.19. LR sampling location for sediment sample 91056.

Vegetation located just outside of square to NE, otherwise square itself is mostly devoid of organic material—there are some roots in southwest corner. Uneven surface, with the highest point of the square in the NE and centre, sloping southward down towards the rill system. Square presents a winnowed distribution of artefacts, which cluster in shallow linear incisions that represent the early encroachment of the southern rilling system. This square provides a clear example of slope wash processes and the reorganisation of artefacts across a surface as a result.

The surface is devoid of calcrete. It is smooth and thinly encrusted (~5 mm thick) with fine desiccation cracks. In situ calcrete veining observed just south of square. The sediment just below the surface crust is more indurated. This layer is heterogeneous and speckled with fine, white, spherical crystallisations (possible soil salt crystallisation).

Sample ID 91056

Equipment	Trowel
Position	Center of square
Photo no.	DSCN 3853
Camera	CoolPix Silver

Munsell Chart Colour (dry)

5/6 10YR (Yellowish brown)

Grain size

≤ 500 µm.

Grain roundedness

Heterogeneous, ranges from low sphericity and subangular (larger grains), to high sphericity and subrounded (smaller grains).

Sorting

Poorly sorted.

Consistency

Form holds when wet (moderate to high). Sandy loam.

4.2.5 Lower Red with $CaCO_3$

rSSQ 25 – 91050 (Lag deposit)

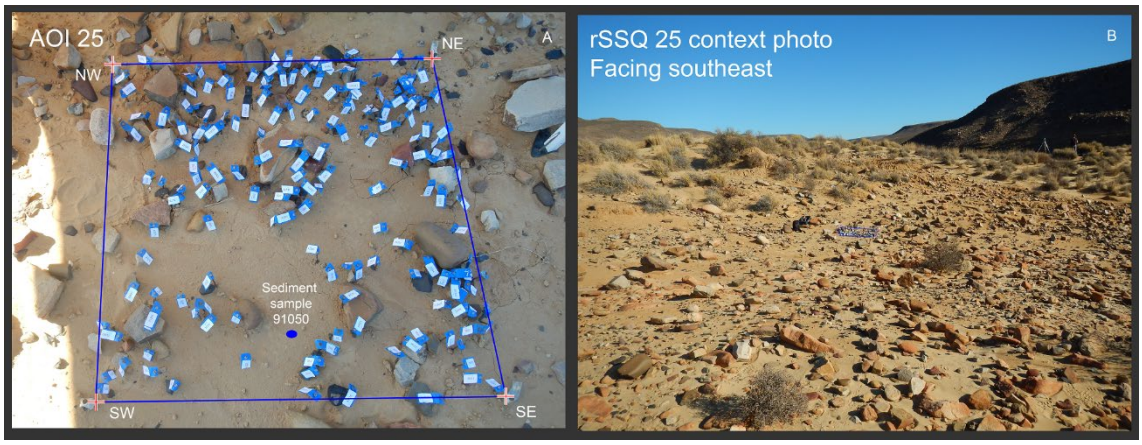

Figure A4.2.20. LRcc sampling location for sediment sample 91050.

The sample square is located close to the transitional zone between calcrete-rich sediment and the heavily colluviated northern hillslope. The surface slopes (declines) from east to west. Although it is generally uniform, the surface of the sample square's south side is slightly more depressed than its north side. Aeolian sand accumulation is also more marked in the north. Most flaked and non-flaked stones cluster in the northern zone of the sample square and vary in size. There is less sandstone float in the sample square compared to the surrounding area. The surface is also sparsely covered by calcrete nodules ranging in size from < 5 mm to 25 mm. Surface sediment is highly consolidated, difficult to excavate with a trowel, with only small fragments excavated at a time.

Sample ID 91050

Equipment	Trowel
Position	Center SW-SE
Photo no.	DSCN 3657
Camera	CoolPix Silver

Munsell Chart Colour (dry)

5/4 and 5/6 on 10YR (yellowish brown)

Grain size

Less than 250 µm. Medium to fine sand. Occasional quartz clast inclusion between 375-500 µm

Grain roundedness

Medium sphericity, subrounded.

Sorting

Well sorted

Consistency

Once broken between fingers, sediment is very fine. Form holds when wet (medium to low). Sandy to sandy loam.

rSSQ 26 – 91049

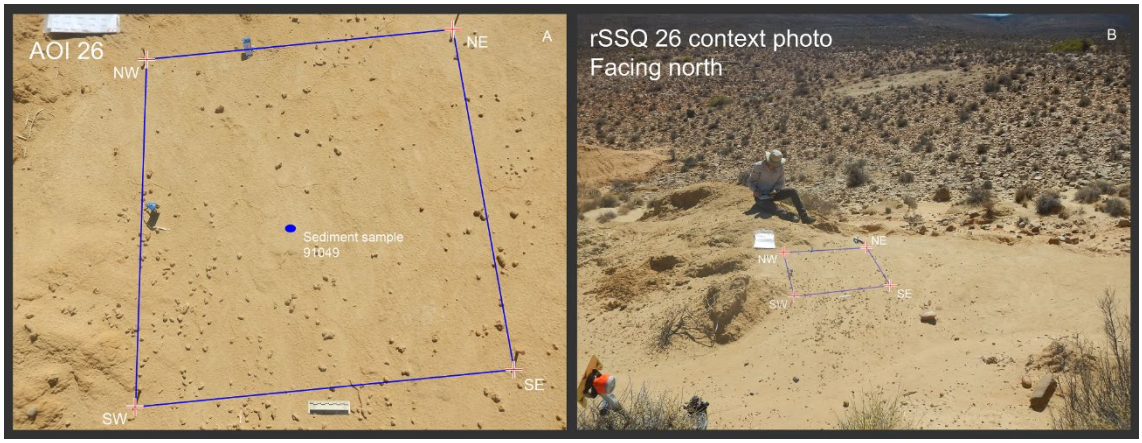

Figure A4.2.21. LRcc sampling location for sediment sample 91049.

Notably lacking in lithic clasts. Only 2 clasts – both artefacts located on extreme margins of the square (western and northern sides). Surface sparsely covered in calcrete nodules – ranging approximately 3-25mm in size. Nodules low sphericity and subangular. Surface very well consolidated. Extremely difficult to excavate with trowel. Crust at least 10mm thick but subsurface remains highly compact. Root casts present.

Sample ID 91049

Equipment Trowel

Position Middle of square

Photo no. DSCN 3574

Camera CoolPix Silver

Munsell Chart Colour (dry)

5/6 10YR

Grain size

Grain size of most clasts less than 250 µm. Quartz inclusions ranging in size between 250-375 µm. Shale inclusions around 375 µm in size.

Grain roundedness

High sphericity, subangular

Sorting

Poorly to moderately sorted

Consistency

Form moderately held when wet. Silty sand.

rSSQ 28 – 91048s28

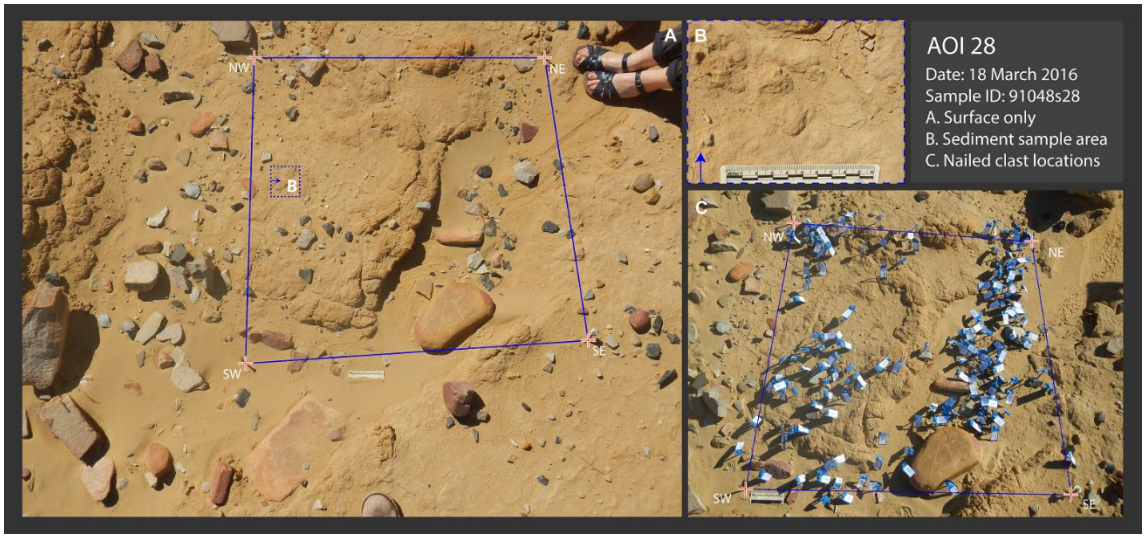

Figure A4.2.22. LRcc sampling location for sediment sample 91048s28**.**

Uneven surface with rill running through south-eastern corner. Majority of artefacts cluster within rill and lower levels of the square. Centre of square effectively devoid of clasts. Small, sparsely scattered calcrete nodules. All nodules are generally <20 mm in size. Calcrete nodules of low sphericity sub angular to sub rounded. Surface outside of rill relatively compact with "desiccation" cracks running throughout. Crust thick and feels concreted – difficult to dislodge with trowel and break between fingers. Thickness at least 15-30 mm. Presence of small number of root casts and fine veining of calcrete filling "desiccation" cracks.

Sample ID 91048s28

Equipment Trowel

Position Middle of western margin

Photo no. DSCN 3568

Camera CoolPix Silver

Munsell Chart Colour (dry)

5/6 10YR (yellowish brown)

Grain size

Less than 250 µm. A few quartz clasts are larger than 250 µm. Small gravel inclusions of about 250 µm.

Grain roundedness

High sphericity – angular to subangular

Sorting

Moderately to well sorted

Consistency

Holds form when wet. Sandy silt.

rSSQ 55 – 91053

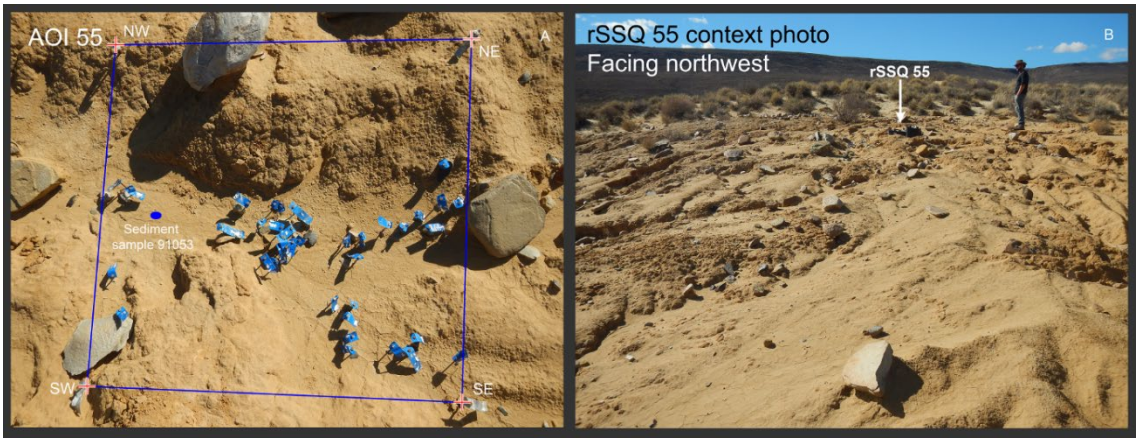

Figure A4.2.23. LRcc sampling location for sediment sample 91053.

Highly concreted – although easier to excavate than previous 2 squares (rSSQ 53 and 28). Surface crust is varied in thickness from about 5-15 mm. Marked lack of vesicles and root casts. Feels relatively sandy and is moderately difficult to break between fingers. Deposit appears to vary in hardness due to uneven distribution of calcareous nodules. Strong surface weathering with higher presence of intact calcrete veining. Deposit feels more like nodular brown sediment of UPK1. Sample taken from edge of rill. Rill slopes from north to south. Calcrete seams and desiccation cracks on surface of surrounding area. Majority of square defined by shallow, moderately incised rill. This rill captures majority of clasts in square except for ID's 32251-3. Extreme range in artefact sizes.

Sample ID 91053

Equipment Trowel

Position Center of western side

Photo no. DSCN 3756

Camera CoolPix Silver

Munsell Chart Colour (dry)

5/6 10YR (yellowish brown)

Grain size

Mostly less than 250 µm with some quartz clasts between 500 and 375 µm

Grain roundedness

Low sphericity - all clasts subangular

Sorting

Well sorted

Consistency

Once broken between fingers feels very sandy. Holds form poorly when wet. Sandy with low silt contribution.

rSSQ 56 – 91054

Figure A4.2.24. LRcc sampling location for sediment sample 91054.

Surface is topographically variable with a rill sloping NE to SW along eastern side of square. Covered in dried vegetation debris. Varied distribution of many calcrete nodules eroded out of desiccated yet semi-intact deposit on either side of rill – predominantly the western side of square. Base of rill has fine veneer of aeolian sand, with a washed surface defined by moderate to fine desiccation cracks. This contrasts with the nodular, concreted sediment of the semi-intact deposit to the west of the rill. Calcrete nodules are generally less than 30 mm in dimension (ranging from large pebbles to granules). Nodules low in sphericity and subangular. Of the eight lithics recorded in square four are in base of rill while four are located in the side of the rill. Two of the larger clasts are partially buried within side of rill – below semi-intact deposit.

Sediment sample was collected from just north of square centre. Sediment surface had a firm upper layer of variable hardness, although it was fairly easy to excavate with a trowel. The crust had a thickness of between 5- and 10-mm. Sediment crust was friable, consisting of vesicles, root casts, and calcrete nodules.

Sample ID 91054

Equipment Trowel

Position Just north of square centre.

Photo no. DSCN 3851 (NE-SE)

Camera CoolPix Silver

Munsell Chart Colour (dry)

5/6 10YR (Yellowish brown)

Grain size

Ranges from less than 100 µm (fine sands) to 500.

Grain roundedness

Larger clasts (quartz and shale) are of low sphericity – angular to subangular. Smaller grains are moderately rounded to subangular

Sorting

Poorly sorted

Consistency

Sandy

rSSQ 57 – 91055 (Heuweltjie?)

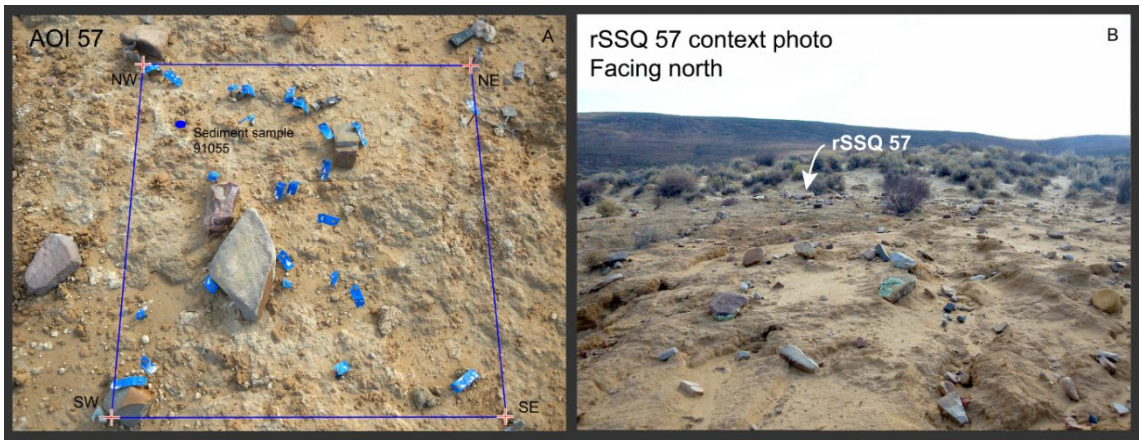

Figure A4.2.25. LRcc sampling location for sediment sample 91055.

Surface fairly level with no notable rilling. Located above major rill system and below current aeolian dune. At the northern margin of exposure. Minimal vegetation. Highly nodular calcrete surface - with concreted sediment nodules and calcareous nodules ranging in size from 35mm or less. Nodules appear moderate to high in sphericity and sub rounded. Prominent calcrete veining throughout surface – suggestive of an in-situ surface architecture. Chalky in nature. Clasts relatively evenly distributed throughout square (albeit with a slight central bias) and of a range of sizes and material. Clasts loosely dispersed over surface with little evidence of burial or pedestaling.

Surface extremely well consolidated and difficult to excavate. Highly heterogenous surface – especially in contrast between calcrete veining and more typically nodulated calcrete. Difficult to break between fingers. Looks similar to the heuweltjie sediments down slope and in the colluvium. This includes the presence of a rugose biocrust (cyanobacteria) indicative of semi-arid conditions and a surface that is moderately resistant to wind and water erosion (Rosentreter *et al.* 2007; Tamm *et al.* 2018). Cyanobacteria was observed on heuweltjies in the area and not in other rSSQ located on LR and LRcc surfaces.

Sample ID 91055

Equipment Trowel and hammer.

Position From north-western corner of square

Photo no. DSCN 3852

Camera CoolPix Silver

Munsell Chart Colour (dry)

5/6 10YR (yellowish brown)

Grain size

Less than 500 µm. Coarse to medium sand and finer.

Grain roundedness

Moderate to low sphericity, angular to sub-rounded.

Sorting

Moderately sorted

Consistency

Sandy. Holds form poorly when wet. Unsure if this is representative of deposit as a whole.

rSSQ 59 – 91057

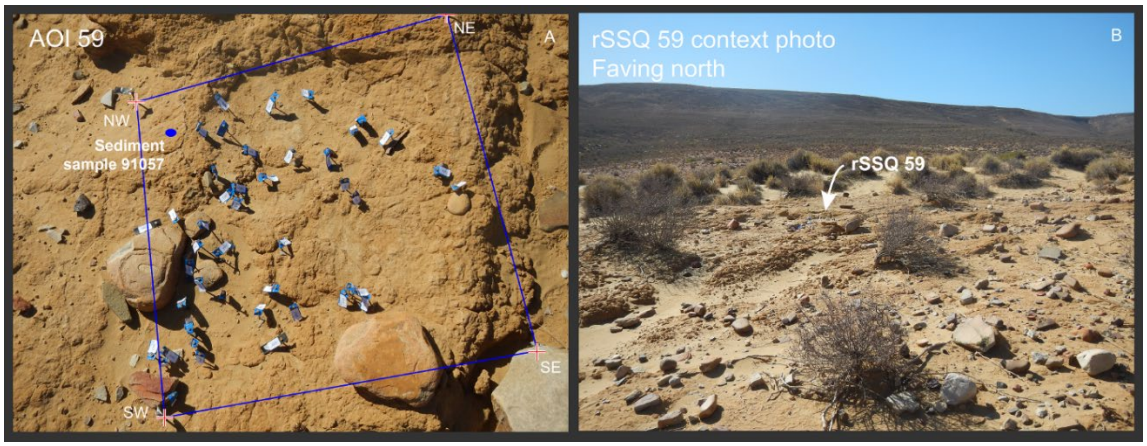

Figure A4.2.26. LRcc sampling location for sediment sample 91057.

Surface highly concreted – very difficult to excavate with only trowel. Uneven topography. Mostly devoid of vegetation, although root system and vegetation present in uphill/northeast of square (same deposit). No aeolian sand present in square. Eroded, desiccated deposit with dense veining of calcrete - although veining finer than that observed in rSSQ 57. However, like 57, this square is located well upslope of washed, rilled exposure and downslope/south of modern, vegetated dune. Clasts relatively evenly spaced within northern half of square, tending towards southwestern depression within southern half of square. Shallow, narrow rill to east of square, touching on south-eastern corner. Evidence of recent decay/breakage of clasts.

Sample ID 91057

Equipment Trowel and hammer

Position North-west corner of square

Photo no. DSCN 3854 (SE-SW)

Camera CoolPix Silver

Munsell Chart Colour (dry)

6/6 10YR (Brownish yellow)

Grain size

750 µm and below – mostly medium to fine sand around 250 µm.

Grain roundedness

Moderate to high sphericity – sub-rounded.

Sorting

Moderately sorted

Consistency

Holds form poorly when wet. Granules coated in white powdery substance.

rSSQ 64 – 91058

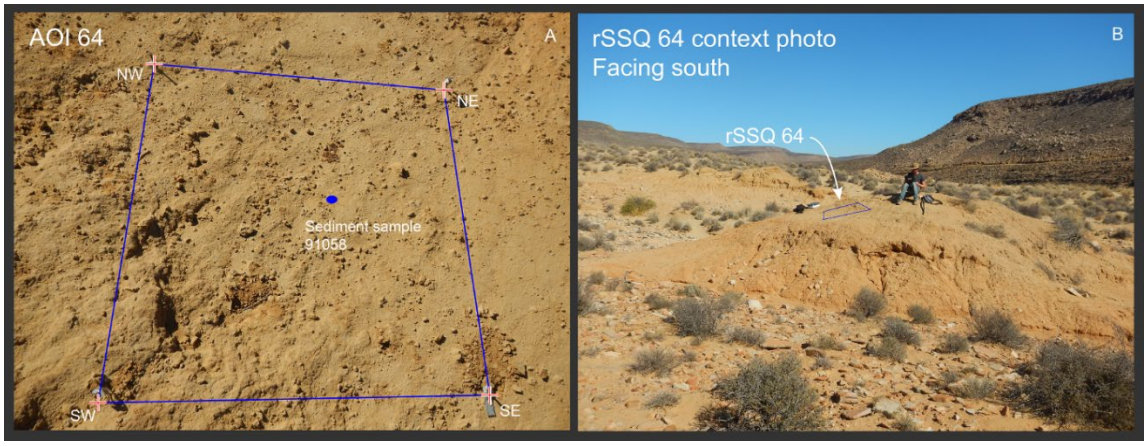

Figure A4.2.27. LR(cc?) sampling location for sediment sample 91058.

Square located towards top of moderately steep slope on the north-eastern side of a residual sediment island, north of the main colluvial stack. Square slopes downward from southwestern corner by approximately 40 degrees. It is devoid of artefact clasts >10mm in diameter. Surface is covered by a fine scatter of very small milky and crystal quartz and quartzite fragments and complete flakes <10 mm in diameter. Surface also consists of numerous calcrete nodules that range in size from 50 mm to less than 5 mm (granules). Nodules are of low sphericity and angular. This surface has an unclear unit association. It could be UY overlying LR or rhizolith-rich LR with calcrete nodules being a possible rhizolith remnant of vegetation. Smaller stone pebbles (<10mm) cover the surface with moderate to high sphericity and sub-angular to sub-rounded. The surface is fairly uniform despite slope. The mound's surface directly down slope of the sample square yields a denser band of both flaked and nonflaked lithics (mostly nonflaked, quartzite). Lithics measure an average maximum dimension of 20 to 50 mm. It is unclear if these lithics are from the top of the mound or eroding out from it.

Sample ID 91058

Equipment	Trowel
Position	Slightly off centre towards northeast corner
Photo no.	DSCN 3860-63
Camera	CoolPix Silver

Munsell Chart Colour (dry)

6/6 10YR (brownish yellow)

Grain size

500 µm or less although mostly between 100-250 µm

Grain roundedness

Moderate to high sphericity – sub-rounded

Sorting

Well sorted

Consistency

Easy to break between fingers. Holds form, but poorly when wet. Sandy with slight silt.

rSSQ 94 – 91149

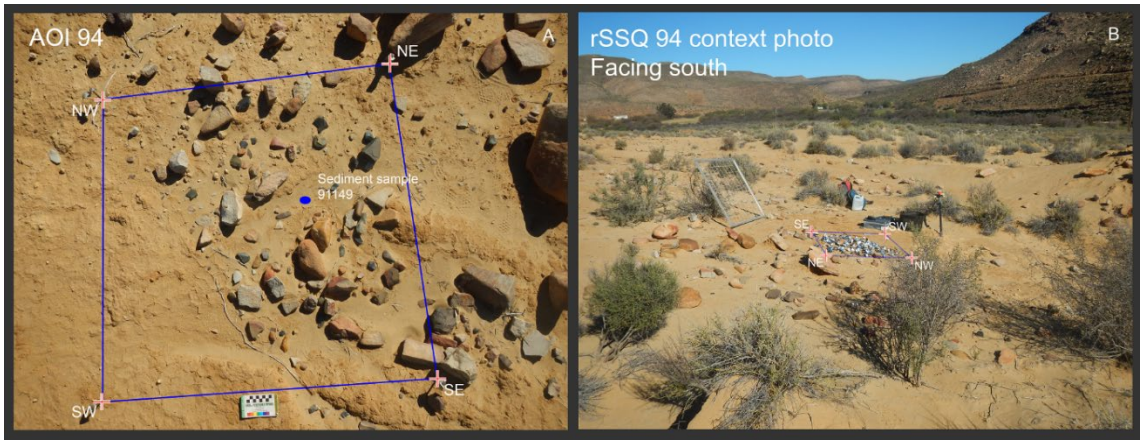

Figure A4.2.28. LRcc sampling location for sediment sample 91149.

Sample square encompasses the calcrete-veined sediment surface and is located on a slope of 10 degrees. Parts of the sample square surface are covered by a fine veneer of sand. North-east of the square is aeolian sand dune. South-east of the sample square is a continuation of the same calcrete-veined surface, with a continuous band of archaeology and non-flaked stone quartzite blocks. South-west of the square is the juncture between the calcrete-veined surface and what appears to be a younger indurated sand deposit. The sandstone and archaeological remains appear adhered to the surface, as opposed to buried. Fairly consistent surface morphology - very homogeneous in terms of topography within the square. Just north of a rill. Archaeology: the square encompasses dense distribution of archaeology across ¾ of the square, dropping off in number towards the south-east corner. Clast size generally ranges from about 150 to above 5 mm. Although calcrete nodules are present, they are sparse and loosely dispersed across the square, ranging in size from 30 to 10 mm with moderate sphericity – being mostly sub-angular. Calcrete nodules increase in number and size towards the north-west corner. Under the veneer of sand, the surface consists of moderate to fine desiccation cracks with small number of fine roots running across. Surface is very firm. Crust is about 5 to 10 mm in thickness - highly indurated with quite a few roots and not easy to break between fingers.

Sample ID 91149

Equipment Trowel

Position Centre of the square (slightly over to the east)

Photo no. DSCN 4933 (sunlight)

Camera CoolPix Silver

Munsell Chart Colour

5/6 in 10YR (yellow to brown)

Grain size

Mostly round, equal to less than 250 µm; couple of quartz clast at 375 µm

Grain roundedness

Moderate to high sphericity; sub-rounded

Sorting

Well to moderately sorted

Consistency

Sandy silt. Form holds when wet: moderate to high.

Reaction to 20% HCl: sediment itself does not react despite its indurated quality; surface nodules react (calcrete). Sediment from the sample square is just above a very calcified sediment.

4.2.6 Heuweltjie

rSSQ 23 – 91046

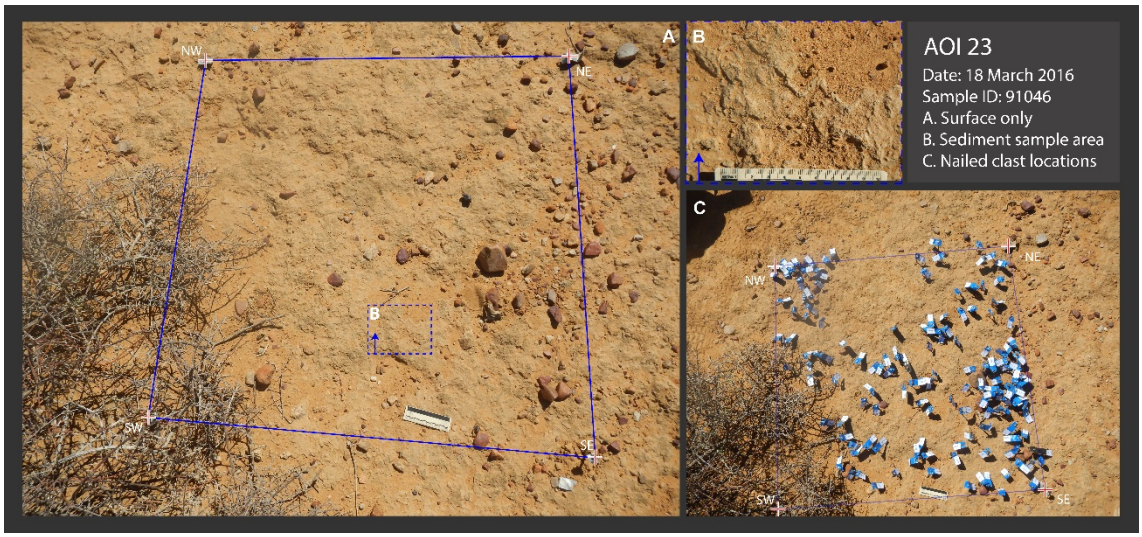

Figure A4.2.29. Heuweltjie/LRcc sampling location for sediment sample 91046.

Surface on a slight slope, declining in a southward direction. Vegetation obscuring the southwest corner. Varying sizes of surface clasts – ranging in size from 50mm to less than 10mm. Clasts sparsely distributed, although clustered along the eastern border. Appear winnowed. Sediment forms a thin crust of about 5-7 mm in thickness on surface – easily broken up by a trowel and into finer sediment under pressure from fingers. Fine sediment feels silty. Calcareous nodules about 20 mm in size throughout sample with root holes throughout. Patches of rugose biocrust (cyanobacteria) cover surface—indicative of semi-arid conditions and a surface that is moderately resistant to wind and water erosion (Rosentreter *et al.* 2007; Tamm *et al.* 2018).

Sample ID 91046

Equipment Trowel

Position Within the southern half, halfway between SW and SE corners.

Photo no. DSCN 3528

Camera CoolPix Silver

Munsell Chart Colour (dry)

10YR 6/4

Grain size

250 µm or less. Mostly 100 µm with quartz clasts sparsely interspersed throughout ranging in size between 250 and 750 µm.

Grain roundedness

High sphericity, sub angular

Sorting

Moderately sorted

Consistency

Clumps slightly when wet; Fine with a slight grit.

rSSQ 24 – 91048

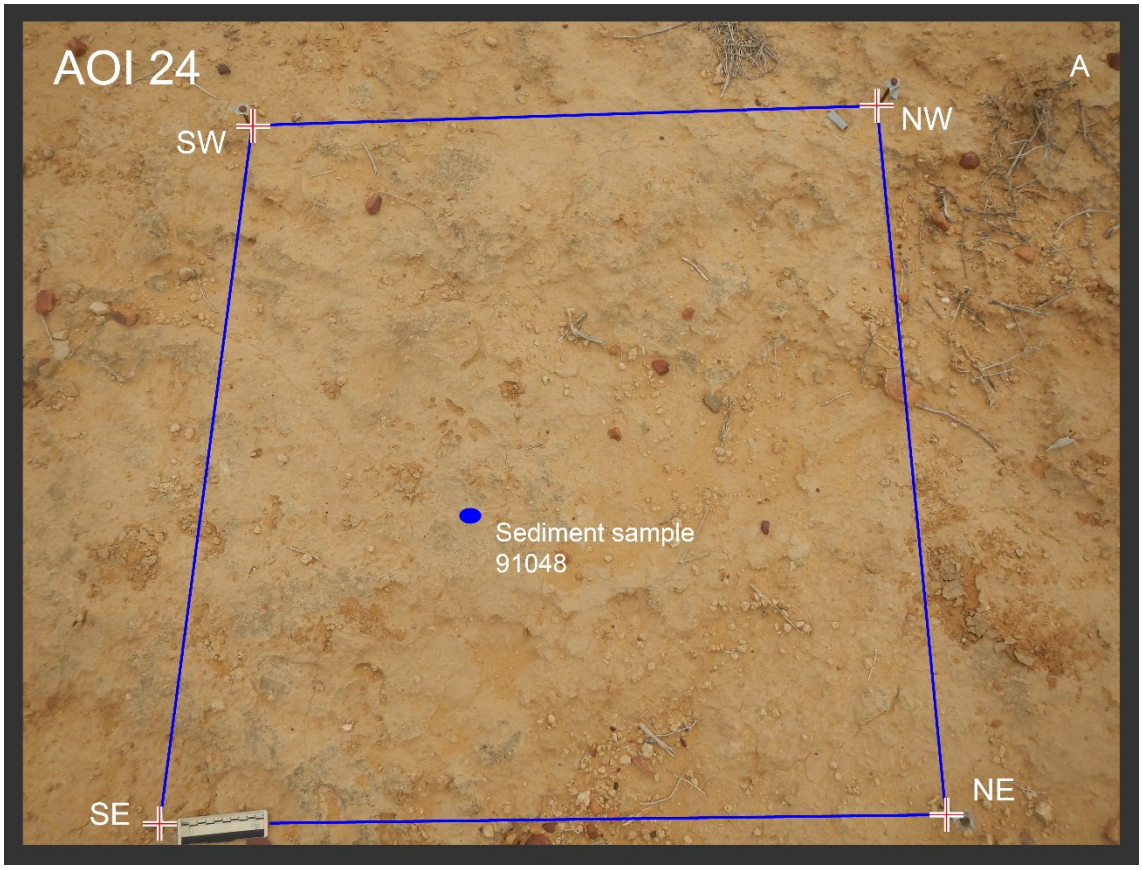

Figure A4.2.30. LR sampling location for sediment sample 91048.

Similar to rSSQ 27. No vegetation or rills. Slightly uneven surface with a general SW downward cant. Deposit potentially less eroded than rSSQ 27 and less *in situ* calcrete observed on surface. Calcrete nodules (25 - <50 mm) scattered across surface. General lithic clasts range in size from 70 to <10 mm and are very sparsely distributed across square. General eastern bias to clasts with a small cluster on SE edge. Crust thickness of about 10-15 mm. Fine roots still present within crust. Crust is easily crushed into a fine sediment between fingers. Surface is covered by patches of rugose biocrust (cyanobacteria) indicative of semi-arid conditions and a surface that is moderately resistant to wind and water erosion (Rosentreter *et al.* 2007; Tamm *et al.* 2018)

Sample ID 91048

Equipment	Trowel
Position	Slightly SE of centre
Photo no.	DSCN 3540
Camera	CoolPix Silver

Munsell Chart Colour (dry)

10YR 6/4 to 6/6

Grain size

< 250 µm. Larger quartz inclusions (375 -750 µm). Clasts of calcrete about 750 µm.

Grain roundedness

High sphericity, subrounded

Sorting

Moderately sorted

Consistency

Sandy laom with slight holding of form when wet

rSSQ 27 – 91047

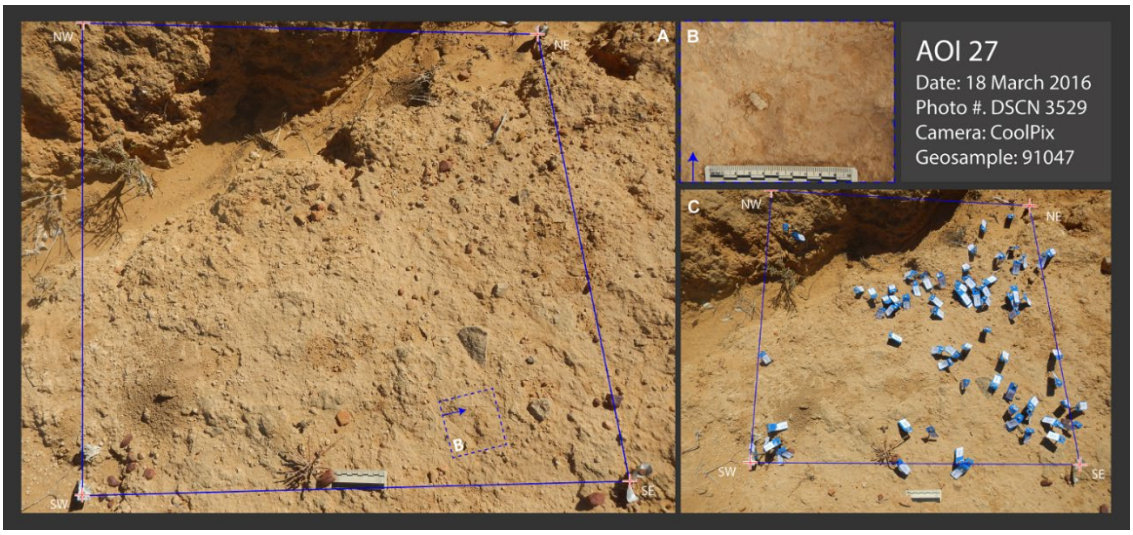

Figure A4.2.31. LR sampling location for sediment sample 91047.

Surface is similar to rSSQ 23. Rill running through northern side of square from NE to NW. Deposit surface is rough with nodules of calcrete. Nodules are larger and more developed along the edge of rill. Surface speckled with small vegetation that does not inhibit visibility. In addition to calcrete nodules (about 5 to 10 mm, sub rounded) surface clasts range in size from about 60 mm to less than 5 mm. Mostly quartzite (completely cortical), many are decayed (highly weathered), angular to subrounded. Sparsely distributed throughout square, clustering along rill edge. Sparse patches of rugose biocrust (cyanobacteria) across surrounding surface—beyond rSSQ—which is indicative of semi-arid conditions and a surface that is moderately resistant to wind and water erosion (Rosentreter *et al.* 2007; Tamm *et al.* 2018)

Sample ID 91047

Equipment	Trowel
Position	Within the SE corner
Photo no.	DSCN 3529
Camera	CoolPix Silver

Munsell Chart Colour (dry)

10YR 5/6 (yellowish brown)

Grain size

250 µm or less than with quartz inclusions (500 – 2000 µm)

Grain roundedness

Quartz inclusion high sphericity, subangular

Sorting

Well to moderate

Consistency

Does not hold form when wet and rolled; sandy with slight silt.

4.2.7 Colluvium

rSSQ 62 – 91059

Figure A4.2.32. Colluvium sampling location for sediment sample 91059.

Located on the colluvial hillslope (northernmost UPK7). The surface of rSSQ 62 is poorly sorted. Its surface consists of many angular sandstone cobbles haphazardly oriented across. Many clasts are partially buried beneath loose sand, within a consolidated sediment. Most sandstone blocks are large to very large in size. Square includes a few large cores (>100 mm). Smaller clasts are primarily composed of nonflaked stone, although a few artefacts (quartzite, hornfels) were found distributed throughout square. Minor occurrences of vegetation within square. Consists mostly of colluvium (large clasts, cobble sized), which made sample extraction difficult. Sediment underlying loose sand is well consolidated and crusted. Clasts include hornfels flakes between 10-15 mm in maximum dimension as well as small quartzite clasts of about 5 mm. The latter are highly decayed (weathered).

Sample ID 91059

Equipment	Trowel
Position	Centre
Photo no.	DSCN 3879, 3881
Camera	CoolPix Silver

Munsell Chart Colour (dry)

6/4 10YR (surface), 5/6 7.5YR (substrate).

Grain size

Less than 750 µm, greater than 250 µm on average (substrate). Less than 500 µm in size, down to about 100 µm (surface). All quartz grain with some gravel contribution (surface).

Grain roundedness

Moderate to low sphericity, sub-rounded (substrate). Moderate sphericity, angular to sub-angular

(surface).

Sorting

Well sorted (substrate). Poorly sorted (surface).

Consistency

Form holds when wet: moderate to high. Sandy with potential (high) clay contribution (substrate). Sandy (surface).

rSSQ 91 – 91151

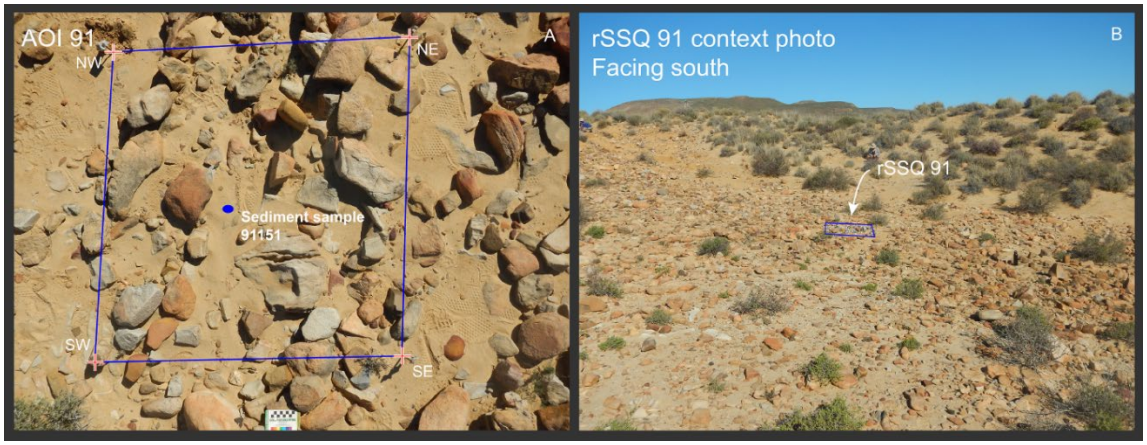

Figure A4.2.33. Colluvium sampling location for sediment sample 91051.

Situated in the colluvium, close to the sand mantle. Clast distribution is not as dense as rSSQ 92. Generally larger clasts. No vegetation inside the square. More stone artefacts than rSSQ 92, but that might be due to visibility as a result of sand veneer. Thicker cover of aeolian sand distributed across the square compared to rSSQ 92. Fairly large outcrop-sandstone contrasting against the size of the archaeological artefacts. Clast size ranges from 10 mm to 300 mm. The sample square slopes towards the magnetic west. More imbrication than in rSSQ 92. Artefacts buried underneath sand veneer. Very heterogeneous surface. Very hard and indurated in some places, firm in others, and softer in some. The sediment consists of small to large air pockets—versicular.

Sample ID 91151

Equipment Trowel

Position Centre of the square

Photo no. DSCN 5006 (sunlight, geosurface), DSCN 5007 (sunlight; top layer removed)

Camera CoolPix Silver

Munsell Chart Colour (dry)

5/4 on the 10YR (yellowish brown)

Grain size

From <100 µm to ≤500 µm

Grain roundedness

Moderate to high sphericity; subangular

Sorting

Moderately to poorly sorted

Consistency

Quartz has a fine coating of peds. Holds form well and contains clay; sandy clay

rSSQ 92 – 91152

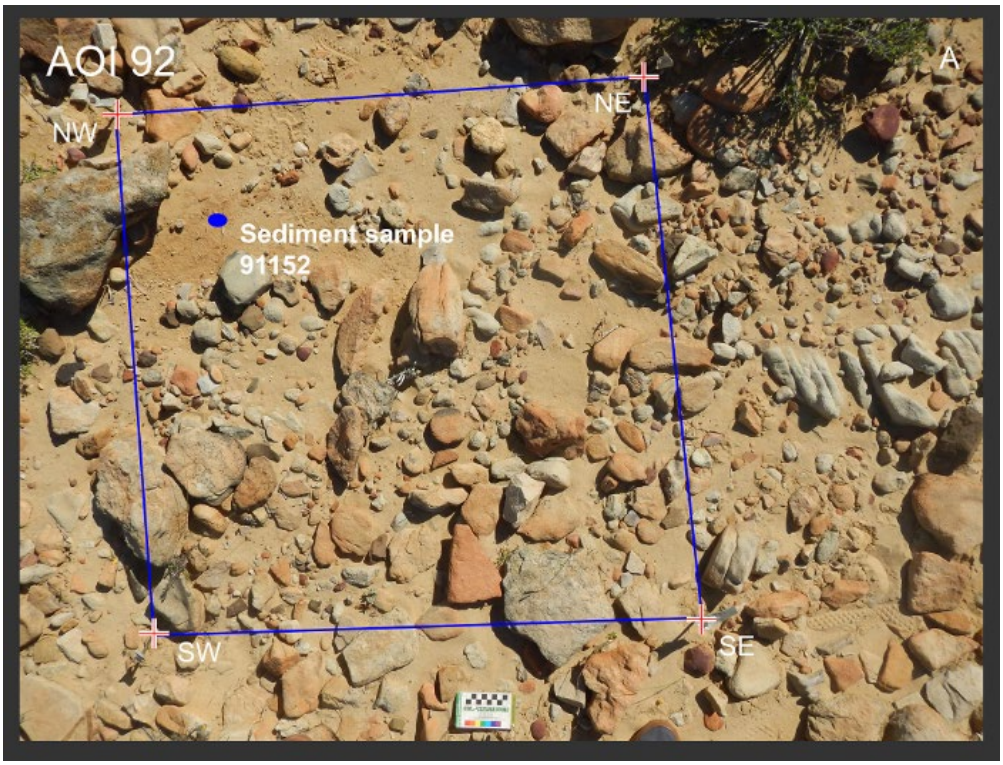

Figure A4.2.34. Colluvium sampling location for sediment sample 91052.

Dense colluvial square. North of the sand dune and archaeological drape (younger, calcrete sediments). Situated on top of and just below outcropping sandstone bedrock (light grey). Dense distribution of clasts, mostly weathered sandstones, that are angular to sub-angular and of low sphericity. Clast size ranges from less than 5 mm up to more than 200 mm. The sample square includes a few artefacts (cores and flakes). Veneer of sand covering more compacted sediment that has desiccation cracks in the surface crust (not well developed). Not much imbrication. The sample square is sloping towards the magnetic west. Similar vegetation coverage in surrounding area as the sand mantle. However, these are a different species.

Sample ID 91152

Equipment	Trowel
Position	North-west of square
Photo no.	(DSCN): 5004 (sunlight, geo surface with sand vaneer); 5005 (sunlight)
Camera	CoolPix Silver

Munsell Chart Colour (dry)

Colour is not homogeneous

From 7.5 YR 7/6 (reddish yellow) to 10 YR 5/6 (yellowish brown)

Grain size

Ranges from 150 µm to less than 100 µm

Grain roundedness

High to moderate sphericity, subrounded

Sorting

Very poorly sorted

Consistency

Form holds when wet (very high).

4.2.8 Summary of frequency of rSSQ with calcium carbonate inclusions and/or features

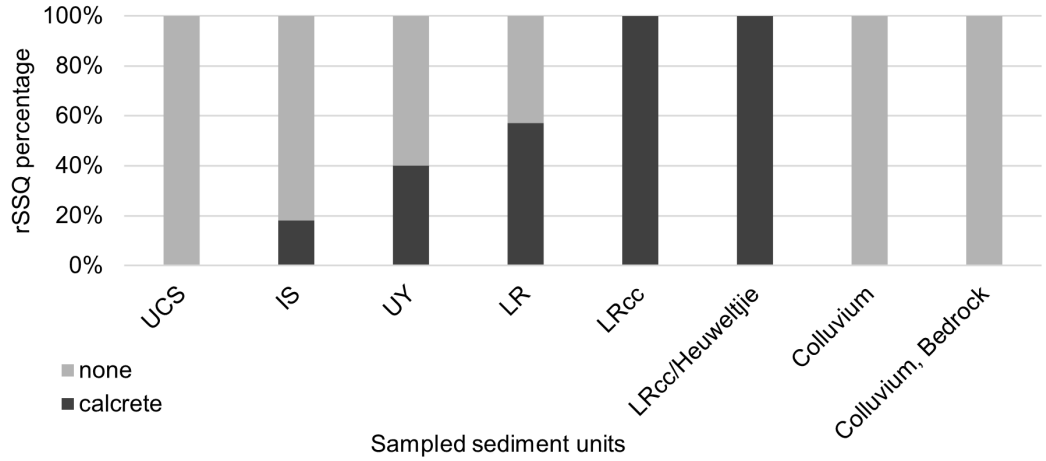

Figure A4.2.35. Frequency of rSSQ with calcium carbonate inclusions and/or features by sediment unit

Table A4.2.1. rSSQ summary tables showing the rSSQ frequency of different surface characteristics by sediment unit:(A) as percentages, and (B) as bar graphs

A

	stony	gravelly	sandy	smooth	cracked	scat	mound	roots	debris	rill	donga	imbricated clasts	precipitates	crusted	vesicles
Unit	%	%	%	%	%	%	%	%	%	%	%	%	%	%	%
UCS															
IS															
UY															
LR															
LRcc															
LRcc/Heuweltjie															
Colluvium															
Colluvium, Bedrock															
All															

B

	stony	gravelly	sandy	smooth	cracked	scat	mound	roots	debris	rill	donga	imbricated clasts	precipitates	crusted	vesicles
Unit	%	%	%	%	%	%	%	%	%	%	%	%	%	%	%
UCS	0%	0%	37%	0%	0%	100%	36%	25%	30%	0%	0%	0%	0%	0%	0%
IS	0%	0%	26%	33%	0%	0%	36%	25%	15%	25%	100%	0%	50%	30%	11%
UY	0%	0%	0%	17%	0%	0%	9%	0%	10%	8%	0%	20%	0%	10%	11%
LR	13%	40%	5%	17%	14%	0%	9%	13%	15%	25%	0%	20%	50%	20%	0%
LRcc	25%	20%	16%	28%	71%	0%	0%	25%	10%	33%	0%	20%	0%	25%	44%
LRcc/Heuweltjie	25%	40%	0%	6%	0%	0%	9%	13%	5%	8%	0%	0%	0%	10%	22%
Colluvium	25%	0%	11%	0%	0%	0%	0%	0%	10%	0%	0%	20%	0%	0%	11%
Colluvium, Bedrock	13%	0%	5%	0%	14%	0%	0%	0%	5%	0%	0%	20%	0%	5%	0%
All	100%	100%	100%	100%	100%	100%	100%	100%	100%	100%	100%	100%	100%	100%	100%

4.3 Grain Size Results

Table A4.3.1. Results of particle size analysis on sediment samples collected from the river and modern terrace and across the sand mantle of UPK7**.**

Unit	Sample	Context	Distance from river (m)	Clay	Silt	Sand	Vol. wt mean (μm)	Mode (μm)			Sorting	Texture
	Field ID | Lab ID			< 4 μm (%)	4-63 μm (%)	63-2000 μm (%)		1	2	3	phi (Φ, Std Dev)	Class*
Alluvium	91084	River channel	16	2.70	4.92	92.4	559	587	80.6	10.9	1.21	Sand
	91085	Terrace	40	1.22	4.46	94.3	374	419	0	0	1.03	Sand
Unconsolidated Sand	91086	South Slope	127	0.00	0.00	100	417	396	0	0	0.58	Sand
	91068	North of Exposure 2	271	1.46	2.49	96.1	203	199	21.4	0	0.68	Sand
	91067	Exposure 1a: far west	NA	1.56	3.04	95.4	338	348	0	0	0.86	Sand
Semi-consolidated sand	91066	West of WT	166	2.49	5.27	92.2	265	286	4.15	8.01	1.20	Sand
	91065	West of WT	167	2.38	3.96	93.7	240	236	3.67	16.7	1.14	Sand
	91069	South of Exposure 2	270	1.03	1.02	97.9	346	337	0	0	0.50	Sand
Indurated Sand	91077	SC1 | 0.1	170	5.41	8.07	86.5	189	196	4.03	0	1.54	Sand

	91078	SC1 | 0.6	170	8.29	13.2	78.5	154	185	5.13	0	2.10	Loamy sand
	91079	SC1 | 1.1	170	6.42	11.7	81.9	140	146	4.40	0	1.53	Loamy sand
	91072	SC1 | 1.7	170	5.52	8.85	85.6	224	248	3.26	0	1.71	Sand to loamy sand
	91073	SC1 | 2.2	170	7.09	9.34	83.6	225	271	3.71	0	1.81	Loamy sand
Upper Yellow	91080 | UOW-2006	OC9 | 0.22	215	6.24	42.0	51.8	119	194	19.1	0	2.20	Loam
	90024 | UOW-1804	OC5 | 0.31	249	4.48	27.2	68.3	125	155	14.3	0	1.98	Sandy loam
	90016 | UOW-1801	OC10 | 0.34	268	4.55	23.9	71.6	157	191	14.8	0	2.10	Sandy loam
Lower Red	91157 | UOW-2014	OC2 | 0.23	217	7.29	35.7	57.0	95.2	145	10.4	0	2.12	Sandy loam
	91155 | UOW-2013	OC1L | 0.60	218	3.99	33.1	62.9	131	179	16.9	0	2.04	Sandy loam
	91153 | UOW-2012	OC1U | 0.35	127	3.29	19.1	77.6	156	179	14.3	0	1.86	Sandy loam to loamy sand
	91070	Exposure 6: Top of residual mound	222	7.17	23.3	69.5	140	176	18.2	0	2.14	Loamy sand
Lower Red with $CaCO_3$	91074	SC1 | 2.7	170	7.59	10.7	81.8	234	308	3.68	0	1.96	Loamy sand

91075	SC1 | 3.2	170	4.25	6.13	89.6	205	208	4.09	21.9	1.42	Sand
91076	SC1 | 3.5	170	11.2	16.6	72.2	160	170	4.29	0	2.56	Sandy loam
90020 | UOW-1802	OC3 | 0.31	214	3.71	19.2	77.1	149	154	12.9	0	1.75	Loamy sand
90018 | UOW-1800	OC11 | 0.33	227	1.86	16.9	81.2	153	158	16.9	0	1.37	Loamy sand
90022 | UOW-1803	OC4 | 0.23	238	4.07	34.6	61.3	137	187	23.1	0	2.00	Sandy loam
90026 | UOW-1832	OC6 | 0.26	230	3.70	32.1	64.2	131	169	23.3	0	1.88	Sandy loam
90028 | UOW-1833	OC7 | 0.22	221	4.34	37.5	58.1	118	167	18.8	0	2.01	Sandy loam
90030 | UOW-1834	OC8 | 0.20	211	3.04	25.4	71.5	140	166	16.3	0	1.89	Loamy sand

Samples are grouped by sediment unit and within each are ordered by Euclidean distance from river channel. In the case of section cut 1 (SC1), samples are ordered by depth below surface (bls), listed under 'context'. *Context abbreviations: OC = OSL cut, SC = Section Cut. context values listed after ' | ' give depth below surface, in meters. *Source: FAO (1990) in Jahn *et al.* (2006).

4.4 XRD Results

Table A4.4.1. Results of XRD analysis on sediment samples collected from the river and modern terrace and across the sand mantle of UPK7 (grouped)

Unit	Sample ID | Lab ID	Context*	Distance from river (m)	Mineralogy					
				Q	F	Ca	Cl	Iron carbonate	Iron oxides
Channel alluvium	91084	River channel	16	91.7	4.90	0.30	1.80	0.20	1.00
Modern terrace alluvium	91085	Modern terrace	40	91.6	4.90	0.30	2.60	0.20	0.50
Unconsolidated sand (UCS)	91086	South slope	127	96.0	2.70	0.00	1.20	0.10	0.00
	91067	Exposure 1a	NA	85.9	8.90	0.00	4.20	0.40	0.70
	91068	North of Exposure 2	271	80.3	15.5	0.00	2.20	0.20	0.80
Semi-consolidated sand (SCS)	91066	West of western tributary	166	86.5	11.9	0.00	1.50	0.00	0.20
	91065	West of western tributary	167	82.3	12.3	0.00	4.80	0.10	0.50
	91069	South of Exposure 2	270	89.8	8.80	0.00	1.10	0.30	0.00
Indurated sand (IS)	91077	SC1 | 0.1	170	81.1	13.2	0.20	4.80	0.30	0.40
	91078	SC1 | 0.6	170	74.0	21.4	0.00	3.80	0.20	0.50
	91079	SC1 | 1.1	170	67.5	28.5	0.00	3.50	0.40	0.10
	91072	SC1 | 1.7	170	80.9	14.8	0.00	3.00	0.40	0.80
	91073	SC1 | 2.2	170	81.3	13.6	0.20	4.40	0.30	0.20
	90020 | UOW-1802	OC3 | 0.31	214	76.1	21.5	0.00	1.70	0.30	0.30
Upper Yellow	91080 | UOW-2006	OC9 | 0.22	215	72.0	18.2	0.00	7.80	0.60	1.10
	90024 | UOW-1804	OC5 | 0.31	249	72.7	24.0	0.00	1.70	0.10	0.50
	90016 | UOW-1801	OC10 | 0.34	268	79.6	15.5	0.00	4.10	0.30	0.50

Lower Red	91157 | UOW-2014	OC2 | 0.23	217	72.5	20.9	0.00	5.30	0.40	0.90
	91155 | UOW-2013	OC1L | 0.60	218	84.1	9.60	0.00	5.30	0.30	0.80
	91153 | UOW-2012	OC1U | 0.35	219	86.0	9.90	0.00	3.40	0.10	0.50
	91070	Top of residual mound (Exposure 6)	222	81.6	12.0	0.00	5.40	0.40	0.60
	91062	Top of residual mound (Exposure 6)	225	84.2	12.6	0.00	2.80	0.20	0.20
	90022 | UOW-1803	OC4 | 0.23	249	77.2	15.6	0.10	5.70	0.50	1.00
Lower Red with CaCO3 (LRcc)	91074	SC1 | 2.7	170	74.4	18.6	0.10	3.70	0.60	2.70
	91075	SC1 | 3.2	170	76.8	17.7	0.00	4.50	0.40	0.70
	91076	SC1 | 3.5	170	72.3	22.0	0.00	4.70	0.30	0.80
	90030 | UOW-1834	OC8 | 0.20	211	76.8	17.6	0.00	4.30	0.60	0.60
	90028 | UOW-1833	OC7 | 0.22	221	69.4	19.8	3.50	5.70	0.40	1.20
	90018 | UOW-1800	OC11 | 0.33	227	78.1	18.2	0.50	2.80	0.10	0.30
	90026 | UOW-1832	OC6 | 0.26	230	81.0	13.5	0.00	4.40	0.30	0.70
Colluvium	91064	Base of mound (Exposure 6)	223	73.8	17.2	0.00	7.50	0.70	0.80

Samples are grouped by sediment unit and within each are ordered by Euclidean distance from river channel. In the case of section cut 1 (SC1), samples are ordered by depth below surface (bls), listed under 'context'. Mineral abbreviations used: Q = Quartz, Ca = carbonates, Cl = clay minerals, F = feldspars, Ch = Chlorite. Groups include: 'Feldspar' = labradorite, orthoclase, microcline, 'Carbonates' = calcite, dolomite, 'Clay minerals' = kaolinite, illite, and chlorite 'Iron carbonate' = siderite, 'Iron oxides' = hematite, goethite. *Context abbreviations: OC = OSL cut, SC = Section Cut. context values listed after ' | ' give depth below surface in meters.

Table A4.4.2. Results of XRD analysis on sediment samples collected from the river and modern terrace and across the sand mantle of UPK7

Sediment unit	Sample ID | Lab ID	Context*	Distance from river (m)	Q	Na-Feldspar		K-Feldspars		Carbonates (Ca)		Clay minerals (Cl)			Iron carbonate	Iron oxides	
					A	L	O	M	Ca	D	K	I	Ch	S	H	G
Channel alluvium	91084	River channel	16	91.7	1.20	0.50		3.20	0.30		0.20	0.60	1.00	0.20		1.00
Modern terrace alluvium	91085	Modern terrace	40	91.6	0.70	2.10	2.10			0.30	1.00	1.60		0.20		0.50
Unconsolidated sand (UCS)	91086	South Slope	127	96.0	2.70							1.20		0.10		
	91067	Exposure 1a	NA	85.9	6.30	0.80		1.80			0.10	3.00	1.10	0.40	0.20	0.50
	91068	North of Exposure 2	271	80.3	9.8	1.1	4.1	0.5			0.30	1.80	1.10	0.20		0.80

Semi-consolidated sand (SCS)	91066	West of WT	166	86.5	11.4		0.5				1.50					0.20
	91065	West of WT	167	82.3	5.5	5.3	1.5			0.90	2.80	1.10	0.10			0.50
	91069	South of Exposure 2	270	89.8	6.30		1.50	1.00		0.20	0.80	0.10	0.30			
Indurated sand (IS)	91077	SC1 | 0.1	170	81.1	13.2				0.2		2.90	1.90	0.30			0.40
	91078	SC1 | 0.6	170	74.0	20.4		1.0			0.10	2.40	1.30	0.20			0.50
	91079	SC1 | 1.1	170	67.5	26.4		2.1			0.40	2.10	1.00	0.40			0.10
	91072	SC1 | 1.7	170	80.9	11.2	0.6	3.0				2.00	1.00	0.40	0.30		0.50

	91073	SC1 | 2.2	170	81.3	12.1		1.5		0.2	0.50	3.20	0.70	0.30		0.20
	90020 | UOW-1802	OC3 | 0.31	214	76.1	16.1		5.4			0.40	1.20	0.10	0.30		0.30
Upper Yellow	91080 | UOW-2006	OC9 | 0.22	215	72.0	13.4	1.2	3.6			0.70	5.30	1.80	0.60	0.10	1.00
	90024 | UOW-1804	OC5 | 0.31	249	72.7	18.1		5.9			0.10	1.30	1.30	0.10		0.50
	90016 | UOW-1801	OC10 | 0.34	268	79.6	12.2	0.3	2.5	0.5		0.20	2.70	1.20	0.30		0.50
Lower Red	91157 | UOW-2014	OC2 | 0.23	217	72.5	12.3	1.7	4.3	2.6		0.60	3.50	1.20	0.40		0.90
	91155 | UOW-2013	OC1L | 0.60	218	84.1	9.30		0.30				4.00	1.30	0.30	0.20	0.60

	91153 | UOW-2012	OC1U | 0.35	219	86.0	6.30	1.30	2.30				2.50	0.90	0.10		0.50
	91070	Top of residual mound (Exposure 6)	222	81.6	10.8		1.2				4.10	1.30	0.40	0.10	0.50
	91062	Top of residual mound (Exposure 6)	225	84.2	9.8		2.8			0.50	1.90	0.40	0.20	0.20	
Lower Red with CaCO3 (LRcc)	91074	SC1 | 2.7	170	74.4	8.9	3.2		6.5	0.1		3.70		0.60		2.70
	91075	SC1 | 3.2	170	76.8	11.0	3.4	3.3				2.40	2.10	0.40		0.70
	91076	SC1 | 3.5	170	72.3	18.1		1.0	2.9		1.50	3.20		0.30	0.20	0.60
	90030 | UOW-1834	OC8 | 0.20	211	76.8	15.7		1.2	0.7		0.30	2.50	1.50	0.60		0.60

	90028 | UOW-1833	OC7 | 0.22	221	69.4	15.6	1.8	2.4	3.5		0.50	3.40	1.80	0.40		1.20
	90018 | UOW-1800	OC11 | 0.33	227	78.1	14.3	3.0	0.9	0.5		0.30	1.70	0.80	0.10		0.30
	90026 | UOW-1832	OC6 | 0.26	230	81.0	12.0	0.6	0.9				3.50	0.90	0.30		0.70
	90022 | UOW-1803	OC4 | 0.23	249	77.2	14.6		1.0		0.1	0.60	3.40	1.70	0.50	0.30	0.70
Colluvium	91064	Base of mound (Exposure 6)	223	73.8	7.4			9.8		0.50	4.30	2.70	0.70	0.20	0.60

Samples are grouped by sediment unit and each sample within a unit is ordered by Euclidean distance from river channel. In the case of section cut 1 (SC1), samples are ordered by depth below surface (bls), listed under 'context'. *Context abbreviations used: OC = OSL Cut, SC = Section Cut. Context values listed after ' | ' give depth below surface in meters. Mineral abbreviations: Q = quartz, A = albite, L = labradorite, O = orthoclase, M = microcline, Ca = calcite, D = dolomite, K = kaolinite, I = illite, Ch = chlorite, S = siderite, H = hematite, G = goethite

4.5 Supplementary Information for Grain Size and Mineralogical Analysis

Analysis of the relationship between stratigraphic level percentage sand and silt (Figure A4.5.1), volume weighted mean and mode 1 (Figure A4.5.2), sorting (phi), percentage quartz, clay, and feldspar (Figure A4.5.3), and mode 1 grains (Figure A4.5.4).

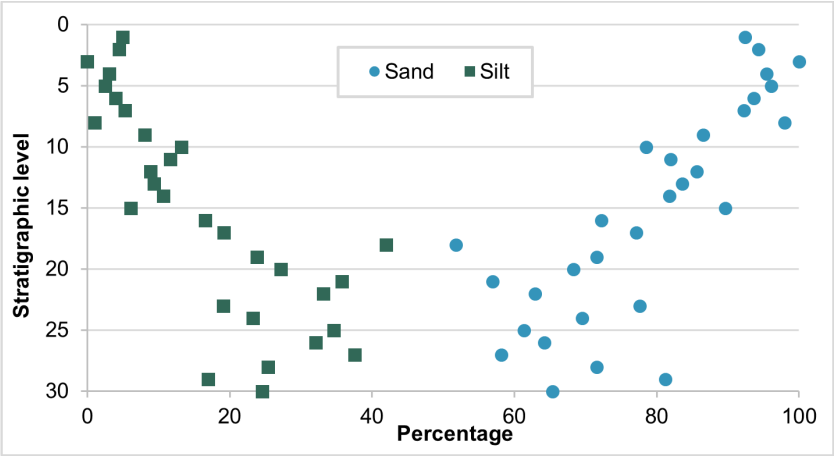

Figure A4.5.1. Scatter plot of the percentages of sand (blue circles) and silt (green squares) plotted as a function of stratigraphic level.

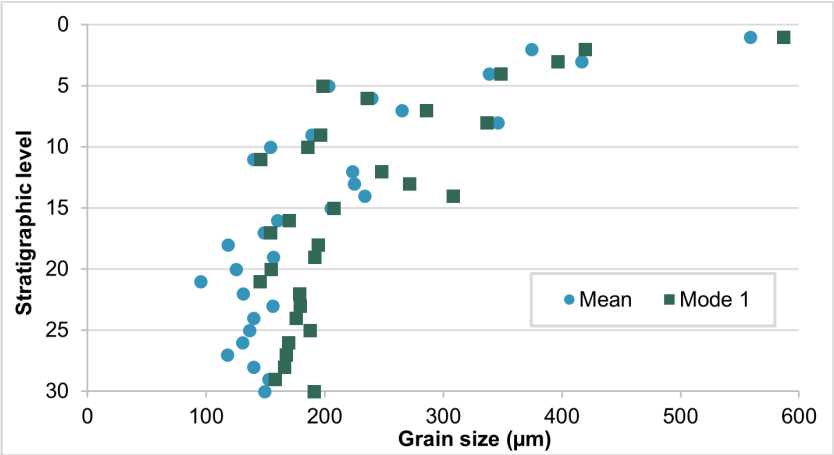

Figure A4.5.2. Scatter plot of mean (blue circles) and mode 1 (green squares) grain size (µm) plotted as a function of stratigraphic level.

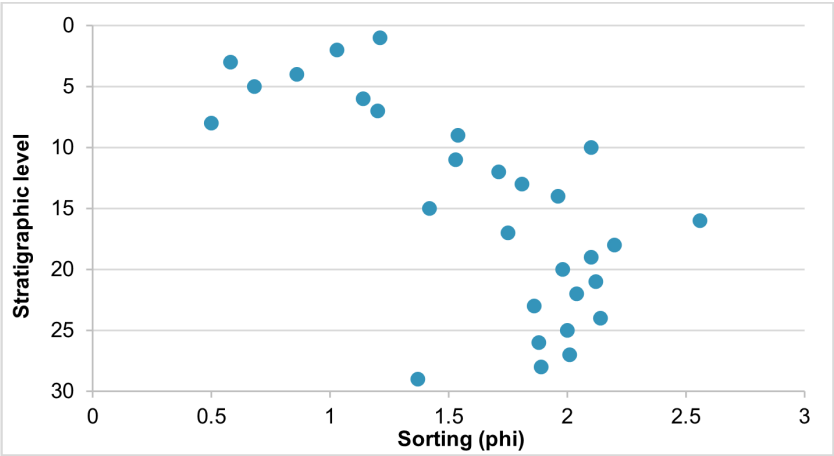

Figure A4.5.3. Scatter plot of sorting (phi) plotted as a function of stratigraphic level.

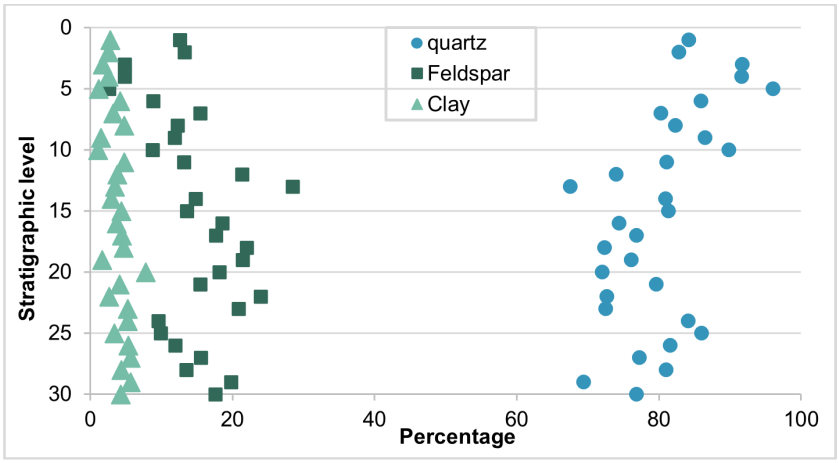

Figure A4.5.4. Scatter plot the percentage of quartz (blue circles), feldspar (green squares) and clay (green triangles) minerals plotted as a function of stratigraphic level.

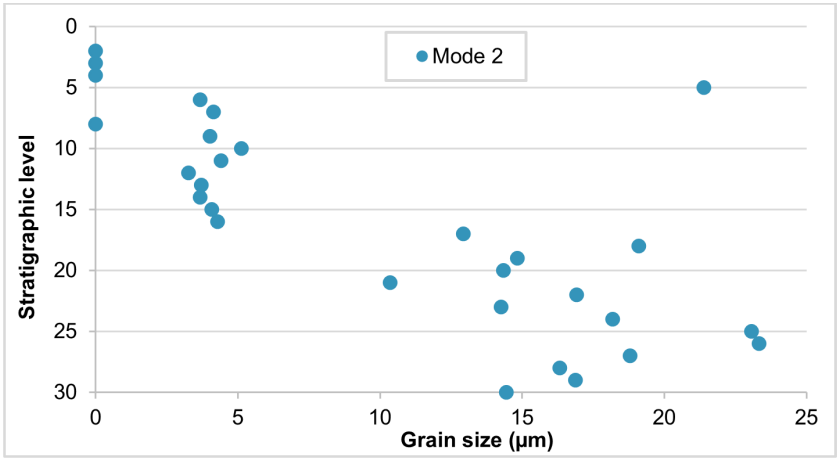

Figure A4.5.5. Scatter plot of mode 2 grain size (µm) plotted as a function of stratigraphic level.

4.6. OSL Sample Context

Table A4.6.1. OSL samples collected from UPK7. Details related to their sedimentary setting, location, matrix characteristics, and collection method are provided. Each sample is organised by deposit, followed by exposure. All samples listed below were collected in steel tubes (see methods Chapter 5).

OSL code	Field ID	OSL Cut	Depth (m)	Elevation (m asl)	Coordinates (dd WGS84)	Field observations of sample context
IS, Indurated sand						
Exposure 1b						
UOW-1802	90020	OC3	0.31	210.47	-32.037103, 19.405168	Collected from a rill section cut. The overlying surface is weathered. The exposed, overlying deposit is harder, more compacted, lacks structure, and is finer in composition from 0-25 cm bls. This caps the sampled sediment. From 25 to 37 cm bls, the sampled substrate is finely laminated. The OSL sample was collected from this finely laminated loamy sand. Calcrete inclusions are absent from both deposits.
UY, consolidated sand						
Exposure 1b						
UOW-2006	91080	OC9	0.22	210.47	-32.037025, 19.405133	Sample collected from the face of rill, on the lower slope of EXP1b. Throughout section, sediment is indurated and sandy, with nodular calcrete inclusions. The base of this cut exposes a very calcareous deposit that is possibly a downslope extension of LRcc. Artefacts are found haphazardly orientated throughout the matrix. Originally recorded as IS, subsequent examination suggests sampled deposit formed prior to UoW-1802—possibly of the UY or LR unit.

UOW-1804	90024	OC5	0.23	215.31	-32.036774, 19.405392	OC5 was cut into the side of a vegetation mound and its underlying consolidated sand. Sampled sediment: silty sand; no calcrete present; hard yet breaks up between fingers into fine sediment. OC is located ~4 m WNW of surface profile line (Figure 6.29). Positioned directly below exposed archaeological surface of late LSA material that includes pottery and an abundance of hornfels. Hypothesized as younger in deposition than 90022 (UOW-1803)
Exposure 2						
UOW-1801	90016	OC10	0.24	214.12	-32.036972, 19.405708	Sample collected from well consolidated sandy sediment that underlies a thin layer of loose surface sand (UCS). No clear bedding structure observed - deposit lacks obvious bedding planes. Early LSA archaeology rest on overlying surface, which was sampled as RNG AOI3 in 2014 and 2015.
LR, consolidated loamy sand						
Exposure 6						
UOW-2012	91153	OC1U	0.35	209.02	-32.036238, 19.404764	Consolidated sandy sediment with fine roots.
UOW-2013	91155	OC1L	0.6	208.76	-32.036238, 19.404763	Sample collected from lower section of OC cut. East wall shows signs of termite activity and speckling of white precipitates. Northeast section has fine white chalky calcareous inclusions. Roots cease just *above* sample tube. This sample and its associated sediment sample 91156 were collected *below* markers of bioturbation.
UOW-2014	91157	OC2	0.23	207.9	-32.036259, 19.404759	Speckling of white precipitates (salt?). Sediment appears to be washed down from upslope (The age dynamic between 91153 and 91155 OC1 is more stratigraphically reliable, while 91157 may not derive from the same depositional sequence).

LRcc, consolidated loamy sand, $CaCO_3$ inclusions						
Exposure 1a						
UOW-1834	90030	OC8	0.2	211.98	-32.036597, 19.404865	Surface is well formed with veins of calcrete within an indurated sandy sediment. Sample taken beneath veined calcrete surface (Figure A4.1.14); section shows veins of calcrete that are not well defined and only appear to extend ~10 cm below the surface of deposit cut (Figure A4.1.14). The remaining substrate yields nodular carbonates and fine roots; Sampled area is a pedestalled remnant of the lower deposit that surrounds it at ground level (Figure A4.1.14), which also includes veined calcrete sediment, but with overlying archaeology. It could relate to sample 90026/UOW-1832.
Exposure 1b						
UOW-1800	90018	OC11	0.33	211.55	-32.037026, 19.405271	Washed, hard surface, with a thin crusted layer. Slope wash evident from pronounced pedestalling and imbrication of small flakes and sandstone cobbles. Substrate is silty and sandy with calcrete veins. Bedding structure is absent. Well-developed shallow roots in the first 30 cm bls. Fine roots present throughout deposit. Sample collected below large calcareous inclusions in highly indurated sand.
UOW-1803	90022	OC4	0.23	213.83	-32.036904, 19.405331	Consolidated sediment with sparse nodules of calcium carbonate. Cut through side of sandy vegetation mound. A lense of artefacts and non-worked stone separate overlying sediment that is finely laminated, bioturbated (roots), and sandy (similar to 90018 or 90020). Sample collected from very hard underlying sediment. OC4 is ~5.5 m south-east of profile line, depicted in Figure 6.29. OSL cut made directly below and downslope of archaeological surface that yields fine materials and laminae, which are often fragmented and small. Fragments of pottery are also present at the top of the exposed slope (downslope of 90024). Upslope of Oct2014 AOI1/2.
UOW-1832	90026	OC6	0.26	213.68	-32.036748, 19.405156	Vein-calcrete sediment. Veins shot vertically throughout section. Quartzite and convergent blades dominate overlying archaeology and appear abundant in MSA quartzite artefacts. Early LSA/hornfels dominated archaeological surface is located upslope of sampled deposit's surface.

UOW-1833	90028	OC7	0.22	212.68	-32.036775, 19.405068	Sediment more solid/concreted than sample 90026/UOW-1932. Brown sediment with calcrete nodules sparsely distributed throughout, no sign of veining. However, XRD results show the presence of calcite. The deposit matrix is very well sorted. Due to hardness of sediment, the OSL sample was taken close to the surface. Surface archaeology overlying sample area is dominated by convergent blades (quartzite dominates). Possibly older than sample 90026. Hornfels naturally backed knives are also present.

4.7 Radial Plots

The following section presents the radial plot assessment of 12 samples from UPK7. Each plot depicts the single-grain D_e values accepted for each sample, the percentage of overdispersion, and the models employed to calculate a sample's paleodose for optical age determination. Radial plots are grouped by sample and ordered by their associated sedimentary unit. Selected plots for age calculation are enclosed by a blue-dashed border. Black dots shown in each radial plot represent individual grains that were included in the D_e and OD estimate. Grey bands are centred on a weighted D_e value using the method listed at the top of each plot: the central age model (CAM), CAM including the normalised absolute deviation (nMAD) (CAM + nMAD), and finite mixture model (FMM; Chapter 6.2). The outliers identified using nMAD are depicted as white triangles, indicating grains they were excluded from the final D_e and OD estimation shown in the relevant plot.

4.7.1 Indurated Sediment (IS): Loamy sand - slope wash/aeolian accumulation

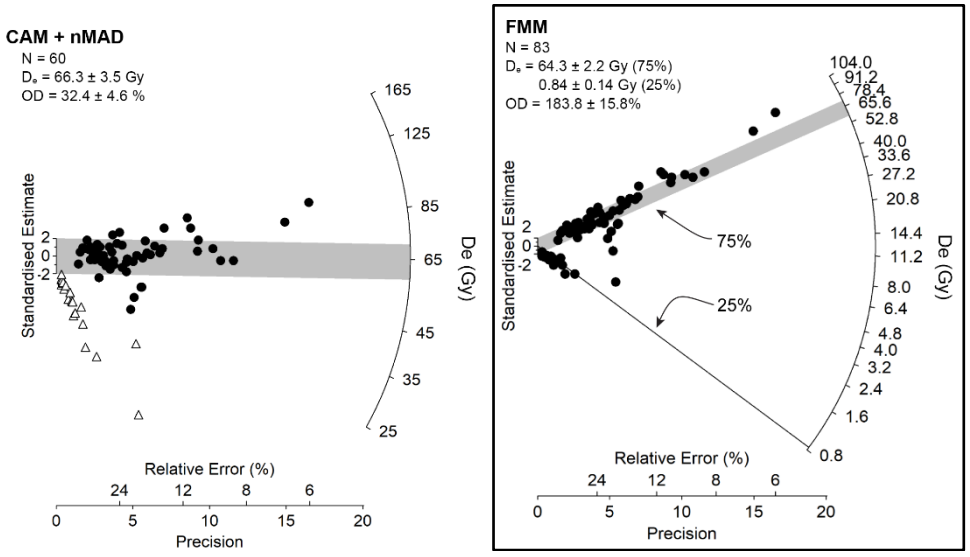

Figure A4.7.1. Radial plots, D_e values, OD, and accepted grain counts for Sample 90020/UOW-1802. Each radial plot depicts a different De value calculated using CAM after the exclusion of outliers, identified using nMAD.

Sample UOW-1802 shows a mixed distribution of accepted D_e values, with two distinct populations dispersed well beyond a central D_e (Figure A4.7.1a). The large OD of 183.8 ± 15.8% further signals to the presence of multiple populations in this sample. Isolating the larger of the two components using nMAD enables the calculation of a central D_e value that likely represents the paleodose of the sample's deposit (Figure A4.7.1b). However, the smaller component consistently clusters around a central D_e value, which warrant its inclusion in D_e estimation. Thus, the FMM was used to determine the number of populations in this sample, the proportion of accepted grains that each component represents, and their weighted means (Figure A4.7.2). The larger of the two populations contributes to 75% of the total accepted grain count, while 25% of grains form the smaller component. There is a substantial difference between the De values of each population with the larger component producing a De value of 64.3 ± 2.2 Gy; slightly less than the central De estimated using CAM plus nMAD (66.3 ± 3.5 Gy). The smaller component shows a distribution of individual De values that tend to be less precise than the first component and produce a much smaller D_e of 0.84 ± 0.14 Gy.

4.7.2 Upper Yellow (UY): Sandy loam – aeolian

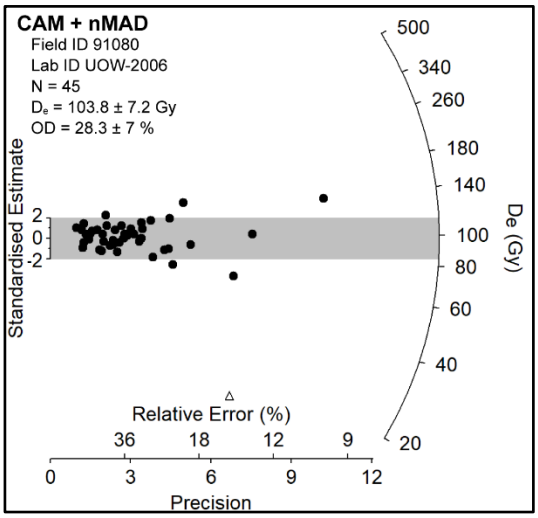

Figure A4.7.2. Radial plots, D_e values, OD, and accepted grain counts for Sample 91080/UOW-2006. Each radial plot depicts a different D_e value calculated using CAM after the exclusion of outliers, identified using nMAD.

Sample UOW-2006 shows a scattered distribution of De values, the majority of which have large relative errors. Of the 47 grains accepted for D_e estimation. The central De is 97.4 ± 8.3 Gy with 52.5 ± 8.3% overdispersion. With the removal of a single outlier, identified using nMAD, resulted in a greatly reduced OD of 28.3 ± 7% and a slightly higher central D_e value of 103.8 ± 7.2 Gy.

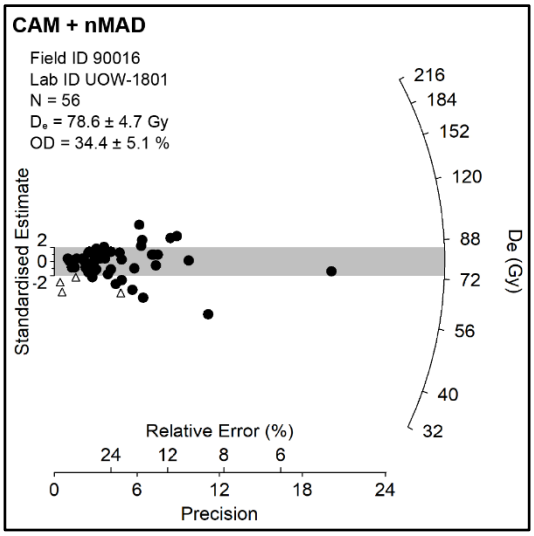

Figure A4.7.3. Radial plots, D_e values, OD, and accepted grain counts for Sample 90016/UOW-1801. Each radial plot depicts a different D_e value calculated using CAM after the exclusion of outliers, identified using nMAD.

Over half of sample UOW-1801's signal-bearing grains (54%) were accepted, while less than 10% were rejected due to saturation. The D_e values have a high OD (37.4 ± 5.3%) that persists even after nMAD outliers were identified and excluded (34.4 ± 5.1%). This suggests possible mixing of the sampled deposit. Bioturbation is suggested by the absence of deposit structure observed throughout the exposed section of OSL cut 10 (see Table A4.6.1). The nMAD-corrected CAM D_e was selected to calculate the burial age of sample UOW-1801.

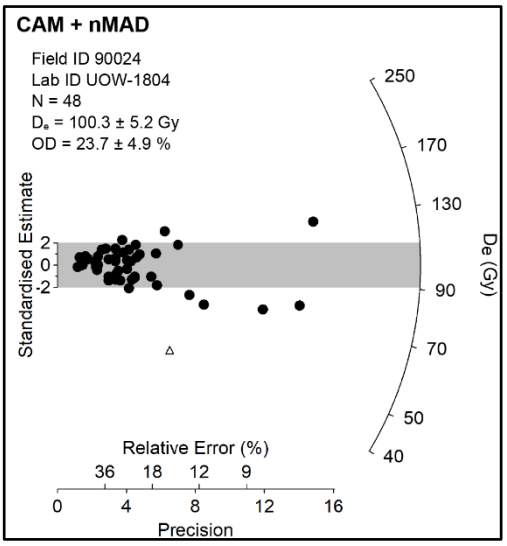

Figure A4.7.4. Radial plots, D_e values, OD, and accepted grain counts for Sample 90024/UOW-1804. Each radial plot depicts a different D_e value calculated using CAM after the exclusion of outliers, identified using nMAD.

Using CAM, the central D_e of sample UOW-1804 (97.6 ± 5.9 Gy) was obtained from a scattered distribution of 49 accepted grains, 37% of all signal-emitting grains. It has a high OD of 30.8 ± 5.3%. After a single outlier was identified using nMAD, its exclusion reduced the OD to 23.7 ± 4.9%. This has minimal effect on the central D_e (100 ± 5.2 Gy). Moreover, the likelihood that the central D_e is truncated due to the exclusion of saturated D_e values is low, with only 13% of grains identified as saturated and 6% yielding extrapolated D_e values (see Tables 6.5 and 6.6). Thus, the nMAD-corrected CAM D_e will be used to calculate the burial age of sample UOW-1804.

4.7.3 Lower Red (LR): Sandy loam – aeolian

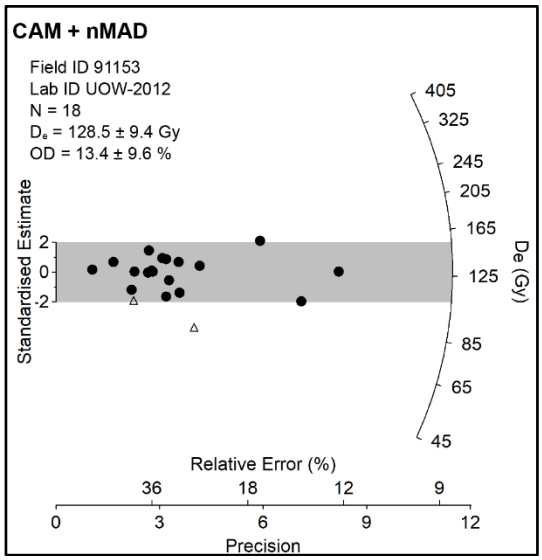

Figure A4.7.5. Radial plots, D_e values, OD, and accepted grain counts for Sample 91153/UOW-2012. Each radial plot depicts a different D_e value calculated using CAM after the exclusion of outliers, identified using nMAD**.**

Only 24% (n = 20) of sample UOW-2012's signal-emitting grains (n = 82) were accepted for analysis (Table 6.7). The radial plot of sample UOW-2012 shows a scattered distribution with an OD of 25.1 ± 9%. Two outliers were identified and excluded from this distribution after applying nMAD, reducing the OD to 13.4 ± 9.6% (Figure A4.7.5 & Table 6.7). The possible truncation of the nMAD-corrected central D_e is likely given that 17% of grains identified as saturated. This is amplified by the additional 22% of grains that were excluded because their L_n/T_n signal failed to intercept the regenerative dose curve (L_x/T_x, see section 'D_e Truncation' for a possible explanation of this type of grain behaviour). Thus, the nMAD-corrected D_e will be treated with caution and the estimated age of this sample interpreted as the minimum age of deposit burial.

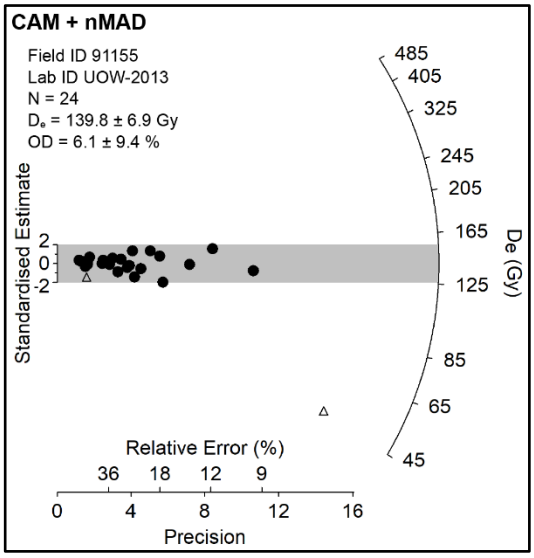

Figure A4.7.6. Radial plots, D_e values, OD, and accepted grain counts for Sample 91155/UOW-2013. Each radial plot depicts a different D_e value calculated using CAM after the exclusion of outliers, identified using nMAD.

Of UOW-2013's signal-emitting grains (n = 88), 30% (n = 26) were accepted for analysis (Table 6.7 & Figure A4.7.6). UOW-2012 has a scattered distribution (Figure A4.7.6) with an OD of 31.5 ± 7.7% (Table 6.7). Two outliers were identified and excluded from this distribution after applying nMAD, reducing the OD to 6.1 ± 9.4% (Figure A4.7.6 & Table 6.7). Truncation of the nMAD-corrected central D_e is likely given 19% of grains in this sample were saturated (Table 6.7). Thus, sample UOW-2013's nMAD-corrected central D_e will be used conservatively and treated as a minimum value when calculating the sediment sample's burial age.

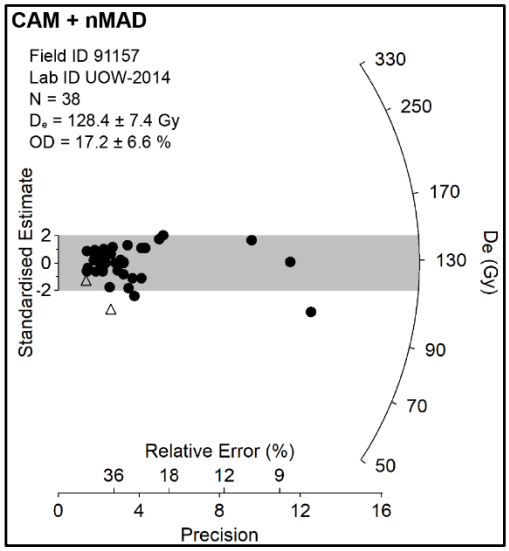

Figure A4.7.7. Radial plots, D_e values, OD, and accepted grain counts for Sample 91157/UOW-2014. Each radial plot depicts a different D_e value calculated using CAM after the exclusion of outliers, identified using nMAD.

The measurement of sample UOW-2014 returned 116 signal-emitting grains, 35% (n = 41) of which were accepted for analysis (Table 6.7). sample UOW-2014 has a moderately scattered distribution (Figure A4.7.7), and an OD of 20.6 ± 6.7% and a central D_e of 124.5 ± 7.6 Gy prior to outlier exclusion (Table 6.7). The D_e distribution appears truncated on the higher end of their distribution. Several high precision grains exaggerate the clustered appearance of the more imprecise D_e values in the dataset. After applying nMAD, only two outliers were identified and excluded (Figure A4.7.7). This reduced the OD to 17.2 ± 6.6% and increased the central D_e value by only a few Gy (128.4 ± 7.4 Gy; Figure A4.7.7 & Table 6.7). Sample UOW-2014's nMAD-corrected central D_e was selected to calculate is optical age. However, this sample also yields a high percentage of saturated grains (19%, Table 6.5) as well as grains that failed to produce D_e values by interpolation (21%, Table 6.5). Thus, its D_e distribution is interpreted as truncated, which will ultimately produce an underestimated age. As a conservative measure, the age produced from the nMAD-corrected central D_e and sample DR will be interpreted as its minimum age of deposition.

4.7.4 Lower Red with CaCO3 (LRcc): Loamy sand - aeolian

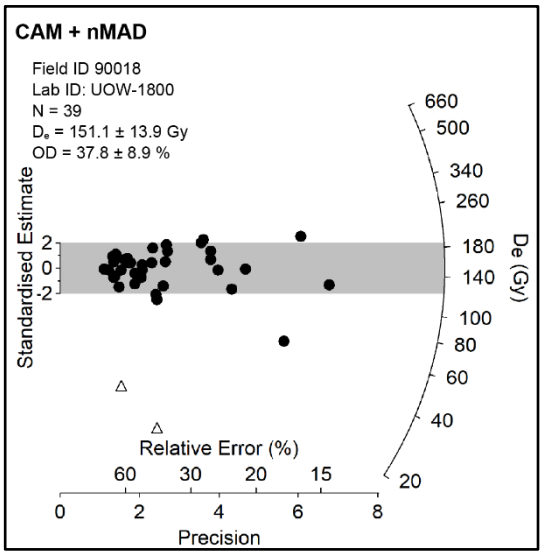

Figure A4.7.8. Radial plots, D_e values, OD, and accepted grain counts for Sample 90018/UOW-1800. Each radial plot depicts a different D_e value calculated using CAM after the exclusion of outliers, identified using nMAD.

UOW-1800 has a scattered distribution (Figure A4.7.8) of 41 (29%) accepted grains (Table 6.5). The CAM derived central D_e of 116.4 ± 23.5 Gy has one of the largest OD's in the sample-set (119.2 ± 15.4%) after the mixed sample UOW-1802 (OD = 183.8 ± 15.8%; Table 6.7). Applying nMAD identified two outlier grains with substantially lower D_e values than the rest of the sample and high relative errors (Figure A4.7.8). Their exclusion increases the central D_e to 151.1 ± 13.9 Gy and reduces the OD to 37.8 ± 8.9% (Table 6.7). The possibility that samples UOW-1800's D_e distribution is truncated due to saturation is suggested by its large percentage of saturated grains (19%, see Table 6.5). Therefore, the nMAD-corrected CAM D_e will be used to calculate the sample's minimum age estimate.

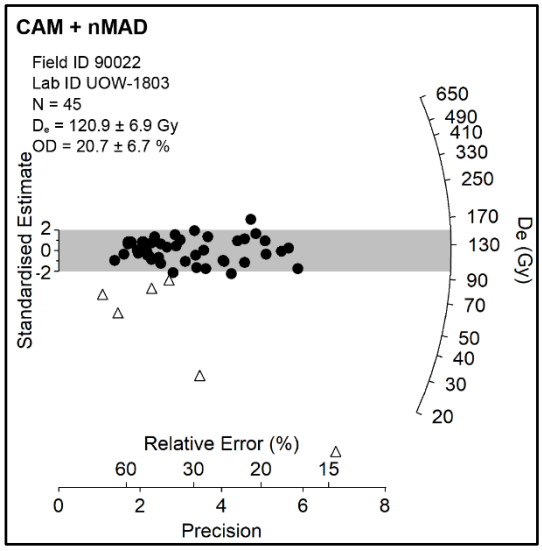

Figure A4.7.9. Radial plots, D_e values, OD, and accepted grain counts for Sample 90022/UOW-1803. Each radial plot depicts a different D_e value calculated using CAM after the exclusion of outliers, identified using nMAD.

Of the 134 signal-emitting grains in sample UOW-1803, 41% were accepted (n = 51, Table 6.5). The radial plot of each grain's D_e value produces a scattered distribution (Figure A4.7.9). They have a central D_e of 90.4 ± 12.1 Gy and large OD (87.7 ± 10.3%, Figure A4.7.9 & Table 6.7). After identifying and excluding outlier grains using nMAD, the OD decreased to 20.7 ± 6.7% (Table 6.7). The precision of the remaining distribution varies. The radial plot in Figure A4.7.9 shows increased variability between individual D_e values as precision increases. Together, individual grains produce a spray of D_e values that become increasingly dispersed as precision increases, a trend observed in all the sedimentary units sampled across the study area. It is possible that sample UOW-1803's D_e distribution is truncated as a result of grain saturation, suggested by the sizable proportion of saturated grains (16%) originally identified and excluded from the dataset (Table 6.5). The nMAD-corrected CAM D_e will be used to calculate the sample's minimum age estimate.

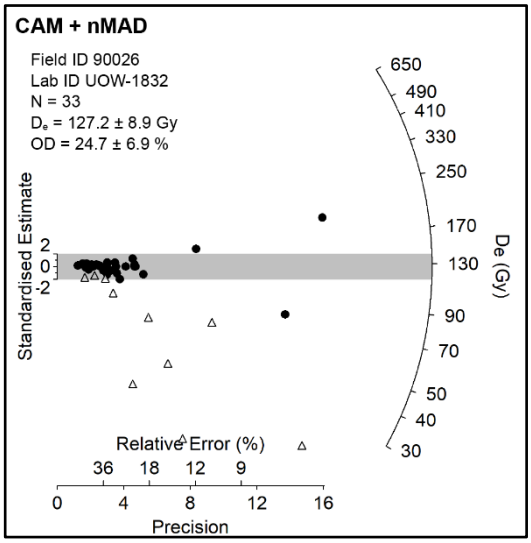

Figure A4.7.10. Radial plots, D_e values, OD, and accepted grain counts for Sample 90026/UOW-1832. Each radial plot depicts a different D_e value calculated using CAM after the exclusion of outliers, identified using nMAD.

Sample UOW-1832 returns similar proportions of accepted (30%) and saturated (29%) grains (Table 6.5 & 6.6). Its D_e distribution shows a clear truncation of higher D_e values, symptomatic of a saturated sample (Figure A4.7.10). The inclusion of a sparse scatter of intrusive grains that vary markedly in D_e value and precision exaggerate the OD (97.9 ± 11.9%), resulting in further underestimation of UOW-1832's CAM D_e. After applying nMAD, the exclusion of outliers decreased the central D_e by ~46 Gy, resulting in a nMAD-corrected D_e of 127.2 ± 8.9 Gy and 24.7 ± 6.9% OD (Figure A4.7.10 & Table 6.7). As with UoW-1803, application of both the minimum and maximum age model failed to return D_e values that differ meaningfully from the nMAD-corrected central D_e. Thus, the nMAD-corrected central D_e will be used to calculate the depositional age of the sample. As a conservative measure, the age derived from the use of this D_e will be interpreted as a minimum value.

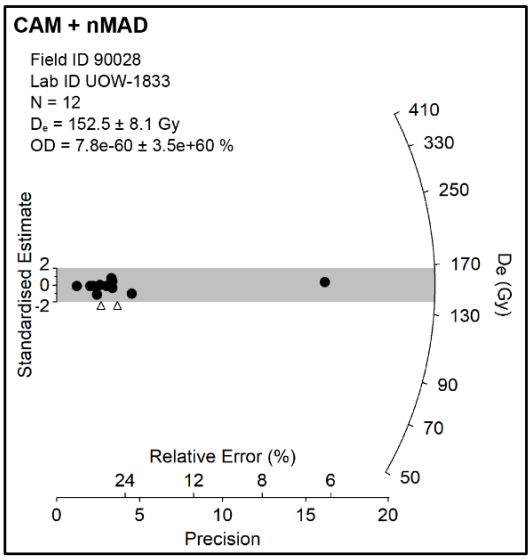

Figure A4.7.11. Radial plots, D_e values, OD, and accepted grain counts for Sample 90028/UOW-1833. Each radial plot depicts a different D_e value calculated using CAM after the exclusion of outliers, identified using nMAD.

As few as 68 signal-bearing grains were identified in sample UOW-1833 and only 21% (n = 14) of these were accepted for D_e analysis (Table 6.5). Its D_e distribution is well constrained to within 2 units of a central value and has the smallest OD values in the sample set (10.9 ± 9.1%, Table 6.7). However, the low number of accepted grains in this sample (n = 14) and the presence of an imprecise D_e value that is >2 units above the central D_e suggest that its D_e distribution is not a reliable representation of the sample's paleodose (Table 6.7). Thus, the D_e of 137.2 ± 10.6 Gy and its resulting age-estimate are excluded from interpretation of the depositional history of LRcc until a larger sample of signal-emitting grains is obtained.

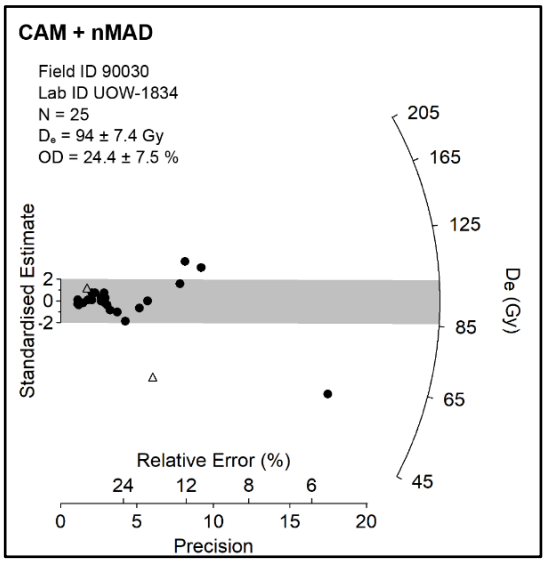

Figure A4.7.12. Radial plots, De values, OD, and accepted grain counts for Sample 90030/UOW-1834. Each radial plot depicts a different De value calculated using CAM after the exclusion of outliers, identified using nMAD.

Sample UoW-1834 has a D_e of 88.9 ± 9.3 Gy and high OD by 34.2 ± 8.2% (Table 6.7). Figure A4.7.12 shows a scattered D_e distribution with the cluster of D_e values overemphasised by the low precision of a few low D_e values. After applying nMAD, only minimal increase in the central D_e and decrease in OD results were observed (Figure A4.7.12 & Table 6.7). The small proportion of grains accepted for this sample makes it difficult to determine if the distribution of grains is representative of the original deposit. Moreover, the percentage of saturated grains (24%) matches the amount accepted for central D_e analysis. A further 15% of grains were also excluded from the final distribution due to the extrapolation of their D_e values, beyond the maximum regenerative dose (Table 6.5). Thus, it is likely that the CAM D_e is truncated by the exclusion of saturated grains. For this reason, the central D_e, modelled after exclusion of nMAD outliers, is treated with caution and will be used in the age equation as a minimum value (Table 6.9).

4.8 Cosmic Dose Burial Depth Scenarios

Table A4.8.1. OSL burial depth scenarios. If overburden is to be included, then the historic scenario is considered the most conservative and reliable scenario for including in the final calculation of each sample's optical age.

Units	Burial Scenarios (S)			S3 Deposit Specific Assumptions
	S1	S2	S3	
	Current	Historic	Stratified	
IS	Current The recorded depth below surface from the current surface to the sediment sample's position.	Current + Historic Overburden includes the current sample depth below surface and the minimum observed amount of deflation (>0.4 m) that has occurred since the introduction of European farming methods (at most, within the last 300 years).	Current + Historic (IS) + UCS	IS occurs today as either exposed or covered by semi consolidated and unconsolidated sand (SCS & UCS). S3 accounts for the removal of overlying IS due to historic erosion (~0.4 m) in addition to a deposit-wide overburden of active unconsolidated sand (UCS, ~1 m in thickness).
UY			Current + Historic (UY) + UCS	UY occurs at higher elevations of UPK7. This deposit is found either in a state of exposure or covered by UCS. It is unclear if the IS unit covers UY, is part of the same deposit, or the result of slope washed UY sediment, redeposited downslope. S3 accounts for the historic loss and exposure of a younger, thicker UY deposit (or possibly an overlying IS unit) and assumes the near constant presence of UCS for most of UY's post-depositional history.
LR			Current + Historic (UY/IS) + UCS	LR and LRcc are considered remnants of a depositional history that was more vegetated, humid, and conducive to sediment stability than the depositional contexts of UY and IS. Thus, S3 assumes minimal erosion of LR and accounts for the long-term addition and consolidation of an overlying UY (or IS), possibly removed by historic erosion. Active UCS is also included as additional overburden.
LRcc			Current + Historic (LR + UY/IS) + UCS	LRcc is considered the basal-most deposit underlying all other consolidated and unconsolidated sandy units at the foot of UPK7's hillslope. OSL samples collected from LRcc either occur directly below an overlying LR unit or beneath an exposed LRcc surface. Here, historic deflation is considered the main erosional force removing the residual overlying units of LR and/or UY. Active UCS is also included as additional overburden.

Table A4.8.2. Estimated burial depths for each sample (a) and averaged burial depths for each sampled deposit (b) at UPK7*.

A

	Sampled unit	IS	UY			LR			LRcc				
	Lab ID (UOW)	1802	2006	1801	1804	2012	2013	2014	1800	1803	1832	1833	1834
	Sample	90020	91080	90016	90024	91153	91155	91157	90018	90022	90026	90028	90030
Depth Scenario (m bls)*	S1. Current	0.25	0.22	0.24	0.23	0.35	0.60	0.23	0.33	0.23	0.26	0.22	0.20
	S2. Historic	0.65	0.62	0.64	0.63	0.75	1.00	0.63	0.73	0.63	0.66	0.62	0.60
	S3. Stratified	1.55	1.52	1.54	1.53	1.65	1.90	1.53	1.63	1.53	1.56	1.52	1.50

B

	Averaged Depths (m bls)				
	Sampled unit	IS	UY	LR	LRcc
Depth Scenario	1. Current	0.25	0.24	0.39	0.25
	2. Historic	0.65	0.64	0.79	0.65
	3. Stratified	1.55	1.54	1.69	1.55

* See Table A4.8.1 for depth scenario descriptions

4.9 DirectAMS Analysis Report

The following appendix presents a report provided by the radiocarbon lab DirectAMS, followed by a description of the radiocarbon samples collected from four combustion features: two from Lungkaal, one from UPK7, and one from UPK9. The materials and structural features of three combustion features—from Lungkaal and UPK9—are characteristic of human-built hearth features. The fourth—from UPK7—only preserves the basal layer of a combustion feature. It was not possible—based on the macro analysis of its structure and content—to determine if this feature resulted from the intentional burning of organic matter by humans, or from unintentional combustion due to anthropogenic and/or natural processes. All coordinates are given in WGS 1984.

4.9.1 Report by DirectAMS conventional radiocarbon age determinations and calculations

Report: 1921-027123-027126 27 March 2018

Customer: 1921
Natasha Phillips
University of Wollongong
School of Earth and Environmental Sciences
Room 268, Building 41
Northfields Ave.
Wollongong, NSW 2522
Australia

Samples submitted for radiocarbon dating have been processed and measured by AMS. The following results were obtained:

Table A4.9.1. Conventional Radiocarbon Age (CRA) Determinations & Calculations

DirectAMS code	Submitter ID	Sample type	Fraction of modern		Radiocarbon age	
			pMC	1σ error	BP	1 σ error
D-AMS 027123	91071	sediment	57.04	0.21	4510	30
D-AMS 027124	91118	charcoal	98.60	0.28	113	23
D-AMS 027125	91119	charcoal	98.33	0.27	135	22
D-AMS 027126	91130	charcoal	99.71	0.33	Modern	-

Results are presented in units of percent modern carbon (pMC) and the uncalibrated radiocarbon age before present (BP). All results have been corrected for isotopic fractionation with an unreported $\delta^{13}C$ value measured on the prepared carbon by the accelerator. The pMC reported requires no further correction for fractionation.

4.9.2 Radiocarbon samples and age calibration

UPK7

Sediment sample 91071 (Lab ID: D-AMS 027123) derives from a remnant charcoal feature on the surface of the Indurated Sand (Figure A4.9.1A-C), in the westernmost exposure (located above the boulder bench) of UPK7 (19°24'18"E 32°2'13"S, GCS: WGS 1984, see Figure A4.1). These ages are determined from charcoal rich sediment, wherein the charcoal was too small and fragmented to isolate under a microscope (e.g., Figure A4.9.1C). Instead, any potential carbon intrusions such as roots, insects and micro fauna were removed, and the sediment sample sent off for bulk analysis. The uncalibrated age for D-AMS 027123 is 4510 ± 30 BP (standard error to within 1 sigma, age corrected for isotopic fractionation [δ13C], Table A4.9.1). D-AMS 027123 was calibrated providing a minimum exposure age for the Indurated Sand in the mid-Holocene (Figure A4.9.2 & Table A4.9.2). Based on the results of the other combustion features (see Table A4.9.2 & below) this was unexpected, as combustion features yielding conventional radiocarbon ages older than 300 years are rare in the Doring River Valley (see 91118-9 from LNGKL 5f and 91130 from hearth feature ‘UPK9b’ below).

Sample/Field ID: 91071

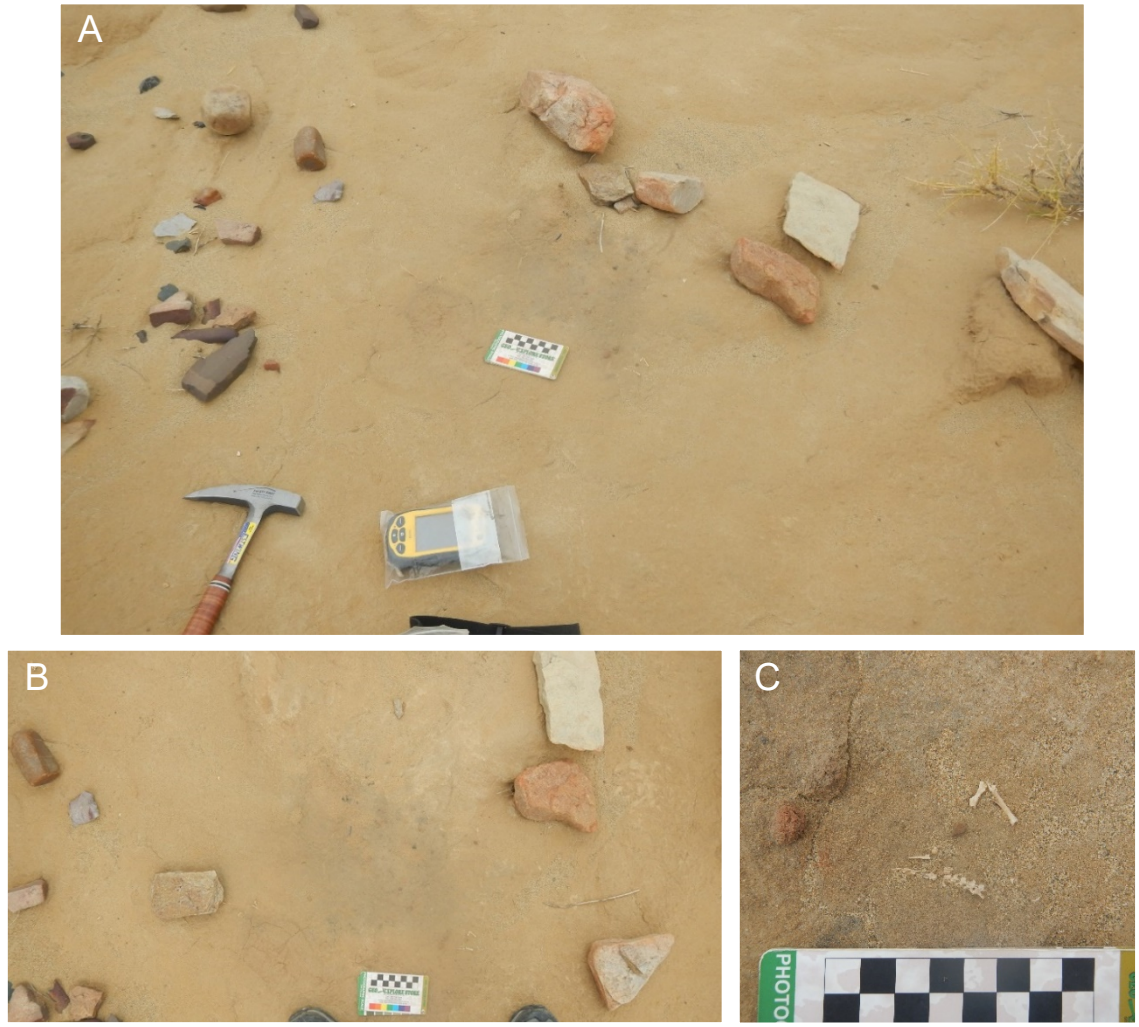

Figure A4.9.1. Photographs of the sampled combustion feature at UPK7 exposed in Indurated Sand (IS), showing (A) the combustion feature and scatter of stones, (B) plan view of the feature, and (C) detail of baked earth, faunal remains, and charcoal. Sample 91071/D-AMS 027123 was collected from 20 mm below the surface this feature. See Figure A4.1 for feature location. Photo facing southwest. Scale is 100 mm.

Laboratory number: D-AMS 027123

Material: Sediment

Lab: DirectAMS

Analysis: Accelerator Mass Spectrometry (AMS), corrected for isotopic fractionation with an unreported δ13C value measured on the prepared carbon by the accelerator

Conventional radiocarbon age (CRA): 4510 ± 30 BP (1σ error)

Calibration

Calibration curve: SHCal13 (Hogg *et al.* 2016)

Software: OxCal version 4.3.2 (Bronk Ramsey 2017)

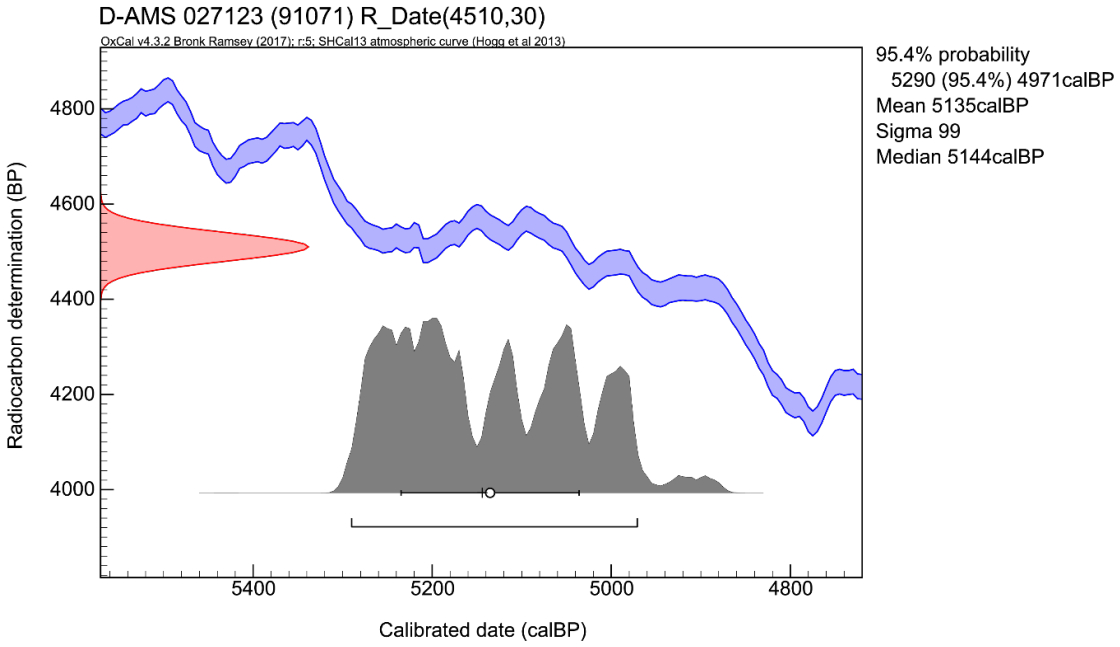

Figure A4.9.2. The CRA of Sample 91071 (D-AMS 021123, 4510 ± 30 BP) is shown intercepting the SHCal13 atmospheric curve (Hogg *et al.* 2016) between 5290-4971 cal BP, at a 95% probability range.

Table A4.9.2. Calibrated Radiocarbon Determinations* Before Present (BP = 1950)^ and in Calendar years (BC and AD)

Lab ID	Field ID	POI	Unmodeled (calBP)			mean	sigma	median
			from	to	probability (%)			
D-AMS 027123	91071	UPK 7	5290	4971	95.4	5135	99	5144

Result: the calibrated age for D-AMS 027123 is between 5290 to 4971 cal BP (95% confidence). The sample's calibrated age has a range of ~300 year as it intercepts with a plateau in the calibration curve.

LNGKL (5f)

Sample 91119 (Lab ID D-AMS 027125) was taken from a built historic stone hearth (Figure 4.9.3a-h). Charcoal was subsampled under a microscope by picking with tweezers. These were sent off to DirectAMS for pre-treatment and analysis. The uncalibrated age is 135 ± 22 BP (standard error 1σ, age corrected for isotopic fractionation [$\delta^{13}C$], Table A4.9.1). This sample was extracted from between structurally intact quarried sandstone, above a layer of lithic artefacts, all of which rest upon a pedestal of sterile, indurated sand (~400 mm above the surrounding ground level, see Figure A4.9.3). OSL sample was not taken from the underlying sediment due to concerns for the structure's integrity.

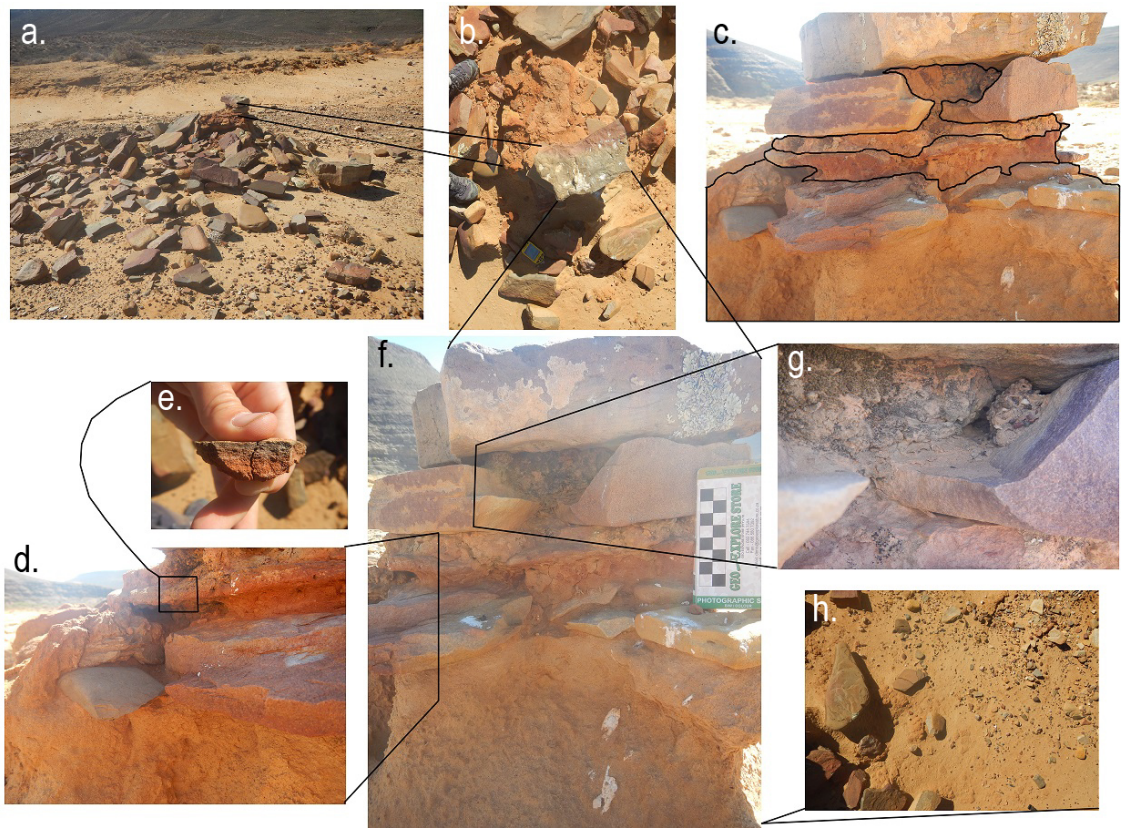

Figure A4.9.3. Photographic compilation of the built hearth at LNGKL shown (a) pedestalled above and in relation to the surround deflated modern surface, (b) from above, and as a series of detailed images of the baked (c-f) and biocrusted sediment (f & g) beneath capping fine-grained sandstone slabs. Photo (d) also shows an artefact protruding from between the base and baked sediment of the overlying hearth and sterile sand below. The surrounding, deflated ground and lithic scatter are depicted in the top-down photo in (h).

Sample 91118 (Lab ID D-AMS 027124) was collected from beneath well clustered, fire cracked sandstones (>100 mm max dimension, Figure A4.9.4). These yielded sizable pieces of charcoal wood, which were isolated out under a microscope with tweezers and sent to the DirectAMS for pre-treatment and analysis. The uncalibrated radiocarbon determination for this sample is 113 ± 23 (standard error to within 1 sigma, age corrected for isotopic fractionation [$\delta^{13}C$], Table A4.9.1). The charcoal from this feature returned a similar uncalibrated ^{14}C determination to 91119. Both radiocarbon ages intercept with the calibration curve three to four times making it impossible to determine when within the last 300 years their associated combustion features were last used.

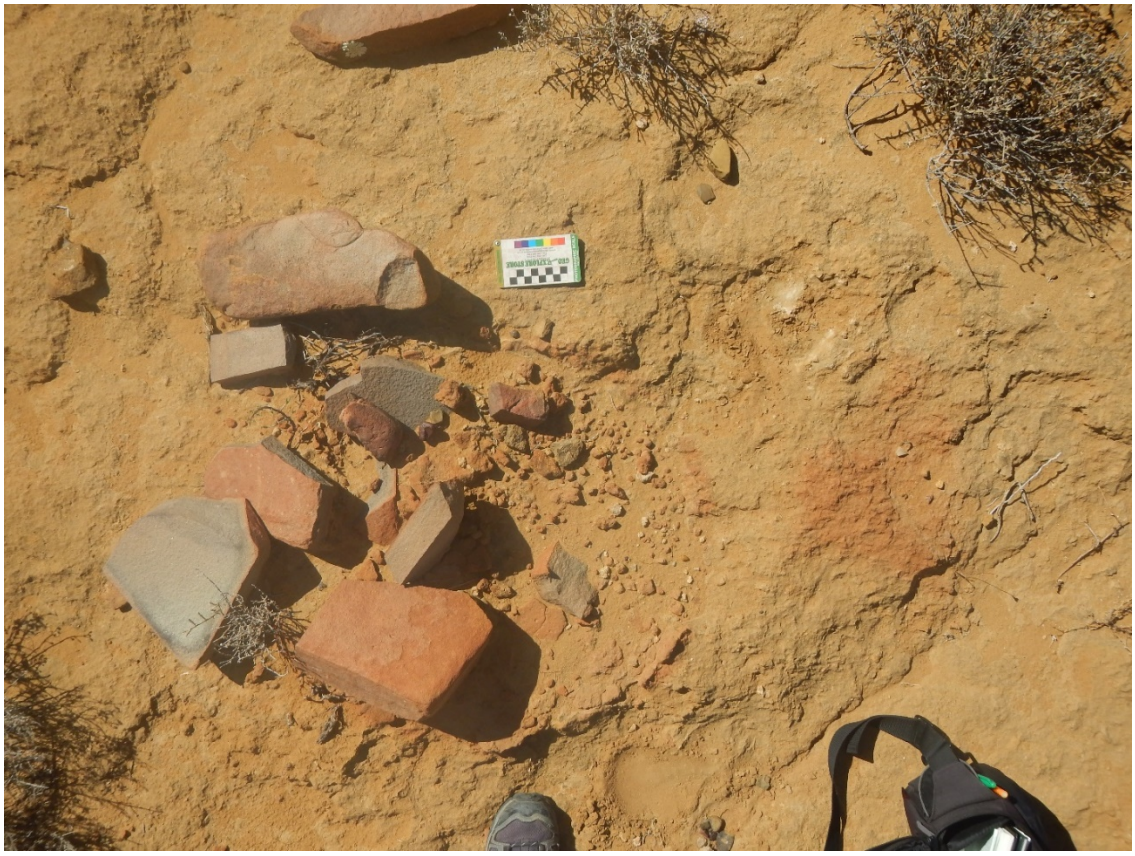

Figure A4.9.4. Photograph of hearth at Lungkaal taken from above. Scale is 100 mm. Sample 91118 was collected from beneath one of the hearth stones. Note the exposure of baked earth to the right of the cluster of hearth stones.

Sample 91118 was originally expected to yield a much older age (like sample 91071 from UPK7) due to its less permeant, fire-scoop-like structure (Figure A4.9.4). This feature appears to reflect the classic buried hearth structure, whereby a hole would have been cut into the underlying sediment and stones placed at the base for heat retention (Figure A4.9.4). Over the last 0-300 years the original sediment surface above the base of this feature has deflated down to expose the base heat retainer stones, which have temporarily capped its substrate, protecting the underlying sediment and charcoal from exposure and erosion.

UPK9 (b)

Charcoal sample 91130 (D-AMS 027126) was collected from beneath heat retainer stones of a hearth feature, overlying a well-defined red baked sediment base (Figure A4.9.5). The calculated CRA for D-AMS 027126 was younger than 1950 and was reported as 'modern' in the DirectAMS report (Table A4.9.1).

Figure A4.9.5. One of two hearths at UPK9. This hearth was sampled for radiocarbon dating (sample 91130), while the built stone hearth (see Figure 8.2) was not sampled. The length of the Trimble Juno is approx. 150 mm. Note how deflation of less resistant substrate has exposed the basal 'scoop' of back earth.